SSD-TR00608
12 May 1989

MULTIPLE BEAM ANTENNA/SWITCH SYSTEM STUDY FINAL REPORT

Submitted to:
NATIONAL AERONAUTICS AND SPACE ADMINISTRATION
GODDARD SPACE FLIGHT CENTER
GREENBELT, MARYLAND 20771

CONTRACT NO. NAS5-30297

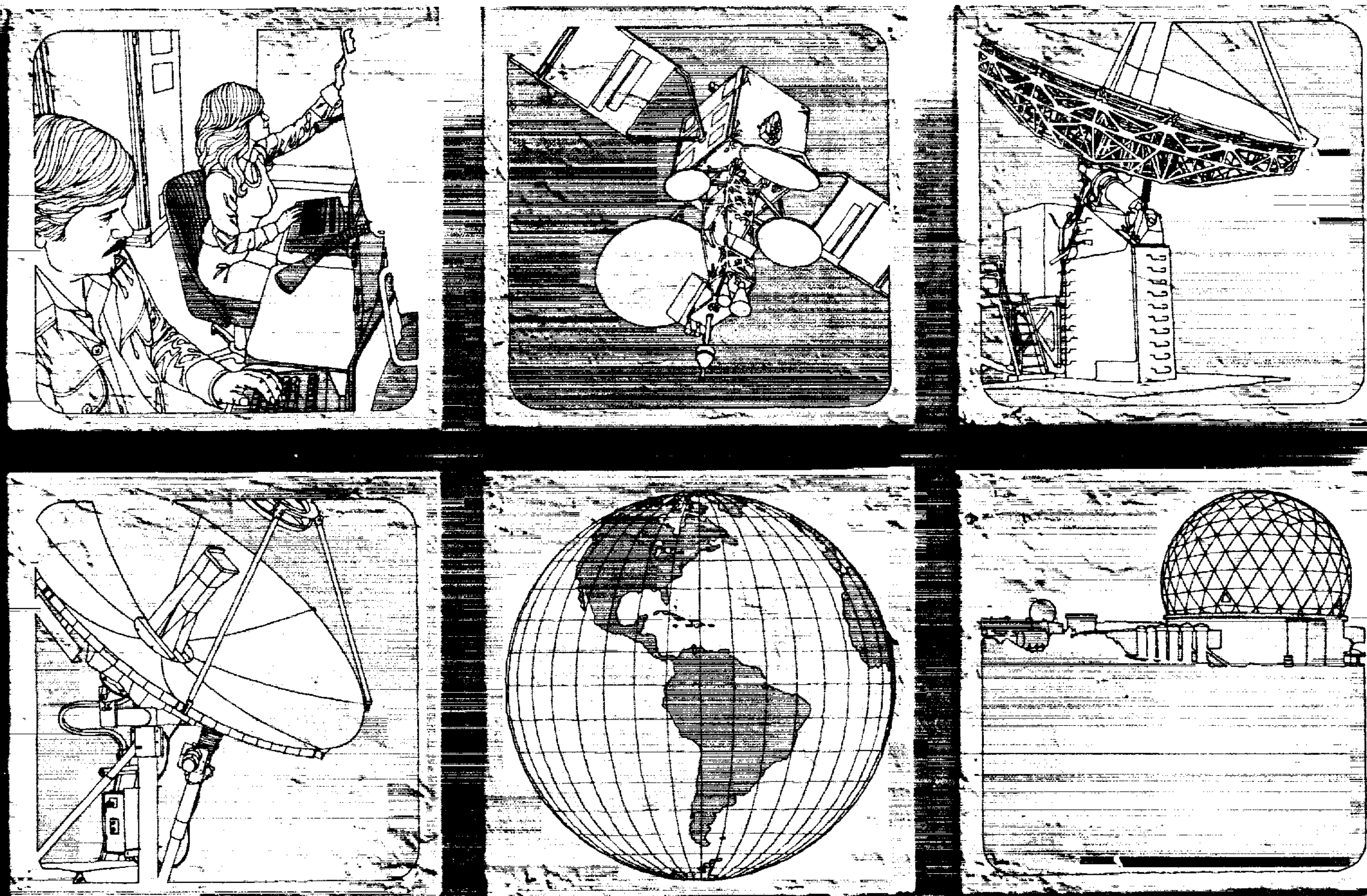

Ford Aerospace/Space Systems Division

SSD-TR00608
12 May 1989

MULTIPLE BEAM ANTENNA/SWITCH SYSTEM STUDY
FINAL REPORT

Submitted to:
NATIONAL AERONAUTICS AND SPACE ADMINISTRATION
GODDARD SPACE FLIGHT CENTER
GREENBELT, MARYLAND 20771

CONTRACT NO. NAS5-30297

FORD AEROSPACE
SPACE SYSTEMS DIVISION
3825 FABIAN WAY
PALO ALTO, CALIFORNIA 94303

STATEMENT OF WORK (SOW) COMPLIANCE MATRIX

Task	Description	SOW Para	Report Section
A	The SGL system		
AA	Analysis of overall SGL system parameters and performance	2.1	2.8
AB	Analyze & perform trade-offs on interconnection schemes between SGL transmitters/receivers and SGL antennas.	2.3	3.9
AC	The SGL antenna subsystem		
ACA	Concept development - definitize requirements	2.1	3.1
ACAA	Effect of different locations of S/C #1 & S/C #2	2.1	2.9
ACAB	Geometrical considerations related to ground stations location		2.5
ACAC	Identification of navigation & attitude requirements	2.1	2.18
ACB	Antenna system electrical & mechanical conceptual design	2.3.1.1	3.3,3.12
ACC	Study candidate antenna systems. Compare performance, complexity, risk, tolerances size, deployment requirements & cost	1.4	3.3,3.11
ACD	Develop high level design & specifications for the selected antenna	2.3.1.1	3.12
ACE	Develop an appropriate antenna acquisition & tracking system and analyze alignment stability	2.3.1.1	3.9,3.10
ACF	Investigate the use of advanced composite materials for feed & antenna fabrication	2.3.1.1	3.6
ACG	Define, describe & analyze all necessary electromechanical mechanisms and drive systems	2.3.1.1	3.8,3.10
ACH	Analyze system level mechanical & thermal errors budget	2.1	3.8
ACI	Specify packaging and stowing requirements for shuttle launch	2.3.1.1	3.7
ACJ	Prepare conceptual design drawings and mass property estimates	2.3.1.1	3.7,3.12
ACK	Define preliminary operational concept from launch through orbital operation	2.1	2.20
ACL	Housekeeping requirements from prelaunch checkout to routine operation	2.1	2.20
ACM	Prepare weight & size estimates of the SGL antenna system	2.3.1	3.12

STATEMENT OF WORK (SOW) COMPLIANCE MATRIX (Continued)

Task	Description	SOW Para	Report Section
ACN	General requirements for the terminal ground support equipment		2.20
ACO	Develop calibration & performance verification concept	2.3.1	2.19
AD	The downlink transmit subsystem		
ADA	An overview of Ka & Ku HPA technology for the 1990s with respect to ATDRSS requirements	2.1	4.2
ADB	Assess phase noise requirements	2.3.1.2	2.12
ADC	Investigate best method of modulation	2.3.1.2	2.3,2.4
ADD	Study possible solutions and generate block diagrams of candidate transmit subsystems, which satisfy ATDRSS requirements	2.3.1.2	4.2,4.3
ADE	Generate a block diagram for each functional unit of the selected design approach	2.3.1.2	4.2,4.3
ADF	Generate general specifications for each functional unit	2.3.1.2	4.2,4.3
AE	The uplink receive subsystem		
AEA	An overview of Ka & Ku LNA and receiver front-end technology for the 1990s with respect to ATDRSS requirements	2.1 2.3.1.2	4.2 4.2
AEB	Assess phase noise requirements	2.3.1.2	2.12
AEC	Study possible solutions and generate block diagrams of optional receive subsystems, which satisfy ATDRSS requirements	2.3.1.2	4.2
AED	Generate a block diagram for each functional unit of the selected design approach	2.3.1.2	4.2,4.3
AEE	Generate general specifications for each functional unit	2.3.1.2	4.2,4.3
AF	Develop a built-in-test concept for the SGL system	2.1	2.19
AG	Calculate life expectancy of major SGL components and consider redundancy	2.1	4,5
AGA	Determine system susceptibility to space radiation environment	2.1	2.14
AGB	Consider modularity for possible in-space servicing	2.1	2.15
AGC	Prepare a reliability prediction for 10 year lifetime	2.3.1.1	4,5

STATEMENT OF WORK (SOW) COMPLIANCE MATRIX (Continued)

Task	Description	SOW Para	Report Section
B	The switch subsystem		
BA	Switch architecture		
BAA	Assessment of ATDRSS connectivity & switching requirements	2.1.1	5.1
BAB	Decomposition of the total switching function into lower order switches	2.2	5.1
BAC	Trade-off study of different switching concepts and interfacing arrangements to the receive/transmit subsystems	2.2	5.2,5.3
BB	Switch implementation methods	2.2	5.3,5.4
BBA	Determine best technologies for microwave switching matrices	2.3.2	5.4
BBB	Study baseband switching matrices and determine best technology for ATDRSS	2.3.2	5.3
BBC	Define multiplexing/demultiplexing requirements and possible implementations	2.3.2	5.3,5.3
BBD	Generate detailed block diagrams of the selected design approach	2.1	5.1
BBE	Define switch control functions, requirements and implementation	2.3.2	5.1
BBF	Define calibration and performance verification concept	2.1	2.19
BBG	Calculate components life expectancy in space radiation environment	2.3.2	2.14
BBH	Prepare a reliability prediction for 10 year lifetime	2.3.2	5.4
BBI	Develop a built-in-test concept for the switch	2.1	2.19
BBJ	Prepare total weight, power & size estimates	2.1	5.4
C	Interface definitions with the host S/C & other subsystems of the communications payload		
CA	Electrical interface	2.1	2.18
CAA	With the S/C's TT&C system	2.1	2.18
CAB	With the master frequency generator	2.1	2.18
CAC	With the S/C's diagnostic & BIT subsystems	2.1	2.18
CAD	With the power subsystem	2.1	2.18
CB	Mechanical/thermal interface		
CBA	Define the antenna mounting interface	2.1	3.7

STATEMENT OF WORK (SOW) COMPLIANCE MATRIX (Continued)

Task	Description	SOW Para	Report Section
CBB	Determine torque disturbance transmitted by antenna to S/C at mounting interface	2.3.1	3.7
CBC	Specify preliminary MBA location on the ATDRS	2.3.1	3.7
CBD	Determine system level thermal budget &		
CBE	Develop thermal control concept & thermal model	2.1	2.16

CONTENTS

CONTENTS (Continued)

CONTENTS (Continued)

CONTENTS (Continued)

CONTENTS (Continued)

ILLUSTRATIONS

ILLUSTRATIONS (Continued)

ILLUSTRATIONS (Continued)

ILLUSTRATIONS (Continued)

ILLUSTRATIONS (Continued)

ILLUSTRATIONS (Continued)

ILLUSTRATIONS (Continued)

ILLUSTRATIONS (Continued)

TABLES

TABLES (Continued)

SECTION 1
INTRODUCTION AND EXECUTIVE SUMMARY

National Aeronautics and Space Administration (NASA) projections indicate that the NASA experiment and mission objectives in the 2000 to 2015 time period will include an expanded Space Station, polar and co-orbiting space platforms, orbiting transfer vehicles, and low-earth orbiting missions. Based on these projections, NASA will require an Advanced Tracking and Data Relay Satellite System (ATDRSS) to meet NASA's mission requirements during the early 21st century.

The ATDRSS will maintain existing Tracking and Data Relay Satellite System (TDRSS) services at S- and Ku-bands and will add new 60 GHz and laser space-to-space links. Multiple space-to-ground links (SGLs) at Ku- and/or Ka-bands will also be added. Figure 1-1 shows two baseline ATDRSS network configurations. Figure 1-2 identifies the satellite communication technology projected to be used in the ATDRSS system architecture, among which are the multiple beam SGL capability and the supporting intelligent on-board switch.

The ATDRSS program plan is to continue to develop the critical technologies to support the space network and satellite configurations illustrated in Figures 1-1 and 1-2. The ATDRSS program plan calls for a 1993 technology cutoff in support of an operational system in the year 2000. A major focus of the ATDRSS technology program is to demonstrate technological feasibility and cost-effectiveness, thereby significantly reducing future implementation risks and maximizing the achievable level of performance.

A baseline for the Multiple Beam Antenna (MBA)/Switch Study is established by the block diagram in Figure 1-3 (per the Statement of Work (SOW)). The hatched area of the block diagram represents the focus area of the MBA/Switch Study. As seen in Figure 1-3, the existing ATDRSS services (S-band multiple access (SMA), S-band single access (SSA), and K-band single access (KSA)) are supported, together with the new 60 GHz single access (WSA) and laser single access (LSA) capabilities. An intersatellite crosslink subsystem is also present to relay ATDRSS telemetry, tracking, and command (TT&C) and user signals between the ATDRSS satellites.

1.1 MBA/SWITCH STUDY OBJECTIVES

During the course of this study, a conceptual design of two ATDRS subsystems, the multiple beam space-to-ground antenna and the switch, will be developed. The requirements of the SOW will be carefully analyzed and candidate system architectures will be defined to the point where crucial

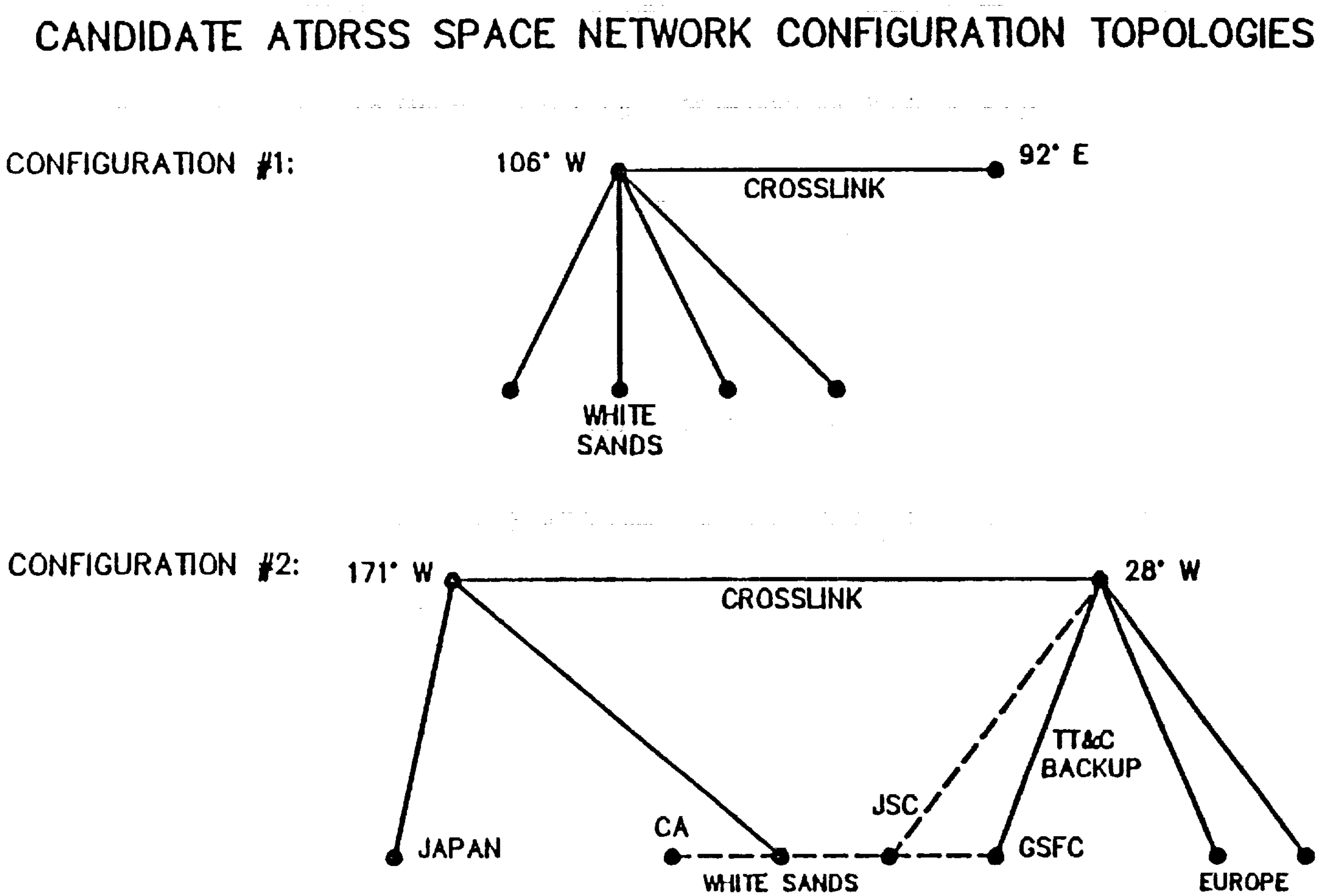

Figure 1-1. Baseline ATDRSS Network Configurations

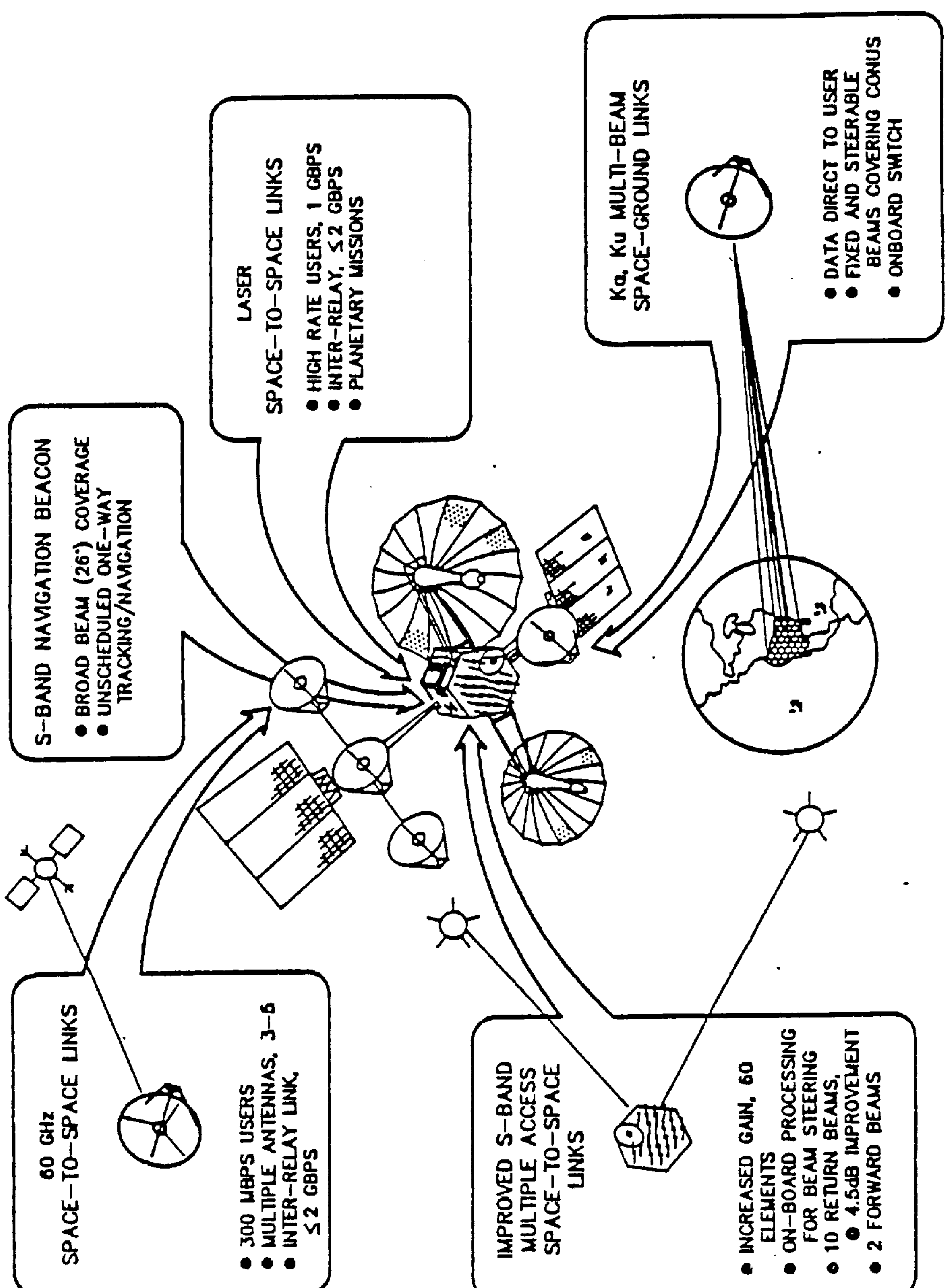

Figure 1-2. ATDRSS Spacecraft Concept and Technological Enhancements

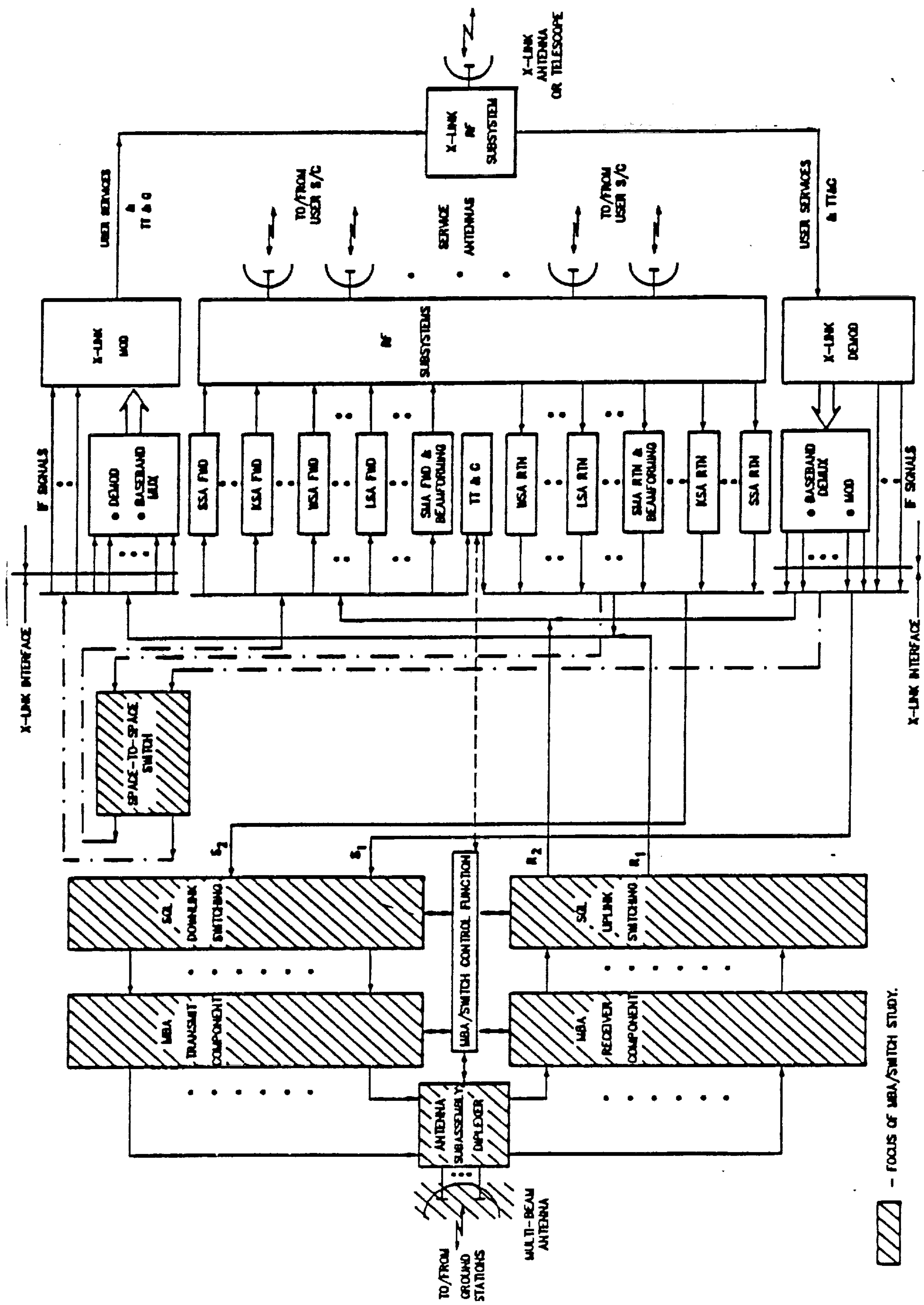

Figure 1-3. ATDRSS Spacecraft Functional Overview

comparisons and tradeoff studies can be performed. The study will produce conceptual designs and block diagrams, both electrical and mechanical, of the main components of the subsystems. Overall system performance will be calculated and interfaces between subsystems and units within the subsystems defined.

Special attention will be given to new technologies to take full advantage of new developments and components subject to a 1993 technology cutoff. Whenever applicable, the study will indicate and define special R&D efforts that, if completed successfully and in time, could benefit the ATDRSS program.

1.2 BASELINE OVERALL SYSTEM PARAMETERS

Figure 1-3 provides the baseline defining the scope of the MBA/Switch Study. Figure 1-4 is a baseline S-band and Ku-band frequency plan for ATDRSS (per the SOW). Similarly, Figure 1-5 shows a baseline for Ka-band and W-band frequency plan for ATDRSS. Table 1-1 defines a baseline for uplink (forward link) service characteristics and Table 1-2 defines a baseline for downlink (return link) service characteristics.

1.3 ORGANIZATION OF THE REPORT

Systems engineering issues are addressed in Section 2. Section 3 addresses the MBA issues. Section 4 focuses on the issues related to the transmit and receive systems. Issues related to the switch system are covered in Section 5. Section 6 draws the conclusions of this study effort and lists suggested future studies.

1.4 EXECUTIVE SUMMARY

In our study of the MBA/switch for the SGL uplink and downlink services, several issues related to systems engineering, antenna, transmit/receive and switch systems have been addressed. In the following few sections, the details of all the results are provided, and the summary of these results is presented.

Bandwidth allocation at Ku-band is inadequate to serve the data rate requirements for the forward and return services. This calls for the frequency reuse by dual-polarization transmissions. This also leads to the conclusion that bandwidth-efficient higher alphabet signaling schemes need to be considered. These considerations, in turn, may mean abandoning the simple "bent-pipe" IF switching concept and resorting to demodulation and remodulation on board each service. This may also affect the link power budgets; this leads to the consideration of power-efficient forward error correction coding techniques.

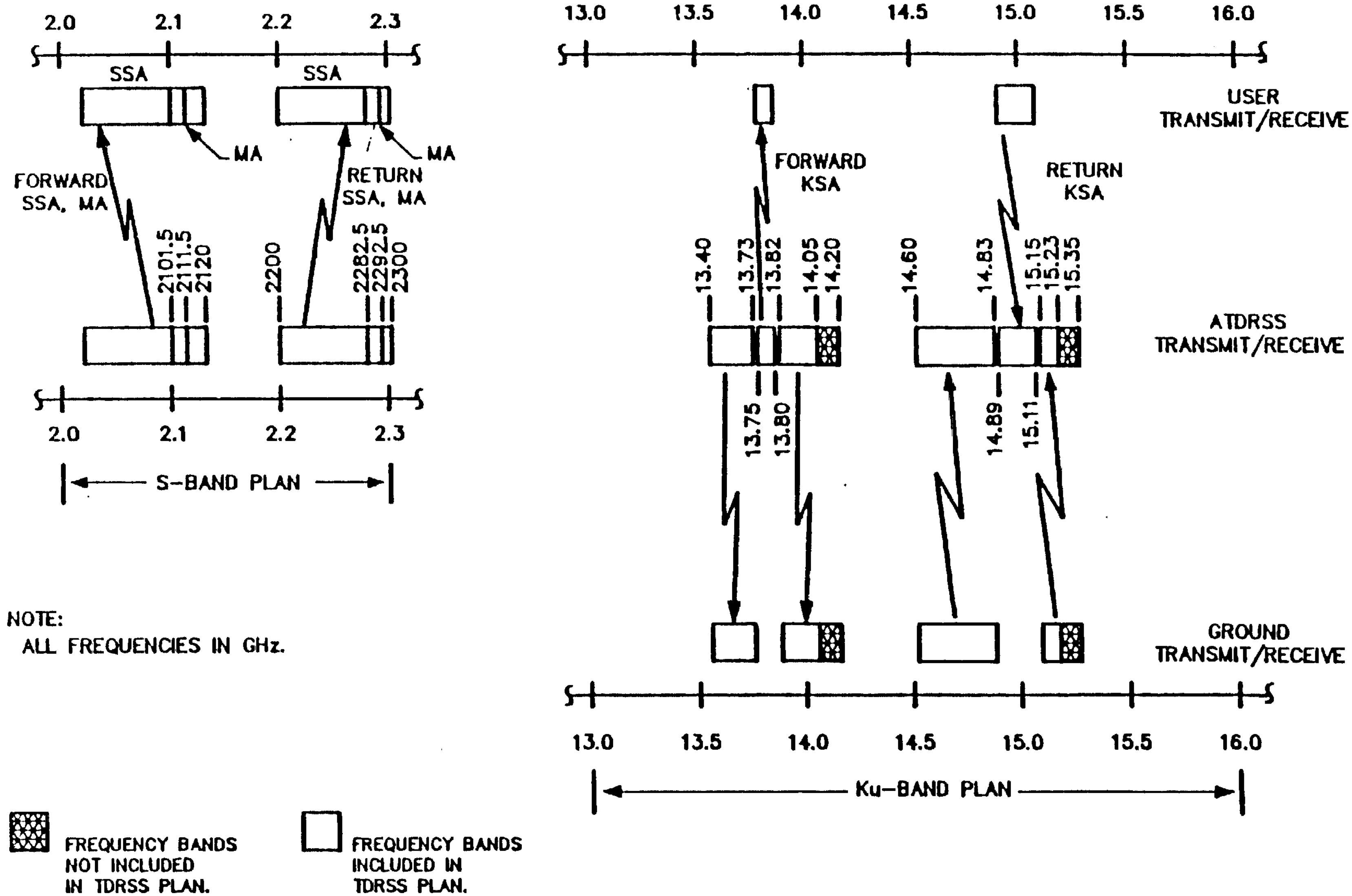

Figure 1-4. Baseline S-Band and Ku-Band Frequency Plan for ATDRSS

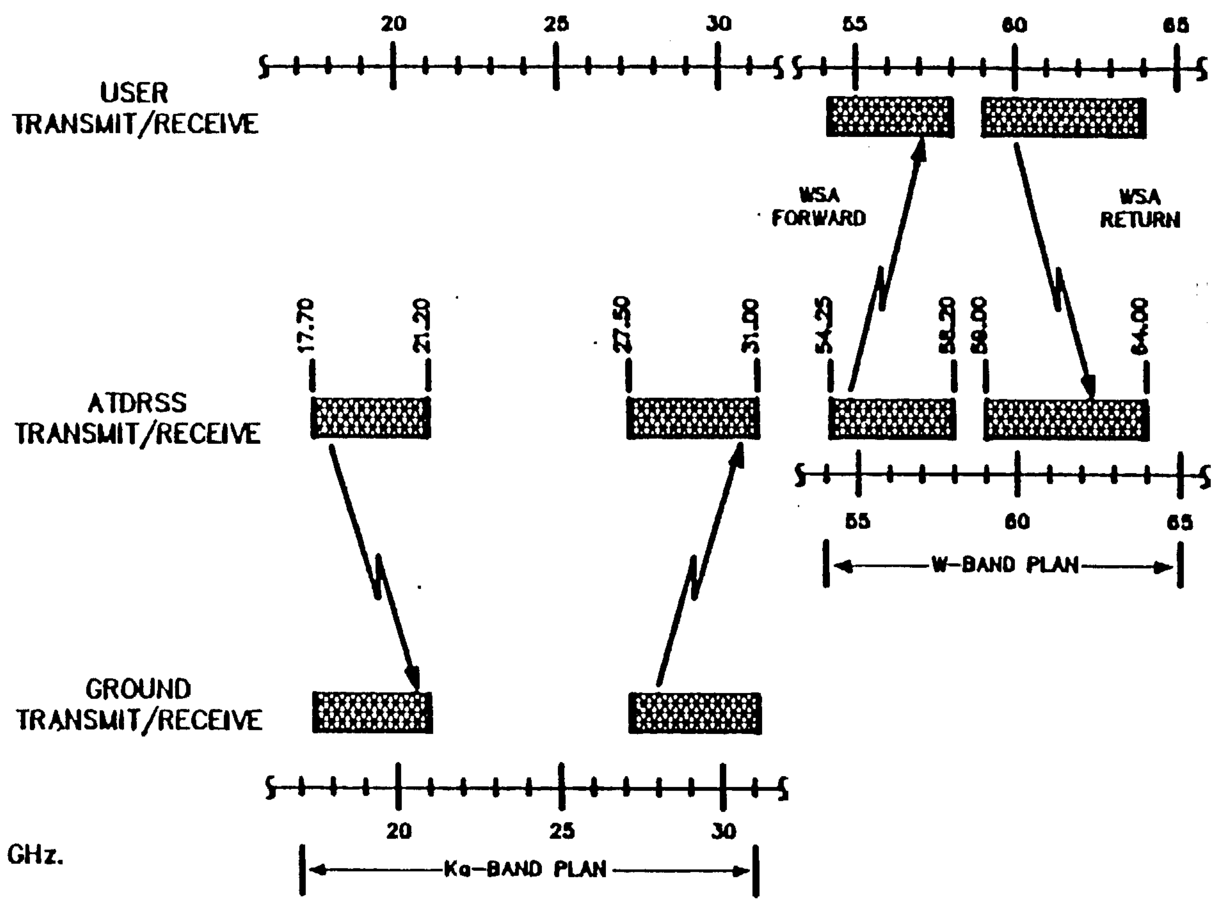

NOTES:

- ALL FREQUENCIES IN GHz.
- OPTICAL OPTIONS, FOR ATDRSS CROSSLINKS AND USER ACCESS, ARE NOT SHOWN.

Figure 1-5. Baseline Ka-Band and W-Band Frequency Plan for ATDRSS

Table 1-1. Baseline Uplink Service Characteristics (Forward Link)

SERVICE	NUMBER OF SERVICES	MAXIMUM BAUD RATE PER LINK (BAUDS)	MINIMUM BAUD RATE PER LINK (BAUDS)	DATA FORMAT	MODULATION
TT&C	2	500 K*	20 K**	NRZ	PCM/PSK/PM
SMA	4	10 K	0.1 K	NRZ	PSK***
SSA	4	11 M	0.1 K	NRZ	PSK***
KSA	4	50 M	1 K	NRZ	PSK***
WSA	10	50 M	1 K	NRZ	PSK
LSA	2	50 M	1 K	NRZ	PSK

NOTE: THIS TABLE REPRESENTS THE COMPOSITE UPLINK CHARACTERISTICS WHICH MAY BE SUPPORTED BY SGLs WITH ONE OR TWO ATDRSS SPACECRAFT.

* ASSUMES A 500 KHz RANGE TONE ON CARRIER.

** ASSUMES A COMMAND SUBCARRIER AT 16 KHz WITH A DATA RATE OF 4 Kbps.

*** MODULATION SCHEMES AS IDENTIFIED IN TDRS USER'S GUIDE.

Table 1-2. Baseline Downlink Service Characteristics (Return Link)

SERVICE	NUMBER OF SERVICES	MAXIMUM BAUD RATE PER LINK (BAUDS)	MINIMUM BAUD RATE PER LINK (BAUDS)	DATA FORMAT	MODULATION
TT&C	2	1.5 M*	1.01 M**	NRZ	PCM/PSK/PM
SMA	20	100 K	1 K	NRZ	PSK***
SSA	4	6 M	1 K	NRZ/B1-ϕ	PSK
KSA	4	150 M	1 K	NRZ/B1-ϕ	PSK
WSA	10	150 M	1 K	NRZ	PSK
LSA	2	1 G	100 K	NRZ	PSK

NOTE: THIS TABLE REPRESENTS THE COMPOSITE DOWNLINK CHARACTERISTICS MAY BE SUPPORTED BY SGL's WITH ONE OR TWO ATDRSS SPACECRAFT.

* ASSUMES A TELEMETRY SUBCARRIER AT 1 MHz AND A 500 KHz RANGE TONE.

** ASSUMES A TELEMETRY SUBCARRIER AT 1 MHz WITH 10 Kbps DATA.

*** MODULATION SCHEMES AS IDENTIFIED IN TDRS USER'S GUIDE.

Rain and depolarization effects at EHF, especially at Ka-band, pose a significant threat to the link availabilities at heavy rain areas such as Johnson Space Center (JSC), Kennedy Space Center (KSC), and Marshall Space Center (MSC). The locations of ATDRSS can be optimized to minimize these effects. Zone of exclusion (ZOE) is also dependent on the locations of the ATDRSS 1 and 2.

Hardware-induced effects such as the nonlinear characteristics of the power amplifiers may necessitate the use of linearizers and limiters. Filter distortion effects, adjacent channel interference, and phase noise effects also degrade the performance and deserve careful consideration.

In addition, the ground stations must be sufficiently separated (at least two beamwidths) in order to minimize the interbeam interference effects.

It is also important to identify the components that are susceptible to the space radiation effects and shield or redesign them with "rad-hard" technologies for meeting the requirements of the space environment. In addition, modular design of the component subsystems is desirable for the possible future in-space replacement, servicing, and repair.

The MBA requirements can be met by two candidate approaches -- the prime-focus fed torus reflector approach and the shaped dual-offset reflector approach. The phased array approach may not be practical in the desired 1993 technology timeframe due to the slow progress of space-qualified MMICs needed for feasible implementations.

Feed designs incorporating dual-polarization and multifrequency (14, 20, and 30 GHz) bands are desired. Reflector surface tolerance requirements are tighter for accommodating higher EHF operations. Packaging, stowing, and deployment considerations may require designing and constructing in pieces, assembling, and folding of the torus antenna (for Configuration 2). This may pose other issues such as overall system reliability and gain loss due to possible misalignment of the pieces.

Multiple beam tracking considerations suggest the use of flexible feed interconnect schemes such as the coaxial cable; however, coax cables are lossy, especially at EHF. Placement of upconverters and downconverters at the antenna assembly may raise other issues such as thermal control and radiation protection. Design of tracking mechanism is simplified if the effects of yaw errors can be assumed to be small, leading to a two degree of freedom implementation. This, however, may place the appropriate requirement on the navigation and attitude control system.

Availability of solid-state devices for low noise and power amplifiers may contribute to substantial performance improvement of the transmit/receive systems. In addition, devices such as linearizers and limiters provide additional performance improvements.

To comply with the SGL communications requirements, the switching system architecture must be complex. Redundant switch configurations are desired to improve the system reliability. IF (bent-pipe) switching concept is simple and does not affect the user communications hardware. However, the unavailability of the desired spectrum, especially at Ku-band, may mean that higher alphabet signaling schemes need to be considered. This would, however, affect both the space and ground users hardware unless on-board demodulation and remodulation with higher alphabet signaling are considered. Major advances in baseband switching hardware technologies are taking place, which will make both power and space efficient implementations feasible with 1993 state-of-the-art parts. Space qualification of these parts, however, may be doubtful by the 1993 timeframe. The leading technologies for these applications are, however, gallium arsenide and ECL bipolar semiconductors (gate array), and these technologies are inherently "rad-hard" and space qualification of the baseband switching circuits may not be too difficult.

While advances in all the relevant technology areas are rapidly taking place, it is of particular concern that system level testing be done of implementations with proven technologies. Further studies of proof concepts in both analog and digital switching hardware are desirable. Transmit/receive hardware implementation using solid-state and integrated devices need to be further explored. In-depth studies of MBA, including the tradeoffs for various approaches for reflectors, feeds, tracking mechanisms, and the frequency selective surfaces, are desirable.

SECTION 2
SYSTEMS ENGINEERING

2.1 Ka-BAND FREQUENCY PLAN - UPLINK/DOWNLINK SERVICES

A frequency plan for the Ka-band uplink and downlink services is developed, based upon the data rate requirements for the forward and return services listed in Tables 1 and 2 respectively of the SOW. This frequency plan forms the basis for the functional decomposition of the switching system architecture to be addressed in detail in a later section.

The data rate requirements for the forward link services are shown in Table 2.1-1 (as given in Table 1 of the SOW). The aggregate data rate requirements for the uplink, then would be 845.04 Mbaud. The uplink frequency allocation from 27.5 GHz to 31.00 GHz constitutes a bandwidth of 3.5 GHz and therefore, each baud of uplink data can be accommodated in approximately 4.14 Hz. Based on this requirement, the frequency plan for the uplink services can be devised as shown in Figure 2.1-1. The allocated frequency band is divided into two equal and identically divided parts R1 and R2; R1 is for ATDRS 1 satellite forward services and R2 is for ATDRS 2 satellite forward services (e.g., see configuration 1 in the SOW). Each of these frequency bands is further sub-divided into a band of 94 MHz for Telemetry, Tracking and Command (TT&C), SSA, and SMA services, and the remaining band is divided equally into 207 MHz each for LSA, KSA1, KSA2, and WSA1 through WSA5 forward services. The 94 MHz band is further broken down into 1 MHz for SMA, 3 MHz for TT&C, and 45 MHz each for the two SSAs. The 1 MHz for SMA forward services is further divided into two equal bands of 500 kHz each for the two SMA forward services.

For the return services, a Ka-band downlink frequency plan can similarly be developed. The data rate requirements for the return link services are shown in Table 2.1-2 (as given in Table 2 of the SOW). By using dual polarization, the return link data from both ATDRS 1 and ATDRS 2 can be accommodated within the allocated band of 17.7 to 21.2 GHz; the ATDRS 1 data being transmitted on the orthogonal polarization from that of the ATDRS 2 data. For each polarization, the aggregate symbol rate requirement is 2064.5 Mbaud. The downlink frequency allocation from 17.7 GHz to 21.2 GHz constitutes a bandwidth of 3.5 GHz and therefore, each baud of downlink data can be accommodated in approximately 1.695 Hz. Based on this requirement, the frequency plan for the downlink services can be devised as shown in Figure 2.1-2. The allocated band for the Ka-band downlink is divided into a band of 1.695 GHz for the LSA return link services, and the remaining band of 1.805 GHz is further subdivided into a band of 25.25 MHz for TT&C, SSA, and SMA services and seven equal bands of 254.25 MHz each for KSA1, KSA2, and WSA1 through WSA5

Table 2.1-1. Forward Links Frequency Band Allocation
(Ref. Table 1 SOW)

Service	Number of Services	Maximum Data Rate Mbauds	Total Mbauds
TT&C	2	0.5	1
SMA	2	0.01	0.04
SSA	4	11.0	44
KSA	4	50.0	200
WSA	10	50.0	500
LSA	2	50.0	100
Total	26		845.04

The band of operation from ground to ATDRS 1 is from 27.5 GHz to 31.00 GHz or 3500 MHz. This has to handle 845.04 Mbaud, thus 1 baud can have 4.14 Hz.

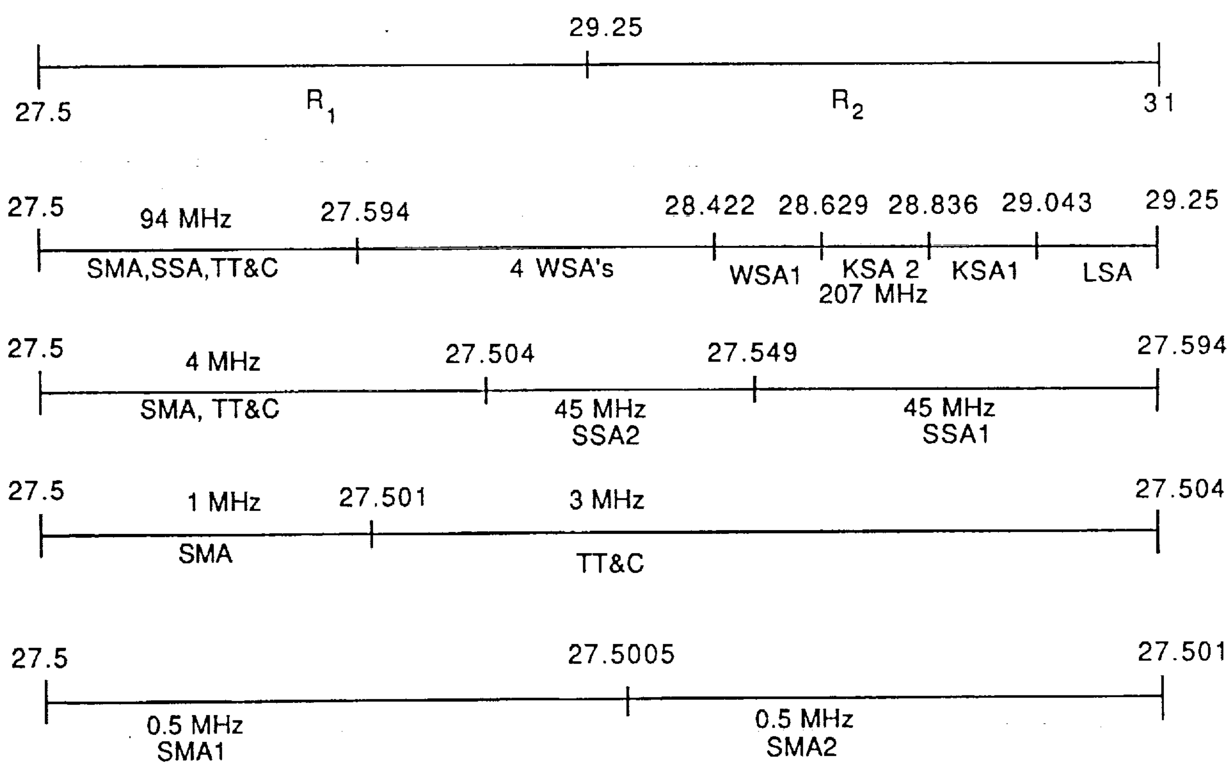

Figure 2.1-1. Frequency Plan, Ka-Uplink, 1 Baud/4.14 Hz

Table 2.1-2. Return Links Frequency Band Allocation for One Polarization

Service	Number of Services	Maximum Data Rate Mbauds	Total Mbauds
KSA	2	150.0	300.0
SSA	2	6.0	12.0
WSA	5	150.0	750.0
TLM	1	1.5	1.5
LSA	1	1000.0	1000.0
SMA	10	0.1	1.0
Total	21		2064.5

Since 3500 MHz are available for transmitting 2064.5 Mbauds then 1 baud can have 1.695 Hz.

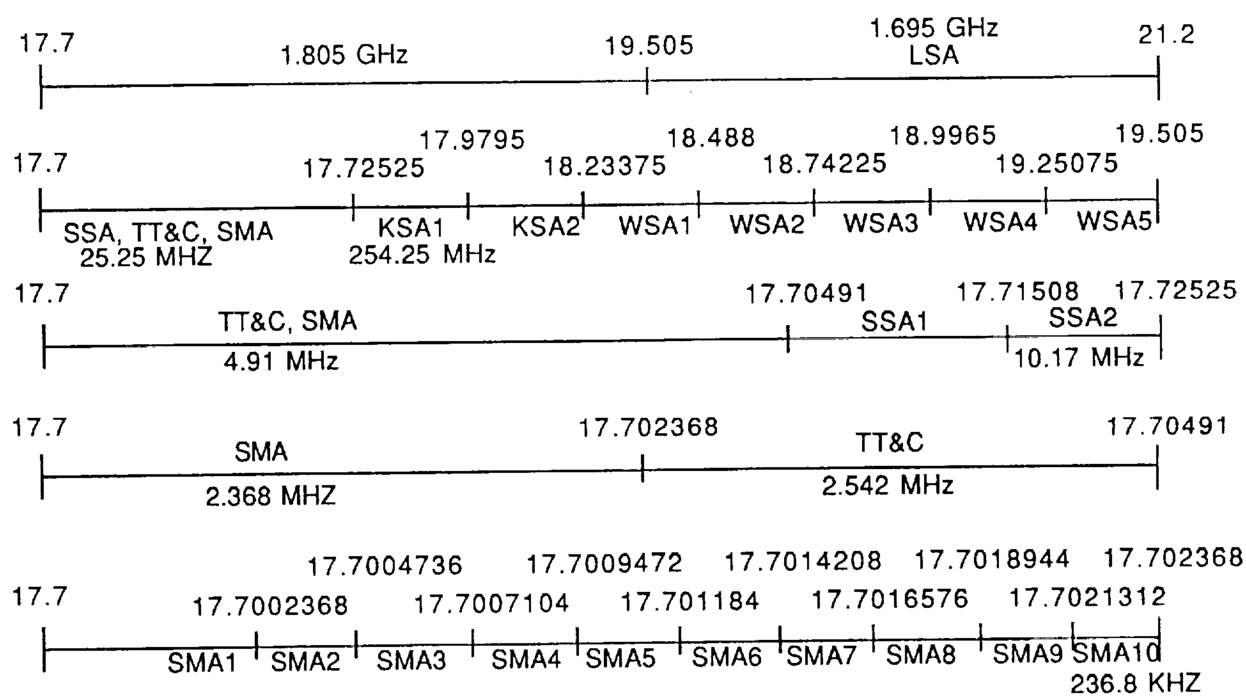

Figure 2.1-2. Frequency Plan, Ka-Downlink, 1 Baud/1.695 Hz, Dual Polarization Required

return services. The 25.25 MHz band is further broken down into 2.368 MHz for SMA, 2.542 MHz for TT&C, and 10.17 MHz each for the two SSAs. The 2.368 MHz for SMA return services is further divided into 10 equal bands of 236.8 kHz each for the 10 SMA return services.

2.2 Ku-BAND FREQUENCY PLANS AND MODULATION FORMATS

In this subsection, frequency plans are developed for the Ku-band uplink and downlink services. The minimum required alphabet size and the possible modulation formats are also discussed here.

2.2.1 Ku-Band Uplink Frequency Plan

From Figure 1-4 (Figure 4 of the SOW), it can be noted that the frequency bands allocated for the Ku-band uplink services are from 14.6 to 14.83 GHz (i.e., a band of 230 MHz) and from 15.15 to 15.35 GHz (a band of 200 MHz). From Table 1-1 (Table 1 of the SOW), we note that the aggregate uplink data rate requirements are 845.04 Mbaud. Even if dual polarizations are to be used, this amounts to a requirement of 422.52 Mbaud per polarization as shown in Table 2.2-1.

The band allocation is not adequate to serve the entire uplink data rate requirements unless higher alphabet modulation formats (than originally planned) are to be used. However, in order to meet the bit error rate requirements, this would require higher transmitted power at the ground terminals and the carrier acquisition, tracking and symbol-synchronization requirements would be tighter (as discussed in the Attachment 3 of Monthly Report 4). The filter distortion, intersymbol interference, and adjacent channel interference effects are also more pronounced.

It is therefore important to keep the alphabet size at the originally planned levels if possible and re-examine the data rate requirements. In the absence of the projected Ku-band/Ka-band uplink data rate requirements for each ground terminal, we proceed as follows. If it can be interpreted that the requirements listed in Table 1 of the SOW are the aggregate uplink requirements from all the ground terminals served by the ATDRS satellites, it is not too unreasonable to assume that the simultaneous Ku-band uplink data rate requirements for the ground terminals, covered by each beam of the MBA are somewhat lower than the aggregate requirements listed in Table 1 of the SOW. The approach taken here, therefore, is to utilize the allocated band for as many uplink services as possible (keeping the alphabet size the same as originally planned).

A frequency plan for the Ku-band uplink services is shown in Figure 2.2-1. Using dual polarizations and a rate of 1.5 Hz per baud of data, all the required services are accommodated. However, from Table 2.2-1 we note that the KSA, WSA, or LSA uplink data rate requirements for each channel are the same (50 Mbaud); therefore, any combination of 10 of these services are simultaneously accommodated in each beam covered by the MBA of the ATDRS. While adding

Table 2.2-1. Forward Links Frequency Band Allocation
(Ref. Table 1 SOW)

Service	Number of Services	Maximum Data Rate Mbauds	Total Mbauds
TT&C	1	0.5	0.5
SMA	2	0.01	0.02
SSA	2	11	22
KSA	2	50	100
WSA	5	50	250
LSA	1	50	50
Total	13		422.52

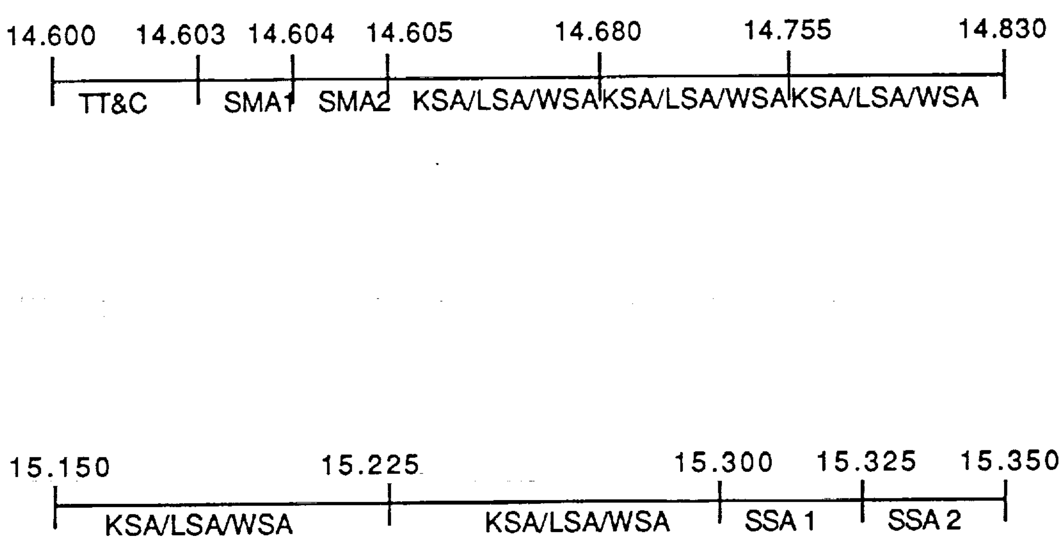

Figure 2.2-1. Frequency Plan, Ku-Band Uplink,
Dual Polarization Required, 1.5 Hz/baud

some complexity to the switching and command systems designs, this approach allows a great deal of flexibility in selecting the type of service that these channels can be used in any given beam coverage area.

As shown in Figure 2.2-1, for each polarization, a possible spectral allocation of the Ku-band for the uplink services is as follows: the TT&C channel is allocated 3 MHz starting from 14.6 GHz, following which are the two SMA channels with an allocation of 1 MHz each. Starting at the frequency of 14.605 GHz, a frequency allocation for three channels each with a band of 75 MHz is made for KSA/WSA/LSA services. Again, starting 15.150 GHz, two such 75 MHz channels are allocated, following which are the two SSA channels, each with an allocation of 25 MHz.

2.2.2 Ku-Band Downlink Frequency Plan

From the Figure 1-4, it can be noted that the frequency bands allocated for the Ku-band downlink services are from 13.40 to 13.73 GHz (i.e., a band of 330 MHz) and from 13.82 to 14.2 GHz (a band of 380 MHz). From Table 1-2, we note that the aggregate downlink data rate requirements are 4129 Mbaud. Even if dual polarizations are to be used, this amounts to a requirement of 2064.5 Mbaud per polarization as shown in Table 2.2-2. The band allocation for the Ku-band downlink services is again inadequate to meet this requirement.

A frequency plan for the Ku-band downlink services is being developed, which will be similar to the plan for the Ku-band uplink services.

Figure 2.2-2 is a frequency plan for the Ku-band downlink services. Using dual polarizations, all the required services are accommodated. However, from Table 2.2-2 we note that the downlink data rate requirements for each of the two LSA channels is 1 Gbaud; therefore, at any given time, if an LSA Ku-band downlink service is required for the ground stations in a beam covered by the MBA of the ATDRS, all other Ku-band services are momentarily suspended in that downlink beam in order to accommodate the LSA downlink transmissions. From Table 2.2-2 we also note that the KSA or WSA downlink data rate requirements for each channel are the same (150 Mbaud); therefore, any combination of six of these services are simultaneously accommodated in each beam covered by the MBA of the ATDRS.

Table 2.2-2. Return Links Frequency Band Allocation for One Polarization

Service	Number of Services	Maximum Data Rate Mbauds	Total Mbauds
KSA	2	150	300
SSA	2	6	12
WSA	5	150	750
TLM	1	1.5	1.5
LSA	1	1000	1000
SMA	10	0.1	1
Total	21		2064.5

Since 3500 MHz are available for transmitting 2064.5 M, then 1 baud can have 1.695 Hz.

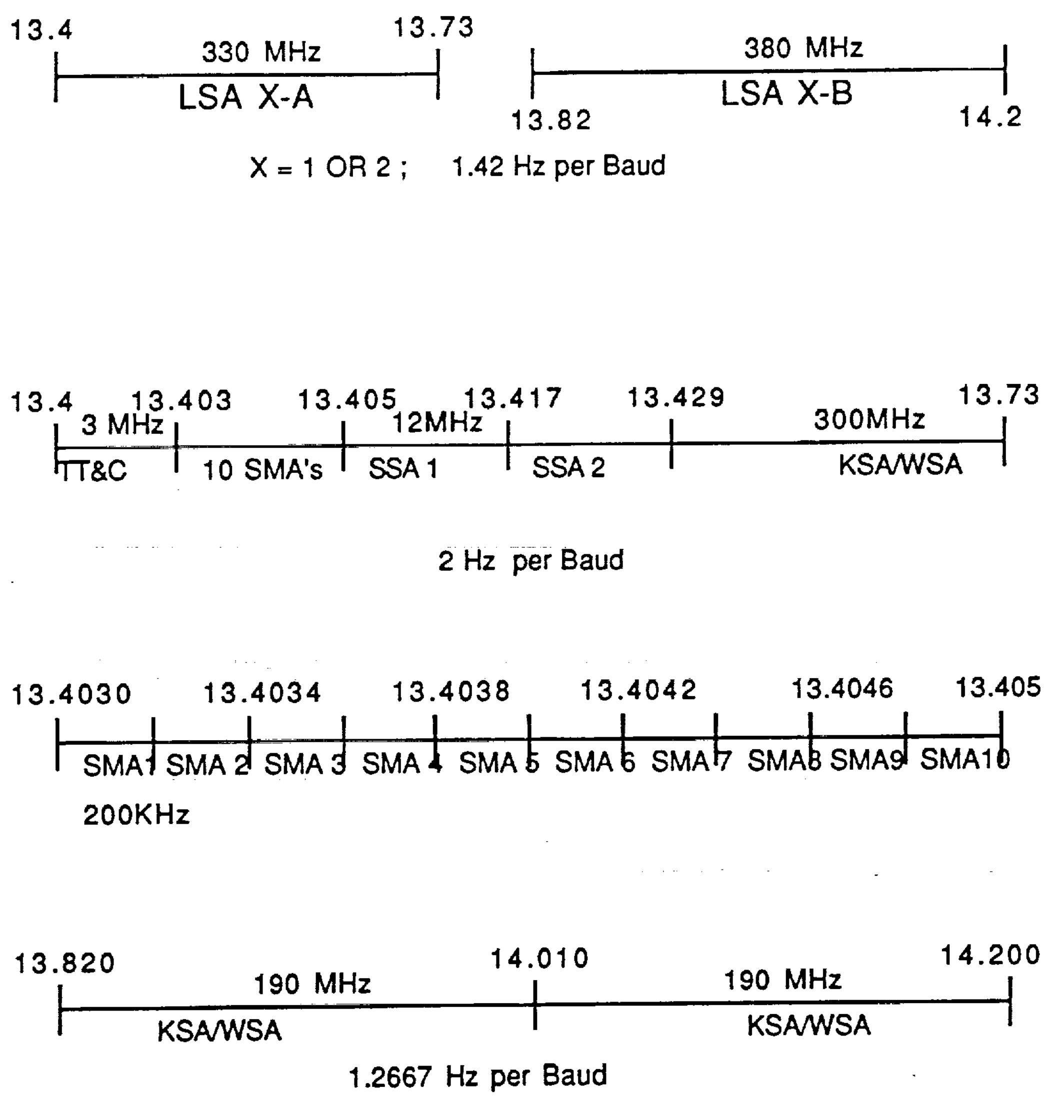

Figure 2.2-2. Frequency Plan, Ku-Band Downlink Dual Polarization Required

As shown in Figure 2.2-2, for each polarization a possible spectral allocation of the Ku-band for the downlink services is as follows. When an LSA downlink transmission to the ground terminals in any beam is desired via the downlink Ku-band, the entire allocated band of 13.40 to 13.73 GHz and 13.82 to 14.2 GHz is used for the LSA downlink transmission with a spectral allocation of 1.42 Hz per baud. Otherwise, in the frequency band between 13.40 and 13.73 GHz, a spectral allocation of 2 Hz per baud is made. The TT&C channel is allocated 3 MHz starting from 13.40 GHz, the 10 SMA channels follow with an allocation of 200 kHz each, and the two SSA channels have an allocation of 12 MHz. Starting at 13.429 GHz, a frequency allocation for a channel with a band of 300 MHz is made for KSA/WSA services. Again, starting at 13.820 GHz, two 190 MHz wide channels are allocated for KSA/WSA downlink services. It is to be noted here that the spectral allocation of only 1.2667 Hz per baud in the frequency band of 13.82 to 14.2 GHz require careful design of the transmit/receive filters to minimize the filter distortion, intersymbol, and adjacent channel interference effects.

2.3 HIGHER ALPHABET MODULATION SCHEMES

In this subsection, the motivations for using higher order modulation formats and the associated issues and concerns are addressed.

As discussed in the previous subsection, higher data rate requirements with limited bandwidth allocations require consideration of higher alphabet modulation schemes. The aggregate return service requirements are 2.065 Gbaud per polarization of a dual-polarized system. If, for example, all the return link communications are to be performed on a downlink at Ku-band, with a downlink allocation of approximately 710 MHz (as per Figure 4 of SOW), it is required that approximately 2.91 symbols/Hz be provided. Assuming a bandwidth expansion factor of 1.5, this translates to about 4.36 baud/Hz. This means that the existing modulation format is to be replaced by a modulation scheme of an order of at least 5 higher. For example, if the original modulation format is binary phase shift keying (BPSK), a 16-phase shift keying (PSK) or a 16-amplitude shift keying (ASK) modulation format is required in order to meet the data rate and bandwidth constraints. As mentioned previously, if the data rate and bandwidth constraints do not permit the possibility of any coding implementations, use of higher alphabet modulation formats permits the use of error correction coding. By considering higher alphabet modulation formats, a system with limited bandwidth constraint can provide more communications capacity (in terms of bits/Hz) and/or permit the implementation of efficient coding schemes, thereby providing more design choices for users, transponders, as well as ground terminals.

Figure 2.3-1 is a plot of probability of bit error as a function of the symbol energy to noise ratio (Es/No) for BPSK, the quadrature phase shift keying (QPSK), 8-PSK, 16-PSK, for 16-quadrature amplitude shift keying (16-QASK) and 64-QASK. It shows that for a given bit error rate requirement, the transmit power is to be increased as the alphabet size increases. It is interesting to note that the performance of 16-PSK is worse than that of 16-QASK; this can be intuitively explained by noting that the phase difference between the adjacent vectors in the phase-plane for the 16-PSK is much smaller, resulting in increased susceptibility for phase errors, whereas 16-QASK has much larger phase separation; (the gray-code implementation of QASK maximizes the distance between adjacent symbol amplitude mapping, thereby minimizing the possibility of errors).

Figure 2.3-2 is a plot of bit rate efficiency in b/s/Hz transmitted as a function of Es/No for PSK and QASK modulation schemes for a specified bit error rate of 10^{-5}. Shannon's limit of channel capacity is also plotted here. It shows that higher bit rate efficiencies require higher

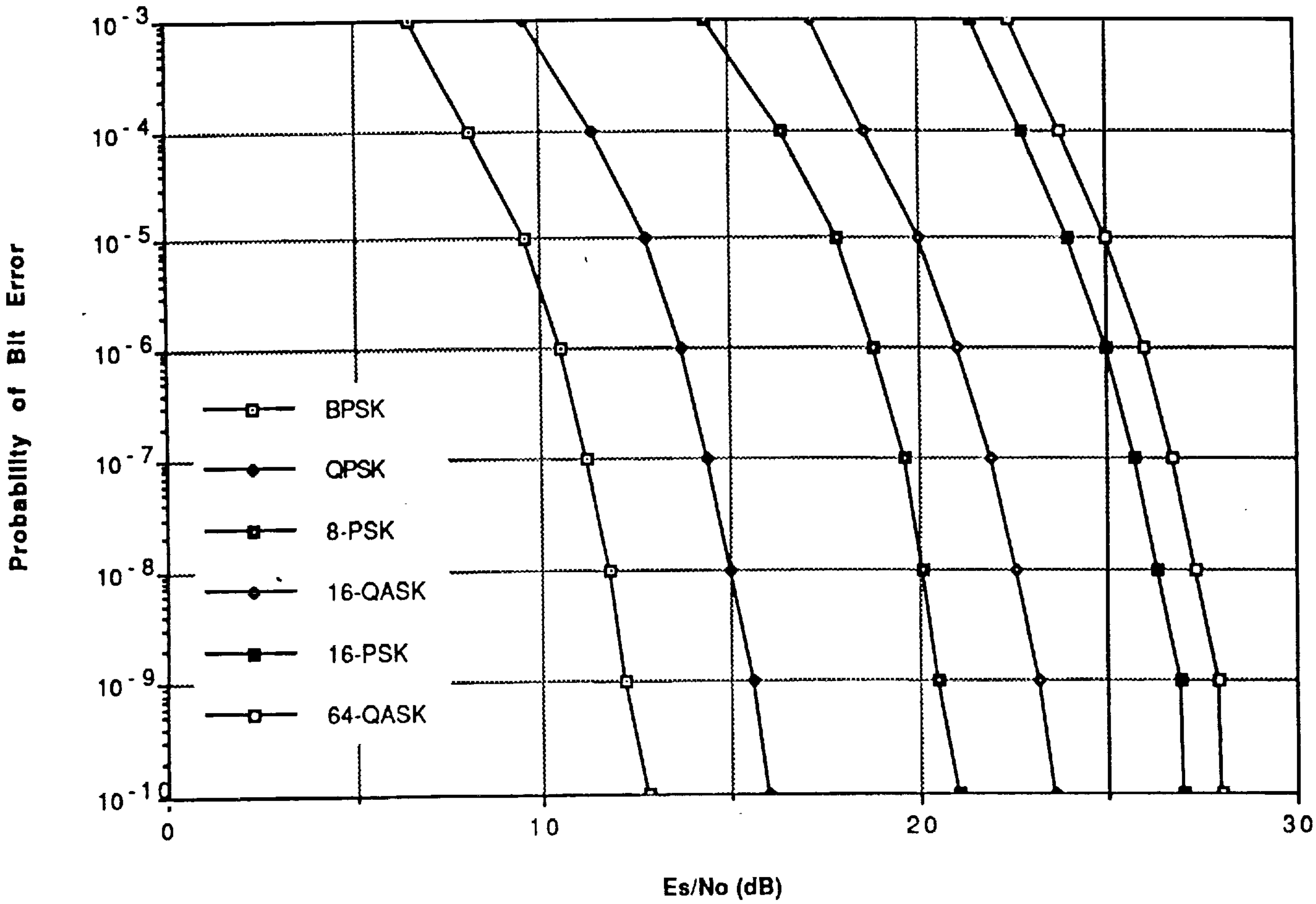

Figure 2.3-1. Probability of Error Versus Es/No Characteristic

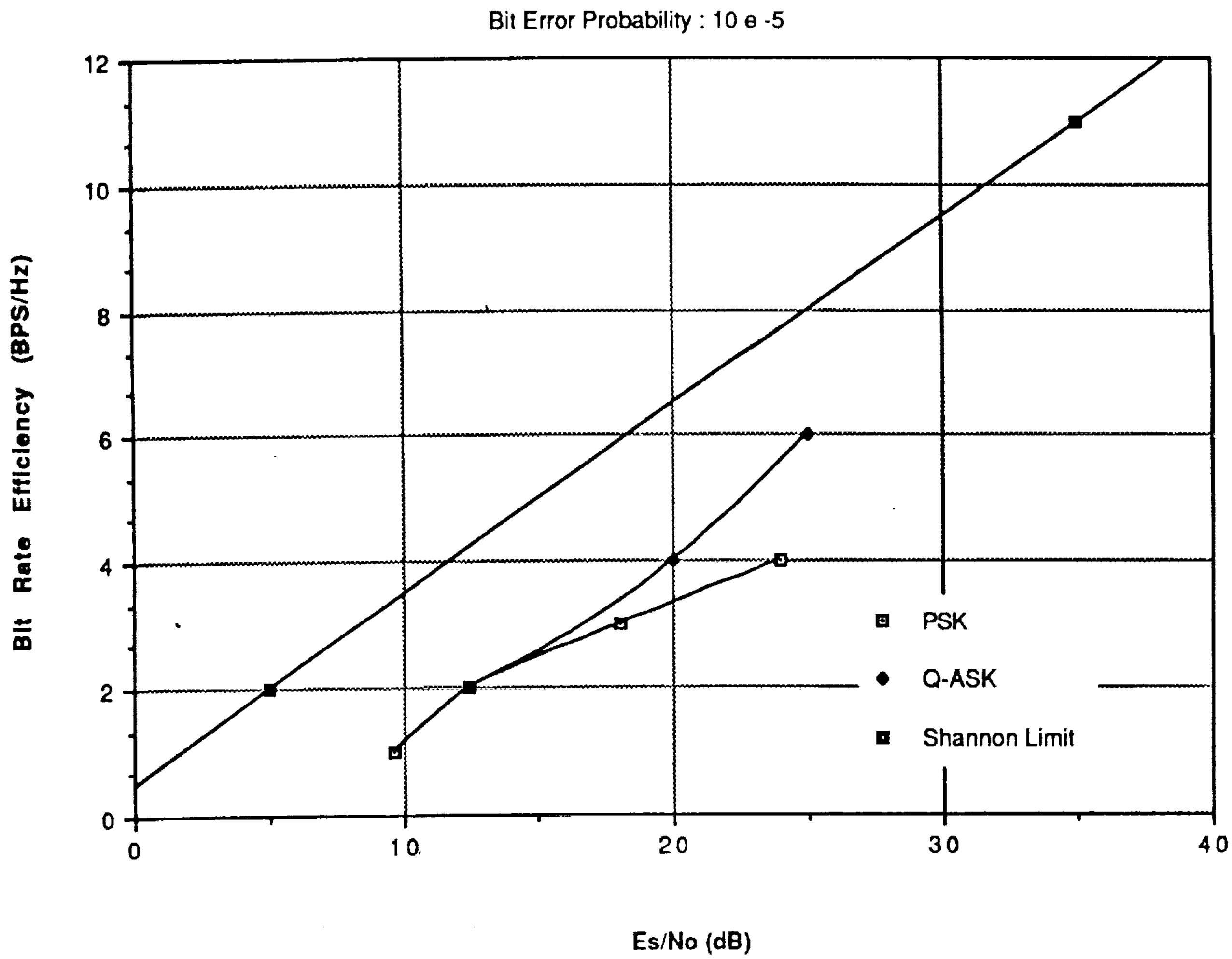

Figure 2.3-2. Bit Rate Efficiency Versus Es/No Plot for M-PSK/QASK

transmitted power. It again shows that QASK modulation schemes provide better performance than PSK schemes as the alphabet size is increased. For example, a 16-QASK modulation scheme provides a bit rate efficiency of 4 b/s/Hz with an Es/No of 20 dB, whereas a 16-PSK requires about 24 dB for the same bit rate efficiency.

It should be noted here that the higher alphabet modulation techniques considered here require much tighter phase error tolerance (than the original modulation formats). QASK modulation schemes additionally require that the amplitude characteristics of the transmitted signals be linear. There is also a need for improved carrier acquisition and tracking as well as symbol synchronization techniques. Higher alphabet modulation schemes are more susceptible to the AM-AM and AM-PM effects, filter distortion effects, intersymbol interference effects, as well as the adjacent channel interference effects.

In conclusion, it can be stated that the higher alphabet modulation schemes considered here provide improved bandwidth efficiency and system design flexibility at the expense of diminished power efficiency and increased system complexity.

SGL Modulation Formats. From the discussions in the above two subsections, we can conclude that there is no advantage in going to higher alphabet modulation formats (than the originally selected format, e.g., QPSK), if the bandwidth constraints permit all the required simultaneous services. Staggered quadrature phase shift keying (SQPSK) provides the same bit-error-rate performance as the BPSK and therefore, if the other system and user constraints permit, this modulation format is recommended for all (uplink/downlink/user) services. This permits compatibility of the links such as the KSA/WSA/LSA uplinks and the KSA/WSA downlinks and provides greater flexibility.

2.4 MODULATION AND CODING ISSUES

As pointed out in several of our monthly reports, the bandwidth allocations for Ku-band uplink/downlink services (even with the use of dual polarizations) are not adequate for providing all the forward/return link user services simultaneously in any given beam coverage area. In the case of Ka-band, on the other hand, the frequency allocation for the return links is adequate if the dual antenna polarizations are utilized; however, the severe rain attenuation and cross polarization degradation effects may place stringent requirements on achievable link margins. Therefore, it may be desirable to investigate the available alternatives such as use of forward error correction (FEC) coding to take advantage of coding gain. This, however, would require higher bandwidths for given user data rates. As discussed in the previous subsection, these considerations provide motivations for higher alphabet modulation formats. Higher alphabet modulation formats provide improved bandwidth efficiencies at the expense of diminished power efficiencies and increased system complexities.

In this subsection, the implications of use of FEC schemes, especially when combined with some specific higher alphabet modulation formats, are explored. Figure 2.4-1 shows the bandwidth efficiency (represented in b/s/Hz) vs the power efficiency (represented by the required symbol energy to noise density ratio Es/No in dB) for PSK and QASK modulation formats. These plots clearly demonstrate the tradeoff between these two parameters i.e., improved bandwidth efficiencies can be provided by higher alphabet modulation formats, but require higher symbol energy to noise ratios. In addition, the plots for QPSK with convolutional encoding with hard-decision/soft-decision Viterbi decoding for rates 1/2, 3/4, and 7/8 are shown. It is clear that soft decision decoding provides better performance than hard decision decoding. These plots show that coding decreases the required Es/No at the expense of diminished bandwidth efficiency. Additionally, the relationship, when a (255, 231) BCH block code is used in conjunction with QPSK, is shown. This shows, for example, that approximately 3 dB gain in the required Es/No can be achieved if a 10% in bandwidth efficiency can be given up. Also shown is the relationship for the case when an 8-PSK modulation format is used in conjunction with a low complexity code (LCC), developed at the University of California [2-1]. These LCCs, although not optimal, provide approximately the same performance as the proposed Trellis-codes proposed for combined modulation and coding schemes [2-2], but with somewhat reduced complexity. The LCC provides approximately 7 dB gain in Es/No with 20% lowering of bandwidth efficiency when compared with an uncoded 8-PSK modulated system. It is interesting to note here that the LCC provides better performance than an uncoded QPSK (see Figure 2.4-1).

Breadboard hardware for both LCC /8-PSK and BCH code with QPSK is developed and demonstrated at Ford Aerospace in our IR&D programs for data rates of up to 500 Mb/s. Very large scale integration (VLSI) implementations of 1 Gb/s devices may take the next 3 to 5 years of development. Space qualification of these devices is probably going to take some additional time.

For our MBA/Switch Study, it is advantageous to consider the higher alphabet modulation schemes (for accomplishing the required bandwidth efficiencies) in conjunction with the coding schemes such as the Trellis coding or the LCC (to provide the required link margins). However, such a choice may affect the design of users' equipment, which may or may not be feasible. In order to avoid this situation, such a choice may necessitate on-board demodulation/remodulation, which in turn, will rule out the possibility of an IF "bent-pipe" switching concept. There are other considerations such as the system complexity, reliability, and the availability of proven space-qualified parts that would make the system design choices much clearer. If the overall system considerations dictate that only QPSK be used, however, the BCH coded QPSK will be a good choice. In conclusion, it can be stated that rapid advances in the area of programmable modulators/demodulators with different levels of modulation/coding may make such a choice much easier (by simply programming and configuring the devices appropriately) not too far in the future.

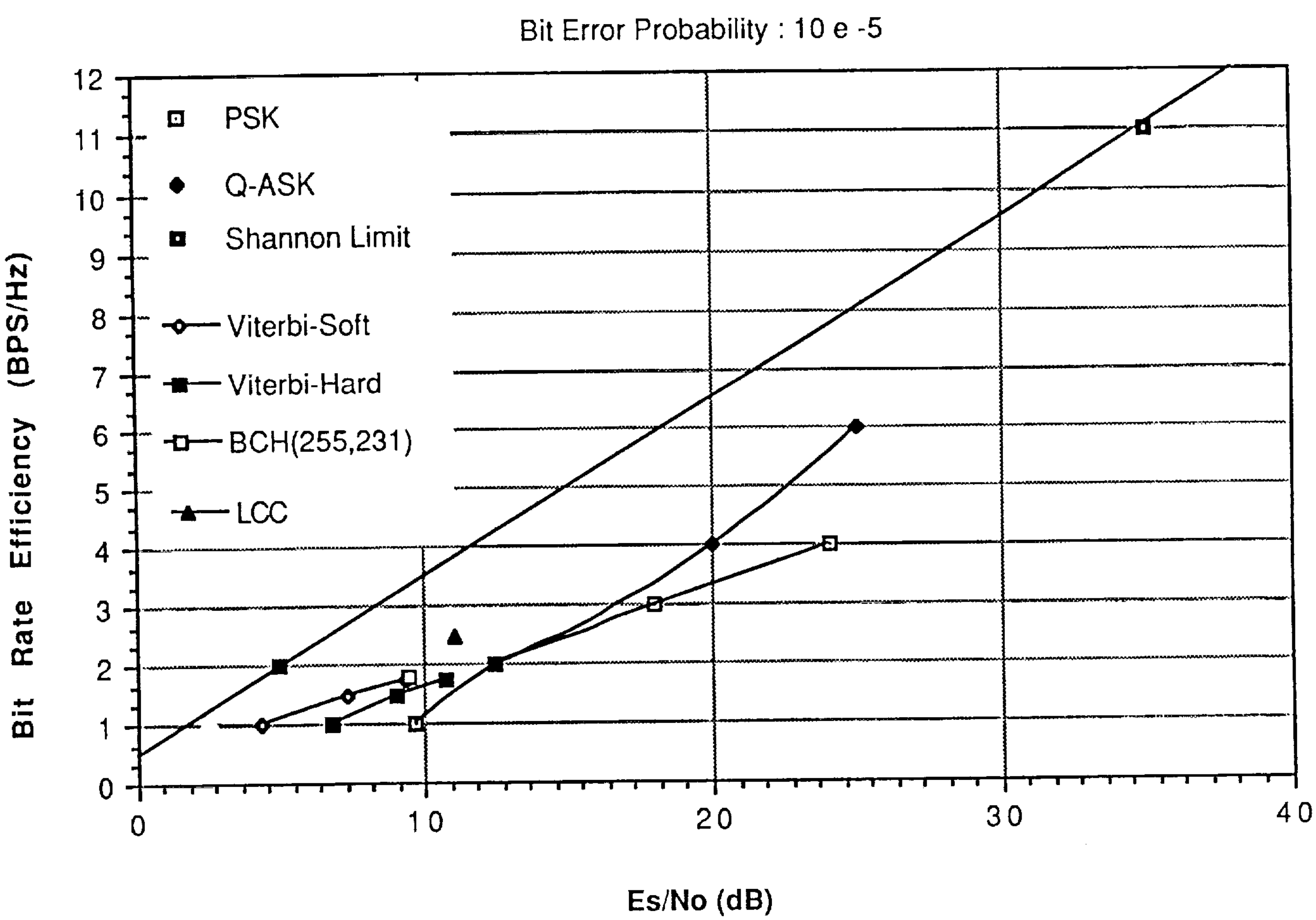

Figure 2.4-1. Bit Rate Efficiency Versus Es/No Plot for M-PSK/QASK

2.5 ZONE OF EXCLUSION (ZOE) STUDIES

Figure 2.5-1 shows the global TDRSS configurations outlined in the SOW. Drawn roughly to scale, it shows alternate locations for a pair of spacecraft in synchronous orbit, chosen so that all of continental United States (CONUS) is visible from one or both spacecrafts (as depicted by the four station locations shown), and the two spacecrafts are in view of each other (to support a data crosslink). Two different sets of configurations are depicted -- one with a spacecraft separation of 162°, and the second with a separation of 143°. The first represents a maximum allowable separation, since the crosslink path clears the edge of the earth by only 139 miles. Two variations of this configuration are apparent, representing crosslinks on opposite sides of the earth. The second configuration is chosen so that parts of CONUS are visible from both spacecrafts.

The "zone of exclusion" represents the portion of the earth from which neither TDRSS spacecraft is visible. The existence and extent of this zone are depicted in Figures 2.5-2 and 2.5-3 for the two configurations. Although the zone would actually encompass an orange-peel-like shape extending north/south from the equator, its width at the equator depends on the minimum elevation angle, below which the spacecraft is considered invisible. This width at sea level is determined to be as follows:

	Configuration 1	**Configuration 2**
Spacecraft location difference	162°	143°
Zone width at 0° elevation	35.4°	54.4°
Zone width at 10° elevation	55.1°	74.1°

These zone sizes would naturally decrease for visibility from user spacecraft in low earth orbit, and would disappear for minimum altitudes of 196 miles for Configuration 1, and 491 miles for Configuration 2.

For intermediate altitudes, the widths of the zone of exclusion would be as follows (assuming 0° elevation angle, but increasing the effective earth radius by 10 km = 6 mi to exclude excessive attenuation paths):

Spacecraft Altitudes (miles)	**Zone of Exclusion Width Configuration 1**	**Zone of Exclusion Width Configuration 2**
50	17.3°	36.3°
100	9.9°	28.9°
150	4.4°	23.4°
200	0	18.7°
300	0	11.1°
400	0	4.9°
500	0	0

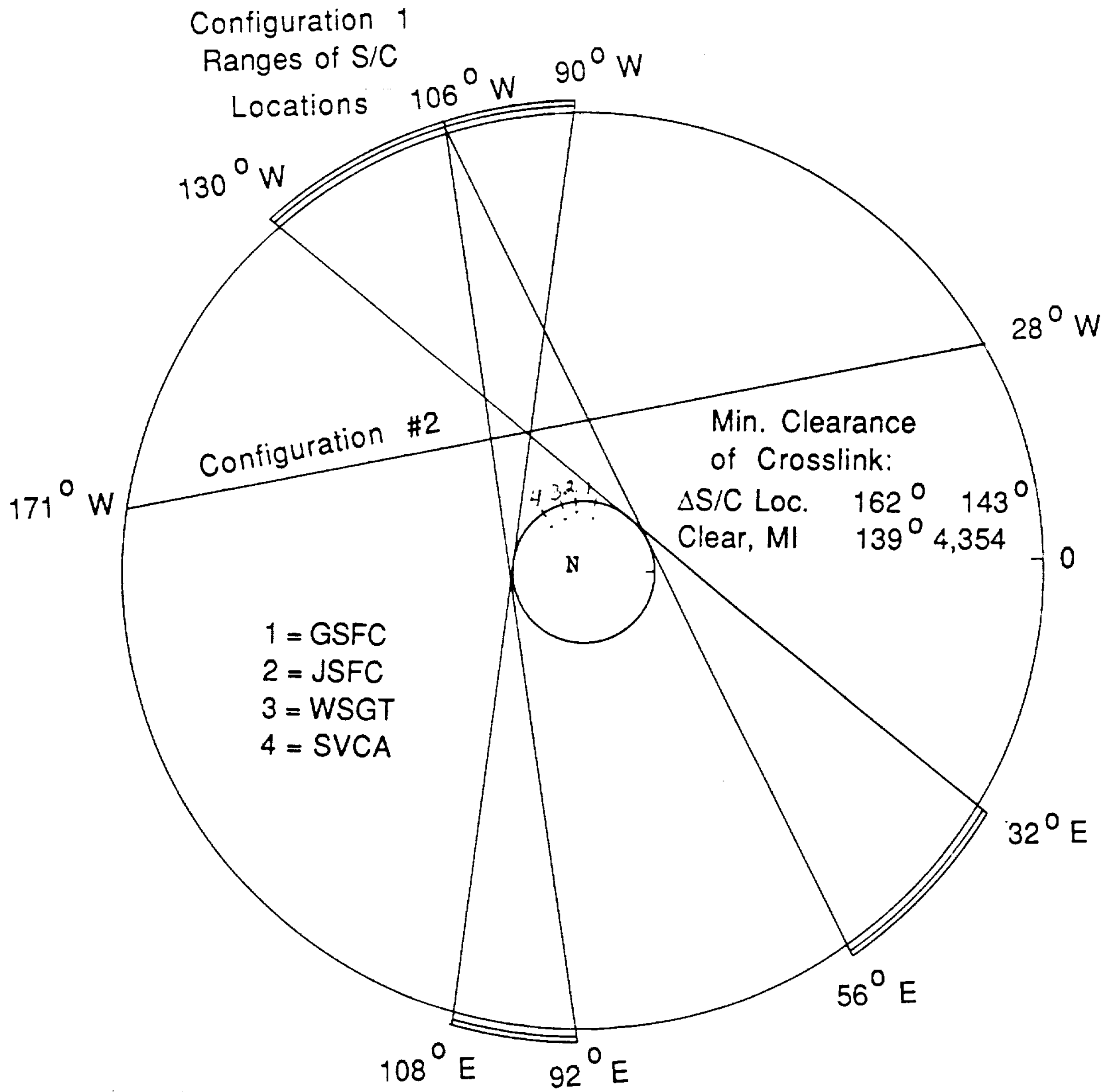

Figure 2.5-1. Configuration 1 Ranges of Spacecraft

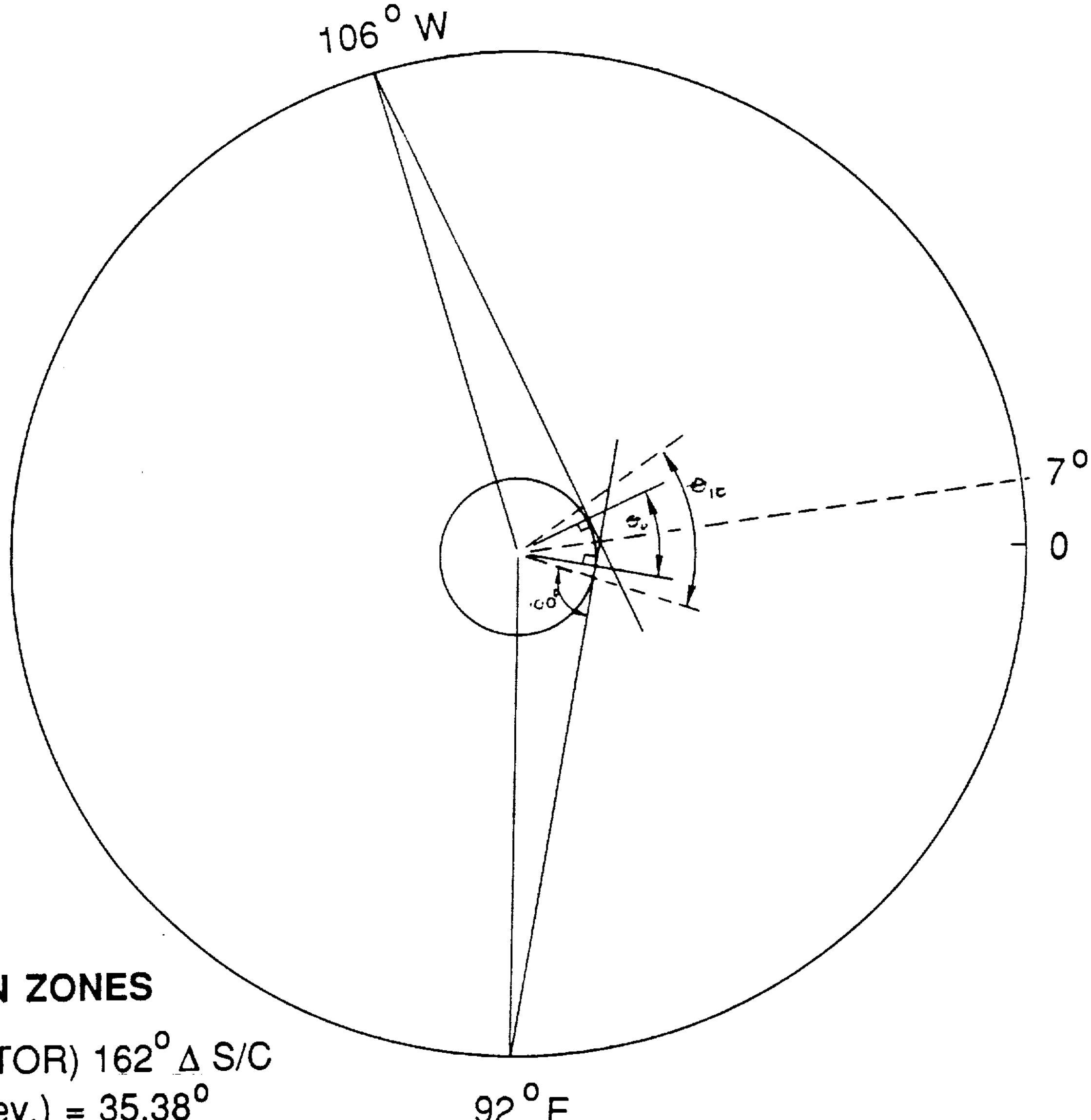

EXCLUSION ZONES

(AT EQUATOR) 162° Δ S/C
0_0 (0° Elev.) = 35.38°
0_{10} (10° Elev.) = 55.12°

(Sea Level)

Zero Excl. Above 196 Mi. Altitude

Figure 2.5-2. Configuration 1

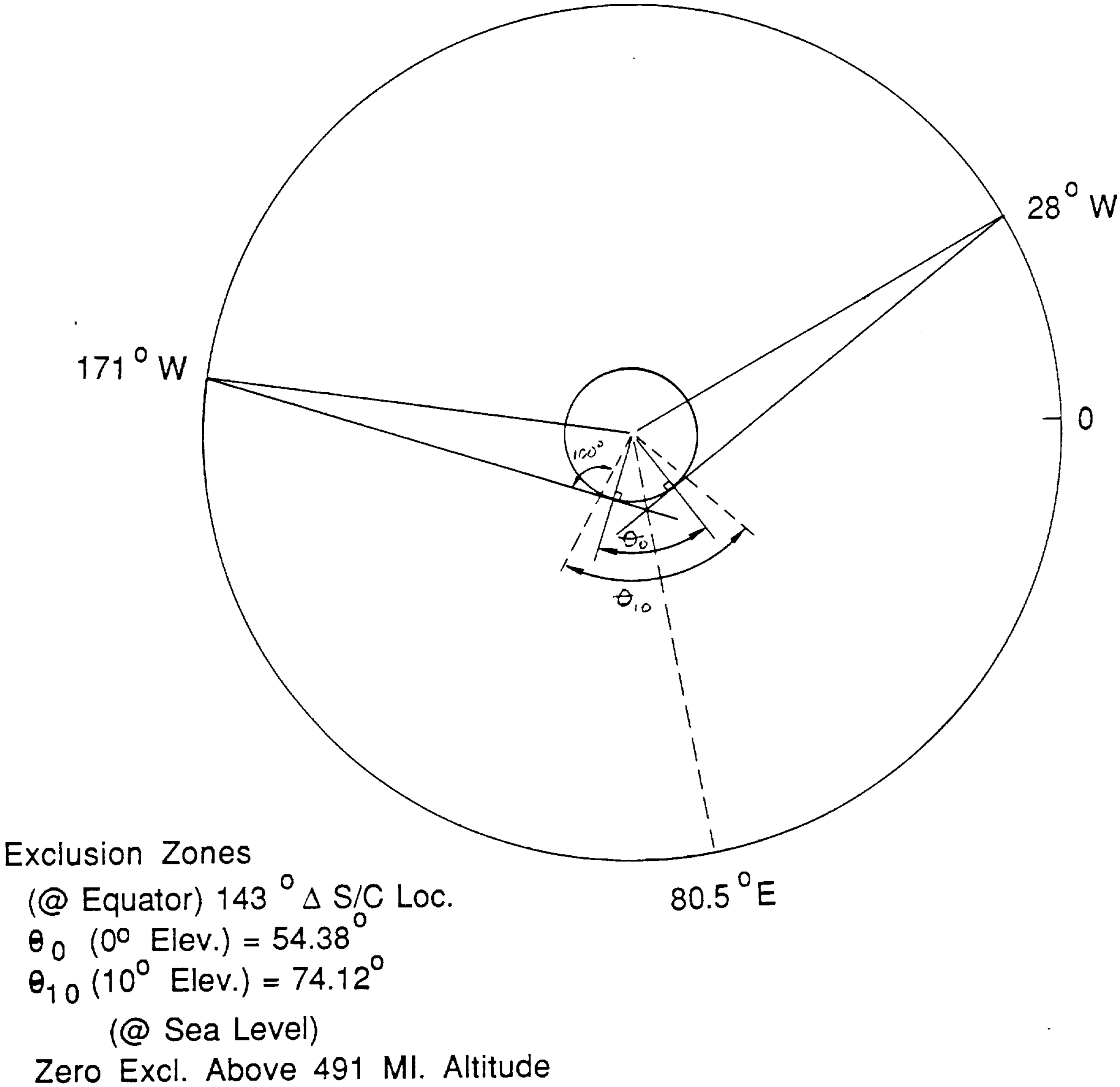

Figure 2.5-3. Configuration 2

2.5.1 ATDRS Location Sensitivity: Configuration 2

STI suggested an alternate location for the ATDRS-East for Configuration 2, namely at either 9° W or 15° W rather than 28° W as stated in the original SOW. In this subsection, we discuss the differences between these two locations in terms of the ZOE.

The change in the ATDRS-East location will result in a change to the ZOE as shown in Figure 2.5-4. While the 9° W choice minimizes the ZOE, the 15° W location allows improved visibility of this satellite from CONUS.

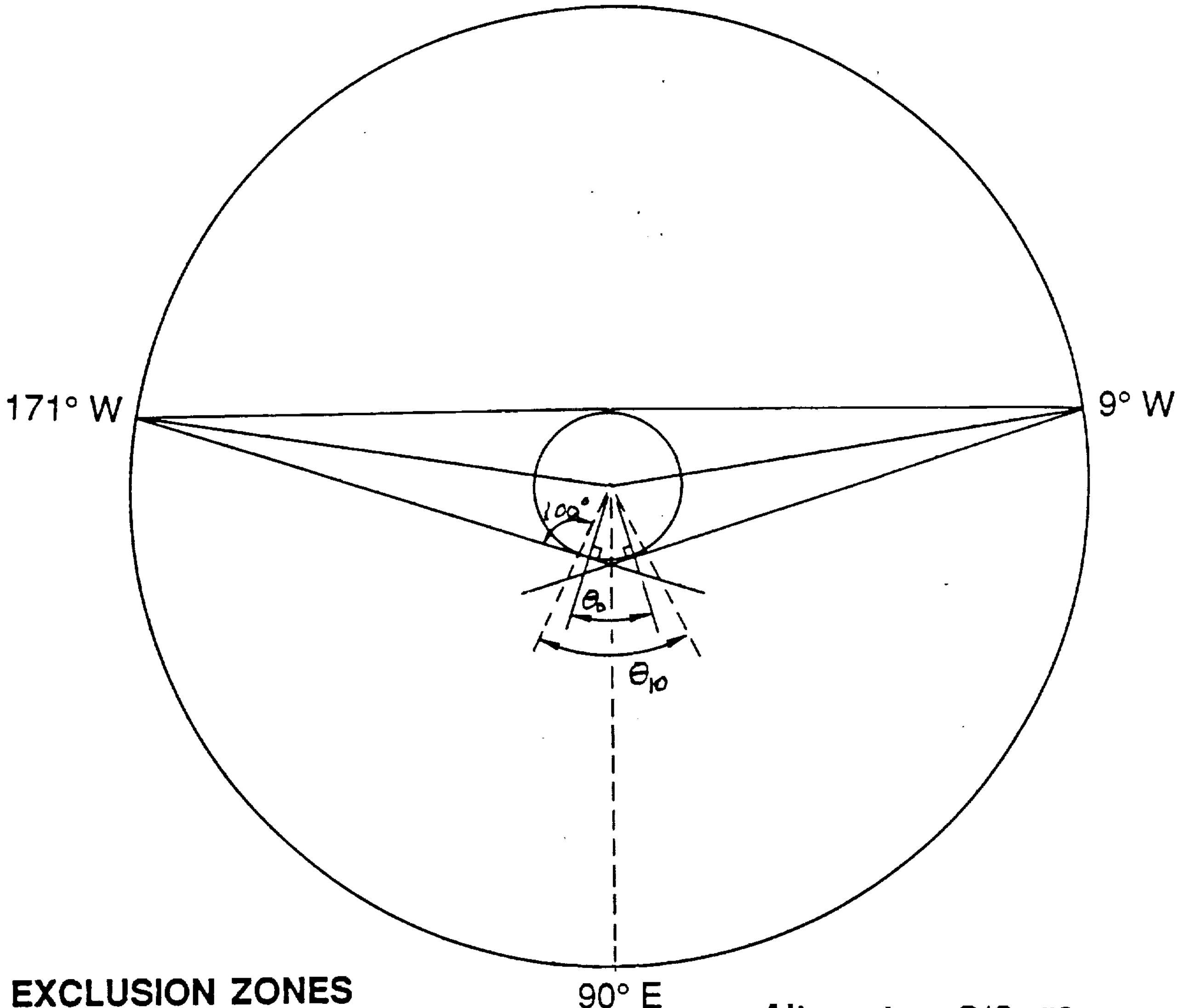

EXCLUSION ZONES

(AT EQUATOR) 162° Δ S/C
θ_0 (0° Elev.) = 35.38°
θ_{10} (10° Elev.) = 55.12°

(Sea Level)

Zero Excl. Above 196 Mi. Altitude

Alternate: S/C #2 at 15° W

Exclusion Zones (@ Equator)

θ_0 (0° Elev.) = 41.38°
θ_{10} (10° Elev.) = 61.12°

(Sea Level)

Zero Excl. Above 276 Mi. Altitude

Figure 2.5-4. Exclusion Zones for Alternate Configuration 2

2.6 EFFECT OF RAIN ON SPACE/GROUND LINK

An analysis has been done to determine the effect of rainy conditions on the ATDRS space-to-ground link (SGL) margin for the following CONUS ground stations: White Sands, Johnson, Goddard, JPL, Sunnyvale, Denver, Andover, and Marshall Centers. Four different orbital locations were assumed for the ATDRS, namely those locations of Configurations 1 and 2 in the SOW. Operating frequencies assumed were 20 GHz for the downlink and 30 GHz for the uplink. Vertical, horizontal, and circular polarizations are considered. Rain loss is dependent upon frequency, elevation angle, and rain zone and altitude of the ground station. Results of a crane model rain attenuation analysis are given in Table 2.6-1 for both 99.5% and 99.8% availability. Loss due to rain, as a function of the availability, is shown in the Table 2.6-1 in dB. For instance, at White Sands with the ATDRS located at 130 W, on the downlink (20 GHz and horizontal polarization) the insertion loss will exceed 0.5 dB for only 0.005% of the time. Similarly, the losses shown for 99.8% availability are those that will not be exceeded for 99.8% of the time.

Loss due to rain is higher if circular polarization is used, and this effect is very noticeable at Ka-band frequencies. (The ground station/satellite geometry must be studied to determine if 0/90° is the rainfall alignment or if some small offset from 0/90 should be used for the orthogonal polarizations.) Higher rain loss is also exhibited with horizontal linear polarization (see the tabulated losses for JSFC).

In addition to actual signal attenuation by raindrops, rain results in an additional area of degradation on the downlink. The sky noise temperature (as seen by the ground antenna) increases with attenuation increase. Increased sky noise temperature results in increased system noise temperature, which in turn results in additional power requirements. Table 2.6-2 gives the results of an analysis into the total link degradation for the downlink communications due to the rain losses of Table 2.6-1, assuming the use of horizontal polarization (which exhibits the worst case rain degradation). The dependence of atmospheric attenuation on frequency is shown in Figure 2.6-1. This clear sky attenuation is computed for each ground station (a function of elevation angle and altitude), assuming a 40% relative humidity and a surface temperature of 21 °C. The clear sky noise temperature for each attenuation and the corresponding system noise temperature (assuming a 129 K receiver noise temperature) are computed. Similarly, sky noise and system noise temperatures for the rain attenuations of Table 2.6-1 are computed and are compared with the system noise temperatures during clear sky operation. The additional degradation in system temperature due to the sky noise increase is given in Table 2.6-2 in dB. Finally, the noise degradation is added to the rain loss to give the total link degradation due to rain for each ground-satellite path.

Table 2.6-1. Loss Due to Rain in dB

Ground Station: White Sands Ground Terminal

Note: Altitude 1.36 km

Frequency	Polarization	Percent Availability	Satellite Longitude (° W) 171	130	106	41
			Elevation Angle 12.8	44.6	52.3	12.0
20.0 GHz	Vertical	99.8	4.6	1.2	1.0	5.0
		99.5	2.3	0.5	0.4	2.5
	Horizontal	99.8	5.3	1.2	1.0	5.6
		99.5	2.6	0.5	0.4	2.8
	Circular	99.8	4.9	1.2	1.0	5.3
		99.5	2.5	0.5	0.4	2.7
30.0 GHz	Vertical	99.8	10.0	2.5	2.1	10.7
		99.5	5.2	1.1	0.9	5.6
	Horizontal	99.8	11.5	2.7	2.2	12.3
		99.5	5.9	1.1	0.9	6.4
	Circular	99.8	10.7	2.6	2.2	11.5
		99.5	5.6	1.1	0.9	6.0
15.0 GHz	Vertical	99.8	2.6	0.6	0.5	2.8
		99.5	1.2	0.2	0.2	1.4
	Horizontal	99.8	2.8	0.7	0.5	3.0
		99.5	1.3	0.2	0.2	1.5
	Circular	99.8	2.7	0.6	0.5	2.9
		99.5	1.3	0.2	0.2	1.4
13.7 GHz	Vertical	99.8	2.0	0.5	0.4	2.2
		99.5	1.0	0.2	0.1	1.0
	Horizontal	99.8	2.3	0.5	0.4	2.4
		99.5	1.1	0.2	0.2	1.2
	Circular	99.8	2.1	0.5	0.4	2.3
		99.5	1.0	0.2	0.2	1.1

Table 2.6-1. Loss Due to Rain in dB (Continued)

Ground Station: White Sands Ground Terminal (Continued)
Note: Altitude 1.36 km

Frequency	Polarization	Percent Availability	Satellite Longitude (° W) 90 Elevation Angle 48.3	10.0	9.0
20.0 GHz	Vertical	99.8	1.0	6.0	6.7
		99.5	0.4	3.1	3.5
	Horizontal	99.8	1.1	6.8	7.6
		99.5	0.4	3.5	3.9
	Circular	99.8	1.1	6.4	7.2
		99.5	0.4	3.3	3.7
30.0 GHz	Vertical	99.8	2.3	12.8	14.4
		99.5	1.0	7.0	7.7
	Horizontal	99.8	2.5	14.8	16.6
		99.5	1.0	8.0	8.8
	Circular	99.8	2.4	13.8	15.5
		99.5	1.0	7.5	8.2
15.0 GHz	Vertical	99.8	0.6	3.3	3.7
		99.5	0.2	1.7	1.9
	Horizontal	99.8	0.6	3.6	4.1
		99.5	0.2	1.8	2.0
	Circular	99.8	0.6	3.5	3.9
		99.5	0.2	1.8	1.9
13.7 GHz	Vertical	99.8	0.4	2.6	2.9
		99.5	0.2	1.3	1.4
	Horizontal	99.8	0.5	2.9	3.3
		99.5	0.2	1.5	1.6
	Circular	99.8	0.5	2.7	3.1
		99.5	0.2	1.4	1.5

Table 2.6-1. Loss Due to Rain in dB (Continued)

Ground Station: Sunnyvale Satellite Test Center
Note: 0 km

Frequency	Polarization	Percent Availability	Satellite Longitude (° W)		
			171	130	106
			Elevation Angle		
			23.5	45.9	43.5
20.0 GHz	Vertical	99.8	4.8	2.5	2.6
		99.5	2.8	1.3	1.4
	Horizontal	99.8	5.4	2.7	2.8
		99.5	3.1	1.3	1.5
	Circular	99.8	5.1	2.6	2.7
		99.5	2.9	1.3	1.4
30.0 GHz	Vertical	99.8	10.2	5.3	5.6
		99.5	6.0	2.8	3.0
	Horizontal	99.8	11.6	5.7	6.1
		99.5	6.8	3.0	3.2
	Circular	99.8	10.9	5.5	5.8
		99.5	6.4	2.9	3.1
15.0 GHz	Vertical	99.8	2.7	1.4	1.5
		99.5	1.5	0.7	0.7
	Horizontal	99.8	2.9	1.5	1.5
		99.5	1.6	0.7	0.8
	Circular	99.8	2.8	1.4	1.5
		99.5	1.6	0.7	0.8
13.7 GHz	Vertical	99.8	2.2	1.1	1.2
		99.5	1.2	0.5	0.6
	Horizontal	99.8	2.4	1.2	1.2
		99.5	1.3	0.6	0.6
	Circular	99.8	2.3	1.1	1.2
		99.5	1.3	0.6	0.6

Table 2.6-1. Loss Due to Rain in dB (Continued)

Ground Station: Sunnyvale Satellite Test Center (Continued)
Note: Altitude 0 km

Frequency	Polarization	Percent Availability	Satellite Longitude (° W) 90 Elevation Angle 35.3	10.0	9.0
20.0 GHz	Vertical	99.8	3.3	10.3	11.2
		99.5	1.8	6.7	7.5
	Horizontal	99.8	3.6	11.8	12.8
		99.5	1.9	7.6	8.5
	Circular	99.8	3.4	11.0	12.0
		99.5	1.8	7.1	8.0
30.0 GHz	Vertical	99.8	6.9	21.8	23.6
		99.5	3.9	14.5	16.1
	Horizontal	99.8	7.7	25.2	27.4
		99.5	4.2	16.6	18.6
	Circular	99.8	7.3	23.5	25.5
		99.5	4.1	15.6	17.4
15.0 GHz	Vertical	99.8	1.8	5.8	6.3
		99.5	1.0	3.7	4.1
	Horizontal	99.8	2.0	6.3	6.9
		99.5	1.0	4.0	4.5
	Circular	99.8	1.9	6.1	6.6
		99.5	1.0	3.9	4.3
13.7 GHz	Vertical	99.8	1.5	4.6	5.0
		99.5	0.8	2.9	3.2
	Horizontal	99.8	1.6	5.1	5.6
		99.5	0.8	3.2	3.6
	Circular	99.8	1.5	4.9	5.3
		99.5	0.8	3.1	3.4

Table 2.6-1. Loss Due to Rain in dB (Continued)

Ground Station: Denver, Colorado

Note: Altitude 1.8 km

Frequency	Polarization	Percent Availability	Satellite Longitude (° W) 171	130	106	41
			Elevation Angle 9.6	37.3	44.2	11.3
20.0 GHz	Vertical	99.8	5.7	1.3	1.1	4.7
		99.5	3.0	0.5	0.4	2.1
	Horizontal	99.8	6.6	1.4	1.2	5.4
		99.5	3.4	0.6	0.5	2.4
	Circular	99.8	6.1	1.3	1.1	5.0
		99.5	3.2	0.5	0.5	2.3
30.0 GHz	Vertical	99.8	11.8	2.7	2.3	9.7
		99.5	6.4	1.1	1.0	4.6
	Horizontal	99.8	13.7	3.0	2.5	11.3
		99.5	7.4	1.3	1.1	5.3
	Circular	99.8	12.8	2.8	2.4	10.5
		99.5	6.9	1.2	1.0	4.9
15.0 GHz	Vertical	99.8	3.2	0.7	0.6	2.7
		99.5	1.7	0.3	0.2	1.2
	Horizontal	99.8	3.6	0.8	0.6	2.9
		99.5	1.8	0.3	0.3	1.3
	Circular	99.8	3.4	0.7	0.6	2.8
		99.5	1.8	0.3	0.2	1.2
13.7 GHz	Vertical	99.8	2.6	0.6	0.5	2.1
		99.5	1.3	0.2	0.2	0.9
	Horizontal	99.8	2.9	0.6	0.5	2.4
		99.5	1.5	0.2	0.2	1.0
	Circular	99.8	2.8	0.6	0.5	2.3
		99.5	1.4	0.2	0.2	1.0

Table 2.6-1. Loss Due to Rain in dB (Continued)

Ground Station: Denver, Colorado (Continued)
Note: Altitude 1.8 km

Frequency	Polarization	Percent Availability	Satellite Longitude (° W) 90 Elevation Angle 41.7	10.0	9.0
20.0 GHz	Vertical	99.8	1.1	5.3	5.7
		99.5	0.5	2.5	3.5
	Horizontal	99.8	1.2	6.1	6.5
		99.5	0.5	2.8	4.0
	Circular	99.8	1.2	5.7	6.1
		99.5	0.5	2.6	3.7
30.0 GHz	Vertical	99.8	2.4	11.0	11.8
		99.5	1.0	5.3	7.5
	Horizontal	99.8	2.6	12.8	13.7
		99.5	1.1	6.1	8.7
	Circular	99.8	2.5	11.9	12.7
		99.5	1.1	5.7	8.1
15.0 GHz	Vertical	99.8	0.6	3.0	3.2
		99.5	0.3	1.4	2.0
	Horizontal	99.8	0.7	3.3	3.6
		99.5	0.3	1.5	2.1
	Circular	99.8	0.7	3.2	3.4
		99.5	0.3	1.4	2.0
13.7 GHz	Vertical	99.8	0.5	2.4	2.6
		99.5	0.2	1.1	1.5
	Horizontal	99.8	0.5	2.7	2.9
		99.5	0.2	1.2	1.7
	Circular	99.8	0.5	2.6	2.7
		99.5	0.2	1.1	1.6

Table 2.6-1. Loss Due to Rain in dB (Continued)

Ground Station: Marshall Space Flight Center
Note: Altitude 0.23 km

Frequency	Polarization	Percent Availability	Satellite Longitude (° W) 130 / Elevation Angle 29.3	106 / 44.8	41 / 27.3	90 / 49.6
20.0 GHz	Vertical	99.8	13.9	10.4	14.6	9.7
		99.5	7.3	5.1	7.7	4.7
	Horizontal	99.8	15.9	11.4	16.8	10.5
		99.5	8.3	5.5	8.8	5.0
	Circular	99.8	14.9	10.9	15.7	10.1
		99.5	7.8	5.3	8.3	4.8
30.0 GHz	Vertical	99.8	27.1	20.2	28.4	18.8
		99.5	14.8	10.3	15.6	9.5
	Horizontal	99.8	31.0	22.0	32.7	20.3
		99.5	16.7	11.2	17.8	10.1
	Circular	99.8	29.0	21.1	30.5	19.6
		99.5	15.7	10.8	16.7	9.8
15.0 GHz	Vertical	99.8	8.4	6.2	8.8	5.8
		99.5	4.3	3.0	4.5	2.7
	Horizontal	99.8	9.2	6.6	9.6	6.1
		99.5	4.6	3.1	4.9	2.8
	Circular	99.8	8.8	6.4	9.2	5.9
		99.5	4.4	3.0	4.7	2.8
13.7 GHz	Vertical	99.8	6.8	5.1	7.2	4.8
		99.5	3.4	2.4	3.6	2.2
	Horizontal	99.8	7.6	5.5	8.0	5.1
		99.5	3.8	2.6	4.0	2.3
	Circular	99.8	7.2	5.3	7.6	4.9
		99.5	3.6	2.5	3.8	2.2

Table 2.6-1. Loss Due to Rain in dB (Continued)

Ground Station: Marshall Space Flight Center (Continued)
Note: Altitude 0.23 km

Frequency	Polarization	Percent Availability	Satellite Longitude (° W) Elevation Angle 10.0	9.0
20.0 GHz	Vertical	99.8	26.6	27.8
		99.5	16.3	17.3
	Horizontal	99.8	31.3	32.7
		99.5	19.0	20.2
	Circular	99.8	28.9	30.2
		99.5	17.6	18.7
30.0 GHz	Vertical	99.8	52.8	55.2
		99.5	33.4	35.5
	Horizontal	99.8	62.2	65.1
		99.5	39.0	41.5
	Circular	99.8	57.5	60.1
		99.5	36.2	38.5
15.0 GHz	Vertical	99.8	15.8	16.5
		99.5	9.5	10.0
	Horizontal	99.8	17.6	18.4
		99.5	10.5	11.1
	Circular	99.8	16.7	17.4
		99.5	10.0	10.6
13.7 GHz	Vertical	99.8	12.8	13.3
		99.5	7.6	8.0
	Horizontal	99.8	14.6	15.2
		99.5	8.6	9.1
	Circular	99.8	13.7	14.3
		99.5	8.1	8.6

Table 2.6-1. Loss Due to Rain in dB (Continued)

Ground Station: Andover, Maine
Note: Altitude 0.21 km

Frequency	Polarization	Percent Availability	Satellite Longitude (° W)			
			130	106	41	90
			Elevation Angle			
			12.8	27.8	30.7	35.1
20.0 GHz	Vertical	99.8	4.3	1.9	1.7	1.4
		99.5	2.2	0.8	0.7	0.6
	Horizontal	99.8	4.8	2.1	1.8	1.5
		99.5	2.5	0.9	0.8	0.7
	Circular	99.8	4.6	2.0	1.7	1.5
		99.5	2.4	0.9	0.8	0.6
30.0 GHz	Vertical	99.8	9.1	4.0	3.6	3.0
		99.5	4.9	1.9	1.7	1.4
	Horizontal	99.8	10.5	4.5	4.0	3.4
		99.5	5.6	2.1	1.8	1.5
	Circular	99.8	9.8	4.3	3.8	3.2
		99.5	5.3	2.0	1.8	1.5
15.0 GHz	Vertical	99.8	2.4	1.0	0.9	0.8
		99.5	1.2	0.5	0.4	0.3
	Horizontal	99.8	2.6	1.1	1.0	0.8
		99.5	1.3	0.5	0.4	0.3
	Circular	99.8	2.5	1.1	0.9	0.8
		99.5	1.3	0.5	0.4	0.3
13.7 GHz	Vertical	99.8	1.9	0.8	0.7	0.6
		99.5	0.9	0.4	0.3	0.3
	Horizontal	99.8	2.1	0.9	0.8	0.7
		99.5	1.0	0.4	0.3	0.3
	Circular	99.8	2.0	0.8	0.7	0.6
		99.5	1.0	0.4	0.3	0.3

Table 2.6-1. Loss Due to Rain in dB (Continued)

Ground Station: Andover, Maine (Continued)
Note: Altitude 0.21 km

Frequency	Polarization	Percent Availability	Satellite Longitude (° W)			
			15	9		
			Elevation Angle			
			15.3	11.2	10.0	9.0
20.0 GHz	Vertical	99.8	3.6	4.9	5.5	6.0
		99.5	1.8	2.6	3.0	3.4
	Horizontal	99.8	4.1	5.6	6.2	6.8
		99.5	2.0	2.9	3.3	3.8
	Circular	99.8	3.8	5.2	5.9	6.4
		99.5	1.9	2.8	3.2	3.6
30.0 GHz	Vertical	99.8	7.7	10.5	11.7	12.9
		99.5	4.0	5.8	6.5	7.5
	Horizontal	99.8	8.8	12.1	13.5	14.8
		99.5	4.6	6.6	7.5	8.6
	Circular	99.8	8.2	11.3	12.6	13.9
		99.5	4.3	6.2	7.0	8.1
15.0 GHz	Vertical	99.8	2.0	2.7	3.0	3.3
		99.5	1.0	1.4	1.6	1.9
	Horizontal	99.8	2.2	3.0	3.3	3.6
		99.5	1.1	1.5	1.7	2.0
	Circular	99.8	2.1	2.9	3.2	3.5
		99.5	1.0	1.5	1.7	1.9
13.7 GHz	Vertical	99.8	1.6	2.1	2.4	2.6
		99.5	0.8	1.1	1.3	1.4
	Horizontal	99.8	1.7	2.4	2.7	2.9
		99.5	0.8	1.2	1.4	1.6
	Circular	99.8	1.7	2.3	2.5	2.8
		99.5	0.8	1.2	1.3	1.5

Table 2.6-1. Loss Due to Rain in dB (Continued)

Ground Station: Jet Propulsion Laboratory

Note: Altitude 0 km

Frequency	Polarization	Percent Availability	Satellite Longitude (° W) 171 / Elevation Angle 22.2	130 / 48.6	106 / 48.3
20.0 GHz	Vertical	99.8	4.0	1.7	1.8
		99.5	2.0	0.7	0.7
	Horizontal	99.8	4.5	1.8	1.9
		99.5	2.2	0.8	0.8
	Circular	99.8	4.3	1.8	1.8
		99.5	2.1	0.7	0.7
30.0 GHz	Vertical	99.8	8.6	3.8	3.8
		99.5	4.5	1.7	1.7
	Horizontal	99.8	9.8	4.1	4.1
		99.5	5.0	1.8	1.8
	Circular	99.8	9.2	3.9	4.0
		99.5	4.8	1.7	1.7
15.0 GHz	Vertical	99.8	2.2	0.9	1.0
		99.5	1.1	0.4	0.4
	Horizontal	99.8	2.4	1.0	1.0
		99.5	1.1	0.4	0.4
	Circular	99.8	2.3	1.0	1.0
		99.5	1.1	0.4	0.4
13.7 GHz	Vertical	99.8	1.7	0.7	0.7
		99.5	0.8	0.3	0.3
	Horizontal	99.8	1.9	0.8	0.8
		99.5	0.9	0.3	0.3
	Circular	99.8	1.8	0.8	0.8
		99.5	0.9	0.3	0.3

Table 2.6-1. Loss Due to Rain in dB (Continued)

Ground Station: Jet Propulsion Laboratory (Continued)
Note: Altitude 0 km

Frequency	Polarization	Percent Availability	Satellite Longitude (° W) 90		
			Elevation Angle		
			40.2	10.0	9.0
20.0 GHz	Vertical	99.8	2.2	8.7	9.3
		99.5	1.0	5.2	5.9
	Horizontal	99.8	2.3	9.9	10.6
		99.5	1.0	5.9	6.6
	Circular	99.8	2.3	9.3	9.9
		99.5	1.0	5.5	6.2
30.0 GHz	Vertical	99.8	4.7	18.8	20.0
		99.5	2.2	11.6	13.0
	Horizontal	99.8	5.1	21.6	23.0
		99.5	2.4	13.2	14.9
	Circular	99.8	4.9	20.2	21.5
		99.5	2.3	12.4	13.9
15.0 GHz	Vertical	99.8	1.2	4.8	5.1
		99.5	0.5	2.8	3.2
	Horizontal	99.8	1.2	5.3	5.6
		99.5	0.5	3.1	3.4
	Circular	99.8	1.2	5.0	5.4
		99.5	0.5	2.9	3.3
13.7 GHz	Vertical	99.8	0.9	3.8	4.0
		99.5	0.4	2.2	2.5
	Horizontal	99.8	1.0	4.2	4.5
		99.5	0.4	2.4	2.7
	Circular	99.8	1.0	4.0	4.3
		99.5	0.4	2.3	2.6

Table 2.6-1. Loss Due to Rain in dB (Continued)

Ground Station: Goddard Space Flight Center
Note: Altitude 0 km

Frequency	Polarization	Percent Availability	Satellite Longitude (° W)			
			130	106	41	90
			Elevation Angle			
			19.6	35.7	31.7	42.8
20.0 GHz	Vertical	99.8	9.2	5.6	6.2	4.7
		99.5	5.2	2.9	3.3	2.4
	Horizontal	99.8	10.5	6.2	6.9	5.2
		99.5	5.9	3.2	3.6	2.6
	Circular	99.8	9.9	5.9	6.5	4.9
		99.5	5.5	3.0	3.4	2.5
30.0 GHz	Vertical	99.8	18.7	11.3	12.5	9.6
		99.5	10.9	6.1	6.9	5.0
	Horizontal	99.8	21.6	12.6	14.1	10.5
		99.5	12.5	6.7	7.7	5.5
	Circular	99.8	20.1	11.9	13.3	10.1
		99.5	11.7	6.4	7.3	5.3
15.0 GHz	Vertical	99.8	5.3	3.2	3.6	2.7
		99.5	2.9	1.6	1.8	1.3
	Horizontal	99.8	5.8	3.4	3.8	2.9
		99.5	3.2	1.7	2.0	1.4
	Circular	99.8	5.6	3.3	3.7	2.8
		99.5	3.1	1.7	1.9	1.4
13.7 GHz	Vertical	99.8	4.3	2.6	2.9	2.2
		99.5	2.3	1.3	1.5	1.1
	Horizontal	99.8	4.8	2.8	3.2	2.4
		99.5	2.6	1.4	1.6	1.1
	Circular	99.8	4.5	2.7	3.0	2.3
		99.5	2.5	1.3	1.5	1.1

Table 2.6-1. Loss Due to Rain in dB (Continued)

Ground Station: Goddard Space Flight Center (Continued)
Note: Altitude 0 km

Frequency	Polarization	Percent Availability	Satellite Longitude (° W)			
			28	15		
			Elevation Angle			
			22.8	13.1	8.5	10
20.0 GHz	Vertical	99.8	8.1	12.5	16.8	15.1
		99.5	4.5	7.5	10.8	9.4
	Horizontal	99.8	9.3	14.5	19.5	17.5
		99.5	5.1	8.6	12.5	10.8
	Circular	99.8	8.7	13.5	18.1	16.3
		99.5	4.8	8.0	11.6	10.1
30.0 GHz	Vertical	99.8	16.5	25.6	34.6	30.9
		99.5	9.5	15.8	22.9	19.9
	Horizontal	99.8	18.9	29.8	40.4	36.1
		99.5	10.8	18.2	26.5	23.0
	Circular	99.8	17.7	27.7	37.5	33.5
		99.5	10.1	17.0	24.7	21.4
15.0 GHz	Vertical	99.8	4.7	7.3	9.7	8.7
		99.5	2.5	4.2	6.1	5.3
	Horizontal	99.8	5.1	8.0	10.7	9.6
		99.5	2.8	4.7	6.7	5.8
	Circular	99.8	4.9	7.6	10.2	9.2
		99.5	2.7	4.4	6.4	5.6
13.7 GHz	Vertical	99.8	3.8	5.8	7.7	7.0
		99.5	2.0	3.4	4.8	4.2
	Horizontal	99.8	4.2	6.6	8.7	7.9
		99.5	2.2	3.8	5.4	4.7
	Circular	99.8	4.0	6.2	8.2	7.4
		99.5	2.1	3.6	5.1	4.5

Table 2.6-1. Loss Due to Rain in dB (Continued)

Ground Station: Johnson Space Flight Center
Note: Altitude 0 km

Frequency	Polarization	Percent Availability	Satellite Longitude (° W)			
			130	106	41	90
			Elevation Angle			
			38.8	53.3	22.7	55.1
20.0 GHz	Vertical	99.8	13.5	11.1	19.0	10.9
		99.5	7.1	5.5	10.7	5.4
	Horizontal	99.8	15.1	11.8	22.0	11.6
		99.5	7.9	5.8	12.3	5.7
	Circular	99.8	14.3	11.5	20.5	11.2
		99.5	7.5	5.7	11.5	5.5
30.0 GHz	Vertical	99.8	26.3	21.5	37.2	21.1
		99.5	14.4	11.2	21.8	10.9
	Horizontal	99.8	29.3	22.9	43.1	22.4
		99.5	15.9	11.8	25.0	11.5
	Circular	99.8	27.8	22.2	40.1	21.8
		99.5	15.1	11.5	23.4	11.2
15.0 GHz	Vertical	99.8	8.1	6.6	11.4	6.5
		99.5	4.1	3.2	6.3	3.1
	Horizontal	99.8	8.7	6.9	12.6	6.7
		99.5	4.4	3.3	6.9	3.2
	Circular	99.8	8.4	6.8	12.0	6.6
		99.5	4.3	3.2	6.6	3.1
13.7 GHz	Vertical	99.8	6.7	5.4	9.3	5.3
		99.5	3.3	2.6	5.0	2.5
	Horizontal	99.8	7.3	5.7	10.5	5.6
		99.5	3.6	2.7	5.6	2.6
	Circular	99.8	7.0	5.6	9.9	5.5
		99.5	3.5	2.6	5.3	2.6

Table 2.6-1. Loss Due to Rain in dB (Continued)

Ground Station: Johnson Space Flight Center (Continued)
Note: Altitude 0 km

Frequency	Polarization	Percent Availability	Satellite Longitude (° W) 28 Elevation Angle 11.3	10.0	9.0
20.0 GHz	Vertical	99.8	27.5	28.9	30.2
		99.5	17.3	18.5	19.3
	Horizontal	99.8	32.3	34.0	35.6
		99.5	20.1	21.5	22.5
	Circular	99.8	29.9	31.4	32.8
		99.5	18.7	20.0	20.9
30.0 GHz	Vertical	99.8	54.6	57.5	59.8
		99.5	35.4	38.0	39.5
	Horizontal	99.8	64.3	67.7	70.6
		99.5	41.3	44.4	46.2
	Circular	99.8	59.4	62.5	65.1
		99.5	38.3	1.2	42.9
15.0 GHz	Vertical	99.8	16.3	17.2	18.0
		99.5	10.0	10.7	11.2
	Horizontal	99.8	18.2	19.1	20.1
		99.5	11.1	11.8	12.4
	Circular	99.8	17.2	18.1	19.0
		99.5	10.5	11.2	11.8
13.7 GHz	Vertical	99.8	13.2	13.9	14.6
		99.5	8.0	8.5	9.0
	Horizontal	99.8	15.1	15.9	16.7
		99.5	9.1	9.7	10.2
	Circular	99.8	14.1	14.9	15.6
		99.5	8.5	9.1	9.5

Table 2.6-2. Degradation in Downlink (20 GHz) Because of Rain

Ground Station: White Sands

Note: Altitude 1.36 km

	Satellite Longitude (°W)						
	106.0	90.0	130.0	171.0			41.0
Elevation Angle (deg)	52.3	48.3	44.6	12.8	10.0	90.0	12.0
Atmospheric Loss (dB)	0.18	0.19	0.20	0.36	0.81	0.89	0.67
Clear Sky Noise Temperature (K)	12.0	12.0	13.0	40.0	50.0	55.0	42.0
Clear Sky System Noise Temperature (K)	141.0	141.0	142.0	169.0	179.0	184.0	171.0
Rain Loss (dB)							
99.8% Availability	1.0	1.1	1.2	5.3	6.8	7.6	5.6
99.5% Availability	0.4	0.4	0.5	2.6	3.5	3.9	2.8
Rainy Sky Noise Temperature (K)							
99.8% Availability	60.0	65.0	70.0	204.0	229.0	240.0	210.0
99.5% Availability	26.0	26.0	32.0	131.0	160.0	172.0	138.0
Rainy System Noise Temperature (K)							
99.8% Availability	189.0	194.0	199.0	333.0	358.0	369.0	339.0
99.5% Availability	155.0	155.0	161.0	260.0	289.0	301.0	267.0
Sky Noise Degradation (dB) Due to Rain							
99.8% Availability	1.27	1.37	1.46	2.96	3.02	3.02	2.97
99.5% Availability	0.41	0.38	0.53	1.87	2.09	2.14	1.93
Total Rain Degradation (dB)							
99.8% Availability	2.27	2.47	2.66	8.26	9.82	10.62	8.57
99.5% Availability	0.81	0.78	1.03	4.47	5.59	6.04	4.73

Assumed Horizontal Polarization on Downlink Includes both Rain Loss and Degradation Because of Increased Sky Noise Temperature.

Table 2.6-2. Degradation in Downlink (20 GHz) Because of Rain (Continued)

Ground Station: Sunnyvale
Note: Altitude 0.0 km

	Satellite Longitude (°W)					
	106.0	90.0	130.0	171.0		
Elevation Angle (deg)	43.5	35.3	45.9	23.5	10.0	9.0
Atmospheric Loss (dB)	0.41	0.48	0.39	0.70	1.61	1.79
Clear Sky Noise Temperature (K)	26.0	31.0	25.0	44.0	91.0	99.0
Clear Sky System Noise Temperature (K)	155.0	160.0	154.0	173.0	220.0	228.0
Rain Loss (dB)						
99.8% Availability	2.8	3.6	2.7	5.4	11.8	12.8
99.5% Availability	1.5	1.9	1.3	3.1	7.6	8.5
Rainy Sky Noise Temperature (K)						
99.8% Availability	138.0	163.0	134.0	206.0	271.0	275.0
99.5% Availability	85.0	103.0	75.0	148.0	240.0	249.0
Rainy System Noise Temperature (K)						
99.8% Availability	267.0	292.0	263.0	335.0	400.0	404.0
99.5% Availability	214.0	232.0	204.0	277.0	369.0	378.0
Sky Noise Degradation (dB) Due to Rain						
99.8% Availability	2.35	262.0	2.32	2.88	2.59	2.48
99.5% Availability	1.39	1.61	1.21	2.05	2.24	2.19
Total Rain Degradation (dB)						
99.8% Availability	5.15	6.22	5.02	8.28	14.39	15.28
99.5% Availability	2.89	3.51	2.51	5.15	9.84	10.69

Assumed Horizontal Polarization on Downlink Includes both Rain Loss and Degradation because of Increased Sky Noise Temperature.

Table 2.6-2. Degradation in Downlink (20 GHz) Because of Rain (Continued)

Ground Station: Denver

Note: Altitude 1.8 km

	Satellite Longitude (°W)						
	106.0	90.0	130.0	171.0			41.0
Elevation Angle (deg)	44.2	41.7	37.3	9.6	10.0	90.0	11.3
Atmospheric Loss (dB)	0.19	0.20	0.21	0.78	0.75	0.83	0.66
Clear Sky Noise Temperature (K)	12.0	13.0	14.0	48.0	47.0	51.0	42.0
Clear Sky System Noise Temperature (K)	141.0	142.0	143.0	177	176.0	180.0	171.0
Rain Loss (dB)							
99.8% Availability	1.2	1.2	1.4	6.6	6.1	6.5	5.4
99.5% Availability	0.5	0.5	0.6	3.4	2.8	4.0	2.4
Rainy Sky Noise Temperature (K)							
99.8% Availability	70.0	70.0	80.0	227.0	219.0	225.0	206.0
99.5% Availability	32.0	32.0	37.0	157.0	138.0	175.0	123.0
Rainy System Noise Temperature (K)							
99.8% Availability	199.0	199.0	209.0	356.0	348.0	354.0	335.0
99.5% Availability	161.0	161.0	166.0	286.0	267.0	304.0	252.0
Sky Noise Degradation (dB) Due to Rain							
99.8% Availability	1.49	1.47	1.64	3.02	2.97	2.93	2.93
99.5% Availability	0.55	0.53	0.65	2.08	1.82	2.26	1.70
Total Rain Degradation (dB)							
99.8% Availability	2.69	2.67	3.04	9.62	9.07	9.43	8.33
99.5% Availability	1.05	1.03	1.25	5.48	4.62	6.26	4.10

Assumed Horizontal Polarization on Downlink Includes both Rain Loss and Degradation Because of Increased Sky Noise Temperature.

Table 2.6-2. Degradation in Downlink (20 GHz) Because of Rain (Continued)

Ground Station: Marshall
Note: Altitude 0.23 km

	Satellite Longitude (°W)					
	106.0	90.0	130.0			41.0
Elevation Angle (deg)	44.8	49.6	29.3	10.0	9.0	27.3
Atmospheric Loss (dB)	0.37	0.34	0.53	1.50	1.66	0.57
Clear Sky Noise Temperature (K)	24.0	22.0	34.0	86.0	93.0	36.0
Clear Sky System Noise Temperature (K)	153.0	151.0	163.0	215.0	222.0	165.0
Rain Loss (dB)						
99.8% Availability	11.4	10.5	15.9	31.3	32.7	16.8
99.5% Availability	5.5	5.0	8.3	19.0	20.2	8.8
Rainy Sky Noise Temperature (K)						
99.8% Availability	269.0	264.0	283.0	290.0	290.0	284.0
99.5% Availability	208.0	198.0	247.0	286.0	287.0	252.0
Rainy System Noise Temperature (K)						
99.8% Availability	398.0	393.0	412.0	419.0	419.0	413.0
99.5% Availability	337.0	327.0	376.0	415.0	416.0	381.0
Sky Noise Degradation (dB) Due to Rain						
99.8% Availability	4.15	4.15	4.03	2.90	2.75	3.98
99.5% Availability	3.43	3.35	3.64	2.87	2.72	3.63
Total Rain Degradation (dB)						
99.8% Availability	15.55	14.65	19.93	34.20	35.45	20.78
99.5% Availability	8.93	8.35	11.94	21.87	22.92	12.43

Assumed Horizontal Polarization on Downlink Includes both Rain Loss and Degradation Because of Increased Sky Noise Temperature.

Table 2.6-2. Degradation in Downlink (20 GHz) Because of Rain (Continued)

Ground Station: Andover

Note: Altitude 0.21 km

	Satellite Longitude (°W)							
	106.0	90.0	130.0	171.0	9.0			41.0
Elevation Angle (deg)	27.8	35.1	12.8	15.3	11.2	10.0	9.3	30.7
Atmospheric Loss (dB)	0.56	0.45	1.17	0.99	1.34	1.50	1.66	0.51
Clear Sky Noise Temperature (K)	35.0	29.0	70.0	60.0	78.0	86.0	93.0	33.0
Clear Sky System Noise Temperature (K)	164.0	158.0	199.0	189.0	207.0	215.0	222.0	162.0
Rain Loss (dB)								
99.8% Availability	2.1	1.5	4.8	4.1	5.6	6.2	6.8	1.8
99.5% Availability	0.9	0.7	2.5	2.0	2.9	3.3	3.8	0.8
Rainy Sky Noise Temperature (K)								
99.8% Availability	111.0	85.0	194.0	177.0	210.0	220.0	229.0	98.0
99.5% Availability	54.0	43.0	127.0	107.0	141.0	154.0	169.0	49.0
Rainy System Noise Temperature (K)								
99.8% Availability	240.0	214.0	323.0	306.0	339.0	349.0	358.0	227.0
99.5% Availability	183.0	172.0	256.0	236.0	270.0	283.0	298.0	178.0
Sky Noise Degradation (dB) Due to Rain								
99.8% Availability	1.65	1.31	2.11	2.10	2.14	2.11	2.07	1.49
99.5% Availability	0.47	0.37	1.10	0.97	1.16	1.20	1.27	0.42
Total Rain Degradation (dB)								
99.8% Availability	3.75	2.81	6.91	6.20	7.74	8.31	8.87	3.29
99.5% Availability	1.37	1.07	3.60	2.97	4.06	4.50	5.07	1.22

Assumed Horizontal Polarization on Downlink Includes both Rain Loss and Degradation Because of Increased Sky Noise Temperature.

Table 2.6-2. Degradation in Downlink (20 GHz) Because of Rain (Continued)

Ground Station: JPL
Note: Altitude 0.0 km

	Satellite Longitude (°W)					
	106.0	90.0	130.0	171.0		
Elevation Angle (deg)	44.3	40.2	48.6	22.2	10.0	9.0
Atmospheric Loss (dB)	0.38	0.43	0.37	0.74	1.61	1.79
Clear Sky Noise Temperature (K)	24.0	28.0	24.0	46.0	91.0	99.0
Clear Sky System Noise Temperature (K)	153.0	157.0	153.0	175.0	220.0	228.0
Rain Loss (dB)						
99.8% Availability	1.9	2.3	1.8	4.5	9.9	10.6
99.5% Availability	0.8	1.0	0.8	2.2	5.9	6.6
Rainy Sky Noise Temperature (K)						
99.8% Availability	103.0	119.0	98.0	187.0	260.0	265.0
99.5% Availability	49.0	60.0	49.0	115.0	215.0	227.0
Rainy System Noise Temperature (K)						
99.8% Availability	232.0	248.0	227.0	316.0	389.0	394.0
99.5% Availability	178.0	189.0	178.0	244.0	344.0	356.0
Sky Noise Degradation (dB) Due to Rain						
99.8% Availability	1.79	1.99	1.71	5.56	2.48	2.37
99.5% Availability	0.64	0.80	0.65	1.45	1.94	1.92
Total Rain Degradation (dB)						
99.8% Availability	3.69	4.29	3.51	7.06	12.38	12.97
99.5% Availability	1.44	1.80	1.45	3.65	7.84	8.52

Assumed Horizontal Polarization on Downlink Includes both Rain Loss and Degradation Because of Increased Sky Noise Temperature.

Table 2.6-2. Degradation in Downlink (20 GHz) Because of Rain (Continued)

Ground Station: Goddard

Note: Altitude 0.0 km

	Satellite Longitude (°W)							
	106.0	90.0	130.0	28.0	15.0	9.0		41.0
Elevation Angle (deg)	35.7	42.8	19.6	22.8	13.1	8.5	10.0	31.7
Atmospheric Loss (dB)	0.48	0.41	0.83	0.72	1.24	1.89	1.61	0.53
Clear Sky Noise Temperature (K)	31.0	27.0	51.0	45.0	73.0	104.0	91.0	34.0
Clear Sky System Noise Temperature (K)	160.0	158.0	180.0	174.0	202.0	233.0	220.0	163.0
Rain Loss (dB)								
99.8% Availability	6.2	5.2	10.5	9.3	14.5	19.5	17.5	6.9
99.5% Availability	3.2	2.6	5.9	5.1	8.6	12.5	10.8	3.6
Rainy Sky Noise Temperature (K)								
99.8% Availability	220.0	202.0	264.0	256.0	280.0	287.0	285.0	231.0
99.5% Availability	151.0	131.0	215.0	200.0	250.0	274.0	266.0	163.0
Rainy System Noise Temperature (K)								
99.8% Availability	349.0	331.0	393.0	385.0	409.0	416.0	414.0	360.0
99.5% Availability	280.0	260.0	344.0	329.0	379.0	403.0	395.0	292.0
Sky Noise Degradation (dB) Due to Rain								
99.8% Availability	3.40	3.28	3.38	3.45	3.07	2.52	2.74	3.44
99.5% Availability	2.44	2.22	2.81	2.77	2.74	2.38	2.54	2.54
Total Rain Degradation (dB)								
99.8% Availability	9.60	8.48	13.88	12.75	17.57	22.02	20.24	10.34
99.5% Availability	5.64	4.82	8.71	7.87	11.34	14.88	13.34	6.14

Assumed Horizontal Polarization on Downlink Includes both Rain Loss and Degradation Because of Increased Sky Noise Temperature.

Table 2.6-2. Degradation in Downlink (20 GHz) Because of Rain (Continued)

Ground Station: Johnson

Note: Altitude 0.0 km

	Satellite Longitude (°W)						
	106.0	90.0	130.0	28.0			41.0
Elevation Angle (deg)	53.5	55.1	38.8	11.3	10.0	90.0	22.7
Atmospheric Loss (dB)	0.35	0.34	0.45	1.43	1.61	1.79	0.73
Clear Sky Noise Temperature (K)	23.0	22.0	29.0	82.0	91.0	99.0	45.0
Clear Sky System Noise Temperature (K)	152.0	151.0	158.0	211.0	220.0	228.0	174.0
Rain Loss (dB)							
99.8% Availability	11.8	11.6	15.1	32.3	34.0	35.6	22.0
99.5% Availability	5.8	5.7	7.9	20.1	21.5	22.5	12.3
Rainy Sky Noise Temperature (K)							
99.8% Availability	271.0	270.0	281.0	290.0	290.0	290.0	288.0
99.5% Availability	214.0	212.0	243.0	287.0	288.0	288.0	273.0
Rainy System Noise Temperature (K)							
99.8% Availability	400.0	399.0	410.0	419.0	419.0	419.0	417.0
99.5% Availability	343.0	341.0	372.0	416.0	417.0	417.0	402.0
Sky Noise Degradation (dB) Due to Rain							
99.8% Availability	4.21	4.21	4.15	2.97	2.79	2.64	3.79
99.5% Availability	3.54	3.53	3.73	2.94	2.77	2.62	3.63
Total Rain Degradation (dB)							
99.8% Availability	16.01	15.81	19.25	35.27	36.79	38.24	25.79
99.5% Availability	9.34	9.23	11.63	23.04	24.27	25.12	15.93

Assumed Horizontal Polarization on Downlink Includes both Rain Loss and Degradation Because of Increased Sky Noise Temperature.

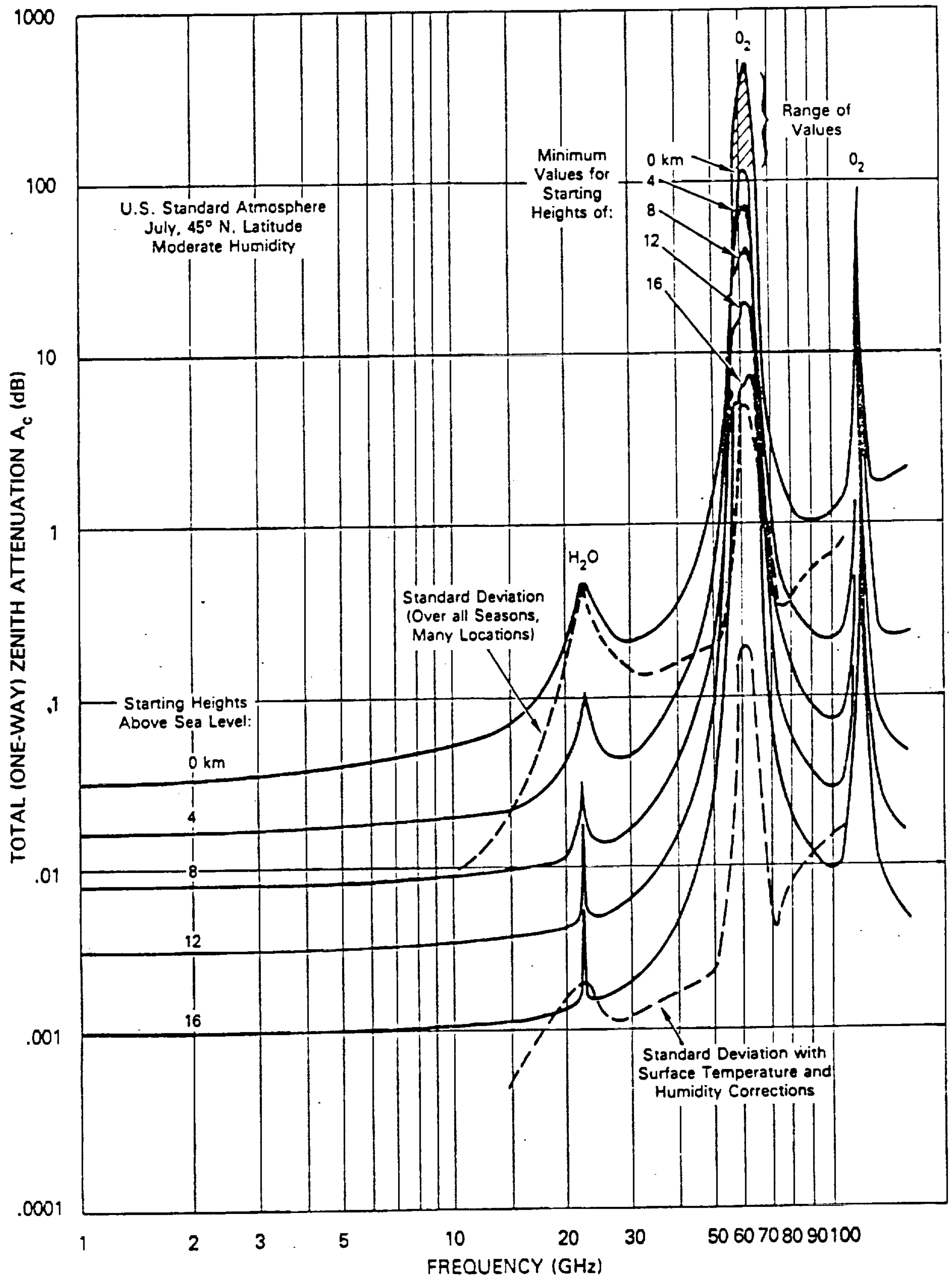

Figure 2.6-1. Total Zenith Attenuation Versus Frequency

Table 2.6-3 provides similar link degradations for the downlinks at 20 GHz, assuming the use of vertical linear polarization. Tables 2.6-4 and 2.6-5 provide the total link degradations at Ku-band, assuming use of horizontal and vertical polarizations respectively.

2.6.1 ATDRS Location Sensitivity: Configuration 2

2.6.1.1 Introduction. Stanford Telecommunications, Inc. (STI) has suggested an alternate location for the ATDRS-East for Configuration 2, namely at either 9° W or 15° W rather than 28° W as stated in the original SOW. In this subsection, we discuss the differences between these two locations in terms of the communication performance to CONUS and to the European ground stations. Comments on the Japanese ground site (as viewed from an ATDRS at 171° are included).

2.6.1.2 Communication Sensitivity to ATDRS-East Location

2.6.1.2.1 Communication to CONUS Sites. Of those CONUS ground stations selected for inclusion in this study, both Goddard and Andover are visible from 15° W but only Andover can be seen from 9° W (the elevation angle from Goddard Space Flight Center (GSFC) to a satellite located at 9° W is only 8.5°). Figures 2.6-2 and 2.6-3 are coverage maps depicting ground visibility from spacecraft located at 15° W and 9° W, respectively.

Rain loss values for CONUS locations as viewed from these two ATDRS positions are presented elsewhere in this report. Summarizing the differences in sensitivity of Andover to these two ATDRS locations, the rain loss increase is as much as 1.5 dB at 20 GHz and more than 3 dB at 30 GHz.

2.6.1.2.2 Communication to European Sites. Because atmospheric and rain attenuation are highly dependent on elevation angle, the change in sensitivity of any ground site to a change in satellite location is a function of elevation angle differences. Figures 2.6-2 and 2.6-3 each show five concentric circles, depicting elevation angle radii of 50, 40, 30, 20, and 10°. All European stations, of course, have better visibility (i.e., higher elevation angles) if the ATDRS is located at 9° W, but even ground sites in extreme southern Scandinavia have elevation angles in excess of 20° if the ATDRS is situated at either location.

Table 2.6-3. Degradation in Downlink (20 GHz) Because of Rain

Ground Station: White Sands

Note: Altitude 1.36 km

	Satellite Longitude (°W)						
	106.0	90.0	130.0	171.0			41.0
Elevation Angle (deg)	52.3	48.3	44.6	12.8	10.0	9.0	12.0
Atmospheric Loss (dB)	0.18	0.19	0.20	0.36	0.81	0.89	0.67
Clear Sky Noise Temperature (K)	12.0	12.0	13.0	40.0	50.0	55.0	42.0
Clear Sky System Noise Temperature (K)	141.0	141.0	142.0	169.0	179.0	184.0	171.0
Rain Loss (dB)							
99.8% Availability	1.0	1.1	1.2	5.3	6.8	7.6	5.6
99.5% Availability	0.4	0.4	0.5	2.6	3.5	3.9	2.8
Rainy Sky Noise Temperature (K)							
99.8% Availability	60.0	60.0	70.0	189.0	217.0	228.0	198.0
99.5% Availability	26.0	26.0	32.0	119.0	148.0	160.0	127.0
Rainy System Noise Temperature (K)							
99.8% Availability	189.0	189.0	199.0	318.0	346.0	357.0	327.0
99.5% Availability	155.0	155.0	161.0	248.0	277.0	289.0	256.0
Sky Noise Degradation (dB) Due to Rain							
99.8% Availability	1.27	1.25	1.46	2.76	2.87	2.88	2.81
99.5% Availability	0.41	0.38	0.53	1.67	1.90	1.97	1.75
Total Rain Degradation (dB)							
99.8% Availability	2.27	2.25	2.66	7.36	8.87	9.58	7.81
99.5% Availability	0.81	0.78	1.03	3.97	5.00	5.47	4.25

Assumed Vertical Polarization on Downlink Includes both Rain Loss and Degradation Because of Increased Sky Noise Temperature.

Table 2.6-3. Degradation in Downlink (20 GHz) Because of Rain (Continued)

Ground Station: Sunnyvale
Note: Altitude 0.0 km

	Satellite Longitude (°W)					
	106.0	90.0	130.0	171.0		
Elevation Angle (deg)	43.5	35.3	45.9	23.5	10.0	9.0
Atmospheric Loss (dB)	0.41	0.48	0.39	0.70	1.61	1.79
Clear Sky Noise Temperature (K)	26.0	31.0	25.0	44.0	91.0	99.0
Clear Sky System Noise Temperature (K)	155.0	160.0	154.0	173.0	220.0	228.0
Rain Loss (dB)						
99.8% Availability	2.6	3.3	2.5	4.8	10.3	11.2
99.5% Availability	1.4	1.8	1.3	2.8	6.7	7.5
Rainy Sky Noise Temperature (K)						
99.8% Availability	131.0	155.0	127.0	194.0	263.0	268.0
99.5% Availability	80.0	98.0	75.0	138.0	228.0	238.0
Rainy System Noise Temperature (K)						
99.8% Availability	260.0	284.0	256.0	323.0	392.0	397.0
99.5% Availability	209.0	227.0	204.0	267.0	357.0	267.0
Sky Noise Degradation (dB) Due to Rain						
99.8% Availability	2.23	2.49	2.20	2.71	2.50	2.40
99.5% Availability	1.29	1.53	1.21	1.88	2.10	2.07
Total Rain Degradation (dB)						
99.8% Availability	4.83	5.81	4.70	7.51	12.80	13.60
99.5% Availability	2.69	3.33	2.51	4.68	8.80	9.57

Assumed Vertical Polarization on Downlink Includes both Rain Loss and Degradation Because of Increased Sky Noise Temperature.

Table 2.6-3. Degradation in Downlink (20 GHz) Because of Rain (Continued)

Ground Station: Denver

Note: Altitude 1.8 km

	Satellite Longitude (°W)						
	106.0	90.0	130.0	171.0			41.0
Elevation Angle (deg)	44.2	41.7	37.3	9.6	10.0	9.0	11.3
Atmospheric Loss (dB)	0.19	0.20	0.21	0.78	0.75	0.83	0.66
Clear Sky Noise Temperature (K)	12.0	13.0	14.0	48.0	47.0	51.0	42.0
Clear Sky System Noise Temperature (K)	141.0	142.0	143.0	177.0	176.0	180.0	171.0
Rain Loss (dB)							
99.8% Availability	1.1	1.1	1.3	5.7	5.3	5.7	4.7
99.5% Availability	0.4	0.5	0.5	3.0	2.5	3.5	2.1
Rainy Sky Noise Temperature (K)							
99.8% Availability	65.0	65.0	75.0	212.0	204.0	212.0	192.0
99.5% Availability	26.0	32.0	32.0	145.0	127.0	160.0	111.0
Rainy System Noise Temperature (K)							
99.8% Availability	194.0	194.0	204.0	341.0	333.0	341.0	321.0
99.5% Availability	155.0	161.0	161.0	274.0	256.0	289.0	240.0
Sky Noise Degradation (dB) Due to Rain							
99.8% Availability	1.37	1.35	1.54	2.84	2.79	2.77	2.74
99.5% Availability	0.39	0.53	0.50	1.88	1.64	2.06	1.48
Total Rain Degradation (dB)							
99.8% Availability	2.47	2.45	2.84	8.54	8.09	8.47	7.44
99.5% Availability	0.79	1.03	1.00	4.88	4.14	5.56	3.58

Assumed Vertical Polarization on Downlink Includes both Rain Loss and Degradation Because of Increased Sky Noise Temperature.

Table 2.6-3. Degradation in Downlink (20 GHz) Because of Rain (Continued)

Ground Station: Marshall
Note: Altitude 0.23 km

	Satellite Longitude (°W)					
	106.0	90.0	130.0			41.0
Elevation Angle (deg)	44.8	49.6	29.3	10.0	9.0	27.3
Atmospheric Loss (dB)	0.37	0.34	0.53	1.50	1.66	0.57
Clear Sky Noise Temperature (K)	24.0	22.0	34.0	86.0	93.0	36.0
Clear Sky System Noise Temperature (K)	153.0	151.0	163.0	215.0	222.0	165.0
Rain Loss (dB)						
99.8% Availability	10.4	9.7	13.9	26.6	27.8	14.6
99.5% Availability	5.1	4.7	7.3	16.3	17.3	7.7
Rainy Sky Noise Temperature (K)						
99.8% Availability	264.0	259.0	278.0	289.0	290.0	280.0
99.5% Availability	200.0	192.0	236.0	283.0	285.0	241.0
Rainy System Noise Temperature (K)						
99.8% Availability	393.0	388.0	407.0	418.0	419.0	409.0
99.5% Availability	329.0	321.0	365.0	412.0	414.0	370.0
Sky Noise Degradation (dB) Due to Rain						
99.8% Availability	4.09	4.09	3.98	2.90	2.74	3.94
99.5% Availability	3.33	3.27	3.50	2.83	2.69	3.50
Total Rain Degradation (dB)						
99.8% Availability	14.49	13.79	17.88	29.50	30.54	18.54
99.5% Availability	8.43	7.97	10.80	19.13	19.99	11.20

Assumed Vertical Polarization on Downlink Includes both Rain Loss and Degradation Because of Increased Sky Noise Temperature.

Table 2.6-3. Degradation in Downlink (20 GHz) Because of Rain (Continued)

Ground Station: Andover

Note: Altitude 0.21 km

	Satellite Longitude (°W)							
	106.0	90.0	130.0	171.0	9.0			41.0
Elevation Angle (deg)	27.8	35.1	12.8	15.3	11.2	10.0	9.0	30.7
Atmospheric Loss (dB)	0.56	0.45	1.17	0.99	1.34	1.50	1.66	0.51
Clear Sky Noise Temperature (K)	35.0	29.0	70.0	60.0	78.0	86.0	93.0	33.0
Clear Sky System Noise Temperature (K)	164.0	158.0	199.0	189.0	207.0	215.0	222.0	162.0
Rain Loss (dB)								
99.8% Availability	1.9	1.4	4.3	3.6	4.9	5.5	6.0	1.7
99.5% Availability	0.8	0.6	2.2	1.8	2.6	3.0	3.4	0.7
Rainy Sky Noise Temperature (K)								
99.8% Availability	103.0	80.0	182.0	163.0	196.0	208.0	217.0	94.0
99.5% Availability	49.0	37.0	115.0	98.0	131.0	145.0	157.0	43.0
Rainy System Noise Temperature (K)								
99.8% Availability	232.0	209.0	311.0	392.0	325.0	337.0	346.0	223.0
99.5% Availability	178.0	166.0	244.0	227.0	260.0	274.0	286.0	172.0
Sky Noise Degradation (dB) Due to Rain								
99.8% Availability	1.49	1.21	1.95	1.90	1.96	1.96	1.92	1.40
99.5% Availability	0.34	0.22	0.90	0.81	0.98	1.05	1.10	0.28
Total Rain Degradation (dB)								
99.8% Availability	3.39	2.61	6.25	5.50	6.86	7.46	7.92	3.10
99.5% Availability	1.14	0.82	3.10	2.61	3.58	4.05	4.50	0.98

Assumed Vertical Polarization on Downlink Includes both Rain Loss and Degradation Because of Increased Sky Noise Temperature.

Table 2.6-3. Degradation in Downlink (20 GHz) Because of Rain (Continued)

Ground Station: JPL

Note: Altitude 0.0 km

	Satellite Longitude (°W)					
	106.0	90.0	130.0	171.0		
Elevation Angle (deg)	48.3	40.2	48.6	22.2	10.0	9.0
Atmospheric Loss (dB)	0.38	0.43	0.37	0.74	1.61	1.79
Clear Sky Noise Temperature (K)	24.0	28.0	24.0	46.0	91.0	99.0
Clear Sky System Noise Temperature (K)	153.0	157.0	153.0	175.0	220.0	228.0
Rain Loss (dB)						
99.8% Availability	1.8	2.2	1.7	4.0	8.7	9.3
99.5% Availability	0.7	1.0	0.7	2.0	5.2	5.9
Rainy Sky Noise Temperature (K)						
99.8% Availability	98.0	115.0	94.0	175.0	251.0	256.0
99.5% Availability	43.0	60.0	43.0	107.0	202.0	215.0
Rainy System Noise Temperature (K)						
99.8% Availability	227.0	244.0	223.0	304.0	380.0	385.0
99.5% Availability	172.0	189.0	172.0	236.0	331.0	344.0
Sky Noise Degradation (dB)						
Due to Rain						
99.8% Availability	1.71	1.92	1.63	2.39	2.37	2.27
99.5% Availability	0.50	0.80	0.51	1.30	1.78	1.79
Total Rain Degradation (dB)						
99.8% Availability	3.51	4.12	3.33	6.39	11.07	11.57
99.5% Availability	1.20	1.80	1.21	3.30	6.98	7.69

Assumed Vertical Polarization on Downlink Includes both Rain Loss and Degradation Because of Increased Sky Noise Temperature.

Table 2.6-3. Degradation in Downlink (20 GHz) Because of Rain (Continued)

Ground Station: Goddard

Note: Altitude 0.0 km

	Satellite Longitude (°W)							
	106.0	90.0	130.0	28.0	15.0	9.0		41.0
Elevation Angle (deg)	35.7	42.8	19.6	22.8	13.1	8.5	10.0	31.7
Atmospheric Loss (dB)	0.48	0.41	0.83	0.72	1.24	1.89	1.61	0.53
Clear Sky Noise Temperature (K)	31.0	27.0	51.0	45.0	73.0	104.0	91.0	34.0
Clear Sky System Noise Temperature (K)	160.0	156.0	180.0	174.0	202.0	233.0	220.0	163.0
Rain Loss (dB)								
99.8% Availability	6.2	4.7	9.2	8.1	12.5	16.8	15.1	6.2
99.5% Availability	2.9	2.4	5.2	4.5	7.5	10.8	9.4	3.3
Rainy Sky Noise Temperature (K)								
99.8% Availability	210.0	192.0	255.0	245.0	274.0	284.0	281.0	220.0
99.5% Availability	141.0	123.0	202.0	187.0	238.0	266.0	266.0	257.0
Rainy System Noise Temperature (K)								
99.8% Availability	339.0	331.0	393.0	385.0	409.0	416.0	414.0	360.0
99.5% Availability	280.0	252.0	331.0	316.0	367.0	395.0	386.0	283.0
Sky Noise Degradation (dB)								
Due to Rain								
99.8% Availability	3.27	3.14	3.28	3.32	3.00	2.49	2.70	3.31
99.5% Availability	2.28	2.10	2.64	2.59	2.60	2.29	2.43	2.40
Total Rain Degradation (dB)								
99.8% Availability	8.87	7.84	12.48	11.42	15.50	19.29	17.80	9.51
99.5% Availability	5.18	4.50	7.84	7.09	10.10	13.09	11.83	5.70

Assumed Vertical Polarization on Downlink Includes both Rain Loss and Degradation Because of Increased Sky Noise Temperature.

Table 2.6-3. Degradation in Downlink (20 GHz) Because of Rain (Continued)

Ground Station: Johnson

Note: Altitude 0.0 km

	Satellite Longitude (°W)						
	106.0	90.0	130.0	28.0			41.0
Elevation Angle (deg)	53.5	55.1	38.8	11.3	10.0	9.0	22.7
Atmospheric Loss (dB)	0.35	0.34	0.45	1.43	1.61	1.79	0.73
Clear Sky Noise Temperature (K)	23.0	22.0	29.0	82.0	91.0	99.0	45.0
Clear Sky System Noise Temperature (K)	152.0	151.0	158.0	211.0	220.0	228.0	174.0
Rain Loss (dB)							
99.8% Availability	11.1	10.9	13.5	27.5	28.9	30.2	19.0
99.5% Availability	5.5	5.4	7.1	17.3	18.5	19.3	10.7
Rainy Sky Noise Temperature (K)							
99.8% Availability	267.0	266.0	277.0	289.0	290.0	290.0	286.0
99.5% Availability	208.0	206.0	233.0	285.0	286.0	287.0	265.0
Rainy System Noise Temperature (K)							
99.8% Availability	396.0	395.0	406.0	418.0	419.0	419.0	415.0
99.5% Availability	337.0	335.0	362.0	414.0	415.0	416.0	394.0
Sky Noise Degradation (dB)							
Due to Rain							
99.8% Availability	4.17	4.17	4.11	2.97	2.79	2.63	3.77
99.5% Availability	3.47	3.46	3.61	2.91	2.75	2.60	3.55
Total Rain Degradation (dB)							
99.8% Availability	15.27	15.07	17.61	30.47	31.69	32.83	22.77
99.5% Availability	8.97	8.86	10.71	20.21	21.25	21.90	14.25

Assumed Vertical Polarization on Downlink Includes both Rain Loss and Degradation Because of Increased Sky Noise Temperature.

Table 2.6-4. Degradation in Downlink (13.7 GHz) Because of Rain

Ground Station: White Sands

Note: Altitude 1.36 km

	Satellite Longitude (°W)						
	106.0	90.0	130.0	171.0			41.0
Elevation Angle (deg)	52.3	48.3	44.6	12.8	10.0	9.0	12.0
Atmospheric Loss (dB)	0.06	0.06	0.07	0.21	0.26	0.29	0.22
Clear Sky Noise Temperature (K)	4.0	4.0	4.0	14.0	17.0	19.0	15.0
Clear Sky System Noise Temperature (K)	133.0	133.0	133.0	143.0	146.0	148.0	144.0
Rain Loss (dB)							
99.8% Availability	0.4	0.5	0.5	2.3	2.9	3.3	2.4
99.5% Availability	0.2	0.2	0.2	1.1	1.5	1.6	1.2
Rainy Sky Noise Temperature (K)							
99.8% Availability	26.0	32.0	32.0	119.0	141.0	154.0	123.0
99.5% Availability	13.0	13.0	13.0	65.0	85.0	89.0	70.0
Rainy System Noise Temperature (K)							
99.8% Availability	155.0	161.0	161.0	248.0	270.0	283.0	252.0
99.5% Availability	142.0	142.0	142.0	194.0	214.0	218.0	199.0
Sky Noise Degradation (dB) Due to Rain							
99.8% Availability	0.65	0.81	0.80	2.40	2.66	2.81	2.44
99.5% Availability	0.29	0.28	0.27	1.33	1.64	1.68	1.42
Total Rain Degradation (dB)							
99.8% Availability	1.05	1.31	1.30	4.70	5.56	6.11	4.84
99.5% Availability	0.49	0.48	0.47	2.43	3.14	3.28	2.62

Assumed Horizontal Polarization on Downlink Includes both Rain Loss and Degradation Because of Increased Sky Noise Temperature.

Table 2.6-4. Degradation in Downlink (13.7 GHz) Because of Rain (Continued)

Ground Station: Sunnyvale

Note: Altitude 0.0 km

	Satellite Longitude (°W)					
	106.0	90.0	130.0	171.0		
Elevation Angle (deg)	43.5	35.3	45.9	23.5	10.0	9.0
Atmospheric Loss (dB)	0.11	0.13	0.11	0.19	0.44	0.49
Clear Sky Noise Temperature (K)	7.0	9.0	7.0	13.0	28.0	31.0
Clear Sky System Noise Temperature (K)	136.0	138.0	136.0	142.0	157.0	160.0
Rain Loss (dB)						
99.8% Availability	1.2	1.6	1.2	2.4	5.1	5.6
99.5% Availability	0.6	0.8	0.6	1.3	3.2	3.6
Rainy Sky Noise Temperature (K)						
99.8% Availability	70.0	89.0	70.0	123.0	200.0	210.0
99.5% Availability	37.0	49.0	37.0	75.0	151.0	163.0
Rainy System Noise Temperature (K)						
99.8% Availability	199.0	218.0	199.0	252.0	329.0	339.0
99.5% Availability	166.0	178.0	166.0	204.0	280.0	292.0
Sky Noise Degradation (dB) Due to Rain						
99.8% Availability	1.64	2.00	1.65	2.50	3.21	3.26
99.5% Availability	0.86	1.11	0.87	1.59	2.51	2.62
Total Rain Degradation (dB)						
99.8% Availability	2.84	3.60	2.85	4.90	8.31	8.86
99.5% Availability	1.46	1.91	1.47	2.89	5.71	6.22

Assumed Horizontal Polarization on Downlink Includes both Rain Loss and Degradation Because of Increased Sky Noise Temperature.

Table 2.6-4. Degradation in Downlink (13.7 GHz) Because of Rain (Continued)

Ground Station: Denver

Note: Altitude 1.8 km

	Satellite Longitude (°W)						
	106.0	90.0	130.0	171.0			41.0
Elevation Angle (deg)	44.2	41.7	37.3	9.6	10.0	9.0	11.3
Atmospheric Loss (dB)	0.06	0.06	0.07	0.26	0.25	0.27	0.22
Clear Sky Noise Temperature (K)	4.0	4.0	5.0	17.0	16.0	18.0	14.0
Clear Sky System Noise Temperature (K)	133.0	133.0	134.0	146.0	145.0	147.0	143.0
Rain Loss (dB)							
99.8% Availability	0.5	0.5	0.6	2.9	2.7	2.9	2.4
99.5% Availability	0.2	0.2	0.2	1.5	1.2	1.7	1.0
Rainy Sky Noise Temperature (K)							
99.8% Availability	32.0	32.0	37.0	141.0	134.0	141.0	123.0
99.5% Availability	13.0	13.0	13.0	85.0	70.0	94.0	60.0
Rainy System Noise Temperature (K)							
99.8% Availability	161.0	161.0	166.0	270.0	263.0	270.0	252.0
99.5% Availability	142.0	142.0	142.0	214.0	199.0	223.0	189.0
Sky Noise Degradation (dB) Due to Rain							
99.8% Availability	0.81	0.81	0.95	2.68	2.58	2.64	2.45
99.5% Availability	0.23	0.27	0.26	1.66	1.37	1.81	1.19
Total Rain Degradation (dB)							
99.8% Availability	1.31	1.31	1.55	5.58	5.28	5.54	4.85
99.5% Availability	0.48	0.47	0.46	3.16	2.57	3.51	2.19

Assumed Horizontal Polarization on Downlink Includes both Rain Loss and Degradation Because of Increased Sky Noise Temperature.

Table 2.6-4. Degradation in Downlink (13.7 GHz) Because of Rain (Continued)

Ground Station: Marshall

Note: Altitude 0.23 km

	Satellite Longitude (°W)					
	106.0	90.0	130.0			41.0
Elevation Angle (deg)	44.8	49.6	29.3	10.0	9.0	27.3
Atmospheric Loss (dB)	0.10	0.09	0.15	0.41	0.45	0.15
Clear Sky Noise Temperature (K)	7.0	6.0	10.0	26.0	29.0	10.0
Clear Sky System Noise Temperature (K)	136.0	135.0	139.0	155.0	158.0	139.0
Rain Loss (dB)						
99.8% Availability	5.5	5.1	7.6	14.6	15.2	8.2
99.5% Availability	2.6	2.3	3.8	8.6	9.1	4.0
Rainy Sky Noise Temperature (K)						
99.8% Availability	208.0	200.0	240.0	280.0	281.0	244.0
99.5% Availability	131.0	119.0	169.0	250.0	254.0	175.0
Rainy System Noise Temperature (K)						
99.8% Availability	337.0	329.0	369.0	409.0	410.0	373.0
99.5% Availability	260.0	248.0	298.0	379.0	383.0	304.0
Sky Noise Degradation (dB) Due to Rain						
99.8% Availability	3.95	3.87	4.25	4.20	4.14	4.28
99.5% Availability	2.82	2.64	3.32	3.87	3.84	3.38
Total Rain Degradation (dB)						
99.8% Availability	9.45	8.97	11.85	18.80	19.34	12.28
99.5% Availability	5.42	4.94	7.12	12.47	12.94	7.38

Assumed Horizontal Polarization on Downlink Includes both Rain Loss and Degradation Because of Increased Sky Noise Temperature.

Table 2.6-4. Degradation in Downlink (13.7 GHz) Because of Rain (Continued)

Ground Station: Andover

Note: Altitude 0.21 km

Satellite Longitude (°W)

	106.0	90.0	130.0	15.0	9.0			41.0
Elevation Angle (deg)	27.8	35.1	12.8	15.3	11.2	10.0	9.0	30.7
Atmospheric Loss (dB)	0.15	0.12	0.32	0.27	0.37	0.41	0.45	0.14
Clear Sky Noise Temperature (K)	10.0	8.0	21.0	18.0	24.0	26.0	29.0	9.0
Clear Sky System Noise Temperature (K)	139.0	137.0	150.0	147.0	153.0	155.0	158.0	138.0
Rain Loss (dB)								
99.8% Availability	0.9	0.7	2.1	1.7	2.4	2.7	2.9	0.8
99.5% Availability	0.4	0.3	1.0	0.8	1.2	1.4	1.6	0.3
Rainy Sky Noise Temperature (K)								
99.8% Availability	54.0	43.0	111.0	94.0	123.0	134.0	141.0	49.0
99.5% Availability	54.0	43.0	127.0	107.0	141.0	154.0	169.0	49.0
Rainy System Noise Temperature (K)								
99.8% Availability	183.0	172.0	240.0	223.0	252.0	263.0	270.0	178.0
99.5% Availability	155.0	148.0	189.0	178.0	199.0	209.0	218.0	148.0
Sky Noise Degradation (dB) Due to Rain								
99.8% Availability	1.20	1.68	2.05	1.82	2.18	2.29	2.33	1.09
99.5% Availability	0.46	0.34	1.00	0.84	1.15	1.28	1.40	0.31
Total Rain Degradation (dB)								
99.8% Availability	2.10	1.68	4.15	3.52	4.58	4.99	5.23	1.89
99.5% Availability	0.86	0.64	2.00	1.64	2.35	2.68	3.00	0.61

Assumed Horizontal Polarization on Downlink Includes both Rain Loss and Degradation Because of Increased Sky Noise Temperature.

Table 2.6-4. Degradation in Downlink (13.7 GHz) Because of Rain (Continued)

Ground Station: JPL

Note: Altitude 0.0 km

	Satellite Longitude (°W)					
	106.0	90.0	130.0	171.0		
Elevation Angle (deg)	48.3	20.2	48.6	22.2	10.0	9.0
Atmospheric Loss (dB)	0.10	0.12	0.10	0.20	0.44	0.49
Clear Sky Noise Temperature (K)	7.0	8.0	7.0	13.0	28.0	31.0
Clear Sky System Noise Temperature (K)	136.0	137.0	136.0	142.0	157.0	160.0
Rain Loss (dB)						
99.8% Availability	0.8	1.0	0.8	1.9	4.2	4.5
99.5% Availability	0.3	0.4	0.3	0.9	2.4	2.7
Rainy Sky Noise Temperature (K)						
99.8% Availability	49.0	60.0	49.0	103.0	108.0	187.0
99.5% Availability	19.0	26.0	19.0	54.0	123.0	134.0
Rainy System Noise Temperature (K)						
99.8% Availability	178.0	189.0	178.0	232.0	309.0	316.0
99.5% Availability	148.0	155.0	148.0	183.0	252.0	263.0
Sky Noise Degradation (dB) Due to Rain						
99.8% Availability	1.17	1.39	1.17	2.12	2.93	2.95
99.5% Availability	0.38	0.53	0.38	1.10	2.05	2.16
Total Rain Degradation (dB)						
99.8% Availability	1.97	2.39	1.97	4.02	7.13	7.45
99.5% Availability	0.68	.093	.068	2.00	4.45	4.86

Assumed Horizontal Polarization on Downlink Includes both Rain Loss and Degradation Because of Increased Sky Noise Temperature.

Table 2.6-4. Degradation in Downlink (13.7 GHz) Because of Rain (Continued)

Ground Station: Goddard

Note: Altitude 0.0 km

	Satellite Longitude (°W)							
	106.0	90.0	130.0	28.0	15.0	9.0		41.0
Elevation Angle (deg)	35.7	42.8	19.6	22.8	13.1	8.5	10.0	31.7
Atmospheric Loss (dB)	0.13	0.11	0.23	0.20	0.34	0.51	0.44	0.14
Clear Sky Noise Temperature (K)	9.0	7.0	15.0	13.0	22.0	33.0	28.0	10.0
Clear Sky System Noise Temperature (K)	138.0	136.0	144.0	142.0	151.0	162.0	157.0	139.0
Rain Loss (dB)								
99.8% Availability	2.8	2.4	4.8	4.2	6.6	8.7	7.9	3.2
99.5% Availability	3.2	2.6	5.9	5.1	8.6	12.5	10.8	3.6
Rainy Sky Noise Temperature (K)								
99.8% Availability	138.0	123.0	194.0	180.0	227.0	251.0	243.0	151.0
99.5% Availability	8.0	65.0	131.0	115.0	169.0	206.0	192.0	89.0
Rainy System Noise Temperature (K)								
99.8% Availability	267.0	252.0	323.0	309.0	356.0	380.0	372.0	280.0
99.5% Availability	209.0	194.0	260.0	244.0	298.0	335.0	321.0	218.0
Sky Noise Degradation (dB) Due to Rain								
99.8% Availability	2.87	2.67	3.51	3.37	3.72	3.71	3.74	3.06
99.5% Availability	1.81	1.52	2.56	2.36	2.96	3.16	3.10	1.97
Total Rain Degradation (dB)								
99.8% Availability	5.67	5.07	8.31	7.57	10.32	12.41	11.64	6.26
99.5% Availability	3.21	2.62	5.16	4.565	6.76	8.56	7.80	3.57

Assumed Horizontal Polarization on Downlink Includes both Rain Loss and Degradation Because of Increased Sky Noise Temperature.

Table 2.6-4. Degradation in Downlink (13.7 GHz) Because of Rain (Continued)

Ground Station: Johnson

Note: Altitude 0.0 km

	Satellite Longitude (°W)						
	106.0	90.0	130.0	28.0			41.0
Elevation Angle (deg)	53.5	55.1	38.8	11.3	10.0	90.0	22.7
Atmospheric Loss (dB)	0.09	0.09	0.12	0.39	0.44	0.49	0.20
Clear Sky Noise Temperature (K)	6.0	6.0	8.0	25.0	28.0	31.0	13.0
Clear Sky System Noise Temperature (K)	135.0	135.0	137.0	154.0	157.0	160.0	142.0
Rain Loss (dB)							
99.8% Availability	5.7	5.6	7.3	15.1	15.9	16.7	10.5
99.5% Availability	2.7	2.6	3.6	9.1	9.7	10.2	5.6
Rainy Sky Noise Temperature (K)							
99.8% Availability	212.0	210.0	236.0	281.0	283.0	284.0	264.0
99.5% Availability	134.0	131.0	163.0	254.0	259.0	262.0	210.0
Rainy System Noise Temperature (K)							
99.8% Availability	341.0	339.0	365.0	410.0	412.0	413.0	393.0
99.5% Availability	263.0	260.0	292.0	383.0	388.0	391.0	339.0
Sky Noise Degradation (dB) Due to Rain							
99.8% Availability	4.01	3.99	4.25	4.25	4.18	4.11	4.42
99.5% Availability	2.89	2.83	3.29	3.96	3.92	3.88	3.78
Total Rain Degradation (dB)							
99.8% Availability	9.71	9.59	11.55	19.35	20.08	20.81	14.92
99.5% Availability	5.59	5.43	6.89	13.06	13.62	14.08	9.38

Assumed Horizontal Polarization on Downlink Includes both Rain Loss and Degradation Because of Increased Sky Noise Temperature.

Table 2.6-5. Degradation in Downlink (13.7 GHz) Because of Rain

Ground Station: White Sands

Note: Altitude 1.36 km

	Satellite Longitude (°W)						
	106.0	90.0	130.0	171.0			41
Elevation Angle (deg)	52.3	48.3	44.6	12.8	10.0	9.0	12.0
Atmospheric Loss (dB)	0.06	0.06	0.07	0.21	0.26	0.29	0.22
Clear Sky Noise Temperature (K)	4.0	4.0	4.0	14.0	17.0	19.0	15.0
Clear Sky System Noise Temperature (K)	133.0	133.0	133.0	143.0	146.0	148.0	144.0
Rain Loss (dB)							
99.8% Availability	0.4	0.4	0.5	2.0	2.6	2.9	2.2
99.5% Availability	0.1	0.2	0.2	1.0	1.3	1.4	1.0
Rainy Sky Noise Temperature (K)							
99.8% Availability	26.0	26.0	32.0	107.0	131.0	141.0	115.0
99.5% Availability	7.0	13.0	13.0	60.0	75.0	80.0	60.0
Rainy System Noise Temperature (K)							
99.8% Availability	155.0	155.0	161.0	236.0	260.0	270.0	244.0
99.5% Availability	136.0	142.0	142.0	189.0	204.0	209.0	189.0
Sky Noise Degradation (dB) Due to Rain							
99.8% Availability	0.65	0.65	0.80	2.18	2.49	2.61	2.31
99.5% Availability	0.09	0.28	0.27	1.21	1.44	1.49	1.18
Total Rain Degradation (dB)							
99.8% Availability	1.05	1.05	1.30	4.18	5.09	5.51	4.51
99.5% Availability	0.19	0.48	0.47	2.21	2.74	2.89	2.18

Assumed Vertical Polarization on Downlink Includes both Rain Loss and Degradation Because of Increased Sky Noise Temperature.

Table 2.6-5. Degradation in Downlink (13.7 GHz) Because of Rain (Continued)

Ground Station: Sunnyvale
Note: Altitude 0.0 km

	Satellite Longitude (°W)					
	106.0	90.0	130.0	171.0		
Elevation Angle (deg)	43.5	35.3	45.9	23.5	10.0	9.0
Atmospheric Loss (dB)	0.11	0.13	0.11	0.19	0.44	0.49
Clear Sky Noise Temperature (K)	7.0	9.0	7.0	13.0	28.0	31.0
Clear Sky System Noise Temperature (K)	136.0	138.0	136.0	142.0	157.0	160.0
Rain Loss (dB)						
99.8% Availability	1.2	1.5	1.1	2.2	4.6	5.0
99.5% Availability	0.6	0.8	0.5	1.2	2.9	3.2
Rainy Sky Noise Temperature (K)						
99.8% Availability	70.0	85.0	65.0	115.0	189.0	198.0
99.5% Availability	37.0	49.0	32.0	70.0	141.0	151.0
Rainy System Noise Temperature (K)						
99.8% Availability	199.0	214.0	194.0	244.0	318.0	327.0
99.5% Availability	166.0	178.0	161.0	199.0	270.0	280.0
Sky Noise Degradation (dB) Due to Rain						
99.8% Availability	1.64	1.91	1.54	2.37	3.07	3.11
99.5% Availability	0.86	1.11	0.72	1.48	2.35	2.43
Total Rain Degradation (dB)						
99.8% Availability	2.84	3.41	2.64	4.57	7.67	8.11
99.5% Availability	1.46	1.91	1.22	2.68	5.25	5.63

Assumed Vertical Polarization on Downlink Includes both Rain Loss and Degradation Because of Increased Sky Noise Temperature.

Table 2.6-5. Degradation in Downlink (13.7 GHz) Because of Rain (Continued)

Ground Station: Denver

Note: Altitude 1.8 km

	Satellite Longitude (°W)						
	106.0	90.0	130.0	171.0			41.0
Elevation Angle (deg)	44.2	41.7	37.3	9.6	10.0	9.0	11.3
Atmospheric Loss (dB)	0.06	0.06	0.07	0.26	0.25	0.27	0.22
Clear Sky Noise Temperature (K)	4.0	4.0	5.0	17.0	16.0	18.0	14.0
Clear Sky System Noise Temperature (K)	133.0	133.0	134.0	146.0	145.0	147.0	143.0
Rain Loss (dB)							
99.8% Availability	0.5	0.5	0.6	2.6	2.4	2.6	2.1
99.5% Availability	0.2	0.2	0.2	1.3	1.1	1.5	0.9
Rainy Sky Noise Temperature (K)							
99.8% Availability	32.0	32.0	37.0	131.0	123.0	131.0	111.0
99.5% Availability	13.0	13.0	13.0	75.0	65.0	85.0	54.0
Rainy System Noise Temperature (K)							
99.8% Availability	161.0	161.0	166.0	260.0	252.0	260.0	240.0
99.5% Availability	142.0	142.0	142.0	204.0	194.0	214.0	183.0
Sky Noise Degradation (dB) Due to Rain							
99.8% Availability	0.81	0.81	0.95	2.50	2.39	2.47	2.24
99.5% Availability	0.39	0.53	0.50	1.88	1.64	2.06	1.48
Total Rain Degradation (dB)							
99.8% Availability	1.31	1.31	1.55	5.10	4.79	5.07	4.34
99.5% Availability	0.48	0.47	0.46	2.75	2.35	3.12	1.96

Assumed Vertical Polarization on Downlink Includes both Rain Loss and Degradation Because of Increased Sky Noise Temperature.

C-2

Table 2.6-5. Degradation in Downlink (13.7 GHz) Because of Rain (Continued)

Ground Station: Marshall

Note: Altitude 0.23 km

	Satellite Longitude (°W)					
	106.0	90.0	130.0			41.0
Elevation Angle (deg)	44.8	49.6	29.3	10.0	9.0	27.3
Atmospheric Loss (dB)	0.10	0.09	0.15	0.41	0.45	0.15
Clear Sky Noise Temperature (K)	7.0	6.0	10.0	26.0	29.0	10.0
Clear Sky System Noise Temperature (K)	136.0	135.0	139.0	155.0	158.0	139.0
Rain Loss (dB)						
99.8% Availability	5.1	4.8	6.8	12.8	13.3	7.2
99.5% Availability	2.4	2.2	3.4	7.6	8.0	3.6
Rainy Sky Noise Temperature (K)						
99.8% Availability	200.0	194.0	229.0	275.0	276.0	235.0
99.5% Availability	123.0	115.0	157.0	240.0	244.0	163.0
Rainy System Noise Temperature (K)						
99.8% Availability	329.0	323.0	358.0	404.0	405.0	364.0
99.5% Availability	329.0	321.0	365.0	412.0	414.0	370.0
Sky Noise Degradation (dB) Due to Rain						
99.8% Availability	3.85	3.78	4.12	4.15	4.09	4.17
99.5% Availability	2.69	2.57	3.15	3.75	3.73	3.22
Total Rain Degradation (dB)						
99.8% Availability	8.95	8.58	10.92	16.95	17.39	11.37
99.5% Availability	5.09	4.77	6.55	11.35	11.73	6.82

Assumed Vertical Polarization on Downlink Includes both Rain Loss and Degradation Because of Increased Sky Noise Temperature.

Table 2.6-5. Degradation in Downlink (13.7 GHz) Because of Rain (Continued)

Ground Station: Andover

Note: Altitude 0.21 km

	Satellite Longitude (°W)							
	106.0	90.0	130.0	15.0	9.0			41.0
Elevation Angle (deg)	27.8	35.1	12.8	15.3	11.2	10.0	9.0	30.7
Atmospheric Loss (dB)	0.15	0.12	0.32	0.27	0.37	0.41	0.45	0.14
Clear Sky Noise Temperature (K)	10.0	8.0	21.0	18.0	24.0	26.0	29.0	9.0
Clear Sky System Noise Temperature (K)	139.0	137.0	150.0	147.0	153.0	155.0	158.0	138.0
Rain Loss (dB)								
99.8% Availability	0.8	0.6	1.9	1.6	2.1	2.4	2.6	0.7
99.5% Availability	0.4	0.3	0.9	0.8	1.1	1.3	1.4	0.3
Rainy Sky Noise Temperature (K)								
99.8% Availability	49.0	37.0	103.0	89.0	111.0	123.0	131.0	43.0
99.5% Availability	26.0	19.0	54.0	49.0	65.0	75.0	80.0	19.0
Rainy System Noise Temperature (K)								
99.8% Availability	178.0	166.0	232.0	218.0	240.0	252.0	260.0	172.0
99.5% Availability	155.0	148.0	183.0	178.0	194.0	204.0	209.0	148.0
Sky Noise Degradation (dB) Due to Rain								
99.8% Availability	1.06	0.84	1.89	1.73	1.97	2.10	2.15	0.95
99.5% Availability	0.46	0.34	0.87	0.84	1.04	1.18	1.21	0.31
Total Rain Degradation (dB)								
99.8% Availability	1.86	1.44	3.79	3.33	4.07	4.50	4.75	1.65
99.5% Availability	0.86	0.64	1.77	1.64	2.14	2.48	2.61	0.61

Assumed Vertical Polarization on Downlink Includes both Rain Loss and Degradation Because of Increased Sky Noise Temperature.

Table 2.6-5. Degradation in Downlink (13.7 GHz) Because of Rain (Continued)

Ground Station: JPL

Note: Altitude 0.0 km

	Satellite Longitude (°W)					
	106.0	90.0	130.0	171.0		
Elevation Angle (deg)	48.3	40.2	48.6	22.2	10.0	9.0
Atmospheric Loss (dB)	0.10	0.12	0.10	0.20	0.44	0.49
Clear Sky Noise Temperature (K)	7.00	8.00	7.00	13.0	28.0	31.0
Clear Sky System Noise Temperature (K)	136.	137.	136.	142.	157.	160.
Rain Loss (dB)						
99.8% Availability	0.7	0.9	0.7	1.7	3.8	4.0
99.5% Availability	0.8	1.0	0.8	2.2	5.9	6.6
Rainy Sky Noise Temperature (K)						
99.8% Availability	43.0	54.0	43.0	94.0	169.0	175.0
99.5% Availability	19.0	26.0	19.0	49.0	115.0	127.0
Rainy System Noise Temperature (K)						
99.8% Availability	172.0	183.0	172.0	223.0	298.0	304.0
99.5% Availability	148.0	155.0	148.0	178.0	244.0	256.0
Sky Noise Degradation (dB) Due to Rain						
99.8% Availability	1.03	1.27	1.03	1.95	2.78	2.78
99.5% Availability	0.38	0.53	0.38	0.97	1.91	2.04
Total Rain Degradation (dB)						
99.8% Availability	1.73	2.17	1.73	3.65	6.58	6.78
99.5% Availability	0.68	0.93	0.68	1.77	4.11	4.54

Assumed Vertical Polarization on Downlink Includes both Rain Loss and Degradation Because of Increased Sky Noise Temperature.

Table 2.6-5. Degradation in Downlink (13.7 GHz) Because of Rain (Continued)

Ground Station: Goddard

Note: Altitude 0.0 km

	Satellite Longitude (°W)							
	106.0	90.0	130.0	28.0	15.0	9.0		41.0
Elevation Angle (deg)	35.7	42.8	19.6	22.8	13.1	8.5	10.0	31.7
Atmospheric Loss (dB)	0.13	0.11	0.23	0.20	0.34	0.51	0.44	0.14
Clear Sky Noise Temperature (K)	9.0	7.0	15.0	13.0	22.0	33.0	28.0	10.0
Clear Sky System Noise Temperature (K)	138.0	136.0	144.0	142.0	151.0	162.0	157.0	139.0
Rain Loss (dB)								
99.8% Availability	2.6	2.2	4.3	3.8	5.8	7.7	7.0	2.9
99.5% Availability	1.3	1.1	2.3	2.0	3.4	4.8	4.2	1.5
Rainy Sky Noise Temperature (K)								
99.8% Availability	131.0	115.0	182.0	169.0	214.0	241.0	232.0	141.0
99.5% Availability	75.0	65.0	119.0	107.0	157.0	194.0	180.0	85.0
Rainy System Noise Temperature (K)								
99.8% Availability	260.0	244.0	311.0	298.0	343.0	370.0	361.0	270.0
99.5% Availability	204.0	194.0	248.0	236.0	286.0	323.0	309.0	214.0
Sky Noise Degradation (dB) Due to Rain								
99.8% Availability	2.75	2.53	3.35	3.22	3.56	3.59	3.61	2.90
99.5% Availability	1.71	1.52	2.37	2.21	2.79	3.00	2.93	1.88
Total Rain Degradation (dB)								
99.8% Availability	5.35	4.73	7.65	7.02	9.36	11.29	10.61	5.80
99.5% Availability	3.01	2.62	4.67	4.21	6.19	7.80	7.13	3.38

Assumed Vertical Polarization on Downlink Includes both Rain Loss and Degradation Because of Increased Sky Noise Temperature.

Table 2.6-5. Degradation in Downlink (13.7 GHz) Because of Rain (Continued)

Ground Station: Johnson

Note: Altitude 0.0 km

	Satellite Longitude (°W)						
	106.0	90.0	130.0	28.0			41.0
Elevation Angle (deg)	53.5	55.1	38.8	11.3	10.0	90.0	22.7
Atmospheric Loss (dB)	0.09	0.09	0.12	0.39	0.44	0.49	0.20
Clear Sky Noise Temperature (K)	6.0	6.0	8.0	25.0	28.0	31.0	13.0
Clear Sky System Noise Temperature (K)	135.0	135.0	137.0	154.0	157.0	160.0	142.0
Rain Loss (dB)							
99.8% Availability	5.4	5.3	6.7	13.2	13.9	14.6	9.3
99.5% Availability	2.6	2.5	3.3	8.0	8.5	9.0	5.0
Rainy Sky Noise Temperature (K)							
99.8% Availability	206.0	204.0	228.0	276.0	278.0	280.0	256.0
99.5% Availability	131.0	127.0	154.0	244.0	249.0	253.0	198.0
Rainy System Noise Temperature (K)							
99.8% Availability	335.0	333.0	357.0	405.0	407.0	409.0	385.0
99.5% Availability	260.0	256.0	283.0	373.0	378.0	382.0	327.0
Sky Noise Degradation (dB) Due to Rain							
99.8% Availability	3.94	3.92	4.16	4.20	4.13	4.07	4.33
99.5% Availability	2.83	2.77	3.15	3.84	3.81	3.78	3.63
Total Rain Degradation (dB)							
99.8% Availability	9.34	9.22	13.86	17.40	18.03	18.67	13.63
99.5% Availability	5.43	5.27	6.45	11.84	12.31	12.78	8.63

Assumed Vertical Polarization on Downlink Includes both Rain Loss and Degradation Because of Increased Sky Noise Temperature.

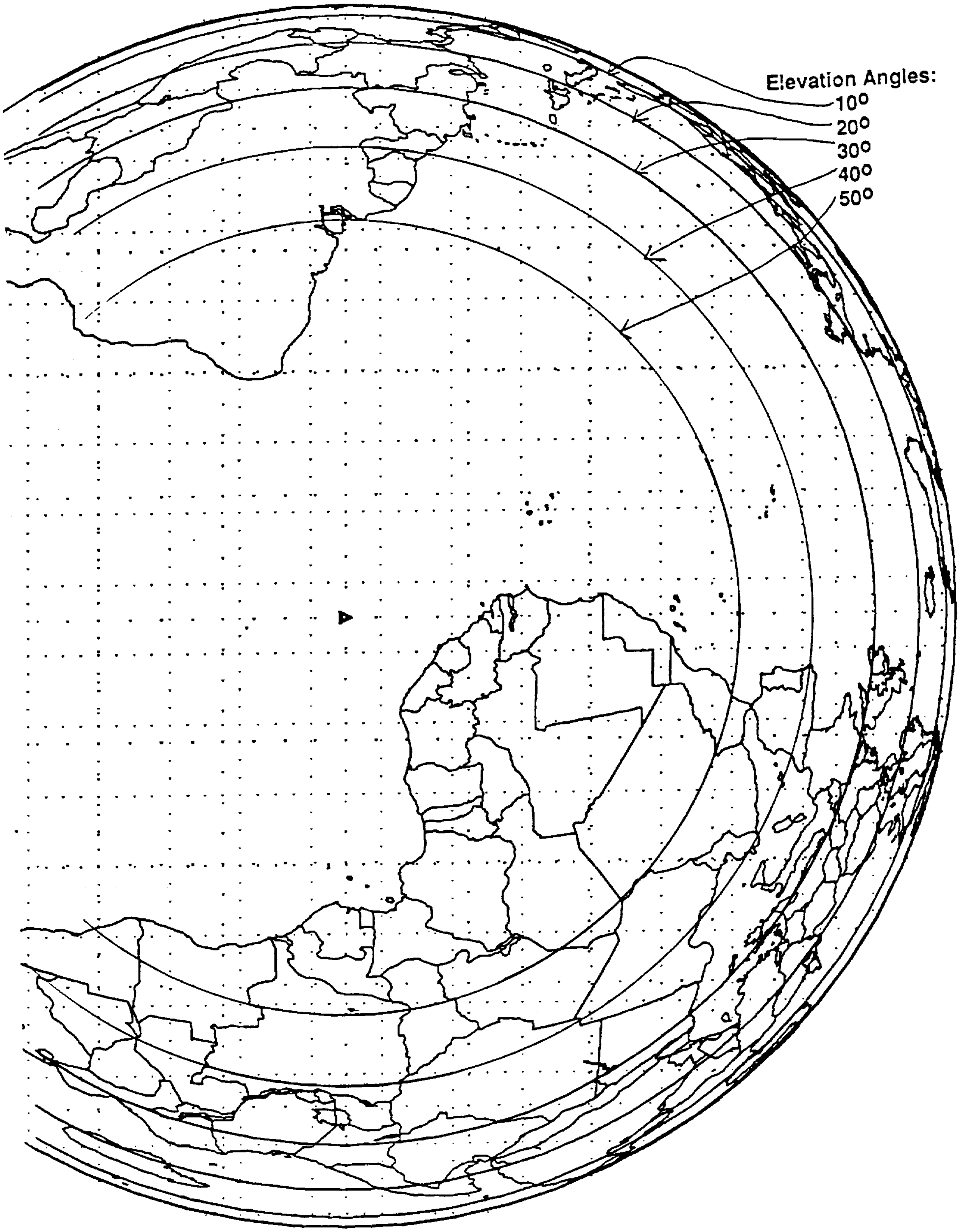

Figure 2.6-2. Coverage from ATDRS at 15° W

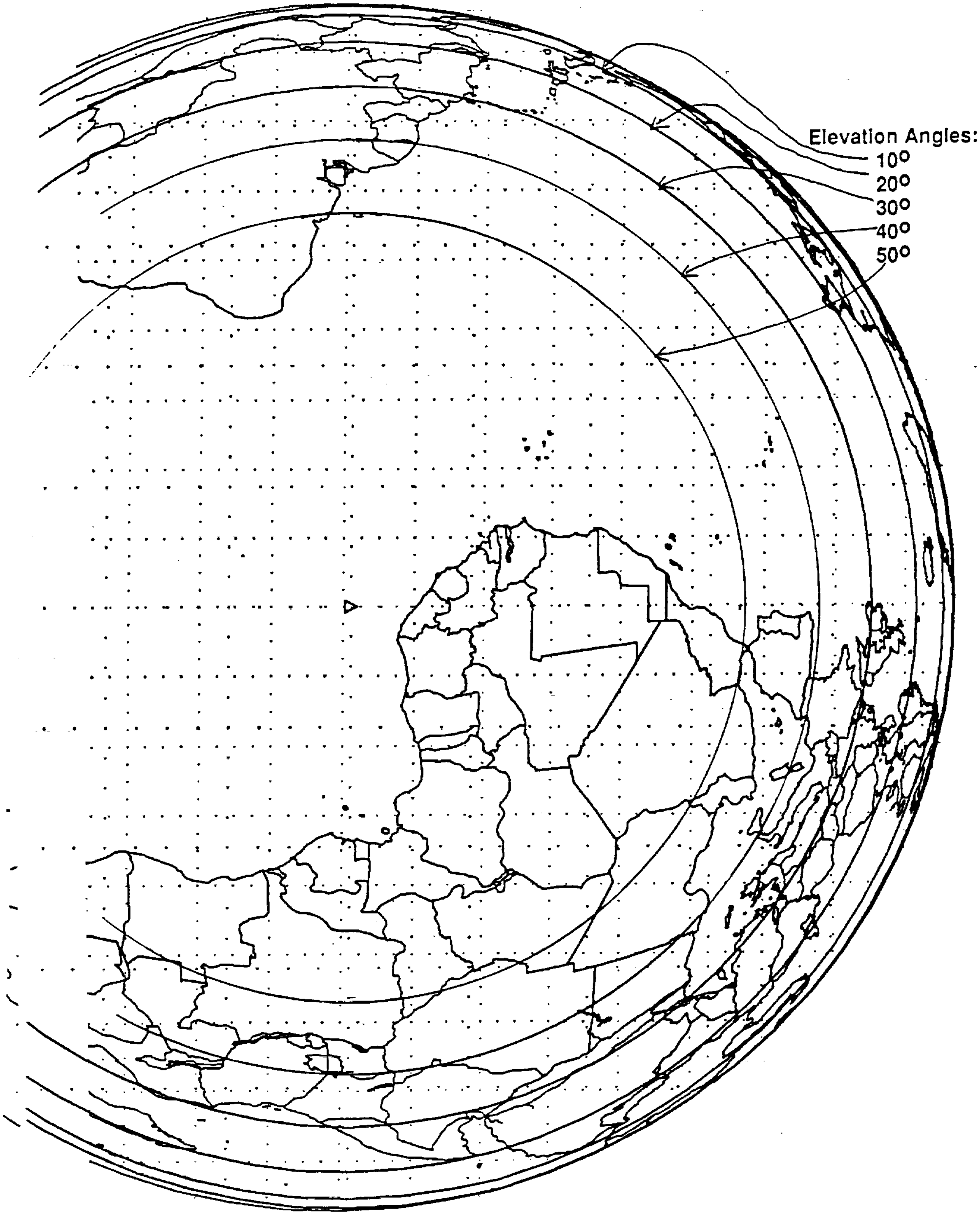

Figure 2.6-3. Coverage from ATDRS at 9° W

Elevation angles and corresponding rain attenuation were computed from five possible European ground stations (Fucino, Geneva, Brussels, Madrid, and Edinburgh) to each of the two alternate ATDRS-East locations. The largest change in elevation angle (2.8°) occurred at the Italy site, and the corresponding maximum increase in rain attenuation at this ground site was 0.3 dB at 30 GHz. Geneva showed the most sensitivity to spacecraft location; the rain attenuation increased 0.4 dB at 30 GHz; 0.3 dB at 20 GHz. At Ku-band frequencies the rain loss change did not exceed 0.1 dB at any ground location. Worst case rain attenuation (99.8% availability) for these European sites is presented in Table 2.6-6.

The CONUS rain attenuation differences (as much as 3 dB) far outweigh those for European ground sites. If the choice between 15° W and 9° W for ATDRS is driven by transmitter power to CONUS, then the 15° W location is clearly better.

2.6.1.3 **Communication to Japanese Sites from ATDRS-West.** Figure 2.6-4 is a coverage map showing visibility from 171° including elevation angle radii of 10°, 20°, and 30°. All of Japan lies within these bounds; Tokyo's elevation angle is 24° while that of the extreme western part of Japan is about 15°. Locating a Japanese ground station near the 24° elevation will minimize the link degradation due to rain. For instance, the rain loss at 20 GHz increases from 8.7 to 12.5 dB as the elevation angle changes from 24 to 15°. At 30 GHz the change can be as much as 9 dB over this elevation angle range. At Ku-band the same phenomena occur but the results are not quite so extreme. At 13.7 GHz the attenuation caused by rain can increase from 4.5 to 6.4 dB, while at 15 GHz the change can be as much as 2.5 dB.

Table 2.6-6. Rain Attenuation For European Ground Sites

			Frequency (GHz)			
			30	20	15	13.7
Ground Site	**ATDRS(°W)**	**El Angle**	Rain Loss (dB)			
Fucino	9	36.4	2.7	1.3	0.7	0.6
	15	33.5	2.9	1.4	0.8	0.6
Geneva	9	34.8	4.8	2.3	1.3	1.0
	15	32.9	5.2	2.5	1.3	1.1
Brussels	9	30.5	4.2	2.0	1.1	0.9
	15	29.0	4.5	2.1	1.1	0.9
Madrid	9	43.0	5.7	2.7	1.5	1.2
	15	42.0	5.9	2.8	1.5	1.3
Edinburgh	9	26.1	3.5	1.6	0.9	0.7
	15	25.4	3.6	1.7	0.9	0.7

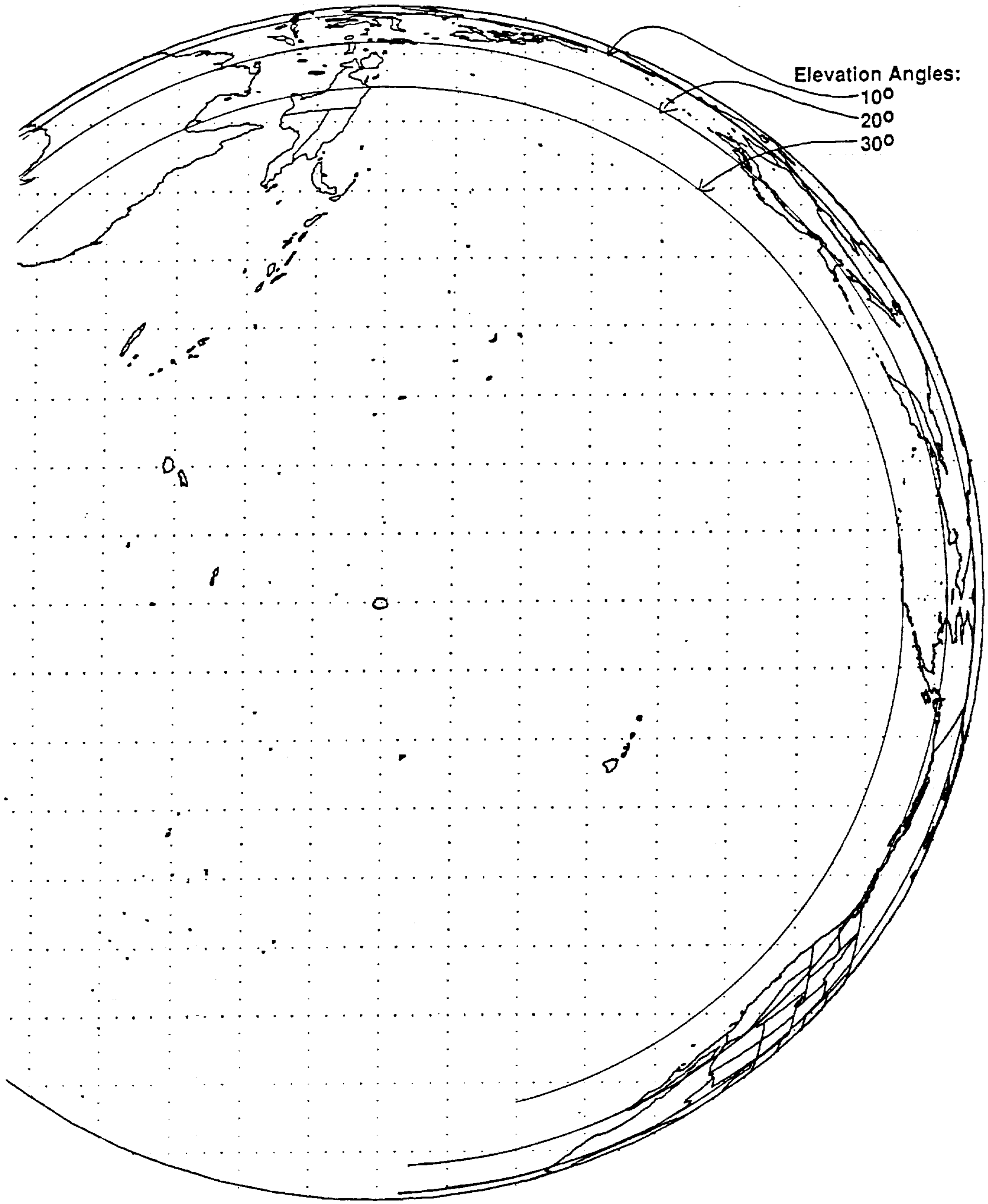

Figure 2.6-4. Coverage from ATDRS at 171° W

2.7 CROSS-POLARIZATION DISCRIMINATION (XPD) ISSUES

Frequency plans for Ku-band uplink/downlink and for Ka-band downlink use both horizontal and vertical polarizations. This is necessitated by the respective forward/return communications requirements with bandwidth allocations that are insufficient to provide these services without resorting to dual-polarization use. This, in turn, requires a careful assessment of the possible XPD at these bands of frequencies at the worst case rain attenuations and elevation angles. These issues are addressed in this subsection.

Based upon the ranges of rain attenuation values at each band for a given elevation angle and availability, XPD can be evaluated following reference [2-3]. The modeling in reference [2-3] was done in Fortran language on a Honeywell mainframe computer.

Figures 2.7-1 shows the XPD versus rain attenuation (AR) relationships (both values being in decibels) for White Sands Ground Terminal (WSGT) coverage at 14, 20, and 30 GHz frequency bands from an ATDRS, located at 90° W (which corresponds to 48.3° elevation angle at WSGT) for the link availability requirements of 99.5% and 99.8% and, for the worst case tilt of the rain drops with respect to the electric fields of 45° and, for the best case tilt of 0° or 90°. These plots show larger degradation in XPD at higher frequencies due to the encountering of larger attenuations. For instance, for a given requirement of 99.8% link availability, the XPD is in the range of 47 dB (for the worst case tilt) to 68 dB (corresponding to the best tilt angle), whereas at 30 GHz, XPD is in the range of 40 to 60 dB. At a link availability requirement of 99.5%, the values of XPDs are better (43 to 68 dB at 30 GHz).

Figure 2.7-2 shows similar plots for WSGT for the worst case elevation angle of 10°. This shows that, at such elevation angles, the worst case XPD is much below a desired value of at least 30 dB at all frequencies, the worst case being at 30 GHz.

Similar plots for Johnson Space Flight Center (JSFC) for elevation angles of 55° and 10° are shown in Figures 2.7-3 and 2.7-4, respectively. They demonstrate that the XPD is much worse at JSFC than at WSGT, due to the much higher rain rates at JSFC. With a link availability requirement of 99.8%, the worst case XPD is much below a desired value of 30 dB at all frequencies, even for the best elevation angles near 55° (corresponding to an optimum ATDRS location of 90° W). The situation is clearly much worse at elevation angles near 10° (as demonstrated by Figure 2.7-4). Again, if we are willing to relax the link availability requirement to 99.5%, the XPD values corresponding to the elevation angles near 55° and for worst case rain-drop tilt angles of 45° are slightly above the 30 dB design goal.

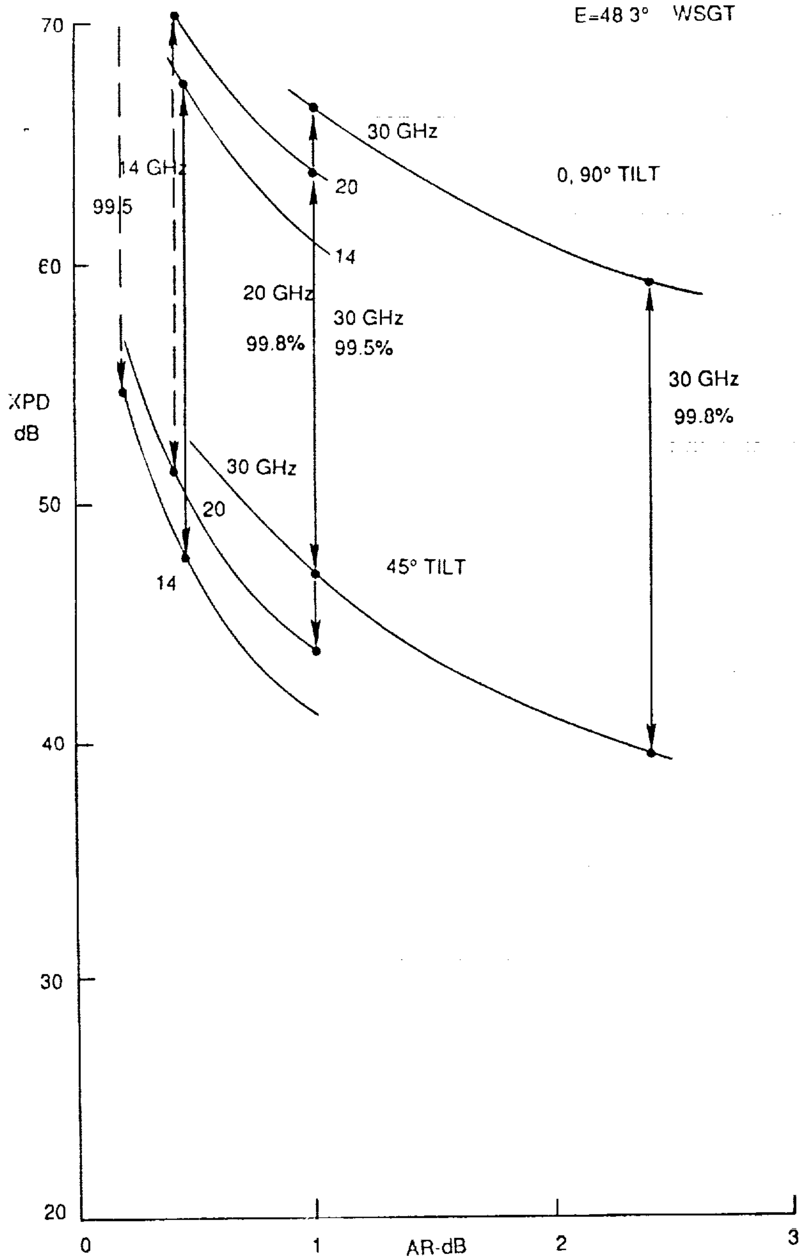

Figure 2.7-1. WSGT E = 48.3°

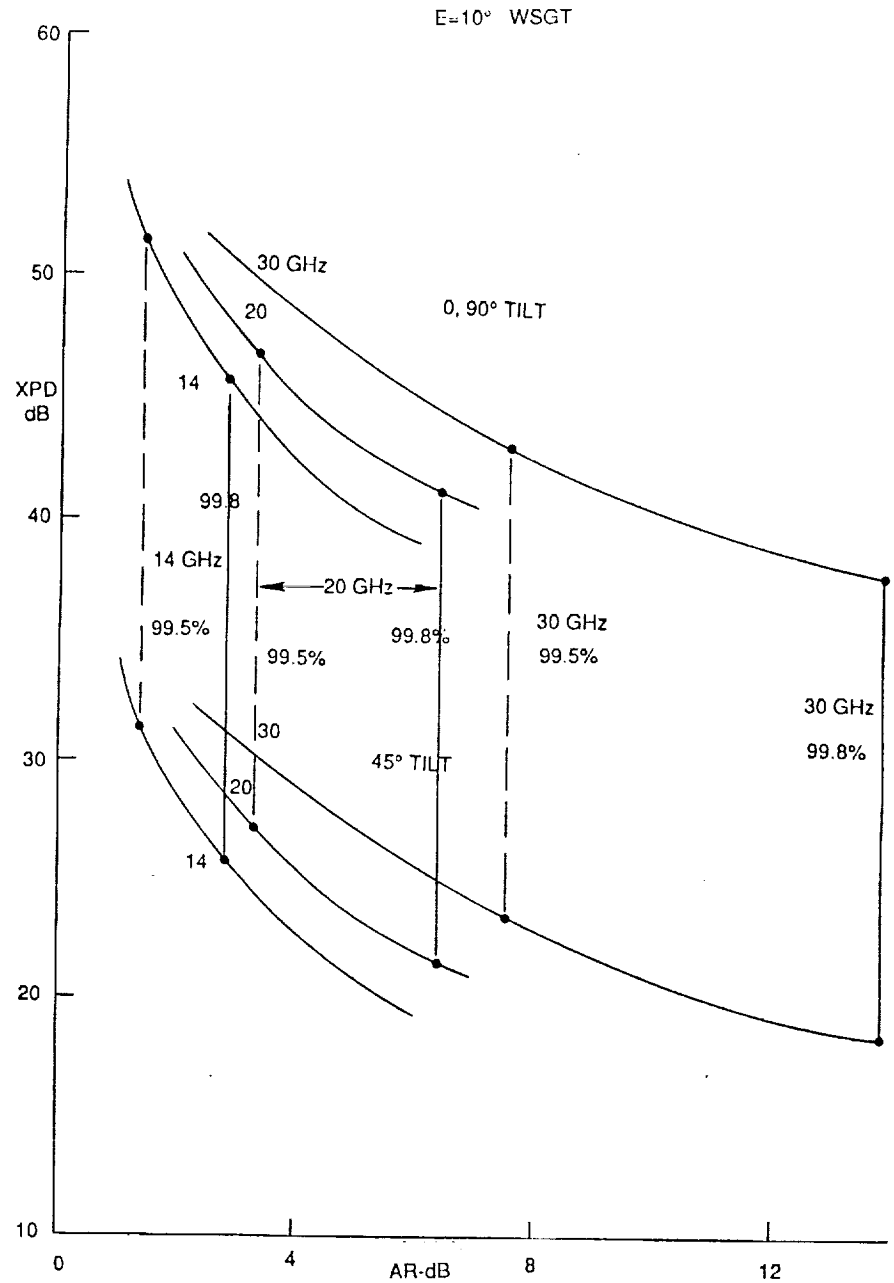

Figure 2.7-2. WSGT E = 10°

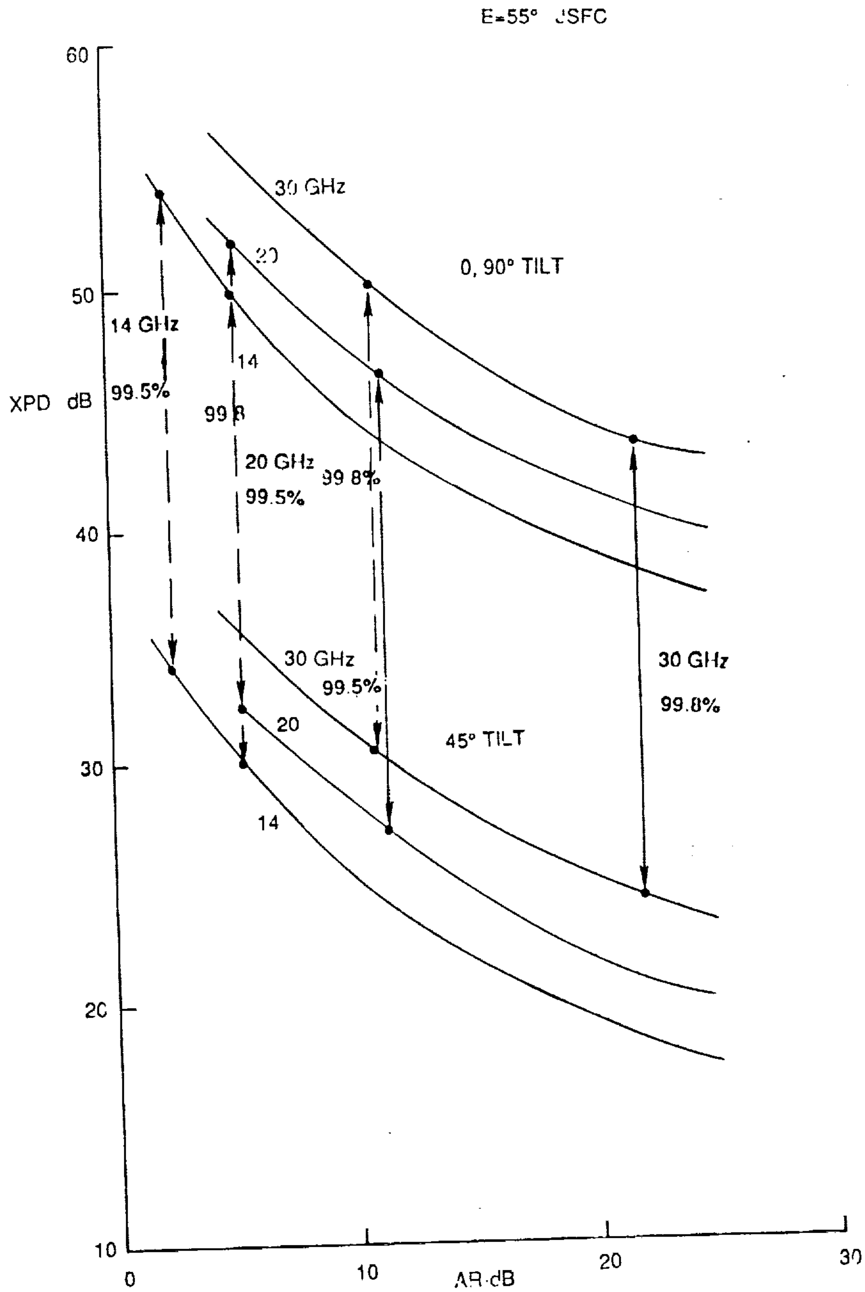

Figure 2.7-3. JSFC E = 55°

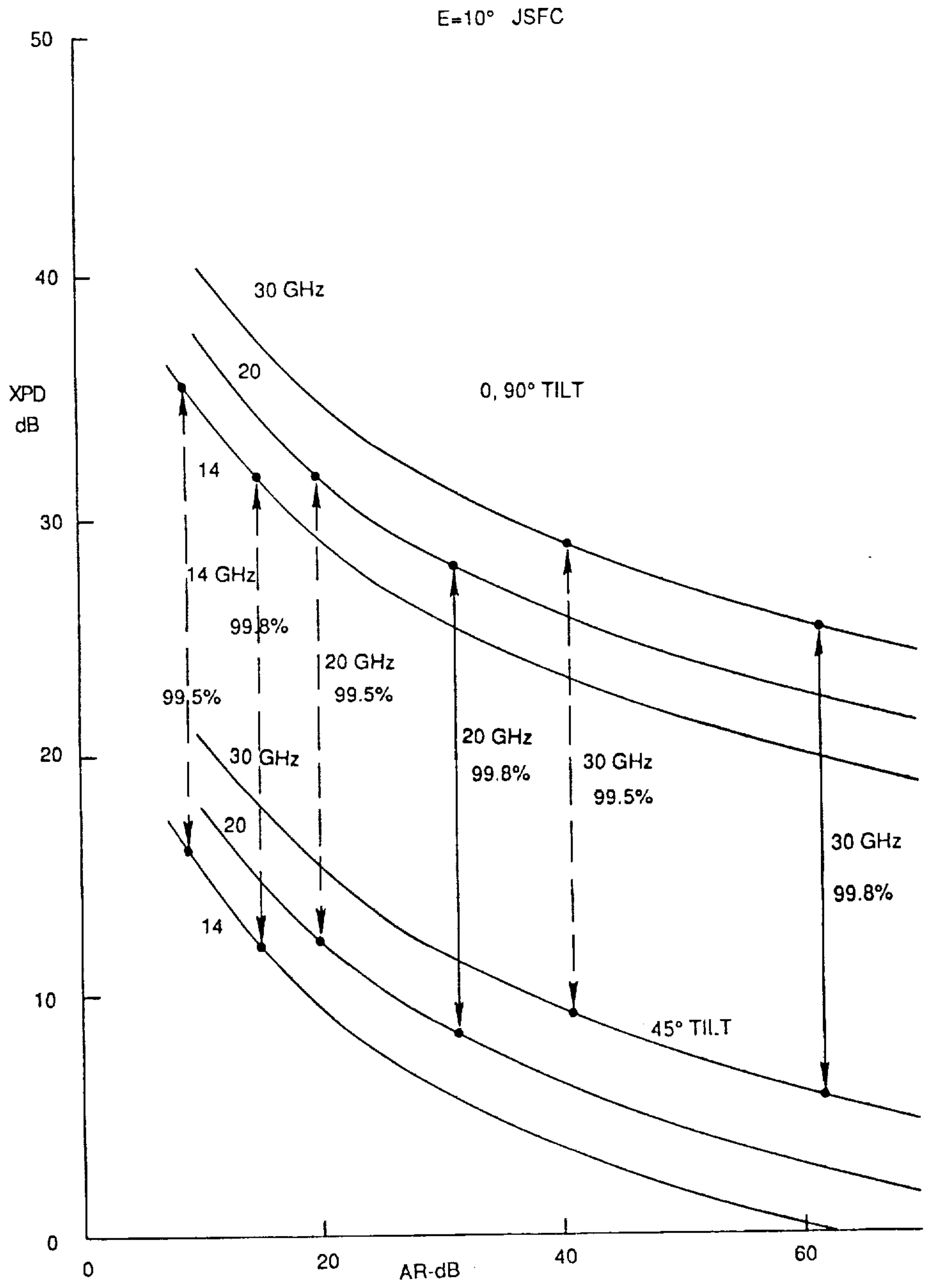

Figure 2.7-4. JSFC E = 10°

Figure 2.7-5 and 2.7-6 show XPD values plotted as a function of frequency, for WSGT and JSFC respectively with a link availability requirement of 99.8%, for the two elevation angles and the two tilt angles considered before in Figures 2.7-1 through 2.7-4. These two figures summarize the concerns about the achievable XPD, especially at ground stations in the rainy regions such as JSFC.

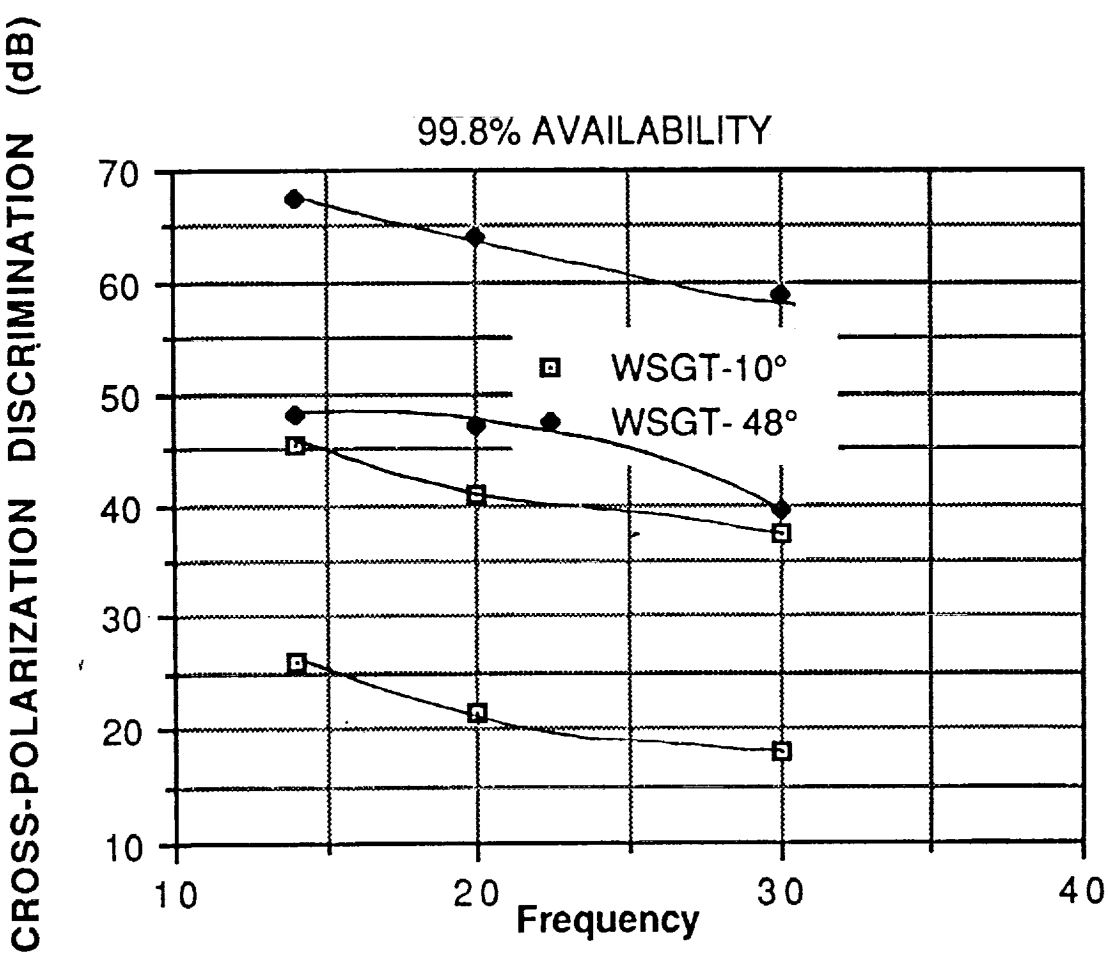

Figure 2.7-5. XPD Versus Frequency Plot
White Sands Ground Terminal

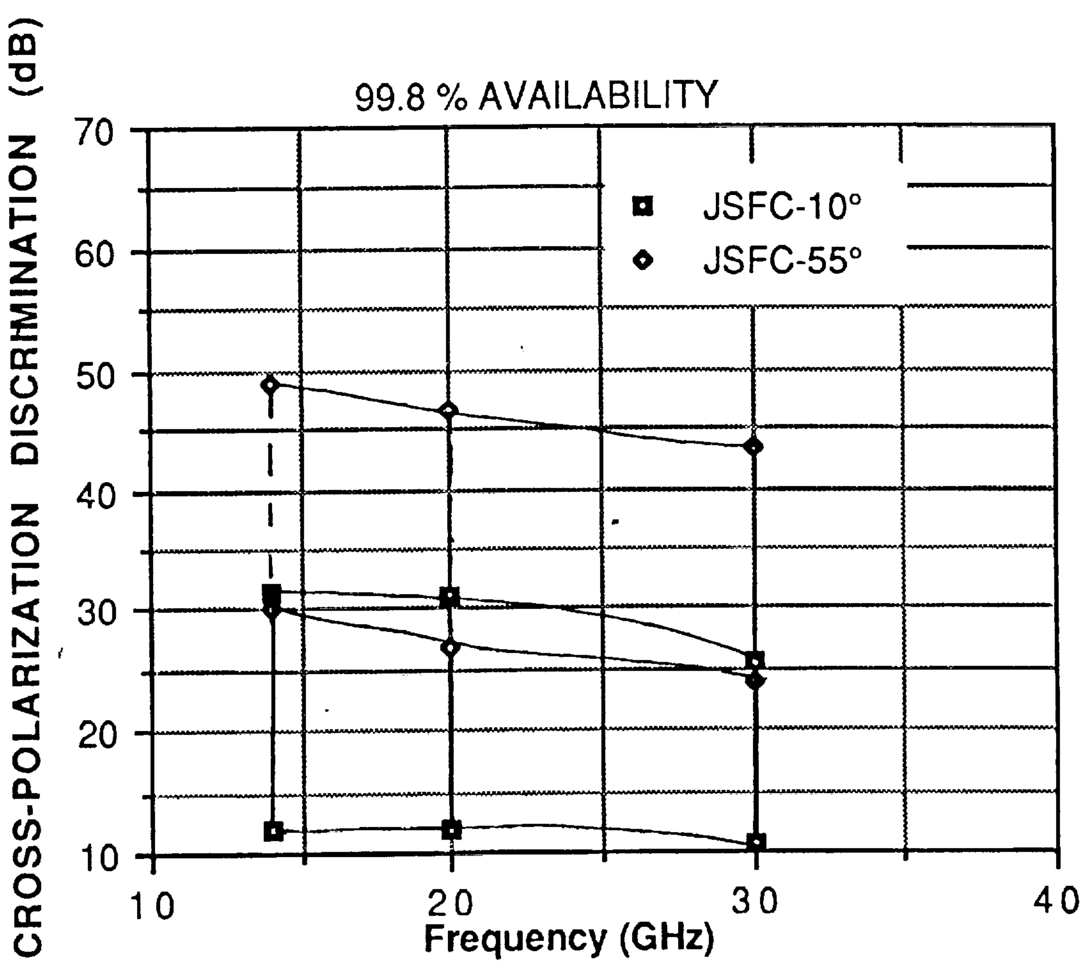

Figure 2.7-6. XPD Versus Frequency Plot
Johnson Space Flight Center

2.8 SUMMARY OF SPACE TO GROUND LINK ANALYSES

This subsection provides the SGL downlink analyses performed for the TNGT (at White Sands) and the various CONUS RGTs at Ku-band and at Ka-band. The baseline assumptions are listed below.

The ATDRSS satellites are assumed to have a transmission capability of -37 dBW/bit of data transmitted, and the spacecraft downlink antenna is assumed to be of 2.4 m diameter (refer to Section 3 for antenna size computations). The modulation format is assumed to be QPSK with no coding. The symbol rate is assumed to be 1 Gbaud for Ku-band links. For Ka-band, however, the symbol rate is assumed to be 2 Gbaud for TNGT links (White Sands terminal) and 1 Gbaud for the RGT links. The bit error rate requirements are set at 1E-5, the link availability requirements are set at 99.8% and a link margin of 3 dB is assumed. Each earth terminal is assumed to have a downlink antenna with diameter of 60 ft and a receive system with a G/T of 70.37 dB/K (at 13.8 GHz).

The results presented here for Ku-band links conform to the STI Configurations 1 and 2. They include CONUS sites as seen from ATDRS located at 106° W, Andover as viewed from 15° W and 9° W, and White Sands as seen from 171° W. Also included are link budgets for various positions of ATDRS locations for JSC. Due to the worst rain attenuation encountered at JSC, the final choice of ATDRS locations may be driven by the G/T requirements at JSC.

For Ka-band, parametric results are provided for downlink to White Sands (TNGT) terminal. For all other terminals, the results of the worst case analysis (corresponding to the 9° elevation angle) and for configuration 1 (satellite longitude of 106° W) are shown.

Figure 2.8-1 plots the G/T requirements at JSC Earth Station as a function of the elevation angle. Also shown in the figure are the worst case requirements for various other CONUS sites. It shows that the worst case G/T requirement corresponding to 9° elevation angle is 53.6 dB/K for Ku-band service meeting the previously mentioned requirements. Coding could improve this situation by several dBs.

One area of concern from this study is the allocated band of 800 MHz at Ku-band. In order to support a symbol rate of 1 Gbaud, a bandwidth of approximately 1.5 GHz is needed. It is possible to use the two polarizations of transmission. This can be accomplished by frequency division multiplexer (FDM) techniques for all the services other than the LSA return link service. For LSA return link, however, a maximum rate of 1 Gbaud per service is specified. If the Ku-band

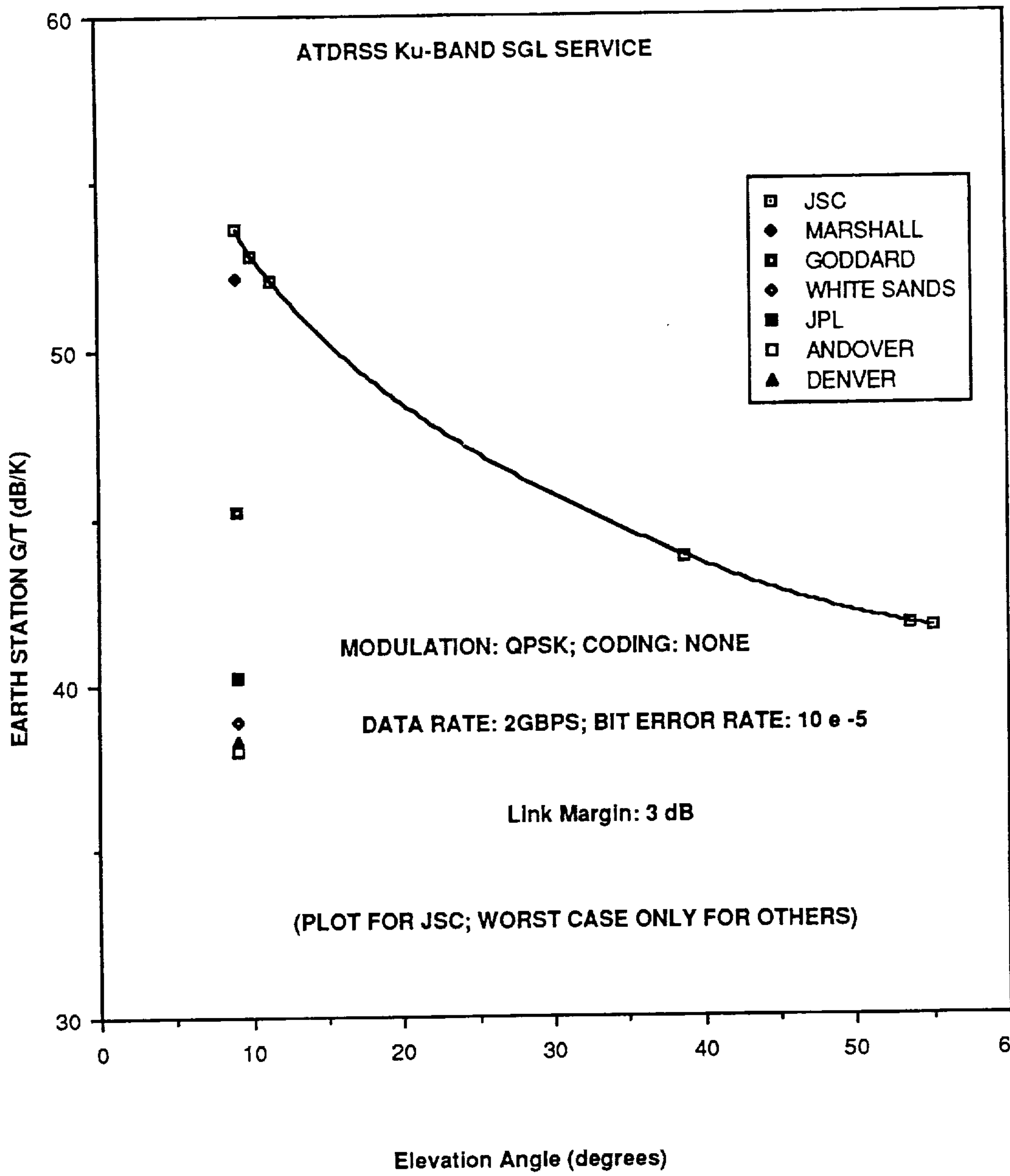

Figure 2.8-1. Elevation Angle Versus Required Earth Station G/T

downlink is to be used for this service, it necessitates on-board demodulation/remodulation with the data stream being split for transmission on each polarization. Alternatively, higher order modulation formats (e.g., M-PSK, M > 4) may be considered.

Figure 2.8-2 shows the G/T requirements plotted as a function of the elevation angle at the TNGT (White Sands) for the Ka-band services. Also shown are the worst case requirements (corresponding to the 9° elevation angle) for various CONUS RGTs. The figure also shows the required G/T for JSC, Marshall Space Flight Center (MSFC) and Goddard Space Flight Center

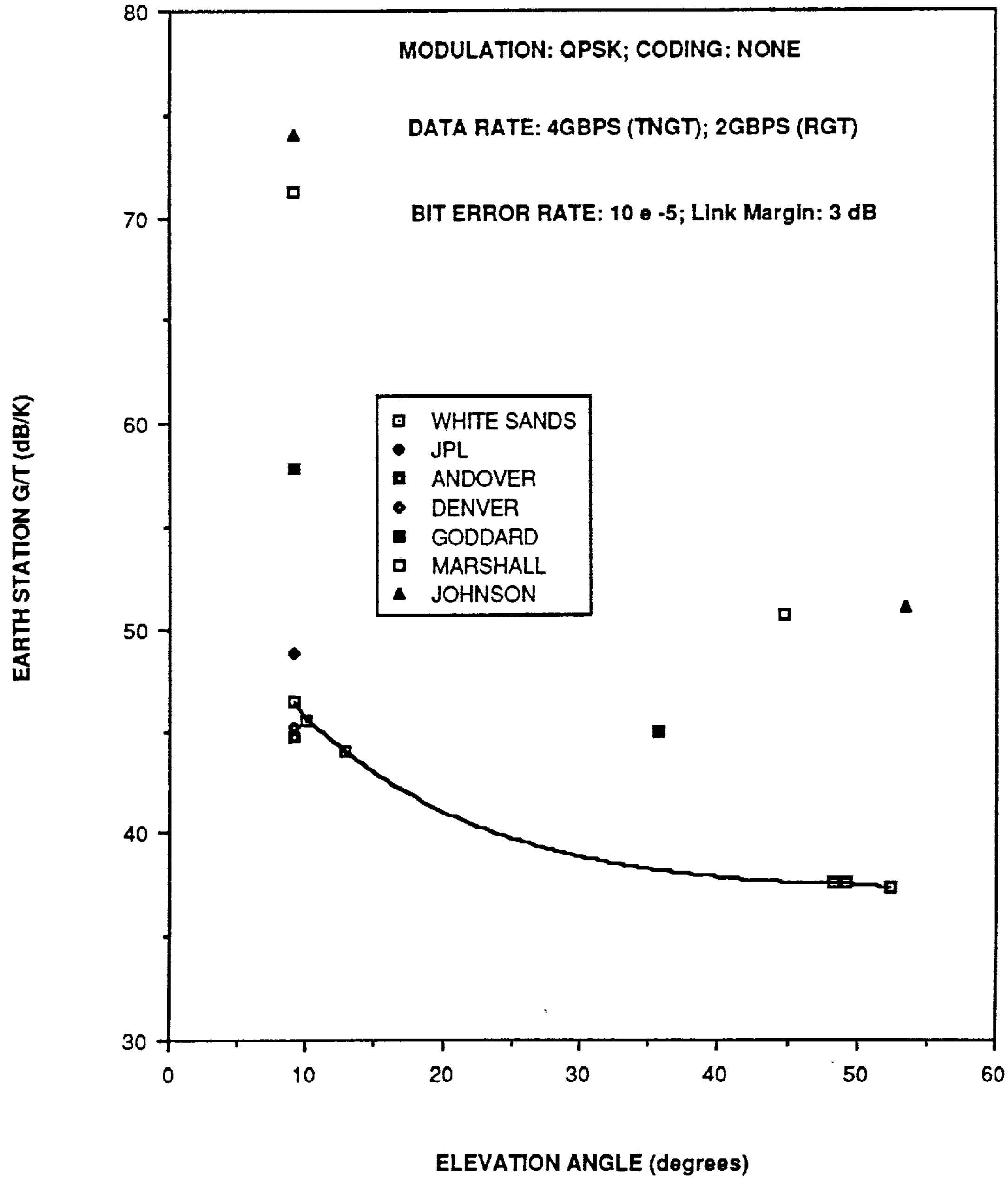

Figure 2.8-2. Elevation Angle Versus Required Earth Station G/T

(GSFC) for the case when the satellite is located at 106° W longitude. A worst case G/T requirement of 46.4 dB/K is needed at the WSGT for meeting all the previously mentioned requirements with a link margin of 3 dB. Again, coding could reduce the requirements by several dBs. As evident from the figure, it will not be practical to provide the Ka-band service to JSC and Marshall Center for elevation angles down to 9° due to the impractically high requirements caused by heavy rain attenuation effects. However, for the case when the satellite is located at 106° W longitude, the requirements for JSC and MSFC are respectively 51 and 50.7 dB/K, which are comparable to the worst case requirement for the WSGT. The associated details of the link analyses are presented in the Appendix A.

2.9 SATELLITE LOCATION SENSITIVITY OF RGT G/T REQUIREMENTS

In this subsection, we study the sensitivity of RGT G/T requirements to the location of the communicating satellites.

We recall here that the rain degradation effects are much more severe at Ka-band than at Ku-band. Figure 2.9-1 shows the G/T requirements plotted as a function of the elevation angle. It shows that of all the ground stations studied, JSFC undergoes the worst degradation. MSFC and GSFC also undergo severe rain degradation, although their degradations are somewhat better than that of JSFC. WSGT undergoes much less rain degradation, although its data rate requirements are doubled (4 Gb/s, WSGT being a TNGT).

In order to study the sensitivity of the G/T requirements for the RGTs, we therefore decided to study the three worst case sites in terms of rain degradation, namely JSFC, MSFC, and GSFC. Figure 2.9-2 plots the G/T requirements for these sites as functions of the satellite longitude for a link availability requirement of 99.8% and a bit error rate requirement of 1E-5 and using QPSK modulation with no coding. It shows that JSFC, undergoing the worst rain degradation, determines the best location of the satellite.

It appears from Figure 2.9-2 that a satellite longitude of 92° W provides the least G/T requirement for JSFC of about 51 dB/K. However, we recall from our link analyses (see Appendix 1) that a receive antenna of 60 ft provides a gain of 68.67 dBi at 19.45 GHz and an assumed system noise temperature of 341 K gives a G/T of only 43.35 dB/K. This is about 7.65 dB lower than the minimum required G/T for the even best possible satellite location. The possible important design alternatives to accomplish this additional required link budget are listed as follows:

a. Replace the power amplifier in the satellite transponder providing 8 W backed off power (which meets the -37 dBW/b EIRP requirement) with a power amplifier providing about 50 W backed off power. This design alternative is easy to implement and poses no technological problems. If the satellite power budget permits, this alternative provides a simple solution.

b. Replace 2.4 m satellite antenna with 5.8 m antenna. This again poses no technological problems in antenna design itself, however, this reduces the beamwidth by that ratio, leading to tighter pointing error requirements. This would also mean that there would be greater scanning loss because the smaller the beamwidth, the larger the number of beams to cover the same area. Also this larger antenna may require launching in smaller pieces and assembling in space leading to alignment problems and surface error tolerance problems. Finally, it would add increased weight on the spacecraft.

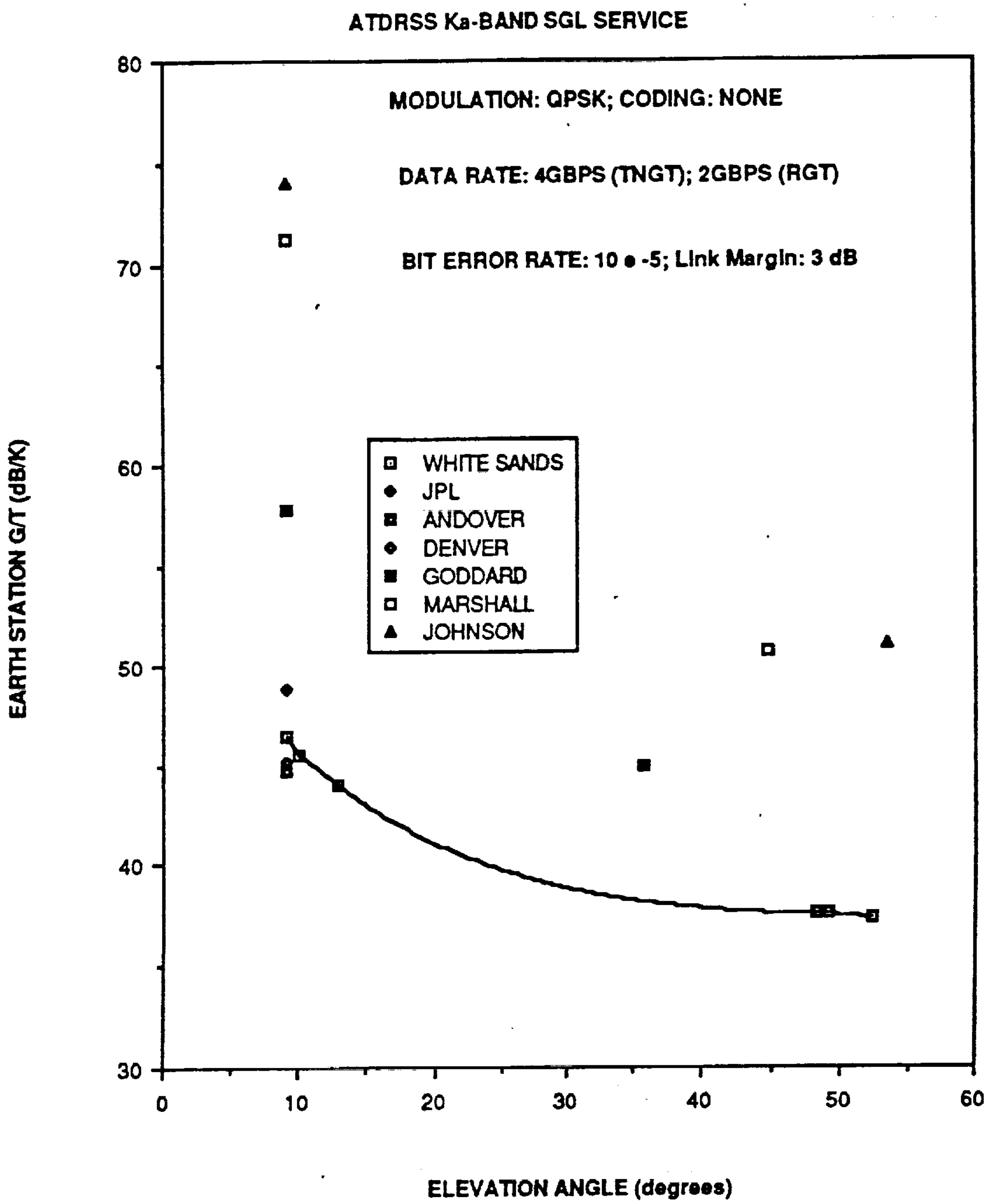

Figure 2.9-1. Elevation Angle Versus Required Earth Station G/T

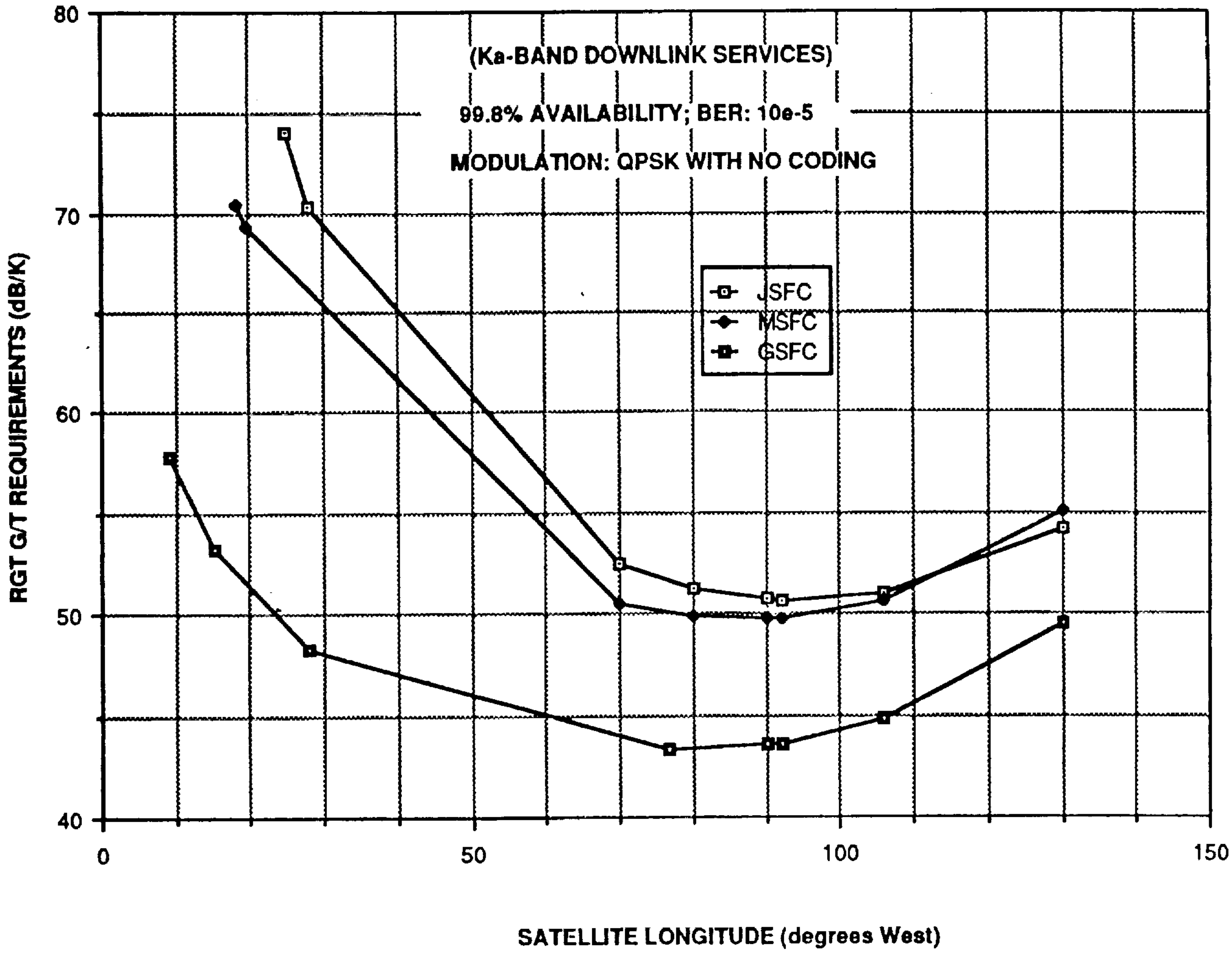

Figure 2.9-2. Satellite Location Sensitivity of RGT G/T Requirements

c. Coding can be used to improve the performance of about 3 to 5 dB. However, this would require additional bandwidth, which is unavailable for the return services. Due to the bandwidth restrictions, higher order modulation formats are to be considered, which may affect the user and ground station architectures. Using higher order modulation formats means that the transmit power is to be increased to meet the bit error rate requirement.

d. Increase the size of the ground terminal antenna to about 150 ft. This alternative would pose surface tolerance and pointing issues and is very expensive.

e. Reduce the system noise temperature of the ground terminal. A reduction of 7.65 dB would require the system noise temperature to be at about 58 K. It is possible to reduce the system noise temperature by incorporating better low noise amplifiers (LNAs) with lower noise figures. However, the lower the noise figure, the higher the complexity and the higher the costs of implementation. A sky noise temperature of 30 K means that an LNA with a noise figure of about 0.4 dB is needed for providing a system noise temperature of 58 K.

f. A relaxation of the link availability requirement from 99.8% to 99.5% provides about 6.5 dB gain in the link budget; however, this would mean that the original goals of designing the system for high link availability are being compromised.

g. A reduction in data rate requirements may be possible by reevaluating the users communications requirements with each ground terminal (especially JSFC, MSFC, and GSFC). However, reduction in data rates by a factor of about 6 would severely restrict the return link communications capability of the users.

From the above discussion, it seems that the most cost-effective alternative is to increase the transponder power (i.e., the first design approach presented above).

2.10 STATION SEPARATION FOR ISOLATION

In a previous memo (Attachment 12, Monthly Report 1) discussing isolation of the MBA beams from calculated patterns of a torus reflector antenna, it was stated that a 30 dB isolation between beams could be maintained if these beams were separated by a minimum of 1°. Although this separation is an arbitrary number and is based on a preliminary antenna design, it is interesting to note what implications this separation requirement might have on potential ground station locations.

The focus of points within 1° of the ground stations mentioned in our first review is shown in Figure 2.10-1, as seen from synchronous satellites at the various positions listed. These cover ground stations for both Configurations 1 and 2. One additional CONUS ground station has been added at Andover, Maine. It is apparent that the only stations listed within 1° of each other are Goddard and Andover for Configuration 1, and Kennedy and Johnson SFCs for Configuration 2. It is also apparent that the only locations within CONUS for a mobile station meeting this 1° separation requirement are in the central states and the northwest.

This separation requirement, essentially to provide spatial isolation between adjacent beams, becomes especially important for a dual-polarized system where polarization isolation is not available between stations.

2.10.1 Interference Analysis

Interference between beams in a multibeam antenna is strictly a function of beam separation and sidelobe structure of the individual beams. No additional polarization isolation is available in the ATDRS case since both senses of polarization are in use, unless some higher modulation than QPSK is used to achieve a reasonable degree of isolation between beams. An early theoretical and experimental study performed by Ford Aerospace at C-band with a bootlace lens configuration [2-4] (one of the easiest with which to control sidelobes, because of the lack of blockage) showed that beam separations of at least two beamwidths are generally required to achieve a reasonable degree of isolation (30 dB). This has been borne out by measurements on Ford Aerospace's 20 GHz dual-reflector antenna developed for NASA Lewis's ACTS Program, [2-5] for which literally hundreds of patterns were measured with different beam positions, polarizations, and frequencies. The conclusions indicate that first sidelobes are often higher than -30 dB, and that achievement of this degree of isolation required that adjacent beams be located beyond this first sidelobe, or about 0.7° apart (representing 2.3 beamwidths). A similar separation would suffice for the ATDRS 30 GHz beams, where the required gain (54.6 dBi) implies a similar beamwidth (0.3°). However, if the same aperture is used for 20 GHz, the beamwidth will be about 0.45°, so that the minimum separation will increase to approximately 1.0°. This figure was used in the last monthly report to

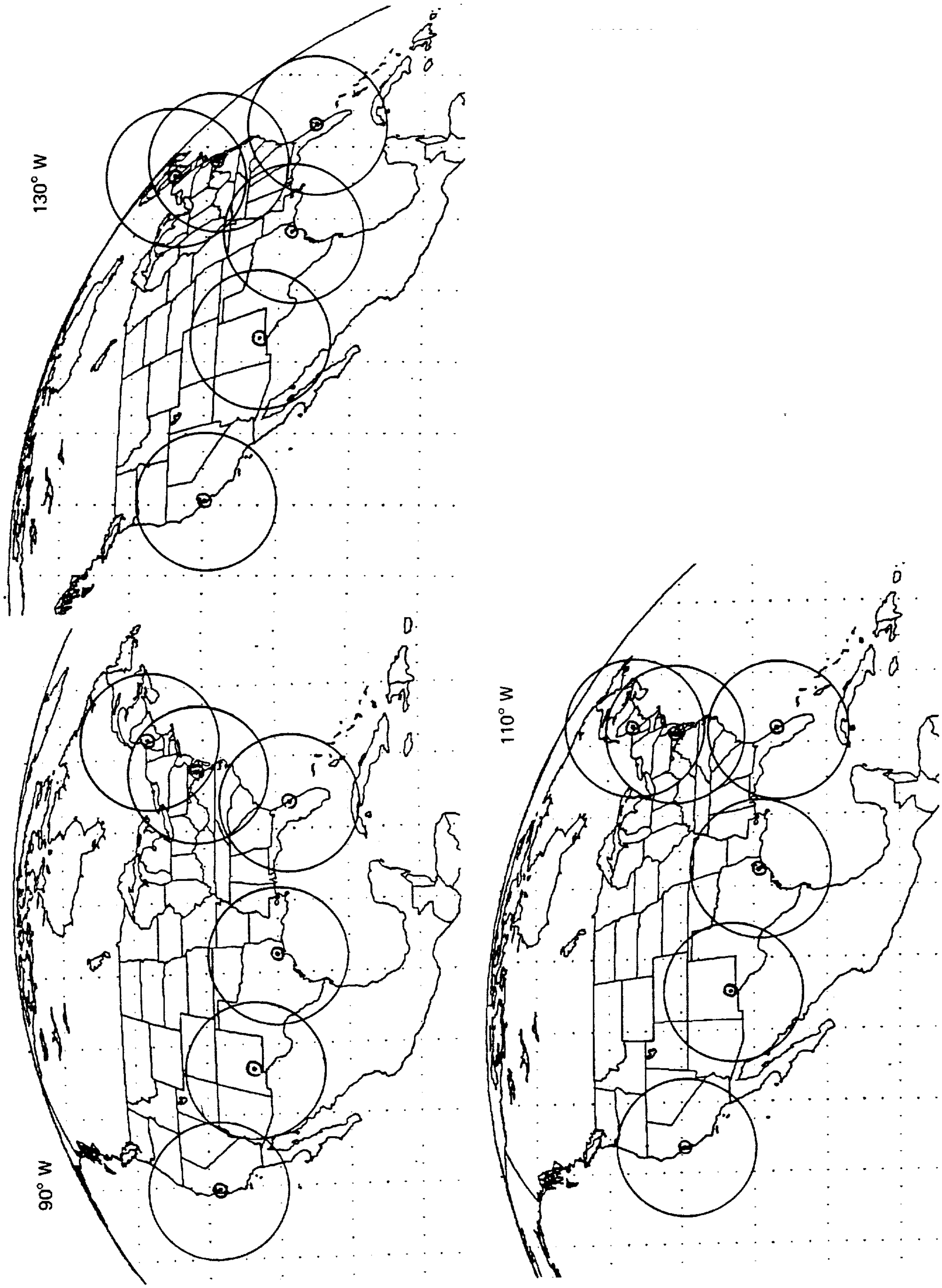

Figure 2.10-1a. Locus of Points within 1° of Potential Ground Stations

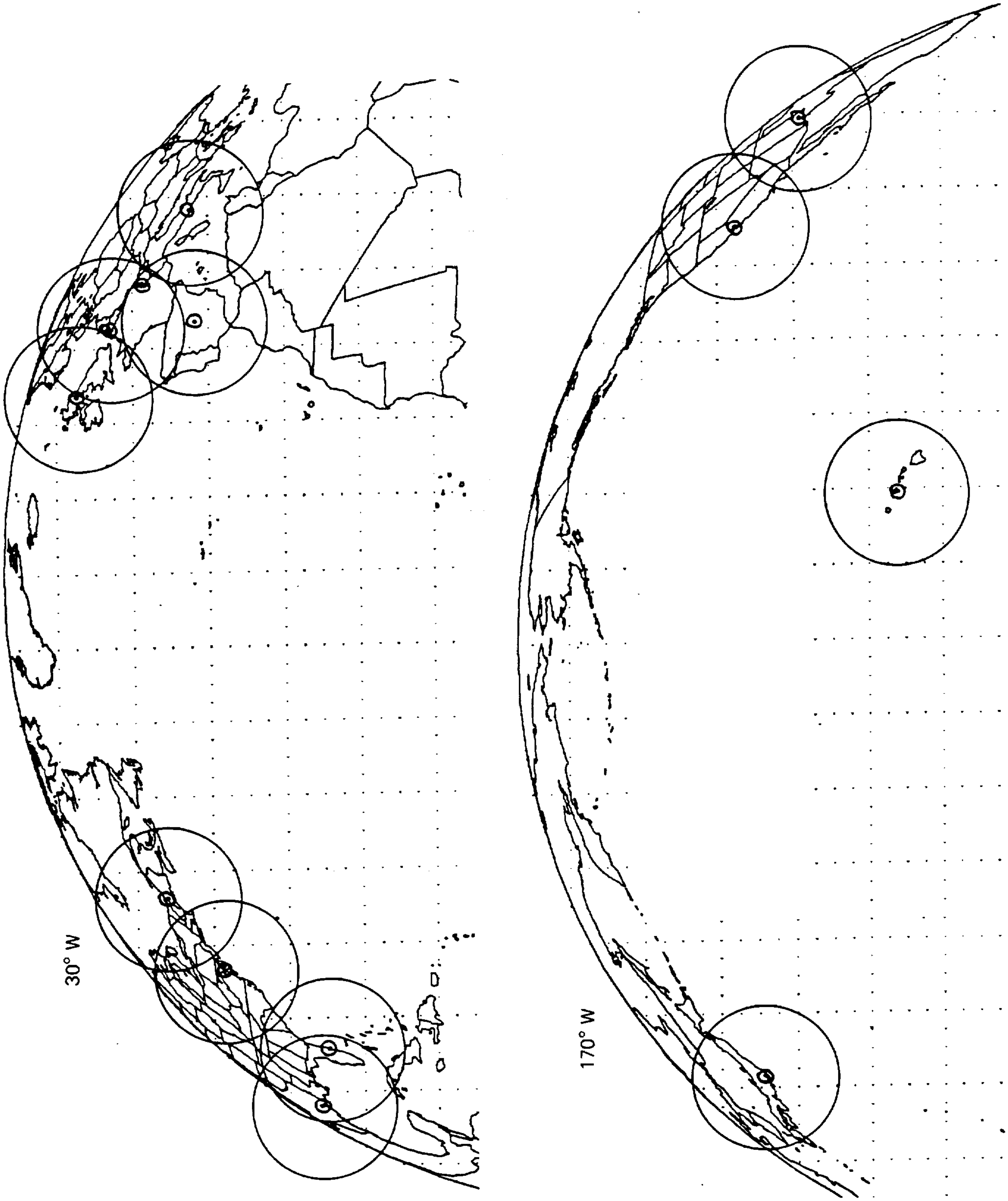

Figure 2.10-1b. Locus of Points within 1° of Potential Ground Stations

draw the 1° contour circles around assumed CONUS ground station locations to identify potential isolation problems. Similar maps for the new ground station locations suggested by STI and for the new satellite locations of 9° and 15° W are shown in Figure 2.10-2. These show that 1° separation criterion is met for all stations except the following two pairs from 110° W, longitude:

a. Goddard GSFC and Andover, Maine
b. White Sands TNGT and Denver, Colorado

The latter pair nearly meet the 1° separation criterion, and could potentially meet the 30 dB isolation goal.

The following station locations were used:

Name	Designation	Latitude (° N)	Longitude (° W)
Andover, Maine	AND	44.64	70.75
Huntsville, Alabama	MSFC	34.72	86.60
Denver, Colorado	DENV	39.58	105.00
Pasadena, California	JPL	34.14	118.16

If the same antenna or one of the same size were to be used for Ku-band (13.7 - 15.2 GHz), the corresponding beamwidths would be some 35% larger, or about 0.6°. The 1° station separation would result in some degradation in isolation, perhaps to 25 dB. The recommended minimum separation of 1.35° in this case, for 30 dB isolation, would be violated by all adjacent stations except JPL/WSGT and WSGT/JSFC. In order to reduce the beamwidth for the Ku-band coverages so that 1° station separation will result in adequate isolation (30 dB), a larger antenna would be required (about 35% larger). Thus, if an 8 ft diameter reflector were used for 20 and 30 GHz (consistent with the required gain), an 11 ft one would be required for Ku-band. Alternatively, the 8 x 15 ft torus reflector described in the first monthly report would have to increase to 11 x 18 ft.

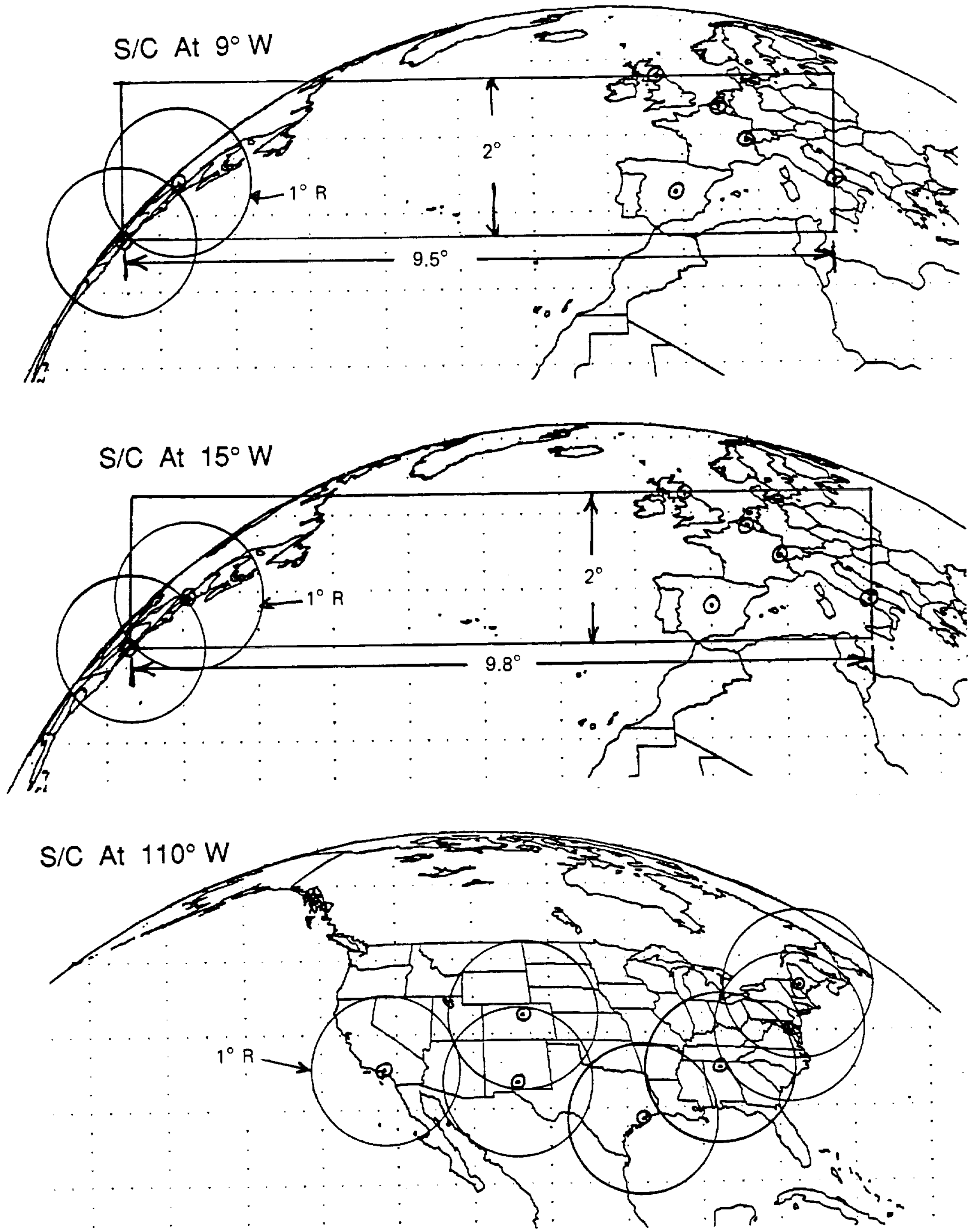

Figure 2.10-2. Interference and Scan Ranges with New Configurations

2.11 FILTER DISTORTION AND ADJACENT CHANNEL INTERFERENCE EFFECTS

The total maximum baud-rate of all the return services combined, according to the SOW Table 2, is 4130 Mbaud, but the total simultaneous data transmission to ground stations is not required to exceed 2000 Mbaud. On the other hand, the bandwidth of the downlink is 3.5 GHz per polarization, or 7 Gbaud if both polarizations are used. It is clearly advantageous to use one polarization for the fixed stations while the mobile stations use the second one, because otherwise interference between downlink beams will limit the geographic areas in which the mobile stations are allowed to operate. (This limitation is shown in Attachment 4 of Monthly Report 2.) Use of one polarization means that:

a. It is necessary to achieve a spectral efficiency of at least
   2000/3500 = 0.571 baud/Hz
b. It is necessary to devise a switching frequency conversion scheme that satisfies the 2.0 Gbaud bound capable of "packing" every possible subset of return signals into a 3.5 GHz band. It is easy to see that this can only be accomplished with a substantial number of on-board synthesizers. Moreover, this scheme violates an implied requirement of the SOW, namely: "Each service indicated in Table 1 has a unique designated carrier frequency" (paragraph 2.2.1). Therefore, we will not consider this possibility further. The other practical alternative (which stops short of on-board demodulation/modulation) is to allow every ground station to use both polarizations. In this case two bands of 3.5 GHz each must support all the return signals totaling 4.130 Gbaud.

Roughly speaking, we need to achieve a spectral efficiency of:

4130/7000 = 0.59 baud/Hz

or 1.69 Hz/baud

while providing the necessary guard bands between the FDM signals.

The spectral efficiency shown above poses a rather critical design issue, because the on-board channel filters used to demultiplex/multiplex the various FDM signal components constitute a part of the user-to-ground channel. These filters can cause considerable bit error rate (BER) performance degradation, unless matched to the other filters of the channel, including the transmit filter, in a way that satisfies Nyquist's criterion for zero ISI and at the same time the "matched filter requirement," so as to optimally filter out the thermal noise of the link. Two interesting cases are identifiable.

a. The on-board filters are relatively wide, so that even when the user is transmitting his highest specified baud rate, the on-board filters do not distort the relayed return signals and at the same time do not reject significantly adjacent channel interference (ACI), which is being taken care of by the user transmit filter. In this case the transmit filter and ground receiver/demodulator filters only determine the BER performance of the system. On-board channel filters are still necessary in order to limit noise contributions from adjacent channels as can be seen in Figure 2.11-1 and 2.11-2.

b. The on-board filters significantly affect the overall channel transfer function and therefore, must in conjunction with the other filters, approximate Nyquist's criterion for zero ISI and the "matched filter" condition.

Assuming that the user to ATDRS link is the one that contributes all the thermal noise supplied to the demodulator in the ground station, while the ATDRS to ground link adds no thermal noise, the on-board channel filters can be treated as part of the receiver, and therefore, filtering on board is equivalent to filtering in the ground-based demodulator. This is the case for a single channel, but when ACI is taken into account, the situation is different. Ground-based filters are ineffective in

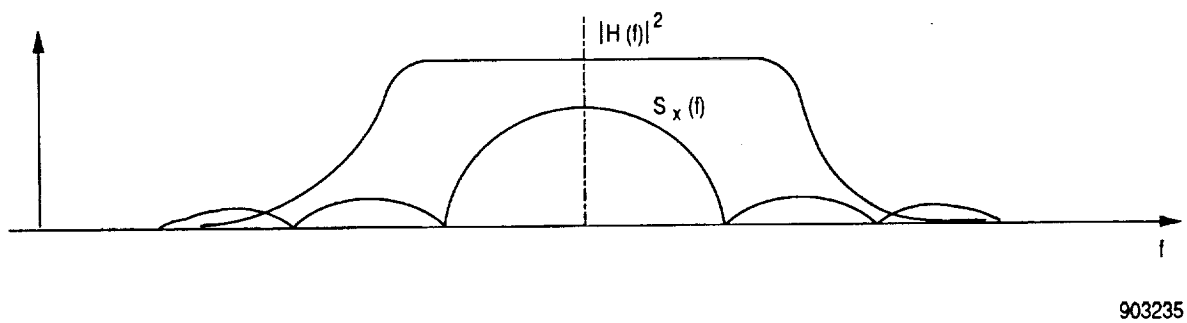

Figure 2.11-1. Spectral Display of Received Signals and On-Board Channel Filters Amplitude Responses

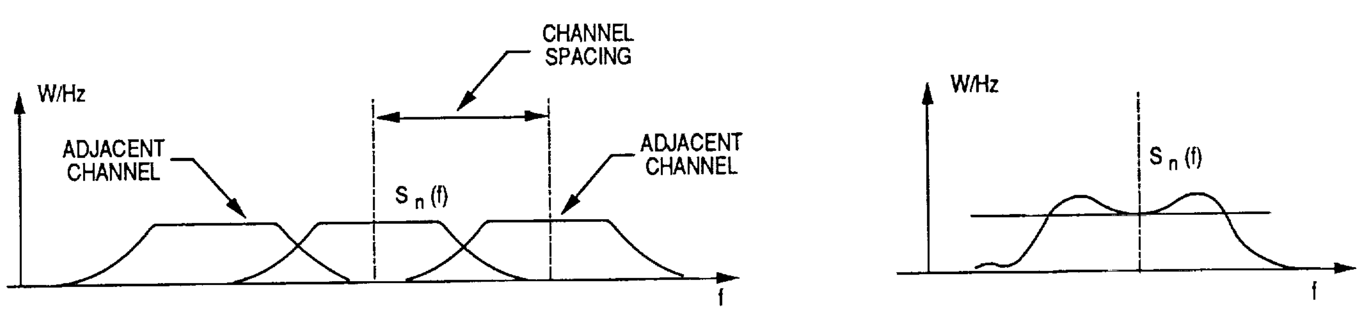

Figure 2.11-2. Noise Contributions of Adjacent Channels Due to Wide On-Board Channel Filters

combating ACI introduced on board as a result of insufficient filtering prior to the FDM process, and in this sense, on-board filtering and filtering in the ground station are not equivalent. ACI can be controlled either by the user (by limiting the spectral mask of his transmitted signal) or by the on-board channel filters or by both. This is evident from the simple model shown in Figure 2.11-3.

In the existing TDRS system the user is not required to use a transmit filter. In fact, the transmitted spectrum is bound from below by the requirement that the symbol rise time will not exceed 5% of signal duration. (See, for instance, TDRSS User's Guide, STDN No. 101.2 Revision 5, September 1984, Table 3-16.) The transmitted spectrum resembles the $(\sin(x)/x)^2$ shape of an unfiltered QPSK modulated signal over a band wider than twice the baud rate. We can choose between two approaches:

1. Leave the user's spectrum "wide open" and severely filter the return signals on-board ATDRSS to achieve an acceptable level of ACI.
2. Limit the spectrum of the user's transmitted signal, so that with a moderate amount of additional filtering on-board ATDRS, an acceptable level of ACI will result.

Approach 1 is compatible with existing user equipment. As shown in Figure 2.11-3, each return signal will be filtered to limit its effective bandwidth and shifted to its downlink frequency (the order is not crucial for the present discussion). Adjacent channels will be stacked 1.69 symbol-rates apart to achieve the required spectral efficiency of 0.59 baud/Hz. The main design issue is the characteristics of all the filters involved both on board and in the ground-based demodulator to optimize the BER performance of the system under specified ACI conditions.

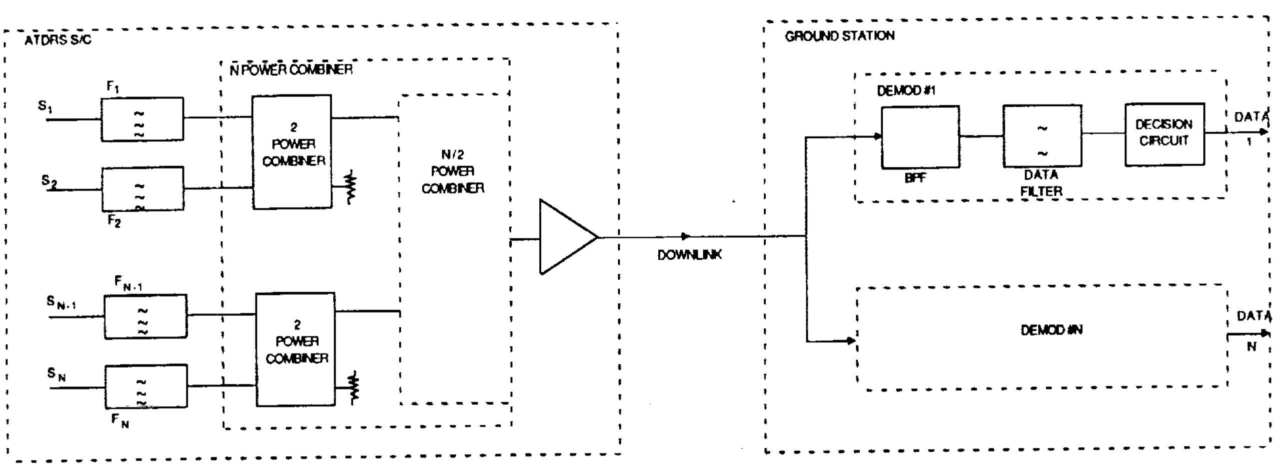

Figure 2.11-3. An ACI Model

The impact of mismatched filters and other link impairments on BER performance has been studied by many authors. Ford Aerospace has several computer programs that were developed at Ford Aerospace by J. Jones and W. K. Leong [2-6] under contract NAS2-8538 and by J. Y. Huang under IR&D project 79010303 [2-7]. These programs calculate the loss in Eb/No of the link due to filter distortion for a selection of desired BER values with respect to ideal theoretical performance. The most popular filter families can be specified independently for the transmitter, the transponder, and the receiver up to a total of 10 filters. Ideal phase equalization could also be exercised as well as finite (but linear only) transmitted waveform rise time. The programs can also accept arbitrarily weighted thermal noise contributions from the uplinks and downlinks (i.e., user to ATDRS and ATDRS to ground).

Mismatch and intersymbol interference loss caused by filtering was computed using the J. Jones, et al, program for some selected values of filters. Certain assumptions were made:

a. The data channels are TDRS-type, the modulation is QPSK and the symbol rate 150 Mb/s.
b. Integration was performed over four lobes of the signal spectrum (the main lobe is considered two lobes). It turns out that the error introduced by this approximation is negligible.
c. We considered interference from two past and two future symbols.

In the following Tables 2.11-1 and 2.11-2 we assumed that:

a. There are two-pole 150 MHz wide (double-sided) Butterworth data filters in the demodulator.
b. Each Chebychev filter is perfectly equalized, i.e., zero time delay distortion is assumed. The filters passband ripple is 0.1 dB.
c. The downlink noise is 20 dB lower than the user-ATDRS link.

Table 2.11-1 gives data for a seven-pole Chebychev filter in the transponder with various bandwidths. The demodulator contains the data filter only. Table 2.11-2 has two identical seven-pole Chebychev filters, one in the transponder, the other in the receiver. Degradation is computed for transmitted symbol rise times of 0% and 5% (worst case TDRS spec). The tables show the power increase required to maintain a BER of 1E-5.

Table 2.11-1 shows that a filter as narrow as 180 MHz can be used in the transponder and the resulting power increase necessary to maintain a BER of 1E-5 in only about 1 dB.

Table 2.11-1. Power Increase Required to Maintain a BER of 1E-5
One 7-Pole Chebychev in Transponder (ATDRS)

RT(%) BW(MHz)	300	270	240	225	200	180	170	160	150	140
0	0.68	0.63	0.59	0.58	0.71	1.05	1.33	1.78	2.63	4.36
5	0.61	0.56	0.52	0.51	0.65	0.98	1.26	1.71	2.56	4.29

Table 2.11-2. Power Increased Required to Maintain a BER of 1E-5
One 7-Pole Chebychev in Transponder (ATDRS)
One 7-Pole Chebychev in Receiver (Demod)

RT(%) BW(MHz)	270	240	225
0	0.86	1.07	1.27
5	0.84	1.00	1.20

Table 2.11-2 shows a degradation of about 1.0 dB for two cascaded seven-pole Chebychev filters with 3 dB bandwidths of 240 MHz. In all cases the degradation is slightly worse for symbol rise times of 0%.

The program was also run to assess the effect of the equalizer. The degradation for two 240-MHz cascaded seven-pole filters with rise time 5% and no equalizer present was 2.04 dB, 1 dB worse than the corresponding 1.0 dB shown in Table 2.11-2. To assess the effect of a degraded downlink, we ran the program with user-ATDRS link noise to downlink noise ratio of 10 dB, (note that the downlink noise is filtered by the demodulator only). With two 240 MHz bandwidth filters, one at the transponder and the other in the demodulator, the loss was 1.01 dB compared to 1.0 dB in Table 2.11-2.

At the moment we have no access to a comparable program for ACI calculation that is as general, flexible, and convenient as the programs mentioned above. To fill the need, a rudimentary program has been written on a SUN workstation. The program calculates the effective increase in total demodulator noise (channel noise) due to interference by adjacent uncorrelated signals having a $(\sin(x)/x)^2$ prefiltered spectrum, i.e., a QPSK or BPSK modulated carriers. The program accepts Butterworth and Chebyshev filters only. Strictly speaking, the output is the loss in Es/No when compared to operation with no ACI (and not the required boost in Es, in order to preserve the same BER). The program takes into account an interfering signal having the same spectral shape as the interfered signal but not necessarily the same signaling rate (i.e., modulation rate) or power. In general, though, there are two adjacent channels and in the worst case the interfering signals might have higher power than the interfered signal. Corresponding corrections must therefore be made in order to bound the worst case ACI.

Some calculated results derived from the model of Figure 2.11-3 are shown below:

a. There are two interfering signals spaced 1.69 x fs MHz above and below the center frequency of the interfered signal.
b. The power of the interfering signals is 5 dB above that of the interfered signal.
c. F_s is the common baud rate of the interfered and interfering signals.
d. Each signal is QPSK modulated and is not filtered by the transmitter.
e. Each signal if filtered on-board ATDRS with a signal Chebychev bandpass filter before being applied to a common power combiner (which is not frequency selective) as shown in Figure 2.11-3.
f. The ground-based demodulator contains one Chebyshev bandpass filter followed by one pair of baseband Butterworth data filters.
g. Es is the received energy per symbol at the input to the spacecraft transponder.
h. No is the thermal noise spectral density at the input of the spacecraft transponder, and the downlink thermal noise in negligible.

Filter Parameters. The transponder and demodulator BPFs are seven-pole Chebyshev filters with 0.1 dB ripple in the passband. The 3 dB bandwidth appears in the table in f_s units (normalized by f_s).

Choosing as an example f_s = 150 Mbaud and channel spacing of 1.69 x f_s = 253 MHz, we can achieve an ACI loss of 0.059 dB at Es/No = 12 dB with transponder and demodulator filters having 3 dB bandwidth of 1.6 x f_s = 240 MHz. If we increase the bandwidth of both BPFs to 270 MHz, the ACI loss increases sharply to 1.35 dB for the same Es/No ratio of 12 dB.

Table 2.11.3. Es/No Loss Due to ACI

Transponder BPF 3 dB Bandwidth	Demodulator BPF 3 dB Bandwidth	Es/No dB	Loss in Es/No dB
2	1.8	10	0.99
2	1.8	12	1.48
2	1.8	15	2.58
2	1.6	10	0.24
2	1.6	12	0.38
2	1.6	15	0.73
1.8	1.8	12	1.35
1.6	1.8	12	0.73
1.5	1.8	12	0.37
1.333	1.8	12	0.092
1.2	1.8	12	0.032
1.8	1.6	12	0.23
1.6	1.6	12	0.059
1.5	1.6	12	0.027
1.333	1.6	12	0.0075

Figure 2.11-4 shows the typical situation discussed above.

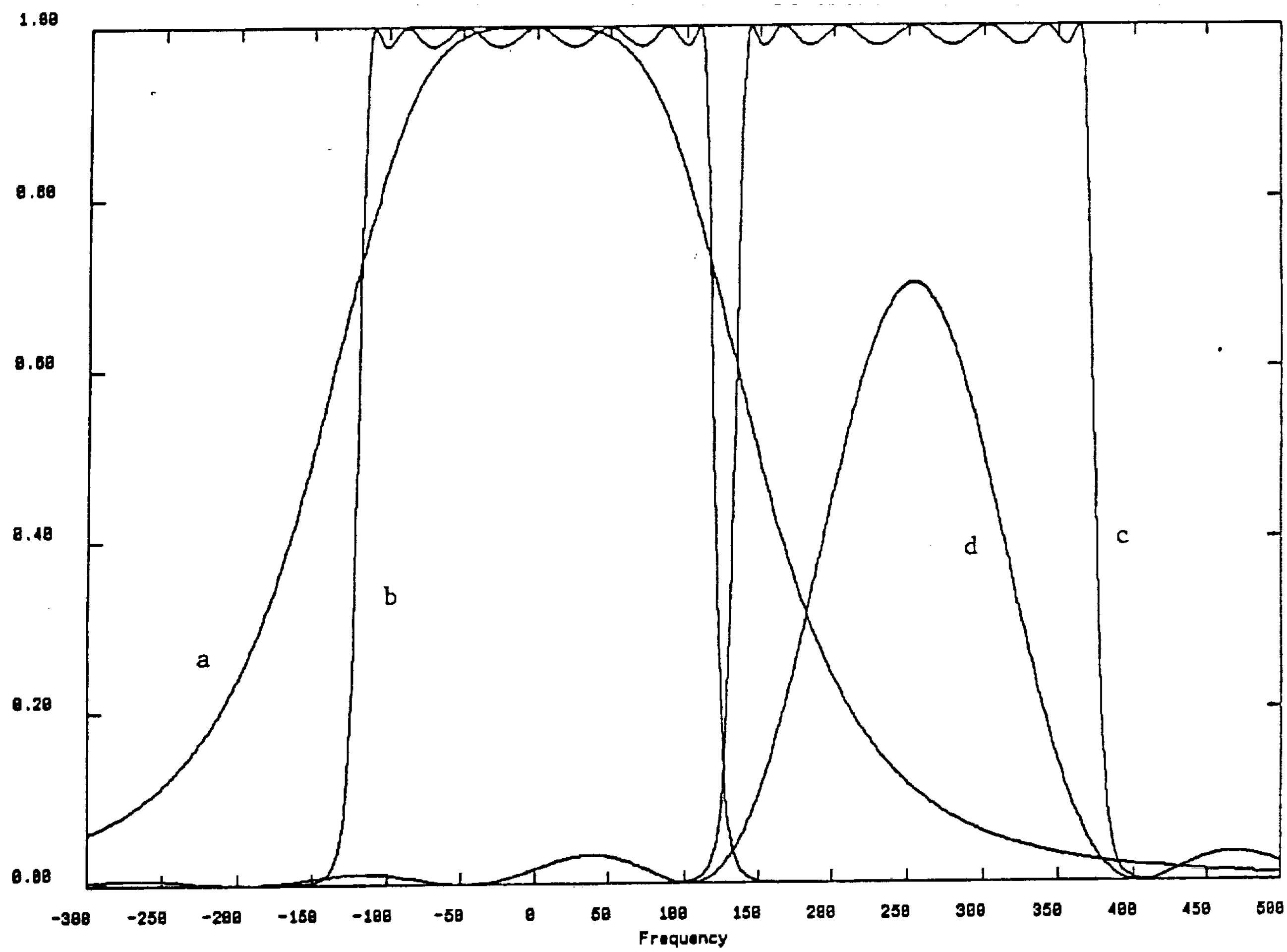

a. Magnitude square response of the demodulator 2 pole Butterworth data filters. 3dB bandwidth is 150 MHz (double sided).

b. Magnitude square response of the demodulator 7 pole Chebyshev filter. 3dB bandwidth is 240 MHz.

c. Magnitude square response of the transponder 7 pole Chebyshev BPF centered on the adjacent channel. 3dB bandwidth is 240 MHz. Channel spacing is 253.5 MHz.

d. Spectrum of interfering signal, f_S = 150 M Baud..

Figure 2.11-4. ACI Model

2.12 ATDRSS - DOPPLER MEASUREMENTS AND PHASE NOISE

2.12.1 Doppler Measurements

Two modes of Doppler measurements are offered to users of ATDRSS, namely one-way and two-way (round trip) measurements. A two-way measurement is performed when the ground station (GS) transmits a carrier to the user spacecraft, which responds by transmitting back a coherent turnaround carrier. The transponder carrier is then received in the GS, mixed with a coherent LO and the beat frequency is counted over a specified time interval to derive the Doppler shift. The actual counting can be done in any convenient frequency as long as the offset is known precisely and can be subtracted. The frequency stability of the GS carrier is of utmost importance in such a measurement, because, if the frequency of the carrier drifts during the round trip propagation time of the signal, a Doppler measurement error results.

An obvious figure of merit for Doppler measurement systems is the mean square measurement error $\Delta f(\tau)$, denoted $D_{\Delta f}(\tau)$, and

$$\sigma_{\Delta f}(\tau) = \sqrt{D_{\Delta f}(\tau)}$$

the rms frequency differential, where τ is the round trip delay. These parameters can be obtained directly from the phase noise spectrum of the recovered carrier upon which the Doppler count is performed:

$$D_{\Delta f}(\tau) = \frac{2}{p\tau} \int_{o}^{\infty} S_{\psi}(\omega)\, \mathrm{Sin}^2(\omega\tau/2)\, \mathrm{Sin}^2(\omega\tau/2)\, d\omega$$

where, $S_{\psi}(\omega)$ is the phase noise spectrum of the recovered carrier, and τ is the measurement time, i.e., the time span over which the recovered carrier frequency is counted. Typically, the phase noise spectrum of oscillators increases very rapidly as the frequency decreases toward zero. Fortunately, the two $\sin^2(\ )$ factors under the integral sign above assume very low values for $\omega << \min(T^{-1}, \tau^{-1})$, and therefore, those spectral components of $S_{\psi}(\omega)$ do not contribute much to the total error. However, as τ increases, lower frequency components of $S_{\psi}(\omega)$ start having a larger effect on the measurement error. This is one reason why Doppler measurements through the X-link are expected to have a higher rms error than when one TDRS spacecraft only is relaying the signal. Clearly, when studying two-way Doppler measurements the phase noise model must include the actual propagation delays through all the links involved. Moreover, the phase noise spectrum of the recovered return signal in ATDRSS includes contributions of all the system oscillators (used for frequency conversions).

Figure 2.12-1 depicts a phase noise model of a two-way Doppler system that includes two ATDRS spacecrafts and an X-link. Several closed loops can be identified; the longest, which is from the GS to ATDRS 1 to ATDRS 2 to the user spacecraft to ATDRS 2 to ADTRS 1 and back to the GS is $\tau = 2x\ \tau_1 + 2x\ \tau_2 + 2x\ \tau_3$ seconds long, but shorter loops also exist. Each source of phase noise contributes to the return carrier noise through its own transfer function obtained by tracing all paths from that particular source to the Doppler counting system.

Due to the complexity of the problem and the large number of noise sources involved, a complete phase noise model is necessary. In particular, the phase noise characteristics of all the oscillators and the contribution of the user spacecraft (in coherent turnaround mode) must be known and taken into account. The system's rms Doppler error as specified by NASA must be somehow converted to phase noise allocations for all the major components and subsystems, including, of course, the upconverters and downconverters of the SGL system, which is the main focus of this study.

2.12.2 A Phase Noise Model for ATDRSS

The only way to satisfy TDRSS stringent specifications with respect to two-way Doppler measurements (WU-00-01B paragraph 3.1.1) is to lock all on-board oscillators (used for frequency conversions) to a ground-based common time and frequency standard (CTFS). In the existing TDRSS a pilot signal is transmitted from WSGT to TDRS, which is used on board by the master frequency generator (MFG) as a frequency reference. The system is shown in Figure 2.12-2.

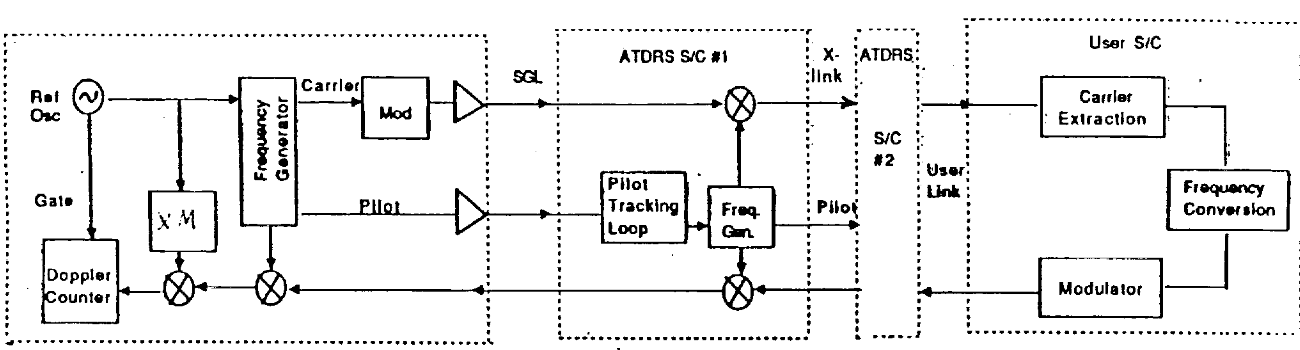

Figure 2.12-1. Two-Way Doppler Measuring System

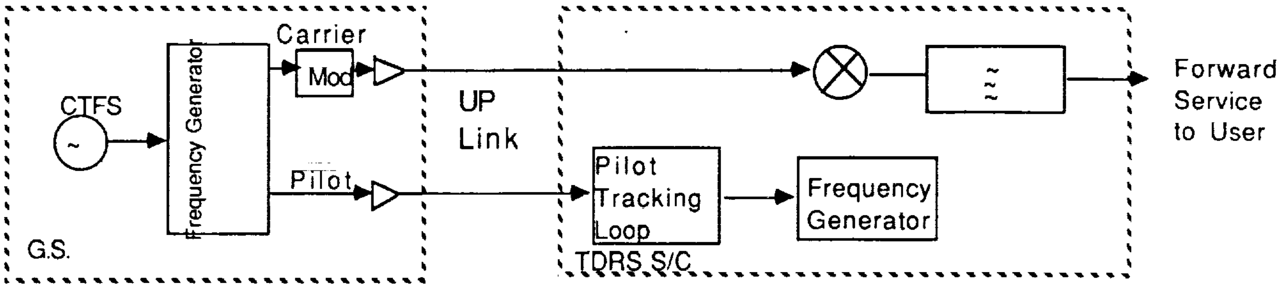

Figure 2.12-2. Pilot Signal in TDRSS

The frequency generator in the GS typically uses a number of VCOs, each phased locked to the CTFS of the station (either directly or indirectly) to generate coherently all the different carriers required for transmission, upconversion, and downconversion. Two circuits of that type are shown in Figures 2.12-3a and 2.12-3b.

The phase noise spectrum of a carrier at frequency f_o can be referred to a frequency $k_1 f_o$ by scaling the spectrum by k_1. This scaling allows us to determine the oscillator phase noise at any desired harmonic or subharmonic of f_1. Scaling also allows the phases of two carriers at different frequencies to be examined for coherency by referring each to a common frequency. A linear phase noise model, which corresponds to Figure 2.12-3 is shown in Figure 2.12-4. There are two independent noise sources in this diagram: The reference oscillator, having the phase noise spectrum $S_o(\omega)$ (in radian^2/Hz) and the VCO with phase noise spectrum that we denote $Sv_1(\omega)$.

Figure 2.12-3 is in fact a fixed frequency synthesizer. The closed loop gain function of the ith circuit, denoted $H_i(S)$ is:

$$H_i(S) = \frac{G_iF_i(S)/K_iS}{1 + GiF_i(S)/K_iS} \tag{2.12.1}$$

It can be shown that the noise spectrum of the output signal is:

$$S_\psi(\omega) = K_i{}^2 S_o(\omega) \, |H_i(\omega)|^2 + S_{vi}(\omega) \, |1-H_i(\omega)|^2 \tag{2.12.2}$$

In other words, the contribution of the reference oscillator to the phase noise spectrum of the output carrier is low-pass filtered by $H_i(\omega)$, while that of the VCO is high-pass filtered by $|1-H_i(\omega)|$. Note, that since Fi(S) describes a low-pass filter, equation 2.12.1 gives:

$$Hi(S) \longrightarrow 1 \text{ when } S \longrightarrow 0 \tag{2.12.3}$$

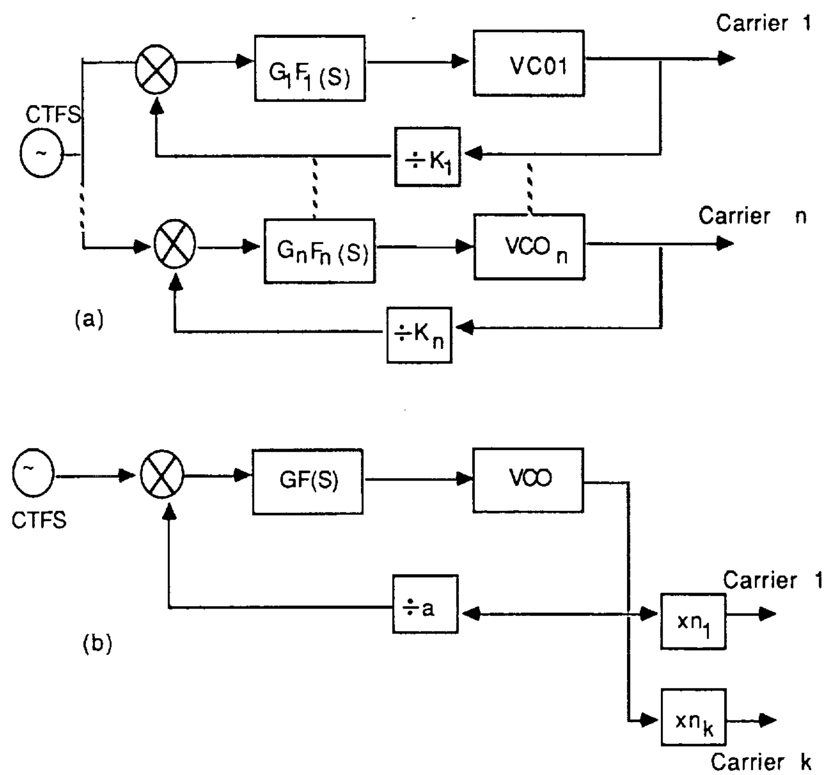

Figure 2.12-3. Two Typical Frequency Generators

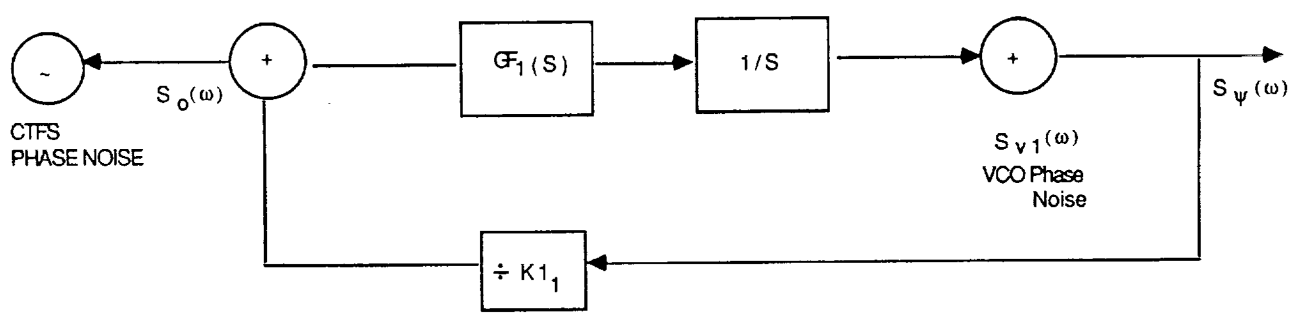

Figure 2.12-4. Phase Noise Model for the Block Diagram 2a.

Since all the single frequency synthesizers of Figure 2.12-3 are using a common reference, all the output carriers are partially coherent, because all possess the phase noise contribution of the common reference. Assuming that the multipliers nl,..,nk are noiseless, the carriers 1 to k of Figure 2.12-3b are fully coherent.

The synthesizer may be fed by a noisy reference, for instance, a reference signal immersed in a white thermal noise of one-sided power spectral density No W/Hz. That part of the thermal noise that penetrates the low-pass filter of the loop modulates the VCO in the same way the error voltage of the loop does, thereby adding phase noise to the output carrier. The contribution of the thermal noise to the phase noise spectrum can be shown to be [Ref. 2-8, eq 8.3.6]:

$$\frac{No}{2P_c} |H(\omega)|^2 \qquad (2.12.4)$$

where, P_c is the received carrier power. The linear phase noise model then becomes that of Figure 2.12-5.

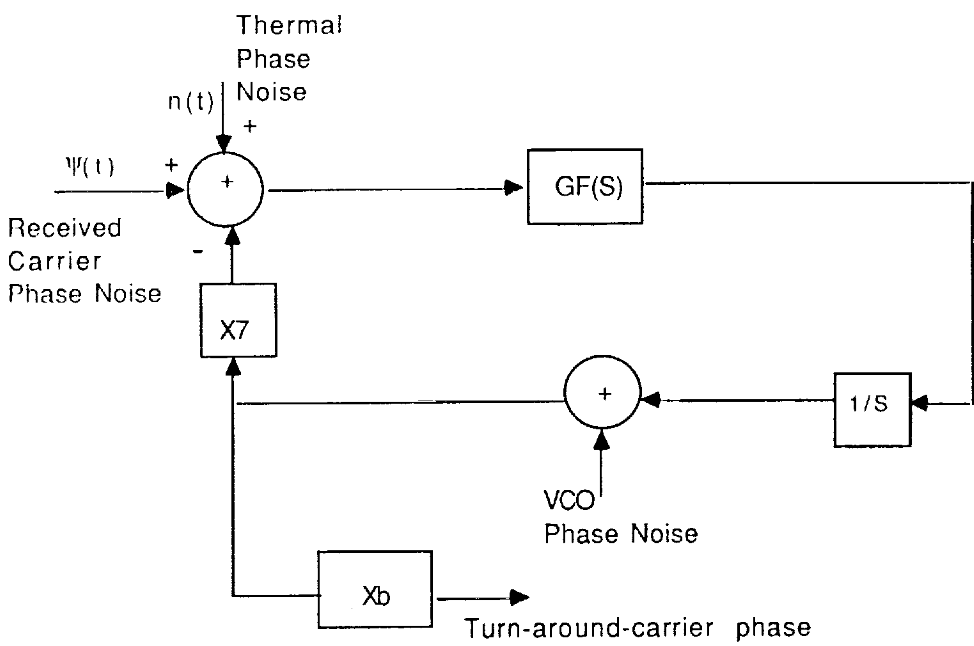

Figure 2.12-5. Linear Phase Noise Model with Thermal Noise

With the harmonic multipliers times r and times b, as shown, the output frequency is now:

$$f_{out} = f_r(b/r) \tag{2.12.5}$$

and the phase noise spectrum is:

$$S_x(\omega) = (b/r)^2\,[S_\psi(\omega) + No/2P_c]\,|H(\omega)|^2 + b^2 S_\upsilon(\omega)|1\text{-}H/(\omega)|^2 \tag{2.12.6}$$

where $S_\psi(\omega)$ and $S_v(\omega)$ are the phase noise spectrum of the input (reference) signal and the VCO respectively. The phase noise variance is:

$$\sigma_x^2 = 2/2\pi \int_0^\infty S_\psi(\omega)d\omega$$

Figure 2.12-2 shows more details of the pilot system on board TDRS. Figure 2.12-6 shows the block diagram and Figure 2.12-7 the corresponding phase noise model.

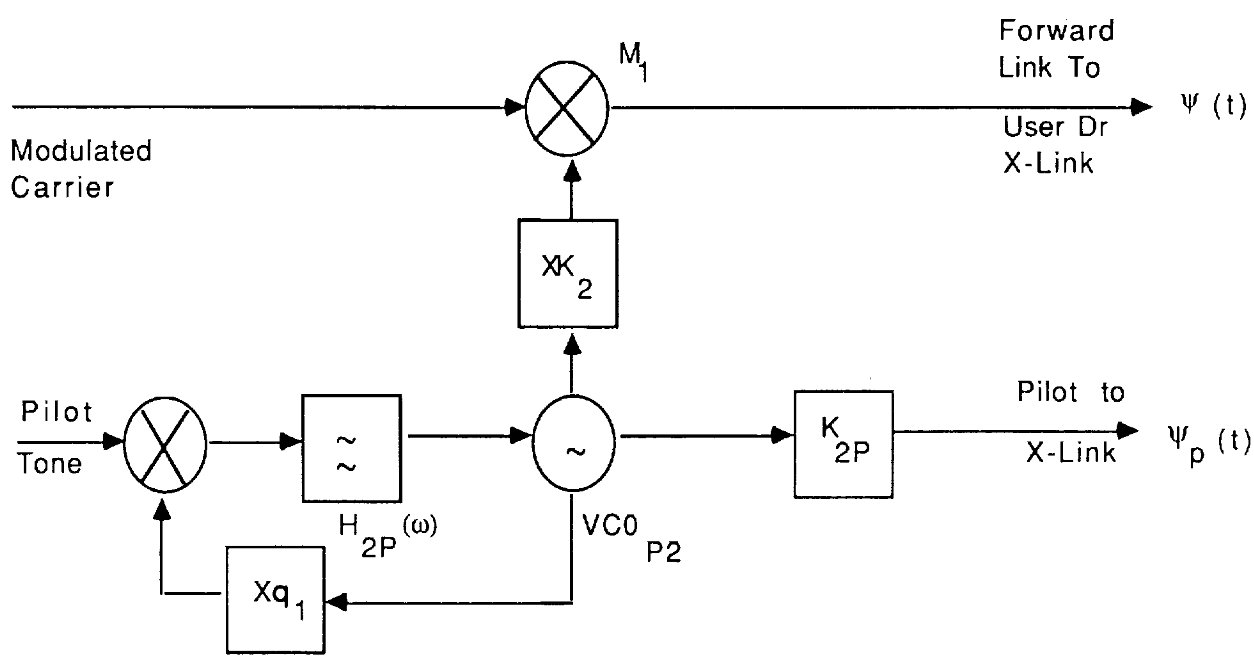

Figure 2.12-6. Pilot Subsystem On-Board TDRS

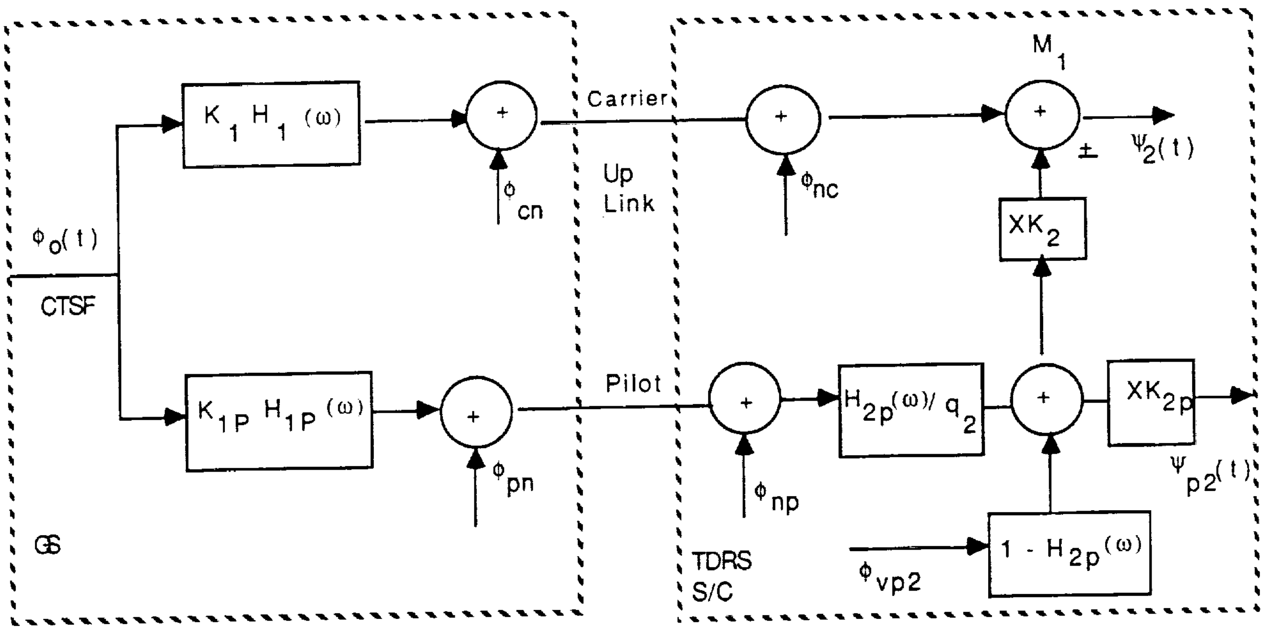

Figure 2.12-7. Linear Phase Noise Model for the Pilot Subsystem

Legend for Figure 2.12-7:

K_1 is the divider in the carrier generating loop (GL) in the GS.
K_{1p} is the divider in the pilot GL in the GS.
$H_1(\omega)$ is the closed-loop gain function in the carrier GL in the GS.
$H_{1p}(\omega)$ is the closed loop gain function of the pilot GL in the GS.
ϕ_{cn} is the noncoherent part of the carrier phase noise (typically, mostly the noise of the VCO in the carrier GL).
ϕ_{pn} is the noncoherent part of the pilot phase noise.
ϕ_{p2} is the phase noise of the VCO in the pilot tracking-loop on-board TDRS.
$H_{2p(\omega)}$ is the closed loop gain function of the pilot tracking loop on board.
ϕ_{nc} is the thermal noise contributed by the carrier uplink
ϕ_{np} is the thermal noise contributed by the pilot uplink

Therefore:

$$S_{\psi 2}(\omega) = K_1{}^2 S_o(\omega)|H_1(\omega)|^2 |1-r_2 H_{2P}(\omega)|^2 +$$
$$+ S_{v1}(\omega)|1-H_{1P}(\omega)|^2 + (No/2P_p)_u + S_{v2}(\omega)K_2{}^2 |1-H_{2P}(\omega)|^2$$
$$+ [(No/2P_p)_u + S_{v1p}(\omega)|1-H_{1P}(\omega)|^2] \cdot |H_{2P}(\omega)|^2 (K_2/q_2)^2$$

Where:

$$r_2 = \frac{H_{1P}}{K_1} \times \frac{K_2}{q}$$

and $S_{v1}(\omega)$ and $S_{v1p}(\omega)$ are the noncoherent parts of the phase noise spectrum of the carrier and pilot GL respectively.

Note that the reference phase noise spectrum is multiplied by the factor $|1-r_2H_2(\omega)|$. This is because the two signals mixed by the mixer M1 (following which, in TDRS the lower sideband is recovered) have a coherent phase noise component contributed by the reference oscillator. Part of this common component, as determined by $H_{2p}(\omega)$ and the factor r_2, is subtracted by M1. (This procedure is strictly correct, of course, only if the propagation delay through the uplink is equal for the carrier and pilot signals).

The effect of the "pilot controlled" downconversion scheme is, therefore, to filter out some of the low frequency phase noise of the reference oscillator at the expense of adding the thermal noise and the noncoherent noise of the pilot link. Since the thermal noise of the pilot link can be made sufficiently small (by allocating sufficient power to the pilot signal), and since the noncoherent noise of the VCOs involved is high-pass filtered, the main contributor of low frequency phase noise is probably the CTFS. Consequently, a substantial reduction in low frequency phase noise should be possible for large values of r_2 (as the case happens to be for the S-band forward services).

When two TDRS spacecrafts operate in cascade, both the forward service signal and the pilot have to be relayed through spacecraft 1 and the X-link to spacecraft 2 as shown in Figure 2.12-6. The phase noise spectrum of the pilot at the input to the X-link can be derived by observation:

$$S_{\psi P2}(\omega) = [K_{1P}^2 S_o(\omega)|H_1(\omega)|^2 +$$
$$+ S_{vP1}(\omega)|1-H_{1P}(\omega)|^2 + (No/2_{Pp})_u] \, |H_2(\omega)|^2 (K_{2P}/q_2)^2 +$$
$$+ S_{vP2}(\omega) K_{2P}^2 |1-H_2(\omega)|^2$$

We now assume that the carrier is upconverted in TDRS 1 by the mixer M1 to the X-link frequency band (WSA) and then downconverted in TDRS 2 by M2 to the user forward service frequency. The pilot tone tracking loop in the second spacecraft, which tracks the pilot received through the X-link, is similar in construction to the one we have shown in Figure 2.12-6, but it might have different parameters due to the different frequency and dynamics of the X-link. In the following equations all the parameters of TDRS 2 will be marked with the subscript 3, while those of TDRS 1 will be marked as before with the subscript 2.

The components of the phase noise spectrum $S_{\psi}(\omega)$ of the forward service carrier transmitted by TDRS2 are shown in Table 2.12-1.

Table 2.12-1. Spectral Phase Noise Components of an X-Link Relayed Forward Service Signal

Noise contributed by the GS's CTFS	$S_o(\omega)\vert K_1H_1(\omega) + K_{1p}H_{1p}(\omega)H_{2p}(\omega)(K_2/q_2) - \frac{K_{1p}K_{2p}K_3}{q_2q_3} H_{1p}(\omega)H_{2p}(\omega)H_{3p}(\omega)\vert^2$
Noise contributed by the VCO of the carrier GL at the GS	$S_{v1}(\omega)\vert 1 - H_1(\omega)\vert^2$
Thermal noise of the carrier uplink	$\left(\frac{N_o}{2_{pc}}\right)_\mu$
Noise contributed by the pilot VCO on-board ATDRS 1	$S_{2p_2}(\omega)K_2^2\vert 1 - H_{2p}(\omega)\vert^2$
Phase noise injected by M1 (not including the "coherent noise")	$\left[\left(\frac{N_o}{2P_p}\right)_\mu + S_{v1p}(\omega)\vert 1 - H_{1p}(\omega)\vert^2\right]\vert H_{2p}(\omega)\vert^2\left(\frac{K_2}{q_2}\right)^2$
Thermal noise in the X-link	$\left(\frac{N_o}{2_{pc}}\right)_x$
Phase noise injected by M2 (not including the coherent noise)	$\left[S_{vp1}(\omega)\vert 1-H_1(\omega)\vert^2 + \left(\frac{N_o}{2p_p}\right)_\mu\right]\vert H_{2p}(\omega)\vert^2\left(\frac{K_{2p}}{q_2}\right)^2\left(\frac{K_3}{q_3}\right)^2\vert H_{3p}(\omega)\vert^2 +$ $+ S_{vp2}(\omega)K_{2p}^2\vert 1-H_2(\omega)\vert^2\left(\frac{K_3}{q_3}\right)^2\vert H_{3p}(\omega)\vert^2 +$ $+ S_{vp3}(\omega)K_3^2\vert 1-H_{3p}(\omega)\vert^2\left(\frac{N_o}{2P_p}\right)_x\vert H_{3p}(\omega)\vert^2\left(\frac{K_3}{q_3}\right)^2$
$S_{\psi 3}(\omega)$	Total

Note that:

$$F_f = F_o\,[K_1 + K_{1p} \times K_2/q2 - K_{1p} \times K_{2p} \times K_3/(q2 \times q3)]$$

Where:

F_f is the user forward service frequency

and F_o is the frequency of the CTFR in the GS.

2.13 EFFECT OF SUN PASSING THROUGH THE SPACE/GROUND LINK SYSTEM FIELD OF VIEW

Two issues to be considered are the effect of sun on the ATDRS uplink receivers, and the effect of sun on the ground station's downlink receivers. The sun's intense heat affects the operating noise temperature of the receivers when it passes through the field of view of the antennas or even when a significant sidelobe is directed toward the sun. It is necessary to determine the effect the sun is expected to have on the performance of ATDRSS at any given time. In addition to the timing and magnitude it is important to know the expected duration of the degradation in performance. Since these parameters depend on the location of the ground station and the ATDRS involved, we need to repeat this calculation for each intended ATDRS location and each ground station considered. We will deal with the downlink first.

2.13.1 Effects of the Sun on the Downlink Performance

The SOW does not provide us with specific information related to the radiation pattern and losses of the ground station antennas nor do we possess information regarding the operating noise temperatures of the ground receivers. Therefore, the most we can do is to investigate the movement of the CONUS defined by the sun and the ground station about the line connecting the ground station and the ATDRS. Depending on the location of the ground station and the ATDRS, it might be the case that the above mentioned CONUS never approaches the ATDRS. As an example, we have chosen a 1° separation as a criterion for good ATDRS versus ground station location (as seen from the earth, the mean angular size of sun is 0.533°). As shown in Figure 2.13-1, the downlink performance could be degraded by about 17.2 dB.

2.13.2 Effects of Sun on the Uplink Performance

Contrary to the downlink case, the sun cannot possibly position itself precisely on the extension of the line connecting ATDRS and a ground station, because a ground station is located inside the globe contour as seen from the ATDRS. Still the degrading effect of the sun might be significant, if the angle between the lines connecting the ATDRS to a ground station and the ATDRS to the center of the sun is of the same order of magnitude as the beamwidth of the ATDRS uplink antenna. There are two issues that must be resolved:

a. The astrogeometric issue, namely, for a given set of ground station and ATDRS locations, what is the minimal angular distance between these lines?

b. The uplink antenna issue, namely, what is the radiation pattern, side lobe level, pointing accuracy etc., that we can safely assume (both for the fixed and mobile ground station?

1. Geometrical Description

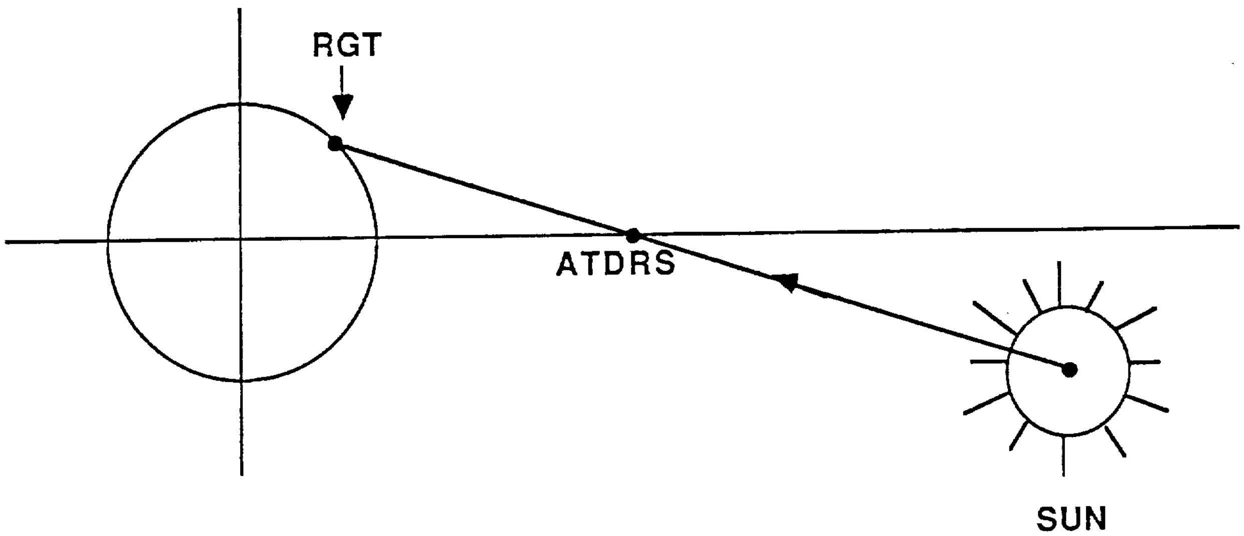

2. Facts and assumptions:

- The angular Diameter of the Sun: $\alpha = 0.533°$
- The Beamwidth of the Ground Station Antenna: $< \alpha$
- The Radio Noise Temperature of the sun over the Downlink Band: $T_{sun} \approx 12{,}500°K$
- Atmospheric Absorption: 0 dB (worst case)
- Fraction of Power Received through the Main Beam to total Received Power: 100%
- Background noise of sky over Downlink Band: 0° K
- Transmission Losses In Antenna and Cable System: a= 0.794 → 1 dB

3. Conclusion:

System Noise Temperature (Based on LNA N.F. of 1.6 dB): 189° K
System Noise Temperature with Sun: 9987° K
"Sun Loss": 10 Log (9987/189) = 17.2 dB

Frequency of occurence and duration wil be studied.

Figure 2.13-1. Effect of the Sun on Downlink

Our analysis is limited to addressing the astrogeometric issue, cited in (a) above. The radio temperature of the sun for the uplink frequency range is:

27.5 to 31 GHz i.e., the wavelength (λ) is in the order of

$$\lambda = (3 \times 10^8)/(30 \times 10^9) = 0.01 \text{ m}$$

For the downlink the frequency range is:

17.7 to 21.2 GHz i.e.,

$$\lambda = (3 \times 10^8)/(20 \times 10^9) = 0.015 \text{ m}$$

According to "Astrophysical Quantities" by C.W.Allen, Third edition, p.192: at 27.5 GHz, T_a = 8900°K while, at 17.7 GHz, T_a = 12,500°K where, T_a is the apparent temperature i.e., the black body temperature of the visible disk (of the sun), which produces the same flux density as the sun. In general, the noise temperature decreases with increasing temperature, so that the low edge of either band is "hotter." The performance degradation due to the sun for uplink communications is about 8.4 dB as shown in Figure 2.13-2.

2.13.3 Frequency and Duration of Sun Effects

Figure 2.13-3 plots the angle of the ground terminals from geostationary earth orbit as a function of their latitudes. Based on the observation that the worst case durations of sun effects happen when the subsatellite point is on the same longitude as the ground station, we proceed to evaluate the worst case frequencies and durations of sun effects.

Figure 2.13-4 plots the sun declination versus days from March 21 (when the sun is directly above the equator). From this figure, we note that the period of sun effects is larger for the ground stations that are closer to the equator. The frequency is unaffected by the location of the ground station, except for the fact that the time of the year at which sun effects occur varies according to the location of the particular ground station. We assume here that the beamwidth of all the ground stations is the same.

a. Effect of the sun is limited to RGTs located at (or near) 10° elevation angle.
b. Important parameters
   1. Uplink beamwidth: ≈0.3°
   2. Pointing error: 0.15° max (est.)
   3. Angular diameter of the sun: 0.533°
   4. Noise temperature of the sun: ≈8,900 K
   5. Atmospheric attenuation at 0° elevation: ≈28 dB (one way) at 30 GHz

Geometrical Description

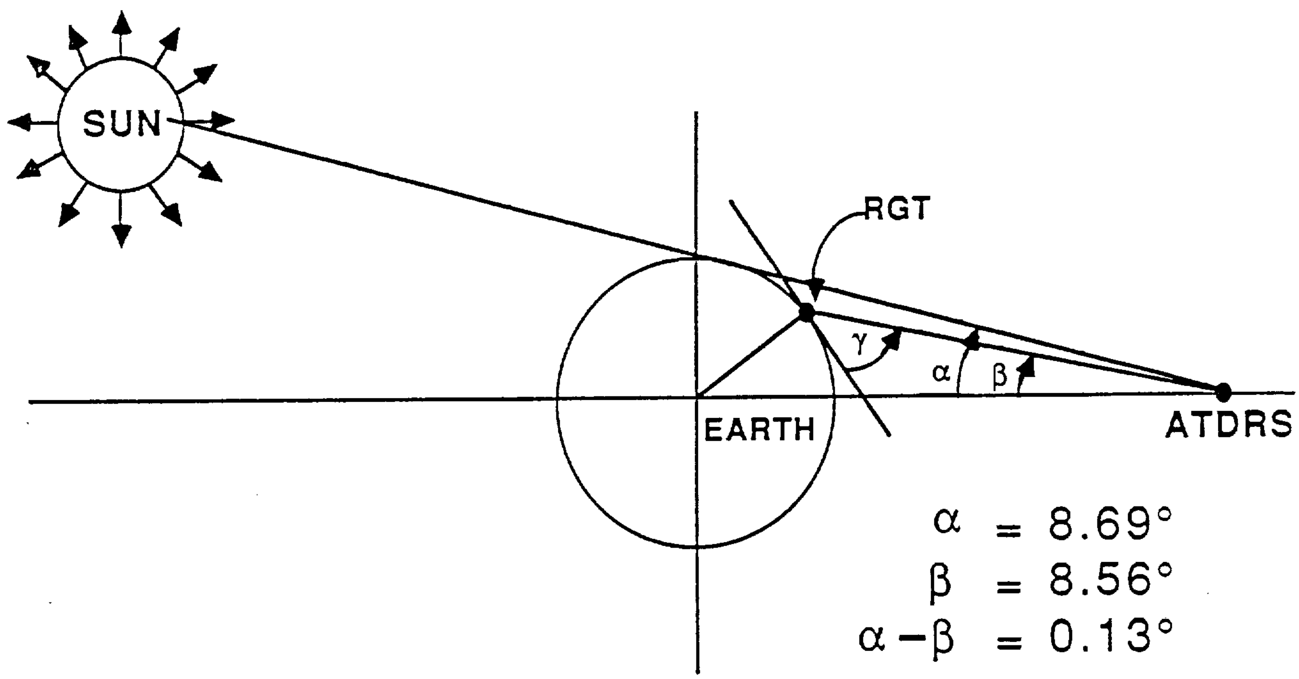

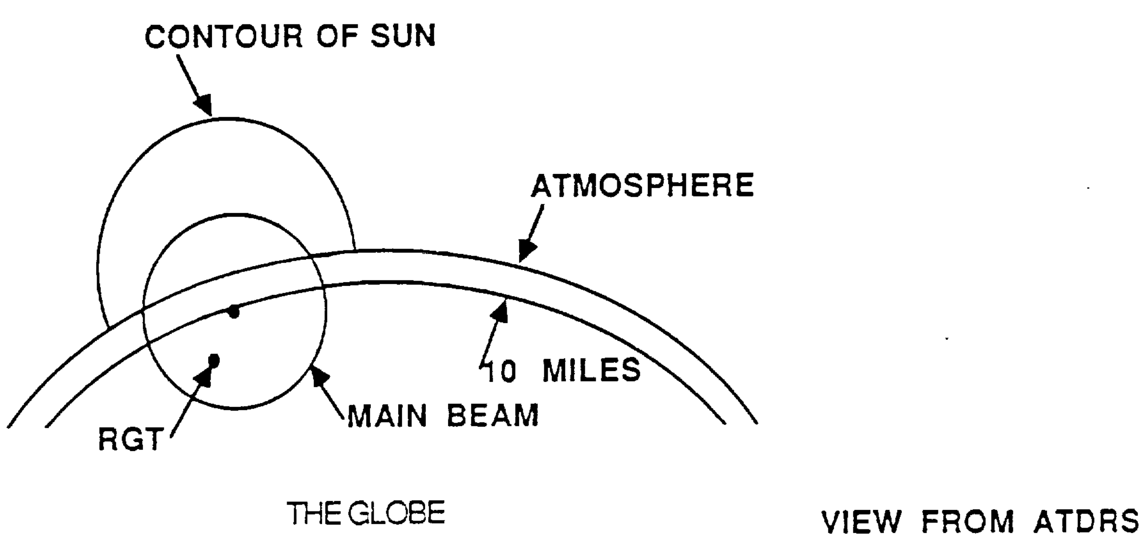

Figure 2.13-2. Effect of the Sun on Uplink (27.5 to 31 GHz)

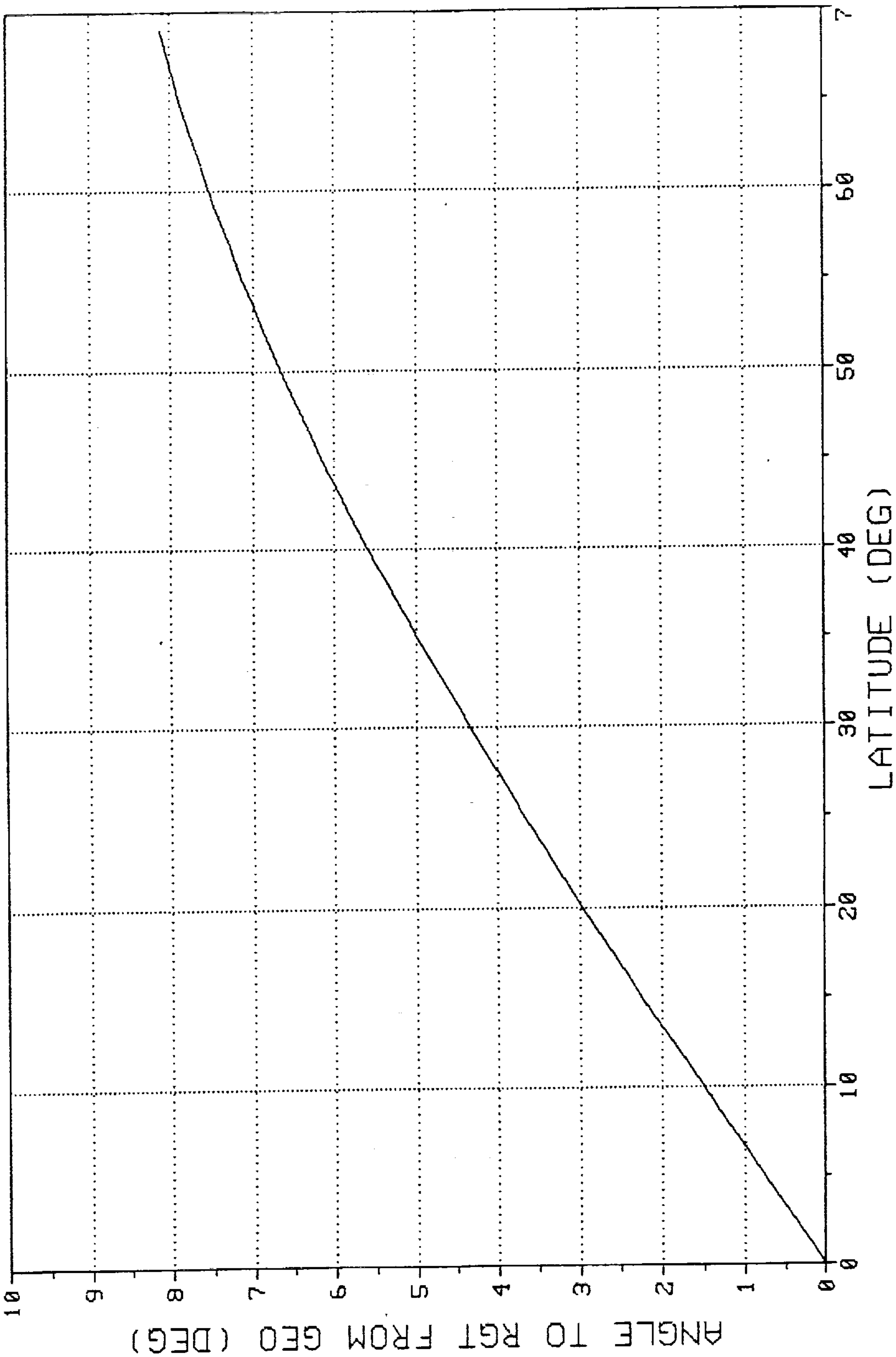

Figure 2.13-3. Angle of Ground Terminals from Geostationary Earth Orbit as a Function of Their Latitudes

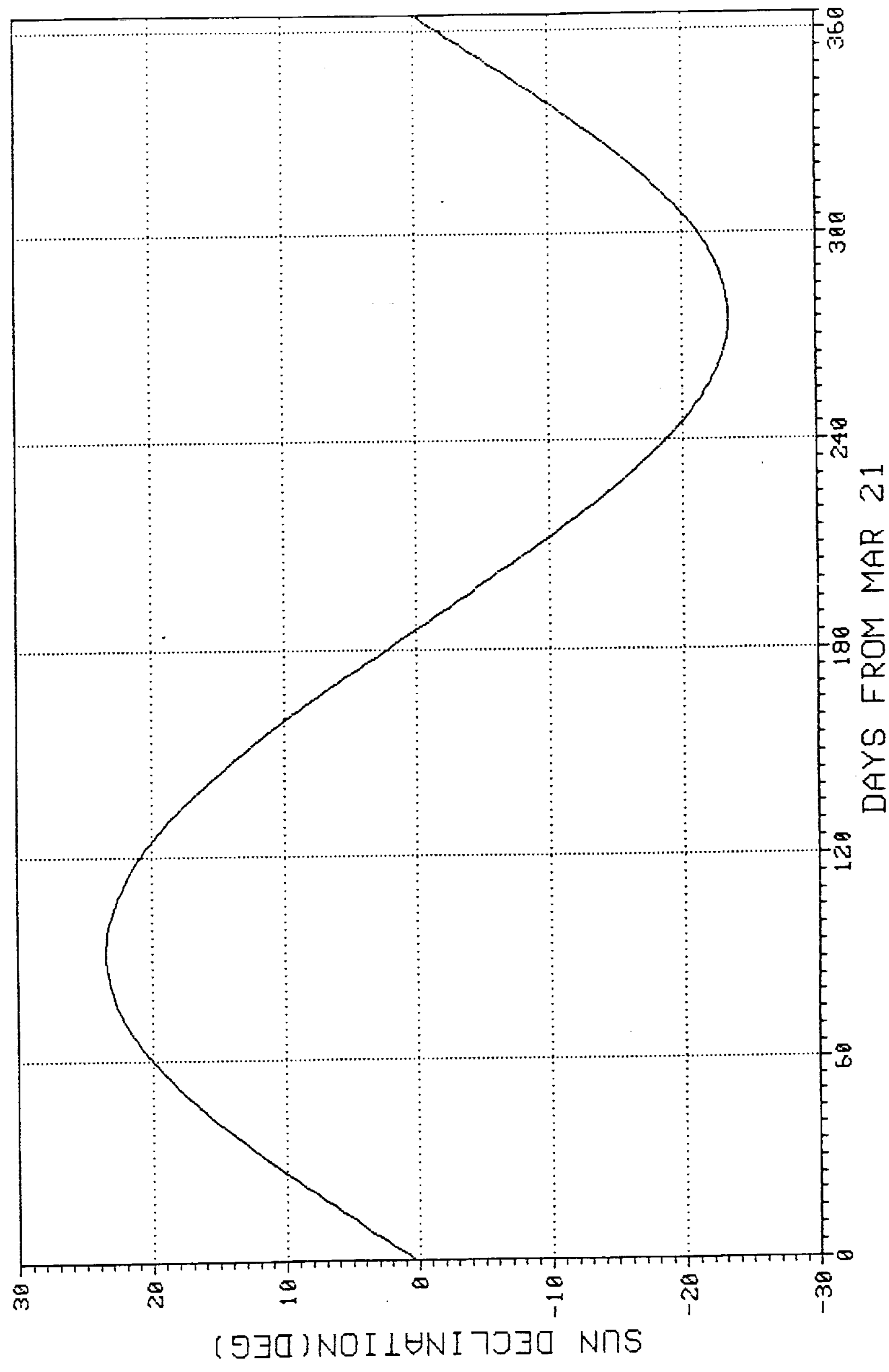

Figure 2.13-4. Sun Declination

c. Analysis
   1. The center of the beam may be directed at a visible part of the sun.
   2. The blocking effect of the atmosphere is small above 10 miles
   3. 10 miles constitute only 0.024° angular separation.

d. Conclusions
   1. In the worst case, one-half the main beam app may have a clear view of the sun.
   2. System noise temperature: 571.5 K
   3. System noise temperature with sun: 3989.6 K
   4. Sun loss: 8.44 dB
   5. Frequency of occurrence and duration will be studied.
   6. Effect on acquisition/tracking will be studied.

Because interference effects are significant during sun effects (see the previous subsection), we need to consider the first sidelobe also in addition to the main lobe. Of all the CONUS sites, JSFC has the lowest latitude and therefore encounters the sun effects for the maximum duration. We therefore consider JSFC for further study as the worst case CONUS location in view of sun effects.

It is to be noted here that for the uplink sun interference scenario, the sun's declination on only one side of the ground terminal is to be considered, because when the sun is on the other side, the earth is blocking the sun and would therefore prevent the interference from happening. However, for the downlink interference scenario, the interference effects from both sides must be considered.

For the downlink interference scenario, assuming a ground station antenna beamwidth is smaller than the angular diameter of the sun (0.533°) and making allowance for the first sidelobe on both sides of the main lobe of the beam, the interference angle can be a maximum of 1°. Noting that the JSFC latitude is 29.53° N, we have the angle from GEO (see Figure 2.13-1) for this case is roughly 4°. For this case, from Figure 2.13-2, we note that the exact periods of the downlink sun effects can be deduced by looking up sun declinations of - 4° $\pm$1°. It appears that the downlink sun effects for JSFC occur during the periods from 194 to 198 days and from 352 to 356 days from the March 21. On each of these 10 days sun effects are predominant for a duration of 8 minutes (based on the observation that sun declination changes at 1°/4 minutes).

For the uplink sun interference scenario, sun declinations of 4° to 5° are to be considered. This appears to happen (see Figure 2.13-2) during the days 10 to 12, and from 173 to 175 days from March 21. On each of these 6 days, sun effects are encountered for a duration of 4 minutes.

2.14 COMPONENT SUSCEPTIBILITY TO SPACE RADIATION ENVIRONMENT

Various electronic components that may be used for the ATDRSS hardware include RF, linear, and digital circuits. Table 2.14-1 lists the inherent radiation hardness levels for various circuit families for surviving the specified ranges of total dose, dose rate, and neutron fluency levels.

For nonmilitary applications, the most important radiation hardness parameter is the total dose level that the circuits need to survive. Figure 2.14-1 and Table 2.14-2 show the inherent total dose levels tolerated by various circuit families. Typically, for nonmilitary applications, a total dose level of 100 krads is specified. RF power devices such as TWTAs have no radiation susceptibility problems. Other RF devices such as the SSPAs, LNAs, mixers, oscillators, and switching circuits can be implemented with inherently radiation-hard technologies such as the gallium arsenide technology. Some linear and digital circuit families do not survive the specified total dose levels of 100 krads. It is, however, possible to shield such devices to make them survivable for total dose levels of 1 Mrads and above.

Table 2.14-1. Inherent Hardness Levels for Discrete Semiconductor Devices

Device Type	Total Gamma Dose-Rads Si	Gamma Flux-Rads Si/sec Permanent	Gamma Flux-Rads Si/sec Upset	Neutron Flux-n/cm^2
Germanium Diode	$>10^4$	$>10^9$*	10^8-10^9	$>10^{12}$
Silicon Diode	10^5-10^6	$>10^9$*	10^9-10^{10}	$>10^{13}$
Zener Diode	10^5-10^6	$>10^9$*	10^9-10^{10}	10^{13} (ΔV_z<10mV)
Schottky Diode	$>10^6$	$>10^{10}$	$>10^9$	$>10^{15}$
Fast Recovery Diode (PIN)	$>10^6$	$>10^{10}$	10^8-10^9	$>10^{15}$
Current Reg. Diode (FET)	$>10^4$	$>10^{10}$	10^8-10^9	$>10^{11}$-10^{12}
SCR's	$>10^4$	$>10^{10}$*	10^4-10^5	10^{11}-10^{12}
Triac's	$>10^4$	$>10^{10}$*	10^4-10^5	10^{11}-10^{12}
Germanium Transistor	-10^4	$>10^{10}$*	10^7-10^9	10^{11} - 10^{12}
Silicon Transistor	$>10^4$	$>10^9$*	10^7-10^9	10^{11} - 10^{12}
Darlingtons	$>10^4$	$>10^{10}$*	10^7-10^9	10^{11} - 10^{12}
FET's	$>10^4$	10^{10}	10^8-10^9	10^{11}-10^{12}
MOSFET's	10^4-10^5	$>10^{10}$	$>10^{10}$	$>10^{15}$
GaSFET's	$>10^6$	10^{10}	-10^9	$>10^{14}$
UJT's	$>10^4$	10^{10}	10^7-10^9	$>10^{12}$

Table 2.14-1. Inherent Hardness Levels for Discrete Semiconductor Devices (Continued)

Device Family	Neutron n/cm^2	Gamma Flux $\frac{rad(Si)}{sec}$ Permanent	Gamma Flux $\frac{rad(Si)}{sec}$ Upset	Total Dose rad(Si)
ECL	$>10^{15}$	$>10^{11}$	$*>10^{8}$	$>10^{7}$
SSI CMOS	$>10^{15}$	10^{9}	$*10^{8}$	10^{4}
LSI CMOS	$>10^{15}$	10^{9}	$*10^{7}$	$*10^{3}$
TTL	$>10^{14}$	$>10^{10}$	$*10^{7}$	10^{6}
STTL	10^{15}	$>10^{10}$	$*10^{7}$	10^{6}
LTTL	$>10^{14}$	$>10^{10}$	$*5x10^{7}$	10^{6}
LSTTL	$>10^{14}$	$>10^{10}$	$*10^{8}$	10^{6}
HTTL	$>10^{14}$	$>10^{10}$	$*10^{7}$	10^{6}
PMOS	$>10^{15}$	$>10^{10}$	$*10^{5}$	$*10^{3}$
NMOS	$>10^{15}$	$>10^{10}$	$*10^{5}$	$*10^{3}$
LED's	10^{13}	$>10^{10}$		10^{5}
SCR	$*10^{10}-10^{12}$	$>10^{10}$	$*10^{3}$	10^{4}
Analog Linear IC's	$*10^{12}-10^{12}$	$>10^{10}$	$*10^{6}$	$10^{4}-10^{5}$
Silicon Diodes	$>10^{13}$		$10^{9}-10^{10}$	$10^{5}-10^{6}$
Zener Diodes	$10^{13}(\Delta V_z<10mV)$		$10^{9}-10^{10}$	$10^{5}-10^{6}$
Linear Hybrid	$10^{12}-10^{13}$	$10^{9}-10^{10}$		$10^{4}-10^{5}$

*Critical characteristics have parameters which must be considered on an individual basis.

Sources: AFWL-TR-78-5
DNA 3246F

TOTAL DOSE DEGRADATION

- Mechanism Is Charge Trapped In Device Oxide Layers
- Voltage Changes
- Gain Changes
- 10^4 to 10^7 rad (Si)
- Longer Life Space Systems Require Higher Hardness Levels

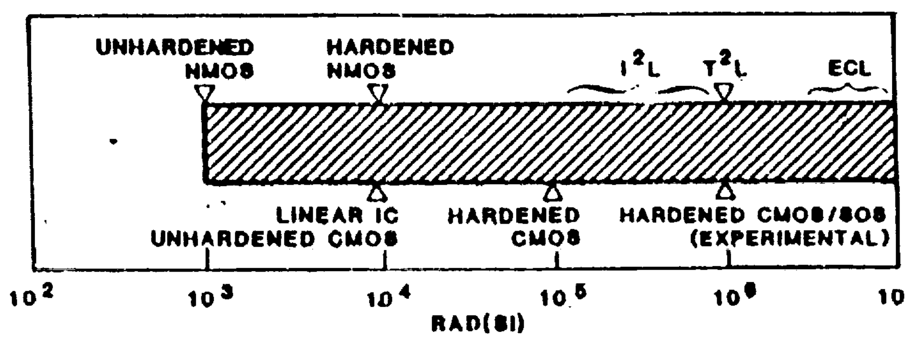

- SEMICONDUCTOR DEVICE MALFUNCTION RANGE IS $10^3 - 10^7$ RAD(SI), DEPENDING UPON CONSTRUCTION
- VERY DIFFICULT TO HARDEN SYSTEM ABOVE 10^6 RAD(SI) (EXCEPT BY SHIELDING)

Figure 2.14-1. Total Dose Degradation

Table 2.14-2. Total Dose Thresholds for Various Electronic Technologies

Technology	Manufacturer
CMOS bulk	Various
RAD hard CMOS	Sandia, Harris, NSC, RCA Honeywell
HCMOS	NSC, MOT others
CMOS/SOS	RCA
RAD hard CMOS/SOS	RCA
NMOS	Various
HMOS I	INTEL
HMOS II	INTEL
HMOS III	INTEL
DMOS	NEC
VMOS	AMI
PMOS	Various
PMOS/SOS	Various
MNOS hardened	Sandia, NCR Sperry
MNOS/SOS hardened	
SNOS	Hitachi
MNOS Commercial	

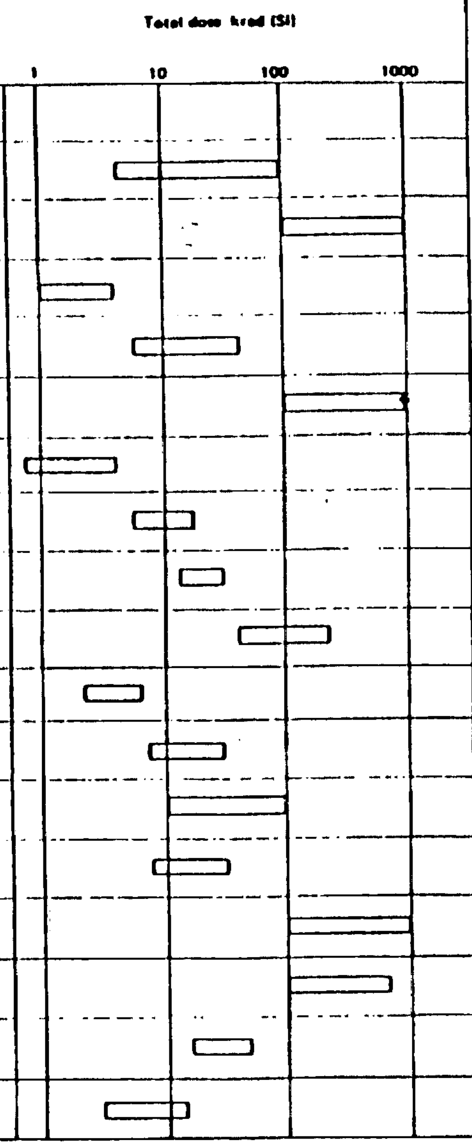

Technology	Manufacturer
Standard TTL	Various
Low-power Schottky TTL (LST²L)	Various
Rad hard (LST²L)	Various TI, Harris
Fairchild Adv-Schottky TTL (FAST)	Fairchild Motorola Signetics
Adv-Schottky logic (ASL)	TI
Integrated Schottky logic (ISL)	Raytheon
Emitter-coupled logic (ECL)	Various
Current injection logic (I²L)	TI
Isoplanar current injection logic (I²L)	Fairchild
Isoplanar Z process ISO-Z	Fairchild
Current mode logic (CML)	Honeywell
Implanted oxide (IMOX)	AMD Various
Triple-diffused (3-D)	TRW
Collector-diffused isolation (CDI)	Ferranti
Dielectric isolated TTL	Harris Various

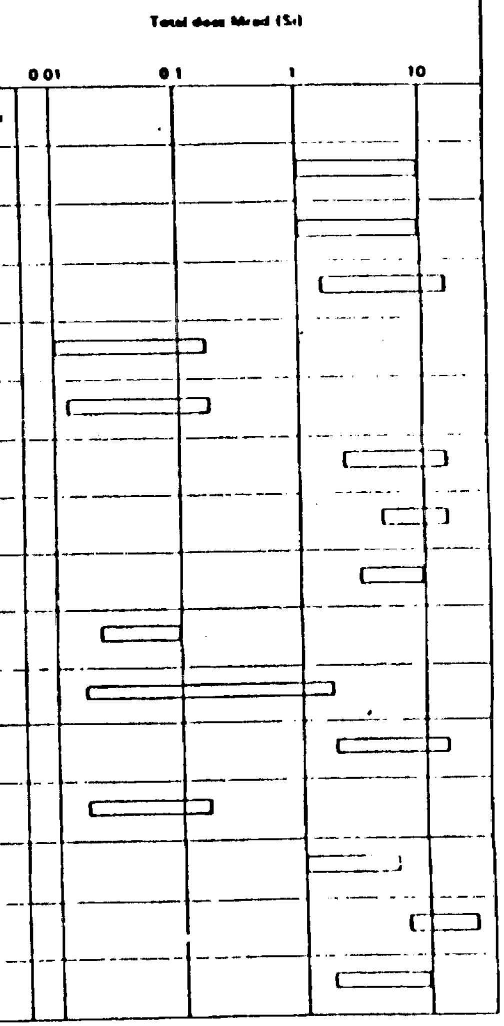

2.15 IN-SPACE SERVICEABILITY CONSIDERATIONS

For all future NASA missions including the ATDR satellite systems, the plans call for the repair or replacement of defective parts in space wherever possible. All future NASA satellites must be designed to facilitate easy isolation and replacement of defective parts.

Modular designs are required of all the subsystems that will possibly require in-space repair/replacement. This, however, will increase the initial cost of the satellites by as much as 12% [ref. 2-9, 2-10, 2-11]. On the other hand, there are indications that spacecraft lifetime extensions beyond 15 years require extensive redesign of the spacecraft to withstand the increased total dosage of radiation exposure [ref. 11]. The increase in mass and the design and manufacturing costs involved in the redesign may be greater than converting to a serviceable spacecraft.

It is therefore very important to identify the subsystems that may require repair/replacement prior to the maximum life expectancy of the spacecraft. An analysis of the ATDRSS system is performed to determine which subsystems can be serviced in space. The subsystems are analyzed to determine the expected lifetime, failure modes, and the possibility of being serviced. The first two criteria are based on historical experience while the last is based on an evaluation of the individual subsystem designs.

The designs are analyzed to determine their adaptability to a modular design, the number and complexity of interfaces required, and compatibility with the servicing/repairing equipment. The results of the analysis are tabulated in Table 2.15-1.

At the end of a 12-year mission, there is a probability of less than 50% that the entire spacecraft will be able to complete the mission. The biggest contributing factor to this figure is the payload.

A large number of failures occur in the TWTAs. As the K-band transponders transition from being TWTAs to SSPAs, the reliability of the payload can be expected to increase significantly. It is therefore important to consider modular designs for permitting easy serviceability/replaceability of these subsystems. The switch-matrices may also have high failure rates; however, the extensive number of RF interconnections will perhaps preclude the possibility of applying in-space servicing concepts to these components. These components are therefore designed to incorporate the required redundancy for meeting the spacecraft lifetime requirements.

Table 2.15-1. Analysis of Serviceable Components on Baseline Satellite

Bus Component	Life Limitations	Cycle Limitations	Consumable Limitations	Technology Limitations	Servicing Required?
Structure				Material properties.	None
Propulsion					
Tanks	Blocked orifices		Fuel		Refuel
Fuel lines	Clogged lines				None
Thrusters	Blocked orifices	Worn valves		I_{sp} of fuel	None
Power					
Generation	Radiation	Thermal cycles of connections.		Cell efficiency	None
Storage	Cell depletion			Batteries; NiH and NaS.	Replace
Distribution	Cycling of relays			Converter design	Replace
Attitude Control					
Sensors	Sensor degrades	Moving parts wearout.		Sensors	Replace
Actuators		Moving parts wearout.			Replace
TT&C	Aging of electronics			Solid state designs, transmitter.	None
Thermal	Aging of coatings and blankets				None
Central electronics	Aging of electronics			Data storage, microprocessors	Replace
Solar array drive		Moving parts wearout.			None
Payload					
Antennas				Materials	None
Transponders	TWTA wear out SSPA aging	Infant failure		Replace TWTAs with SSPAs.	Replace
Switch Matrices	Switch failure rates require redundant designs				None

2.16 THERMAL CONTROL CONCEPTS

The baseline thermal control concepts are:

a. The electronic module containing all the electronic components including the transmitters, receivers, switch matrices, and microprocessors will be boxes of truss structures that contain panels constructed of aluminum faceskins covering an aluminum honeycomb core. Variable conductance heat pipes (VCHP) are embedded in the panels. All electrical and electronic components are mounted to the interior of the panels. The exterior of the panel will contain optical solar reflectors (OSRs). All surfaces not covered in OSRs and the truss structure will be covered by multilayer aluminized Kapton multilayer blankets. A heater system will be employed. A tradeoff of required electronic module radiator area (a function of module dissipation for various spacecraft locations, sun angles) is indicated by Figures 2.16.1 through 2.16-3.

b. The beam waveguide assembly is internal to the dual-axis electronic module, which will be covered by aluminized Kapton multilayer blankets. No heater system will be employed for thermal control of these assemblies (unless mounting of the transponder assemblies is desired).

c. The electromechanical systems will employ a thermistor controlled heater system and will employ a multilayer blanket system where the two-axis movement will allow.

d. The antenna reflector system will have aluminized Kapton multilayer blankets attached to the back side of the main reflector and on the concave side of the subreflector. All other surfaces will be coated with white paint to act as a second surface mirror system and to provide diffuse reflections in the solar spectrum. All areas that are to employ multilayer blankets will be examined to determine if the blankets could cause multiple equivalent insulation to other critical spacecraft surfaces. Any blanket that could contribute to such an effect will be painted with a diffuse black coating, which is standard Ford Aerospace practice. All blankets will be grounded to the spacecraft structure.

e. Some of the high-speed electronic circuits may require additional thermal management procedures such as heat-sinking. The application, from gigabit logic in Appendix B, details the design procedures for thermal managing of very high speed GaAs digital IC families.

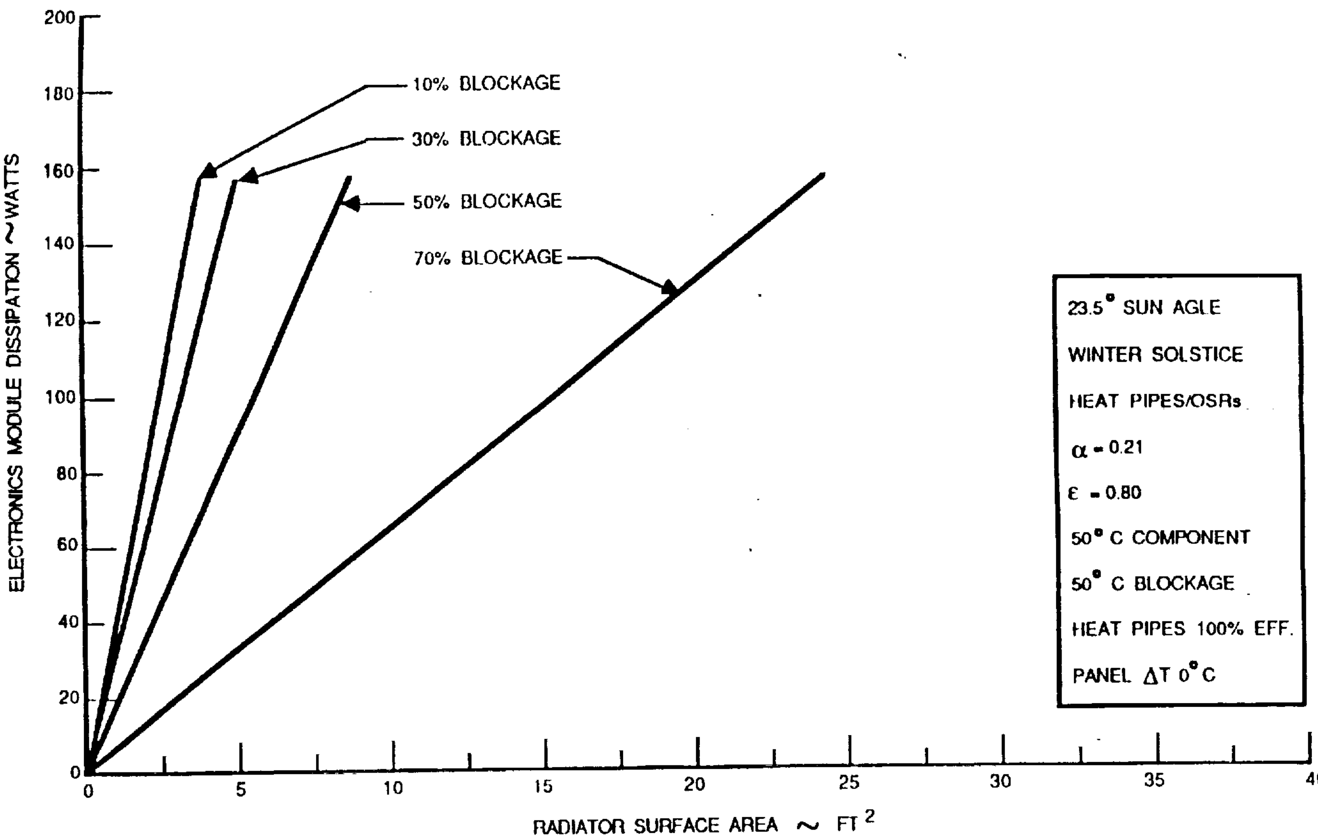

Figure 2.16-1. Module Dissipation in Watts Versus Radiation Surface Area in Ft^2

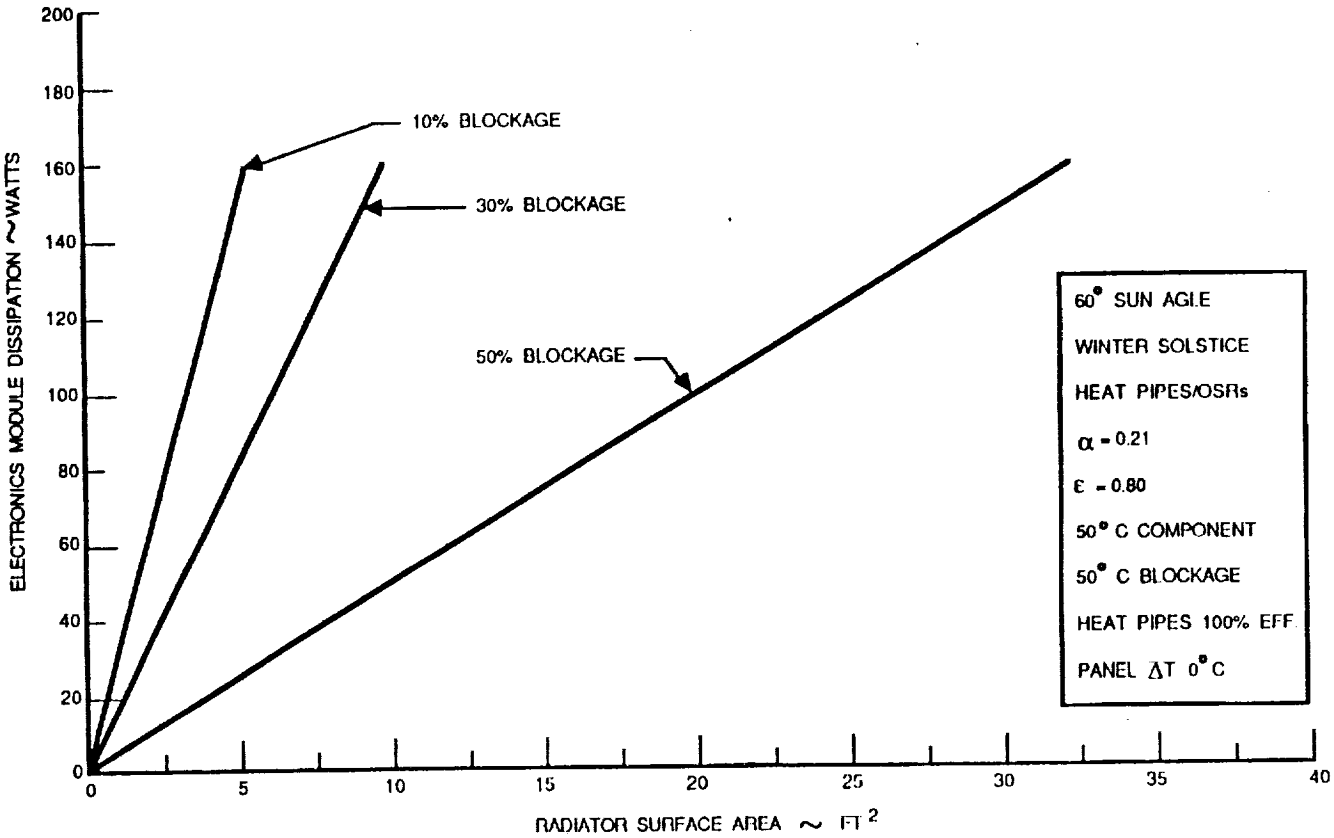

Figure 2.16-2. Module Dissipation in Watts Versus Radiation Surface Area in Ft^2

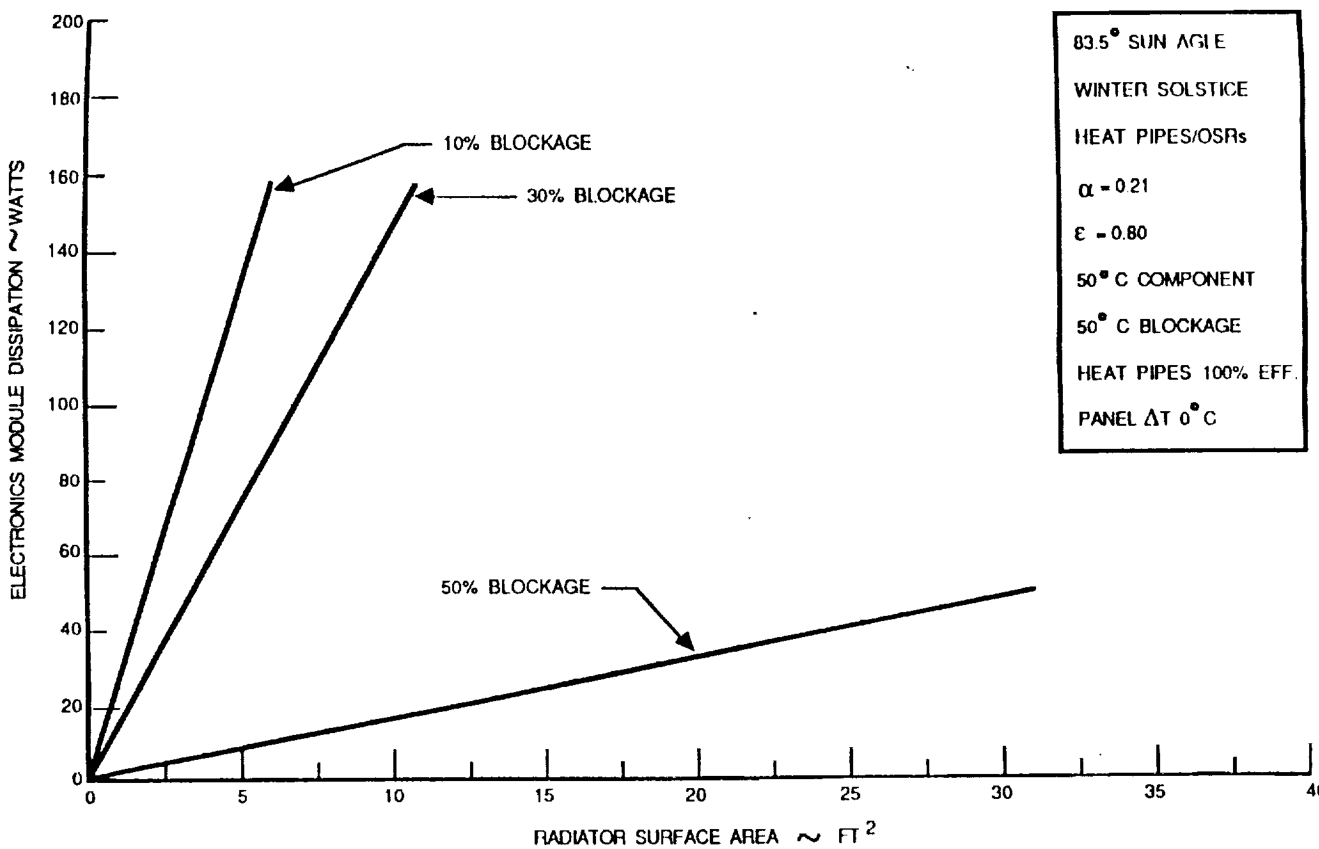

Figure 2.16-3. Module Dissipation in Watts Versus Radiation Surface Area in Ft^2

2.17 NAVIGATION AND ATTITUDE CONTROL SYSTEM ISSUES

The MBA is required to point within 0.15° of nominal to ensure satisfactory performance.

Ford Aerospace's INTELSAT VII communications satellite is currently being designed to maintain the following pointing accuracies:

Pitch = 0.0795°
Roll = 0.0759°
Yaw = 0.1370°

When errors due to yaw excursions and E-W, N-S station drift are included and transformed into E-W and N-S pointing error, the worst case is:

E-W = 0.1191
N-S = 0.1128

The present TDRS spacecraft uses large steerable antennas which make significant attitude disturbances to the spacecraft when they are moved during operation. The spacecraft pointing errors are larger than those quoted for the Ford Aerospace satellite, the major contributor being the large yaw error. Current TDRS spacecraft attitude pointing requirements for the normal mode are:

Without Disturbances	Pitch = 0.15°
	Roll = 0.15°
	Yaw = 1.0°
With Disturbances due to SA antenna slewing	Pitch = 0.35°
	Roll = 0.45°
	Yaw = 1.6°

These correspond to azimuth and elevation errors of 0.44° and 0.52°, respectively.

Ford Aerospace studies of future (1993) versions of TDRS satellites predict azimuth and elevation errors of 0.15° during normal operation and 0.20° during stationkeeping.

The MBA could be flown on an INTELSAT VII-type of spacecraft design having fixed antennas without an active MBA pointing system. On the current TDRS with its less accurate attitude control system, active pointing of antenna systems is required. For future (1993-2000 year) Ford Aerospace's versions of an advanced TDRS spacecraft pointing accuracies of 0.15° for a fixed MBA are achievable during normal operations.

An active pointing system for the MBA may be desirable because of projected spacecraft attitude control systems capabilities marginally approaching the stated antenna requirements.

2.18 HOST SPACECRAFT INTERFACES

In this subsection, we briefly address the issues related to the host spacecraft (electrical) interfacing.

Figure 2.18-1 is a functional block diagram of the host spacecraft interfaces. Each of the functional control units represented in the figure communicates with others via the common satellite bus (e.g., 1553 type). The electrical power needs for each unit are provided by the spacecraft power bus shown in the figure. MBA/switch functions are broken down into two broad areas for convenience: multiple beam antenna control unit, which performs the beam formation, acquisition, and tracking of the various beams; the other unit, MBA communications and switching control unit performs the configuration control of the uplink/downlink communications and switching functions. Each of these units also may perform the built-in test, fault-detection, and correction by switching to redundant functional units. These two units may communicate with other spacecraft control units such as the host spacecraft controller, (which usually controls the satellite bus access) the navigation and attitude control unit (which may provide the pointing and the ephemeris information) and the telemetry tracking and control unit (which provides the command inputs and receives the telemetry data from each of the other units on the spacecraft). Other spacecraft units such as built-in test and maintenance units for the entire spacecraft may be performing the health/sanity check for the entire spacecraft operations.

Each of the control functions can possibly be performed by a single-chip microcomputer unit such as Intel 8051, which is available in space-qualified and radiation-hardened form. It is expected that there will be no significant technology impact issues in the area of host spacecraft electrical interfacing for the MBA/switch.

Interfacing with master frequency generator (MFG) is required by various local oscillator values shown in the transmit/receive system (Section 4) and switch system (Section 5). A detailed design of these systems defines the LO frequency requirements, which in implementation are derived from the MFG.

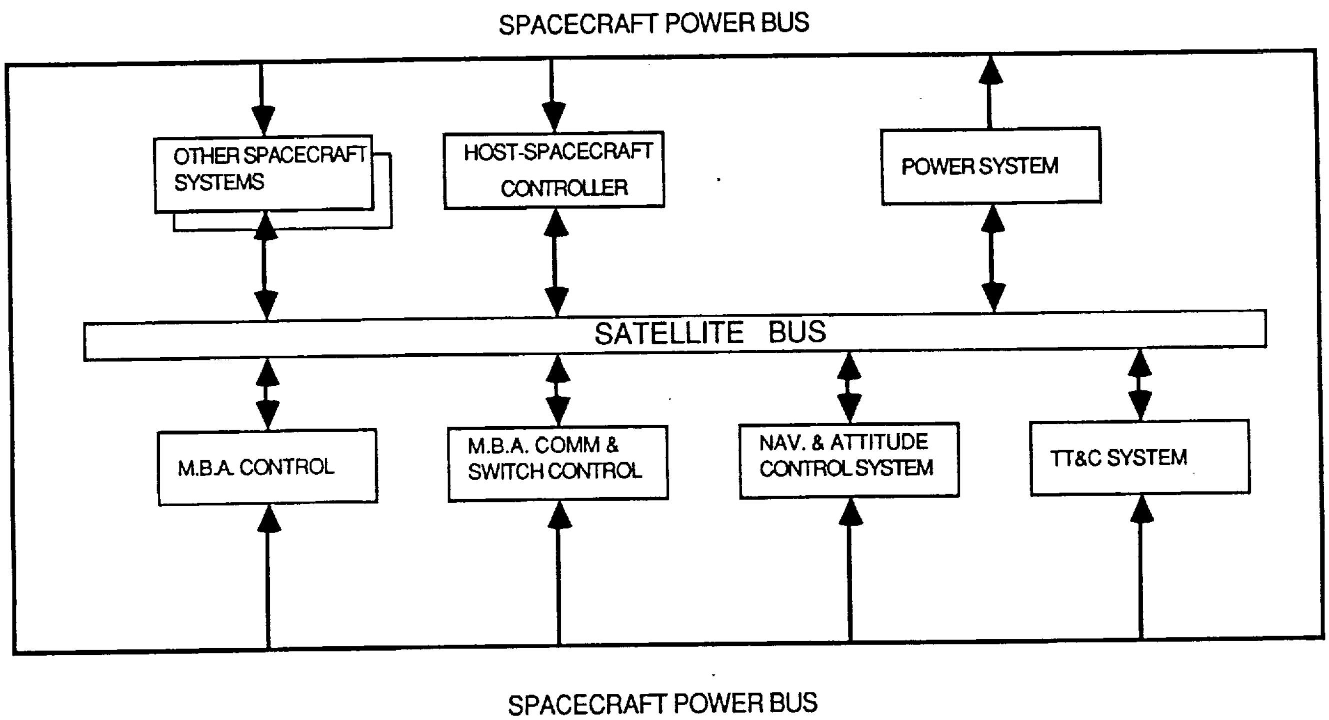

Figure 2.18-1. Host Spacecraft Interfaces

2.19 CALIBRATION, VERIFICATION, AND BUILT-IN TESTING

In this subsection, a brief account of the system testing needed from prelaunch to the flight performance verification is provided. A sample testing procedure is given in the Tables 2.19-1 and 2.19-2.

Additionally, ATDRSS requires as a minimum the following tests:

2.19.1 End-to-End Bit Error Rate Test

The end-to-end bit error rate performance of the ATDRSS is measured in a near continuous mode. An RF carrier with QPSK modulated with a pseudo-random sequence of length (2^x -1) (where x is TBD) is applied to one of the inputs. The MBA/switch matrix connects this input to the test downlink. This downlink signal is demodulated and the BER test is performed with a special custom-made test set used for lower level tests.

2.19.2 Switch Interconnectivity

During flight system tests, each of the possible return and forward switches, crosslink input and output switches, and the space-to-space connectivity switch interconnect paths will be exercised to demonstrate the integrity of the switching functions.

2.19.3 Electromagnetic Compatibility Test

Abbreviated radiation and susceptibility measurements will be conducted on all the panels with all communications and TT&C subsystems installed.

2.19.4 Built-in Testing

Test couplers will be installed at the uplink and downlink as well as the crosslink and user-link antenna/transmit/receive interfaces. Besides, end-to-end air link to air link measurements will be facilitated for testing communications performance parameters with air link up/hardline down, hardline up/air link down and hard line up/hard line down configurations.

Table 2.19-1. Flight System Test Descriptions

Measure Number	Measurement Name	Description
	Input Section Tests:	
101	Ground Delay	A microwave signal will provide the input to the transponder. The output point of measurement for this test will be the input to the transmitter (i.e., the TWT input connector). The test signal will be swept over the transmission bandwidth. Amplitude modulation at a representative baseband frequency will be applied to the uplink signal and the phase difference between the modulation on the input signal and the output will be measured to determine group delay. The baseband frequency will be sufficiently small so that no significant error is introduced in calculating group delay. The measurement will be made at a level TBD below saturation for each transmission channel.
102	Frequency Response	A microwave signal source will provide the input to the transponder. The output point of measurement for this test will be the input to the transmitter (i.e., the TWT input connector). The amplitude response will be measured by an analog sweep at saturation and at TBD input backoff. The frequency range will extend over a range sufficient to show the response to TBD below peak response. A computer controller will set the channel start and stop frequencies and level of the input to the transponder. The output will be fed to a spectrum analyzer and converted to digital format for data reduction by the computer. (Measurement accuracy: TBD MHz). The analog plots of unreduced data will be made on an X-Y recorder. The reduced data will be available on a line printout and a CRT plot with hardcopy capability. Gain slope of transmission channels (dB/MHz) will be determined from the measurement plot and compared to the graded specifications within the usable bandwidths. (Measurement Accuracy: TBD)

Table 2.19-1. Flight System Test Descriptions (Continued)

Measure Number	Measurement Name	Description
103	Out-of-Band Attenuation	Each input multiplexer will be tested for out-of band response beyond the usable bandwidth of each channel. Command response will also be verified. Each preselector bandpass filter at the input to the receivers will be tested for rejection of out-of-band channels. A swept response including bandwidth TBD MHz and TBD dB dynamic range will be recorded for verification of specified performance. (Measurement accuracy: TBD dB)
104	Output Power vs Input Power	A microwave signal source will be used to provide the input to the transponder. The output point of measurement for this test will be the input to the transmitter (i.e., the TWT input connector). The input frequency will be set to the center of each channel. A single carrier power transfer curve will be generated for each channel.
	Hardline	
105	Input/Output Reflection Coefficient	For these measurements, swept frequency techniques or an automated network analyzer will be used. Calibrated directional couplers are used for measurement of incident and reflected signal levels at the input and output of the transponder.
106	Frequency Response vs Drive	A microwave signal source will provide the input to the transponder. The amplitude response will be measured by an analog sweep at saturation and at TBD input backoff. The frequency range will extend over a range sufficient to show the response to TBD dB below peak response. A computer controller will set the channel start and stop frequencies and level of the input to the transponder. The output will be fed to a spectrum analyzer and converted to digital format for data reduction by the computer (Measurement accuracy: TBD MHz).

Table 2.19-1. Flight System Test Descriptions (Continued)

Measure Number	Measurement Name	Description
107	Group Delay	A microwave signal source will provide the input signal to the transponder. The test signal source will provide the input signal to the transponder. The test signal will be swept over the transmission bandwidth. Amplitude modulation at a representative baseband frequency will be applied to the uplink signal and the phase difference between the modulation on the uplink signal and the downlink will be measured to determine group delay. The baseband frequency will be sufficiently small so that no significant error is introduced in calculating group delay. The measurement will be made at a level TBD dB below saturation for each transmission channel.
108	Out-of-Band Attenuation	The method of measurement 103 will be used to plot the total overall sum of receive and transmit responses. A single input level in the linear range will be used as input to the transponder. The swept frequency response will have TBD dB dynamic range and include at least twice the usable bandwidth.
109	Gain Steps/Deltas & Gain Transfer	A microwave signal source will be used to provide the input to the transponder. The input frequency will be set to the center of each channel. Saturation will be determined for each channel frequency by insertion of a small percentage of AM. The transponder output carrier will be sampled and detected, and the TBD kHz demodulated signal fed to a VSWR meter. When the maximum power saturation point is reached, the AM component will go through a null. Measurement of the switched attenuators will be performed during this test by switching each attenuator and measuring the change in level to obtain saturated output power. The single carrier transfer curve will be measured once per each TWTA and will consist of increments of 1 dB (input signal) from TBD dB to TBD dB input drive with respect to saturation. The X and Y axis scale factors will be flux density at the transponder input vs EIRP.

Table 2.19-1. Flight System Test Descriptions (Continued)

Measure Number	Measurement Name	Description
109	Gain Steps/Deltas & Gain Transfer (Continued)	Data at saturation and TBD dB backoff at the center frequency, if available, will be compared to determine the peak-to-peak variations per day. The communication module test temperature range will be compared with the predicted daily variations and the measured variations prorated for comparisons with the specifications. (Measurement Accuracy: TBD dB; repeatability: TBD dB)
109a	Thermal Vacuum Transitional Gain Monitoring (Linear Gain)	All comm subsystem receivers that are required to be active during T/V transitions will be repetitively monitored for variations in gain vs temperature as the transition progresses. Monitoring will be suspended when thermal engineering determines that transponder drive is hampering plateau acquisition.
110	RF Isolation	A microwave frequency synthesizer will be used to drive the input to the transponder. A computer will set the input frequency for each channel and set the signal level for saturation. The ASA will look for spurious signals in the channels occupying the same frequency band as the driven channel. Any spurious signals less than TBD dB below the level of the output signal will be documented for frequency and level. The data will be available on a line printout. (Measurement accuracy: TBD dB)
111	Spurious Outputs	A microwave frequency synthesizer will be used to drive the input to the transponder. The ASA will check for channel spurious signals with a saturated output and without any signal access. A computer will set a single input frequency for each channel center and set the signal level for saturation. The ASA will look for spurious signals in the channel in TBD kHz increments and in the same bandwidths. Then the input signal is removed and the ASA will again look for spurious signals in TBD kHz increments. Any spurious signal above the output noise level will be documented for frequency and level. The data will be available on a line printout. The specification, in TBD kHz bandwidths, will be prorated in direct ratio to the ASA noise bandwidth to establish criteria. An additional allowance may be required for spurious detection, because actual channel noise approximates the specified maximum noise density. (Measurement Accuracy: TBD dB).

Table 2.19-1. Flight System Test Descriptions (Continued)

Measure Number	Measurement Name	Description
112	Translation Frequency	A microwave frequency source will be used to drive the transponder input. The frequency of the downlink and uplink signals will be measured. The difference between the two frequencies will be calculated and will be the translation frequency of the receiver or receiver/upconverter combination being tested. Results of the measurement will be displayed as receiver LO and downconverter LO frequencies. (Measurement accuracy: TBD)
113	Noise Figure	Repeater noise figure will be measured using the C/N technique. A known carrier will be compared with noise power in a known noise bandwidth. Carrier levels will be in the linear drive range and at the same frequencies used in the gain transfer measurement. The noise figure will also be measured in selected channels using a baseload noise measurement technique. A minimum of one channel for each receiver type, i.e., will be measured for each spacecraft. Compliance to requirements in a TBD MHz baseband will be verified by measuring noise power in stepped increments up to TBD MHz from the reference carrier. (Measurement accuracy: TBD dB; repeatability to TBD dB)
114	Test Coupler Calibration	The coupling factor of each communication transponder flight test coupler will be determined at the unit test level. This data will be available to facilitate the analysis of higher level test data. To provide a test coupler reference measurement, the communication transponder gain will be obtained using both the test coupler "through" port and its "coupled" port at the center frequency of each channel.
115	Command & Telemetry Uniqueness	All appropriate commands will be sent through the command generator in the STE. Cross strap combinations of command units and receivers will be exercised. Proper command operation will be checked via the S/C status display, primary power monitoring, or whatever appropriate indication exists. In any given test phase, only those commands not previously exercised in that phase will be sent as part of this measurement.

Table 2.19-1. Flight System Test Descriptions (Continued)

Measure Number	Measurement Name	Description
115	Command & Telemetry Uniqueness (Continued)	PCM-TLM operation and dwell mode will be verified during normal satellite tests. TLM will be displayed onto the spacecraft status display panel, PCM decommutator, and word select and display unit. The displayed data will be checked against commands sent to verify status. All telemetry will be recorded on magnetic media. Also, all telemetry, either real time or recorded, can be displayed by the DAS in engineering units.
116	Third Order Intermodulation	Two equal amplitude carriers are applied to the TWTA and the level of each third order IM product is measured at the output. For each channel measured, the output carrier level (for each carrier) will be varied from saturation to saturation -TBD dB in tbd dB steps. The data will be plotted with the measured carrier levels as a function of drive level. (Measurement accuracy: TBD dB)
117	Phase Shift vs Drive	This parameter will be verified by measurement of each TWTA. The total relative phase shift will be measured at the center frequency of all TBD MHz channels and at the center and band edges of all channels with greater than TBD MHz usable bandwidth. The response will be plotted continuously versus input drive. Input drive levels from zero to those corresponding to an output of saturation TBD dB will be used. A plot in two sections may be required to obtain satisfactory data. (Measurement Accuracy: TBD)
118	Adjacent Channel and Multipath Interference	During the performance of communications module gain flatness/usable bandwidth and group delay tests, the potential multipath interference will be evaluated at the time of ambient condition reference testing for the prototype and flight equipment. For pathways indicated on the test matrix, frequency response plots will be made of individual channels alone and with all others in the same multiplexer enabled to permit occurrence of multipath interference. This will be evaluated as a function of input level to obtain the envelope of the multipath effect for the measured channel.

Table 2.19-1. Flight System Test Descriptions (Continued)

Measure Number	Measurement Name	Description
119	Beacon Output Power	The carrier power of the beacon transmitter is measured and recorded. A microwave power meter is used for power measurement of the TBD GHz carrier. (Measurement accuracy: TBD dB; repeatability: TBD dB during thermal vacuum)
120	Beacon Frequency	The carrier frequency of the beacon transmitter is measured on a microwave frequency counter. (Measurement accuracy: TBD)
121	RF Path Verification	While driving the transponder inputs with a microwave signal generator and monitoring the transponder outputs, commands will be issued to the transponder to configure the RF pathways to redundant pathway configuration. Proper pathway configuration will be verified by detection of the RF signal at the appropriate output(s). During integration, each RF path is verified after the connections are made.
End-to-End Tests With Antennas		
122	EIRP	An uplink carrier will be applied to the transponder at a level to produce saturated output power. The EIRP will then be obtained using the range calibration. This measurement will be made at the same center frequencies as used for gain measurements.
123	Saturation Flux Density	A microwave synthesizer will be used to illuminate the input to the transponder. Saturation will be determined for each channel frequency by insertion of a small percentage of AM modulation. The transponder output carrier will be sampled and detected, and the TBD kHz demodulated signal fed to a VSWR meter. When the maximum power saturation point is reached, the AM component will go through a null. Frequencies will be assigned from that set used for gain and gain transfer measurements. Saturation flux density will be calculated from the measured uplink power at saturation and range calibration data.

Table 2.19-1. Flight System Test Descriptions (Continued)

Measure Number	Measurement Name	Description
124	Receive G/T	An uplink carrier will illuminate the transponder at a know flux density specified in the system specification (about TBD dB below saturated output). An IF receiver will measure signal and noise in a calibrated noise bandwidth. The uplink signal will then be removed and only the output noise measured. Using the resulting system signal-to-noise ratio, the G/T can be obtained using the measured antenna range calibration factors.
125	Spurious Output	A microwave frequency synthesizer will be used to drive the input to the transponder. The spectrum analyzer will check for channel spurious signals with a saturated output and without any signal access. The transponder input and output accesses will be via hardline. A computer will set a single input frequency for each channel center and set the signal level for saturation. The spectrum analyzer will search for spurious output in the channel bandwidth. Then the input signal is removed and the spectrum analyzer will again look for spurious output. Any spurious output exceeding specifications will be documented for frequency and level. The data will be available on a line printout. The specification bandwidths will be prorated in direct ratio to the spectrum analyzer noise bandwidth to establish criteria. An additional allowance may be required for spurious detection, because actual channel noise approximates the specified maximum density.
126	Frequency Response vs Drive	A microwave synthesizer will be used to illuminate the input to the transponder. The amplitude response will be measured in TBD discrete steps over the frequency range both at saturation and at TBD dB input backoff. A computer controller will set the channel start and stop frequencies and level to the transponder. The output will be measured with a power meter. Gain slope of transmission channels (dB/MHz) will be computed (and plotted) from the measurement plot and compared to the specifications within the usable bandwidths.

Table 2.19-1. Flight System Test Descriptions (Continued)

Measure Number	Measurement Name	Description
126	Frequency Response vs Drive (Continued)	Air link uplink and hardline downlink This phase of the frequency response test is intended to verify transponder operation and integrity of all different antenna subsystem paths between the receive test coupler and antenna feed. A minimum number of channels will be selected to sufficiently cover the application bandwidth of each unique receive RF path between feed and coupler. The antenna beam pointing will be adjusted for a flat zone near beam peak. This test will be performed at the TBD dB backoff level. Hardline uplink and air link downlink. This phase is intended to verify transponder operation and integrity of all different antenna subsystem paths between the transmit test coupler and antenna feed. A minimum number of channels will be selected to sufficiently cover the application bandwidths of each unique transmit RF path between feed and coupler. This test will be performed at saturation. This phase verifies the transponder gain flatness/ gain slope performance of those transponder configurations not tested in the previous two phases. These tests will be performed at the TBD dB backoff level.
127	Repeater Isolation	A microwave frequency synthesizer will be used to drive the input to the transponder. The spectrum analyzer will check for spurious signals. A computer will set the input frequency for each channel and set the signal level for saturation. The spectrum analyzer will look for spurious output in the channels occupying the same frequency band as the driven channel. Any spurious output exceeding the specified level will be documented for frequency and amplitude. The data will be available on a line printout. Antenna radiation will be directed out through the radome during this test. Both uplink and downlink signals will be via hardline to the test complex.

Table 2.19-1. Flight System Test Descriptions (Continued)

Measure Number	Measurement Name	Description
128	Passive Intermodulation	Two uplink signals will be injected simultaneously into one or two separate channels. The downlink of adjacent channels will be searched with a spectrum analyzer to verify absence of unwanted intermodulation products. Selection of frequencies and combination of channels will be determined on the basis of an analysis. Frequency pairs will be selected to generate products which will fall within adjacent channel passbands. Both uplink and downlink signals will be routed via hardline. Output radiation will be directed out through the radome.
129	Beacon EIRP	Each beacon EIRP will be measured on a calibrated system test range in the same manner as measurement 122.
130a	Antenna Patterns	Co-polarized and cross-polarized antenna contour patterns will be taken for this antenna. Receive patterns are measured by illuminating the spacecraft and measuring the response of the appropriate antennas. Transmit patterns are generated by measuring the radiated signal from the spacecraft with the range antenna. Patterns will consist of contours plotted over a 20° by 20° field of view. Data will be recorded in a raster scan at 0.5> intervals. The antenna patterns will be measured at 13.4, 14.315, and 15.23 GHz frequencies in each element beam (three co-polarized and four cross-polarized per beam). Polarization will then be reversed and then measurements will be repeated.
130b	Ka-band Transmit Antenna Pattern	Co-polarized and cross-polarized antenna contour patterns will be taken for this antenna. Transmit patterns are generated by measuring the radiated signal from the spacecraft with the range antenna. Patterns will consist of contours plotted over a 20° by 20° field of view. Data will be recorded in a raster scan at 0.5° intervals. The antenna patterns will be measured at 17.7, 19.45, and 21.2 GHz frequencies in each element beam (three co-polarized and four cross-polarized per beam). Polarization will then be reversed and then measurements will be repeated.

Table 2.19-1. Flight System Test Descriptions (Continued)

Measure Number	Measurement Name	Description
130c	Ka-band Receive Antenna Pattern	Co-polarized and cross-polarized antenna contour patterns will be taken for this antenna. Receive patterns are generated by measuring the radiated signal from the spacecraft with the range antenna. Patterns will consist of contours plotted over a 20° by 20° field of view. Data will be recorded in a raster scan at 0.5° intervals. The antenna patterns will be measured at 27.5, 29.25, and 31.0 GHz frequencies in each element beam (three co-polarized and four cross-polarized per beam). Polarization will then be reversed and then measurements will be repeated.
130d	Mobile Beam Antenna Pattern	Measurements detailed in 130a-130c apply. In addition, the dc voltages which drive the antenna pointing mechanism must be recorded to verify the pointing accuracy.
131a	Swept Frequency Gain for Antenna	The antenna responses will be swept for single element beam peak from low to high end of frequencies at each band. Station locations will be determined by examination of antenna contour data. A frequency synthesizer will be used to generate the sweep (TBD frequency steps over channel bandwidths). Reverse polarization and repeat the measurements. Sweep reference will be recorded.
131b	Swept Frequency Cross-polarization	The antenna cross-polarization responses of 130a will be repeated on a swept frequency basis for six worst case station locations.
131c	Swept Frequency Sidelobes	The antenna sidelobe responses of 130a will be repeated on a swept frequency basis for six worst case station locations.
132a	Beam Swept Cross-polarization	A minimum number of channels will be accessed to cover the antenna frequency range. The same set of channels will be swept once each for each of the four locations per beam. The above tests will be performed in the nominal antenna scan positions only (one position).
132b	Beacon Patterns	Co-polarized and cross-polarized contour patterns will be plotted for the beacon antenna. Contour patterns will be plotted over a TBD x TBD field of view in TBD increments.
132c	Global Telemetry Antenna Patterns	Co-polarized and cross-polarized contour patterns will be plotted over a TBD x TBD field of view in TBD increments. This measurement will be performed at one telemetry frequency.

Table 2.19-2. TC&R Flight System Test Description

Measure Number	Measurement Name	Description
	RF Tests	
201	EIRP/RF Output	The telemetry transmitter beacon output power will be measured in both the high power and low power modes and at all antenna ports using the TLM test couplers. (Measurement accuracy: TBD dB) Air link measurements of radiated power will be performed on the slant range via all earth-facing telemetry antennas and all downlink paths. EIRP performance will be verified using the range calibration. Measured EIRP data will be correlated with measured output power measurements to validate antenna gain performance. RF compatibility with the repeater subsystem will be verified during the test.
202	Frequency and Frequency Stability	The two unmodulated carrier frequencies will be measured on a frequency counter. Data for long-term frequency stability will be maintained throughout the test program. (Measurement accuracy: TBD Hz)
203	Spurious Outputs	The transmitter RF outputs will be monitored on a spectrum analyzer and the output examined over the communication transmission band. The frequency and amplitude of spurious signals will be recorded.
204	TM Mod. Index	The transmitter output will be examined on a spectrum analyzer and using the carrier to first sideband ratio, the modulation index will be determined for all subcarrier combinations.
205	Minimum Flux Density	This test will verify that the spacecraft command system does not respond to commands at flux density level of TBD dBW/m^2 or lower. Command signals will be injected via antenna couplers into each of the command antenna feed lines at a signal level equivalent to the specified flux density threshold.

Table 2.19-2. TC&R Flight System Test Description (Continued)

Measure Number	Measurement Name	Description
206	Command Threshold Execute Threshold	Air Link - This measurement is performed when the spacecraft is on the slant range and serves as a calibration point for command antenna pattern data. At receiver acquisition threshold acquire an unmodulated carrier. After acquisition, modulate the RF carrier with a TBD kHz subcarrier. Increase the RF signal level in TBD dB steps until the command in-lock status point on telemetry indicates a subcarrier lock. This level is command threshold. This test will be performed in the angular range of ±TBD AZ and ±TBD EL from the Z axis. Coupler - This threshold measurement is performed at times in the test sequence when the spacecraft is not on the slant range. A carrier modulated with the executed tone is transmitted to the spacecraft via the test coupler in the command receiver antenna line. All command paths will be tested. The power level is set to provide a signal level at the receiver input corresponding to an incident flux density below threshold and it is increased gradually until the telemetry indicates that the command unit has accepted the execute tone. At the threshold just determined, verify that the command unit will accept a valid command.
207	Command Bandwidth	At receiver acquisition threshold acquire an unmodulated carrier. After acquisition, modulate the RF carrier with a TBD kHz subcarrier. Increase the RF signal level in TBD steps until the command in-lock status point on telemetry indicates a subcarrier lock. Repeat this measurement in TBD kHz steps above the center frequency to fo +TBD MHz. Repeat the measurement in TBD kHz steps below the center frequency to fo-TBD MHz.
208	Command Deviation	Set the carrier at center frequency and the deviation at TBD kHz. At receiver acquisition threshold, acquire an unmodulated carrier. After acquisition, modulate the RF carrier with a TBD kHz subcarrier. Increase the RF signal level in TBD dB steps until the command in-lock status point on telemetry indicates a subcarrier lock. Repeat the test with the deviation reduced in TBD MHz increments to ±TBD MHz.

Table 2.19-2. TC&R Flight System Test Description (Continued)

Measure Number	Measurement Name	Description
209	Command Receive Signal Strength	This test will verity the calibrations of the command receiver signal strength telemetry point(s) obtained during unit test as a function of uplink power or flux density. Command signals will be injected into each of the command antennas over a range of signal levels corresponding to the specified range of flux density.
210	Ranging Phase Delay	Ranging phase shift data will be carried forward from tests performed on the transponder for various drive levels at high, low, and ambient temperatures and in vacuum. Ranging phase shift tests at spacecraft level will be obtained by measuring the difference in phase between the TBD and TBD kHz modulation tones on the downlink carrier compared with those modulation frequencies on the uplink carrier. These measurements will be made at flux density levels of -TBD dBW/m^2. Measurements will be made via the test couplers for all possible ranging paths (antennas) (measurement accuracy: TBD)
211	Ranging Mod. Index	An uplink carrier will be modulated with the ranging tones in sequence, and the downlink modulation index will be measured for each tone. Measurements will be made via the test couplers for all possible ranging paths (antennas).
212	VSWR	Using an automated network analyzer or equivalent swept frequency techniques, the input and output return loss of the system will be measured through the test couplers and plotted vs frequency on a X-Y recorder.
213	TC&R Test Coupler Calibration	The coupling factor of each TC&R flight system test coupler will be determined at the unit test level. This data will be available to facilitate the analysis of higher level test data.

Table 2.19-2. TC&R Flight System Test Description (Continued)

Measure Number	Measurement Name	Description
214	T&C Antenna Coverage	Telemetry broadbeam antenna coverage will be verified by a combination of individual telemetry antenna pattern measurements, transmit power measurements at each antenna port via calibrated antenna test couplers, and radiated EIRP measurements via all of the +Z axis facing antennas.
		Telemetry directional antenna coverage will be verified by measurement of radiated EIRP during spacecraft slant range tests over an angular range of $\pm 10°$ AZ and $\pm 10°$ EL from the +Z axis.
		The radiated air link TC&R tests will provide an end-to-end RF performance verification over a +10° angular range from $\pm$Z axis, validate the linear combining of hardline RF measurements and antenna pattern measurements, and verify RF compatibility of the TC&R and Communications subsystem.
		T&C broadbeam coverage measurements will be performed in elevation increments of TBD degree centered on the earth coverage direction.
215	T&C Antenna Gain Ripple (Broadbeam) Antennas)	Antenna gain ripple will be predicted on the basis of antenna unit tests plus gain versus angle measurements of the telemetry and command antennas on a scale model spacecraft which is representative of the on-orbit spacecraft configuration. Scale model spacecraft tests will include those elevation and azimuth pattern cuts which characterize the transfer orbit attitude and aspect angle geometry. Gain patterns will be measured on all individual telemetry and command broadbeam antennas.
		EIRP and command threshold variation will be predicted on the basis of baseband combining of the composite gain patterns, with allowance for the performance difference between flight and scale model hardware.

Table 2.19-2. TC&R Flight System Test Description (Continued)

Measure Number	Measurement Name	Description
		Baseband Tests
216	T&C Antenna Axial Ratio	Axial ratio performance for each of the T&C broadbeam antenna elements will be measured during unit test of development and flight units. This performance data will be used to analytically determine the impact on the system level performance. Axial ratio performance of the directional telemetry antennas and broadbeam telemetry and command antennas will be verified in the +Z direction ±10° during slant range testing.
217	Command Functional (Side 1 & Side 2)	Baseband acquisition range of TBD kHz +TBD ppm (TBD kHz + TBD Hz). Verify acceptance of all valid commands and rejection of invalid commands and cross strap operation. Verify all block and time tagged commands. Test will include switch-over to secure mode and verification of TBD% of commands in secure mode. The remaining TBD% will be verified in clear text mode.

2.20 PRELIMINARY OPERATIONS CONCEPT AND GENERAL GROUND SUPPORT REQUIREMENTS

In the early phases of the design and development, a detailed operations concept for ATDRSS is needed. The details of this concept are beyond the scope of this study.

The ATDRSS spacecraft equipment, including the MBA, the SGL payload, and the switch matrix along with all the other payloads and bus equipment will be designed to be flown on either an STS mission or on an expendable launch vehicle (such as the Atlas Centaur). Stowing and deployment issues must be adequately addressed. The launch and missions support plan must be developed well in advance. The launch planning must allow for a launch window facilitating a launch at least once a day.

The launch sequence specifies the coverage and performance of the TT&C antennas in the transfer orbit and the final synchronous orbit. The operation performance of other spacecraft equipment (eg., navigation and attitude control equipment) in the transfer orbit must also be specified. All the relevant performance parameters must be monitored at the mission control center or the TNGT as appropriate, throughout the launch phase. In the final synchronous orbit, the deployment procedure of all the antennas including the space-to-ground multiple beam antenna, is to be planned, tested, and administered during the final phases of launch sequence.

Ground support equipment at the TNGT includes the equipment performing the tracking services and the simulation and verification services. The current tracking equipment has the capability of providing up to 19 simultaneous tracking services.

Simulation/verification (SIMVER) services at the TNGT include, in addition to SIMVER of all the user services, the SIMVER of all other ground terminals including the RGTs: the fixed beam covering TNGT as well as the mobile coverage beam(s) can be used for performing these services. Simulations of crosslink communications between ATDRS 1 and ATDRS 2 can be performed at Ka-band (60 GHz communications through the atmosphere undergo significant attenuation) by switching the crosslink payloads to the Ka-band antenna/upconverters and downconverters. At a future date, it may be conceivable that the Space Station will be able to provide SIMVER function of the crosslink communications at 60 GHz.

REFERENCES

2-1 R. M. Tanner. "A Recursive Approach to Low Complexity Codes," IEEE Trans. Inform. Theory, Vol IT-27, No. 5, pp. 533-547, Sep 1981.

2-2 G. Ungerboeck. "Trellis-Coded Modulation with Redundant Signal Sets," IEEE Communications Magazine, Vol 25, No. 2, pp. 5-21, Feb 1987.

2-3 "A Summary on Depolarization of Radio Wave Propagation in the Frequency Band 10 to 30 GHz," Ford Aerospace IR&D Report, WDL-TR10872, 1986.

2-4 "Multiple Beam Frequency Reuse Antenna," Final Report, COMSAT Contract Number IS-474, Aug. 1977 - Nov 1979.

2-5 "30/20 GHz Spacecraft Multibeam Antenna System," Final Report, Contract Number NAS3-22498, Jan 1984.

2-6 J. Jay Jones and W.K.S. Leong. "Analysis of Performance Degradation for a PSK Communication Satellite Channel," Final Report, Prepared under Contract Number NAS2-8538, 15 Dec 1974.

2-7 J. Y. Huang. "Filter Distortion and Intersymbol Interference Effects on BPSK/QPSK/SWPSK/MSK Signals," Ford Aerospace Corporation, Technical Memo 289, Sep 1986.

2-8 R. M. Gagliardi. "Satellite Communications," Lifetime Learning Publications, Chapter 8, 1984.

2-9 "The Multi-Mission Modular Spacecraft and Its Derivatives," Fairchild Space Company, Briefing Information of NASA/GSFC Sponsored Study (currently ongoing).

2-10 "Hubble Space Telescope Study," Lockheed Missiles and Spacecraft Company, Report of NASA/MSFC Sponsored Study.

2-11 "Communications Satellite Systems Operations With the Space Station," Ford Aerospace Corporation, Final Report of NASA/LeRC Sponsored Study.

SECTION 3
ANTENNA ENGINEERING

In this section, all the issues related to the antenna, including the reflector, feed, tracking mechanism, advanced materials, packaging, stowing and deployment tradeoffs are considered. Design summary and performance specifications for the recommended configurations are also presented.

3.1 ANTENNA COVERAGE REQUIREMENTS

MBA design starts with the exact coverage requirements. The network configuration topologies are shown in Figure 1 of the SOW, and specific requirements for spacecraft and ground station locations are listed in paragraphs 2.1 and 2.2 of the SOW. These requirements are summarized in Figure 3.1-1, which includes the fixed ground stations listed in the SOW, plus ground stations covering areas in Europe and Japan. A list of these ground stations and their geographic locations is given in Table 3.1-1.

Relative satellite locations are also shown in Figure 3.1-1 for the specified ranges given in paragraph 2.1 and for the specific locations designated in Figure 1, Configuration 2, of the SOW. Coverage from these spacecraft locations can extend 71.44° both east and west at the equator to maintain a ground station elevation of at least 10° as specified in paragraph 2.2. This range is also shown in Figure 3.1-1.

The antenna designer must understand what the coverage requirements mean in terms of angular coverage from the spacecraft (in synchronous orbit). The information available on the maps of Figure 3.1-2 represents the world as seen from a synchronous spacecraft at various orbit locations. The coordinates are in degrees, N/S and E/W, measured from the nadir of the spacecraft. The scan range required to cover the ground stations listed is shown in Figure 3.1-2 by the boxes surrounding the stations. These scan ranges are summarized in Table 3.1-2 for the various cases. For Configuration 1 (all stations within CONUS), the maximum scan range required is 1.46° N/S and 6.0° E/W. Expanding this range to 2.5° N/S and 6.3° E/W (as shown by the dotted box in Figure 3.1-2b) would allow full CONUS coverage, excluding the southern tips of Florida and Texas.

The required scan range for Configuration 2, as shown on Figures 3.1-2d and 3.1-2e, is considerably greater than for Configuration 1, extending to 3.24° N/S and 12.7° E/W. The N/S range can be reduced to approximately 2.0° by rotating the scan axes of the antenna about 10°.

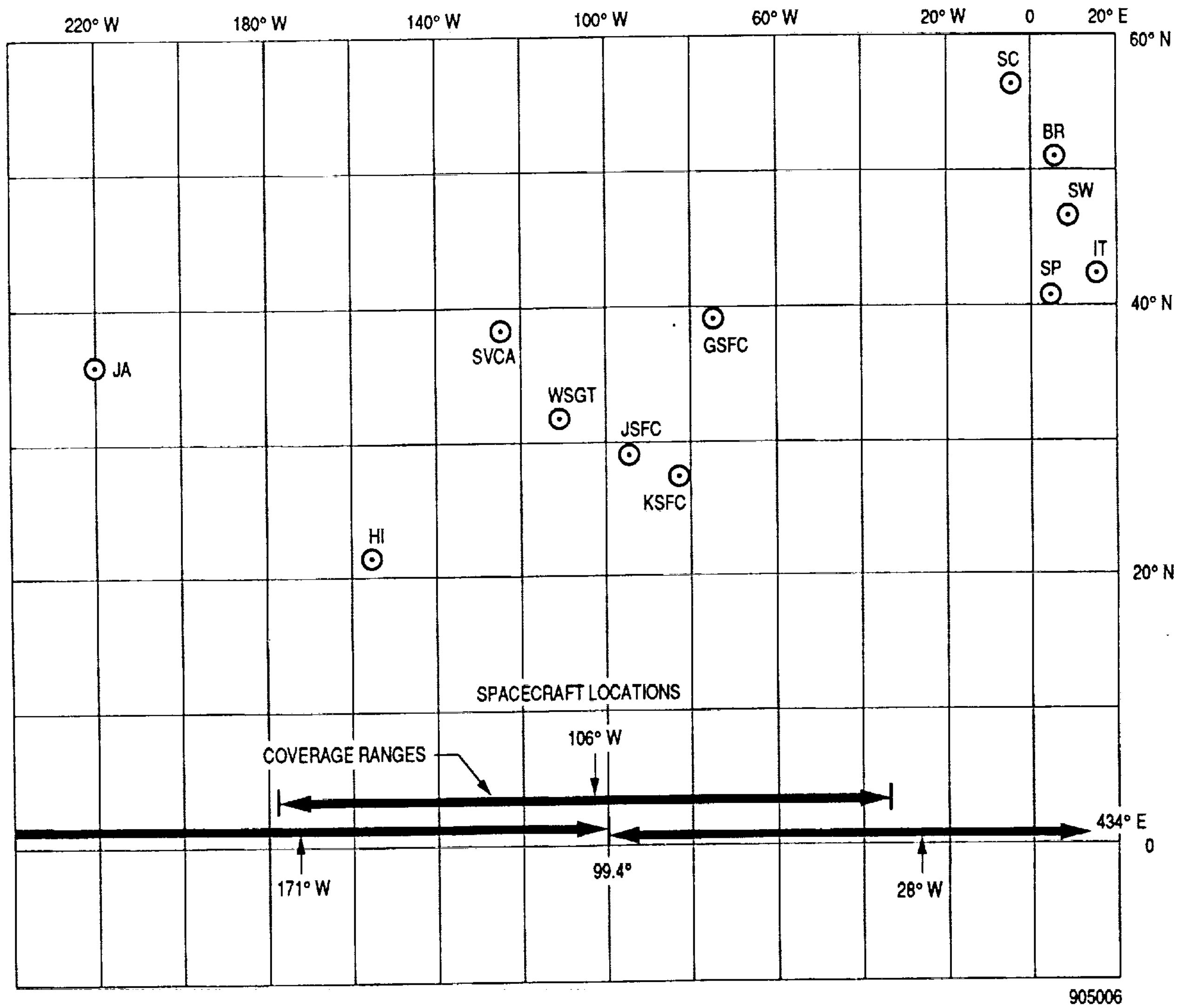

Figure 3.1-1. Designated Coverages

Table 3.1-1. Possible Ground Station Locations

Name	Designation	Latitude	Longitude
White Sands, New Mexico	WSGT	32.365 N	106.49 W
Johnson SFC (Houston)	JSFC	29.53 N	95.10 W
Goddard SFC (Greenbelt)	GSFC	39.0 N	76.83 W
Sunnyvale, California	SVCA	37.38 N	122.02 W
JPL (Pasadena, California)	JPL	34.08N	118.08W
Denver, Colorado	DENV	39.44N	104.59W
Andover, Maine	AND	44.38N	70.45W
Kennedy SFC (Florida)	KSFC	28.51 N	80.70 W
Honolulu, Hawaii	HI	21.4 N	157.9 W
Tokyo, Japan	JAP	35.6 N	220.4 W
Fucino, Italy	IT	42.0 N	13.5 E
Geneva, Switzerland	SW	46.2 N	6.14 E
Brussels, Belgium	BR	50.8 N	4.3 E
Madrid, Spain	SP	40.4 N	4.3 E
Edinburgh, Scotland	SC	55.9 N	3.2 W

This rotation could be accomplished by a mechanical rotation of the downlink antenna, or by a rotation of the entire spacecraft about its yaw axis, if the downlink antenna were rigidly mounted to the spacecraft. This choice would require more careful study, since pointing the downlink antenna to the center of the scan area in each case is required to minimize the scan ranges. Minimizing these scan ranges is important for antenna designs. It impacts the type of scan mechanism allowed, overall antenna size and complexity, and possible loss in gain due to scanning (relative to the midpoint of the scan range).

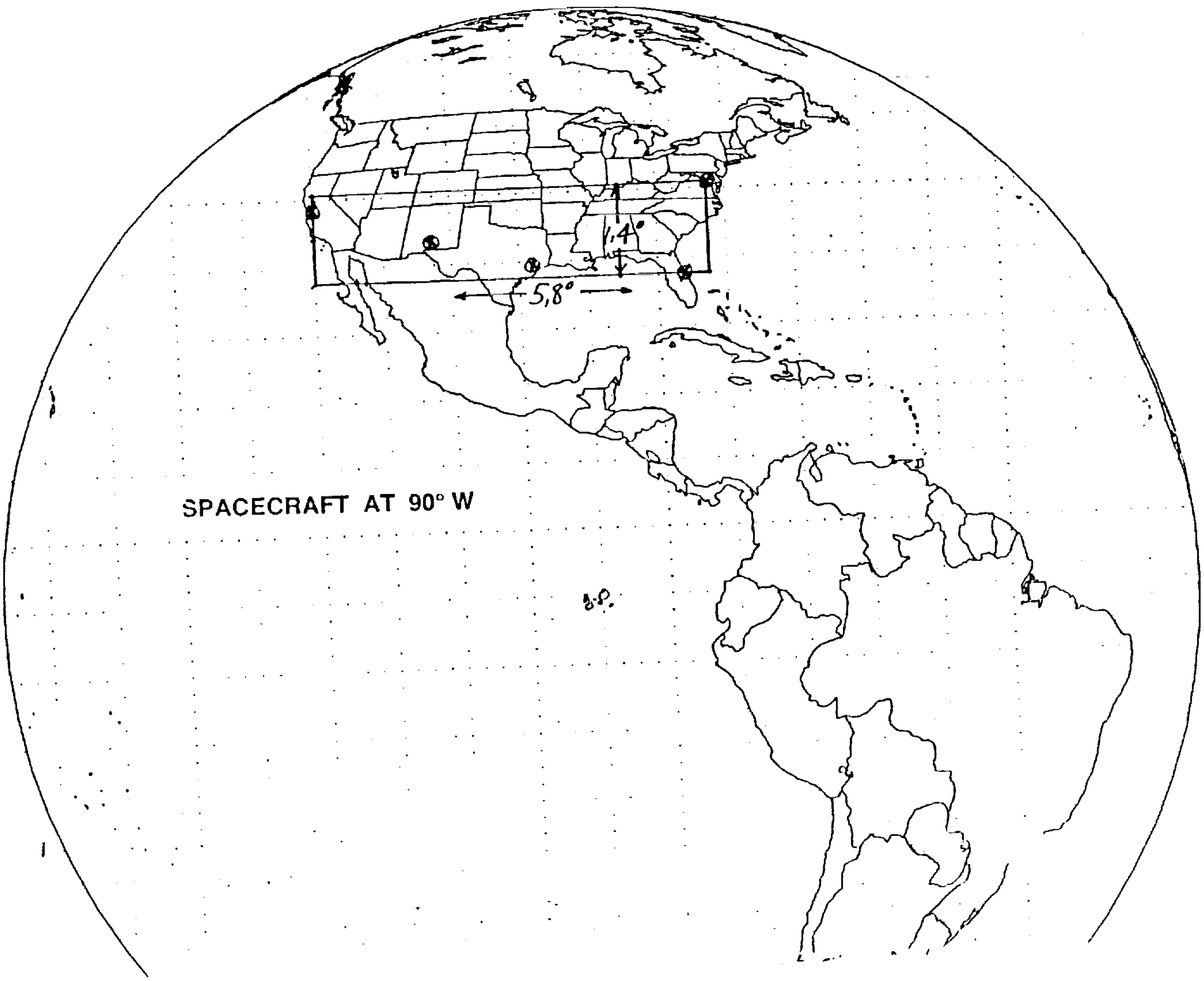

Figure 3.1-2a. Spacecraft at 90° W

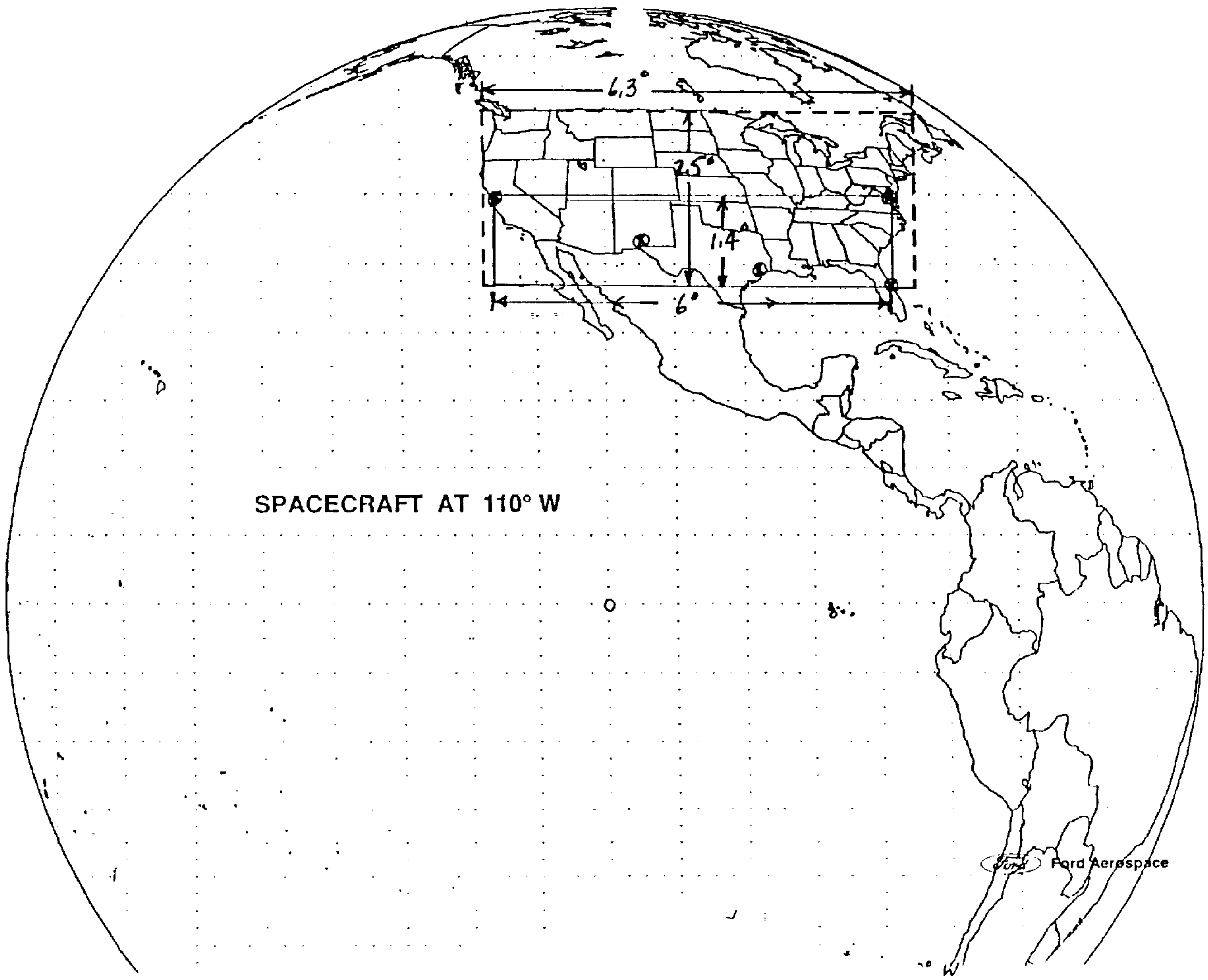

Figure 3.1-2b. Spacecraft at 110° W

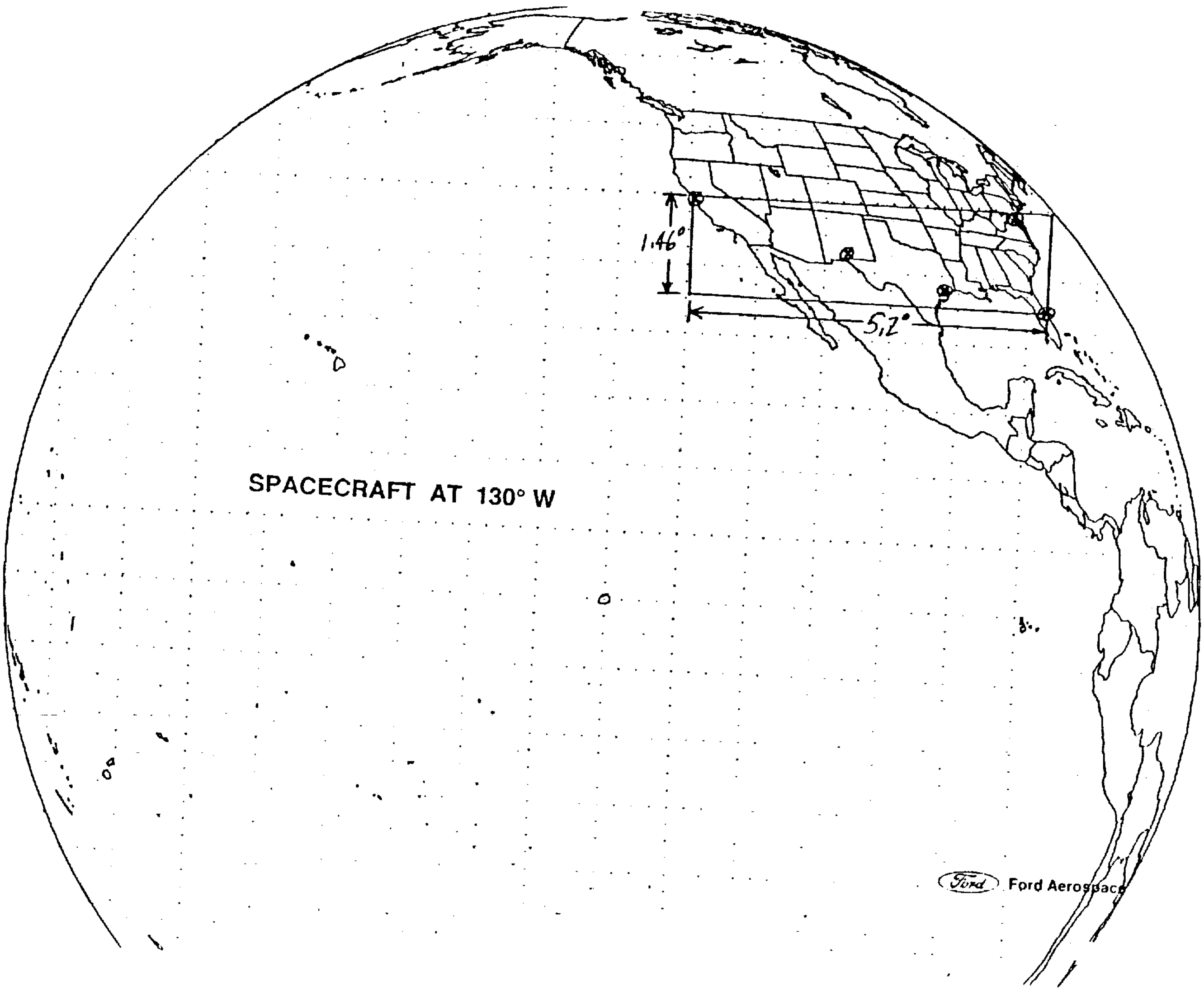

Figure 3.1-2c. Spacecraft at 130° W

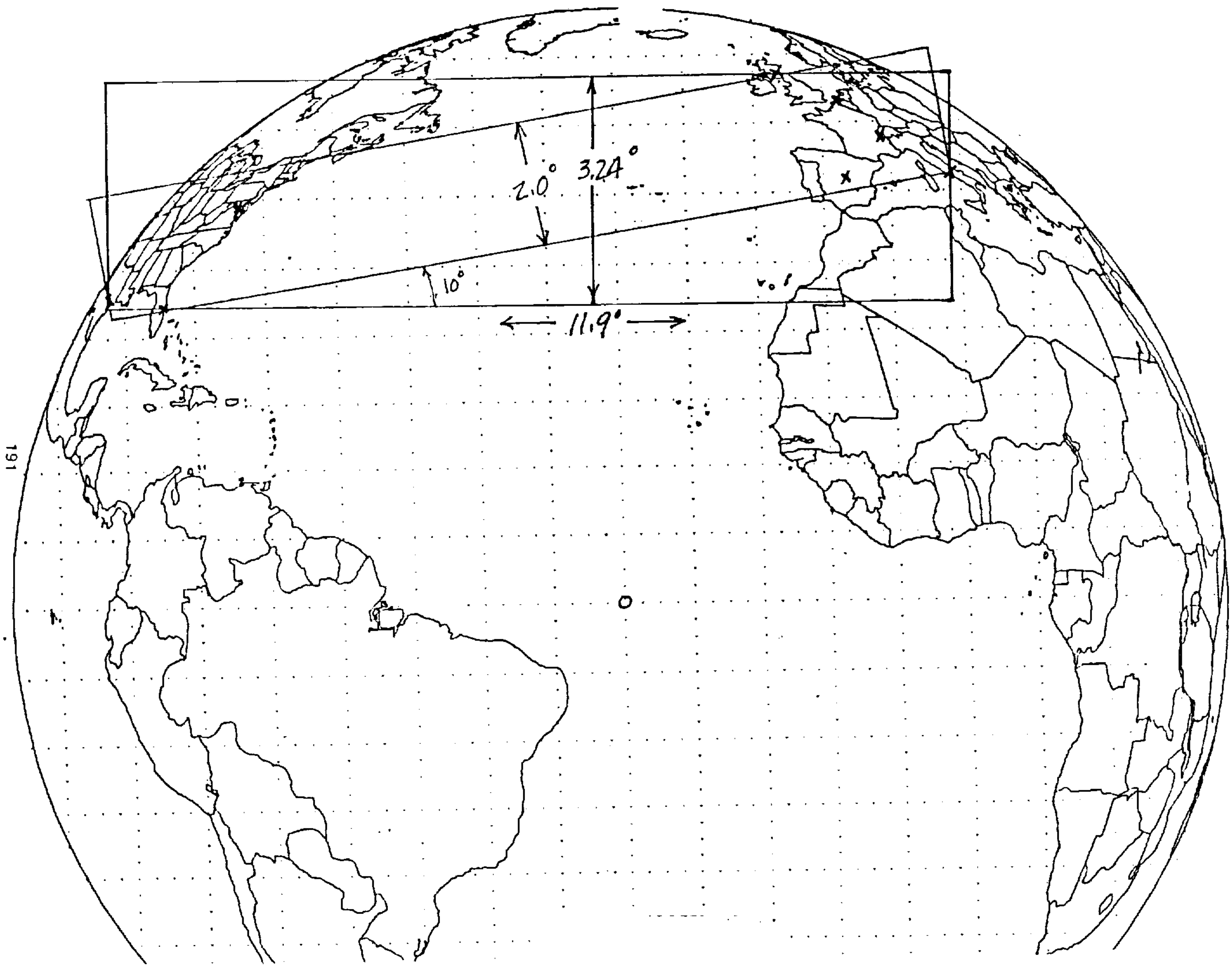

Figure 3.1-2d. Spacecraft at 30° W

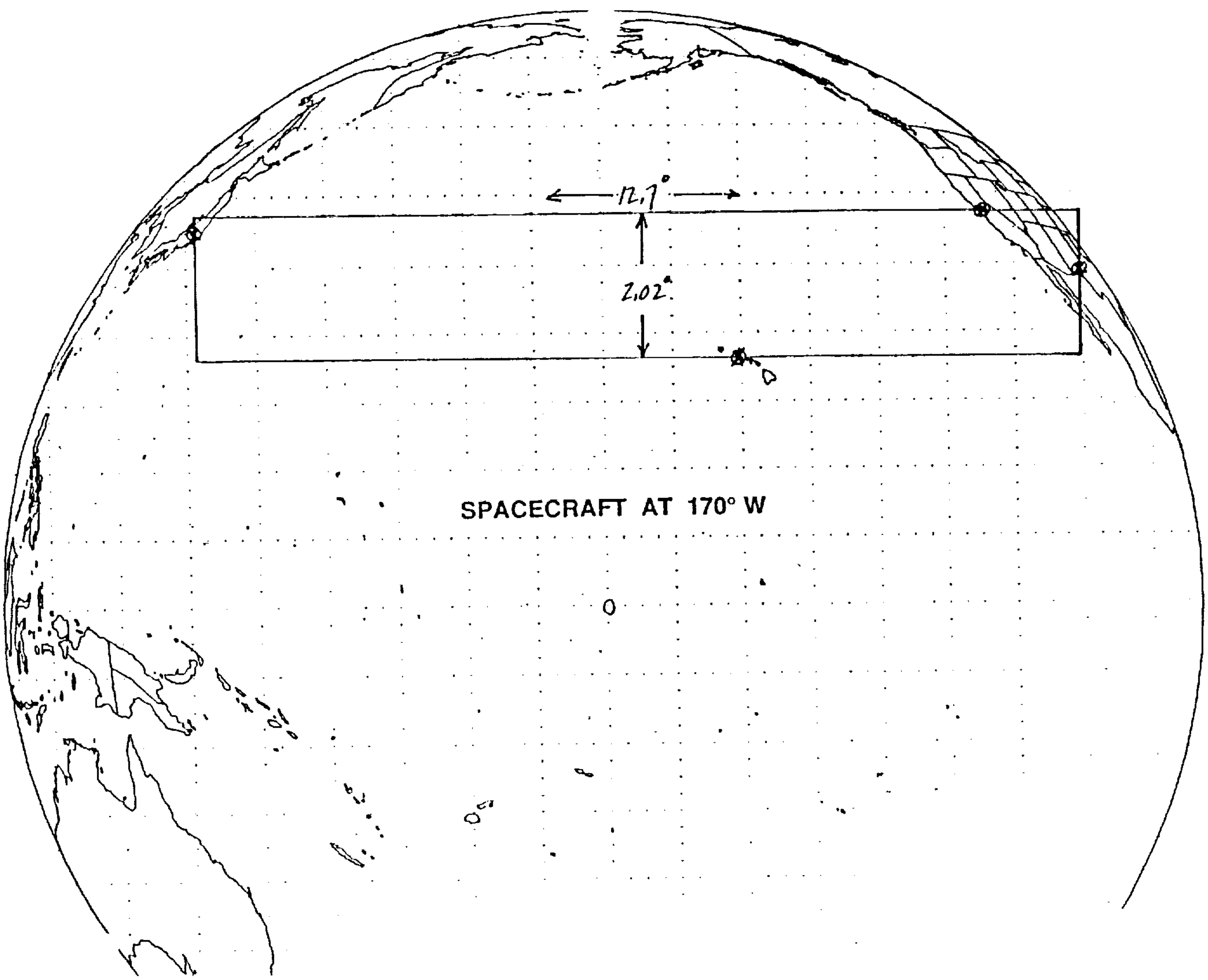

Figure 3.1-2e. Spacecraft at 170° W

Table 3.1-2. Required MBA Scan Ranges

Configuration	Spacecraft Location	Scan-Ranges N/S	Scan-Ranges E/W
1	90°W	1.4°	5.8°
1	110°W	1.4°	6.0°
1	130°W	1.46°	5.2°
1	90-130°W - Full CONUS	2.5°	6.3°
2	30°W	3.24°	11.9°
2	30°W (Rotated)	2.0°	12.0°
2	170°W	2.02°	12.7°

3.2 COMPUTATION OF ANTENNA GAIN AND DIAMETER

In this subsection, the gain and size of the MBA are computed using two different system requirements, viz., the EIRP requirement and the G/T requirement.

3.2.1 Computation of Antenna Gain and Diameter Using Considerations of EIRP

This paragraph shows the details of computing the required antenna gain and diameter for compliance with the EIRP requirement.

On page 2-13 of the SOW the EIRP requirement is -37 dBW/Hz. On the same page the maximum data rate is specified to be 4 Gb/s. At this time the exact bandwidth is not known and to continue the estimation it was assumed that it will be 3.5 GHz. The relation used here is

$$EIRP = 10 * Log[Pt * Ga/BW] = -37 \text{ dBW/Hz}$$

where Pt is the combined RF power of all transmitters
Ga is the antenna gain we are seeking
BW is the maximum bandwidth; already estimated 3.5 GHz

The combined RF power of all transmitters is bound by the dc available power and depends on the efficiency of converting dc energy to RF.

On page 2-6 of the SOW we find that the dc available power is 460 W. Setting aside 160 W for the low power circuits (assumed) we have left 300 W. Assuming a 20% efficiency for the transmitters we have 300*.2 = 60 W of total RF power - this is Pt.

Now the equation is :

$$10 * Log [Pt * Ga/BW] =$$
$$10 * Log [60 * Ga/3.5E9] = -37 \text{ dBW/Hz}$$

Solving for Ga we get

$$Ga = 3.5E9 * 10 \exp (-37/10)/60 = 11639 = 40.66 \text{ dBi}$$

With the antenna gain established the diameter of the dish is found by using the relation:

$$Ga = 0.6 * (D * PI/Lambda)^2$$

where 0.6 is assumed efficiency of the antenna
D is the dish diameter in meters
Lambda is the wavelength in meters = C/F

where C = 3E8 velocity of light in m/s
F = 17.7E9 frequency in Hz

solving for D yields:

$$D = (3E8/(17.7E9*3.14))*SQR\ (11639/0.6) = 0.75 \text{ meters}$$

3.2.2 Computation of Antenna Gain and Diameter Using Considerations of G/T

This paragraph shows the details of computing the SGL antenna gain and diameter using the G/T requirements.

Requirement. Paragraph 2.2.1 of the SOW specifies that G/T for each link should be from 26 to 29 dB/K.

The expression for G/T we are using is

$$10*Log\ (Ga/Ts) = 26 \text{ dB/K}$$

where Ga is the antenna gain
Ts is the system noise temperature in K.

The relation for finding the system noise temperature is:

$$T_s = T_a*(\alpha) + T_l*(1-(\alpha)) + T_r$$

where T_a is the antenna noise temperature - assumed here 290 K
α is line losses from antenna to preamplifier including diplexer and other losses - assumed here 1 dB (or 0.794)
T_l is line temperature assumed here 200 K.
T_r is the receiver noise temperature assumed here 300 K equivalent to 3.1 dB.

These values are now substituted in the expression for Ts

$T_s = T_a*(\alpha) + T_l*(1-(\alpha)) + T_r =$

$= 290 * 0.794 + 200 * (1-0.794) + 300 =$

$= 571.5$ K

Now we use the expression for G/T

10*Log(Ga/Ts)=26

10*Log(Ga) = 26 + 10*Log(571.5) = 53.57 dB

However, in order to compensate for the 1 dB line loss suffered by the signal, the antenna gain necessary should be increased to 54.57 dB.

The gain as a power ratio is 10 (54.57/10)=286418

Antenna Diameter

$Ga = 0.6 * (D*\pi/\lambda)^2$

where 0.6 is the efficiency of the antenna - assumed

D is the antenna diameter in meters

λ is the wavelength in meters = C / F

C is velocity of light in meters = 3E8

F is the frequency in Hz = 27.5E9

$Ga = 0.6 * (D*3.14*27.5E9/3E8)^2$

solving for D yields

D = (3E8/(27.5E9*3.14))*SQR (286418/0.6) =2.40 meters

Since the G/T requirement results in a larger antenna size than the EIRP requirement, this value (of 2.4 meter diameter) is used for all our further studies.

3.3 MBA -- ALTERNATIVE DESIGN CANDIDATES

The principal antenna types to be considered for the ATDRSS application are shown in Figure 3.3-1. These include the simple prime-focus-fed parabolic reflector, two dual-reflector types -- the familiar Cassegrain and a modification with specially shaped reflectors, and the torus reflector, as well as the direct radiating phased array (not shown). All of the reflector type antennas may be either center fed or offset fed to reduce blockage; this offset configuration is generally preferable with an array feed or an extended subreflector to reduce blockage effects. A comparison of their relative performance must include their ability to produce a scanned beam - that is one which is displaced from the position of optical focus. This feature is generally related to the number of beamwidths which must be scanned, as well as the maximum scan angle, which affects such details as the size of the subreflector and placement to avoid blockage. For this, one must determine both the maximum scan angles required, as well as the relative beamwidth, which is related to the gain requirement.

An examination of the system sensitivity requirements together with noise performance expected from 30 GHz devices in the 1993 timeframe has led to the conclusion that an antenna gain of approximately 54.6 dBi will be required (refer to subsection 3.2). This is commensurate with an antenna beamwidth of approximately 0.3°. The scan ranges required, from the previous section, are ±3.5° for Configuration 1, and ±6.0° for Configuration 2; these correspond to scan ranges of ±12 to 20 beamwidths for the two cases.

As the feed from an optically focussed antenna system is displaced from the focal point, its gain generally drops and its pattern degrades (resulting in broadening of the beam and increased sidelobes). The extent of such degradation depends upon the optical system design, and especially upon the f/D parameter (focal length to diameter ratio). A larger f/D results in better scan performance; a practical limit based on spacecraft size constraints appears to be in the range of f/D = 1. For this case, relative gains of the four reflector candidates are shown in Figure 3.3-2 for scans of up to 20 beamwidths. At this maximum scan angle, the simple parabola exhibits a gain loss of over 6 dB, while the Cassegrain loss is of the order of 4 dB[3-1]. These losses are considerably less for scans of only 12 beamwidths. In the next few sections, a detailed examination of torus, dual reflector and phased array approaches are presented.

3.3.1 Torus Designs

Extended scan angles (approaching 180°) are possible with the torus reflector antenna, which is designed with a spherical reflector shape, rather than parabolic, in one or both orthogonal planes. Such a design is commonly used in ground stations to access multiple satellites in synchronous orbit.

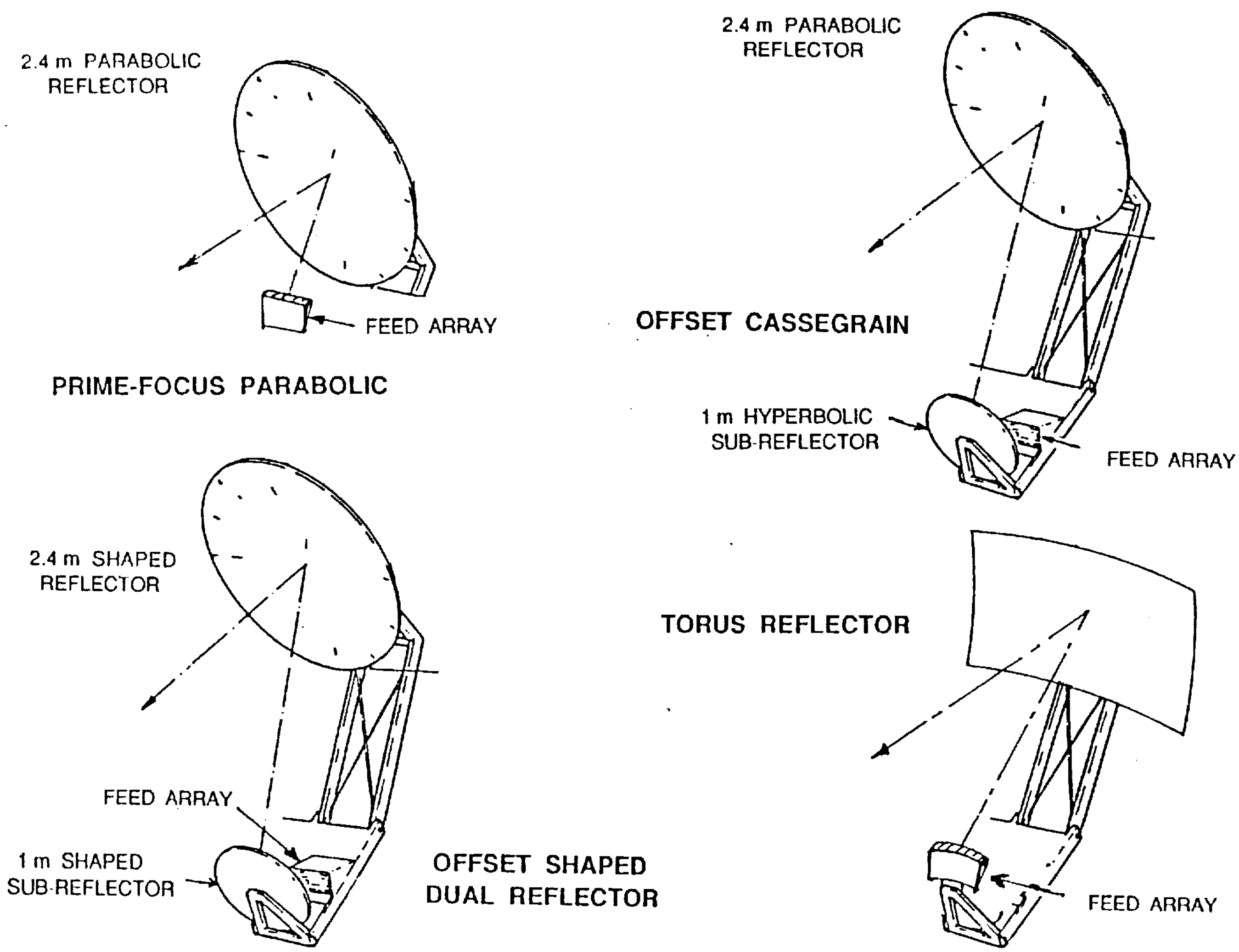

Figure 3.3-1. Multibeam Reflector Antenna Systems

BASIC REQUIREMENTS

GAIN: 54.6 dBi @ 29 GHz for G/T -- Beamwidth = 0.3°

SCAN RANGES: Config. #1 -- ± 3.6° = ± 12 Beamwidths
Config. #2 -- ± 6.0° = ± 20 Beamwidths

SCAN PERFORMANCE OF BASIC REFLECTOR-TYPE MBA's

1. **PARABOLA** -- Limited to small scan range -- ± 4 Beamwidths

2. **Offset Cassegrain** -- Limited to moderate scan range -- ± 12 BW

3. **Dual Offset Shaped Reflectors** -- Adequate for ± 20 Beamwidths

4. **TORUS** -- Unlimited scan range in one dimension, same as parabola in other.

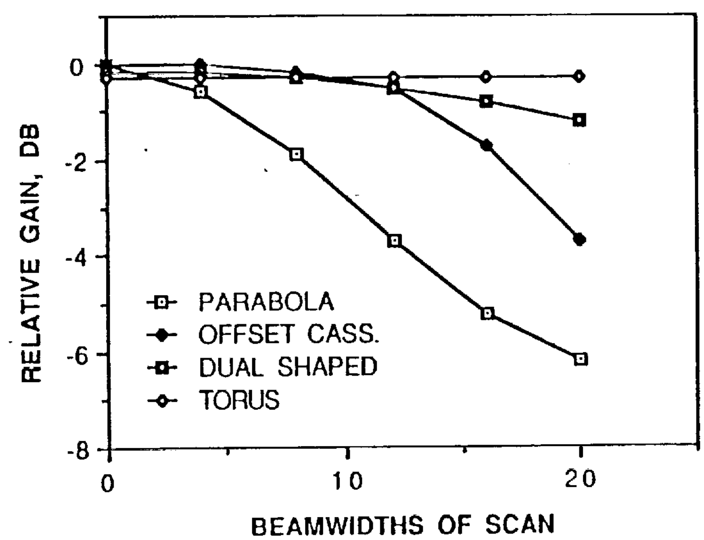

Figure 3.3-2. Multiple Beam Antenna Comparisons

The penalty paid for this ability to scan is a slight loss in gain, since the rays are not as well focussed as with a parabola. A compromise is possible if appreciable scan is required in one direction only (as in the TDRSS case). The reflector may be formed as a parabola in one dimension and a circle in the other. The penalty paid for this so called "torus" design is an enlarged reflector in the scan direction, since the reflector must be extended to intercept rays in different beam directions.

A preliminary design for this torus reflector system has been prepared as shown in Figure 3.3-3. It was designed to afford a minimum of 54.6 dBi directional gain at 29 GHz over a scan range of ±7.5°. The basic area illuminated for a beam in a given direction is about 96 inches in diameter. The focal length (144 inches) and radius of curvature (300 inches) have been selected to produce a maximum path length error of only 0.078 inch with an rms value of 0.032 inch, which corresponds to .08 wavelengths at 30 GHz. This error should be small enough to produce negligible gain loss. The reflector width required to allow the desired scan range is 176", which is considerably greater than the corresponding parabolic reflector, but not necessarily unmanageable.

In order to verify the electrical performance of this torus design, calculations were made of its patterns in two orthogonal planes, and corresponding gains, for beams on axis and scanned in both elevation (N/S) and azimuth (E/W). Typical patterns are shown in Figures 3.3-4 through 3.3-6.

These patterns were calculated using Ford Aerospace's GPAT reflector analysis program, which uses the aperture field method as described by Silver [3-3]. The reflector surface is specified by an input table, and integration is performed over a set of 2500 separate points within the boundaries of the reflector. No account is made of edge effects. The feed pattern is generated from a routine describing the field of a simple waveguide horn.

The calculated gain performance is summarized in Table 3.3-1 at both 20 and 30 GHz. A 2 inch square horn was used to illuminate the reflector at 20 GHz, with excellent results (Figure 3.3-4). The same size horn at 30 GHz produced under illumination with a drastic loss in gain, increase in beamwidth, and dual peaks in the main beam is shown in Figure 3.3-5. Reducing the horn size to 1 in^2 considerably improved the performance at 30 GHz as seen in Figure 3.3-6. It is also observed that the sidelobes are higher and the beamwidth narrower in the horizontal plane since the spherical reflector shaping is not as effective as the parabolic in the vertical dimension.

Sidelobes appear to be below 30 dB beyond 1° from the beam peak, indicating that adequate beam isolation would be available with this design for beams separated by at least 1°, which is consistent with the 2 inch feed horn size spaced to avoid physical interference.

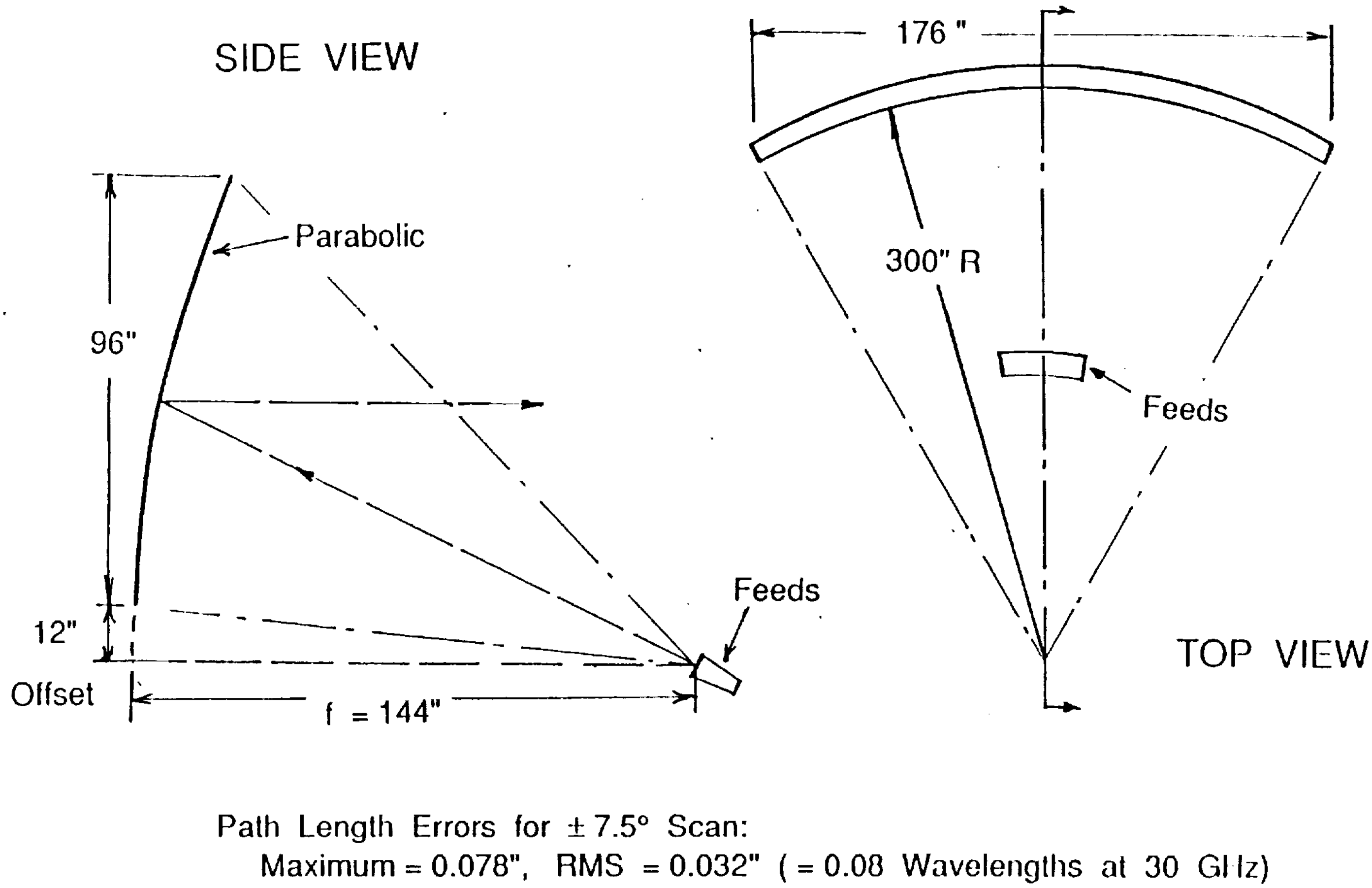

Figure 3.3-3. Preliminary Torus Antenna Design

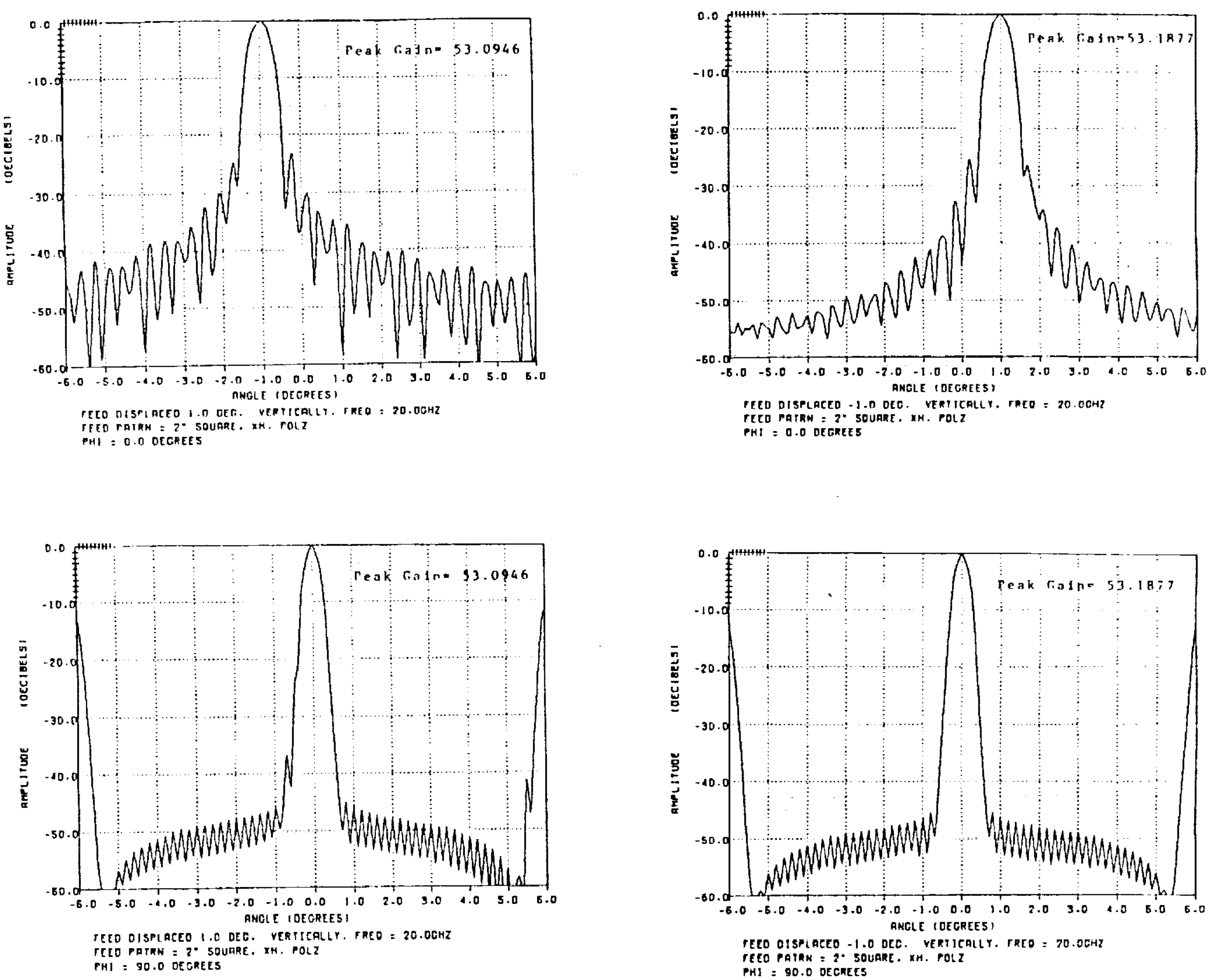

Figure 3.3-4a. Calculated Torus Patterns @ 20 GHz with 2 Inch Feed Horn

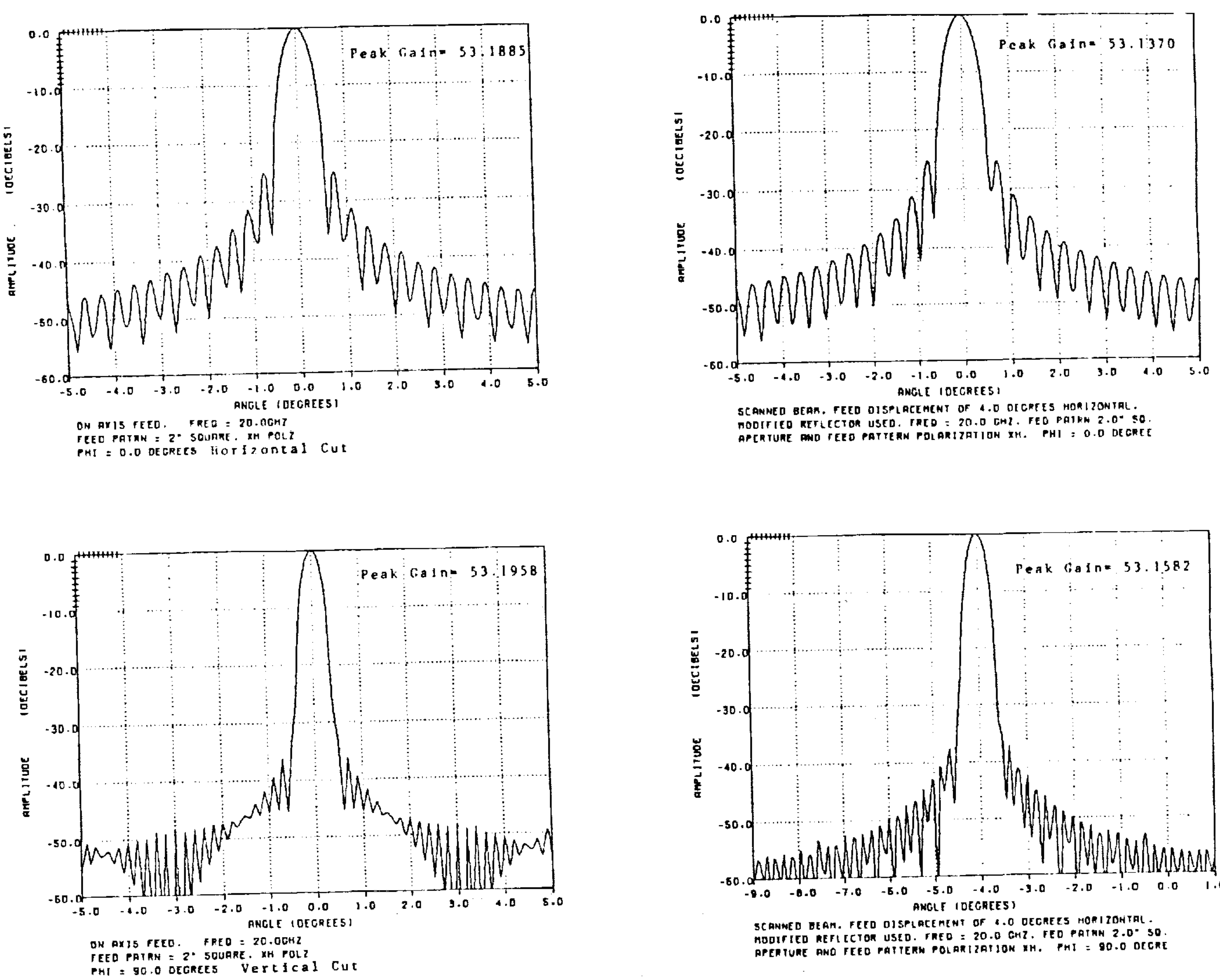

Figure 3.3-4b. Calculated Torus Patterns @ 20 GHz with 2 Inch Feed Horn

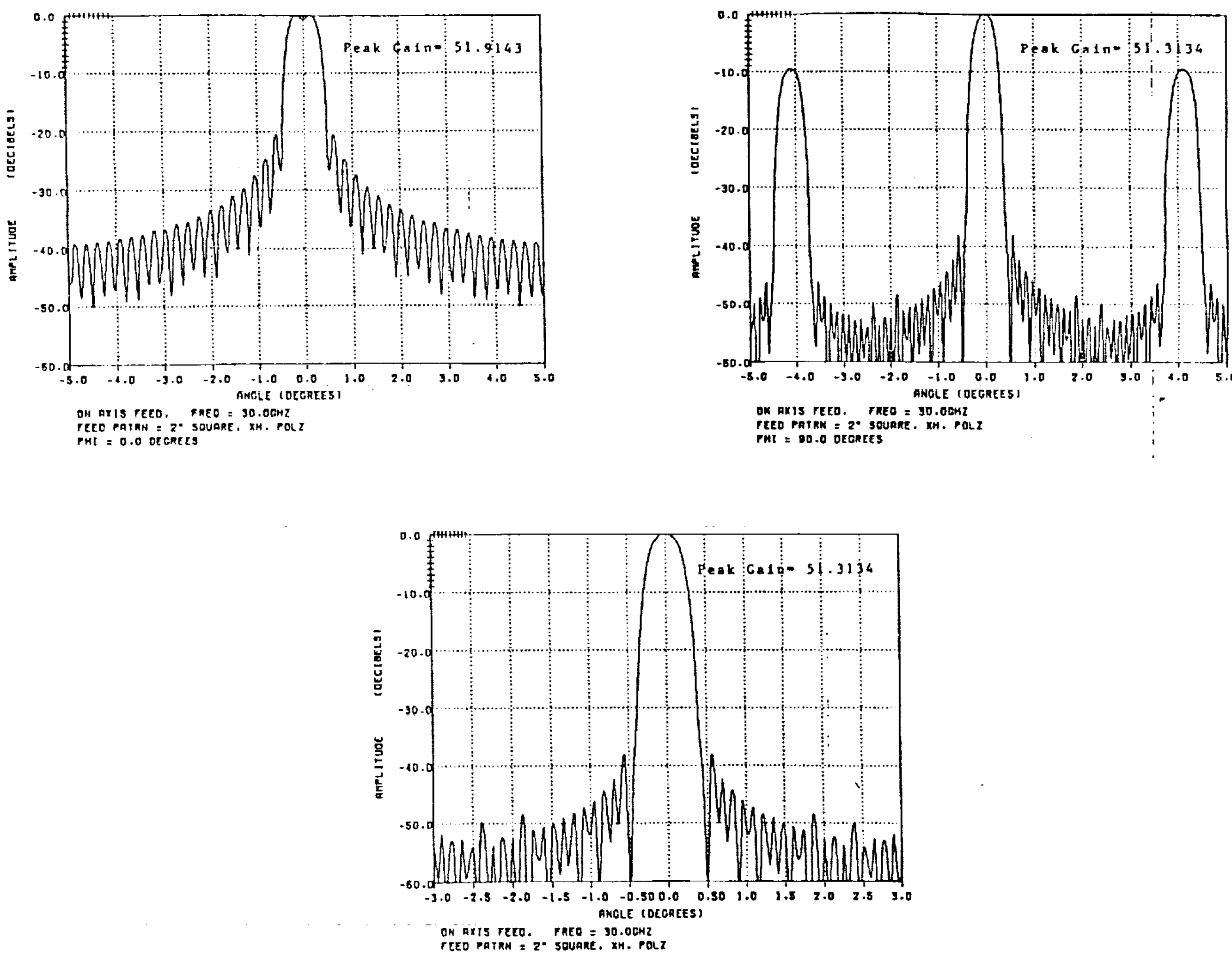

Figure 3.3-5a. Calculated Torus Patterns @ 30 GHz with 2 Inch Feed Horn

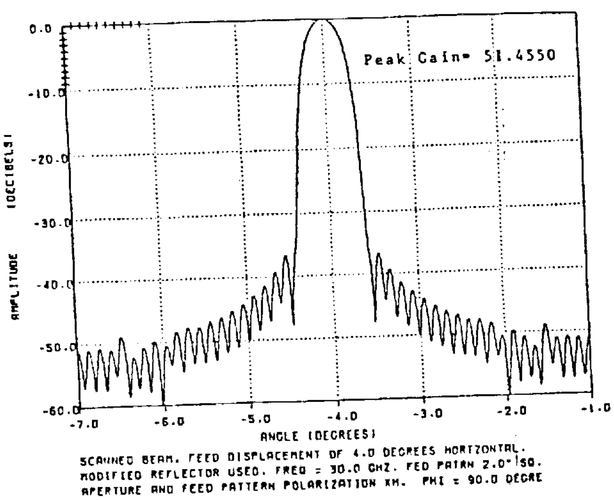

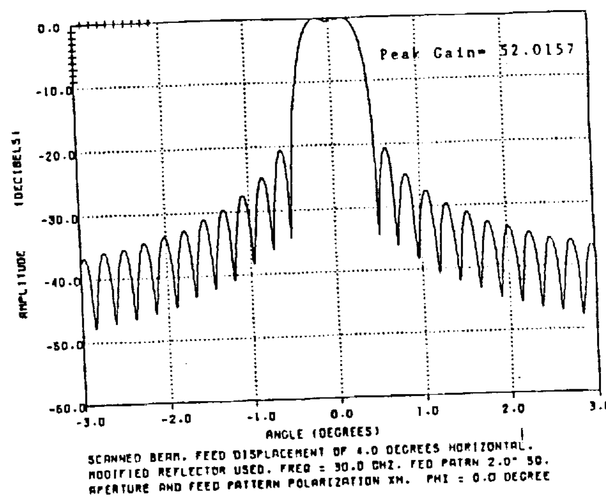

Figure 3.3-5b. Calculated Torus Patterns @ 30 GHz with 2 Inch Feed Horn

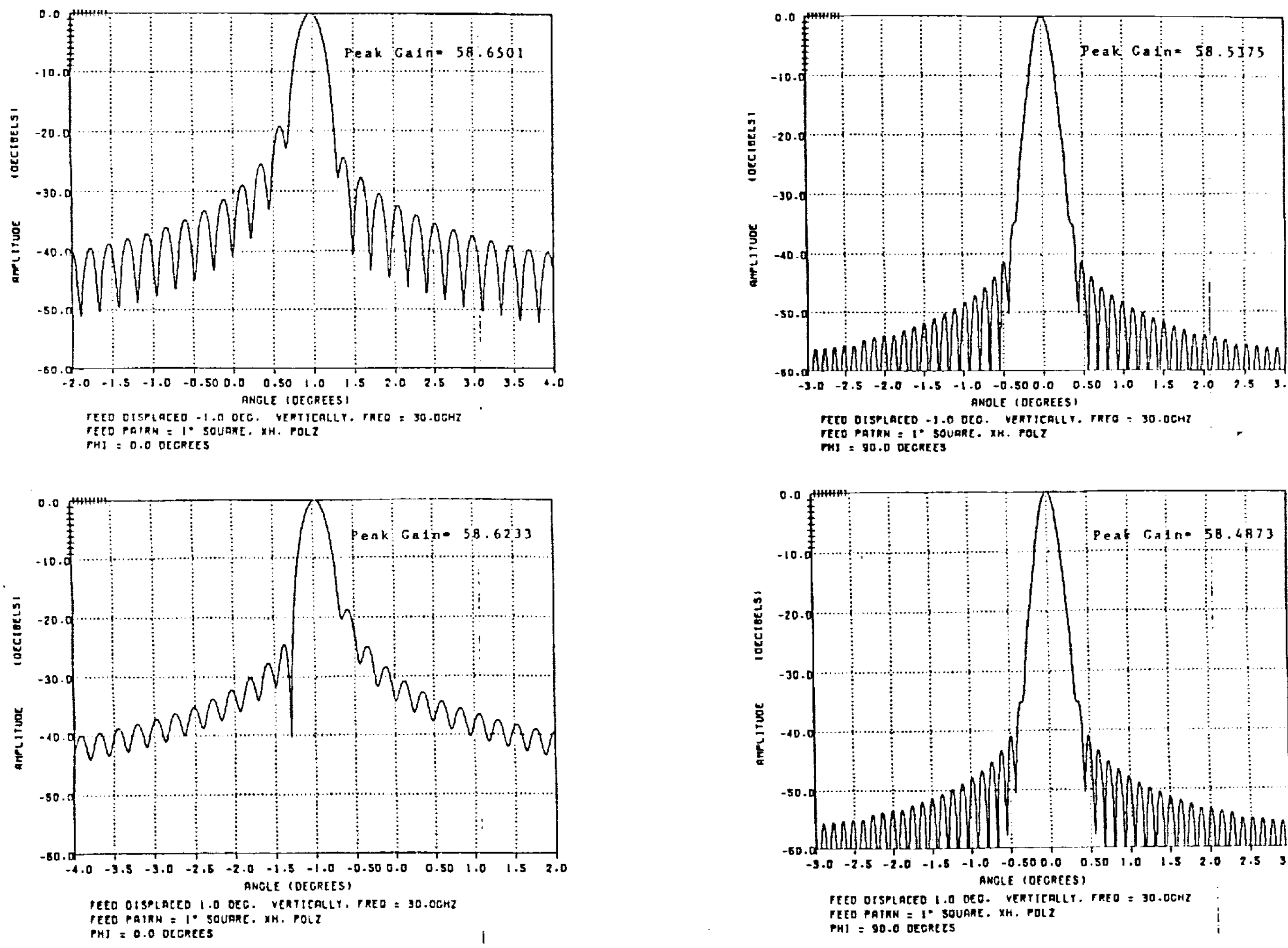

Figure 3.3-6a. Calculated Torus Patterns @ 30 GHz with 1 Inch Feed Horn

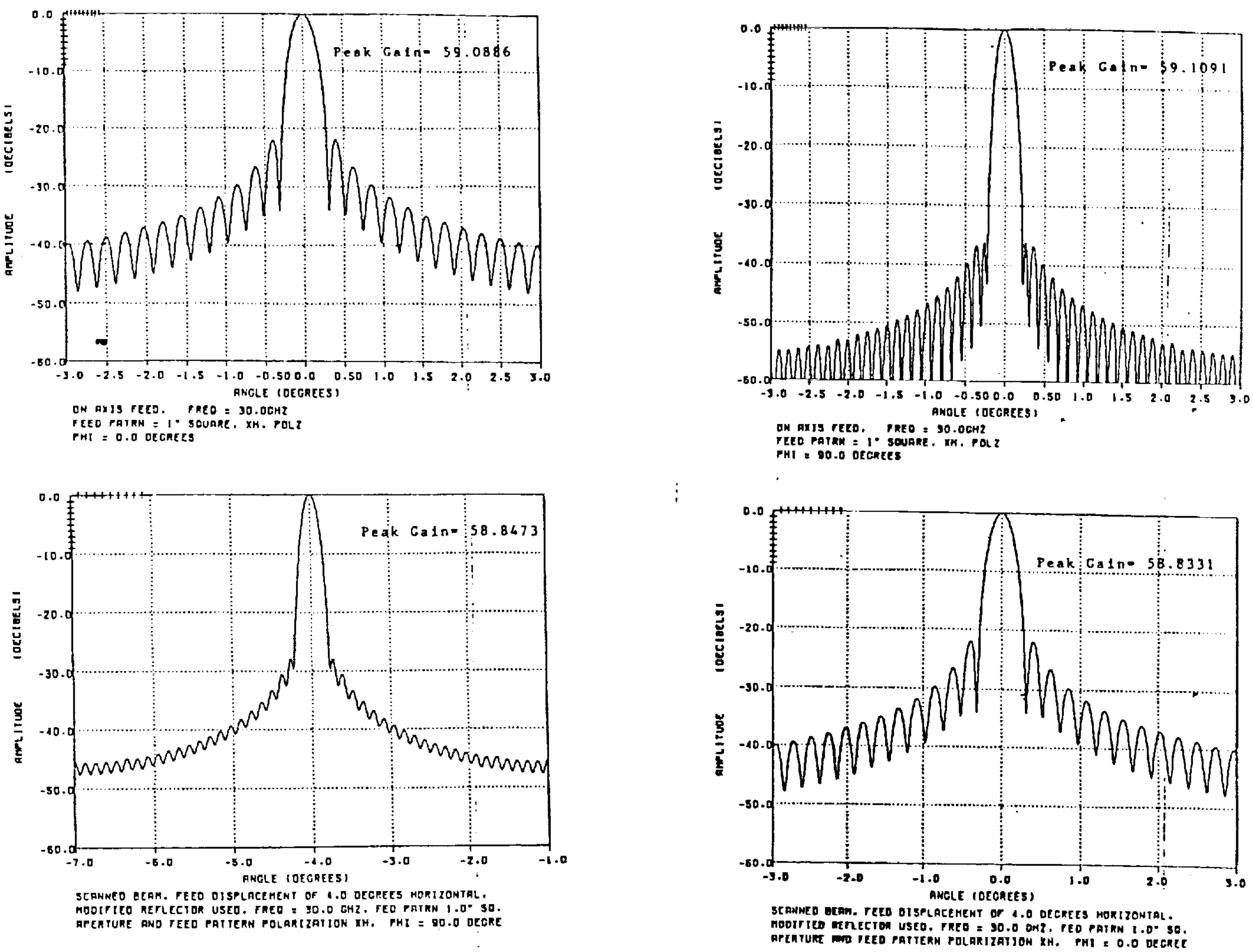

Figure 3.3-6b. Calculated Torus Patterns @ 30 GHz with 1 Inch Feed Horn

Table 3.3-1. Calculated Performance for Torus Antenna

Reflector size (in) = 96 x 176
Focal length (in) = 144
Radius of curvature (in) = 300

Characteristics at 30 GHz with 1 inch square horn feed, horizontal polarization

	Peak Gain dBi	10 dB Beamwidth Horiz.	10 dB Beamwidth Vert.	1st Sidelobe Horiz.	1st Sidelobe Vert.
Beam on axis	59.1	0.45°	0.3°	-23	-37 dB
Scanned 4° horiz	58.8	0.45°	0.3°	-22	-28 dB
Scanned 1° vert	58.6	0.45°	0.32°	-19	-25 dB

Characteristics at 20 GHz with 2 inch square feed horn, horizontal polarization.

	Peak Gain dBi	10 dB Beamwidth Horiz.	10 dB Beamwidth Vert.	1st Sidelobe Horiz.	1st Sidelobe Vert.
Beam on axis	53.2	0.81°	0.58°	-25	-36 dB
Scanned 4° horiz	53.15	0.81°	0.58°	-26	-37 dB
Scanned 1° vert	53.1	0.8°	0.6°	-24	-37 dB

Theoretical maximum gain of 96 x 176 inch aperture = 61.37 dBi @ 30 GHz

Calculated gain of torus = 59.0 dBi average
Apparent aperture efficiency = 58%
Phase errors apparently not too severe
Theoretical gain of 96 inch diameter circular aperture = 57.7 dBi
Apparent aperture efficiency @ 20 GHz = 47%
Feed horn too large in proportion

3.3.2 Dual Reflector MBA

As mentioned in our first monthly report, a dual reflector antenna may be adequate for our multibeam requirement to produce beams separated by as much as 12°, which represents 40 beamwidths at 30 GHz. While a torus reflector may be able to provide a better performance at this extreme scan limit, its greater size may be unattractive. Evaluation of expected performance from the dual reflector approach for various scan limits is the purpose of this section.

The most pertinent data available on the performance of scanned dual reflectors is that developed on Ford Aerospace's Contract NAS3-22498 with NASA Lewis for development of a MBA for full CONUS coverage from a synchronous satellite. After considering a number of different approaches, a method was devised to develop a pair of specially-shaped surfaces for use as dual reflectors in order to minimize the performance degradation (gain loss and increased sidelobes) usually associated with producing a beam from a focused reflector antenna system at a position off the focal point. This was done through an optimization process to minimize phase errors, determined through simple geometrical optics with a given pair of reflector shapes from a number of sample points over the desired coverage area. At the same time, the constraint of producing a planar focal surface was introduced in order to simplify construction of the feed array. The resulting surfaces, represented by a set of 10th-order polynomials, were fabricated as a proof-of-concept (POC) model which was extensively tested, verifying the theoretical design. This POC model is pictured in Figure 3.3-7. Typical measured patterns are shown in Figure 3.3-8, both on axis and scanned to the edge of CONUS, verifying that low-sidelobe patterns were maintained over this field of view. A limited number of gain measurements at some 15 points over this area were used to prepare the approximate gain contour chart shown in Figure 3-3-9, which represents the peak gain available for the narrow 0.3° beam over its field of view. This shows that the gain was maintained within 0.5 dB of the peak value over the entire 3° x 6° scan area, except for two small areas near the corners, where the gain loss approaches 1.0 dB. This contour plot superimposed on several CONUS maps from different spacecraft locations, in Figure 3.3-10, shows that the entire CONUS area required for ATDRSS coverage could be serviced with an antenna of this design with a gain variation of less than 0.5 dB for all stations except a possible mobile one near Seattle, Washington. Measured gain on this model was a maximum of 55.0 dB, consistent with the measured beamwidth of approximately 0.3°, and representing an aperture efficiency of 45% from theoretical for this 13 foot diameter main reflector operating at 19 GHz [3-2].

Extending this design to one optimized for scanning ±6.0° in one dimension only, as required for Configuration 2, appears feasible, with an estimated maximum scan loss of perhaps 1.0 dB. Thus this approach appears very attractive for the ATDRSS MBS application, and should be evaluated further relative to its mechanical integratibility and overall efficiency.

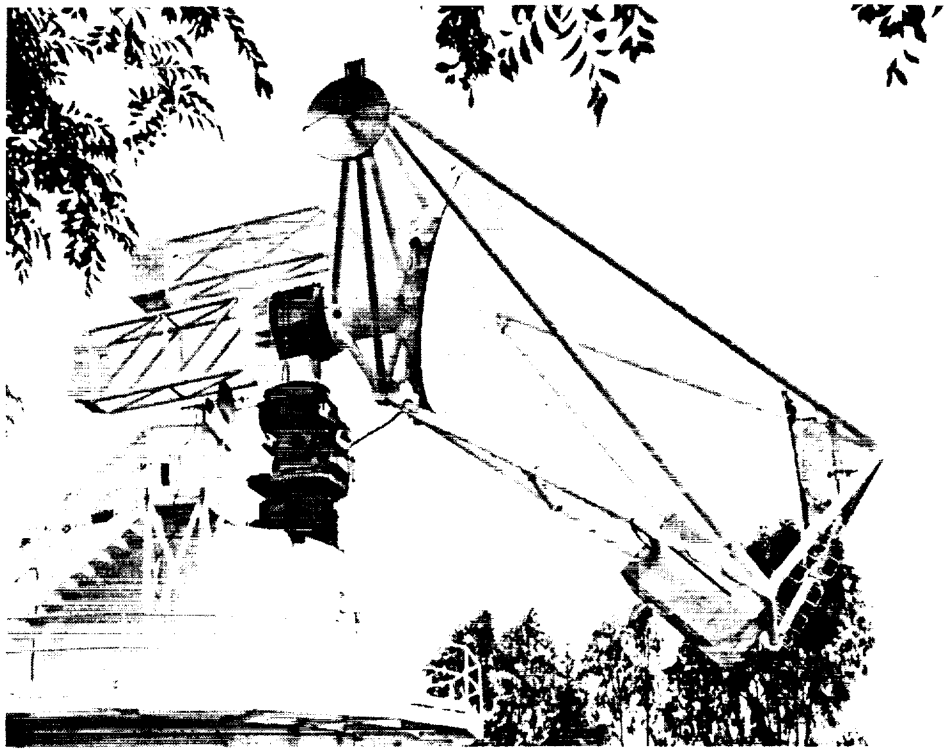

Figure 3.3-7a. NASA-ACTS POC Model 30/20 GHz MBA

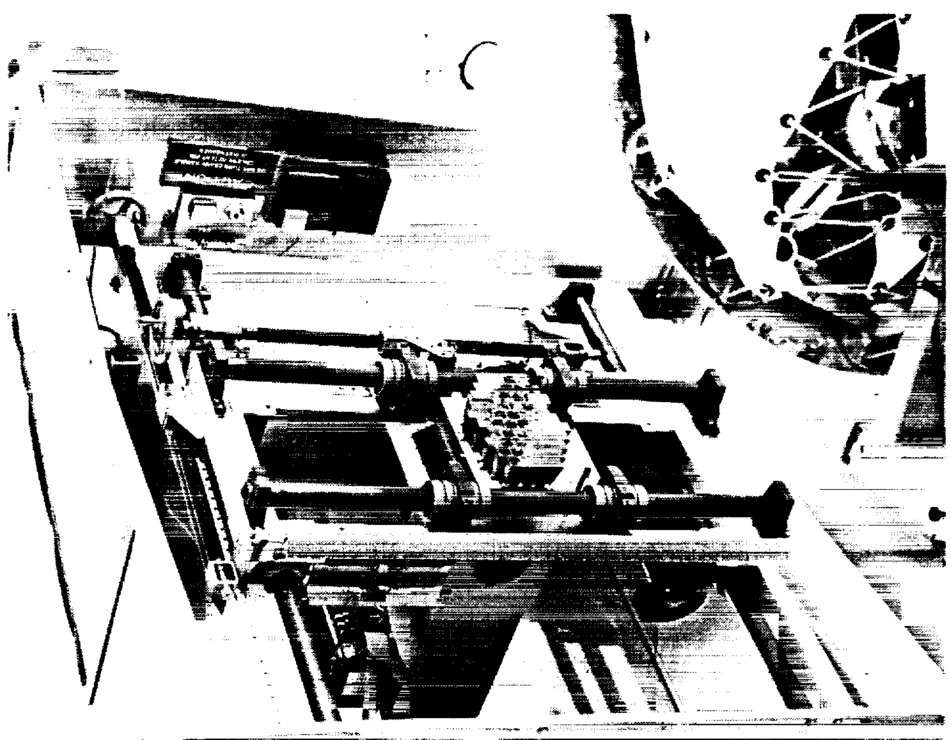

Figure 3.3-7b. NASA-ACTS 30/20 GHz MBA Feed Array

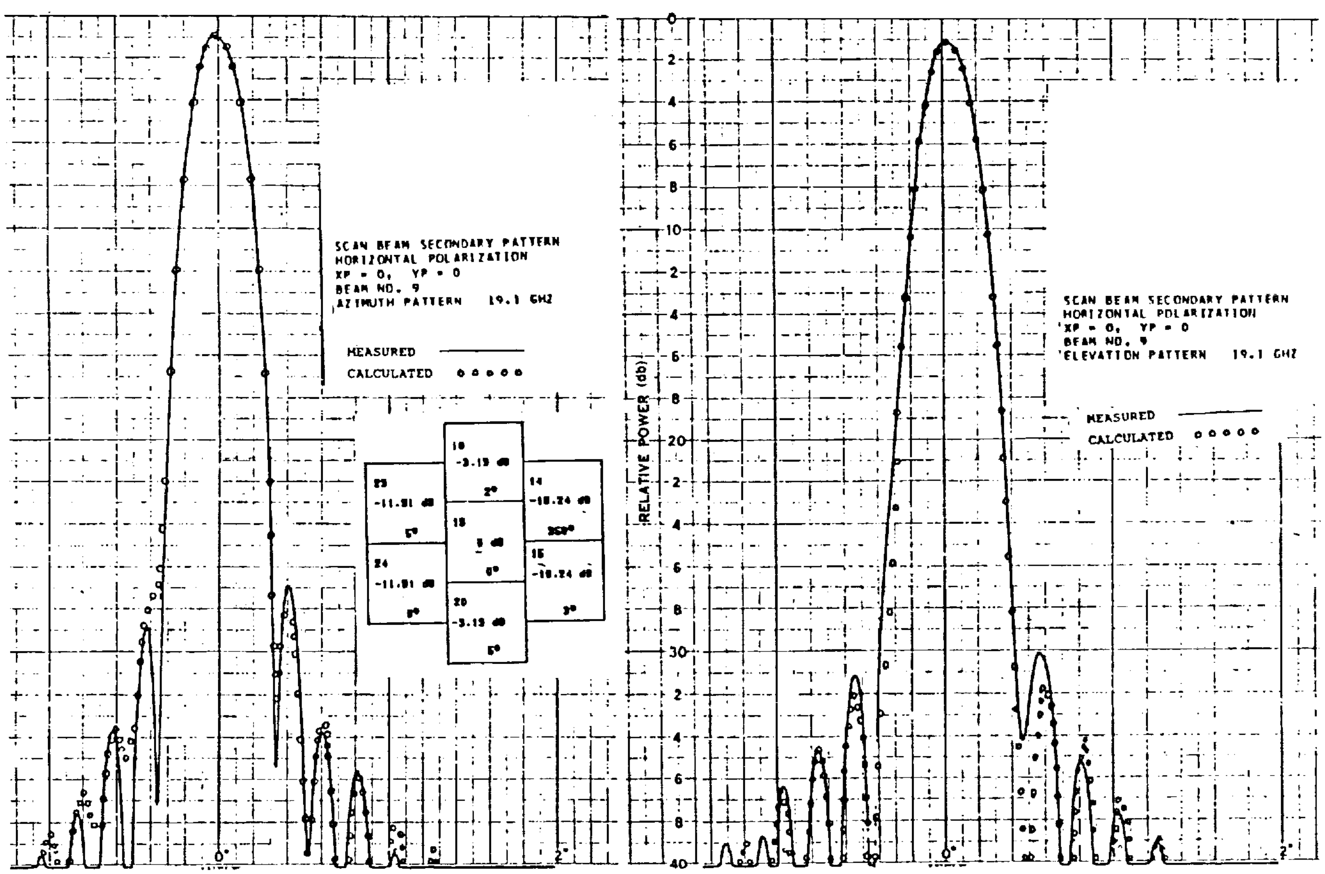

Figure 3.3-8a. NASA-ACTS 30/20 GHz MBA Patterns -- On Axis

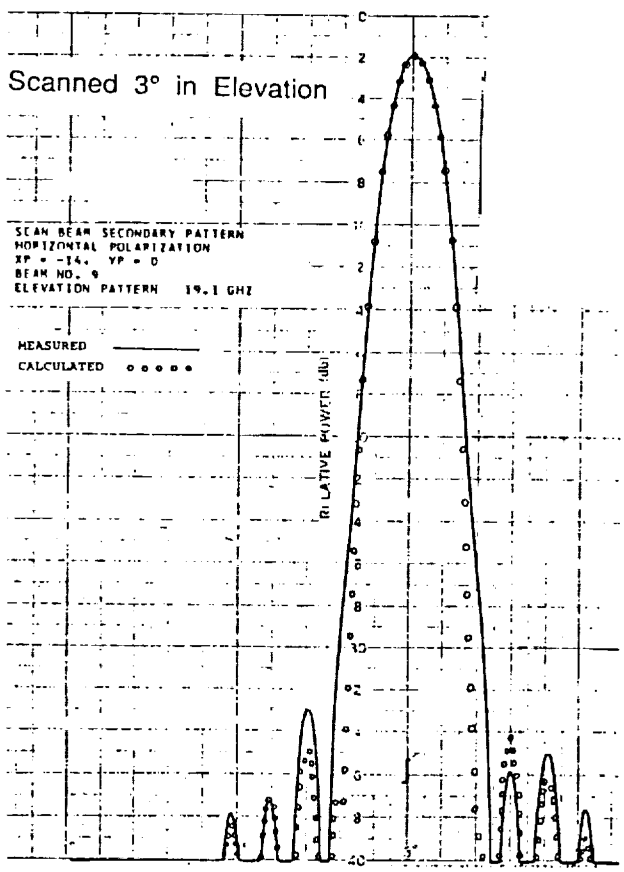

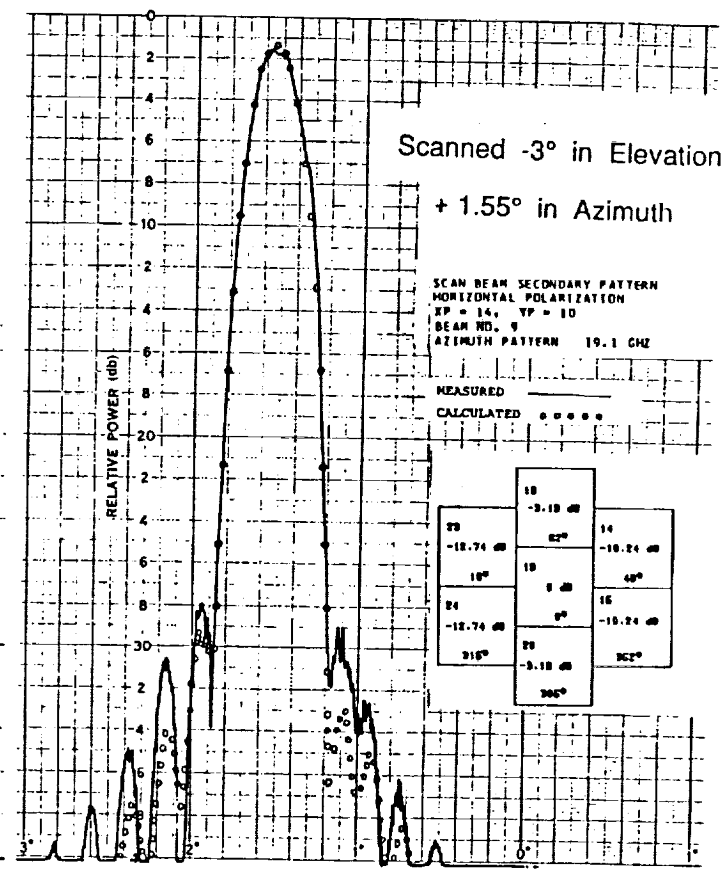

Figure 3.3-8b. NASA-ACTS 30/20 GHz MBA Patterns -- Off Axis

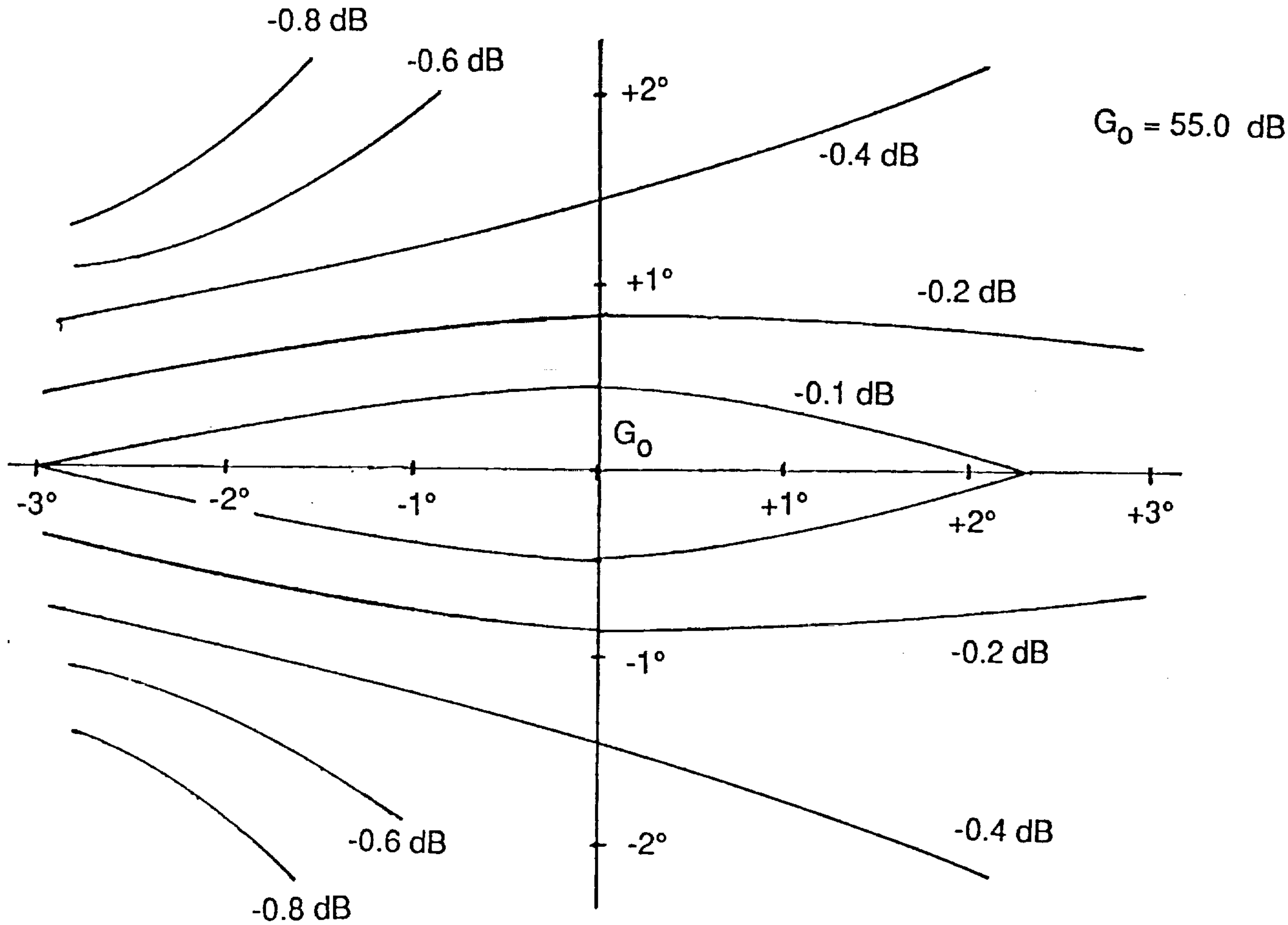

Figure 3.3-9. Measured Gain Contours -- ACTS POC Model Antenna

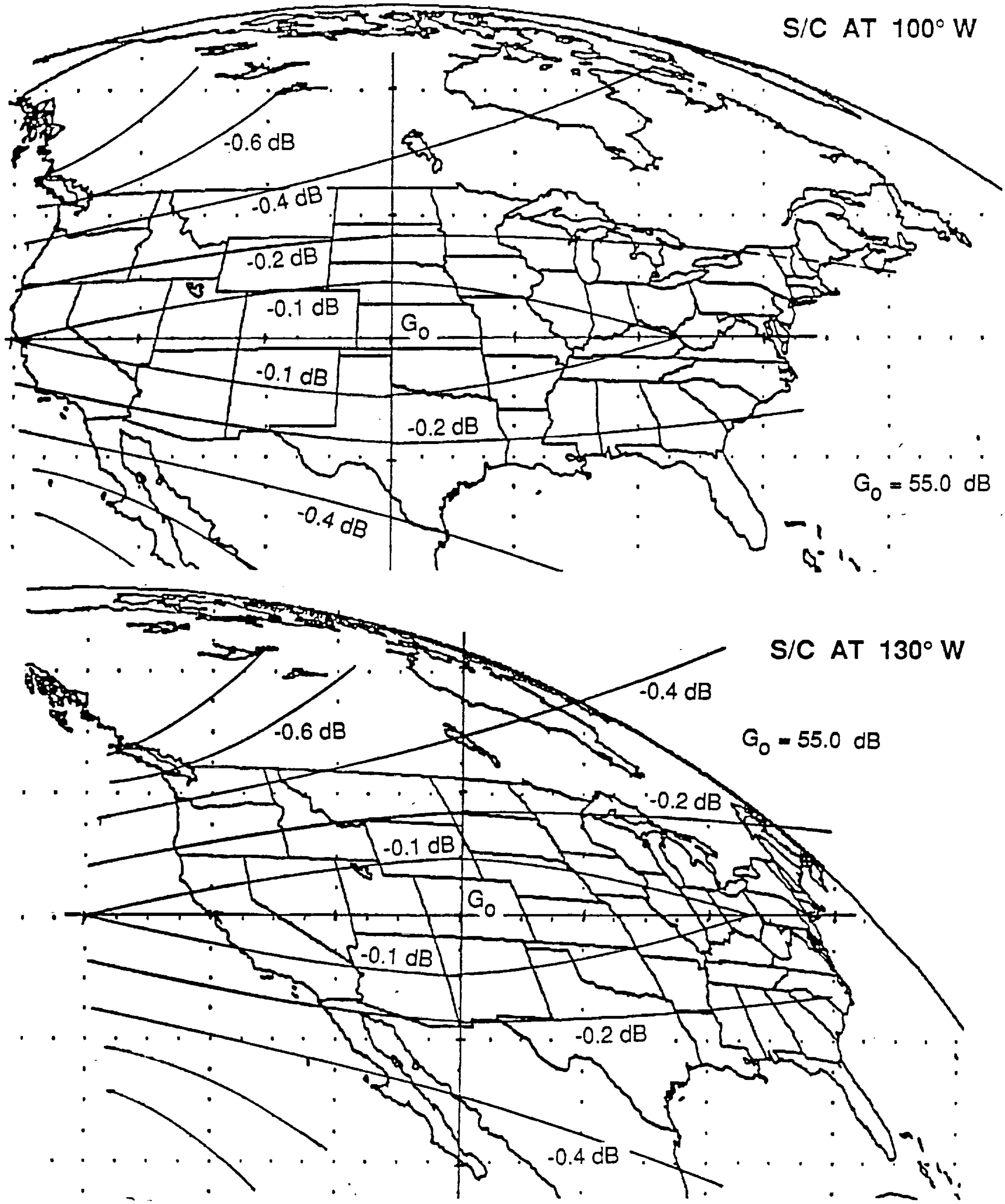

Figure 3.3-10. CONUS Coverage With NASA/ACTS-Type MBA

3.3.3 Multiple Beam Phased Array

The use of a phased array for the ADTRS multiple beam downlink antenna appears attractive, since the same set of array elements may be used for creating multiple beams merely by adjusting the phasing between elements in an appropriate manner. The basic size of the array will be governed by the gain requirement, which has been shown to lead to a radiating aperture size of approximately 8 feet in diameter. This aperture produces a beam with a beamwidth of approximately 0.3°. A conventional design with elements spaced less than one wavelength apart would lead to an array with nearly 60,000 elements at 30 GHz, which appears unmanageable. However, clever design with the use of subarrays can greatly reduce this number, depending upon scan requirements.

For an array which is required to scan over only a limited range, Patton [3-4] has shown that a reasonable minimum number of elements is given by:

$$N_{min} \cong \frac{\sin(\theta_1)\sin(\theta_2)}{\sin^2(\theta_3)}$$

Where θ_1 and θ_2 are the maximum scan angles in two orthogonal directions, and θ_3 is the 3-dB antenna beamwidth. We have shown previously that a scan range of 2° x 6° would be sufficient to cover most of CONUS from synchronous orbit. For an array beamwidth of 0.3°, the above relation indicates that a minimum number of array elements would be around 167. Because of the unequal E/W and N/S scan requirements, the array should naturally be composed of unequal numbers of elements in orthogonal planes. A 8 x 24-element array filling the 8-foot aperture would include 192 elements, just above the minimum. However, these elements would each be 4 x 12-inches in size, and would exhibit 3 dB element beamwidths of about 2.3° x 6.7°, producing nearly 3 dB gain degradation at the scan limits. To limit this scan loss to 1 dB, the element beamwidths would have to be 3.5° x 10.4°, corresponding to a size of about 7.8 x 2.6 inches, representing an array of 12 x 36 elements for a total of 432.

In order to implement dual-polarization capabilities, the elements must normally be symmetrical; this could be accomplished by making each element as an array of three 2.6-in square elements, whose outputs could be combined into a common port for each polarization. The total number of square elements would thus be 1296. A receive-only array using this concept to create six simultaneous beams for both polarizations could be configured as shown in Figure 3.3-11. This concept would require the following hardware:

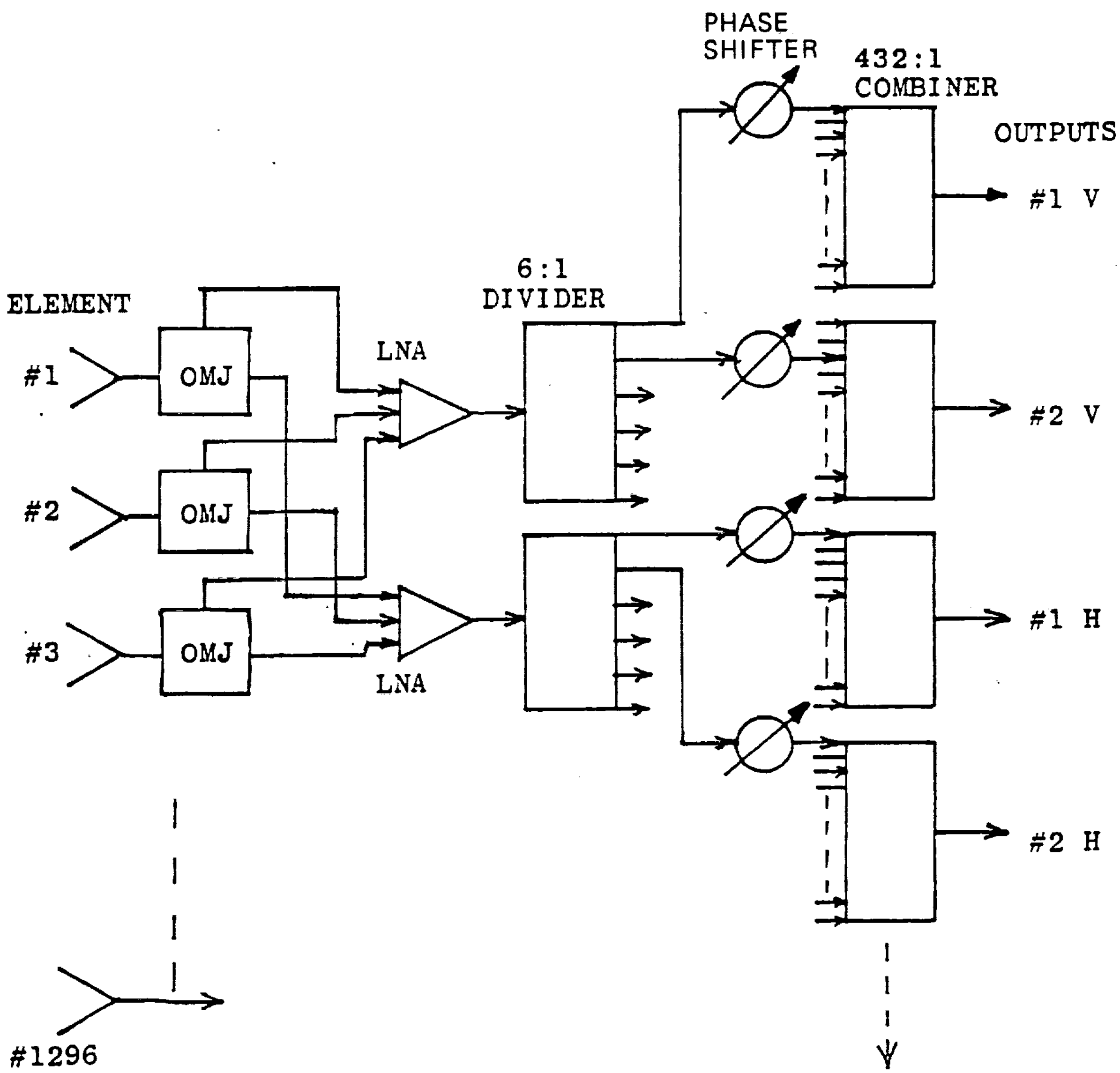

Figure 3.3-11. Phased Array MBA Receive Configuration

1296	radiating elements (horns, or other types)
1296	orthomode junctions to separate dual polarizations
864	three-way combiners to form composite elements
864	low-noise amplifier (phase coherent)
5184	phase control elements
12	power combiners, 432:1

All of these components would be required to operate over the full 3.5 GHz band, maintaining proper operating characteristics in both phase and amplitude for proper beam combining.

If the first three items in the above list could be realized in a form which would cover both the transmit and receive bands (17.7-21.2 GHz and 27.5-31.0 GHz), then a common receive/transmit array could be realized by introducing diplexers (864) in each path illustrated in Figure 3.3-11, and duplicating all the components beyond this point with appropriate transmit-band versions, replacing the low-noise amplifiers with power types. Otherwise, the entire configuration in Figure 3.3-11 would have to be duplicated for the transmit array. This would probably be preferable, since it would eliminate the need for 864 phase-matched diplexers, and for wideband components preceding these, and would also allow independent optimization of the design for the two bands.

One potential advantage of the phased array design for the MBA is the fact that the six beams for each polarization could be steered independently of each other, which would allow coverage of 12 different locations simultaneously, even with half the data rate capabilities of the dual-polarized design. However, the very great number of individual components represents a distinct disadvantage of the phased array approach, unless MMIC designs become feasible in these bands by 1993.

An alternative phased array approach favoring the use of MMICs is to incorporate downconverters (mixers) following the LNAs as shown in Figure 3.3-11, allowing all the power dividing and phase shifting to be done at a convenient IF (probably at X-band to accommodate the 3.5 GHz bandwidth). The front-end hardware (radiating elements and orthomode junctions) would probably best be accomplished in waveguide, because of the bandwidth and polarization purity requirements. One of the remaining problems in the use of MMICs is that of three-dimensional interconnections with these waveguide ports.

Another disadvantage of the phased array is that independent polarization rotation of the individual beams is not possible, unless it were done at IF by combining orthogonal components generated by the suggested circuit. The amount of isolation which could be maintained over the 3.5-GHz bandwidth with this scheme is questionable.

3.3.4 Phased Array Tolerances

A concern for the possible deleterious effects of phase tolerances on the performance of a phased array for the ATDRSS multiple beam downlink led us to the task of preparing a number of contour plots of beams from a typical array as follows: A hexagonal array of 91 elements which had been set up for another project, appears close enough to a possible ATDRSS design to be useful for this evaluation. This design consisted of a set of 8.4-inch diameter elements arranged as shown in Figure 3.3-12 for an effective array diameter of about 7 feet for the ATDRSS uplink gain requirement. Patterns for this array were generated at 12.5, 18, and 28 GHz with equal amplitude and phases for all elements using element patterns of a circular horn. These are shown in Figures 3.3-13, 3.3-14, and 3.3-15. In addition, a set of random variables was set into the phases, and the patterns recalculated, as also shown in these figures. Both positive and negative errors were allowed. Several runs were calculated for peak error values changing from 18° to 90°.

The random error values were derived from the relationship:

$$\Delta\phi = \Delta\phi_{max} \times DP^2 \times SIGN\ (DP), \text{ where } DP = 2.0 \times (RAND\ (1.0) - 0.5)$$

Where RAND(1.0) is a random variable uniformly distributed in the range 0 to 1. These phase perturbations are listed in Table 3.3-2.

At 12.5 GHz, very little difference is seen in the main beam patterns, even down to the -20 dB levels, for as much as 90° maximum phase errors. However, the sidelobe patterns drastically change for the 45° and 90° cases, showing nulls which are not as deep as originally and additional peaks up to he-20 dB level. This suggests that a maximum phase error goal of 18° should be adopted. The only set of patterns calculated at 18 and 28 GHz is for this case. Even this degree of error has considerable effect on the near-in sidelobes at 28 GHz. Is is also interesting to note that even the 90° maximum phase error case at 12.5 GHz had only 0.1 dB effect on the calculated peak gain.

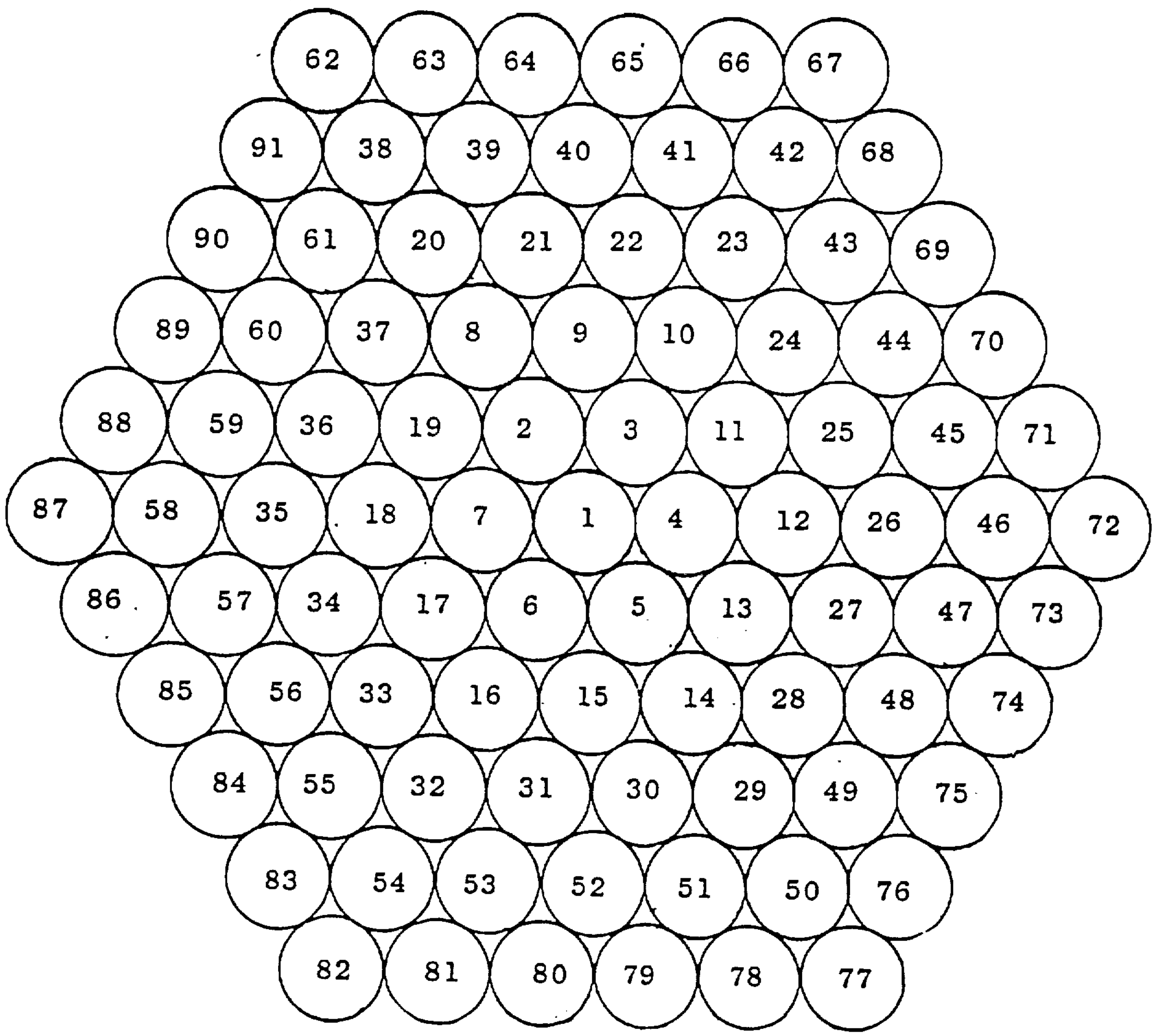

Figure 3.3-12. 91-Element Array Configuration

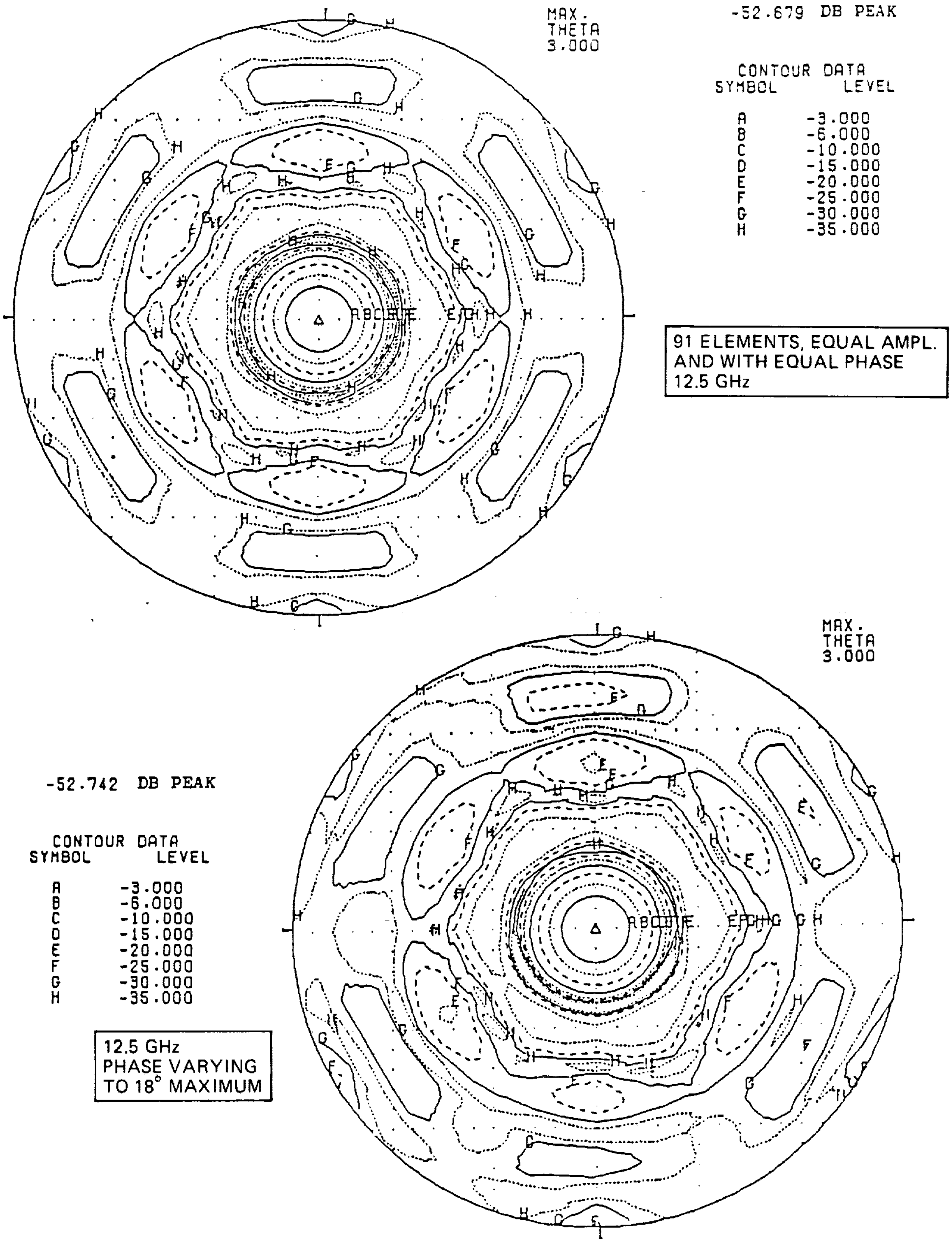

Figure 3.3-13a. 91 Elements, Equal Amplitude and Various Phases

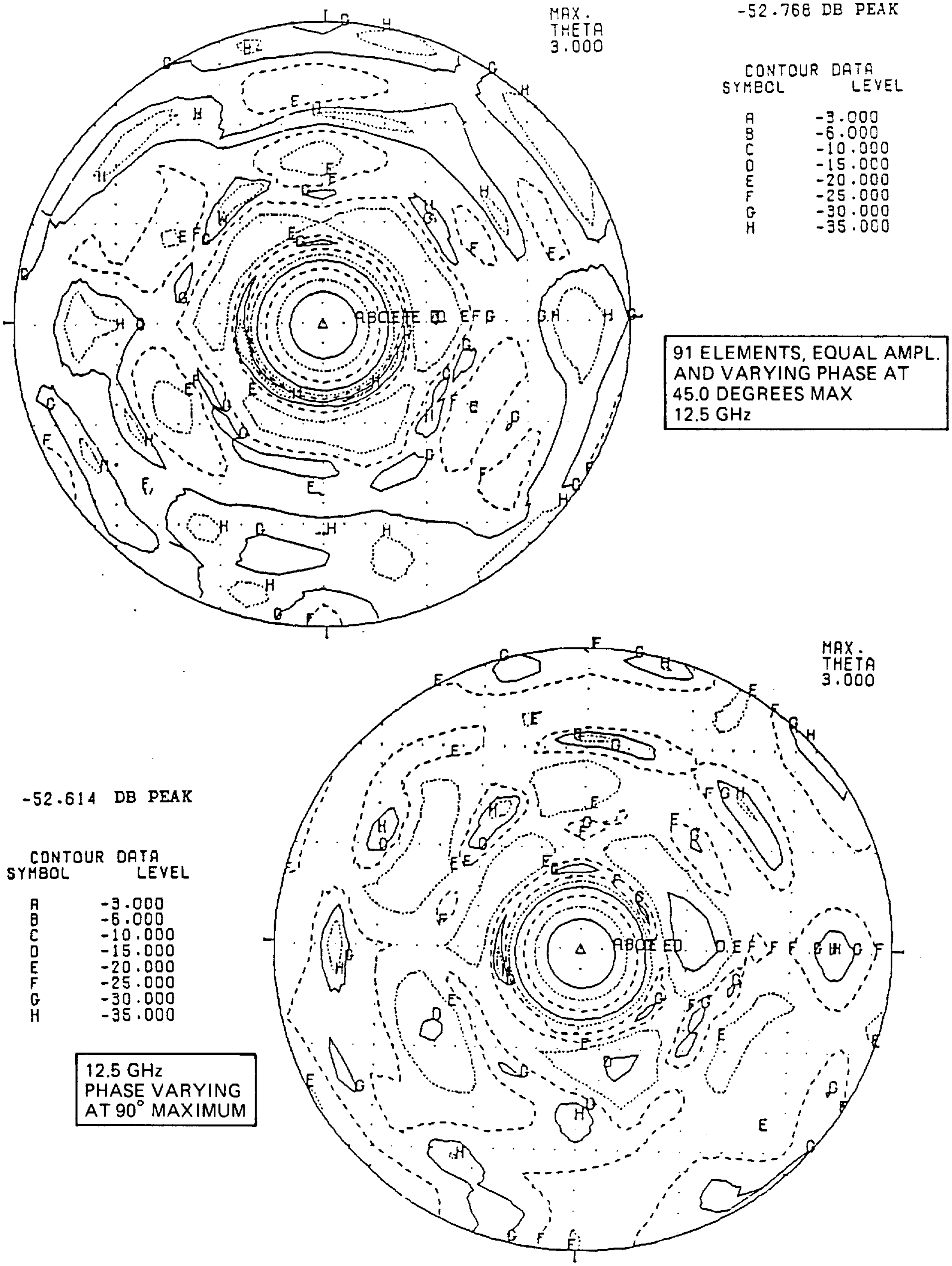

Figure 3.3-13b. 91 Elements, Equal Amplutide and Various Phases

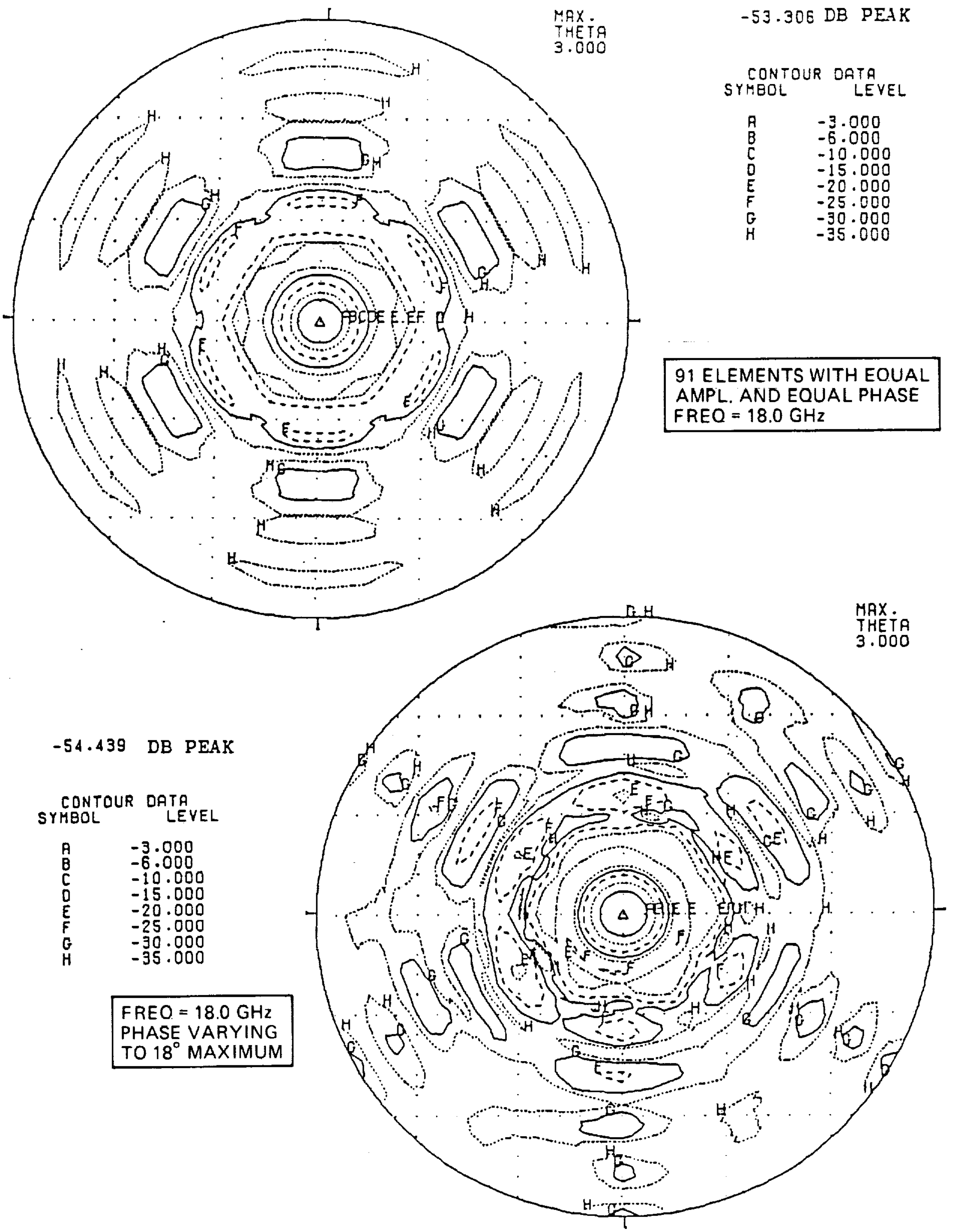

Figure 3.3-14. 91 Elements, Equal Amplitude and Various Phases

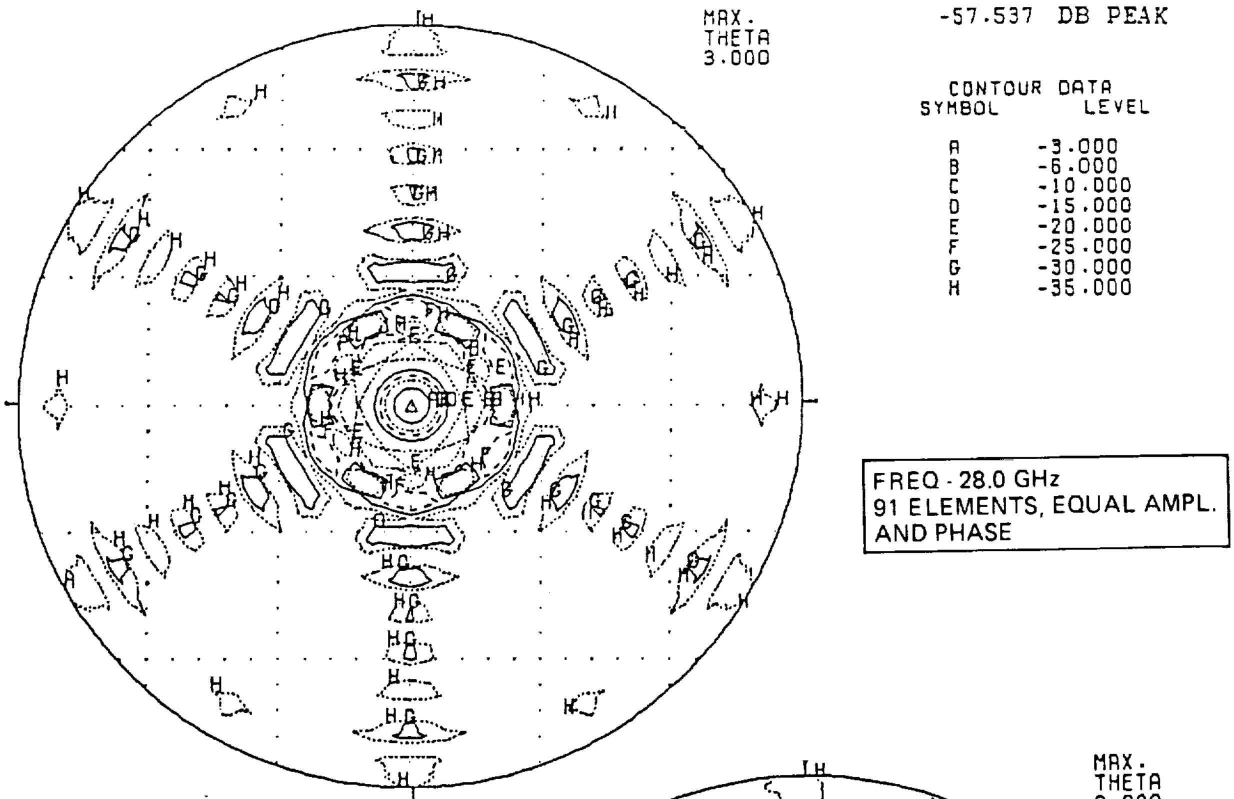

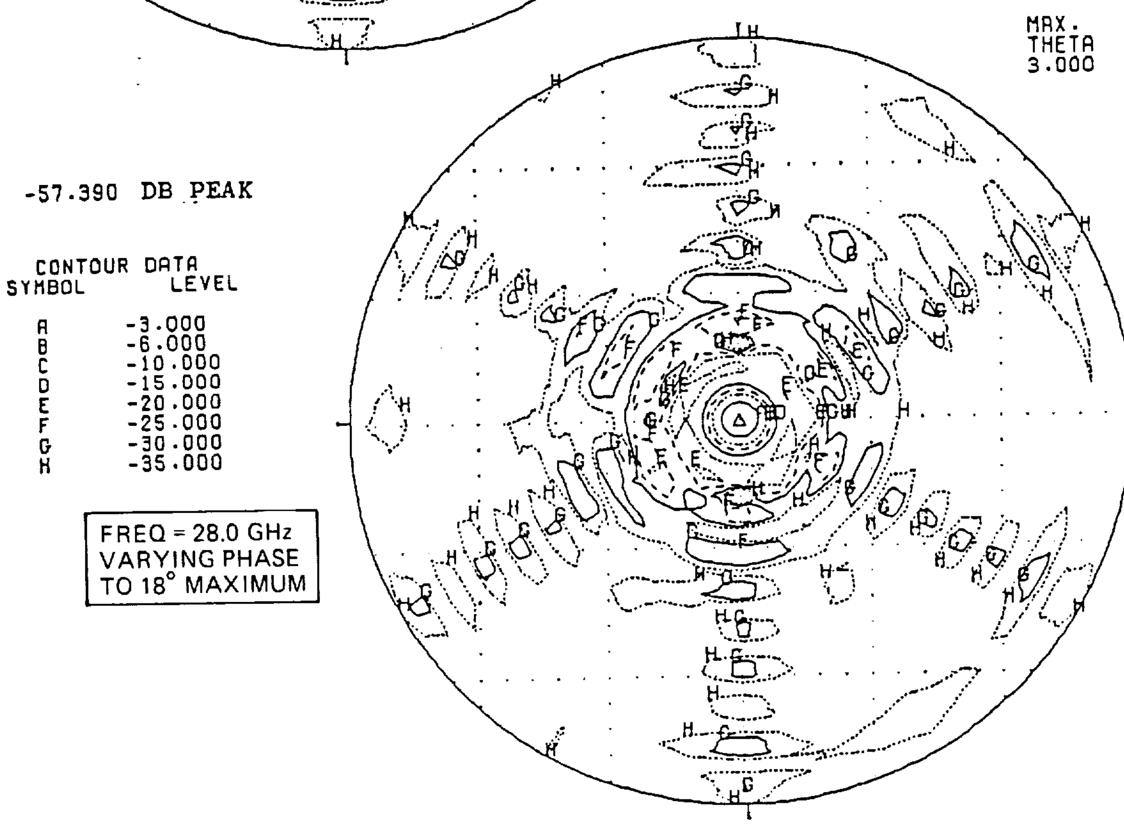

Figure 3.3-15a. 91 Elements, Equal Amplitude and Various Phases

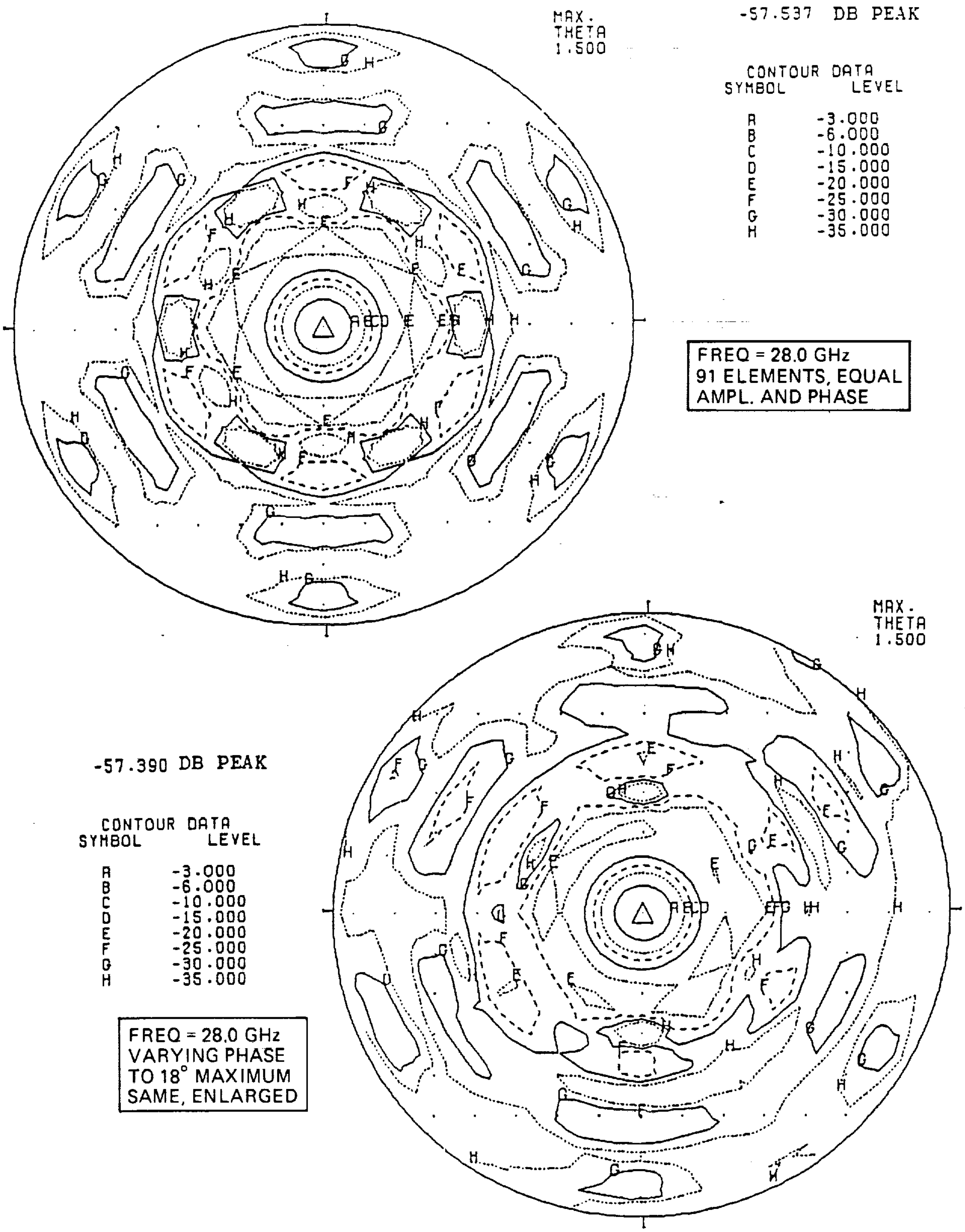

Figure 3.3-15b. 91 Elements, Equal Amplitude and Various Phases

Table 3.3-2. Random Phase Errors Used

EL. NO.	$\phi_{max} = 18°$	$\phi_{max} = 45°$	$\phi_{max} = 90°$	EL. NO.	$\phi_{max} = 18°$	$\phi_{max} = 45°$	$\phi_{max} = 90°$
1	1.85	4.63	9.27	51	-17.56	-43.90	-87.81
2	-0.72	-1.82	-3.64	52	-13.99	-34.98	-69.96
3	9.83	24.59	49.18	53	0.38	0.96	1.92
4	-0.39	-0.98	-1.97	54	0.20	0.51	1.02
5	-10.07	-25.17	-50.35	55	-1.38	-3.45	-6.91
6	-5.60	-14.02	-28.04	56	0.00	0.00	0.00
7	-9.33	-23.32	-46.65	57	9.39	23.47	46.95
8	-1.48	-3.71	-7.42	58	-1.76	-4.41	-8.82
9	-0.15	-0.39	-0.79	59	-2.14	-5.36	-10.72
10	-0.87	-2.19	-4.38	60	-7.72	-19.31	-38.62
11	5.45	13.63	27.27	61	2.09	5.24	10.49
12	0.00	0.02	0.04	62	-0.00	-0.00	-0.00
13	14.94	37.36	74.72	63	7.83	19.58	39.17
14	-4.19	-10.48	-20.96	64	-15.19	-37.98	-75.96
15	0.00	0.00	0.01	65	-0.81	-2.03	-4.06
16	11.87	29.67	59.35	66	7.12	17.80	35.60
17	5.58	13.96	27.93	67	11.03	27.58	55.16
18	0.13	0.33	0.67	68	1.35	3.39	6.79
19	-4.04	-10.11	-20.22	69	-7.58	-18.96	-37.93
20	0.16	0.41	0.82	70	2.86	7.16	14.32
21	-2.62	-6.56	-13.13	71	5.52	13.81	27.63
22	17.56	43.90	87.80	72	0.06	0.15	0.30
23	1.20	3.01	6.30	73	-10.10	-25.25	-50.51
24	-11.60	-29.01	-58.03	74	-5.84	-14.60	-29.20
25	14.84	37.12	74.24	75	-12.40	-31.00	-62.00
26	-4.69	-11.74	-23.48	76	7.52	18.81	37.63
27	-1.22	-3.05	-6.11	77	16.38	40.97	81.94
28	0.48	1.20	2.40	78	-0.07	-0.19	-0.39
29	1.34	3.36	6.73	79	0.04	0.11	0.22
30	-7.86	-19.66	-39.32	80	-12.16	-30.42	-60.84
31	1.45	3.64	7.28	81	9.39	23.47	46.95
32	-5.55	-13.88	-27.76	82	-1.75	-4.39	-8.79
33	-8.62	-21.57	-43.14	83	-2.08	-5.20	-10.41
34	-0.00	-0.01	-0.03	84	-6.64	-16.60	-33.20
35	4.51	11.28	22.56	85	11.63	29.09	58.19
36	-3.80	-9.51	-19.02	86	4.14	10.37	20.74
37	0.99	2.47	4.95	87	-7.82	-19.56	-39.12
38	16.66	41.65	83.30	88	1.62	4.06	8.12
39	0.00	0.00	0.00	89	-2.88	-7.21	-14.43
40	11.21	28.03	56.06	90	11.77	29.43	58.87
41	2.03	5.07	10.15	91	4.96	12.42	24.84
42	-0.05	-0.14	-0.28				
43	0.37	0.93	1.86				
44	0.12	0.31	0.62				
45	-4.57	-11.43	-22.87				
46	-0.69	-1.72	-3.45				
47	11.27	28.19	56.39				
48	2.31	5.77	11.55				
49	0.46	1.15	2.30				
50	1.03	2.58	5.17				

Some thought needs to be given to the type of phase shifters which would be employed for such an array. For a 7-foot array at 30 GHz, a 3° scan would require a maximum phase variation across the array of over 11 wavelengths. If a modulo-360° phase shifter were used, it would introduce an error of 235° at the edges of a 3500-MHz band at 30 GHz, which would be intolerable. Thus, it is concluded that a true time delay phase shifter would be required. For a digital-type device with a minimum bit size of 9° (half the suggested maximum error tolerable), this range of delay would require a 9-bit phase shifter (0.025 to 6.4 wavelengths). Although devices of this type could be built reliably and reproducibly using MMIC techniques, this longest bit would require a line length of 2.5 inches (in air), difficult to implement on an MMIC substrate. One potential alternative to this dilemma would be to incorporate most of this line-length differential directly in the power dividers/combiners for individual beams for a predetermined set of beam positions. Small variations could be handled with, perhaps, 6-bit variable phase shifters on each element; these could also incorporate adjustments for initial calibration of the longer line elements.

Although the maximum phase error of 18° would represent an impossible tolerance to hold on a 6.5-wavelength (2304°) bit, initial calibration could remove the major portion of any errors in fabrication, while temperature-induced variations would affect all elements equally and so would not require compensation.

3.4 ANTENNA FEEDS

3.4.1 Requirements

All of the reflector approaches for the multibeam downlink antennas will require a number of multiband feeds to create the individual beams. It is the purpose of this section to examine possible designs for these feeds. The requirements may be summarized as follows:

Antenna Feed Requirements

Frequencies:	13.4 - 15.23 GHz (Ku) -- 12.8% 17.7 - 21.2 GHz (Ka Transmit) -- 18.0% 27.5 - 31.0 GHz (Ka Receive) -- 12.2%
Polarizations:	Dual orthogonal linear in each band
Beamwidth and Shape:	Adequate for illumination of reflector with typical f/D = 1.0, shaped for high efficiency and low sidelobes (typical beamwidths of 45° to 50°)

3.4.2 Configurations

The form that the feed may take is restricted by the proximity of adjacent beams. Some applications require that a continuous array of beams be available with crossovers between beams at approximately the -3 dB levels for continuous area coverage, as for the NASA Lewis ACTS antenna referenced in paragraph 3.3.2. This design utilized a contiguous array of some 500 square horns, each about 2 wavelengths in aperture size. Individual horns produced relatively high-sidelobe beams; in order to achieve low sidelobes, a cluster of seven adjacent horns was excited for each beam with proper amplitudes and phases. This allowed adjacent beams to be positioned only one beamwidth apart with measured sidelobes approaching -30 dB. Our present application restricts adjacent beams to be at least two beamwidths apart, for adequate isolation; thus horn sizes of at least four wavelengths are allowable, which is certainly adequate for producing the beamwidths desired without requiring the rather awkward cluster feed approach.

An examination of the frequency requirements for the feeds shows that the three multiple bands cover a range of greater than an octave, so that simple rectangular waveguide components designed to support the lowest band will support multiple higher modes in the upper bands. Thus it is highly recommended that some alternate approach be taken so that a single feed is not required to cover all three bands. This may be done either by utilizing a separate reflector for one of the bands (as suggested by the isolation problems), or by spatial filtering (as with the use of a frequency-selective reflector (FSS)).

One feed actually built by Ford Aerospace for the Japanese CS spacecraft antenna combined four bands (4, 6, 20, and 30 GHz) into one large tapered conical feed horn illuminating a spinning offset-fed shaped reflector. The lower bands were introduced into the horn through slots at the appropriate locations along the horn with special filtering to prevent excessive losses in higher bands. However, the complexity, criticality, and bandwidth performance achieved suggest that this would not be an appropriate approach for the multiple closely spaced feeds required for the present application.

If a common aperture were to be used for all three bands, separate feeds for at least one of the bands could be provided by inserting a planar FSS between the reflector system and the feeds to create a virtual focal point for the reflected bands as depicted in Figure 3.4-1. Optimum performance would be achieved by separating the bands which are farthest apart in frequency by the FSS; these are the 20 and 30 GHz bands. Thus the 14 and 20 GHz bands would be combined into a common feed horn, automatically minimizing the bandwidth required for this horn. Ford Aerospace has developed an FSS for separating the 20 and 30 GHz bands on an IR&D program. The design consists of two sheets of crossed dipoles printed on thin mylar, separated by appropriate thickness of low dielectric material as shown in Figure 3.4-2. Measured performance of a model of this structure is given in Figure 3.4-3, showing that losses in each of the bands are less than 0.2 dB. Note that the higher frequency band is reflected from the FSS due to resonance of the dipoles, while the lower frequency is transmitted. This method of operation automatically ensures even better performance at frequencies below the lower band, since the dipoles are farther from resonance at 14 GHz.

Details were made available relative to the calculated performance of a typical FSS design developed for another program, which was intended to separate the 20 and 44 GHz bands. Calculated amplitude and phase of waves transmitted through the FSS over a 20% band around 20 GHz are shown in Figures 3.4-7 and 3.4-8 for various polarizations and angles of incidence (θ_i). These show that the loss is under 0.1 dB over most of this band, except for one polarization case, and that the phase response is well behaved (nearly linear) for all cases. There is some difference in phase (up to 25°) for orthogonally-polarized signal for incidence angles of 45°, which could cause some signal distortion; however, this could be minimized by orienting the FSS so that incidence angles are minimized for transmitted bands.

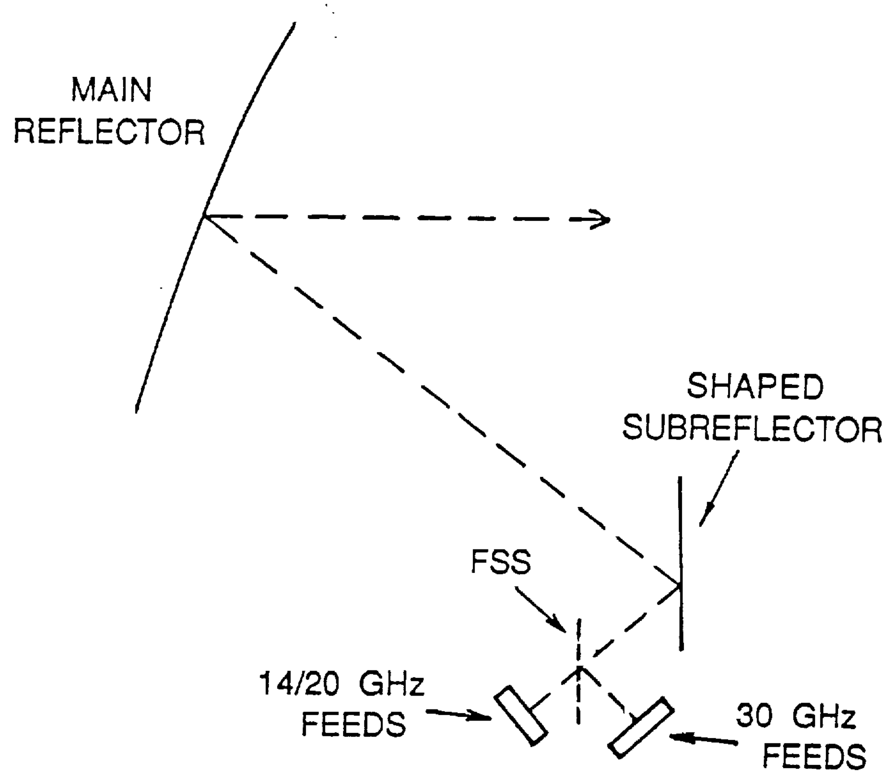

Figure 3.4-1. Dual-Reflector Antenna with FSS for Band Separation

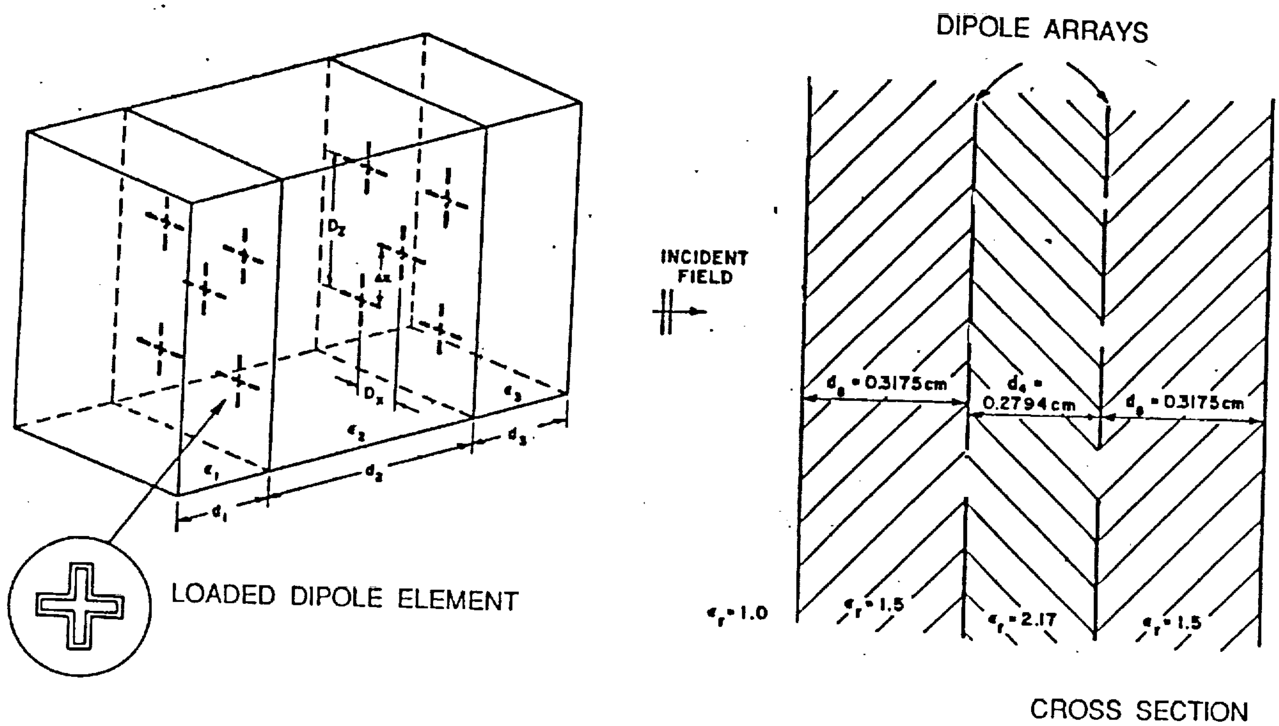

Figure 3.4-2. FSS Configuration: Two Planar Arrays of Crossed Dipoles Between Three Dielectric Sheets

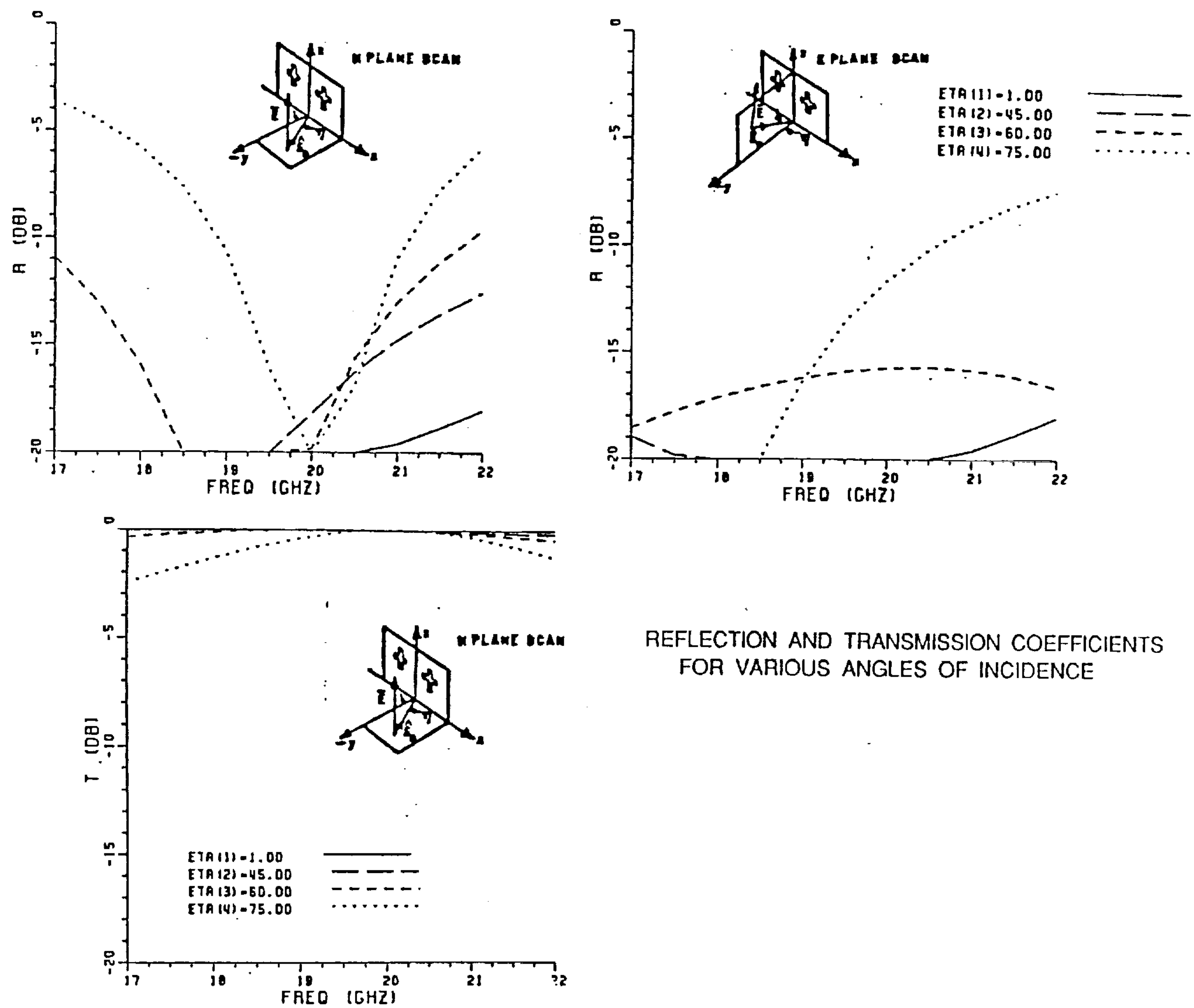

REFLECTION AND TRANSMISSION COEFFICIENTS FOR VARIOUS ANGLES OF INCIDENCE

Figure 3.4-3a. Calculated FSS Performance -- 20 GHz Band

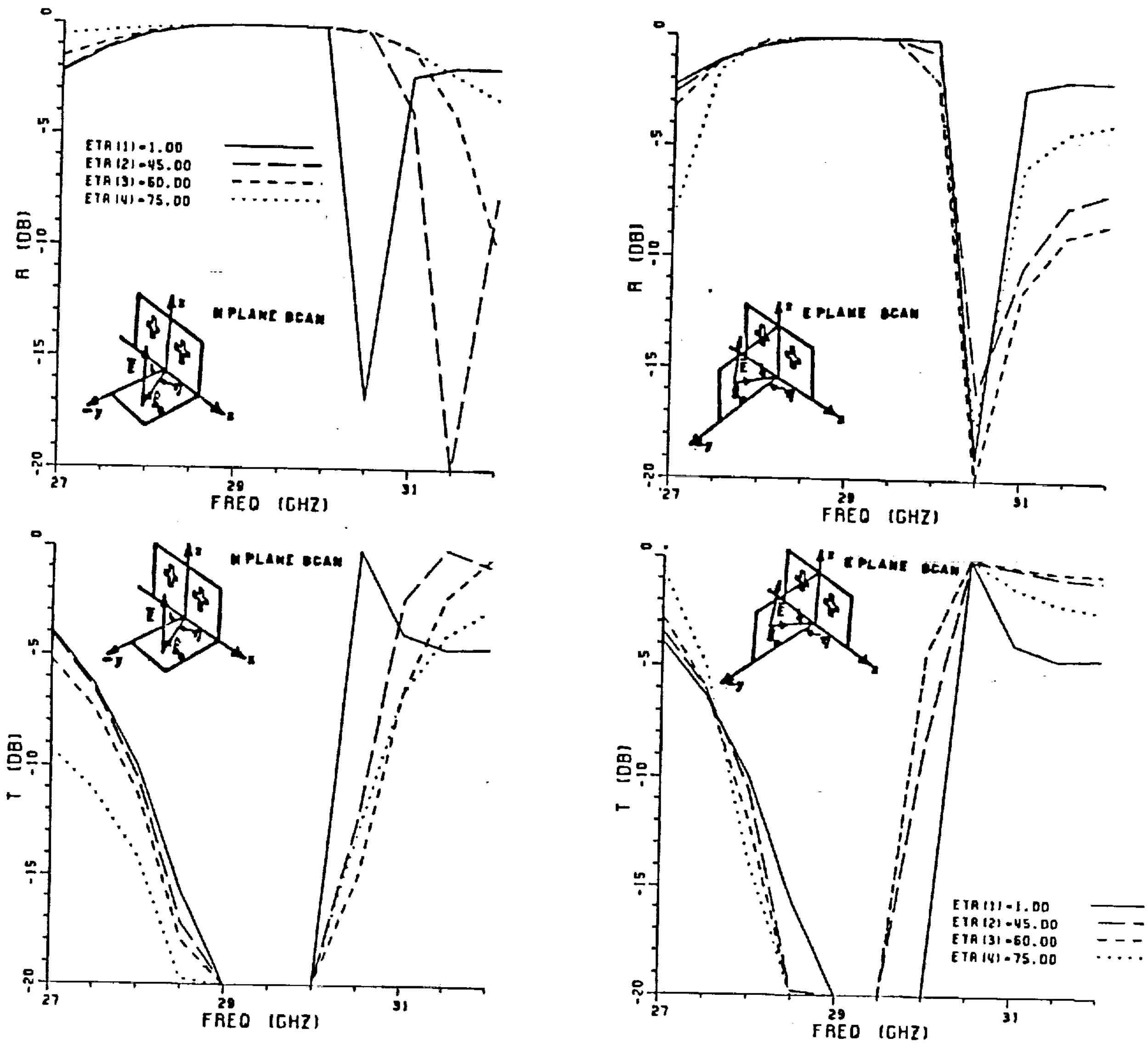

Figure 3.4-3b. Calculated FSS Performance – 30 GHz Band

3.4.3 Feed Design

Two possible approaches are suggested for a dual-band feed for either 14/20 GHz or 20/30 GHz: (1) a cascaded set of orthomode junctions (OMJs) (one for each band), or (2) a pair of concentric horns, each with its own orthomode junction (for polarization separation). The first approach was used for the Japanese CS antenna to cover the 20 and 30 GHz bands. A model of this device is shown in Figure 3.4-4. The OMJs are separated by a stepped section of waveguide, so that the lower band is reflected from this section. The larger OMJ may have to incorporate resonant irises at the side port apertures and bandpass filters to prevent loss of the higher frequency energy into these ports. These two OMJs are then coupled into a single tapered horn as shown in Figure 3.4-5 with possible higher-order mode control for pattern shaping.

The second approach for the dual-band feed, that of two concentric circular horns, makes use of the fact that the higher band normally does not require as large an aperture to produce the same beamwidth as the lower to illuminate the same reflector system. This approach was considered for a number of ground antenna systems at Ford Aerospace and is depicted in Figure 3.4-6. The center horn may be reduced in size even farther to allow more aperture control in the lower band by incorporating dielectric loading, which may extend beyond the horn aperture as a "polyrod" device. Neither of these devices currently exists (to our knowledge) in dual-polarized versions for the designated bands; however, the design principles are sufficiently straightforward that development should not prove difficult.

Either of these suggested designs appears feasible, and a separate study program should be undertaken to determine which would yield the better performance.

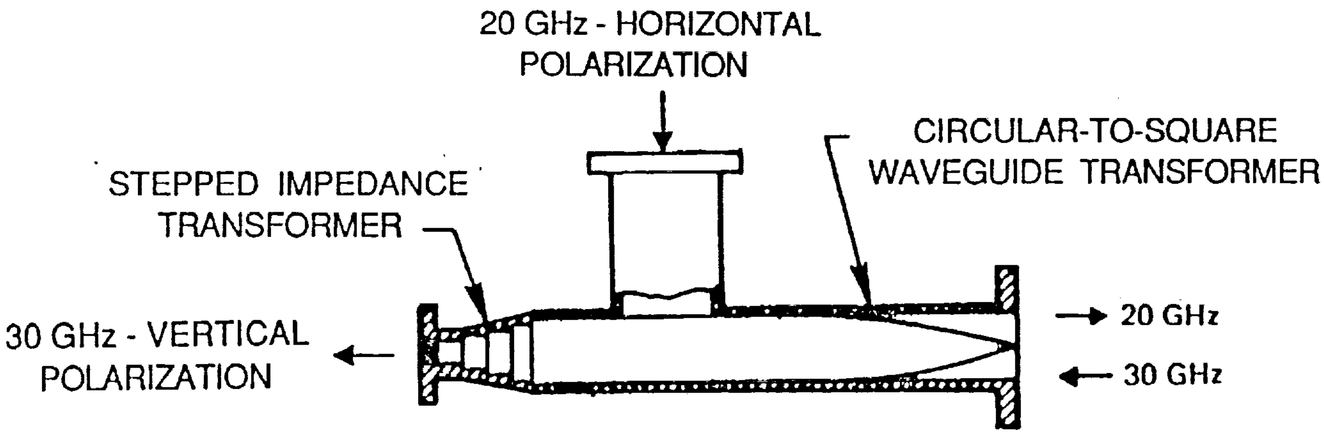

Figure 3.4-4. CS Orthomode Transducer (OMJ)

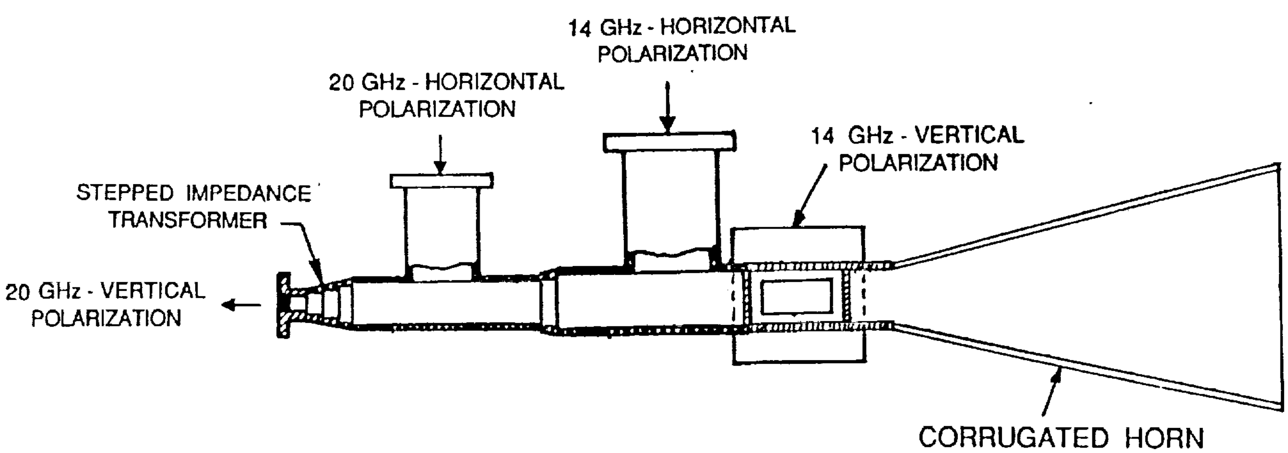

Figure 3.4-5. Dual-Polarization 14/20 GHz Feed Element

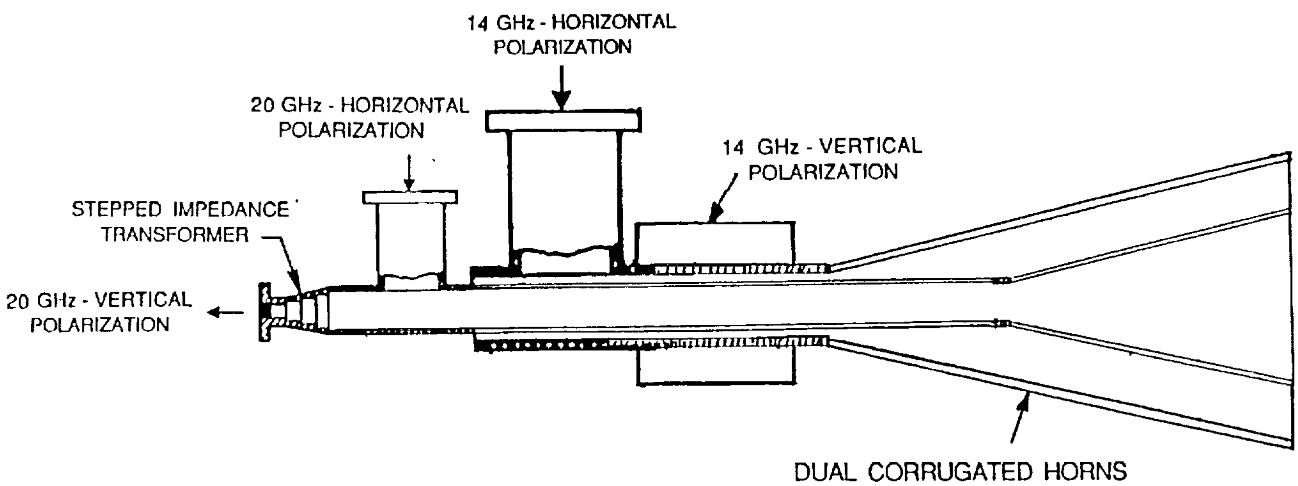

Figure 3.4-6. Alternate Dual-Polarization 14/20 GHz Feed Element

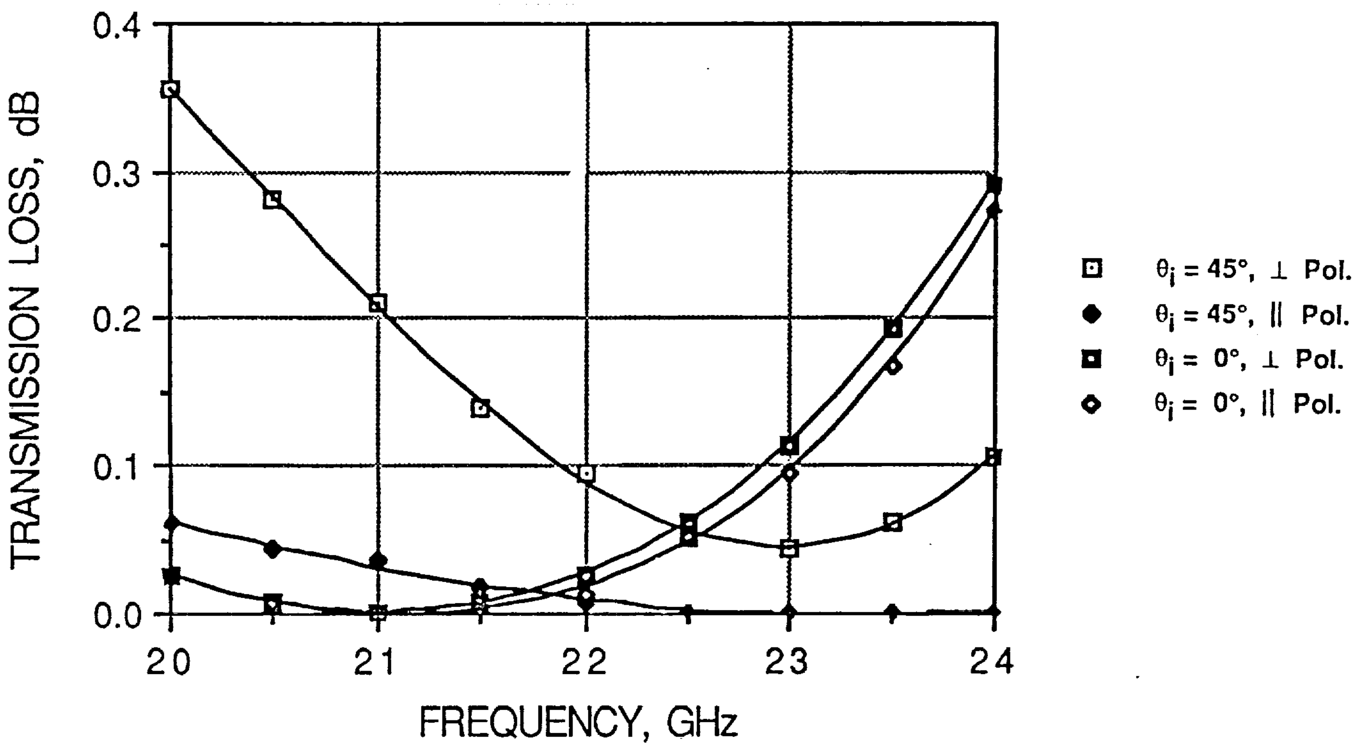

Figure 3.4-7. FSS Amplitude Coefficients

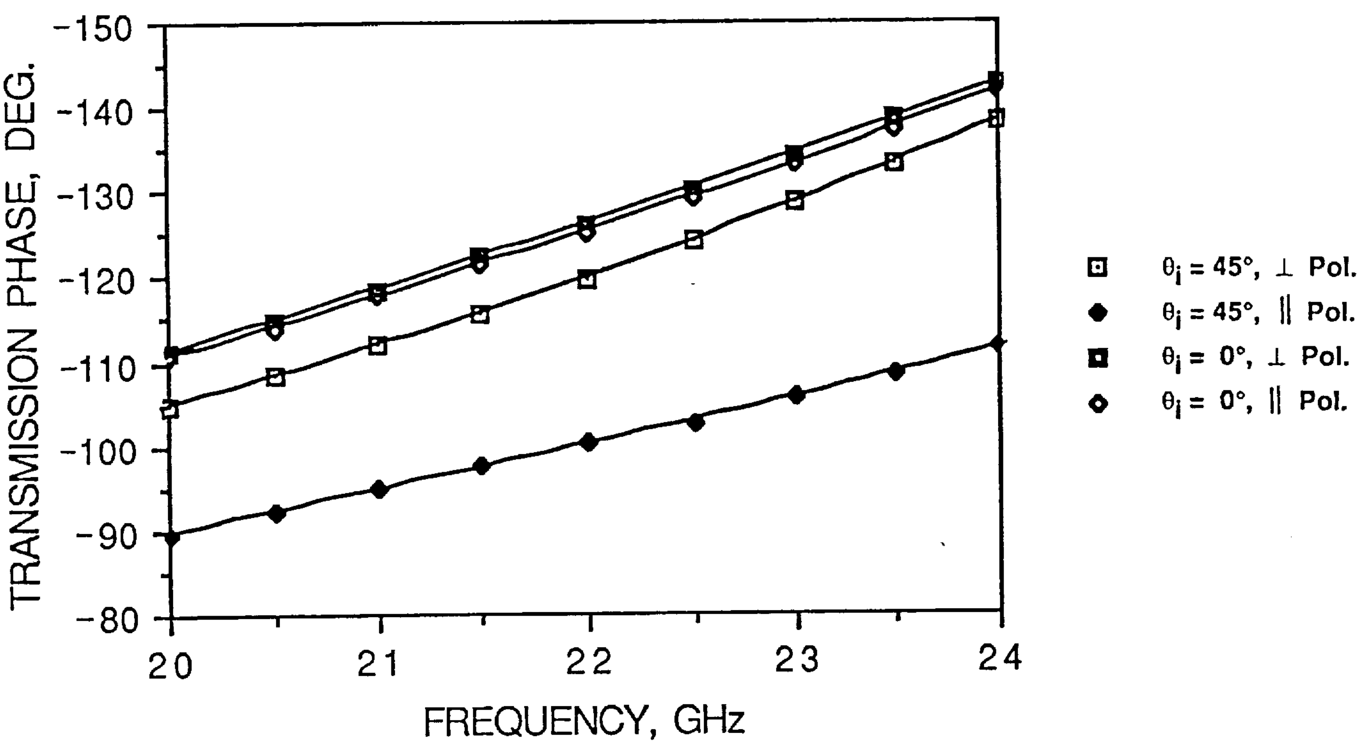

Figure 3.4-8. FSS Phase Coefficients

3.5 REFLECTOR TOLERANCE CONSIDERATIONS

Some concern exists for possible gain degradations of reflector-type antennas due to surface tolerance errors. Theoretically, Ruze [3-5] predicts the gain losses depicted in Figure 3.5-1 for typical reflectors with RMS surface accuracies in the range of 3 to 60 mils for the three frequency bands of interest.

In order to determine the range of surface tolerances to expect, we have assembled the data shown on Figure 3.5-2 representing measured tolerances on a number of typical reflectors as a function of diameter. Predicted tolerances in orbit are also shown, as a result of taking into account expected thermal distortions. These two values are represented by showing a range of values for tolerances in each case. For instance, measured tolerances for the 8-foot reflector to be used for the INTELSAT VII multibeam communications antenna (I-7) averaged around 10 mils; this is expected to increase to perhaps 12 mils in orbit with thermal distortions. Actually, on-orbit degradations are usually quite small for typical space-type antennas made of graphite epoxy, which has a very low coefficient of thermal expansion. The four points designated by "(x)" represent a set of reflectors whose contours were measured, and a "best-fit" parabola determined for each, allowing the focal point to be moved slightly to minimize apparent surface errors. This process often reduces the effective tolerances of a given surface by a factor of 2 or 3, for a small adjustment.

Three additional interesting cases are shown in Figure 3.5-2, the first being NASA ACTS-Program 20/30 GHz 13.5-foot main reflector constructed by Ford Aerospace as a POC model. This reflector was custom fabricated of aluminum by an optics laboratory, and showed a measured RMS error of only 0.8 mil with a maximum peak-to-peak error of 4.5° mils. This unit was very expensive to fabricate, but shows what can be accomplished if required. If this unit were used as a mold to fabricate a graphite-epoxy flight model, the errors would probably increase to perhaps the 3-mil range, on orbit.

The other two unique cases shown are the ATS-6 and the TDRSS-SA antennas, which are unfurlable and made of conducting mesh.

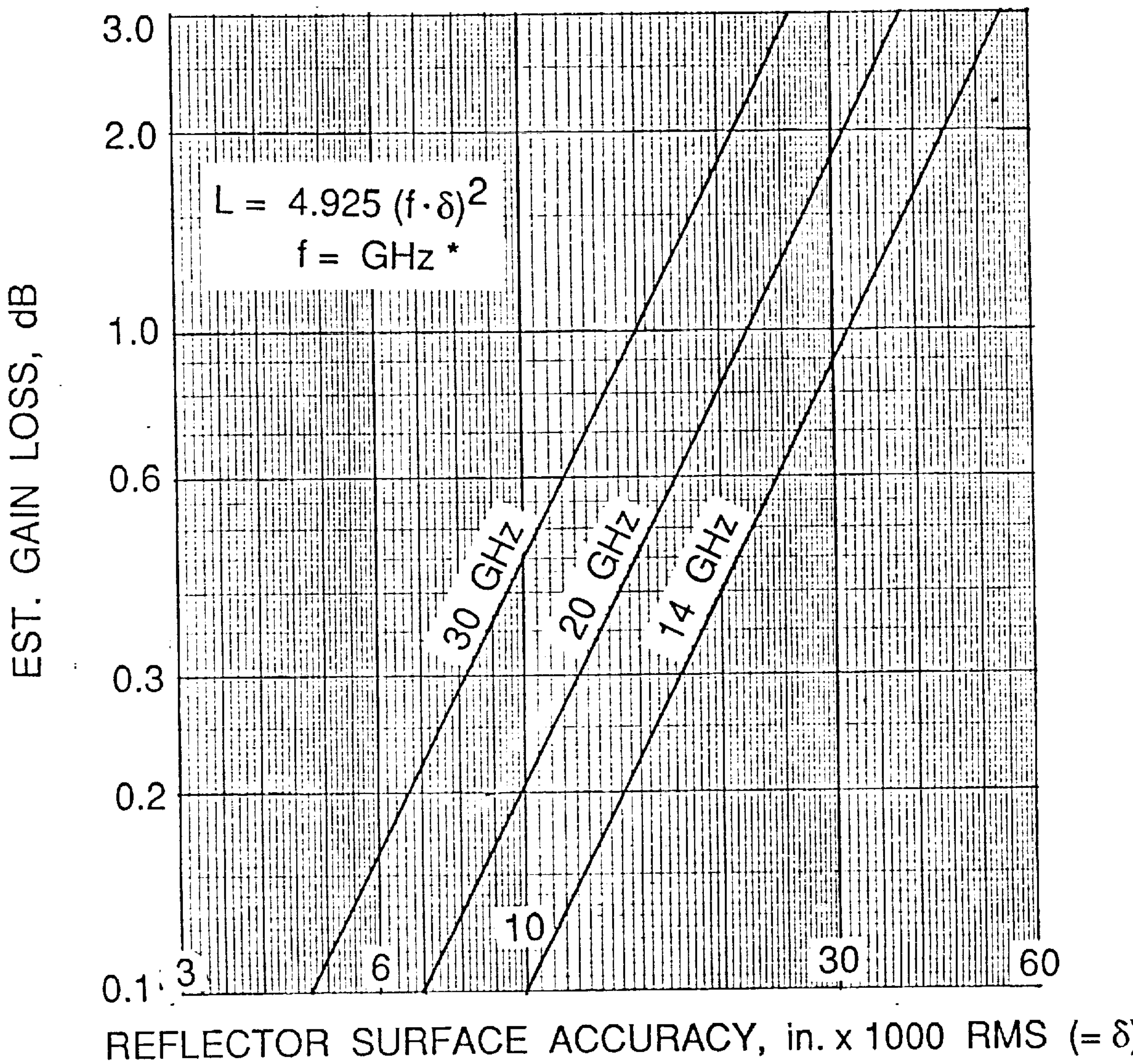

* Ruze, "Antenna Tolerance Theory", PROC. IEEE, Apr. 1966

Figure 3.5-1. Gain Loss Due to Reflector Tolerances

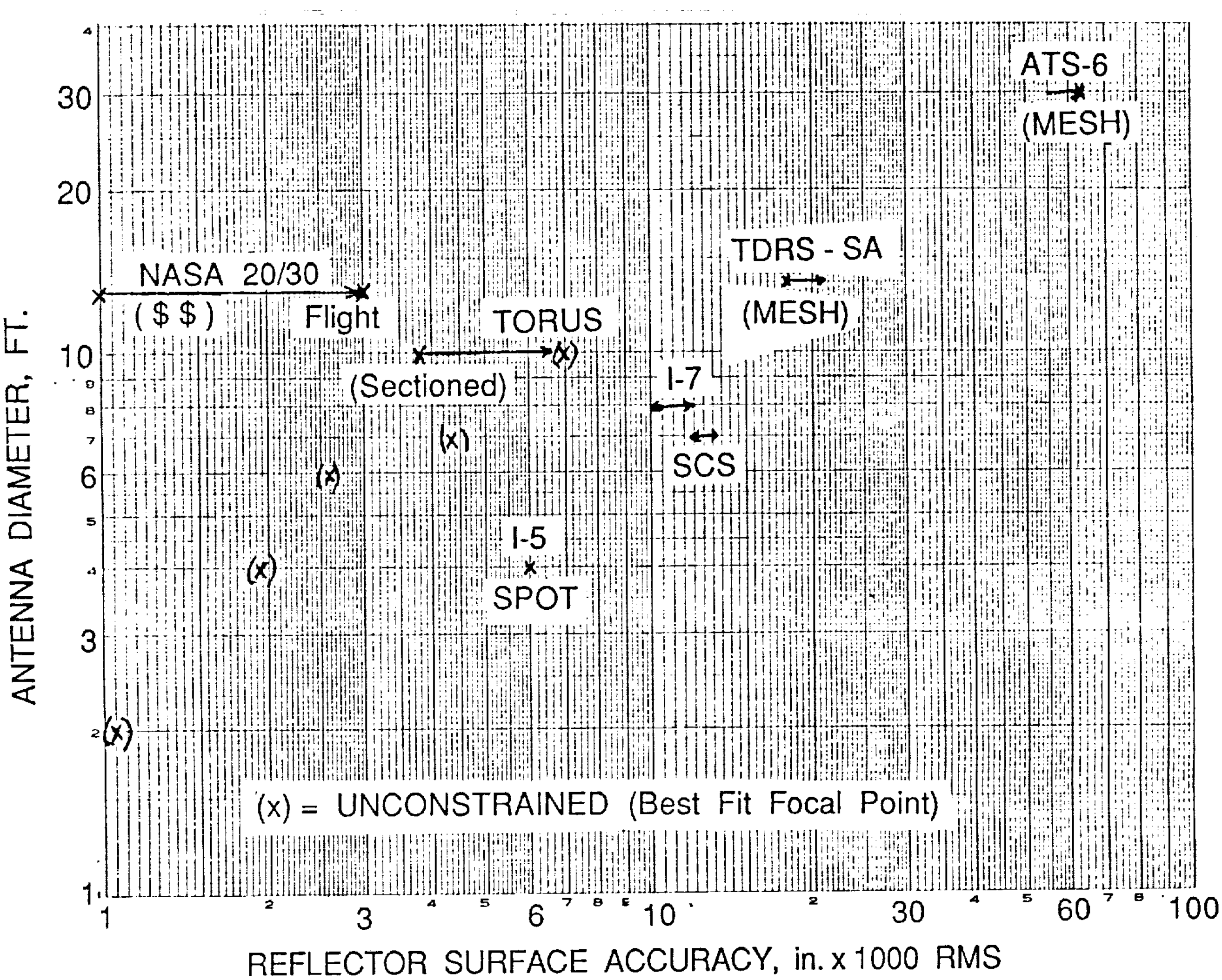

Figure 3.5-2. Reflector Tolerances Achievable

Predictions of anticipated tolerances for the two antenna types identified as prime candidates for this program are also shown on Figure 3.5-2: the 10-foot torus (for Configuration 1) and the 7-foot (2.4 m) shaped dual reflector. These expectations are shown as 7 mils and 4.5 mils, respectively. If the torus were constructed in three smaller sections of 3.3 feet each, the tolerances would improve to around 4 mils, as shown, assuming that the deployment system could properly position these three sections.

Our conclusions relative to the gain degradation to be expected for the TDRSS MBA can be determined by using the above expected tolerance values in conjunction with the predicted losses of Figure 3.5-1. Surface tolerance values of 4 to 4.5 mils would result in losses of less than 0.1 dB even at the highest frequency of interest (30 GHz). A 7-mil tolerance would yield a gain loss of only 0.2 dB at 30 GHz, and 0.1 dB or less at 20 and 14 GHz. These values are probably inconsequential to the overall system performance.

3.6 ADVANCED COMPOSITE MATERIALS FOR ANTENNAS AND FEEDS

Advanced composite materials such as carbon fiber/epoxy are already being used for satellite components such as the antenna reflectors, structures, feeds, solar arrays and RF hardware. Examples are shown in Figures 3.6-1 through 3.6-8. Table 3-6-1 summarizes advances in light weight materials for antenna reflectors. Carbon fiber material has the fine qualities of light weight, and good RF and thermal performance, which are very important for satellite designs. When used for EHF applications, however, surface accuracy requirements may be difficult to meet with the current state of technology. However, rapid progress in this area is taking place.

In some applications (e.g., Japanese SUPERBIRD satellites), two sets of feeds - one for each polarization - may be desirable, when a high polarization isolation at Ka-band is desired. In such applications, both the sets of feeds may illuminate the same reflector, provided the surface of the reflector is made of dual-gridded RF-transparent material. Graphite fiber is not suitable for such applications, since this material is not RF transparent. For such applications, materials such as Kevlar are used. Kevlar is an excellent choice for applications requiring RF transparency. Kevlar is used for the (Japanese) SUPERBIRD satellite antennas. Kevlar also has the fine qualities of light weight, good RF and thermal performance; however, Kevlar material is prone to degradation effects due to hydroscopic absorption, and therefore care must be taken to prevent absorption of moisture during the prelaunch phase.

Feed elements can be made of copper, copper-plated graphite, or aluminum materials. Aluminum and copper have good conductivity characteristics, but aluminum is somewhat lighter and cheaper than copper. Copper-plated graphite provides the best features of both materials, viz., the good thermal characteristics and light weight of graphite and the good electrical characteristics of copper. However, accurate machining and molding of copper plated graphite at EHF may be difficult and expensive, and may result in lower feed efficiencies. For applications which are cost and/or link-budget sensitive, aluminum feeds may provide a compromise between good performance, low cost, and light weight.

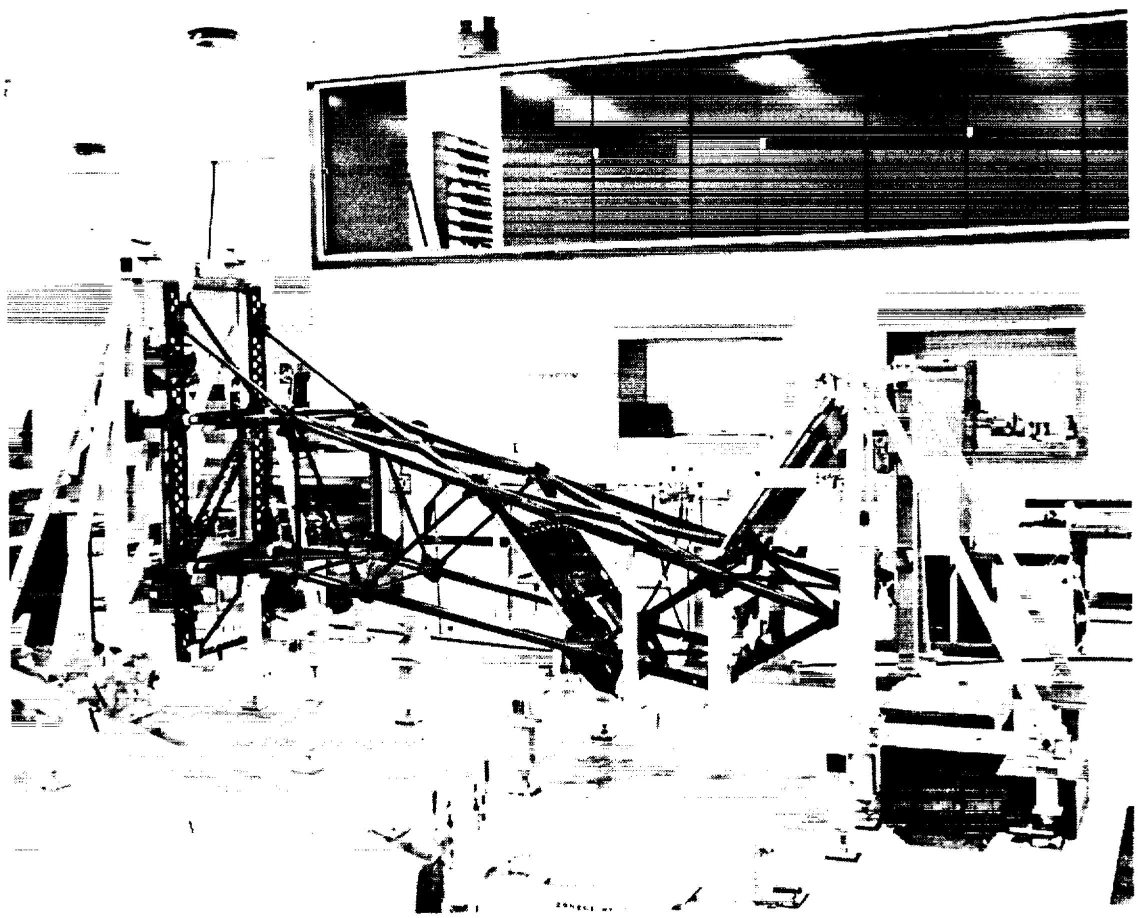

Figure 3.6-1. INTELSAT V Carbon Fiber/Epoxy Antenna Tower

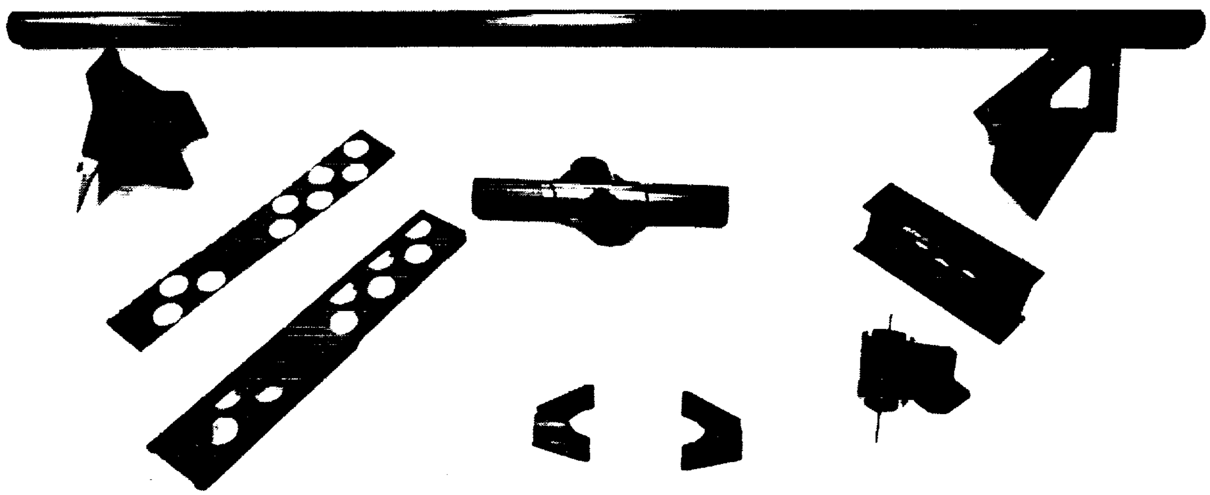

Figure 3.6-2. INTELSAT V Carbon Fiber/Epoxy Antenna Tower Piece Parts

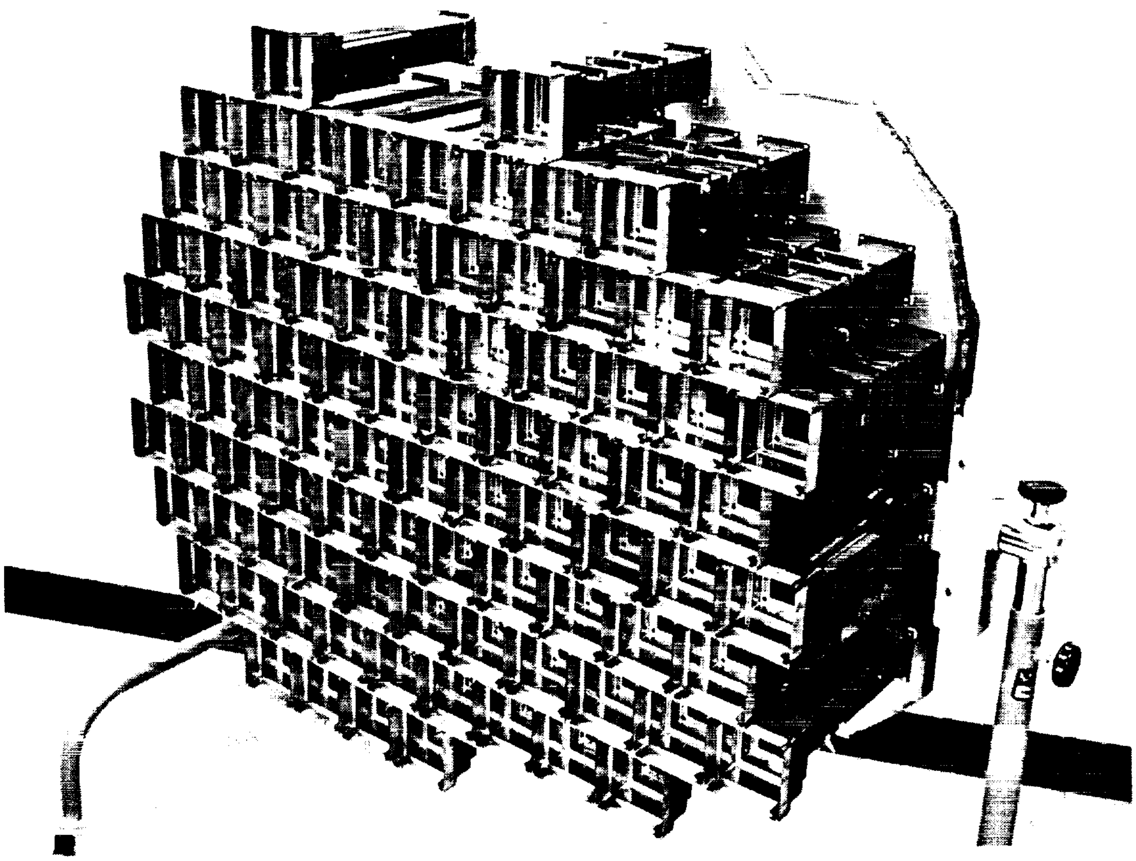

Figure 3.6-3. INTELSAT V Carbon Fiber/Epoxy 4 GHz Feed Array

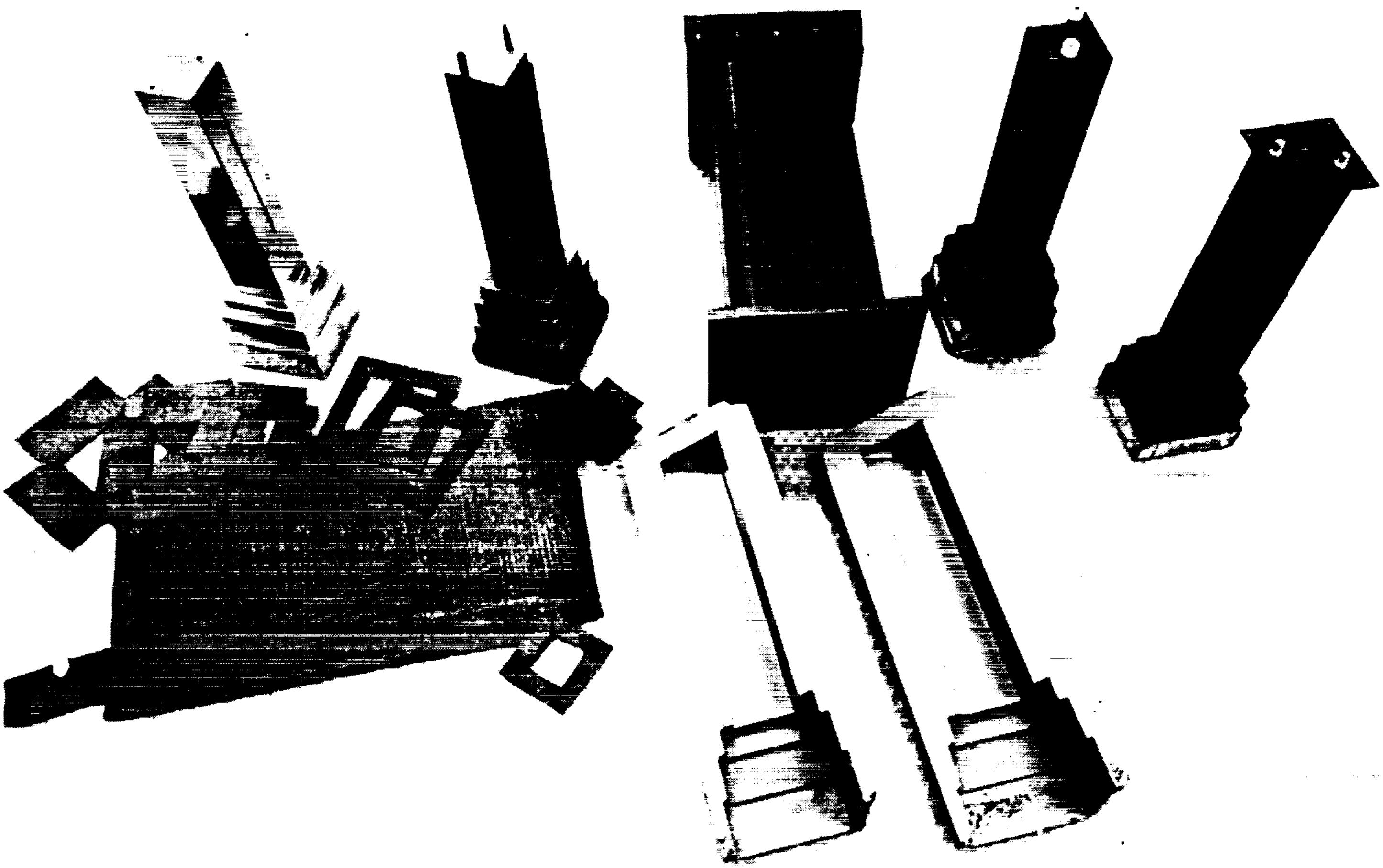

Figure 3.6-4. INTELSAT V Carbon Fiber/Epoxy Feed Elements and Tooling

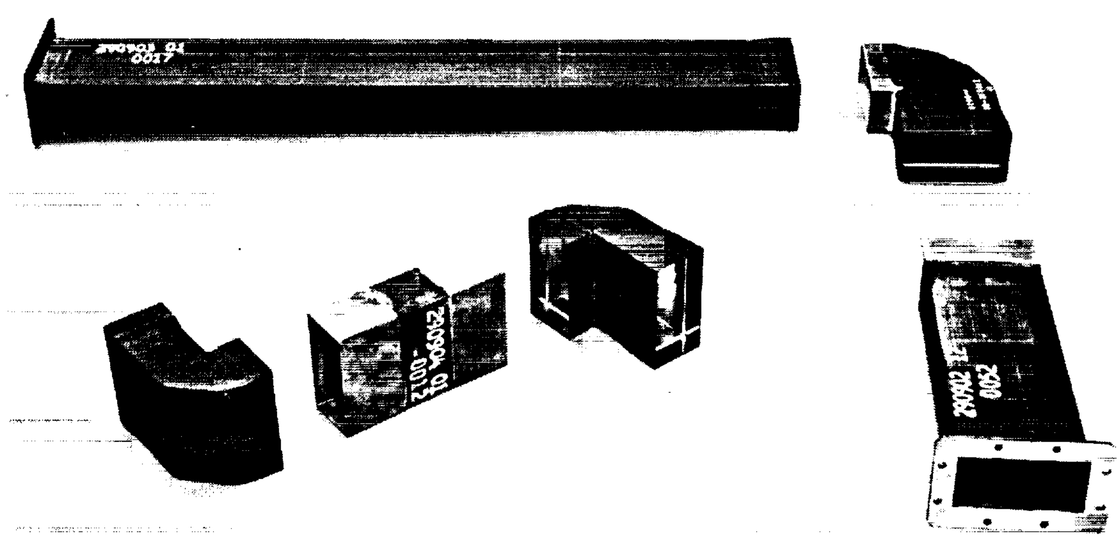

Figure 3.6-5. INTELSAT V Carbon Fiber/Epoxy Waveguides

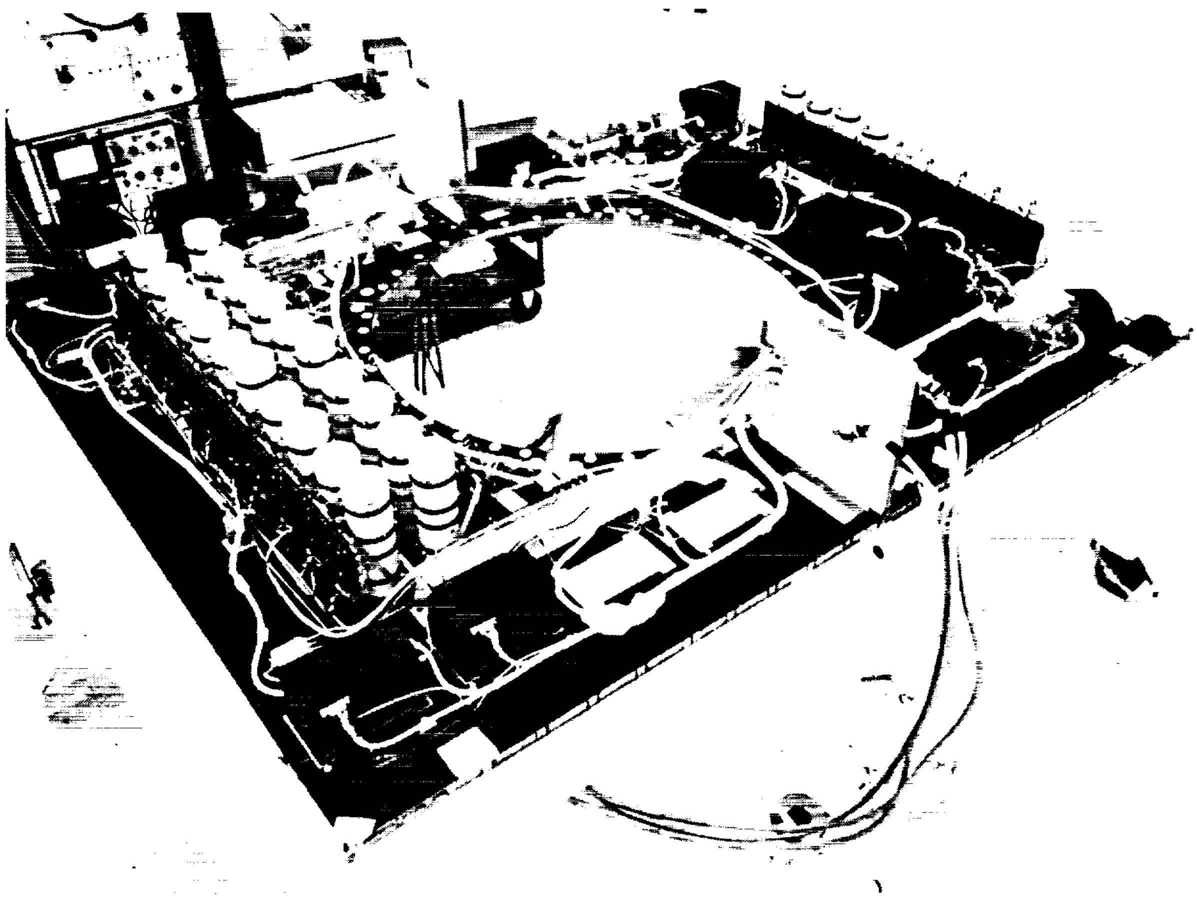

Figure 3.6-6. INTELSAT V Antenna Deck with Carbon Fiber/Epoxy Multiplexers

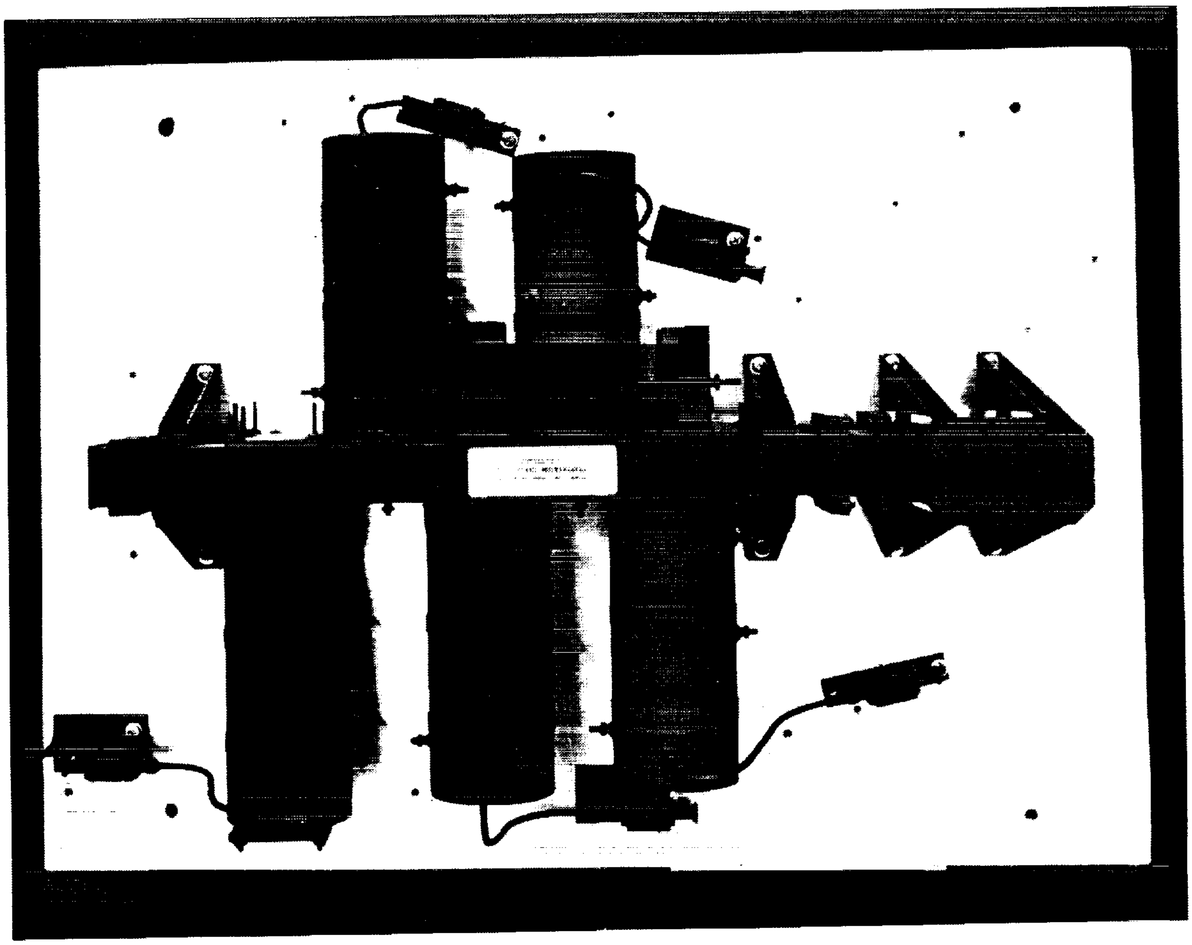

Figure 3.6-7. INTELSAT V Carbon Fiber/Epoxy Hemi Output Multiplexers

Figure 3.6-8. INTELSAT V Carbon Fiber/Epoxy Solar Array

Table 3.6-1 Advancements in Lightweight Materials for Antenna Reflectors

Year First Used at Ford Aerospace	Graphite Fiber Type	Honeycomb Core	Programs
1971	HMS (high modulus)	3.0 lb/ft^3 aluminum	NATO III, VIKING, CS, ETS II, ECS
1977	GY-70 (ultra-high modulus)	2.0 lb/ft^3 aluminum	INSAT-1
1983	Pitch-75 (ultra-high modulus)	2.0 lb/ft^3 aluminum Kevlar-49	ARABSAT, SKYNET-IV, I-VA/IBS
1985	Pitch-100 (ultra-high modulus)	2.0 lb/ft^3 aluminum Kevlar-49	IR&D
1986	Pitch-100 Carbon-carbon	Monocoque	Aerospace Corp

3.7 DEPLOYMENT AND PACKING ISSUES

In this subsection, deployment, packaging, stowing and other related issues are addressed.

3.7.1 Deployment Issues

A major contribution to antenna pointing error is the thermally-induced distortion of the deployment arm. The hinges used on INTELSAT V were made of aluminum. SUPERBIRD, a Ford Aerospace satellite currently being built, uses titanum hinge arms, which have improved thermal stability and stiffness. New designs are being generated to use graphite to further reduce thermal distortions. Thermal distortion of the reflector is the other large contributor to pointing error. The remaining reflector and feed supporting structure is made from graphite and is tailored to meet stiffness and strength requirements while limiting thermally-induced distortions to virtually negligible levels.

The offset shaped dual reflector might require deployment of both reflectors and would incorporate hinges of similar design with changes to accommodate the size/mass differences of the two reflectors. Deployment of the subreflector is to be avoided, and tradeoff studies involving the spacecraft configuration and the launch vehicle would be necessary to optimize the overall system. If deployment of the subreflector is required, it will complicate alignment (hinge repeatability) and adversely affect antenna pointing (thermally-induced hinge distortions).

A torus reflector has only one reflector, but its large size (176 wide x 96 inches) makes packing within the launch vehicle envelope more difficult. If the spacecraft/launch vehicle configuration would allow a single deployment, the same hinge configuration discussed previously would be used. If the packaging requirements would necessitate folding the reflector, it would introduce potentials for additional alignment errors and temperature gradients that would cause larger thermal distortions.

For all antenna configurations it is desirable to make the feeds and reflectors all in one module. This expedites fabrication, spacecraft integration, and alignment. Each antenna system is shown as a module (and includes feed, reflectors, support structure and deployment mechanism) in Figure 3.7-1. It is best if the feeds are kept close to the spacecraft mainbody to provide the most benign thermal environment possible as well as to minimize the distance between the feeds and the transponder output sections. This antenna module is joined to the spacecraft primary structure by simple attachments designed to minimize alignment errors while still maintaining ease of integration.

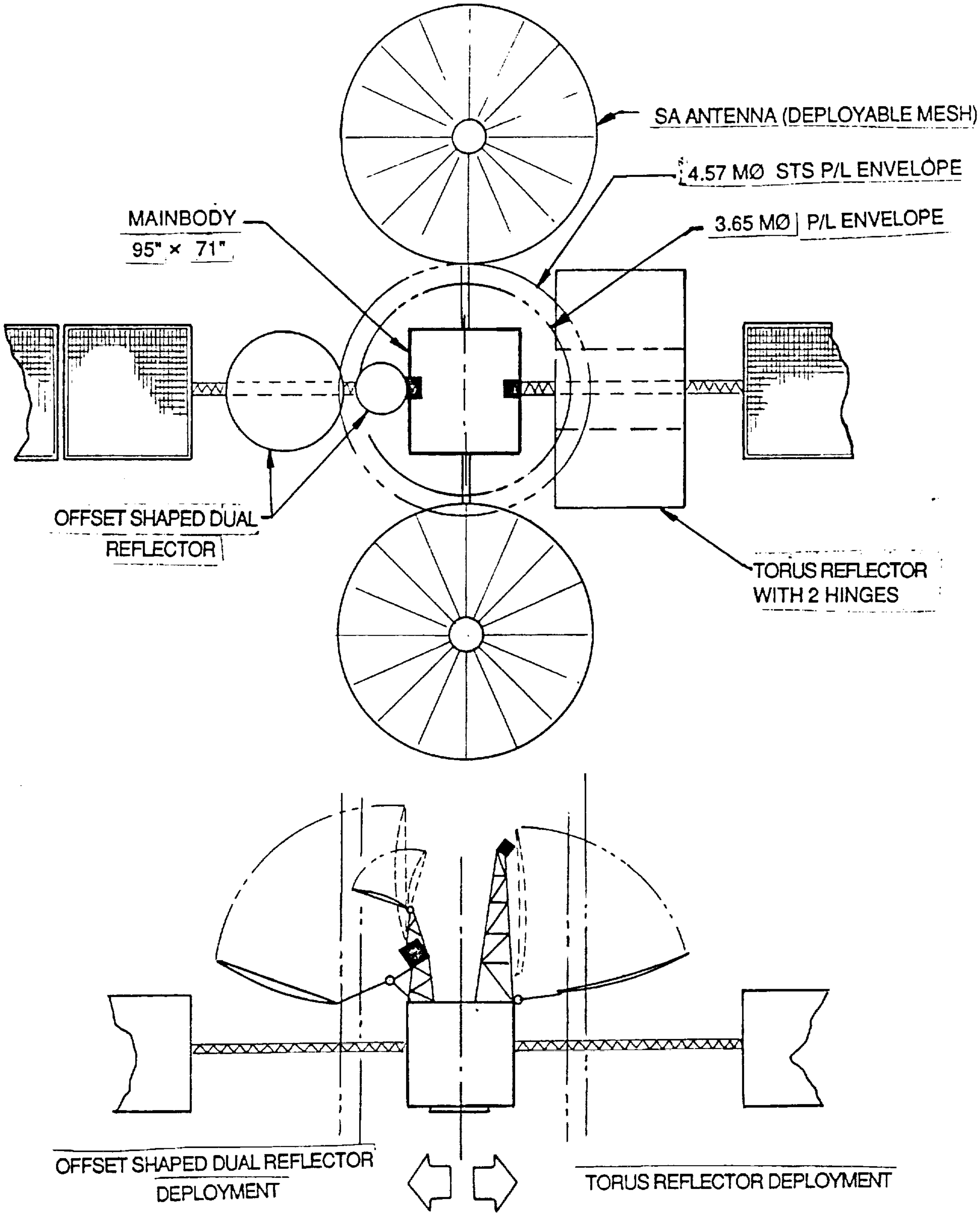

Figure 3.7-1. Two MBA Configurations of TDRSS

3.7.2 Deployment Mechanisms

Integrating large antennas into a communications satellite requires consideration of the launch vehicle payload envelopes, launch vehicle environments, and the requirements of the on-orbit spacecraft configuration. Some of the factors influencing the spacecraft configuration are thermal control, solar torques, thruster plumes, sensor fields of view, mass properties, etc.

The MBAs two leading configurations are both shown on a generic type of TDRS in Figure 3.7-1. This is a composite picture for illustration of size comparison only (only one multibeam would be flown on TDRS). The torus reflector configuration is shown on top (north) while the dual-shaped reflector configuration is on the bottom side (south).

It is apparent that the large torus reflector (176 inches) would take the entire 4.57 m diameter of the STS (shuttle) payload envelope and that the reflector would not fit within the 3.65 m diameter of the smaller expandable launch vehicle (ELV) payload envelope. Even fitting in the STS is unlikely because of the inefficient use of space and the necessity of stowing other antenna systems. Therefore the folding of the torus reflector in some manner is required for stowage in the shuttle or an ELV (unless its width can be reduced).

A single hinge or dual hinge line as shown in Figure 3.7-1 on the torus reflector would be a likely means of folding the reflector. While folding this reflector is relatively simple mechanically, the RF complications are not easily predicted. After folding the reflector, an additional rotation would be required to stow the folded reflector within the launch vehicle envelope as shown in the side view of the spacecraft in Figure 3.7-1.

There have been numerous designs of deployable or folding reflectors. A prime example is the mesh antenna used for the single access antennas on TDRS. These 16 foot diameter antennas deploy from a small package. Their major drawback, as with all deployable reflectors, is high cost and mechanical complexity.

An alternative configuration would utilize the offset shaped dual reflectors with rigid reflectors and simple single axis deployment hinges. This configuration has a more compact design because of the folded optics and also the smaller (2.4 m and 1.0 m diameter) reflectors. These small reflectors allow stowage in the smaller 3.65 m diameter fairing without disturbing the reflector surfaces (Figure 3.7-1). An additional advantage of the dual reflector configuration is the proximity of the feed to the mainbody. This minimizes the distance of RF connection to the transponder as well as allowing for a more controlled thermal environment for the feed.

From this brief and simple spacecraft configuration study, it appears that the simple single axis deployment mechanisms of the dual reflector configuration could be virtually the same as those used on present Ford Aerospace satellites.

The reflector mechanisms support the stowed reflectors during launch and, when on orbit, release and deploy the reflectors to their operational position. They consist of two pyrotechnically released holddowns and two spring-driven deployment hinges for each reflector. Figure 3.7-2 shows a reflector with its mechanisms in the stowed and deployed positions. The deployment is a simple single-axis rotation. Deployment goes quickly (6 to 8 seconds); the reflector stops suddenly and latches positively at the desired position. The sudden stop generates latchup loads which the hardware is designed and tested to sustain. For simplicity and reliability, dampers or brakes are not used.

Requirements of the reflector mechanisms are summarized in Table 3.7-1. The mechanisms must be strong enough to sustain the launch and latchup loads, and stiff enough to meet frequency requirements when stowed and deployed. On orbit, they must accurately hold the position of the deployed reflectors under temperature extremes. Mechanisms design includes the effects of ground handling and testing environments. In general, ground handling is controlled to be less severe than operational loads.

For high reliability, the deployment is based on simple, redundant mechanical springs and low-friction bearings. Friction torques are maintained small compared to spring torques. When deployed, the hinges lock positively with no backlash or play for stable antenna pointing.

Sizing of the deployment springs is bounded by two constraints: the springs must provide sufficient energy to overcome resistance from all sources by a margin of at least three under worst-case conditions, yet the energy must not be so large that structural loads at latchup are excessive. Momentum or kinetic energy of the deploying reflectors is not considered in developing the torque margin. Furthermore, the worst-case torques are evaluated under both hot and cold extreme conditions. The spring sizing yields a minimum torque margin of 4-to-1.

Latchup loads are calculated assuming no friction with maximum spring settings. Latchup loads have high structural margins and are well within the hardware capability.

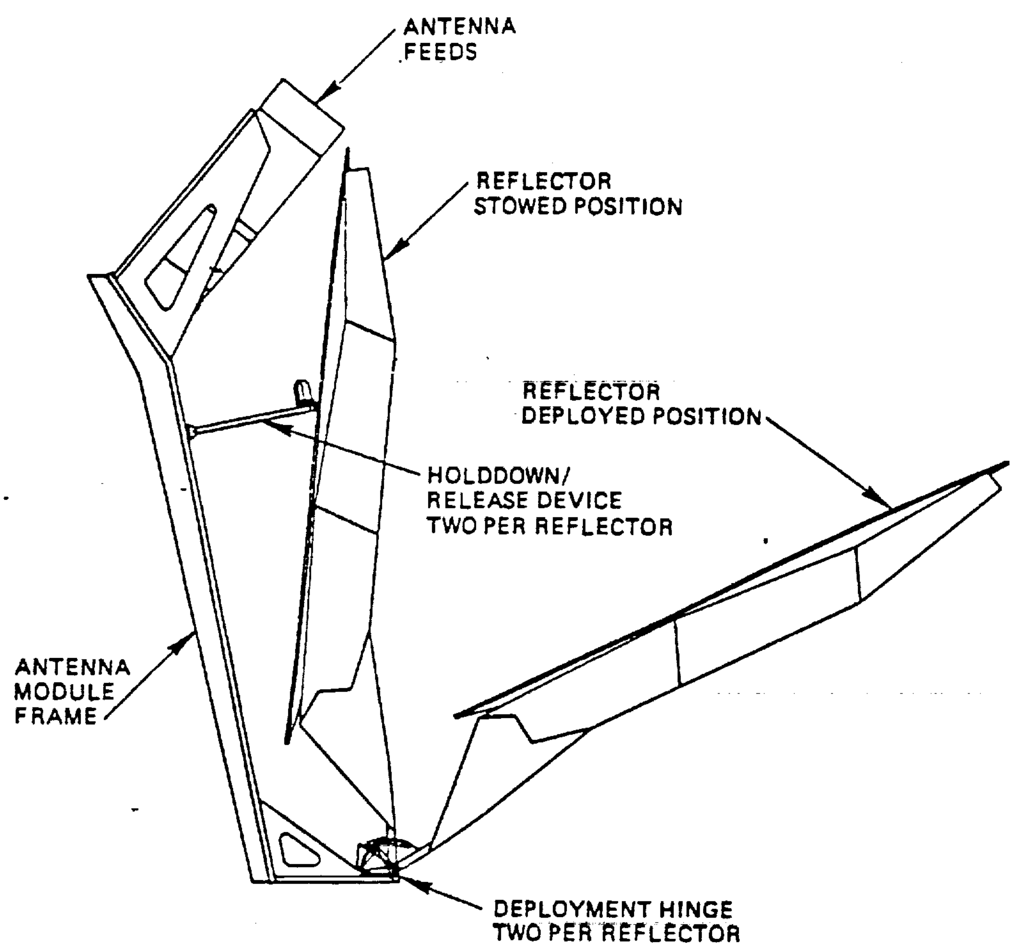

Figure 3.7-2. Reflector Deployment Uses Mechanisms from INTELSAT V and FS-1300 Designs

Table 3.7-1. A Requirements Summary for Deployment Mechanisms for Large Antenna Reflectors

Requirement	Comments
Torque margin greater than 3-to-1 at any position in the range of potion	Typically, 4-to-1
Torque margin based on zero kinetic energy	Momentum and kinetic energy are not considered in torque margin determination
Mechanism design considers ground handling and test environments	----
Accessibility to stowage and deployment devices without disturbing their position of thermal control hardware	----
Fully redundant	Four deployment springs per hingeline
Positive latching	Latching lever catches in slot
Design life based on ground test plus on-orbit functional cycles with 1.5 safety factor or minimum of 50 cycles	Deployment mechanisms must work only once on orbit
No thermal constraints on mechanism operation during spacecraft orbital design life	Deployment temperatures -80 to + 70 °C
Telemetry and commands	Release commands and latchup telemetry
Derived Requirements	
Survive launch loads	Mechanisms sized for 1/5 factor of safety on yield, with positive margins of safety
Stiff enough to satisfy overall stowed and deployed frequency requirements	----
Accommodate differential thermal distortions stowed	Design uses flexures, pivots, and floating bearings
Withstand latchup loads at deployment	----
Reflector repeatability less than 0.015 (beam error)	----
Small antenna pointing error from hinge thermal distortions	Reflector hinges made of titanium for low thermal expansion
No looseness or free play in deployed and latched hinges	Latched hinges are preloaded to eliminate looseness

3.7.2.1 **Launch Holddown and Release Devices.** In the stowed position, the reflector is held from deploying by two holddown/release struts. Each strut is held together by a pretensioned rod. At deployment, severing of the rods by pyrotechnic cutters releases the reflectors for rotation to their deployed positions. There are two types of struts.

The struts attach to the satellite and reflector by spherical monoball bearings to allow pivoting. This permits differential thermal expansion between satellite and the reflector without building up large forces. One of the struts at each reflector is triangulated to provide lateral support for the stowed reflector. The struts are made of 2024-T81 aluminum.

The aluminum holddown rod is pretensioned to approximately 2.2 kN (500 lb) to provide a preload larger than the worst-case launch load. The rod is locked by nuts located at the reflector end of the strut. It has two independent knives and squibs for full cutting redundancy.

3.7.2.2 **Deployment Hinges.** Figure 3.7-3 is annotated sketch showing the deployment and latching functions. The hinge consists of two parts: the stationary part that mounts to the satellite and the rotating part that mounts to the reflector. These parts are hinged together by spherical, monoball bearings (12.7 mm diameter). This provides self-alignment of the axis of rotation and dual bearing surfaces for redundancy. The bearings are dry-film lubricated with molybdenum disulfide. Titanium (6A1-V) is used throughout the hinges for low thermal distortion and, thereby, small antenna pointing error when deployed. For low thermal stresses, hinge mounting uses flexures to accommodate differential thermal distortion between the titanium hinge and the composite structures. Further, to allow for differential thermal motions between the reflector and satellite, one of the hinges is designed to float along the axis of rotation; the other hinge is fixed to maintain proper position of the reflector.

Deployment is driven by the unwinding of two redundant, beryllium-copper, helical torsion springs at each hinge. The spring windup is adjustable for control of deployment torque. Four independent springs are active about each hinge line.

The hinges have a latching mechanism that stops the deployment and holds the reflector in its proper deployed position with zero backlash. This mechanism can be seen in Figure 3.7-3. It consists of a clevis-mounted roller that rides on a guide during deployment and drops into a slot in the guide at the deployed position The clevis is pivoted from the stationary part of the hinge. The

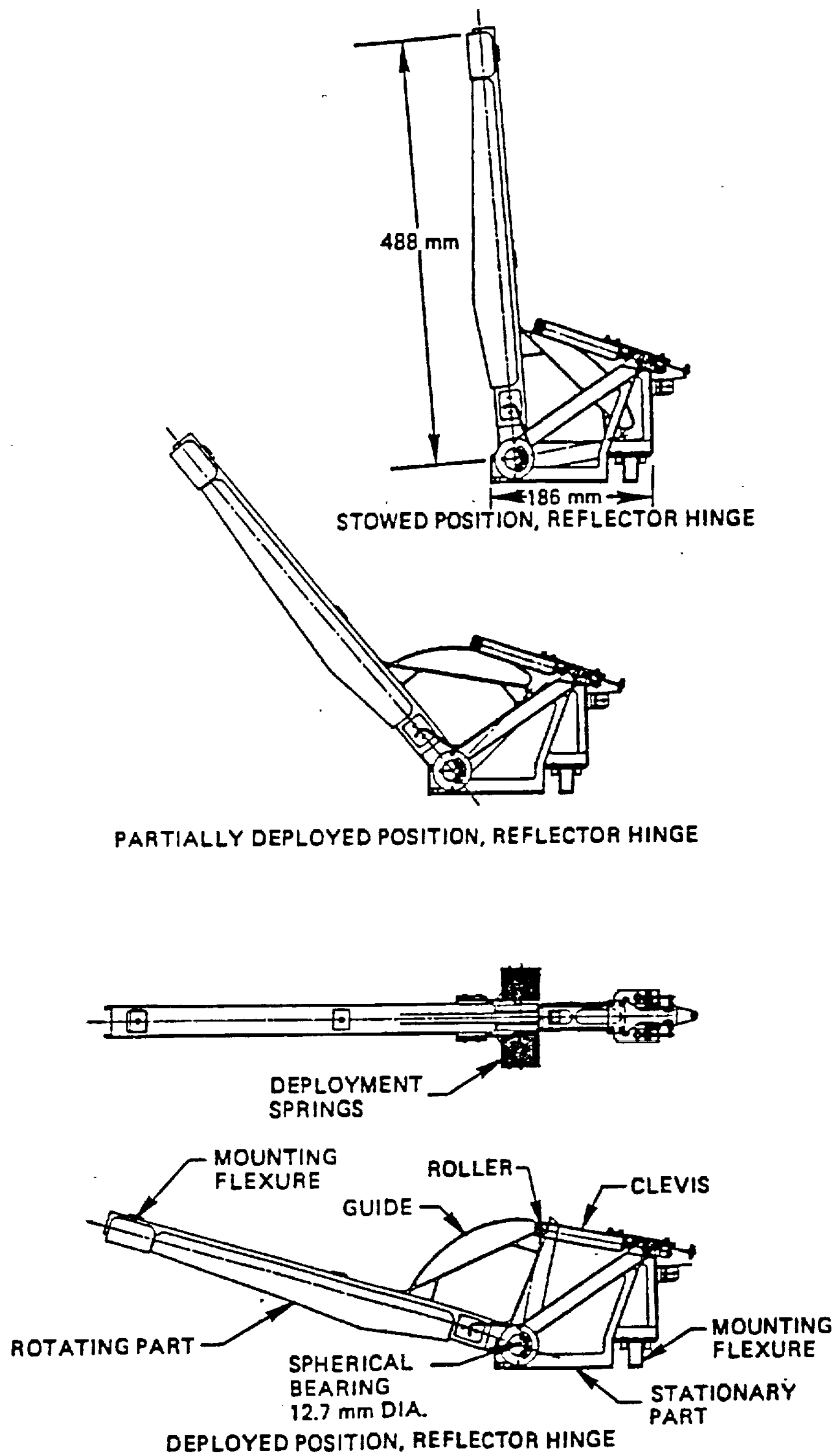

Figure 3.7-3. Reflector Deployment Hinge Uses Simple Rotation and Positive Latching

guide surface is lubricated with molybdenum disulfide for low friction. Two redundant torsion springs mounted about the clevis pivot hold the roller against the guide during deployment and drive the roller into the locking slot. A threaded link in the clevis permits the length of the clevis to be adjusted for synchronization of lockup between the pair of hinges and for accurate alignment of the reflector.

A microswitch mounted on one of the hinges on each reflector signals proper latchup by telemetry.

3.7.3 Packaging--Spacecraft Configuration

The ATDRSS presently has a number of payload configurations, all of which have large antennas. The numerous antennas present a challenge to stow and secure them for the launch environments as well as deploy in a manner that allows satisfactory operation on orbit. The final ATDRSS configuration determination is beyond the scope of this study, however, several configurations incorporating one of the possible ATDRSS payloads are shown to illustrate the relationship of the MBA to the rest of the spacecraft.

A possible ATDRSS payload has two large single access (SA) antennas that deploy about the mainbody as well as a hexagonal shaped multiple access (MA) antenna. The present TDRS 2.0 m diameter space to ground antenna is replaced by the MBA.

The STS orbiter provides the largest payload envelope and therefore provides the simplest packaging task for the ATDRSS incorporating the MBA. Figure 3.7-4 shows an ATDRSS with the MBA in the launch configuration in the STS orbiter. Present ATDRSS studies include the possibility of using expendable launch vehicles. The Atlas Centaur payload envelope is shown along with the shuttle envelope for comparison with the orbiter.

The ATDRSS spacecraft proposed for this study is similar to present Ford Aerospace spacecraft having a central cylinder propellant module, a rectangular mainbody, and separate antenna modules. Figure 3.7-4 shows that the length precludes the use of this configuration in the Atlas Centaur. In this version of the ATDRSS it is necessary that the 16 ft diameter SA antennas be of the unfurlable type. Some versions of ATDRSS being studied use rigid SA antennas to reduce cost and complexity, but these versions would be extremely difficult or impossible to include the MBA.

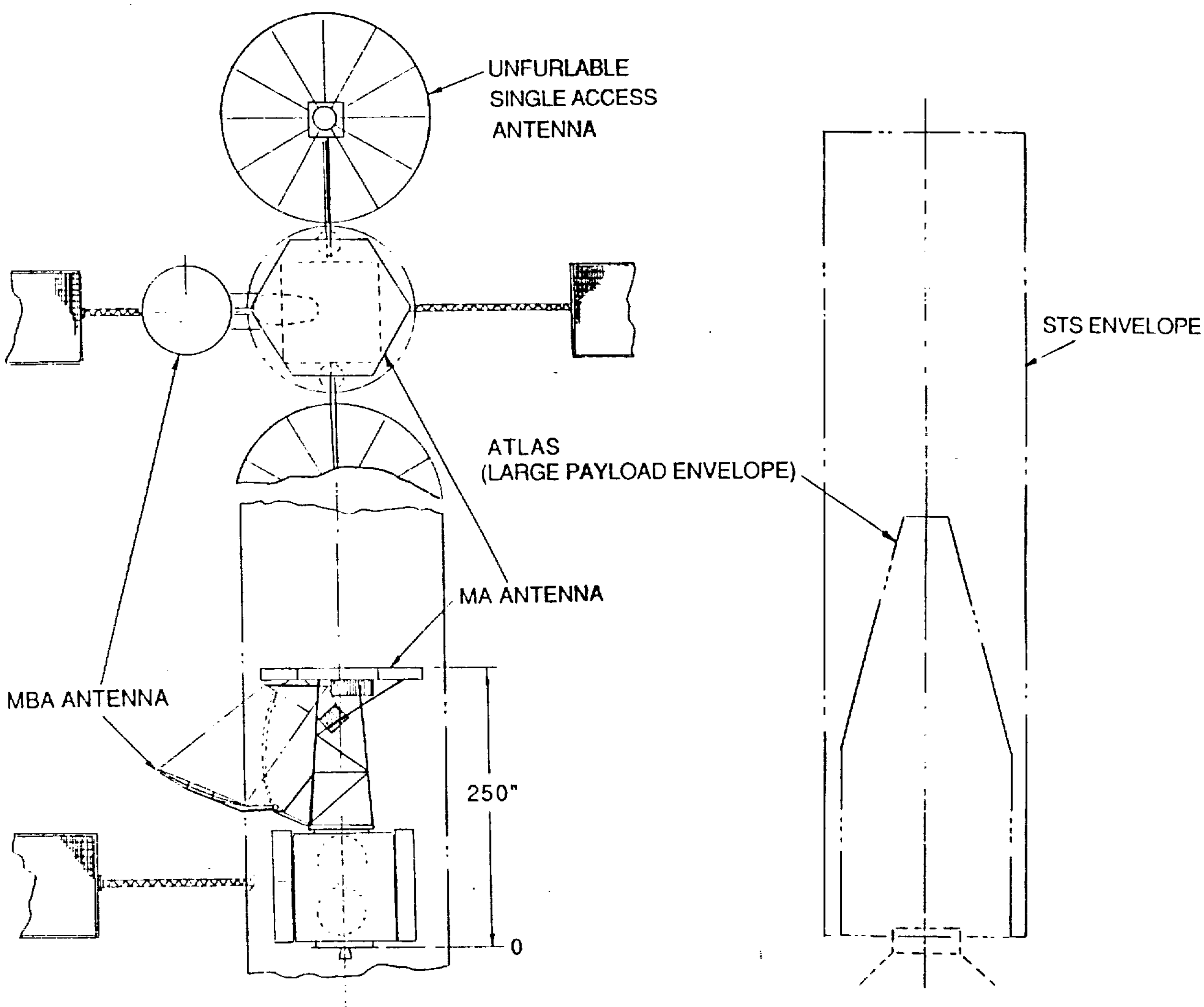

Figure 3.7-4. MBA Spacecraft in STS

A version of the ATDRSS stowed in the Atlas Centaur (ELV) payload envelope is shown in Figure 3.7-5. The MA antenna must be deployed and the mainbody must be shortened from the configuration shown in Figure 3.7-4. Additionally, the solar array panels must be reduced in height and doubled in number. To have enough equipment mounting and radiator area, some equipment may have to be mounted inside the antenna support structure.

All of the factors influencing a spacecraft configuration such as thermal control, solar torques, thruster plumes, sensor fields of view, mass properties, power requirements and so forth have not been considered in detail for these configurations. It can be concluded that the MBA will have a very significant impact on the spacecraft configuration and must be considered at the very earliest stages of the spacecraft design.

3.7.4 Torque Disturbances: Deployment and Pointing

The INTELSAT V satellite's attitude control system maintains satisfactory control during deployments of antennas similar to the MBA. The ATDRSS is not expected to have any unacceptable disturbances due to the MBA deployment.

Detailed analysis could be done to determine the effect of the feed motion during antenna pointing; however, the resulting disturbance due to the small mass and slow motion of the feed is expected to be insignificant.

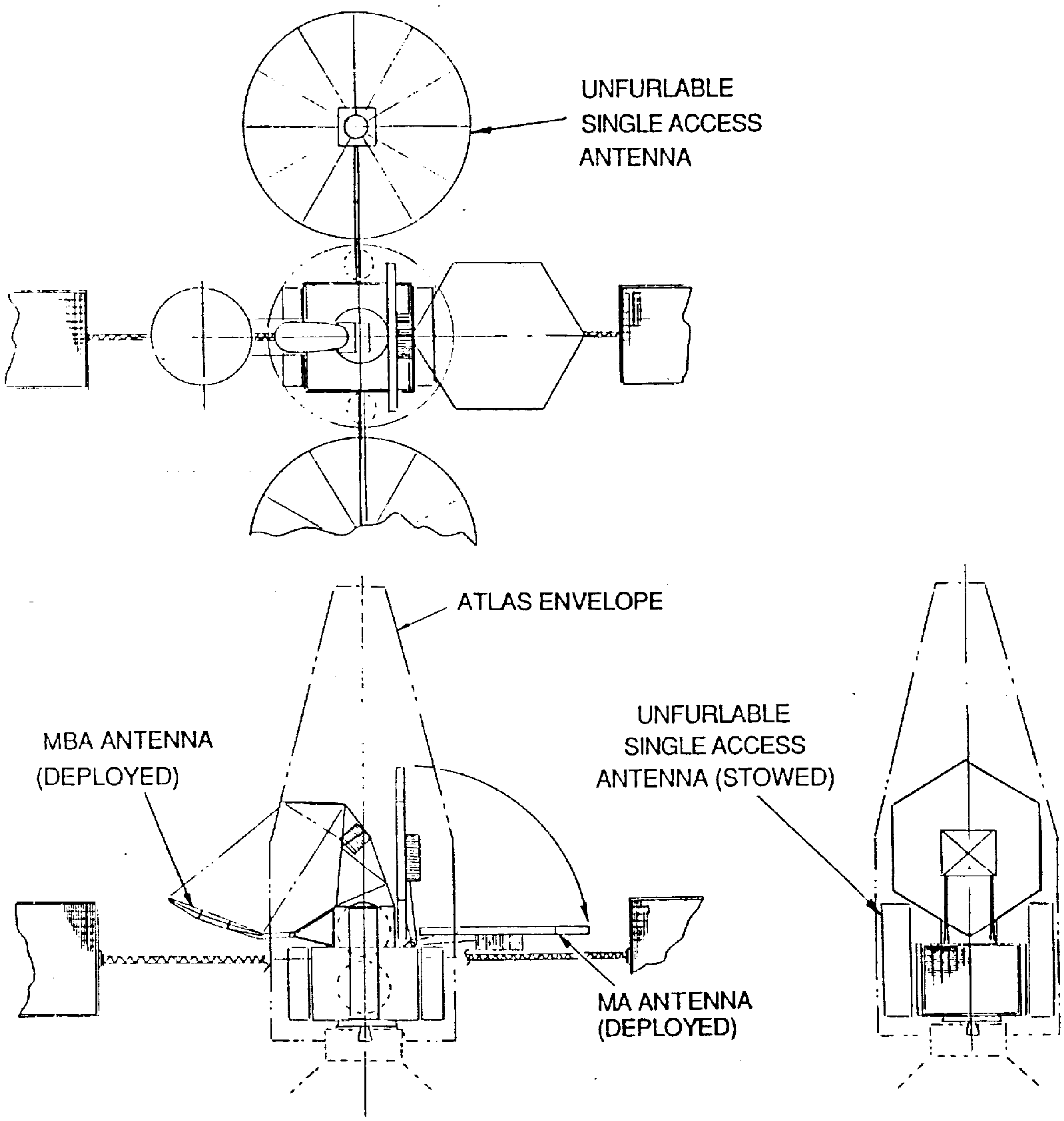

Figure 3.7-5. MBA Spacecraft in Atlas Centaur

3.8 ANTENNA POINTING ERROR ANALYSIS

The antenna pointing error analysis accounts for the total range of the RF boresight pointing excursions for the antenna system. The contributions of individual sources of errors are computed about each of the spacecraft pointing axis (pitch, roll, and yaw) for each spacecraft operating mode. Deterministic error sources that can be reduced by use of programmed spacecraft bias generators are identified (e.g., orbital inclination). Residual errors from these error contributors are computed and used in the pointing excursion assessment.

The pointing error sources are:

- Earth sensor errors
- Attitude Determination and Control System (ADCS) error contributions
- Thermal distortions
- Mechanical alignments

The time behavior of each error contributor is analyzed. The errors are grouped into one of five time categories as shown below.

Title	**Time Period or Duration**
Short Term	Less than 24 hours
Diurnal	24-hour period
Seasonal	1-year period
Long Term	10-year period
Alignment	Constant

The errors are then combined in each category to account for the worst-case RF boresight excursion. Error combinations that arise from hardware that lack a thorough and rigorous analysis are identified, and margins are established for these error contributors. The resulting errors from each time category (including the margins) are added to arrive at a worst-case assessment for the RF boresight excursion about the pitch, roll, and yaw axes. The appropriate time category errors are next combined to arrive at the following assessments:

- Maximum RF boresight excursion over life of spacecraft
- Maximum RF boresight excursion in 24-hour period
- Maximum RF boresight excursion in 12-month period

Table 3.8-1 is a summary of antenna pointing error for the normal attitude control mode with both momentum wheels operating. Table 3.8-2 gives the error budget for one mode (mode magnetic storm) for the 10-year life of a large three-axis communications satellite. The L-mode configuration is the backup model if a momentum wheel failure occurs.

Table 3.8-1. Normal Mode Antenna Pointing Errors with V-Wheel Configuration

	10 Year	12 Month	24 Hour
Roll	0.070	0.040	0.038
Pitch	0.080	0.043	0.042
Yaw	0.067	0.043	0.043

The resulting pitch, roll, yaw pointing errors must be converted into azimuth (EW) and elevation (N-S) variations on the earth disk. The pitch and roll errors transform directly into E-W and N-S deviations. Antenna yaw errors produce pointing error components in both E-W and N-S directions with relative magnitudes depending on the location of a particular ground target.

Descriptions of errors due to earth sensors and ADCS are beyond the interest of this report and are not included. A discussion of errors due to thermal distortions and mechanical alignments follows.

3.8.1 Thermal Distortion Errors

These errors are caused by distortions due to shadowing of the reflectors, feeds, and support structure with the antenna system. The values used in the antenna pointing error analysis are based upon Ford Aerospace's experience with reflectors of similar size and construction to the MBA. The reflectors are approximately the same size as the INTELSAT V reflectors. The thermal distortion effects of the attached offset feed are separately analyzed and accounted. A very detailed thermal distortion analysis was performed on the INTELSAT V antennas and this analysis computed the angular displacement of more than 200 nodes accounting for the following effects.

- Spacecraft time of day (shadowing)
- Seasonal effects
- Long-term aging (change of coefficient of thermal expansion)

Table 3.8-2 Antenna Pointing Error During Normal Mode

		Pitch	Pitch	Pitch
Random Alignment Errors				
Earth sensor electrical axis to reference mirror		0.0050	0.0050	0.0000
Earth sensor reference mirror to S/C reference axis		0.0050	0.0050	0.0000
Antenna boresight to antenna reference mirror		0.0150	0.0150	0.0150
Gravity compensation fixture		0.0100	0.0150	0.0100
Deployment repeatability		0.0150	0.0150	0.0100
Momentum wheel alignment		0.0000	0.0000	0.0100
Earth sensor change due to vibration		0.0050	0.0050	0.0000
Momentum wheel change due to vibration		0.0000	0.0000	0.0070
	RSS	0.0250	0.0274	0.0240
Random Long-Term Errors (10-year exposure)				
Earth sensor accuracy		0.0120	0.0020	0.0000
	SUM	0.0120	0.0020	0.0000
Random Seasonal Errors (1 year)				
Earth sensor mounting		0.0000	0.0010	0.0000
Solar torque tracking (L mode)		0.0000	0.0050	0.0200
Earth sensor accuracy		0.0010	0.0010	0.0000
	SUM	0.0010	0.0020	0.0200
Random Diurnal Errors (24 hours)				
Antenna thermal distortion		0.0110	0.0120	0.0100
Antenna thermal distortion contingency		0.0210	0.0200	0.0020
Earth sensor mounting		0.0000	0.0010	0.0000
Solar torque tracking (L mode & magnetic storm)		0.0000	0.0070	0.0800
Residual earth sensor calibration accuracy		0.0025	0.0025	0.0000
	SUM	0.0345	0.0425	0.0920
Random Short Term Errors (less than 24 hours)				
Control loop jitter (L mode & storm)		0.0070	0.0020	0.0010
	SUM	0.0070	0.0020	0.0010
MBA pointing error in normal mode		0.0795	0.0759	0.1370
		E-W	N-S	
Spacecraft pitch and roll errors		0.0795	0.0759	
Errors due to yaw excursions		0.0359	0.0359	
Errors due to $\pm 0.1^{\circ}$ E-W & N-S station drift		0.0037	0.0010	
Worst-case E-W and N-S pointing error		0.1191	0.1128	

Notes:
1. Error budget assumes N-S stationkeeping.
2. The normal mode budget is for worst case condition in which the L-mode backup wheel configuration is used in the presence of a severe magnetic storm.
3. Short-term effects due to wheel unloads and stationkeeping are not considered in this chart.

The results of the NASTRAN analysis were nest inputted to a "best fit" program that determine the resultant pitch, roll, and yaw pointing errors.

Thermal distortion of the reflector support hinge arms contribute to the antenna thermal distortion errors. The worst-case displacement of the reflector occurs during conditions near solstice, at midnight, when one hinge arm of a particular reflector is in full sunlight while the other is shadowed by the spacecraft mainbody.

The thermal distortion values were obtained by linear addition of the effects of reflector, feed, and hinge distortion. Because some of the components thermal distortion values have not been fully verified either by a detailed NASTRAN "best fit" computer simulation and/or a hardware test demonstration, Ford Aerospace carries a contingency factor for the contribution of antenna system thermal distortion into the antenna pointing error budget based on the size and geometry of the antenna system.

3.8.2 Alignment Errors

Alignment errors result from imperfections in positioning the RF boresight relative to the electrical axis of the reference attitude sensor. These errors are constant throughout the life of the spacecraft. In the case of the reflectors, the contributors result only from location uncertainties between the attitude reference sensor, structural elements, and antennas.

Ford Aerospace's design does not require in-orbit measurements and spacecraft repositioning in order to achieve the required RF boresight accuracy. Instead, we rely on careful ground construction and precision alignment tooling (including zero-G fixtures), exhaustive and repeated ground calibrations, and the use of accurate deployment mechanisms.

The composite alignment error for the antennas is computed by RSSing of the individual contributors. Justification of using an "RSS sum" of the individual "3 sigma errors" is based upon the fact that they are both statistically independent and uncorrelated. Estimation of the alignment error by an "RSS sum" was similarly done on the INTELSAT V spacecraft programs.

3.9 ANTENNA TRACKING AND FEED INTERCONNECT ISSUES

In this subsection, the tracking and feed interconnect issues of the MBA are discussed.

3.9.1 Tracking Issues

Investigation of the antenna tracking issues are addressed in this subsection. System level characteristics for the pointing mechanism are also defined. In order to define these characteristics, the following assumptions have been made.

The mechanism will require a pointing resolution less than the anticipated beamwidth of 0.3° to keep pointing error induced signal level losses within acceptable ranges. A pointing resolution goal of 0.05° has been established.

A two degree of freedom mechanism will be required. The spacecraft pointing errors in pitch and roll are assumed large enough to cause significant signal degradation, necessitating servo control of the pointing mechanism in these axes. Pointing errors in yaw are assumed insignificant.

A closed loop tracking system will be used. Spacecraft sensor data does not give adequate pointing information to remove the pitch and roll errors. By using a closed loop monopulse tracking system, with the signal possibly originating from the White Sands earth station, these errors can be removed. A closed loop system will also relax assembly, deployment, and thermal induced pointing error requirements. Note that a closed loop system will relax the required mechanism accuracy, but not the required resolution.

The orbital location of the mechanism is known well in advance. One concept that is being investigated mounts the antenna feeds in a fixed array with the location of each feed corresponding to a particular ground station. A unique feed array configuration will be required for each spacecraft orbital location, which must be determined prior to hardware construction.

A movable feed will provide coverage for the upper CONUS region. The dual-reflector system has a flat focal plane, hence a planar mechanism can position the feed. For the torus reflector system, the focal plane is curved in two axes, requiring a somewhat more complex mechanism to properly position the feed.

3.9.2 Feed Interconnect Choices

Rigid waveguide, coaxial cable, or flexible waveguide will connect the feed with the spacecraft. The advantages and disadvantages of each system have been identified. Rigid waveguide will provide the lowest signal losses, but will also require a number of rotary joints to accommodate the motion of the CONUS feed. Coaxial cable is the highest loss system, but is also the most flexible. A coaxial cable system may require that amplifiers be mounted at the feeds, which introduces a possible thermal issue for those components. Flexible waveguides may be too rigid to allow for anticipated CONUS feed motions.

3.10 MULTIPLE BEAM ANTENNA TRACKING MECHANISM

In this subsection system level characteristics for the TDRSS MBA pointing mechanisms are defined. Several approaches to positioning the antenna system have been investigated and a summary of each will be presented in the mechanism tradeoffs section. Issues common to all systems are listed below. Studies in this subsection are, however, limited to Configuration 1.

Two mechanisms, a tracking positioner and a CONUS positioner, will be required. The TDRSS MBAs will track a total of six targets, all within CONUS. Six feeds are required, five of which always track the same earth stations. These feeds can be mounted and aligned in a fixed orientation with respect to each other, but will require either an antenna or feed positioner mechanism to point them with respect to the spacecraft. This mechanism will be referred to as the tracking positioner. The sixth feed, mounted on the CONUS positioner, is required to cover upper CONUS with a range of approximately $\pm 1°$ N/S and $\pm 3°$ EW.

A two degree of freedom mechanism will be required. Our analysis shows spacecraft pointing errors in pitch and roll large enough to cause significant signal degradation, necessitating servo control of the pointing mechanism in these axes. Pointing errors in yaw are not large enough to cause significant signal degradation. The mechanism will require a pointing resolution less than the anticipated beamwidth of 0.3° to keep pointing error induced signal level losses within acceptable ranges. A pointing resolution goal of 0.05° has been established.

A closed loop tracking system must be used. Spacecraft sensor data does not give adequate pointing information to remove the pitch and roll errors. By using a closed loop monopulse tracking system, with the signal possibly originating from the White Sands earth station, these errors can be removed. A closed loop system will also relax assembly, deployment, and thermal induced pointing error requirements. Note that a closed loop system will relax the required mechanism accuracy, but not the required resolution.

The orbital location of the spacecraft must be known well in advance. One concept which is being investigated mounts the antenna feeds in a fixed array, with the location of each feed corresponding to a particular ground station. A unique feed array configuration may be required for each spacecraft orbital location, which must be determined prior to hardware construction.

Rigid waveguide, coaxial cable, or flexible waveguide will connect the feed with the spacecraft. The advantages and disadvantages of each system have been identified (see previous subsection). Rigid waveguides provide the lowest signal losses, but will also require a number of rotary joints to accommodate the motion of the CONUS feed. Coaxial cable system may require that amplifiers be mounted at the feeds, which introduces a possible thermal issue for those components. Flexible waveguide may be too rigid to allow for anticipated CONUS feed motions. This issue has not been resolved.

3.10.1 Mechanism Tradeoffs

Two antenna systems have been proposed for the MBA antennas: a torus system and a dual reflector system. A description of tracking mechanisms for each system is presented below for both the tracking and CONUS positioners.

3.10.1.1 Torus Antenna

3.10.1.1.1 Tracking Positioner. Four methods have been investigated: position the main reflector, position the entire antenna system, position all feeds simultaneously, and position each feed independently. Table 3.10-1 summarizes the approaches for the tracking positioner.

a. **Position the Main Reflector.** Pivoting the main reflector by means of a two degree of freedom mechanism is a relatively simple approach to meet tracking requirements. However, RF alignments will change when the reflector is pivoted, introducing signal degradation. This approach will also require a larger mechanism to position the relatively heavy dish, resulting in a mass penalty. The primary advantage to this approach is that the feeds are stationary, and allow the use of low loss rigid waveguide.

b. **Position the Entire Antenna.** This approach is very similar to "a" above. The antenna and feeds are mounted on a common baseplate, and are attached to the spacecraft through a two degree of freedom mechanism. The mass penalty for this approach is larger than "a", and rigid waveguide may no longer be used. As the feeds and antenna are moved as a complete unit, no RF misalignments occur while positioning.

Table 3.10-1. Torus Antenna Positioner Options Comparisons

Option	a	b	c	d
Mass	Med	Med	Low	Low
System complexity	Low	Low	Med	High
RF misalignment	Yes	No	No	No
Cost	Low	Med	Med	High
Flexible waveguide	No	Yes	Yes	Yes
Tracking difficulty	Low	Low	Low	High
Spacecraft impact	Low	Med	Low	High

c. **Position all Feeds Simultaneously.** Changing the pointing direction of the feeds can be achieved by mounting them on a movable baseplate. Ideally, this can be achieved without misaligning the RF path. The focal plane for the torus system, however is nonplanar, indicating that a nonplanar mechanism is needed to achieve this goal. As the shape of the focal plane for the antenna has not been defined, the difficulty of implementing such a system cannot be assessed. This system would be relatively lightweight, and would require flexible waveguide.

d. **Position each Feed Independently.** This system is identical to "c" above, except that each feed is mounted on its own two degree of freedom, nonplanar mechanism. This allows great operational flexibility, albeit at great cost and complexity. In addition, each feed would require its own tracking system to offer any advantages over method "c".

3.10.1.1.2 **Conus Positioner.** The CONUS positioner will be of the movable feed type, and will require a remote center pivot point and flexible waveguide as in "c" and "d" above.

3.10.1.2 **Dual Reflector System.** Five methods have been investigated: position the main reflector, position the subreflector, position the entire antenna system, position all feeds simultaneously, and position each feed independently. Table 3.10-2 summarizes the approaches for the case of dual reflector system.

3.10.1.2.1 **Tracking Positioner**

a. **Position the Main Reflector.** Pivoting the main reflector by means of a two degree of freedom mechanism is a relatively simple approach to meeting tracking requirements. However, RF alignments will change when the reflector is pivoted, introducing signal degradation. This approach will also require a larger mechanism to position the relatively heavy dish, resulting in a mass penalty. The primary advantage to this approach is that the feeds are stationary, and allow the use of low loss rigid waveguide.

b. **Position the Subreflector.** A stationary reflector is combined with a steerable subreflector for this approach, which offers the same advantages and disadvantages as described in the previous subsection, Position the main reflector. The positioner mechanism for the subreflector would be lighter than one for the main reflector.

Table 3.10-2. Dual Reflector System Positioner Options Comparisons

Option	**a**	**b**	**c**	**d**	**e**
Mass	Med	Med	Med	Low	Med
Mechanism complexity	Low	Low	Low	Low	Med
RF misalignment	Yes	Yes	No	No	No
Cost	Low	Low	Med	Low	High
Flexible waveguide	No	No	Yes	Yes	Yes
Tracking difficulty	Low	Low	Low	Low	High
Spacecraft impact	Low	Low	Med	Low	Low

c. **Position the Entire Antenna.** The antenna and feeds are mounted on a common baseplate, and attached to the spacecraft through a two degree of freedom mechanism. The mass penalty for this approach is larger than "a" or "b", and rigid waveguide may no longer be used. As the feeds and antenna are move as a complete unit, no RF misalignments occur while positioning.

d. **Position all Feeds Simultaneously.** This approach is identical to that proposed for torus approach, with one important difference. The dual-reflector system has a flat focal plane, allowing the use of a simple, planar two degree of freedom mechanism.

e. **Position each Feed Independently.** This approach is identical to that proposed in the previous subsection. A planar mechanism would be suitable for each feed.

3.10.1.2.2 **Conus Positioner.** The CONUS positioner will be of the movable feed type. Again, a planar mechanism would be used for positioning.

3.10.2 Recommendations

For the torus system, option "a", position the main reflector, is the simplest, lowest cost solution. A thorough systems trade study would be needed to determine that the RF misalignment losses are small, and that the additional system mass is not a problem. Should RF misalignment prove to be a problem, options "b", position the entire system, and "c", position all feeds simultaneously, become viable candidates. Of these two, option "c" is preferred due to its lower mass and minimal spacecraft impact. Option "d", position each feed individually, is preferred only if individual feed positioning is required. While this is the only system which can remove spacecraft yaw errors, our projections do not indicate that this capability is required.

For the dual-reflector system, option "d", position all feeds simultaneously, is the preferred choice. The flat focal plane of the dual-reflector system allows the feed positioner mechanism to be planar, making this option more attractive for the dual-reflector system than the torus. Should a solution which does not require flexible waveguide be desired, option "b", position the subreflector, is the lightest and simplest positioner mechanism.

Of all the systems investigated, the simplest, lowest risk mechanism is a dual-reflector antenna with a feed positioner. A system with a reflector or subreflector positioner is the easier to implement, but positioning these items causes misalignments in the RF path. At this time, the effects of optical misalignments are unknown, making it a higher risk choice.

3.10.3 Tracking System Implementation

Figure 3.10-1 is a schematic of a mechanism concept for a dual-reflector feed positioner. The system consists of two planar mechanisms, each with two degrees of freedom. The tracking positioner feed horns are mounted to a plate which is free to translate in both the pitch and roll directions. The plate is moved by stepper motors and ball screws. Total travel is ± 0.5 inch. Mounted to the tracking positioner feed plate is the CONUS positioner mechanism, which uses a similar arrangement of ball screws and stepper motors; however, total travel is approximately ± 5° in pitch and ± 2° in roll.

Using a standard 10 pitch ball screw and 1.8° stepper motor yields a resolution of 0.00050°/step. At a sensitivity of 1°/inch mechanism resolution is more than adequate at 0.0005°/step. Absolute position encoding can be provided by linear potentiometers on the lead screws.

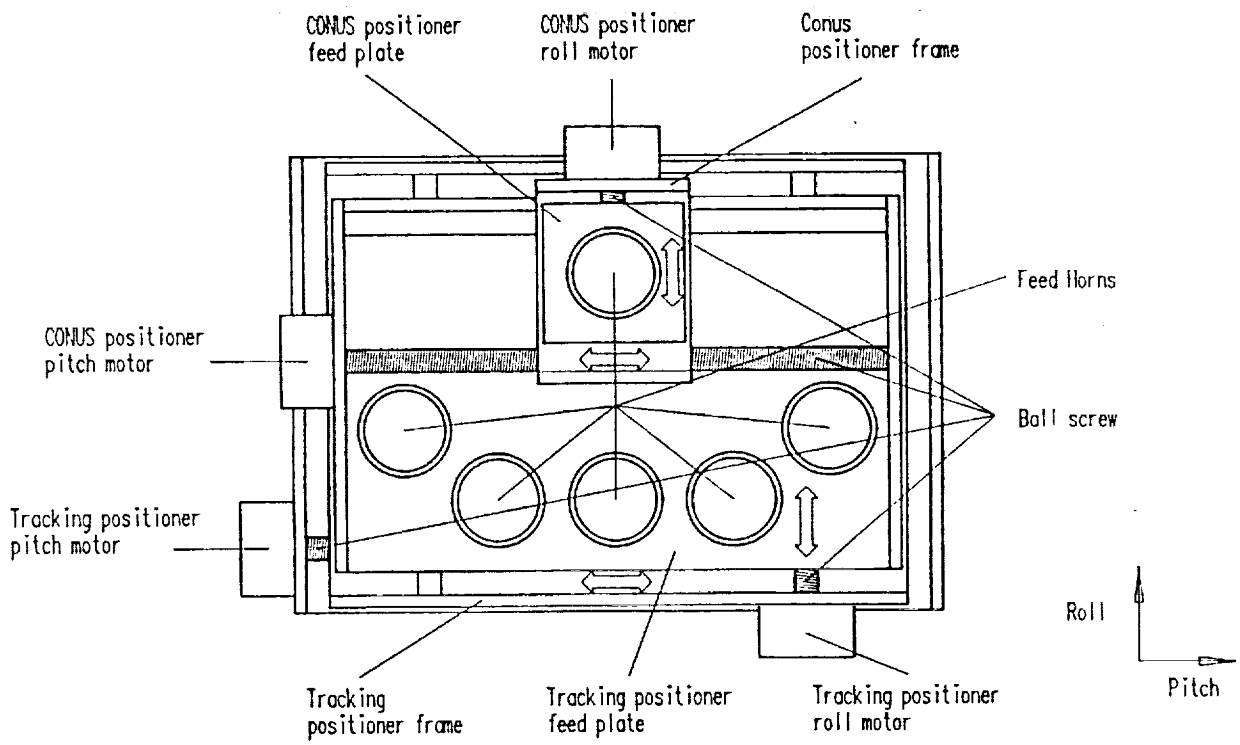

Figure 3.10-1. Feed Mechanism Combines CONUS and Tracking Positioners

3.11 MBA ALTERNATIVE DESIGN COMPARISONS

In this subsection, the various alternative design approaches considered in subsection 3.3 are compared, taking into account the impact of the considerations described in paragraph 3.4.3.10.

We begin this subsection by briefly reviewing the results presented in subsection 3.3, Figure 3.3-2, comparing gain degradation of various reflectors as a function of scan. Figure 3.11-1 is a revised version of the previous figure, refined to incorporate results of the contour plot of the dual-shaped reflector system shown in Figure 3.11-2. A comparison is difficult to make, since the gain degradation varies with direction away from the central axis (nominal focal point). According to the contour plot of Figure 3.11-2, the gain remains nearly flat in the East-West direction (the asymmetrical plane of the dual-reflector system) for ± 3°, which is roughly 11 beamwidths. However, scans of ± 2° N-S (7.4 beamwidths) cause a gain degradation of 0.4 dB. Furthermore, diagonal scans of 3° E and ± 2° N-S cause the worst-case degradation of 1.0 dB. Thus Figure 3.11-2 shows both the worst-case condition as well as a more favorable one, representing conditions along the E-W axis. Plots for the paraboloid and Cassegrain reflectors are similarly averages of scan losses in various directions.

Three of the most promising antenna design approaches, viz., phased array, dual-shaped offset reflector and torus antenna designs, were analyzed in some detail in Section 3.3. These three approaches can all meet the basic requirements. It appears desirable at this point to attempt some comparison of the three to help in making a choice among them. This comparison can include quite a number of parameters, some of which are difficult to evaluate quantitatively, but an attempt has been made to initiate such a comparison for a number of factors, as shown in Table 3.11-1.

Basic designs for the three candidates were originally developed for a common size -- 8-feet diameter -- which was considered necessary to meet the basic gain requirement of 54.7 dBi at 30 GHz. Gain estimates for this size differ for the three approaches, and so some size adjustment could be made for a comparison of different structures with the same gain.

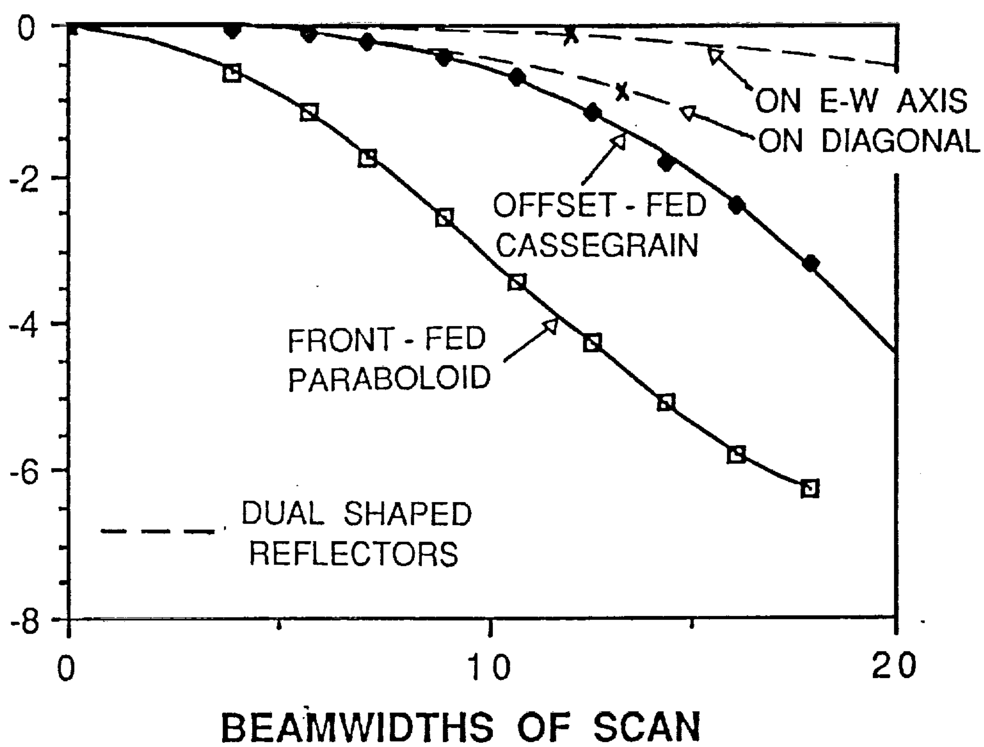

Figure 3.11-1. Antenna Scan Performance

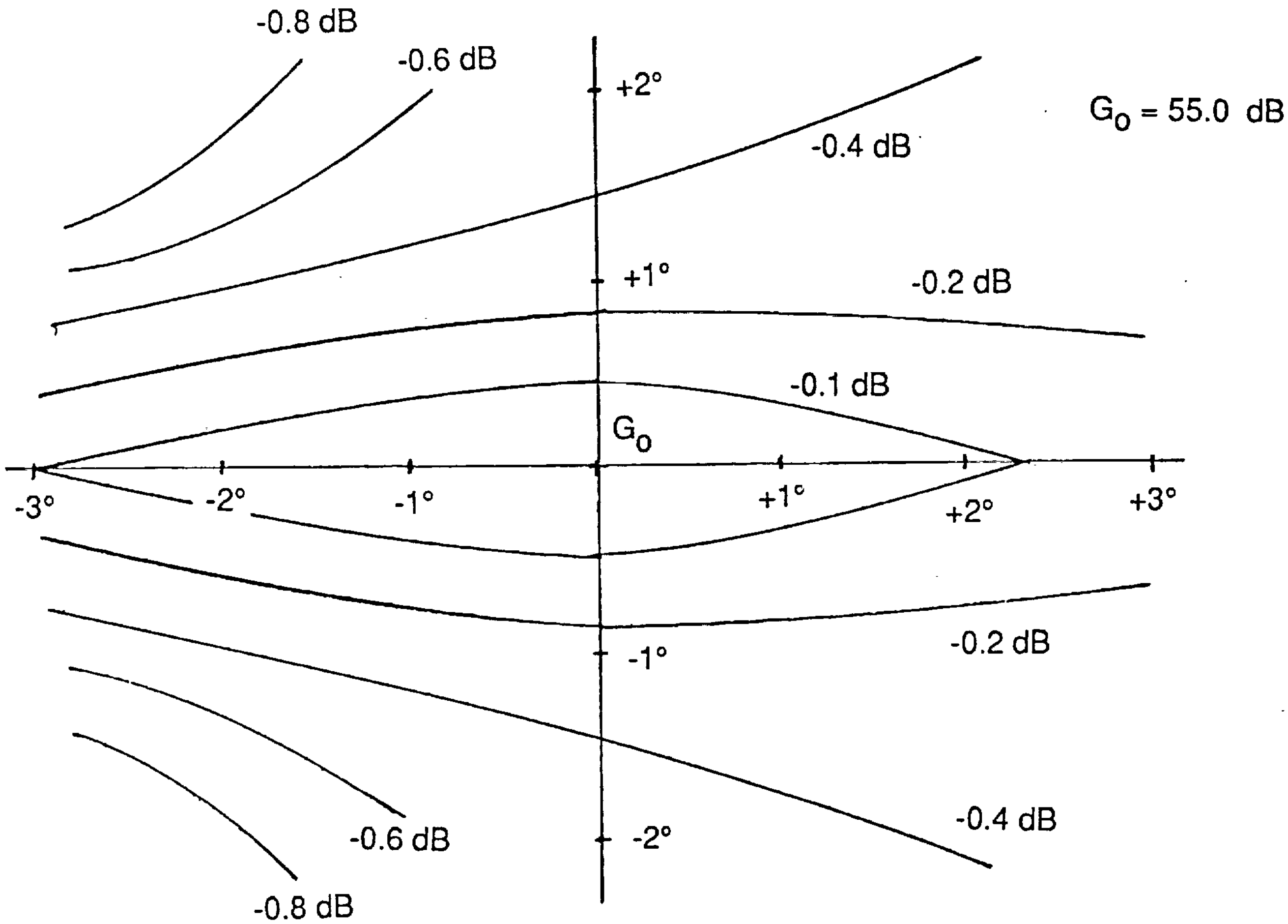

Figure 3.11-2. Measured Gain Contours -- Acts POC Model Antenna

Table 3.11-1. TDRSS SGL MBA Comparisons

	PHASED ARRAY		SHAPED DUAL REFLECTOR		TORUS REFLECTOR	
	CONFIG #1	CONFIG. #2	CONFIG #1	CONFIG. #2	CONFIG #1	CONFIG. #2
SCAN RANGE REQ'D	3° X 6°	2° X 13°	3° X 6°	2° X 13°	3° X 6°	2° X 13°
MULTIBEAM MECHANISM	SEPARATE CIRCUITS FOR EACH BEAM		MULTIPLE FEEDS - MOVEABLE FOR MOBILE STA.		MUTIPLE FEEDS - MOVEABLE FOR MOBILE STA.	
OVERALL SIZE - MAIN STRUCTURE SUB-REFLECTOR	3 X 96" SQUARE		96" D 24" X 60"	96" D 24" X 72"	96" X 136" —	96" X 176" —
MECHANISM FOR MULTIPLE BANDS (F12-14, 20, 30 GHz)	SEPARATE STRUCTURES FOR EACH		BROADBAND FEEDS OR FSS		BROADBAND FEEDS OR FSS (MODIFIED DESIGN)	
PERFORMANCE:						
GAIN @ 30 GHz - PEAK (DB) MIN., EDGE/SCAN	57 56	57 56	55 54.5	55 54	58 57.5	59 58.5
COMPLEXITY 12/14 GHz 20 GHz 30 GHz	6 BEAMS 270 HPA & LNA, 3200 Δ♦ 384 HPA, 230 Δ♦ 864 LNA's, 5200 Δ♦	3 BEAMS SAME # LNA'S & HPA'S HALF # Δ♦	6 BEAMS 6/12 FEED HORNS, 1/2 MOVABLE DUAL REFLECTORS POSSIBLE FSS		6 BEAMS 6/12 FEED HORNS, 1/2 MOVABLE SINGLE REFLECTOR POSSIBLE FSS	
DEPLOYMENT	MORE DIFFICULT		RELATIVELY SIMPLE		COMPLICATED	
EASE OF BEAM STEERING (ATTITUDE CORRECTIONS)	EASIEST (ELECTRONIC)		MORE DIFFICULT REQUIRES MECHANICAL MOTION OR REFLECTOR(S) OR FEED ARRAY		MORE DIFFICULT REQUIRES MECHANICAL MOTION OR REFLECTOR(S) OR FEED ARRAY	
COST	HIGHEST - DEVELOPMENT OF MMIC'S - SEPARATE STRUCTURES FOR EACH BAND		MEDIAN SHAPED REFLECTOR COSTLY TO FABRICATE		LOWEST SIMPLEST REFLECTOR	
RISK	HIGHEST - MAY HAVE THERMAL & PACKAGING PROBLEMS • INTERCONNECTIONS - DEVELOPMENT OF MMIC'S STATE-OF-THE-ART		LOWEST - ALIGNMENT OF DUAL REFLECTORS SOME PROBLEM - DUAL BAND FEEDS DIFFICULT		MEDIAN - LARGER REFLECTOR MAY REQUIRE FOLDING FOR STOWAGE - CONFIGURATION WITH FSS MORE COMPLEX - MOVING FEEDS ON CIRCULAR ARC MORE DIFFICULT - DUAL BAND FEEDS DIFFICULT	

The major challenges in this antenna are the multiband and multibeam requirements. Multiple beams are accommodated in the phased array design by duplicating all of the beamforming elements for each beam -- phase shifters, combiners, etc., and dividing the received signal for processing by each set. This division process produces unacceptable losses unless it occurs after the first set of preamplifiers, which set the noise performance of the receiving system. Thus LNAs are required for each basic element of the phased array. On transmit, this translates into a requirement for power amplifiers at each element, each of which must handle all of the separate transmit channels. To avoid excessive intermodulation effects, these amplifiers may have to be operated at an appropriate backoff level from saturation, which results in lower efficiencies. Furthermore, the duplication of beamforming components leads to the requirement for a great number of such components, which could thus most easily be realized in MMIC form.

For the reflector-type antennas, accommodating multiple beams merely means duplicating feeds, all of which can use the same reflector. However, positioning these beams off the focal axis may result in gain degradation, unless some special measures are taken, such as the use of dual-shaped reflectors or an extended-size torus reflector.

Operating these antennas at multiple frequency bands poses some special problems. First of all, using a common aperture over the range from 12 to 30 GHz results in an inherent gain variation of some 3 dB, which may or may not be acceptable. Furthermore, designing a common feed structure to operate over this band presents a major problem, especially for dual-polarization operation. The reflector-type antennas can avoid this problem to some extent by use of an intermediate frequency-selective subreflector, which would allow individual feeds to operate over one or two bands at most. This option for the torus reflector presents somewhat of a geometrical problem, since the feeds would have to be considerably offset from the reflector to avoid blockage.

It is not considered desirable to operate the phased array over the desired 12-30 GHz band, because of the compromise in array geometry which it would impose. Thus three separate arrays should be considered for this multiband system, covering 12-14, 20 and 30 GHz separately. This would also allow optimum sizing of each for its particular gain requirements.

The costs of the torus designs and implementations are expected to be the lowest mainly due to the simplicity of the reflector fabrication; the dual-reflector approach is expected to be more expensive due to the associated costs of fabrication of the shaped reflector; the phased array approach is estimated to be the most expensive because of the requirement of separate structures for each band and because of the development and space-qualification costs of the MMIC.

The dual-reflector configuration is expected to provide the least risk approach, while the phased arrays configurations are judged to be the most risky of the three approaches.

Attitude corrections and beamshaping/steering are most easily accomplished by the phased array approach, whereas they are more difficult to achieve with the other two approaches due to the inherent (mechanical) steering mechanisms required.

The deployment of the dual-reflector configuration is expected to be the easiest, whereas the torus approach is the most complicated. (For a discussion in this area, refer to subsection 3.7.

3.12 ATDRSS MBA -- DESIGN DESCRIPTION SUMMARY

Two alternative designs are being recommended to meet the multibeam requirements of the space-ground link antenna for a future ATDRS spacecraft -- either a shaped dual-reflector design, or a parabolic torus reflector. Both designs utilize multiple feeds to accommodate the multiple beams; several of these would be movable to service the mobile ground stations. A choice could not be made between these two designs because of the variability of the requirements (differences between alternate system configurations), and because of the arbitrary weights which need to be assigned to various tradeoff factors (such as size, weight, and electrical performance). A sketch of the two alternate designs is shown in Figure 3.12-1. The torus produces slightly higher gain, but at the expense of a larger structure, which may have to be folded to fit into the launch envelope.

The basic problem which must be faced in designing a focussed antenna system (reflector or lens) for a multibeam application is the gain degradation produced when a beam is formed far off the focal axis of the antenna. Because of gain requirements, the beamwidth of the antenna will be on the order of 0.3° at 30 GHz. This beam must be scanned ± 6.5° to cover stations specified for Configuration 2, which represents ± 22 beamwidths. This amount of scan would produce considerable loss of gain for a simple Cassegrain reflector system. However, a torus reflector system can be designed which will allow this scan with very little gain loss, at the expense of a larger reflector in the direction of scan. This reflector has a circular shape in the scan direction, and a parabolic in the orthogonal direction. The parabolic dimension must be 2.4 m (96 inches) to produce the desired beamwidth, while the maximum circular dimension depends upon the extent of scan and radii of curvature. For the design parameters selected, this dimension would be 136 inches (3.45 m) for Configuration 1, and 176 inches (4.47 m) for Configuration 2. The feeds for the multiple beams are dispersed along a circular arc at about half the radius of the main reflector (which was selected as 300 inches = 7.6 m for high efficiency). Each feed illuminates a different portion of the reflector, which is properly focussed, and explains the need for the extended reflector size.

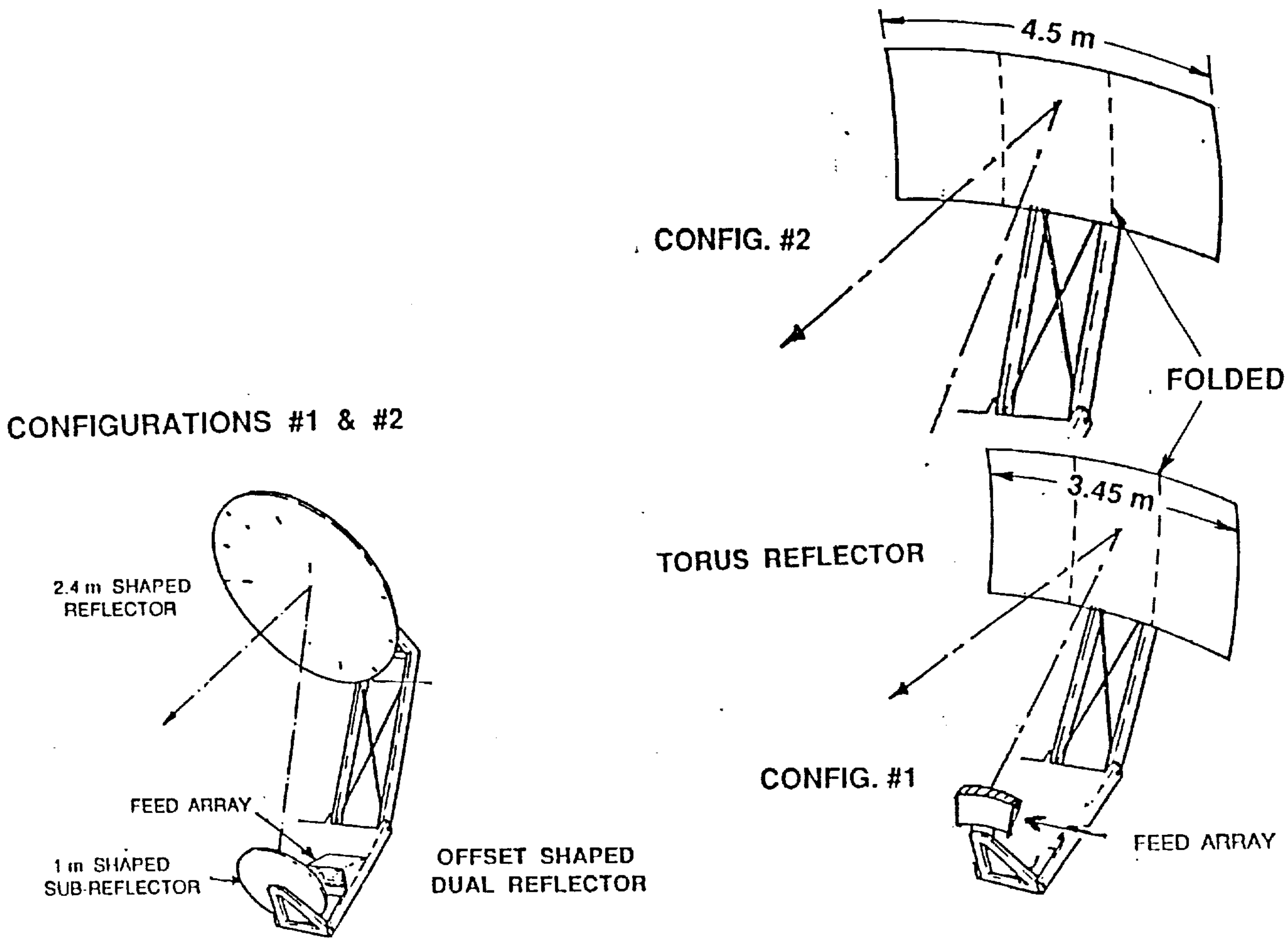

Figure 3.12-1a. MBA Design

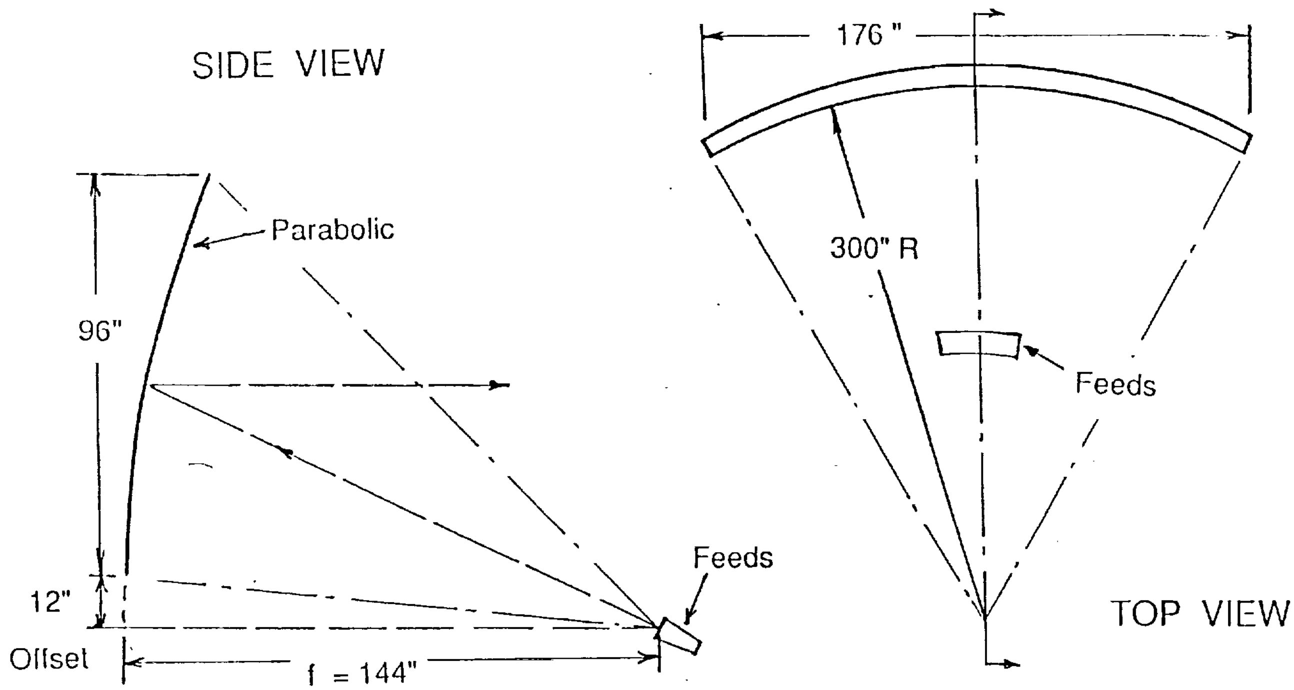

Path Length Errors for ± 7.5° Scan:
Maximum = 0.078", RMS = 0.032" (= 0.08 Wavelengths at 30 GHz)

Figure 3.12-1b. Preliminary Torus Antenna Design

The alternate design makes use of a pair of shaped dual-reflectors, offset-fed (to prevent blockage), whose shapes are determined by an optimization program which minimizes path length errors for scanned beams. This concept has been proven by design and measurements on a POC model built for NASA Lewis Research Center, and operating at 20 GHz. This model demonstrated ± 12 beamwidths scan with a similar beamwidth (0.3°), and a maximum gain degradation at scan edge of less than 0.5 dB. This design could be extended to cover ± 22 beamwidths of scan with a projected loss of less than 1.0 dB. The main reflector for this design is again 2.4 m = 96 inches in diameter, while the subreflector is elliptically shaped, 24 x 60 inches for Configuration 1, and 24 x 72 inches for Configuration 2. The extended dimension again is required because feeds for different beams illuminate different portions of the subreflector. The feeds are located on a planar surface for ease of positioning.

The feeds for both of these designs will depend critically upon the final requirements for the MBA system -- which orbital configuration is chosen, which bands are required (Ku and Ka in all feeds?), and the number and location of the ground stations selected. A basic dilemma still exists relative to required isolation between beams -- although the antenna designs produce low sidelobes, beams must still be separated by about two beamwidths to realize 25 to 30 dB isolation. For Ka-band operation, at 20 GHz, this requires a minimum beam separation of 1°, which severely limits the selection of ground station locations permitted. For Ku-band, even larger separations would be required. Thus it is not clear that both bands would be required for all feeds, or how closely the feeds would have to be spaced, which limits the feed sizes. If both bands are desired for all feeds, the most attractive arrangement is to use a planar FSS between individual feeds and the first reflector as sketched in Figure 3.12-2. This allows separate feed horns to be used for different parts of the band, which would allow optimization of feed sizes for each and matching over a more restricted band for each. If only Ka-band is required, both 20 and 30-GHz signals can probably be radiated from a common feed horn with little compromise. Those feeds which service mobile ground stations will be mechanically positioned to create beams in the proper locations; interconnections can probably be made by means of flexible waveguides because of the limited range of motion required.

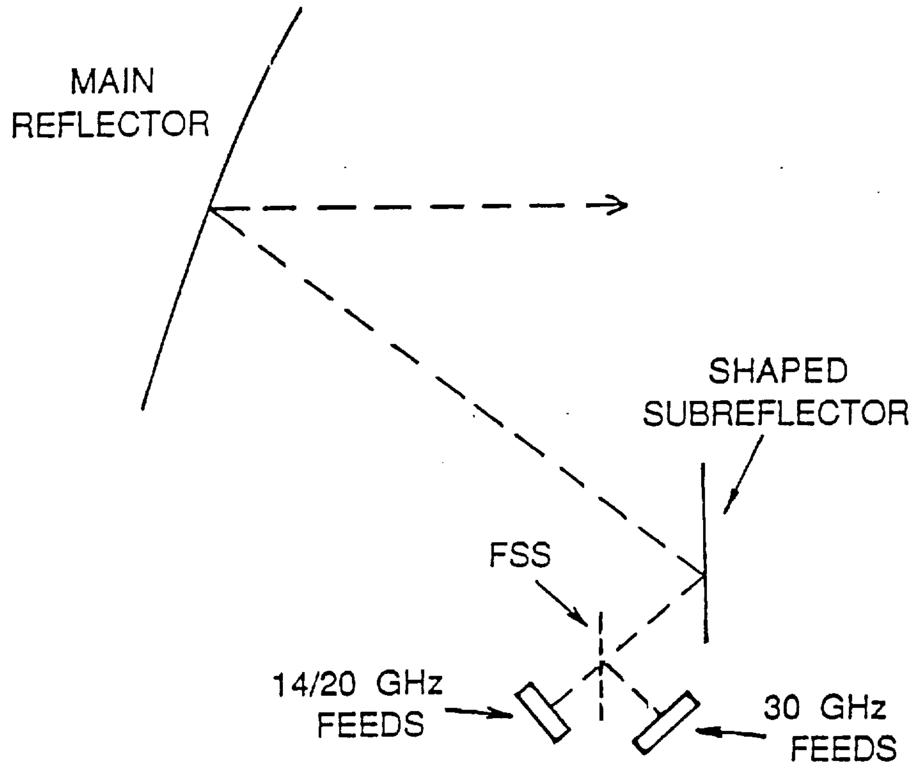

Figure 3.12-2. Dual Reflector Antenna with FSS for Band Separation

The mechanical configuration of the Dual Reflector System is shown in Figure 3.12-3. The structure hardware is based on existing technology, flight proven on the Ford Aerospace INTELSAT V spacecraft. The prime reflector, its support structure, and the reflector deployment mechanism would be similar to the 4 GHz reflector and hinge used on INTELSAT V, differing only in the shape of the reflector and that INTELSAT V has no subreflector. Both the prime and subreflectors would be constructed of aluminum honeycomb core with graphite skins. Backup structure or stiffening ribs would be similarly constructed of an aluminum core, graphite skin sandwich.

A more detailed discussion of the deployment mechanism was presented in subsection 3.7.

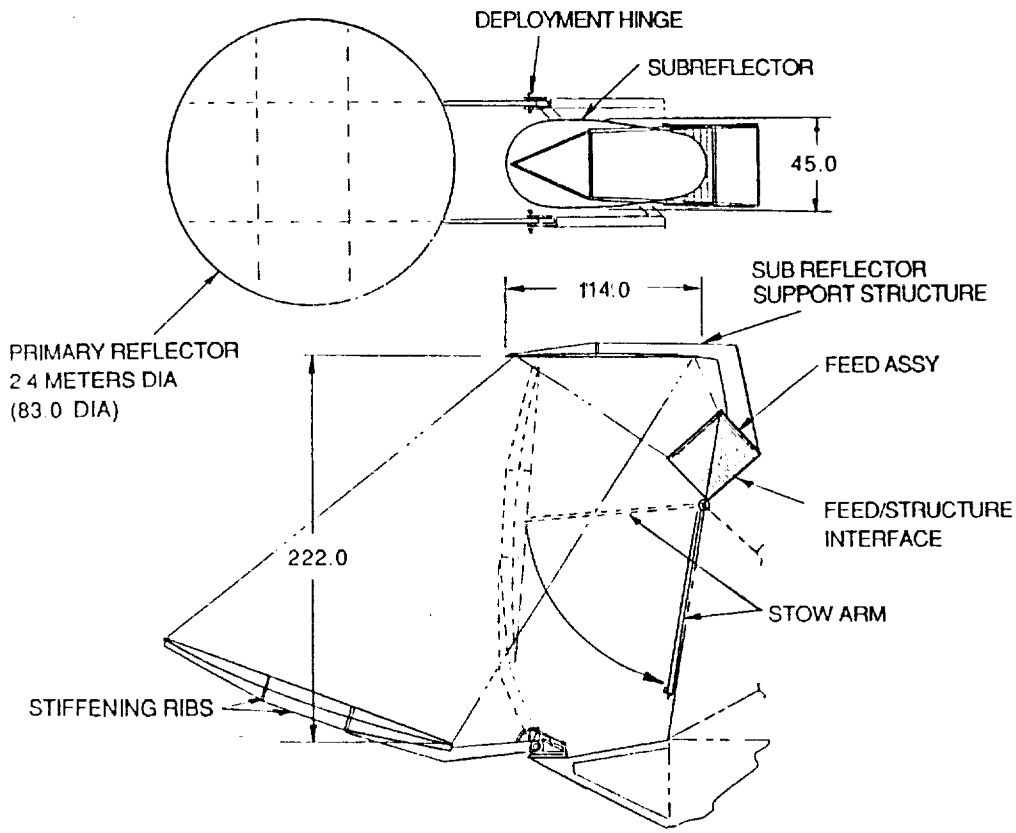

Figure 3.12-3. MBA Dual Reflector Mechanical Configuration

Mass Summary

		kg
a.	Shaped dual-reflector antenna assembly	52.3
	Primary reflector	17.6
	Subreflector	10.7
	FSS assembly	0.5
	Deployment hinges	1.8
	Stow arm assembly	0.7
	2 feed assemblies	21.0
	Feed assembly	10.5
	Feeds	1.8
	Mechanism	6.8
	Structure	1.9
b.	Torus reflector antenna assembly*	50.8 (Configuration 1)
		61.8 (Configigration 2)
	Reflector:	
	Configuration 1 = 96" x 136"	37.8
	Configuration 2 = 96" x 176"	48.8

(*This assumes approximately the same mass for feed and deployment hardware as above for the shaped dual-reflector approach. The torus approach, however, requires a prime-focus single feed assembly and does not use the FSS.)

These figures assume use of 2.0 lb/ft^3 aluminum 1/4 inch cores with 20-mil graphite faceskins, and include backup structure and thermal paint or blankets.

Performance specifications for the two antenna alternates are as follows:

	Shaped Dual Reflector		Torus Reflector	
Configuration	1	2	1	2
Gain, dBi				
30 GHz, peak	55	55	58	59
Edge of scan	54.5	54	57.5	58.5
20 GHz, peak	53.5	53.5	56.5	57.5
Edge of scan	53	53	56	57
Polarization	Dual Linear		Dual Linear	
Polarization Isolation, dB	25	25	25	25
Interbeam isolation*				
@ 20 GHz	25 dB			
@ 30 GHz	30 dB			
@ 15 GHz	20 dB			

*Estimated by closest stations in Configuration 1 (Goddard/Andover); approximately 5 dB enhanced isolation for 1° minimum separation.

REFERENCES

3-1 TRW Report on Contract NAS3-22499, 20 Apr 1982.

3-2 Ford Aerospace Final Report on Contract NAS3-22498, 10 Jan 1984.

3-3 S. Silver, Microwave Antenna Theory and Design, New York: McGraw-Hill, 1949, p. 159.

3-4 W. T. Patton. "Limited Scan Arrays," Phased Array Antenna Symposium, 1970.

3-5 Ruze. "Antenna Tolerance Theory," Proc. IEEE, Apr 1966.

SECTION 4
TRANSMIT/RECEIVE SYSTEM ENGINEERING

The transmit/receive system issues, the associated technology issues, and the reliability figures for each major component are presented in this section.

4.1 DOWNLINK TRANSMISSION ARCHITECTURES

The focus in this subsection is the downlink transmission system architectures. Uplink receive systems are much less complex and implementations are straightforward because the (forward) uplink data rate requirements for each of the services are much lower than those of the corresponding (return) downlink services. Therefore the component and device technologies of the uplink receive systems are covered.

We assume that transmission to a RGT is limited to 1 Gbaud (2 Gb/s with uncoded QPSK signaling) and similarly that transmission to the TNGT is limited to 2 Gbaud.

There are seven ground terminals that will receive data, one TNGT with a maximum data rate of 2 Gbaud, and six RGTs with a maximum data rate of 1 Gbaud. There is an additional restriction of a total downlink data rate of 2 Gbaud. Several downlink transmission architectures are examined to meet the SOW design goal of a maximum prime power consumption of 460 W for the entire MBA/Switch subsystem.

In calculating the required output of each high power amplifier (HPA) (P_T), the factor 1.5 to convert baud rate to spectral bandwidth is used, e.g., 1 Gbaud corresponds to 1.5 GHz bandwidth. Using the required antenna diameter of 2.4 m derived in Attachment 4 and the SOW requirement that the effective isotropic radiation power (EIRP) of each downlink signal be not less than -37 dBW/Hz, then at the minimum downlink frequency of 17.5 GHz the required downlink transmit power is derived from

$$10\text{Log}[P_T \times G_T / \text{Bandwidth}] > -37 \text{ dBW/Hz}$$

$$10\text{Log}P_T > -37 + 10\text{Log}(\text{Bandwidth}) - 10\text{Log } G_T$$

But: $G_T = \eta(D \text{ Pi } F/c)^2$

Where D = antenna diameter = 2.4 meters

η = antenna efficiency = 60%

F = downlink frequency = 17.5 GHz

c = speed of light = 3×10^8 m/s

Pi = 6.28

Therefore $G_T = 0.6\,(2.4)^2\,(Pi)^2\,(17.5\ 10^9)\ \ (3 \times 10^8)^2$

= 116066.5 or 50.65 dB

Adding 1 dB to compensate losses in the feed system, we obtain

$10\text{Log}\ P_T > -37 + 10\text{Log(Bandwidth)} + 1 - 50.65\ \text{dBW}$

or

$10\text{Log}P_T > 10\text{Log(Bandwidth)} - 86.65$

If the HPA must support composite signals, add 7 dB to P_T for backoff to avoid distortion. (This is a rule of thumb figure, assuming use of no linearizers and limiters.)

Table 4.1-1 gives the bandwidths and transmit power necessary to support data rates for the various signal structures dictated by the transmission schemes under consideration. For instance, an LSA service, with a signaling rate of 1 Gbaud, will use 1.5 GHz of spectral bandwidth and will require a transmit power of 3.25 W. Since the LSA is a single signal, the 7 dB backoff does not apply, but a composite 1 Gbaud signal will require a 16.3 W transmitter. A 500 Mbaud composite signal will require an 8.1 W transmitter to transmit the 750 MHz wide signal.

For each of the following transmission architectures, the worst case data distribution that will force the highest prime power consumption is analyzed. Results of the study, number of transmitters, and prime power for each architecture are summarized in Table 4.1-2.

Figure 4.1-1 depicts the single transmitter per ground station architecture. A 32.5 W transmitter is used for the TNGT to support the maximum 2 Gbaud data rate; 16.3 W transmitters are used for each RGT to support the maximum 1 Gbaud composite signal. The worst case data distribution is data being transmitted to each ground station, necessitating all the transmitters be turned on for a total transmit power of 130.3 W. Assuming 20% efficient solid-state power amplifiers (SSPAs), this architecture consumes 651.5 W of prime power, a great deal more than that allowed for the entire MBA/Switch subsystem; therefore this scheme is clearly unacceptable.

Table 4.1-1. Power Required Versus Signaling Rate

$$10 \log P_T = 10 \log (BW) - 86.65 \text{ (dBW)}$$

Services	Signaling Rate	BW (Hz)	P_T (dBW)	P_T (W)	P_T including 7 dB backoff (W)
LSA	1 Gbaud(2)	1.5×10^9	5.11	3.25	16.3
WSA, KSA	150 Mbaud(14)	225×10^6	-3.13	0.5	2.5
SSA	6 Mbaud(4)	9×10^6	-17.1	0.02	0.1
Telemetry	(2)	2.25×10^6	-23.1	0.005	0.025
SMA	100 kbaud(20)	150×10^3	-34.9	0.0003	0.0015
4 X SSA + 2 X TLM		40.5×10^6	-10.6	0.09	0.44
20 X SMA	2000 kbaud	3×10^6	-21.9	0.0065	0.0325
Composite Signals	500 Mbaud	0.75×10^9	2.1	1.6	8.1
	250 Mbaud	0.375×10^9	-0.9	0.81	4.1
	125 Mbaud	0.1875×10^9	-3.92	0.4	2.0
	2 Gbaud	3×10^9	6.12	6.5	32.5

Table 4.1-2. Performance Summary

Transmission Scheme		Prime Power Required (W)	Number of Transmitters
1	Single transmitter per ground station	651.5	7 (32, 16 W)
2	Switched transmitters	528.5	7 (32, 16, 8 W)
3	Dedicated transmitters	476	294 (0.3 mW to 3.25 W)*
4	Hybrid	490	196 (32 mW to 3.25 W)*
5	Varying power transmitters Version 1	406	15 (32, 16, 8)
6	Varying power transmitters Version 2	325.5	29 (32, 16, 8, 4, 2)
7	Varying power transmitters Version 3	221	8 TWTA (32, 16) 21 SSPA (8, 4, 2)

* 2 Gbaud max downlink data rate does not apply

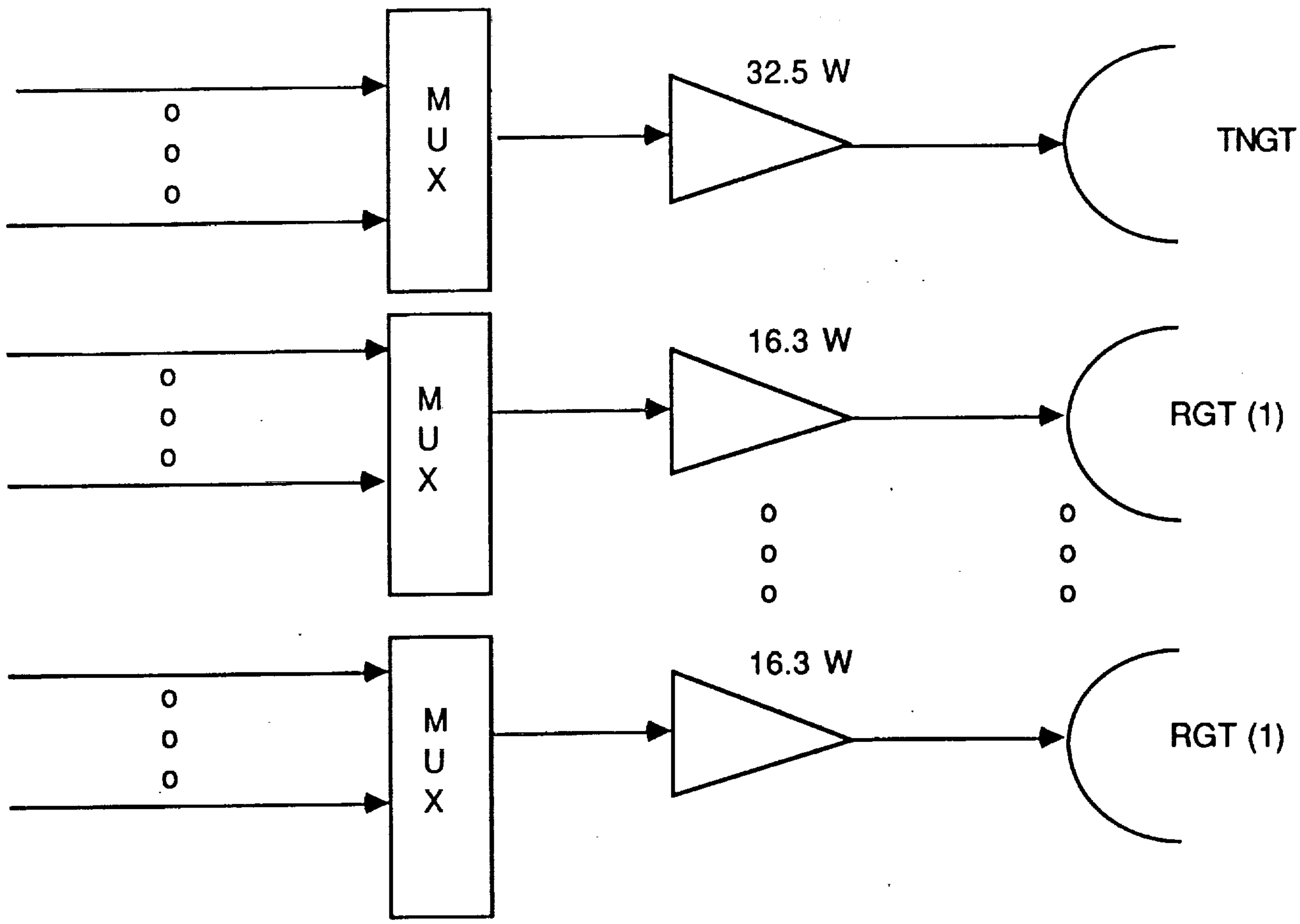

Worst Case Data Distribution:

1 - TNGT @ 32.5 W

6 - RGT @ 16.3 W each

P_{TOT} = 130.3 W

P_{prime} = 651.5 W

Transmitters = 7

Figure 4.1-1. Transmission Scheme 1, Single Transmitter per Ground Station

The architecture shown in Figure 4.1-2 again uses one 32.5 W transmitter for the TNGT but uses switched transmitters for the RGTs. For instance if a RGT is supporting a 1 Gbaud transmission, one of the 16.3 W transmitters would be switched to its antenna feed, while an 8.1 W transmitter would be used for data rates less than 500 Mbaud. Note that three 16.3 W amplifiers are sufficient, because if four signals were each more than 500 Mbaud, the maximum total downlink rate of 2 Gbaud would be exceeded. The worst case data distribution for this architecture is three of the RGTs each receiving slightly more than 500 Mbaud, and three of the RGTs and the TNGT each receiving less than 500 Mbaud of data, again with a total downlink rate less than 2 Gbaud. The total transmit power is 105.7 W and the prime power 528.5 W, again larger than that allocated for the entire subsystem.

Transmission architecture 3 is depicted in Figure 4.1-3. It contains a single transmitter per service. The worst case will be all transmitters in operation at the same time which will require a transmit power of nearly 14 W per terminal. (Note that the maximum downlink restriction of 2 Gbaud does not apply to this architecture, because all return services can be simultaneously supported irrespective of the data rate of each service.) The prime power consumed by this architecture is 476 W, which is closer to the SOW design goal, but still too high. Figure 4.1-4 shows a similar scheme but with the lower data rate signals combined. The prime power is somewhat higher than in Figure 4.1-3, but the number of transmitters has been reduced appreciably.

Figure 4.1-5 depicts the fourth type of architecture described above. Three transmitters are assigned to the TNGT, a 32.5 W for data rates above 1 Gbaud, a 16.3 W for data rates less than 1 Gbaud but in excess of 500 Mbaud, and an 8.1 W for data rates less than 500 Mbaud. Similarly, each RGT has two transmitters, one for data rates in excess of 500 Mbaud and one for lower data transmission rates. As in architecture 2 (Figure 4.1-2), the worst case data distribution is three of the RGTs receiving more than 500 Mbaud of data, while the other three RGTs and the TNGT each receive a fraction of the rest. Total transmit power in this scheme is 81.3 W and prime power is 406.5 W.

The scheme in Figure 4.1-6 is the same as that of Figure 4.1-5 except that more transmitters are allocated to each terminal so that less power will be used for the low data rates. Twenty-nine amplifiers are required instead of the 15 of Figure 4.1-5, but the additional ones are lower power and should present less of a reliability risk. The prime power consumption has been reduced from 406.5 W to 325.5 W. This is a substantial reduction and the technique of adding lower power amplifiers could be continued, but this is a diminishing returns situation.

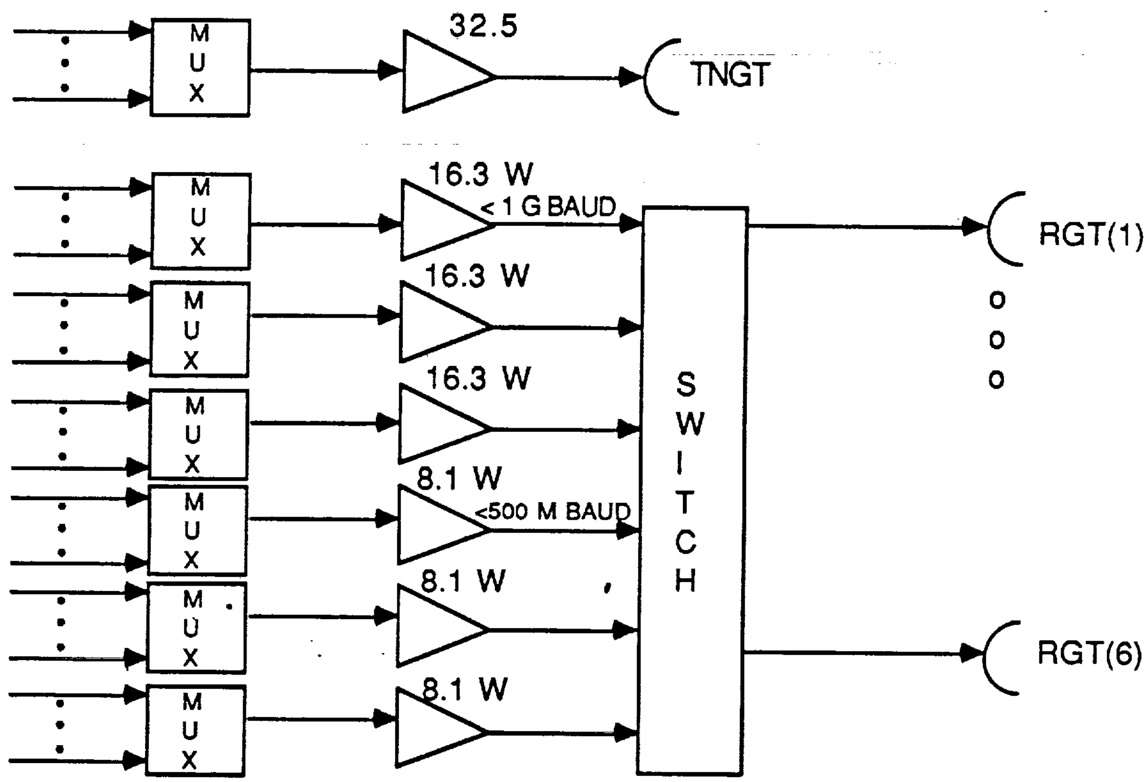

Worst Case Data Distribution

	Data Rate	Power (W)
1 - TNGT	negligible	32.5
3 X RGT	>500 M Baud	48.9
3 X RGT	<500 M Baud	24.3

P_{TOT} = 105.7 watts

P_{prime} = 528.5

transmitters = 7

Figure 4.1-2. Data Transmission Scheme 2, Switched Transmitters

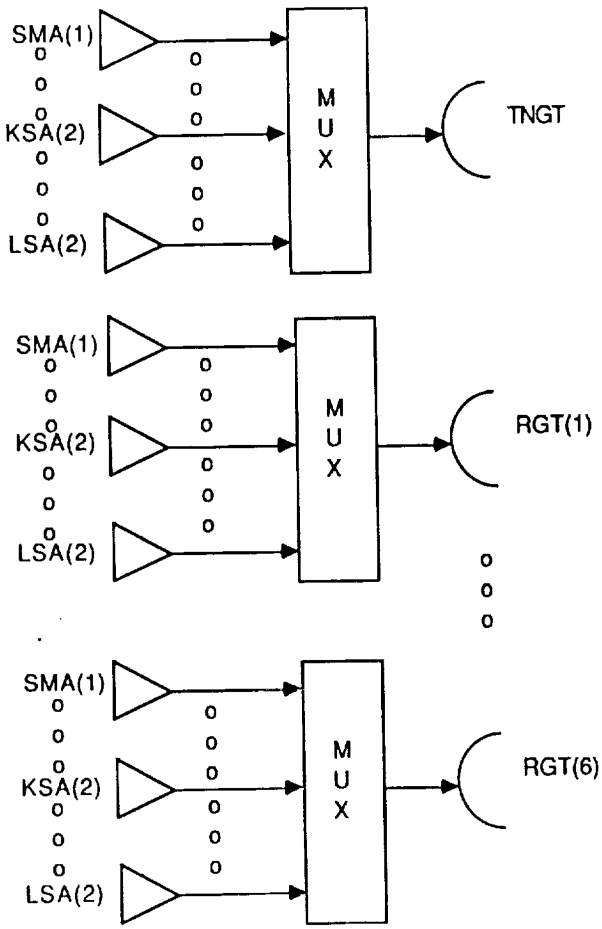

Worst Case Data Distribution

All transmitters operating

#	Signaling Rate	Power (W)	P_{TOT}(W)
2	1 G Baud	3.25	6.5
14	150 M Baud	0.5	7.0
4	6 M Baud	0.02	0.08
2	Telemetry	0.005	0.01
20	100 K Baud	0.0003	0.006
			13.596 Watts/terminal

P_{prime} = 476 W

42 X 7 = 294 Transmitters

Figure 4.1-3. Transmission Scheme 3,
Dedicated Transmitters: Single Transmitter per Service

- Similar to Scheme 3 except
  - Combine 20 MA services into a single signal
  - Combine SSA and TT&C into a single signal

Worst Case Data Distribution

#	Data Rate	Power (W)	P_{TOT}(W)
2	1 G Baud	3.25	6.5
14	150 M Baud	0.5	7.0
1	27 M Baud	0.44	0.44
1	2 M Baud	0.0325	0.0325
			14.0 Watts/terminal

P_{prime} = 490 Watts

18 X 7 = 126 transmitters

Figure 4.1-4. Transmission Scheme 4, Dedicated/Hybrid

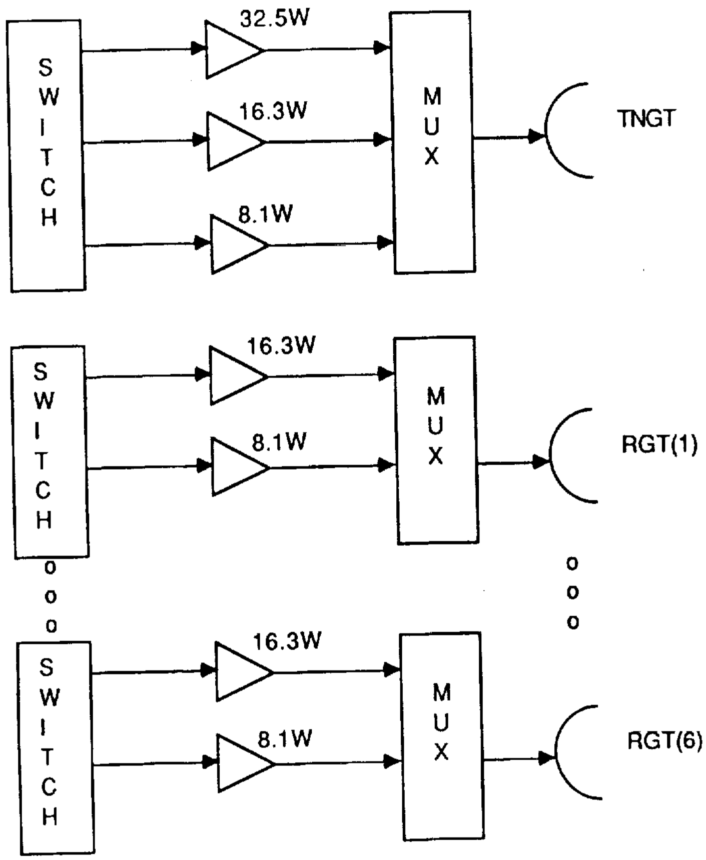

WORST CASE DATA DISTRIBUTION

Station	Data Rate	Power "on"
TNGT	negligible	8.1
3 X RGT	>500 M Baud	48.9
3 X RGT	<500 M Baud	24.3
		P_{TOT} = 81.3W

P_{prime} = 406.5

15 transmitters

Figure 4.1-5. Transmission Scheme 5, Varying Power Transmitters

- Similar to Scheme 5 except add 4.1 and 2.0 watt transmitters for each terminal

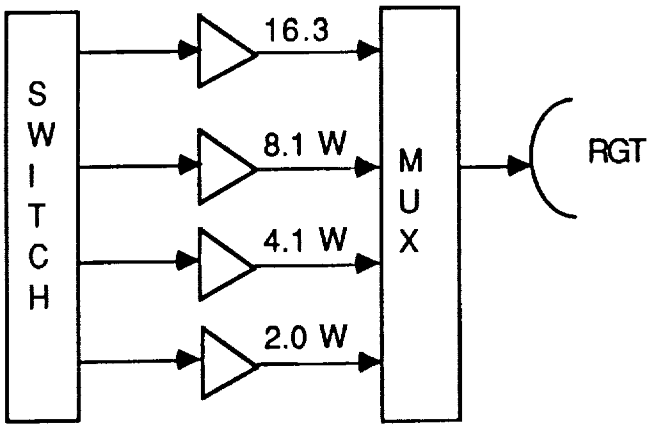

- There are thus 4 X 6 + 5 = 29 transmitters

Worst Case Data Distribution

Station	Data Rate	Power "on"
TNGT	negligible	2.0
3 X RGT	>500 M Baud	48.9
1 X RGT	>250 M Baud	8.1
1 X RGT	>125 M Baud	4.1
1 X RGT	<125 M Baud	2.0
		P_{TOT} = 65.1 Watts

P_{prime} = 325.5 Watts

Figure 4.1-6. Transmission Scheme 6

More power savings could be achieved using the architecture of Figure 4.1-7. This scheme is identical to that of Figure 4.1-6, except the higher power amplifiers, i.e., 32.5 and 16.1 W, could be implemented wth traveling wave tube amplifiers (TWTAs) instead of SSPAs. TWTA efficiency approaches 35%. Assuming 35% efficiency for those 8 units and 20% for the remaining 21 SSPAs, only 221 W of prime power is required.

However, whether or not 35% efficiency at 20 GHz is indeed realizable deserves further study. Reliability and weight are also affected and these topics need to be included in the tradeoff. Switching architectures also need to be analyzed to determine if the remaining allotted 240 W is sufficient for the other components in the MBA and switch subsystems.

Identical to Scheme 6 except

- TWTA for 32.5 W and 16.3 W transmitters
- Efficiency of those units 35%
- $P_{prime} = \frac{48.9}{0.35} + \frac{16.2}{0.2} = 221$ Watts
- Weight and reliability impacts to be studied

Figure 4.1-7. Transmission Scheme 7

4.2 SATELLITE TRANSPONDER HARDWARE

This subsection describes the hardware used for satellite transponders. It also presents typical equipment specifications: typical size, weight, and power required. Possible future solutions are discussed pending the development of new technology.

Figure 4.2-1 shows a simplified block diagram of a transponder - the type of transponder used up to now operating as bent pipe and not used on board processing. The main components of the transponder include a preselector which protects the rest of the equipment from unwanted signals. Sometimes this preselector filter is a diplexer (or multiplexer) with one filter for receiving and one filter for transmitting. Following the preselector is the receiver which will be described in the next paragraph. The input multiplexer is the unit where signals split to different channels to be amplified individually. Usually the channel amplifiers continue to the power amplifiers. At this point, all channels merge to one by the output multiplexer. From here on, the signals are applied to the antenna for transmission.

Preselectors. The discussion of the preselectors is included in subsection 4.3.

Receivers. The receiver is usually a broadband design accommodating all channels. It has to have a low noise front end. Because it carries all channels, it has to be linear so that no intermodulation products will be generated. A typical receiver contains a low noise preamplifier, a downconverter, and an IF amplifier as shown in Figure 4.2-2.

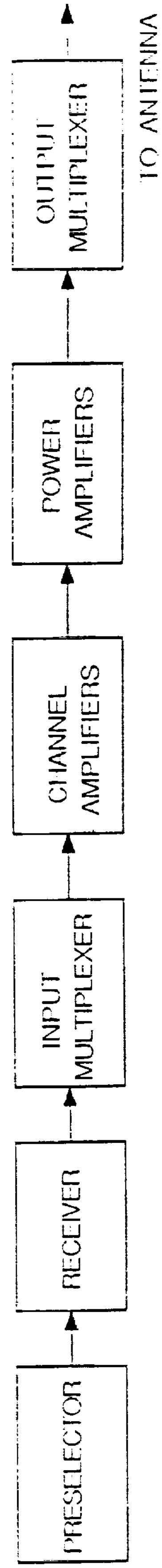

Figure 4.2-1. Simplified Transponder Block Diagram

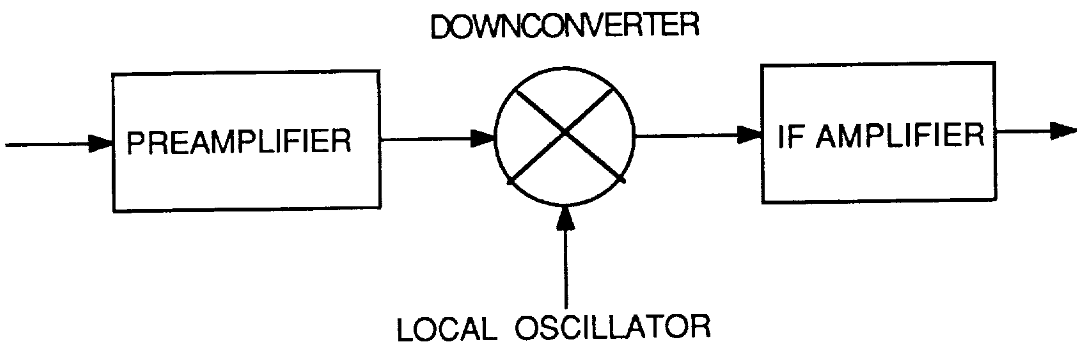

Figure 4.2-2. Typical Receiver Block Diagram

The first stage of the preamplifier is designed to obtain the lowest possible noise figure at the expense of the gain. To accomplish this, the transistor must be of discrete character. Monolithic integrated circuits are inferior to discrete designs if extremely low noise is required. Moreover, even discrete components with excellent capabilities are not permitted if not space qualified. Thus the designer must try to achieve excellent results with relatively old components. We selected four examples of components that in our opinion are presently the best in the industry. The noise figure with these components is shown in Figure 4.2-3.

While the gain of the first stage may be sacrificed in favor of the noise figure, the gain of the preamplifier must be very carefully considered. It has to be as high as possible to minimize the noise contribution of the following stages but should not be too high to avoid nonlinear distortion. Ford Aerospace has designed and built low noise amplifiers for all its satellites, including practically all bands used for satellites.

Further information about the four transistors follows:

Transistor NE20200 - Product of Nippon Electric Company (NEC). This is a high electron mobility transistor (HEMT). The device has been marketed for 2 years and can be purchased as an off-the-shelf item for commercial quality. To our knowledge the device has not been flown, nor is data for its qualification available. Traditionally, however, NEC does the qualification at

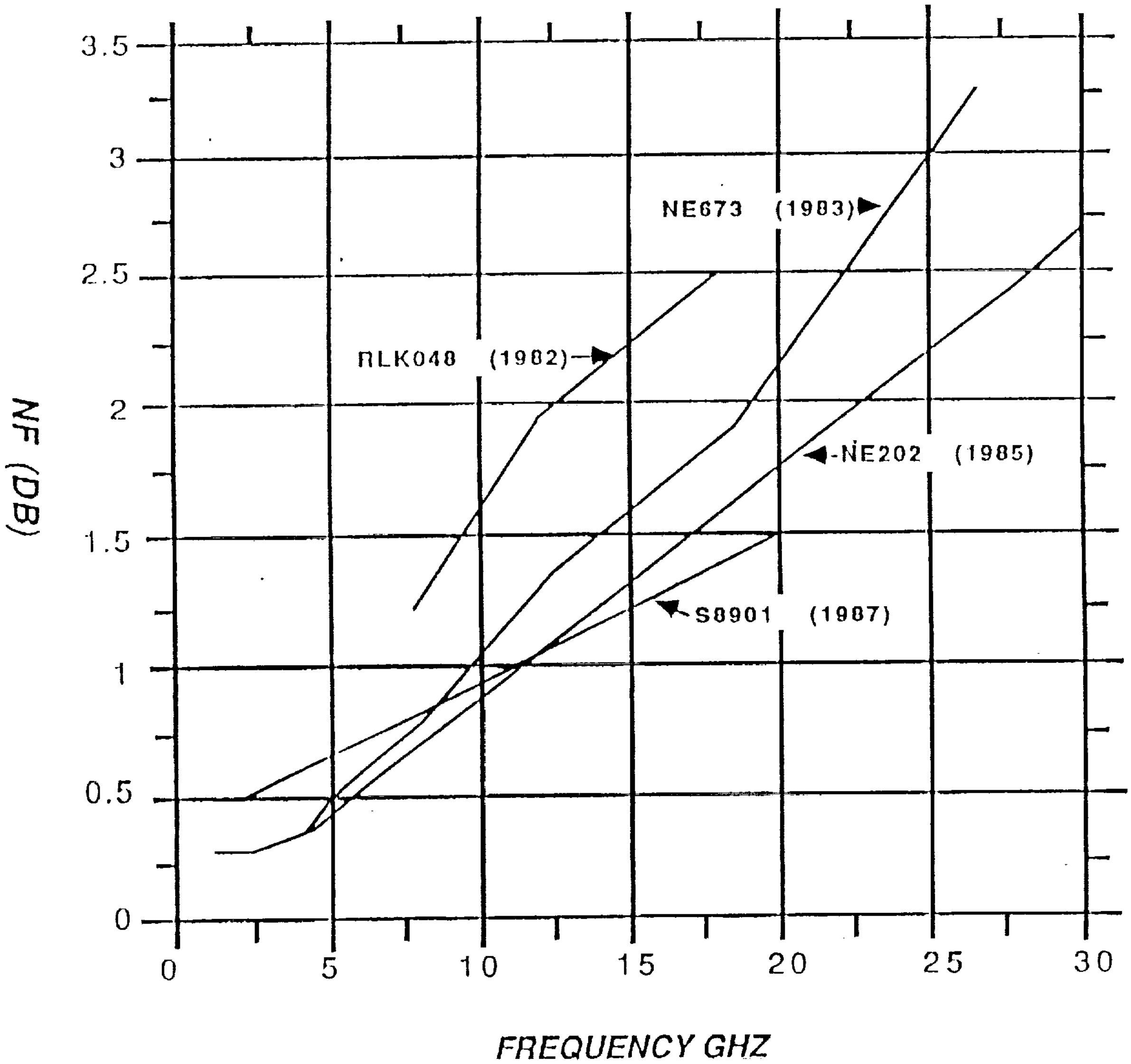

Figure 4.2-3. NF versus Frequencies for NE673, RLK048, NE202, and S8901

the manufacturing plant, and only when they are completely satisfied do they start selling flight quality devices. We have no doubt that the device will be available in 1993 and we predict it will become the standard of this industry. NEC is a reliable and worldwide supplier of flight transistors.

Transistor S8901 - Product of Toshiba. This is also a HEMT device and at high frequencies the electrical characteristics are even better than those for the NE20200. This is very encouraging, since there are at least two devices that can be used. The device is available as an off the shelf item. Ford Aerospace is now experimenting with this device. While the device is excellent and the Toshiba Company has been growing in importance as a reliable supplier, the company has not been in the business of flight transistors. Thus the process of qualification may be a little time consuming.

Transistor RLK048 - Product of Raytheon. This device from 1982 is still a good device but certainly not the best. It is presented here to help show the progress in low noise devices.

Transistor NE673 - Product of NEC. This is a product dating from 1983. The device has been widely used for space application and is a very good gallium arsenide field effect transistor. It is included not only to show the progress in this industry but to show progress within the same company.

Observing the four devices and their performance, one can conclude that the capability has gone toward higher frequencies and lower noise. This trend is expected to continue.

Noise Figures Achievable. The above devices are presently available and they reflect the present status, but they are only an introduction to future projections. In projecting future products, we have surveyed available literature, and here are the findings:

- In a paper by Cappy [4-1] we have found that at 30 GHz General Electric (GE) and Thompson, Ramo Woolridge, Inc. (TRW) are working on devices of noise figure (NF) below 1.8 dB. This is 0.9 dB better than device NE20200 has been showing.
- Interestingly, the same reference indicates that GE has achieved NF of approximately 2.8 dB at 62 GHz.
- In another paper Kawasaki [4-2] has reported NF of 0.75 dB at 12 GHz and 1.2 dB at 18 GHz.

- Schellenberg [4-3] has reported an amplifier with NF of 3.1 dB and 17 dB gain. This is not a device NF but an amplifier characteristic. This is an update of a previous paper by Watkins [4-4] 1 year earlier, where a three stage 30 GHz amplifier had been described with a NF of 3.2 dB and a 23 dB gain.
- Sholley [4-5] describes two amplifiers, one at 60 GHz with 6 dB NF and a 6 dB gain. The second operating at 71 GHz with NF of 7.8 dB and 5 dB gain.

These papers have extensive references and indicate what has been accomplished in the research laboratories.

Low Noise Predictions Summary. We have attempted to summarize the results reported in the literature in order to make consistent assumptions. Table 4.2-1 presents the present status and future projections for 1993:

Table 4.2-1. Noise Figure and Gain Predictions for 1993

	15 GHz	30 GHz	60 GHz
Device NF at present	1.3	2.7	----
Device NF projected	1.2	1.9	3.0
Gain per stage	9	7.0	4.0
NF of two-stage amplifier	1.3	2.2	3.8
Total gain for two stages	18.0	14.0	8.0

In a subsequent effort we attempted to explore the status of the semiconductor industry at 30 to 60 GHz. These results are summarized in Table 4.2-2.

Table 4.2-2. Typical Ku-Band Receiver Specifications

Parameter	Specification
Input frequency (GHz)	14.00-14.40
Output frequency (GHz)	12.35-12.75
LO frequency (GHz)	1.65
RF input power (for 10 channels) (dBm)	-78 to -48
Overdrive (no damage) (dBm)	-28
Gain (dB)	45
Gain slope (dB/MHz)	0.006
Noise figure (dB max)	3.5
Carrier/3IM at P_{out} +2dBm/carrier (dBc max)	-26
RF spurious - in band (dBc max)	-70
Input/output return loss (dB min)	19
Operating temperature (°C)	-10 to +55
Dc power (including dc/dc converter) (W)	8.3

We include some comments for each of the devices in this table

Device 1. Reference [4-6]. A single stage amplifier is described in broadband operation. The lower bandwidth covers 20 to 38 GHz and the higher band covers 26.5 to 38 GHz - the second having a gain of 6 dB and NF of 5 dB. The circuit is implemented in a monolithic design and is contained in a chip, 2 by 1.1 mm. It is expected that by using a narrowband design, a significant improvement in the NF can be achieved.

Device 2. Reference [4-7]. The paper describes a single stage and a dual-stage monolithic amplifier operating from 30 to 40 GHz. The single stage exhibits a gain of 6.5 dB with NF of 4 dB, the dual-stage accomplishes a gain of 10.5 dB and NF of 6 dB. At narrower bandwidths better NF is expected.

Device 3. Reference [4-8]. Eight products are described operating from 1.3 to 43.5 GHz. All of them are for the needs of the National Radio Astronomy Observatory and include ground equipment for low noise amplifiers, cooled by special refrigerators to 13 K. The authors claim that compared at ambient temperature with other products, these products have the lowest noise figures reported. At 13 K and frequency of operation from 42.3 to 43.5 GHz, the amplifier noise temperature is 70 K, corresponding to a NF of 0.95 dB.

Devices 4 and 5. Reference [4-1]. This is an invited paper dealing with noise modeling and measurement including comparisons between the noise performance of MESFETS and HEMT devices. In addition, this paper is probably the best source for finding the state of the art of low noise transistors. The author includes almost every manufacturer, the frequency covered, and the NF achievable. In Table 1 of this source we found that at 30 GHz there is one device by GE, one by TRW with NF of 1.8 dB, and a third device by GE with 1.4 dB. We found that at 60 GHz there is one device by GE with 2.8 dB of NF. It may be worth mentioning that the devices have not been identified.

Device 6. Reference [4-3]. The paper describes a three-stage amplifier operating from 34.25 to 35.75 GHz with a 3.1 dB of NF and 17.4 dB gain. The amplifier is built with HEMT devices (not explicitly identified). The paper claims that device capabilities have been described in previous literature, but this is the first time implementation in an amplifier is reported. For reference they claim that the device measures 1.8 dB NF with 7.2 dB associated gain. When implemented as a three-stage amplifier, the numbers change to 3.1 dB NF and 17.4 dB gain.

Device 7. Reference [4-9]. This is a new source that deals with the most recent advancements by GE which seems to be leading the low noise device technology. This source reports devices that can have NF of 1.2 dB at 32 GHz with 10 dB gain, and NF of 1.8 dB at 60 GHz and associated gain of 6.4 dB. We find these are the best predictions at 30 and 60 GHz. Here, too, the names of the devices have not been disclosed.

We have selected a typical preamplifier and a photograph is shown in Figure 4.2-4. This is a 14 to 14.5 GHz preamplifier with waveguide input and isolator in front of it. It uses Avantek transistors and its NF is 3.5 dB maximum for worst conditions of high temperature. The gain of this preamplifier is nominal 20 dB. These characteristics satisfy the needs of the SUPERBIRD project, thus there are no compelling reasons to use new transistors. With modern devices the noise figure can easily be improved.

Downconverter. The symbol we used for the downconverter is the symbol of a mixer. This is the main component of the downconverter, but usually there are matching isolators and filters to control spurious to propagate down the receiver chain. The mixer is one of the most delicate components of the receiver. Its dynamic capability is lower than that of the transistors if implemented with diode signals. Double balanced mixers are preferred because they have lower spurious. Ford Aerospace has built most of its mixers especially those in the signal path, but a variety of commercially available units are good candidates for use. Diode mixers have proven to be completely satisfactory for space application. Various manufacturers have shown schemes of multidiodes for medium or high levels of operation. Probably the biggest disadvantage of the diode mixers is the need for a high level of local oscillator injection - typically 10 mW for the low level mixers (and 100 mW for the high level units). In this respect the FET mixer offers considerable advantages with much lower low level injection, providing gain rather than loss. The FET mixers are justified for systems that require hundreds of mixers reducing the low power and general power requirements.

We have selected a typical MIC coupled lines type of filter to follow the mixer (see Figure 4.2-5). This and similar MIC-type postmixer filters are presented in the filter section. As stated, the filter is intended to reject the out-of-band spurious signals, but more importantly the filter provides known reflection for these spurious products. The usual termination that an isolator provides is variable with the electrical temperature path. A mixer tuned properly at room temperature exhibits ripples in the passband at different temperatures.

ORIGINAL PAGE
BLACK AND WHITE PHOTOGRAPH

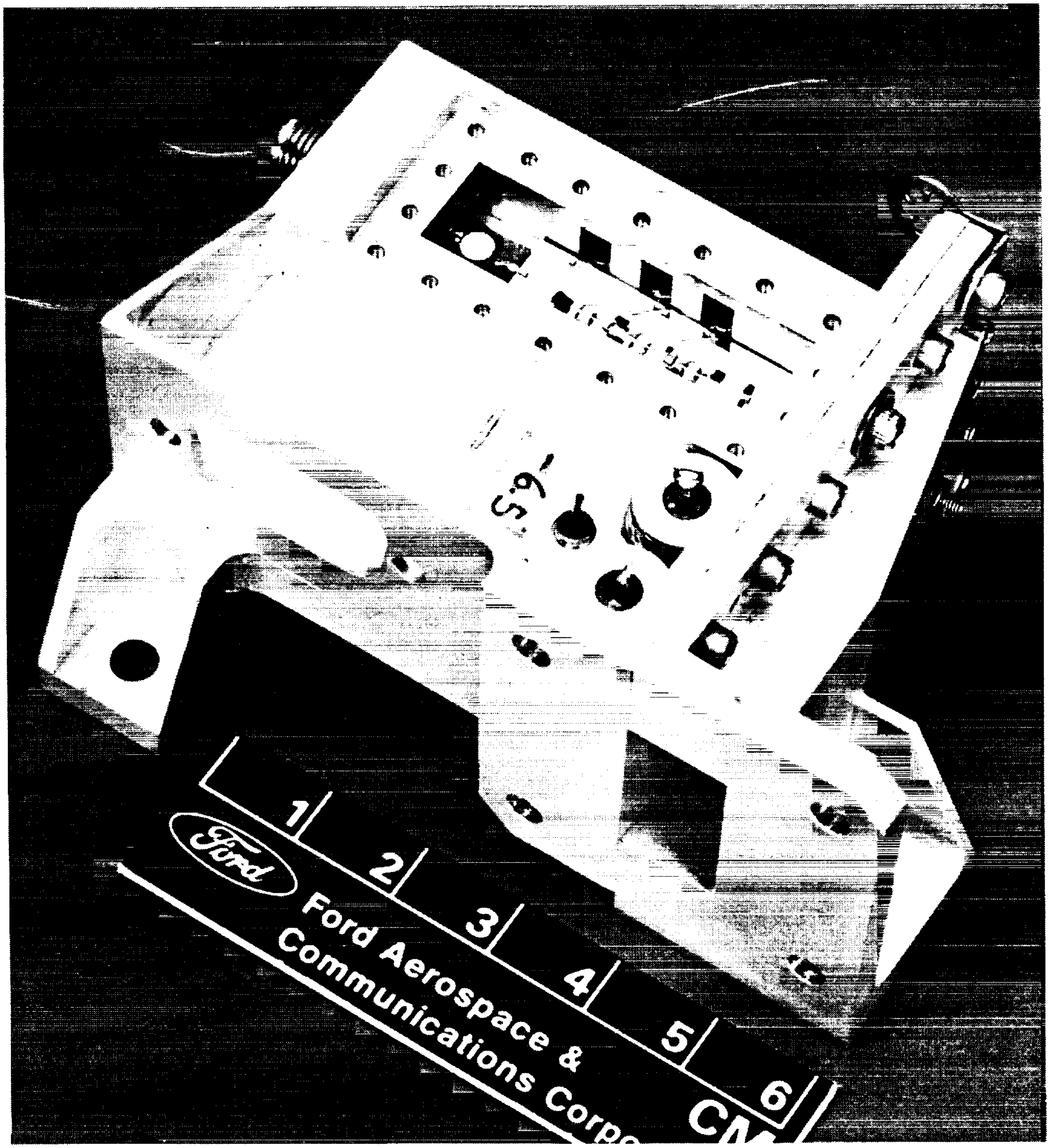

Figure 4.2-4. Ku-Band LNA

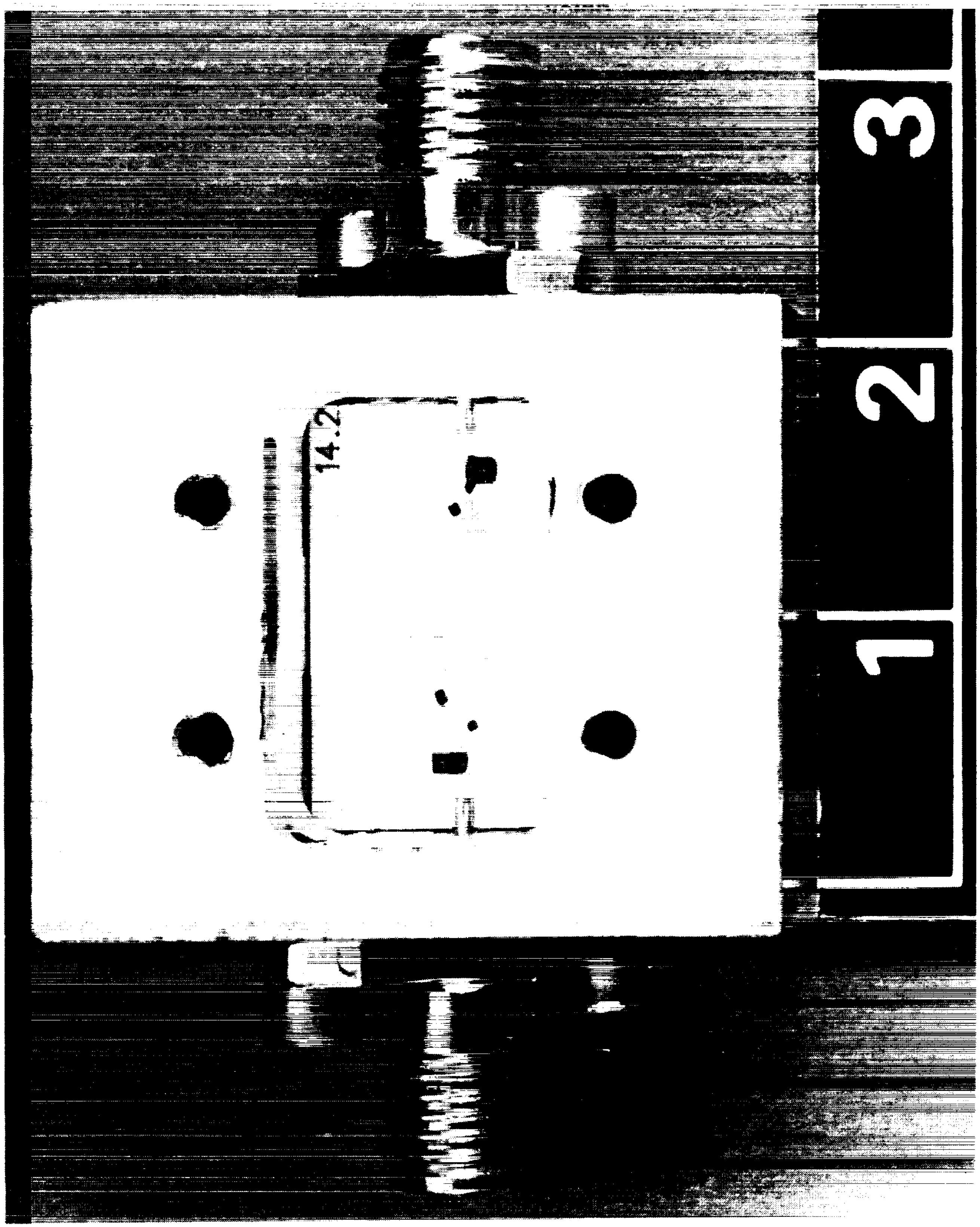

Figure 4.2-5. MIC Type Postmixer Filter

IF Amplifier. The IF amplifier following the downconverter is still broadband passing all the channels without causing IM problems. Its noise figure is of very little importance, since its gain should be sufficient to overcome the losses in the input multiplexer, but not high enough to avoid nonlinear operation.

These receiver components describe present and past technology. New components are already in the market. One component, the monolithic microwave integrated circuit (MMIC) implementation, has three stages of radio frequency (RF) amplification at 6 GHz, a mixer with its low driver stage, and a three-stage IF amplifier - all this in one single chip, 1 mm^2. No such part has been space qualified and will not be flown until some organization will take the initiative to space qualify this or similar parts. But it is very clear that the future satellite receiver will use MMIC technology. Not only size and weight will be reduced but reliability will be much improved. The present technique relies on manual labor, which in most cases is excellent, but can be different and not exactly repeatable. The MMIC technique may have to have more iterations until a component is successful, but then the components will be identical, no soldering joints should be different.

The Dec 1988 issue of the IEEE Transactions of Microwave Theory and Techniques reports progress with MMIC components, including participation of companies like General Electric, Raytheon, COMSAT, Ma/Com, and others. We are convinced some of these components will find their way to future satellites.

Some of the most important specifications of this receiver are presented in Tables 4.2-2 through 4.2-4.

Figures 4.2-6 through 4.2-10 are photographs of existing flight hardware. Equipment names are marked on the photographs. These pictures demonstrate how the hardware is integrated from an individual module to the tray and then to the receiver.

Input Multiplexer. The discussion on the input multiplexer is provided in subsection, 4.3.

Table 4.2-3. Typical Ka-Band Preamplifier Specifications

Quantity	Specification
Frequency (GHz)	27.5 to 28.7
Noise figure (dB at -5 °C)	4.9
Gain (dB min)	26
Gain flatness	0.2 dB/100 MHz 0.7 dB/1200 MHz
Dc power	+5 V/130 mA -5 V/10 mA

Table 4.2-4. Typical Ka-Band Receiver Specifications

Quantity	Specification
Input frequency (GHz)	27.5 to 28.7
Useful bandwidth (GHz)	1200
LO frequency (GHz)	15.1
LO stability	
Short term	78 Hz RMS max 100 Hz to 12 kHz
Long term	$+0.9/-1.3 \times 10^{-6}$
Phase noise (dBC/Hz 1 kHz offset)	-85
(dBC/Hz 10 kHz offset)	-91
(dBC/Hz 100 kHz offset)	-98
Input level (dBm/channel)	-85 to -65
Gain (dB)	55
Gain flatness (dB over any 100 MHz)	0.2
Gain slope (dB/MHz)	0.006
Noise figure (dB at ambient)	5.5
(dB at -10 °C)	4.7
Group delay variation (ns max)	0.45
C/3IM	
At Po=+5dBm (dB min)	26
At Po=+0dBm (dB min)	36
At Po=-5dBm (dB min)	46
Separation (kHz)	1.3
Spurious	
In band (dBC min)	-70
Out of band (dBC min)	-40
VSWR (1.25:1)	
Dc power (W)	6.5
Weight (kg)	1.5

ORIGINAL PAGE
BLACK AND WHITE PHOTOGRAPH

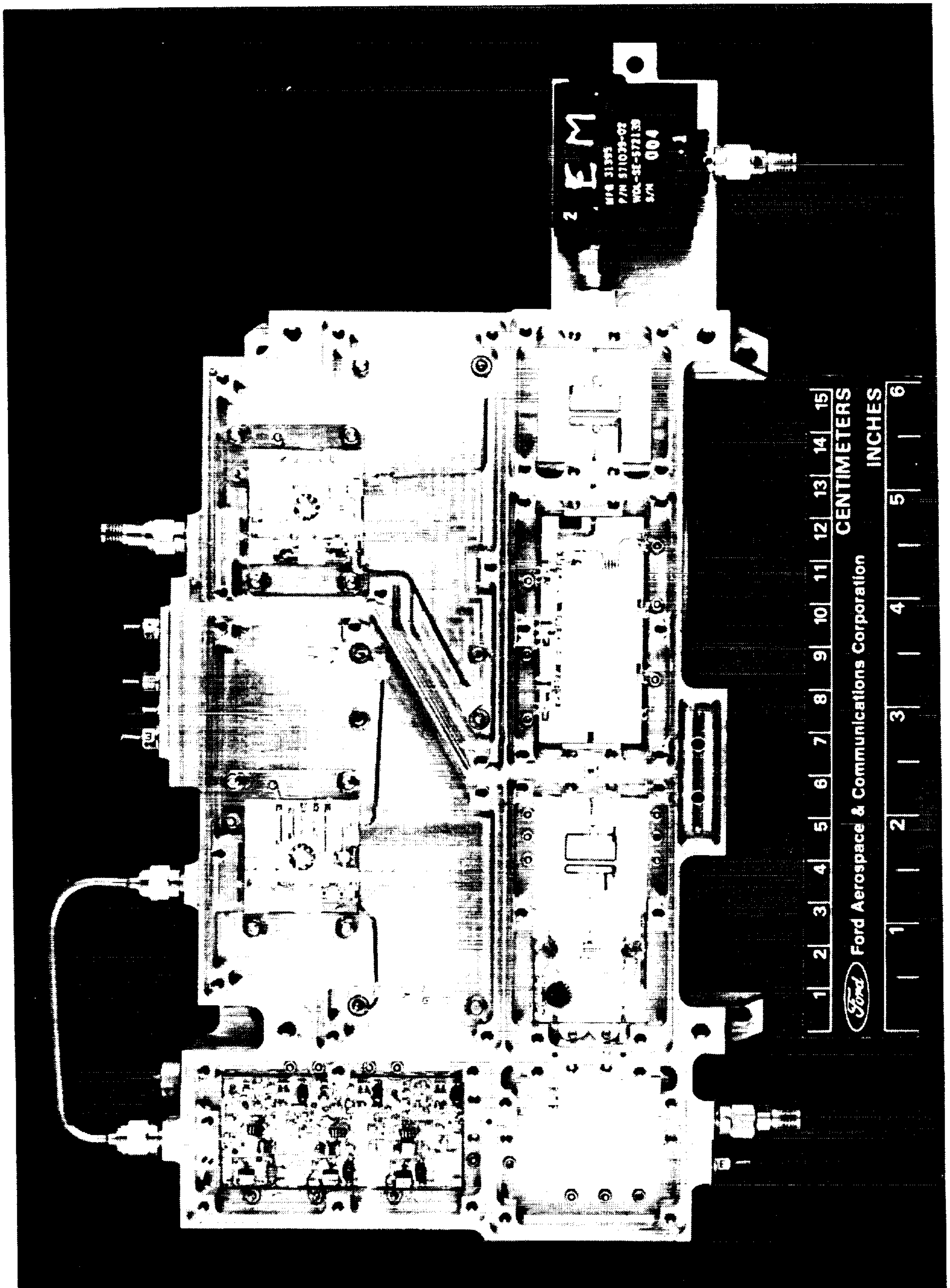

Figure 4.2-6. SAR Receiver Preamplifier

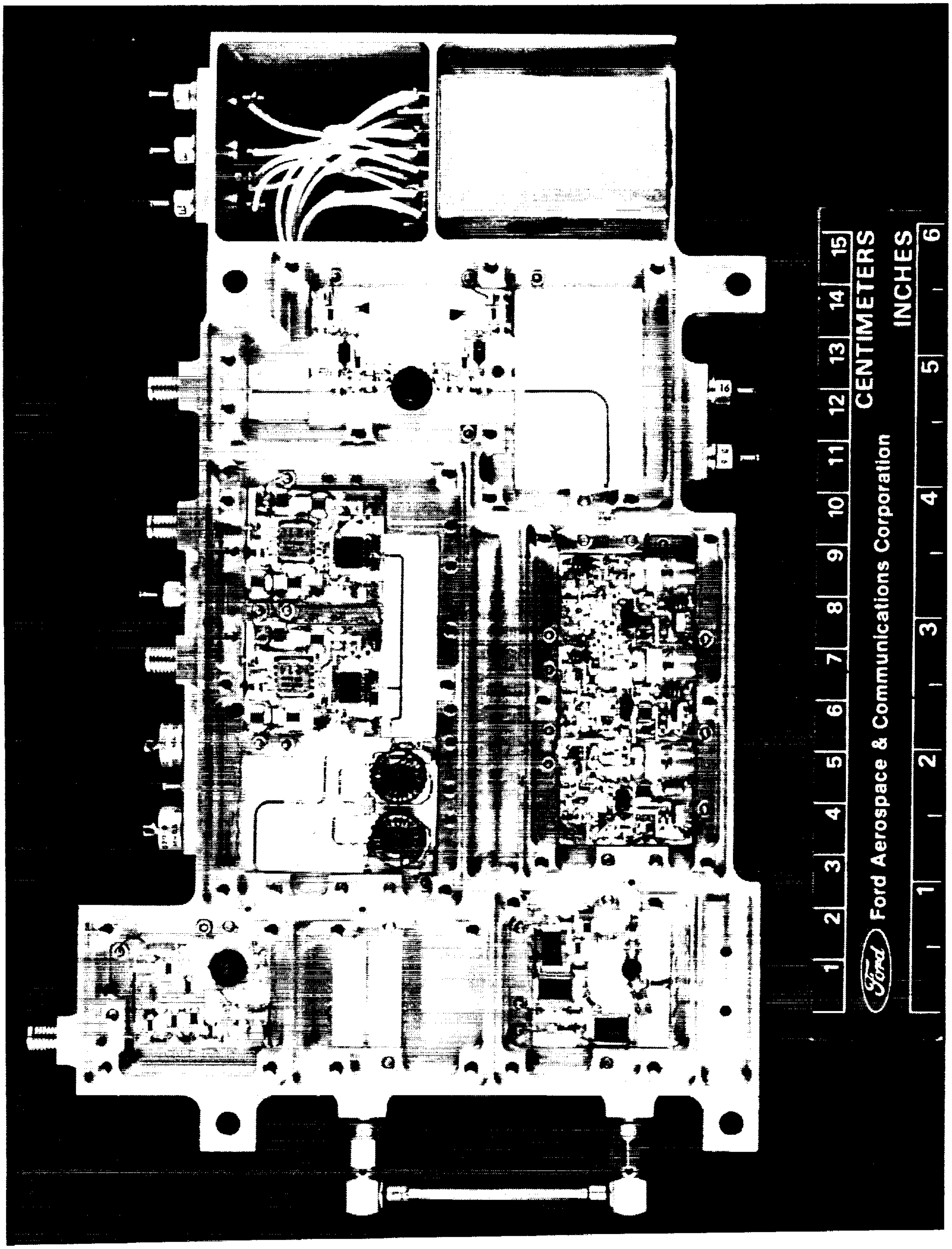

Figure 4.2-7. SAR Receiver IF

ORIGINAL PAGE
BLACK AND WHITE PHOTOGRAPH

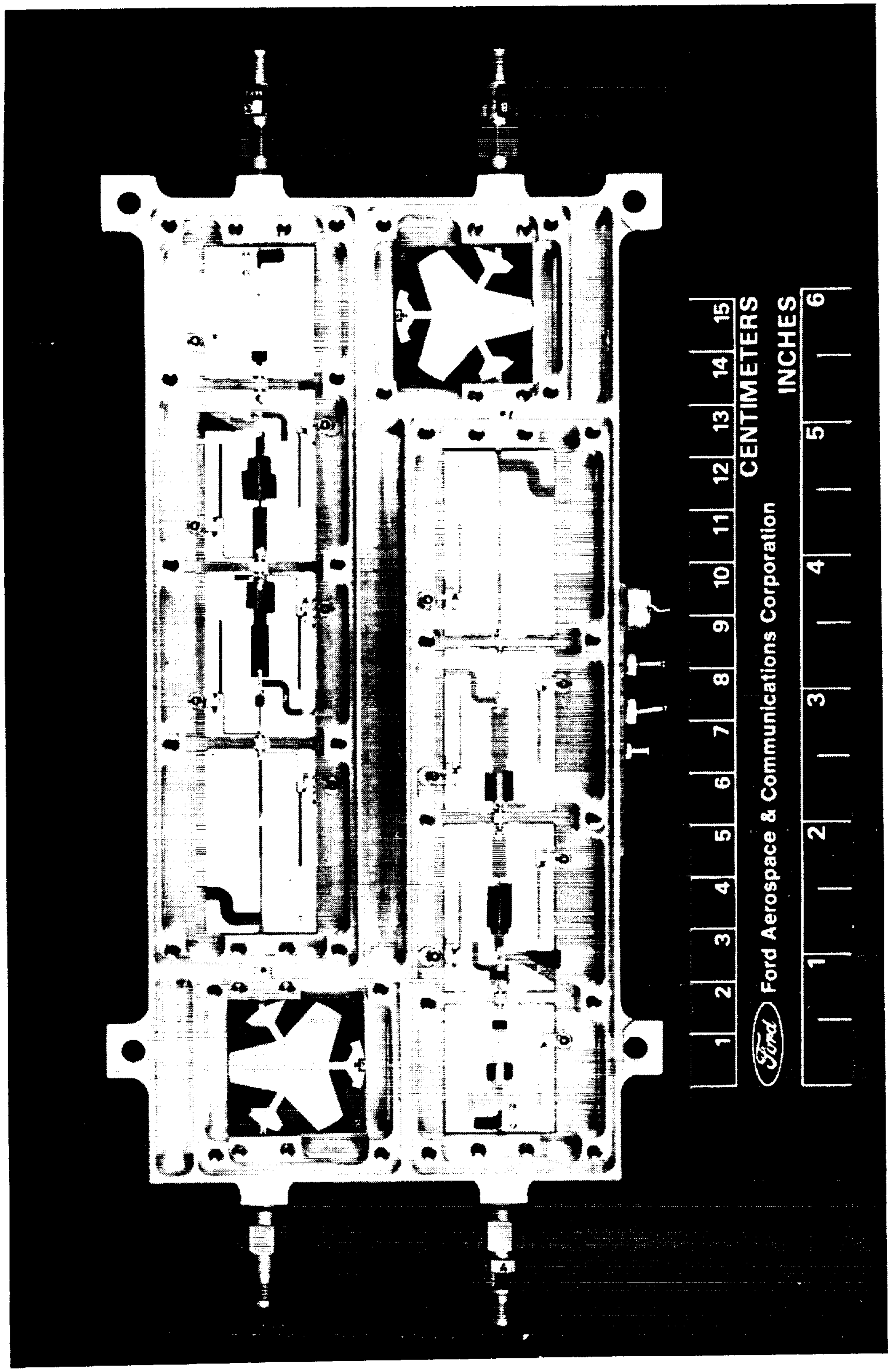

Figure 4.2-8. S-Band Receiver LNA

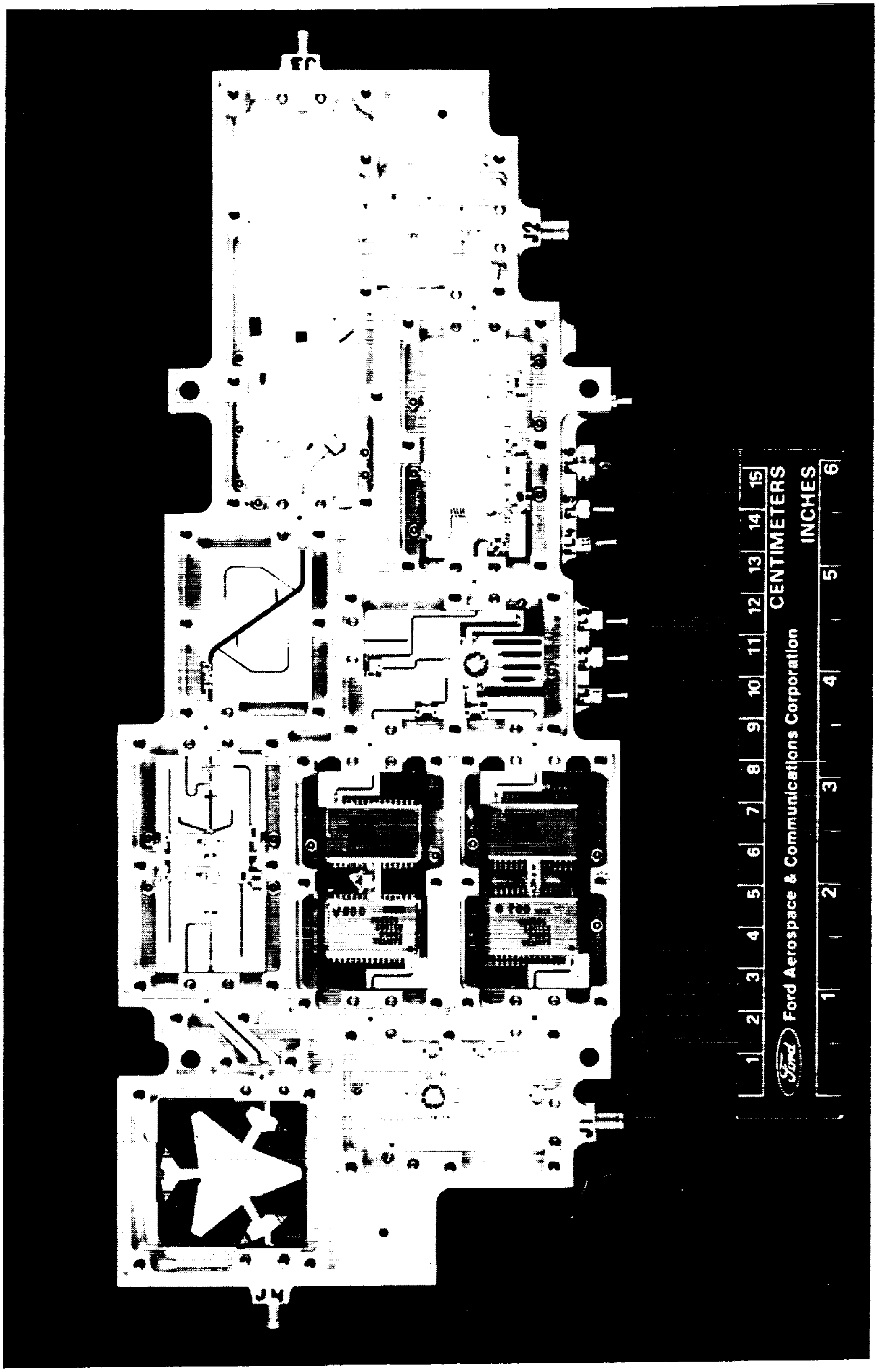

Figure 4.2-9. 400 MHz-1.7 GHz Upconverter

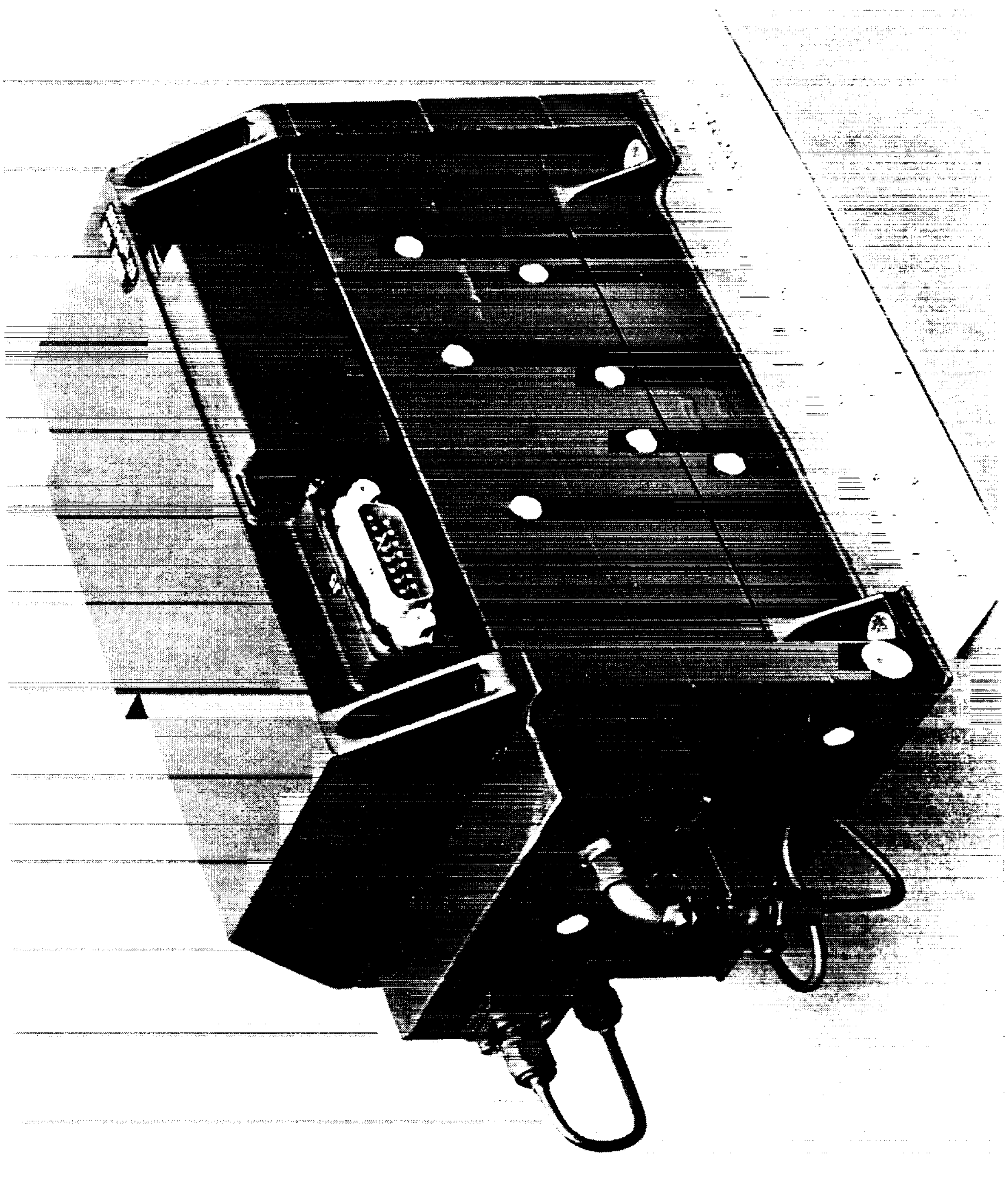

Figure 4.2-10. INTELSAT V Assembled Receiver

Channel Amplifiers. Channel amplifiers are units operating for each individual channel created by the input multiplexer. One receiver may have 10 or more channels and each channel gets its own amplifier. These units are usually considerably narrower in bandwidth, with large gain and very often with some extra requirements as automatic gain control (AGC), limiting, or variable gain control. Noise figures are usually not important, unless the input multiplexer is particularly lossy or the gain in front of the multiplexer is too low. Third order intermodulation products are also not a problem, since there is only one carrier in the band. The last stages have to be able to produce relatively large levels from 5 to 10 dBm to be able to drive the power amplifier that follows. Because of the large gain it is good practice to use bandpass filters implemented as MIC coupled lines. This keeps the noise propagation out of the band. Ford Aerospace uses variable gain amplifiers (VGAs) for this purpose. One VGA has two or three stages - one channel amplifier may have five to six stages. The VGA is implemented with a dual-gate transistor, one gate is used as the single gate FET, the other is used for gain control.

Important features of the channel amplifier are presented in the Table 4.2-5.

Table 4.2-5. Channel Amplifier Specifications

Parameter	Specification
Frequency (GHz)	12.395 - 13.215
Channel BW (MHz)	100
RF input power (dBm)	-45 to -27
Noise figure (dB)	6
Gain commandable (dB)	22 to 40
DC power (W)	3.8

Figure 4.2-11 is a photograph of the VGA - the basic unit for the channel amplifier. The channel amplifier is shown in Figure 4.2-12.

Power Amplifiers. In the past, the satellite power amplifiers were implemented with TWTAs. With progress in semiconductor components, there is gradual conversion to SSPAs first implemented with bipolar transistors and more recently with FETs. At the time of this writeup, FET power amplifiers can be realized up to 15 GHz. This statement is supported by a study of the available transistors for power amplifiers. The results of this study are shown in Table 4.2-6.

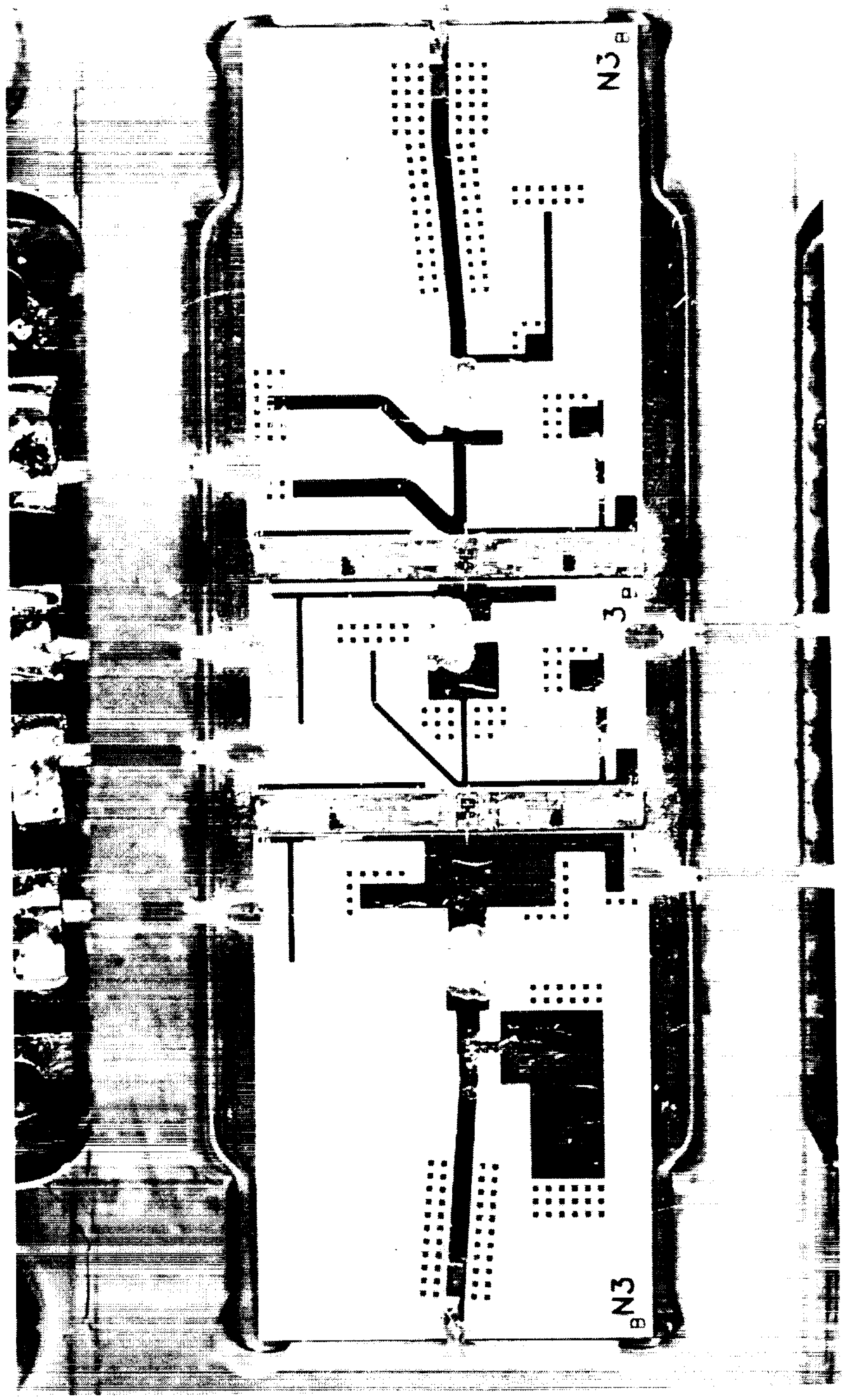

Figure 4.2-11. Channel Amplifier - VGA

ORIGINAL PAGE
BLACK AND WHITE PHOTOGRAPH

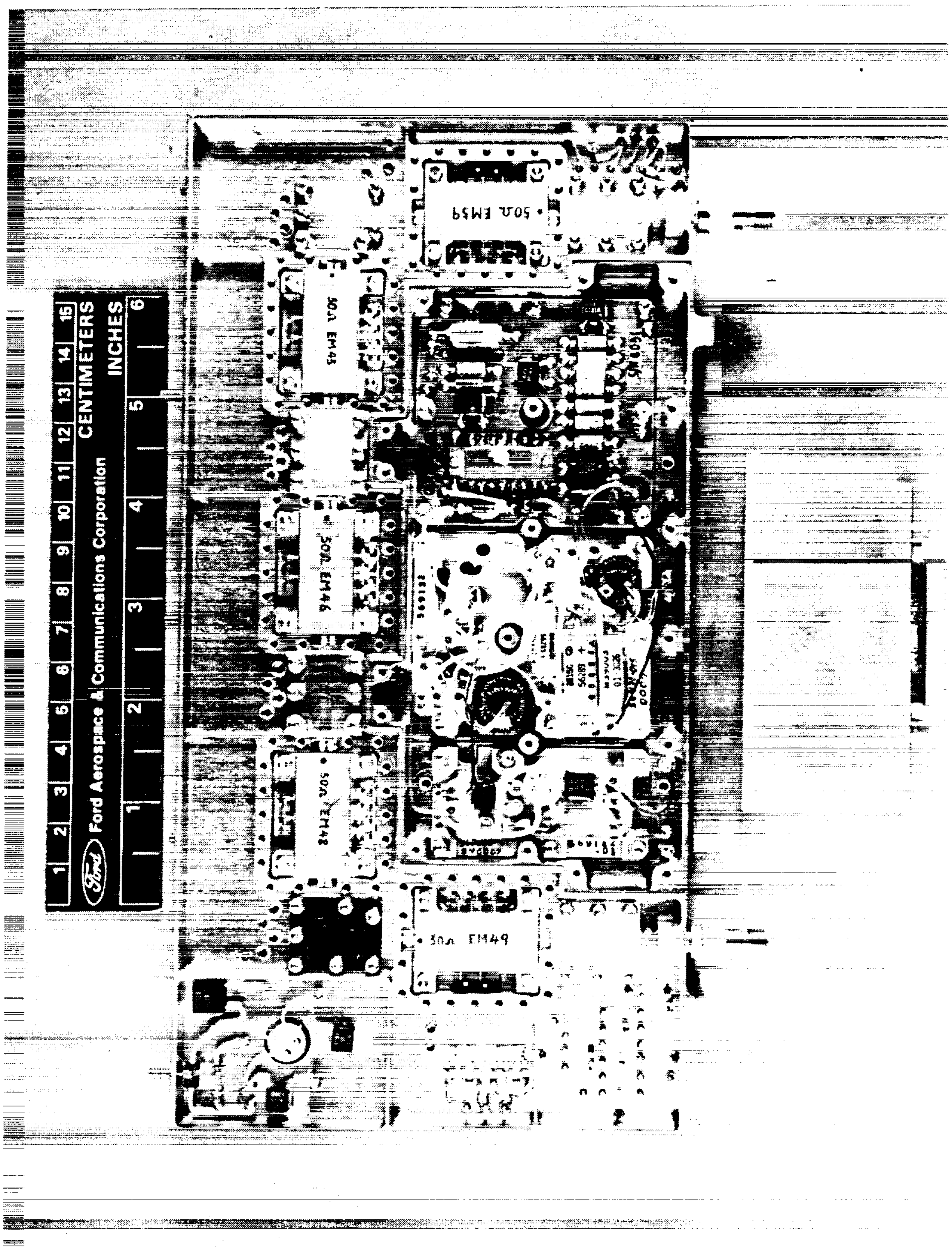

Figure 4.2-12. Ku-Band Channel Amplifier

Table 4.2-6. Commercially Available Transistors for Power Amplifiers

Manufacturer	Part Number	Power
Devices for 15 GHz		
NEC	NEZ1414-6A	6 W
Toshiba	S8861	10 W
Devices for 20 GHz		
Toshiba	JS8894	0.5 W
Toshiba	TIM2121-1	1.0 W in development
NEC	NE985400	0.4 W
NEC	NE357	2.0 W in development
Raytheon	RPK2000	1.0 W space qualified
Raytheon	----	2.0 W in development
Harris SEM	HMF0610	0.25 W
Avantek	----	1.0 W in development
Avantek	----	2.0 W in development
MSC	MSC2031/00	1.12 W (update 22 Apr 88)
Devices for 30 GHz		
Toshiba	JS8864-AS	0.178 W
Toshiba	MMIC	1 W (1988 IEEE MTT-S P413)
Texas Instruments	MMIC	1 W (1988 IEEE MTT-S P179)

As the table indicates, there are now transistors capable of delivering 10 W at 15 GHz, thus making power amplifiers feasible at this frequency. At 20 GHz, there is a transistor delivering only 1 W and there are 2 W units under development. This indicates that the devices for SSPAs are becoming more available.

As part of the ATS-6 program, Ford Aerospace has produced and flown 100 W UHF, 40 W L-band and 20 W S-band transmitters as far back as 1974. Later, as part of INTELSAT V, Ford Aerospace had designed and flown 50 W L-band transmitters. At the present time, there is a new generation of transmitters, the most significant of which is a 12 W S-band transmitter for the NASA GOES program. We selected this last unit for typical specifications and photographs. Table 4.2-7 summarizes typical specifications for this 12 W transmitter.

Table 4.2-7. Typical S-Band Transmitter Specifications

Parameter	Specification
Frequency (MHz)	1683 to 1691.5
Input power (dBm)	-23 to -6
Input/output return loss (dB)	20
Gain flatness/channel (dB max)	0.2
AM/PM (dB)	0.2
Output power (dBm)	40.7
Dc power (W)	51.4
Weight (lb)	4.97

Figures 4.2-13 and 4.2-14 are photographs of the transmitter tray, including the drivers and the power amplifier stage at the output, where a single transistor is delivering the full power.

For higher frequencies the tubes are still the best choice. We have surveyed the industry and the findings are presented in Tables 4.2-8 and 4.2-9.

This table indicates a lot of effort is going on to satisfy demands for high frequencies. It also shows that to operate a tube at these high frequencies, one has to use very high voltages, which presents a problem to the power supply designers i.e., a problem of insulation failure not satisfactorily resolved at this time.

Reliability Information. When reliability is discussed, one has to be reminded that every program has its own specifications. Thus the reliability numbers we are mentioning are not a reflection of what can be accomplished, instead they reflect what was required. Another way of approaching these numbers is to remember that every customer wants excellent reliability, but any improvement adds prohibitive amounts of redundant equipment and this makes the satellite heavy and expensive. Thus these numbers reflect what customers have considered as "good enough." Table 4.2-10 presents typical reliability figures.

ORIGINAL PAGE
BLACK AND WHITE PHOTOGRAPH

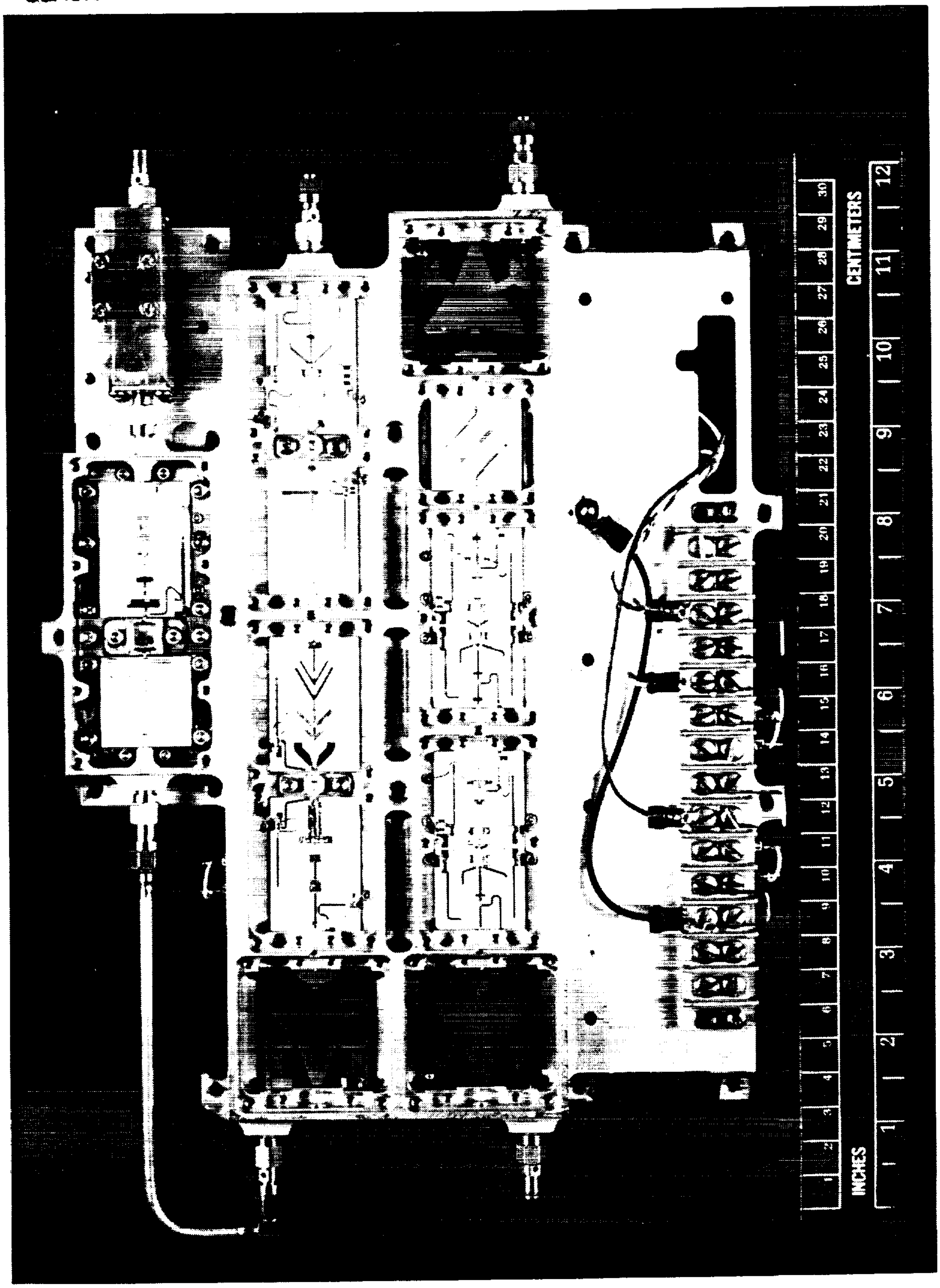

Figure 4.2-13. S-Band Transmitter

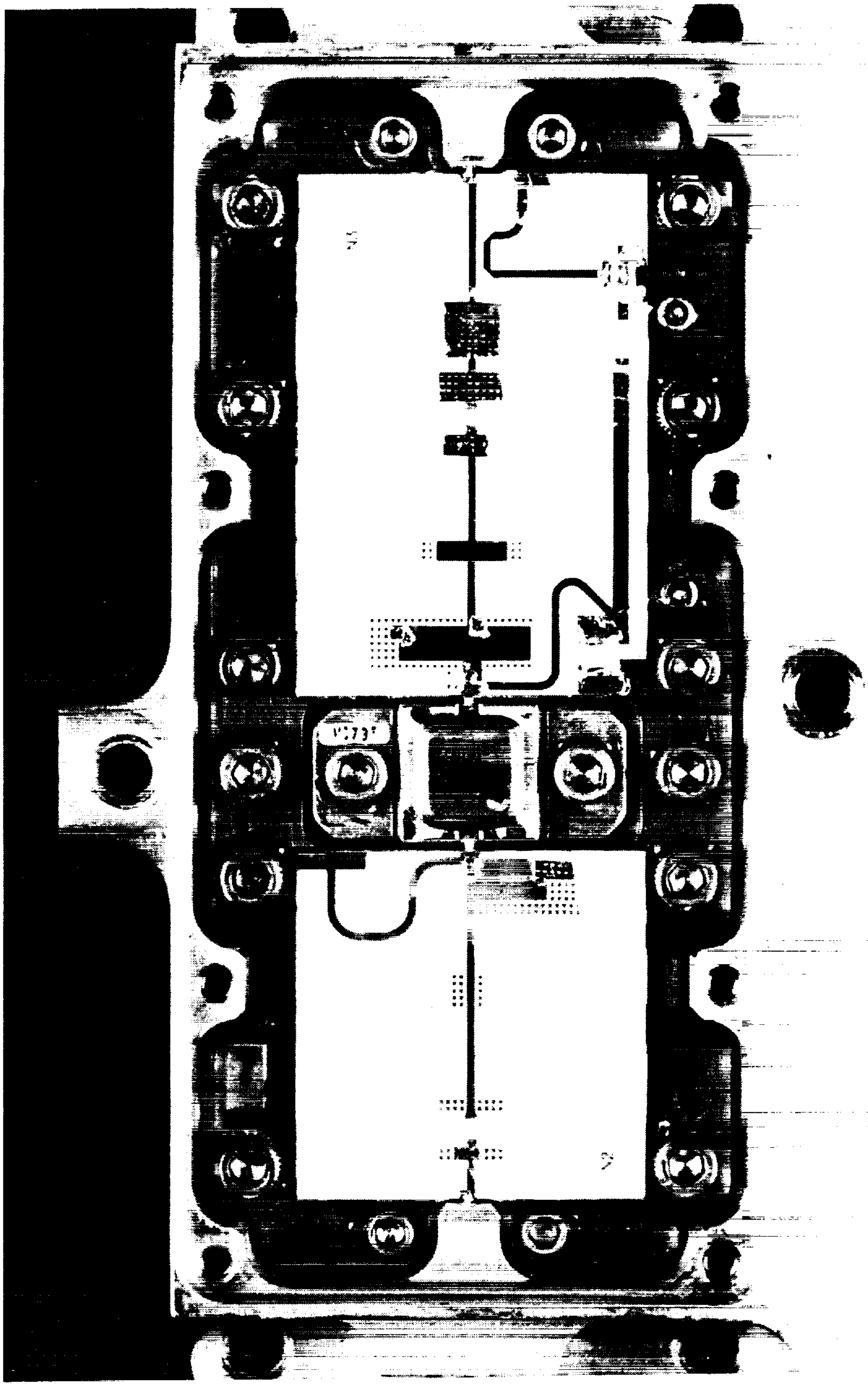

Figure 4.2-14. S-Band SSPA

Table 4.2-8. Traveling Wave Tube Amplifiers for 20 GHz Application

Manufacturer	Tube Name	Frequency (GHz)	Power (W)	Efficiency (%)
AEG	TL20031	17.7-18.8	30	--
AEG	TL20032	18.0-21.5	34	34
AEG	TL20060	18.0-21.5	60	35.5
WJ	WJ3712-4	19.2-20.2	43	40
WJ	WJ3712-5	19.2-20.2	65	--
Hughes	"Hot bottle"	Classified	25-40	--
Hughes	---	---	75	--

Note: The efficiency of the TWTA is a product of the efficiency of the tube and the EPC (usually 85%).

Table 4.2-9. Power Tubes at 60 GHz

Power Output(3)	10W	20W	30W	40W	60W	
Bandwidth(2)	3%	3%	3%	3%	3%	
Saturated gain	50	50	40	50	50	
AM/PM (degrees/dB)	4	4	4	4	4	
Cathode voltage	15	16.5	18.5	18.5	19	kV
Cathode current	10	30	32	44	54	mA
Anode voltage	15.5	17.0	14	19	20	kV
Collector #1 voltage	2300	2700	--	3300	3400	
Collector #2 voltage(4)						
Overall efficiency	26%	28%	28%	32%	33%	
Length	14"	14"	13.5"	15"	15"	(1)
Width	2.5"	3"	3"	3"	3"	
Height	3"	3"		3"	3"	
Weight (lb)	8	8	9.5	9	9	

(1) Note short length means low gain. They can increase the gain as required, but then the tube gets longer.

(2) Wider or narrower bandwidths can be provided, depending on acceptable variations for gain and power. If, for example, a 10 W minimum power output is required over a wider bandwidth, selection of a 20 W version may meet your specification.

(3) Add 1.5 dB for power output at mid band

(4) A second collector stage would add approximately 3% in efficiency.

Table 4.2-10. Typical Reliability Figures

Equipment	Program	Failure rate	P_s(7 years)	P_s(10 years)
6 GHz receiver (with LO)	I-V	1550	0.9093	0.8730
S-band receiver	GOES	1811	0.8949	0.8533
S-band transmitter	GOES	1628	0.9050	0.8671
14 GHz receiver (with LO)	SCS	1103	0.9346	0.9079
14 GHz CH. Ampl.	SCS	446	0.9730	0.9617
Local oscillator	SCS	464	0.9719	0.9602
30 to 50 W Ka-band TWTA	SCS	2400	0.8631	0.8104
10 W C-band SSPA	I-VII	800	0.952	0.9323
16 W C-band SSPA	I-VII	910	0.9457	0.9234
20 W C-band SSPA	I-VII	1060	0.9371	0.9113
30 W C-band SSPA	I-VII	1190	0.9296	0.9010

4.3 FILTER AND MULTIPLEXER HARDWARE

This subsection discusses the hardware aspects, construction capabilities, materials, and expectations of various designs of filters and multiplexers. The order of the presentation follows the simplified transponder block diagram, Figure 4.2-1.

Preselectors. This is the receiver input filter and is positioned before amplification. Its loss adds directly to the NF, thus the loss must be as small as possible. The preselector, like the receiver in general, is usually a broadband device, since it passes all channels. This device is intended to protect the receiver from out-of-band interferences. Usually the preselector has a waveguide implementation and is large and heavy. Figure 4.3-1 shows a preselector filter. The bandpass filter has a low pass filter in front of it. Cascading two filters realizes very high attenuation for the interfering signal without causing an excessive loss for the received signal.

Postmixer Filters. A mixer is a very nonlinear component. Two input frequencies, one the signal and one the local oscillator, produce the third frequency, the intermediate frequency (IF). The nonlinear component produces other frequencies that, if possible, should be constrained within the mixer itself. These frequencies propagate to all ports of the mixer. Frequencies to the signal port may be in the antenna and radiate outside. Some will go to the local oscillator and produce new products. Finally, some frequencies will propagate along the IF path and form undesirable spurious products that can reach the output and be radiated together with the desired signal. The mixer is usually a very poorly matched device. Every design contains an isolator at each port. Spurious products and the isolator produce spurious products that are outside of the isolator bandwidth. They are reflected back to the mixer, passing forward and back to the isolator twice. The propagation through the ferrite, however, is a long electrical path with variable temperature. A mixer tuned for flat response at room temperature gets a ripple response with a change of temperature. Up to 3 dB ripple in the band has been observed. By positioning a filter between the mixer and the isolator, the spurious products are getting a known discontinuity, invariant with temperature. It may be difficult to tune the mixer, but once tuned, it does not change with temperature. The filters described here are the components used.

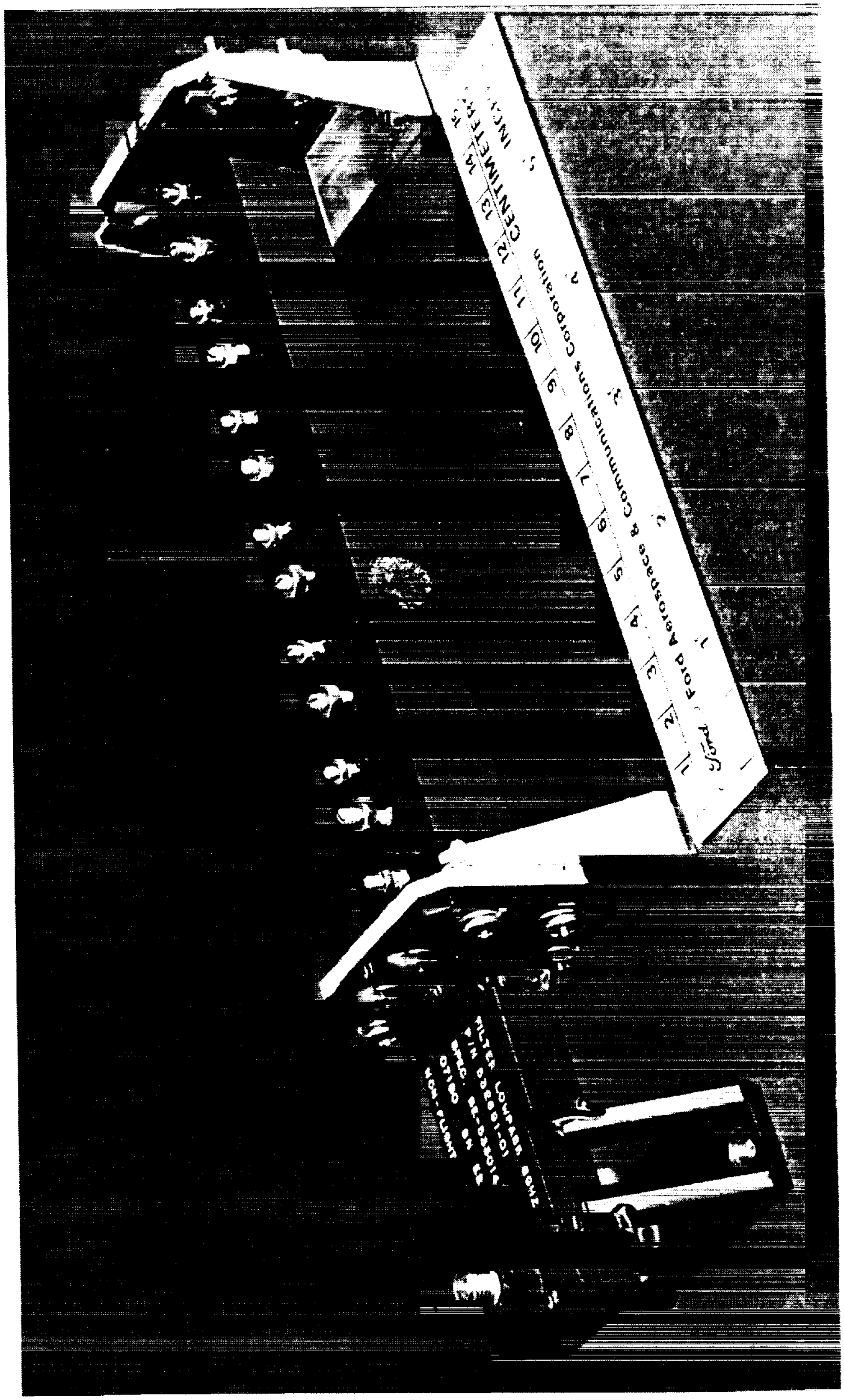

Figure 4.3-1. Preselector 4 GHz

A mixer filter for 14 GHz operation with a bandwidth of 500 MHz is shown in Figure 4.2-5. It is a design of coupled lines. Since the frequency is rather high, the lines are reasonably small. Figure 4.3-2 is a photograph of a mixer filter for 1.6 GHz operation. The lines are relatively long and positioning them side by side makes the substrate very long. In the design shown, the coupled lines appear in pairs. Between the coupled lines are transportation lines leading to the next pair. This results in better use of the surface substrate. Obviously, these types of filters are of planar configuration and can be handled in trays with other circuits. The filters are lossy and cannot be used in front of the preamplifier. Furthermore, they have multiple bandwidths, as at the third harmonic frequency, and will not protect the receiver. However, at the place used within this component, there are no adverse effects and the filters fit perfectly with the rest of the equipment.

Input Multiplexers. The front ends of the receiver are usually broad band and contain all the channels. After sufficient amplification, the channels need to be separated. The place where channel separation occurs is the input multiplexer, a low loss splitter that is selective in frequencies.

In every multiplexer there are as many filters as the number of channels. All filters have common input and individual output. One obvious problem is whether the individual filters interfere with each other. That is, how far apart in frequency should the two adjacent filters be in order to avoid interference. Ford Aerospace started using contiguous filters that permit the closest operation between two channels. An example of contiguous filters is presented in Appendix C.

The input mutliplexers are usually a narrowband design and, because of this, temperature variations may change the passband. To combat this effect the material used for the mutliplexers was invar. Special thin walled invar filters operate well, but they are still relatively heavy. These filters do not handle high power, and therefore other materials may be used. For approximately 10 years Ford Aerospace has used graphite epoxy material that is very strong and very light, with zero expansion, and therefore operating identically at every temperature. Although filters made of this material operate well, they are gradually being replaced by a dielectric filter. The cavity of the filter contains a dielectric body, the pack, that has high dielectric constant and thereby reduces the size of the filter. Figure 4.3-3 illustrates the evolution in filter design by comparing the waveguide implementation, a fiber epoxy cavity filter, and dielectrically loaded filters. All of these operate at 4 GHz and are designed for identical specifications. Size reduction and weight improvement are remarkable.

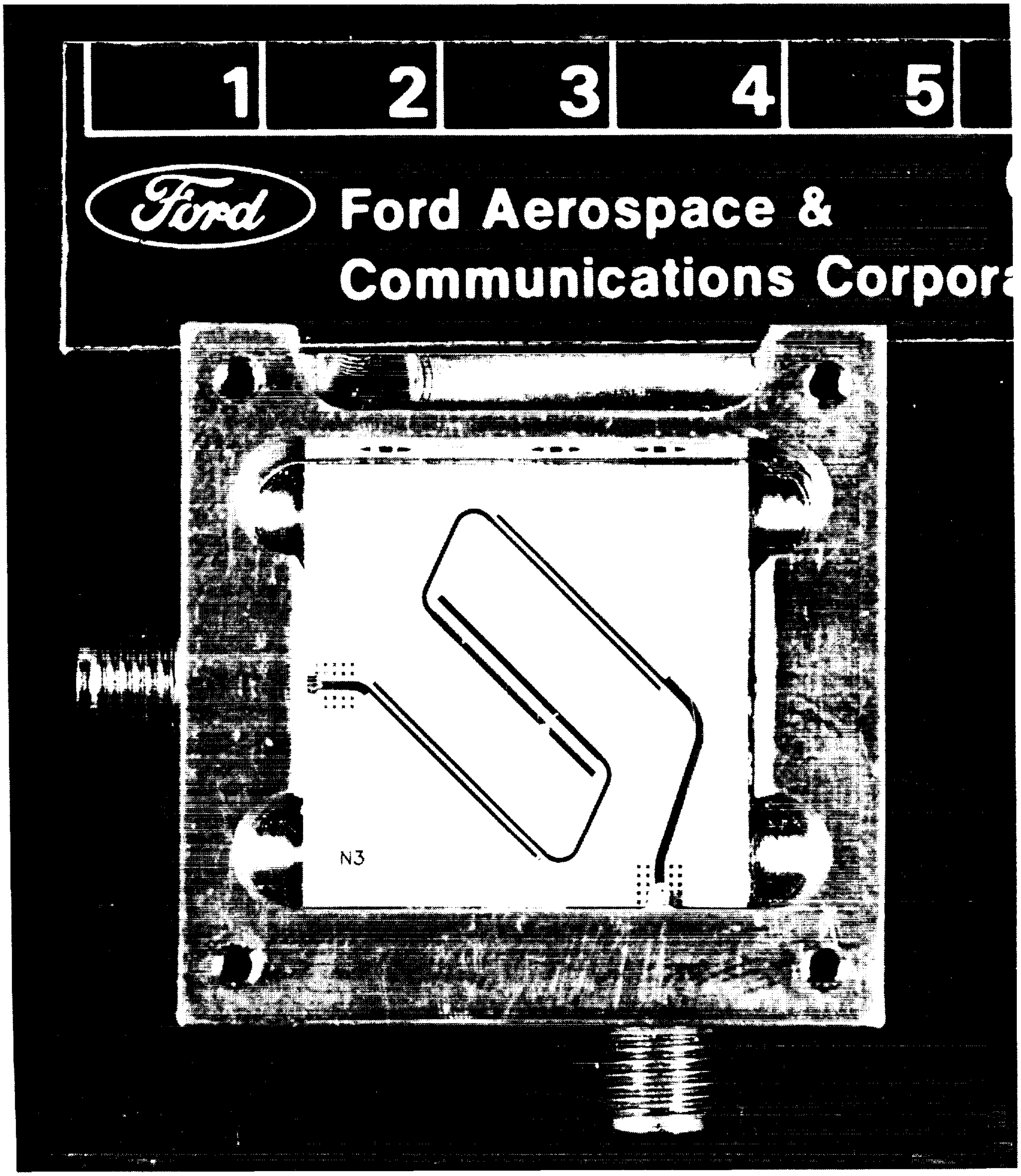

Figure 4.3-2. 16 GHz Postmixer Filter

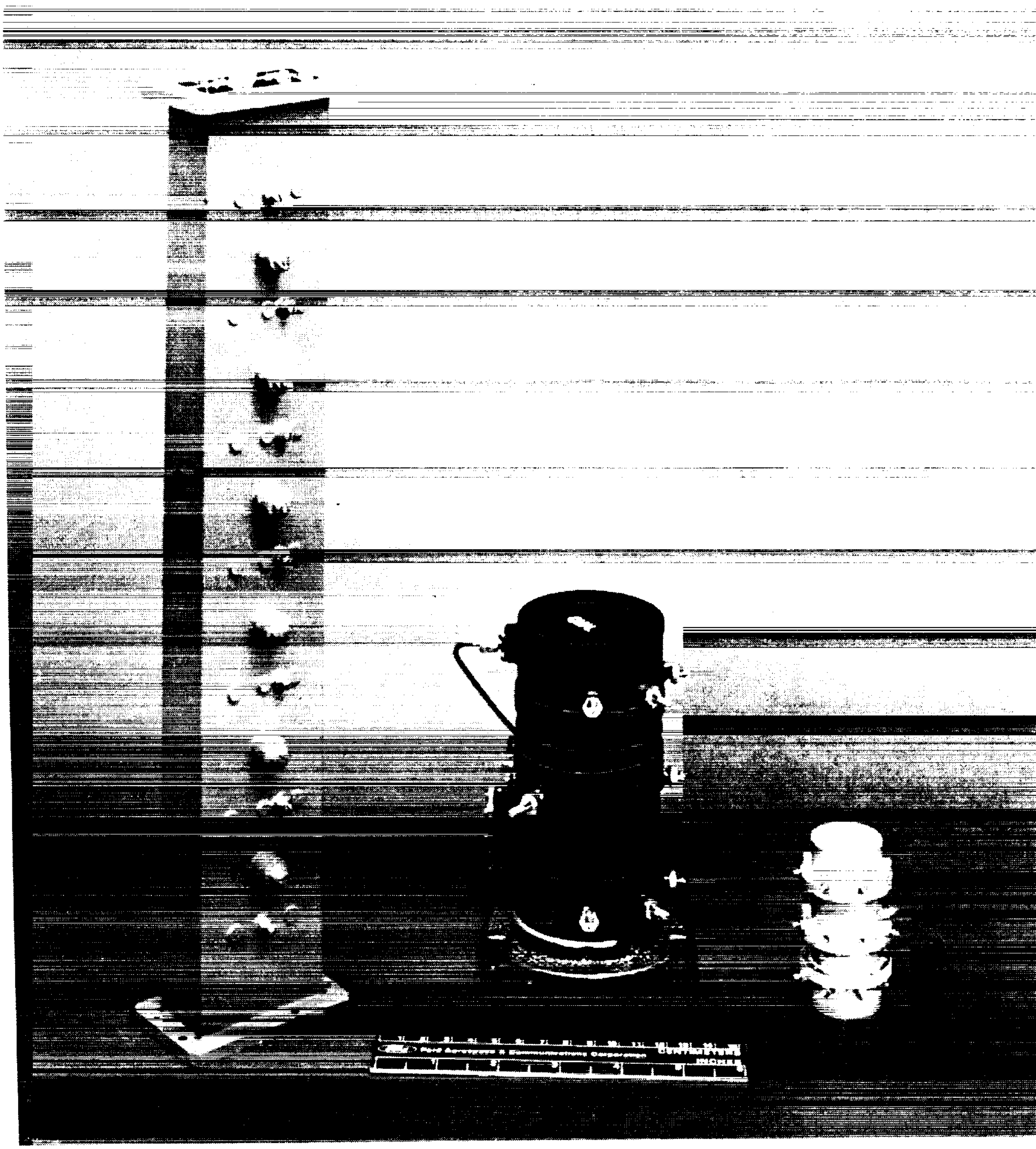

Figure 4.3-3. 4 GHz Waveguide, Cavity, and Dielectric Filter Comparison

Figure 4.3-4 shows three filters at 1.6, 4, and 12 GHz with dielectric loaded cavities. This type of filter can be built for almost every frequency used in satellites. Figure 4.3-5 displays the interior of the dielectric filters, the packs, the coupling irises, and the cavities.

Figure 4.3-6 is a photograph of an input multiplexer used in the SUPERBIRD program at Ku-band. The unit is small because it uses dielectrically loaded cavities.

Output Multiplexers. The output multiplexers perform the reverse operation of the input multiplexers. At the input the channels have to be split, and at the output, after power amplification, the channels have to merge in order to be transmitted by one antenna. In theory both types of multiplexers do not differ, but practical implementation shows some important differences. The filters of the output multiplexers have to handle high power. If lossy, they will generate heat that has to be sinked. The primary requirement is for very low loss. In order to dissipate the heat, the material most often used is invar. Figure 4.3-7 shows the SUPERBIRD Ka-band output multiplexer. Connections are done in waveguide configuration to reduce losses.

The low-pass filters are also visible. These increase attenuation for some out-of-band frequencies, while keeping the insertion losses low in band. A similar unit for INTELSAT V is shown in Figure 4.3-8. Here, too, the material is invar, the connections are waveguide, and the presence of the low-pass filters is obvious.

Topics related to space application filters include passive intermodulation generation, corona discharge, and multipactor effects.

The passive intermodulation effect and the active device effect have the same mechanism, but the effect in active devices is much lower amplitude. In tubes or power amplifiers these products may be 20 dB below the carrier, and in the passive generation they may be 100 dB or more below the carrier. A careful estimate for each design may reveal whether its amplitude may be objectionable. This estimate should be verified by proper tests.

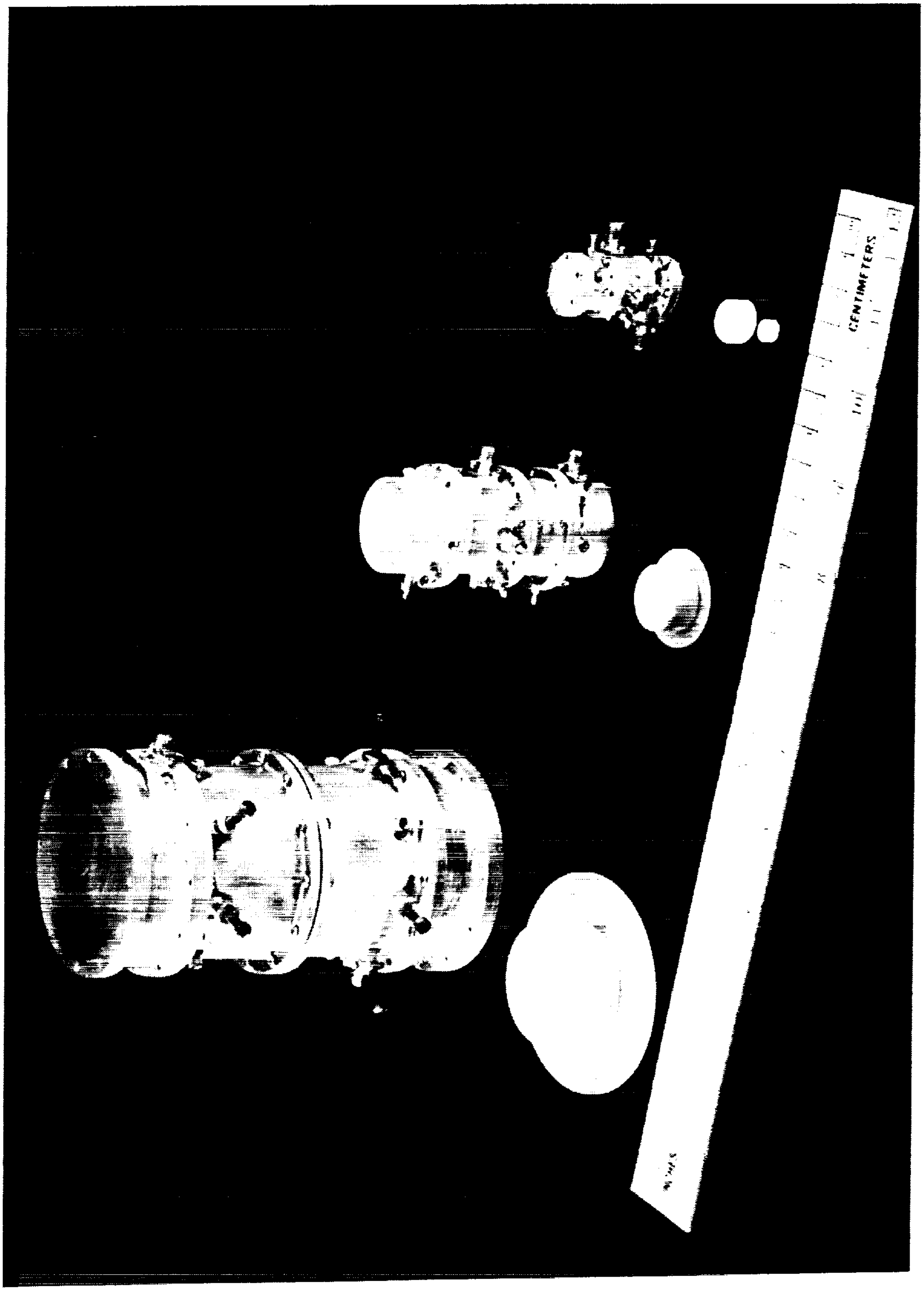

Figure 4.3-4. Dielectric Filters at 1.6, 4, and 12 GHz

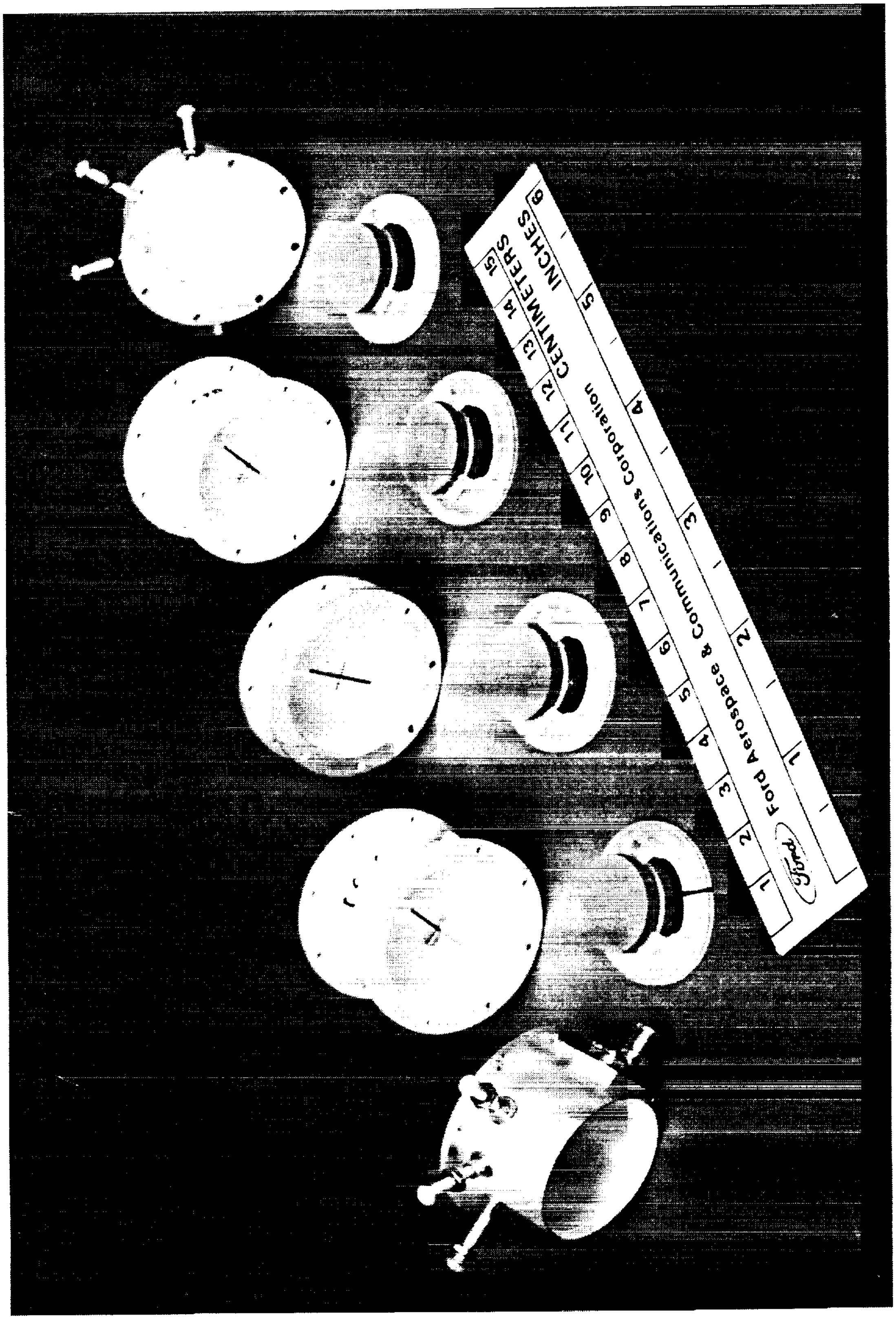

Figure 4.3-5. Interior of Dielectric Filters

ORIGINAL PAGE
BLACK AND WHITE PHOTOGRAPH

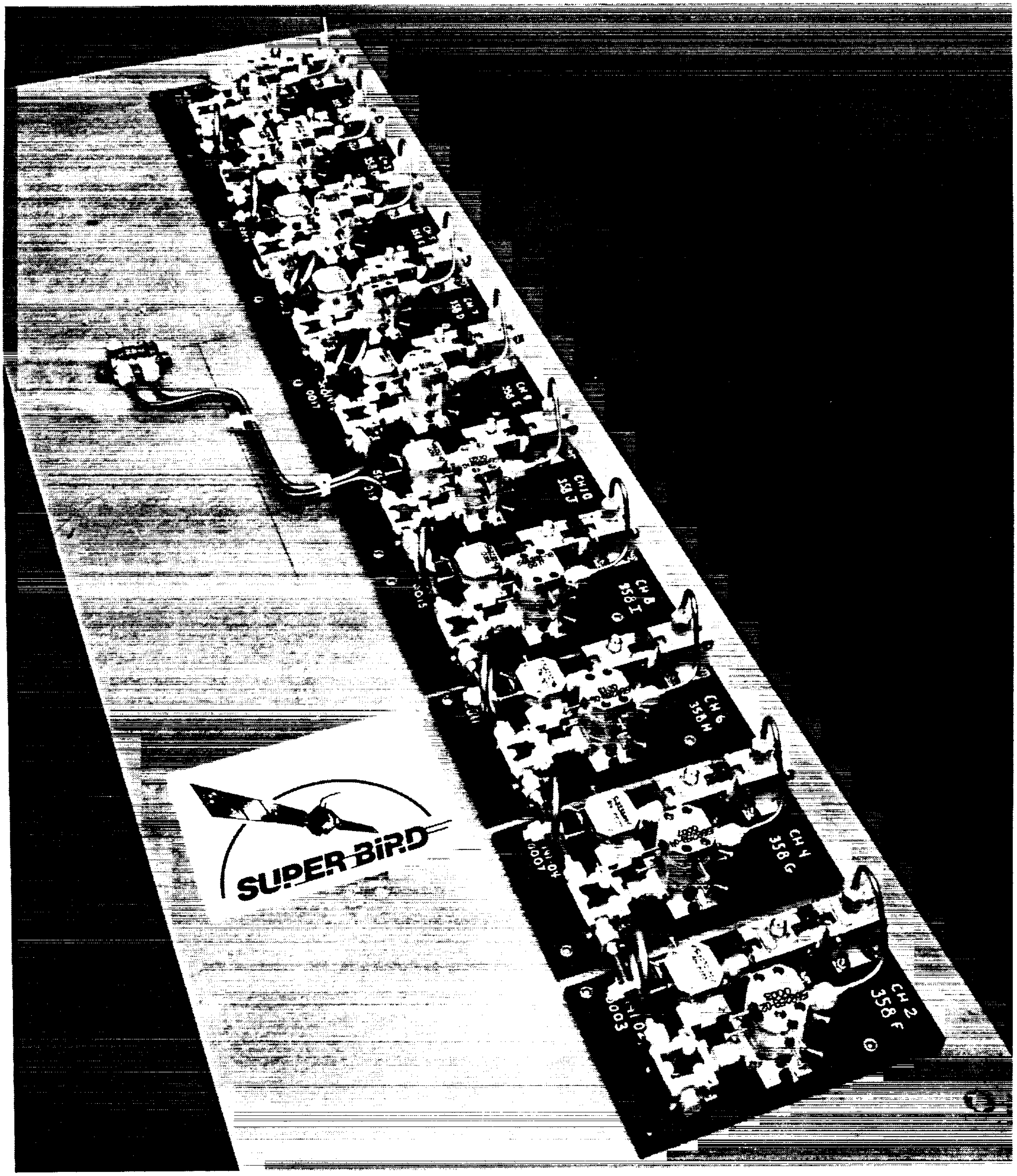

Figure 4.3-6. SUPERBIRD Ku-Band Input Multiplexer

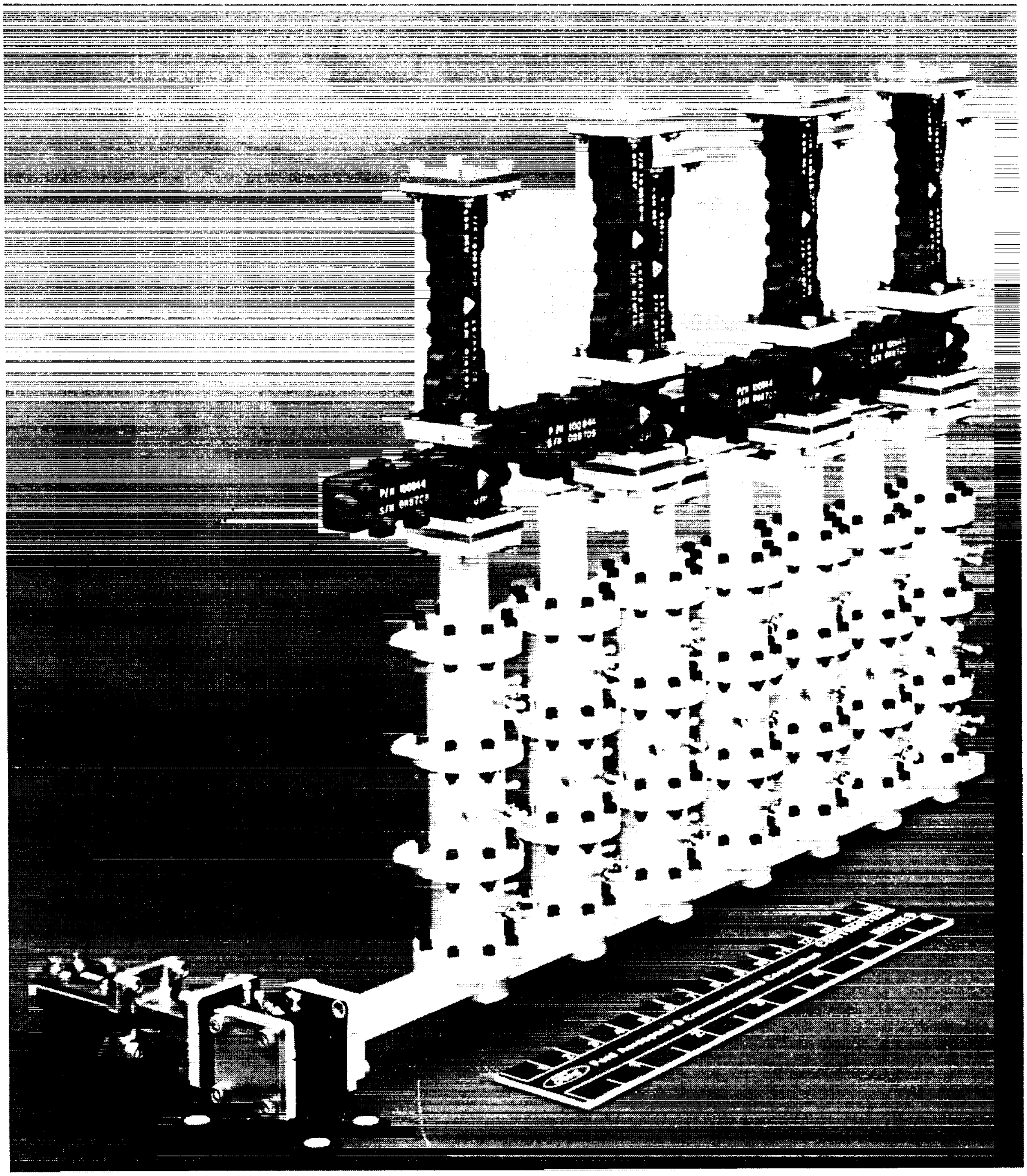

Figure 4.3-7. Ka-Band Output Multiplexer

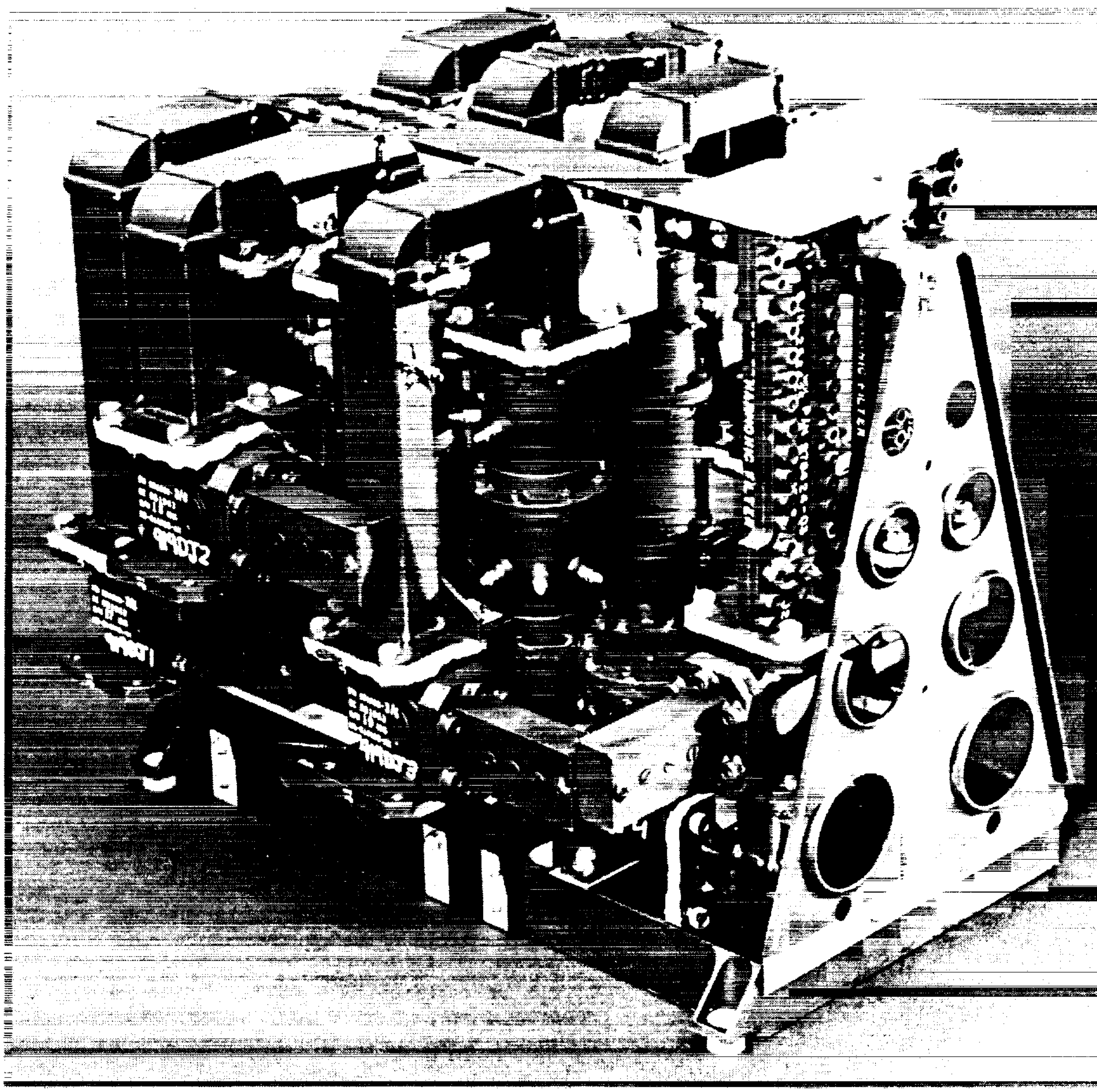

Figure 4.3-8. INTELSAT V 12 GHz Multiplexer

ORIGINAL PAGE
BLACK AND WHITE PHOTOGRAPH

Corona discharge occurs when equipment is operating at reduced pressure. Communication equipment is not turned on until a week after launch. By then the filters are degassed. The telemetry, tracking, and command (TT&C) equipment must be on during ascent. Filters designed for operation during ascent, where air pressure is reduced, must be protected against corona discharge, which is a destructive effect. There are various ways to design filters for preventing corona discharge; one way is to use the dielectric loaded filters.

Multipactor effect is exhibited by a large increase of noise that desensitizes the receivers. A test must be performed to verify that desensitizing is not taking place, since a noise level increase of 20 dB has been observed.

This discussion covers aspects of general importance. Specific solutions are outside the scope of this report.

4.4 LINEARIZERS

Saving dc power in satellites is often a stringent requirement because there is limited capacity to generate this power by solar cells or to store the energy in space qualified batteries. The biggest consumers of power are the power amplifiers. When addressing the question of how to save power, increasing power amplifier efficiency is of prime importance.

When using a system, it is often necessary to have linear operation. To achieve this, transmitter nominal power is usually oversized and then backed off. Depending on the degree of nonlinearity desired, backoff of 5 to 10 dB is acceptable practice, with 7 dB a typical average. But in doing this backoff, transmitter efficiency decreases a great deal. This discussion is intended to show that by using a linearizer the backoff is reduced, transmitter efficiency is improved, and savings in dc power are realized.

4.4.1 Nonlinearities and their Impact on System Operations

There are two types of nonlinearities that can be objectionable: amplitude and phase. The test for amplitude nonlinearity includes the two carrier intermodulation measurement. Two carriers are applied simultaneously to the input of the amplifier under test. When the operation is linear, the same two carriers appear in the amplifier output. This, however, is almost never the case because the output signal contains other frequencies not existing in the input. These frequencies are the product of third order nonlinearities of the device, as shown in Figure 4.4-1. The dB difference between these new frequencies and the original frequencies as they appear in the amplifier output is the third order intermodulation (IM). The existence of new frequencies in the output is very harmful, since energy of one channel penetrates the other channel and reduces the quality of the intelligence. It is very difficult to completely eliminate the generation of new frequencies but it is possible to reduce them to or below a certain level. Backing off the input power is one means of reducing the IM product level.

Phase linearity can be demonstrated by measuring the phase difference between input and output signals. When signals are at low level, the phase difference is constant. By increasing input signal levels, this phase difference begins to change and this is objectionable. The phase nonlinearity will not always cause degradation.

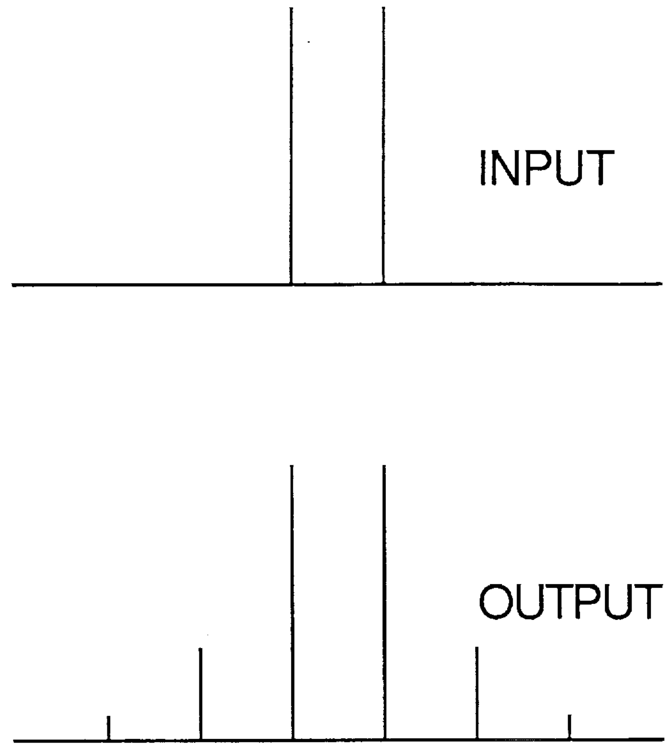

Figure 4.4-1. Intermodulation Distortion in Power Amplifier Input and Output Spectrums

As long as the envelope of the radio frequency (RF) signals is constant, the phase change due to the transmitter is zero. However, in many types of modulation (AM or QPSK), the envelope of the RF is constantly varying. AM is not sensitive to phase variations, but QPSK is. The information is contained in the change of the phase and when the envelope collapses to zero, the phase variations cause degradation of the channel and errors in the transmission. Backing off input power is one way to reduce the phase nonlinearity.

4.4.2 Linearizer Types

4.4.2.1 Feedback Linearizer. If an amplifier is nonlinear, using negative feedback will improve linearity features. Negative feedback reduces the gain, thus additional amplification is required. Since this can be done at low level signal, it does not present a significant handicap. At microwave frequencies, maintaining negative feedback is not a very easy task. The phase of the feedback signal changes very rapidly and at certain frequencies it becomes positive feedback, causing an instability problem. When wideband operation is required, feedback is not recommended. Figure 4.4-2 is a block diagram of a feedback linearizer.

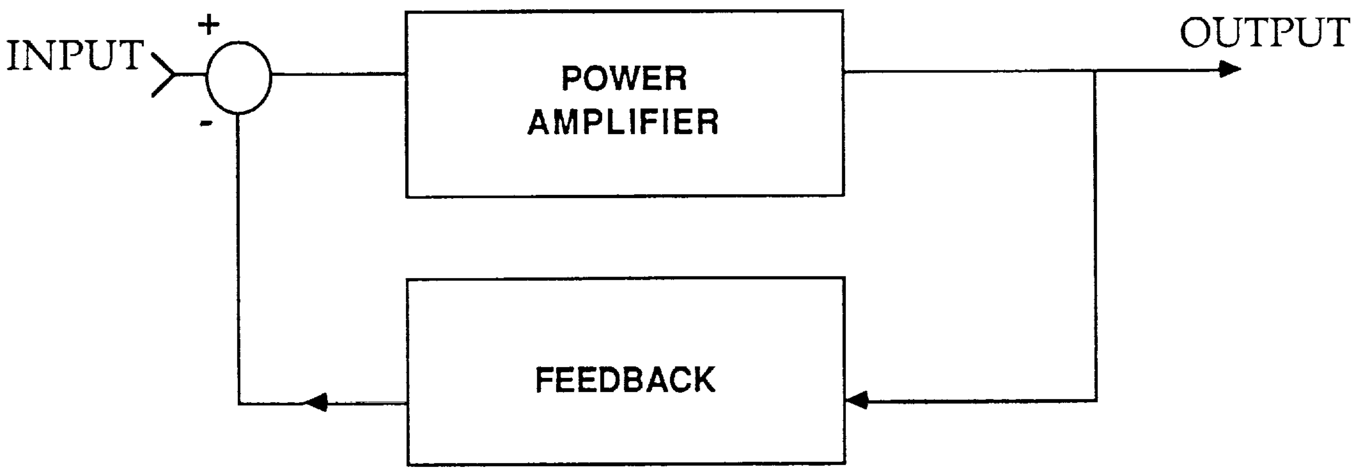

Figure 4.4-2. Feedback Linearizer

4.4.2.2 **Feedforward Linearizer.** Figure 4.4-3 is a block diagram illustrating the principle of operation of this type of linearizer.

Two carriers are applied to the input coupler at point A. The majority of the energy is directed to the input of the main amplifier that is assumed to be nonlinear. Some portion of the input power is directed to a unit called input processor and then to a summing device The output of the amplifier, point B, contains not only the two input frequencies but also all other frequencies generated by the nonlinearities. This is now applied to a directional coupler, so that the main energy is forwarded to a second directional coupler, and some portion of the energy is applied to the summing device. The processor in front of the summer adjusts the amplitude and phase of the two original input signals so that at the output of the summer these two frequencies are cancelled. The output now contains only the products of nonlinearity and is the error signal, point C. The error signal is fed to a second signal processor and then to a second auxiliary amplifier. The output of the second amplifier is added to the output of the main amplifier in the output coupler. The second processor adjusts the amplitude and phase of the error signal so that at the linearizer output the unwanted frequencies are cancelled. Thus only two clean carriers remain.

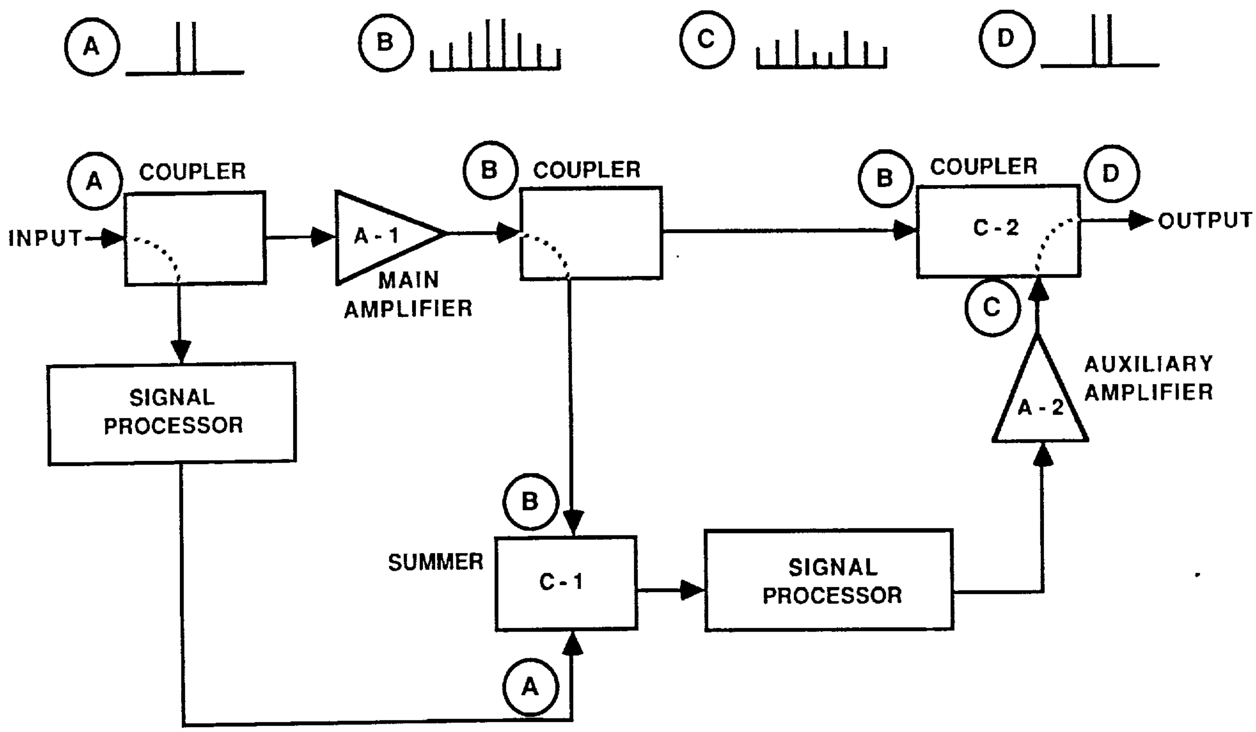

Figure 4.4-3. Feedforward Circuit Block Diagram

This type of linearizer uses a second amplifier and the combined efficiency is rather poor. It is further complicated by two processors and directional couplers, additions that make it heavy. For these reasons the linearizer has not been used in spacecrafts. Its use has been limited to ground equipment, where size, weight, and power requirements are not important.

4.4.2.3 **Predistortion Linearizers.** Figure 4.4-4 is a block diagram of a predistortion linearizer. This type of linearizer contains an input hybrid that splits the signal in two equal amplitudes in 90° phases. Each branch contains an amplifier, attenuator, and eventually, a phase shifter. Both branches are added in a second 90° hybrid of identical design as the first one. The operation of the predistortion linearizer is rather simple. In the upper branch the signal, point A, is applied directly to the amplifier, and it is strong enough to make the operation of this amplifier nonlinear. The output spectrum, point B, contains the products of the IM together with the original two input frequencies. The level and phase of this output can be controlled by the attenuator and phase shifter. The lower branch contains the same components in a different order. The amplifier is connected after an attenuator to prevent it from becoming nonlinear. Its output, point C, is the

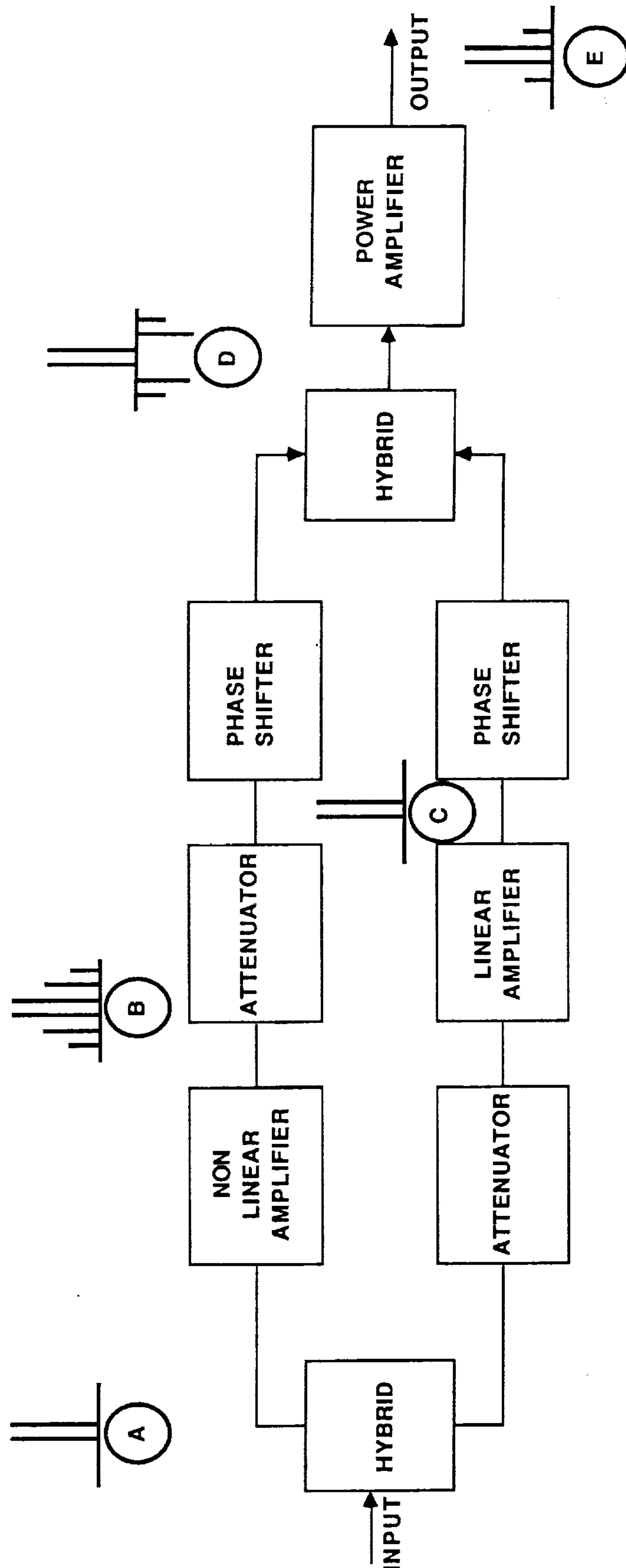

Figure 4.4-4. Predistortion Linearizer

replica of the input, except for the amplitude. Adding the signals of the two branches in the output hybrid becomes subtraction, since the first hybrid caused 90 ° of phase shift and the second hybrid caused another 90 °of phase shift. Point D shows the spectrum in the output. The original two carriers are partially subtracted and the spurious products are with reverse phase. This is the predistortion. The signal is now fed to the final power amplifier, assumed to be nonlinear. However, this time the IM products of the amplifier are reduced, if not completely cancelled. This type of linearizer is compact, simple in operation, and very useful for space applications. With proper electrical design and packaged for space applications the size of this linearizer is 2.5 x 1.5 x 0.5 inches, its weight is less than 50 grams, and its power requirement is 0.4 W.

4.4.2.4 **Amplitude Characteristics Improvement Due to the Linearizer.** Figures 4.4-5 and 4.4-6 show the improvement of amplitude characteristics due to linearizer use. Curve A at the top of Figure 4.4-5 represents the relationship of output power to input power of a typical TWTA. As the figure shows, as long as the signals are at low level the relation is linear - the output changes 1 dB for 1 dB change of the input power. As the levels of the input signals increase, the output changes less than 1 dB per dB - the straight line bends indicating the operation is getting nonlinear. A tangential line to curve B is plotted on the same figure and it represents the output power if the operation had remained linear. By using the straight line and the curve we can find the one dB compression point. In the figure this point occurs at input -12 and output -7 dB (relative scales). The curve has a maximum power that the tube can provide. This is the saturation point for this tube. When the tube is driven further with higher input, the output not only does not increase but actually decreases. Part of the energy of the carrier now goes to the distortion products.

The two lines alone hardly can describe which region is linear and what linear operations really mean. If however the input/output power test is performed using two carriers then we get a different curve - C which saturates earlier and allows us to measure the level of the IM products - curve D. The third order intermodulation (IM) product is the vertical distance between the two-carrier saturation and the third order IM. For the nonlinearized tube for input level 5 dB below the saturation, the IM is 22.5 dB. A tangential straight line to the third order IM product curve is plotted on the same figure - line E. At the common point of the two tangential lines (B and E) we find the intercept point. If this point is given and the slope of line E is known to be 3 dB per dB, then we can estimate the IM capabilities of the tube. Figure 4.4-6 contains the same type of curves but this time a linearizer is used. For 5 dB backoff from saturation, the IM is 32 dB or an improvement of 10 dB, which is a significant improvement.

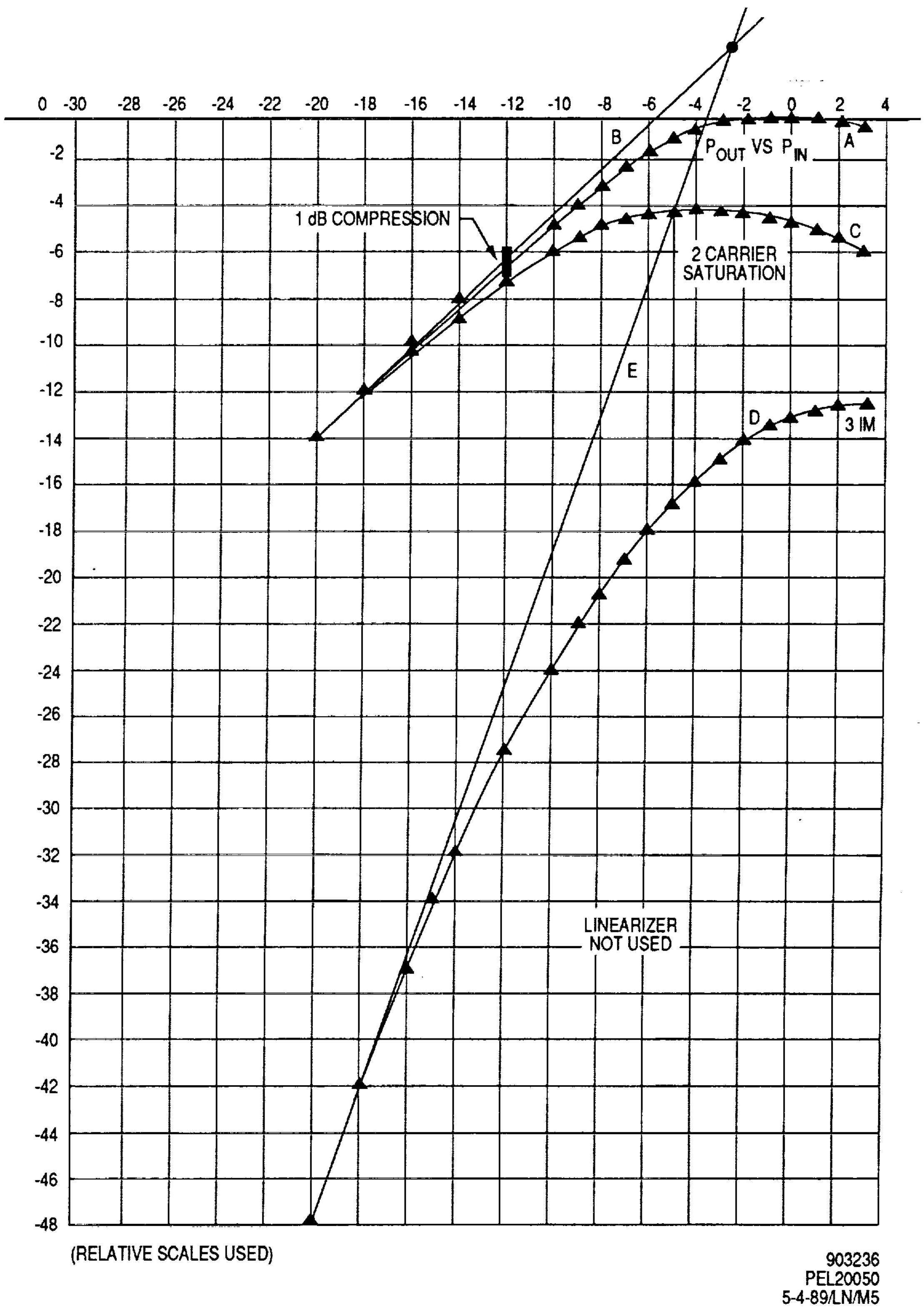

Figure 4.4-5. Output Power Versus Input Power for a Typical TWTA

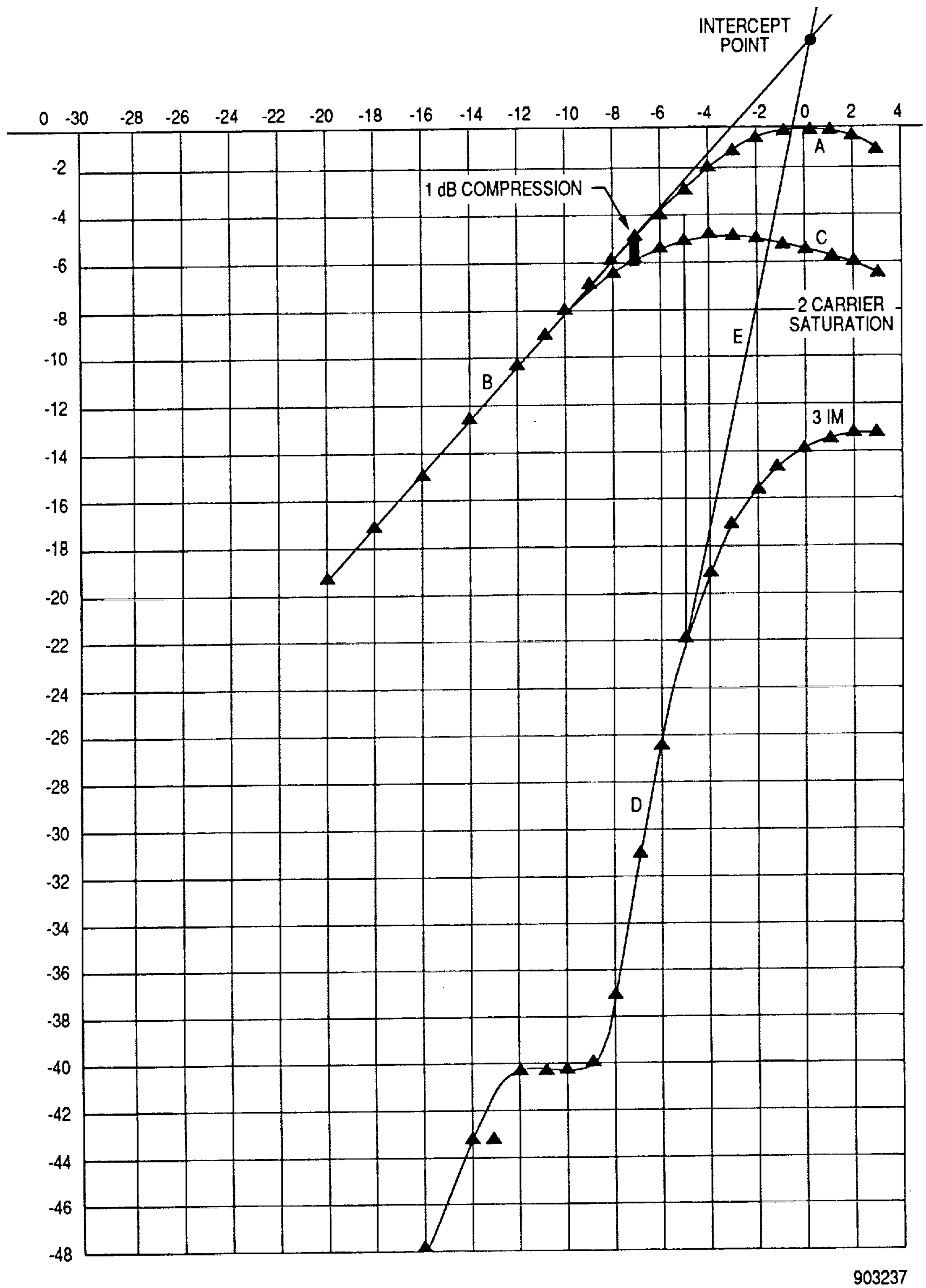

Figure 4.4-6. Output Power Versus Input Power for a Typical TWTA When Used with a Linearizer

These curves are very useful for setting the levels of operation. From system requirements, the output power must be 10 watts and IM levels must be below 30 dB. If this tube is used without a linearizer (Figure 4.4-5), then the input power must be backed off by 8 dB and the output power has lost 3 dB. We should start with a 20 watt tube to meet the requirements. In comparison, if we use the linearizer (Figure 4.4-6) in order to get -30 dB for the IM, the input power must be backed off by 4.5 dB at which point the output power has been reduced by 2 dB. Then we could select a 16 watt tube, with a significant savings in power. The results can be more dramatic if the requirement is to have IM products below 35 dB. Figure 4.4-5 shows that the input power must be backed off by 10 dB reducing the output power 4.5 dB, then we have to start with a 28 watt tube. If the linearizer is used, the input power has to be backed off by 5 dB reducing the output power by 2.5 dB, which means we have to start with a tube of 18 watts.

4.4.3 Phase Improvements Due to Linearizer

Every TWTA or SSPA exhibits changes in the phase difference between the input and output when devices are driven to nonlinear operation. Figure 4.4-7 is a typical curve illustrating the change. As the figure shows, values as high as 40° are often encountered. The same linearizers that are effective in canceling the amplitude nonlinear effects are also effective in improving the phase nonlinear effects. Typically the phase nonlinearity can be reduced from 40° to 5° or less.

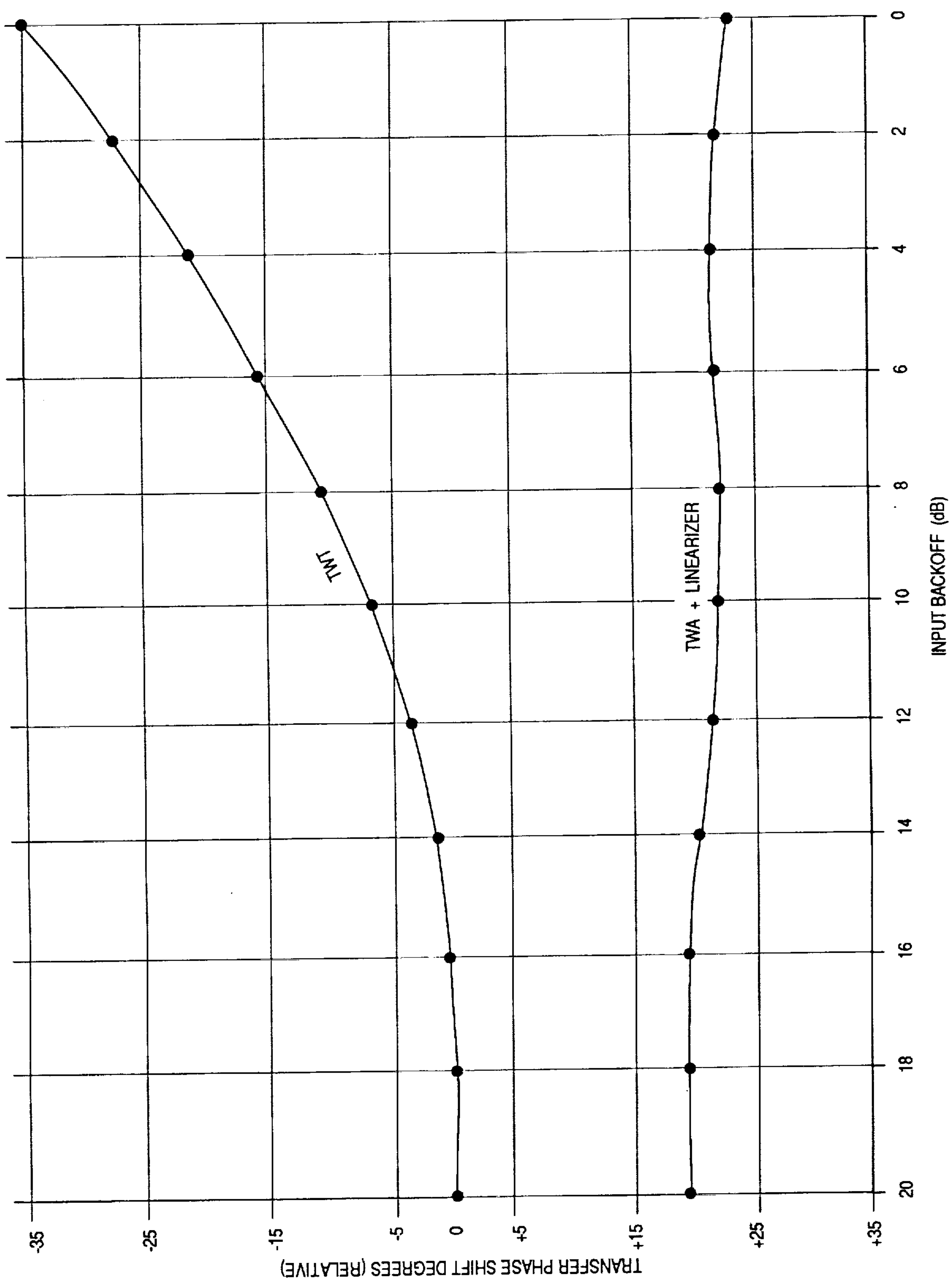

NOTE: PHASE SHIFT CHANGES IN A "MORE-NEGATIVE" DIRECTION INDICATE AN INCREASE IN TIME DELAY

Figure 4.4-7. Typical Curve Illustrating Changes in Phase Differences

REFERENCES

4-1 Alain Cappy. "Noise Modeling and Measurement Techniques," IEEE Transactions on Microwave Theory and Techniques, Vol. MTT-36 No. 1, Jan 1988, p. 1.

4-2 Kawasaki, Inami, Tanaka, Tokuda, Higashiura, Nori and Kamet. "Extremely Low Noise HEMT Fabricated on MOCVD Epi-Wafer," The Transactions of the IECE of Japan, Vol. E 69, No 4, April 1986.

4-3 Schellenberg, Maher, Wang, Wang, and Yu. "35 GHz Low Noise HEMT Amplifier," 1987 IEEE Microwave Theory and Techniques Symposium Digest, p. 441.

4-4 Watkins, Schellenberg, and Yamasaki. "A 30 GHz Low Noise FET Amplifier," 1986 IEEE Microwave Theory and Techniques Symposium Digest, p. 321.

4-5 M. Sholley, A. Nicols. "60 and 70 GHz HEMT Amplifier," 1986 IEEE Microwave Theory and Techniques Symposium Digest, p. 463.

4-6 C. Yuen, C. Nishimoto, M. Glenn, Y. C. Pao, S. Bandy and G. Zdasiuk. "A Monolithic Ka-band HEMT Low Noise Amplifier," 1988 IEEE MTT-S Digest, p. 247.

4-7 S. Bandla, G. Dawe, C. Bedard, R. Tayrani, D. Shaw, L. Raffaeli, and R. Goldwasser. "A 35 GHz Monolithic MESFET LNA," 1988 IEEE MTT-S Digest, p. 259.1.

4-8 S. Weinreb, M. W. Pospieszalski and R. Norrod. "Cryogenic HEMT, Low-Noise Receivers for 1.3 to 43 GHz Range," 1988 IEEE MTT-S Digest, p. 945.

4-9 K. H. G. Duh, P. C. Chao, P. M. Smith, L. F. Lester, B. R. Lee, J. M. Ballingall and M. K. Kao. "Millimeter-Wave Low-Noise HEMT Amplifiers," 1988 IEEE MTT-S Digest, p. 923.

SECTION 5
SWITCH SUBSYSTEM

This section discusses the switching aspects of the SGL MBA/switch for the ATDRSS. The following subsections present a functional overview of the switching architecture. As a baseline, the crosslink interface for communications between the ATDRSS-East and ATDRSS-West is assumed to be at baseband (as depicted in the baseline of Figure 3 of the SOW). The "bent-pipe" crosslink approach, which requires interfacing at IF as opposed to interfacing at the baseband, is addressed in a subsequent subsection. The concept of Ku-band uplink and downlink processing will be addressed in a subsequent subsection.

5.1 INTRODUCTION

The operation of the switch subsystem of the TDRSS network is explained in Figure 5.1-1. There are two ATDRS satellites in operation. The design of the two satellites is identical. Each can communicate with seven ground stations. The same ATDRS can transmit to and receive from users; it can establish communication between two users through the space-to-space links; and can transmit to or receive from the other ATDRS satellite. ATDRS 2 can do everything exactly like ATDRS 1 except communicate with the CONUS ground station since this satellite is not visible from CONUS ground stations.

The functional partition of the switch subsystem is presented in Figure 5.1-2, a block diagram presented in previous reports. The units in this figure should not be identified as hardware boxes. They rather indicate a function and in the process of realization any of these blocks may be quite complicated. This subsection describes how these functions can be translated to conceivable realizable hardware.

5.1.1 Uplink Switch (Ka-Band)

The services of the uplink switch and the frequencies involved are discussed in this subsection. Figure 5.1-3 is identical to Figure 5.1-2, but has shaded areas to show what part is now being discussed. Figure 5.1-3b shows the inclusion of Ku/Ka-band uplinks/downlinks. In this subsection, the discussion is limited to the Ka-band. There are seven inputs to this switch, originating from the seven ground stations. Each input, however, contains 26 services as Table 5.1-1 (p 2-9) of the SOW specifies. To simplify the discussion we will concentrate on the signals of one antenna and then expand to include all of them. Figure 5.1-4 illustrates the frequency plan

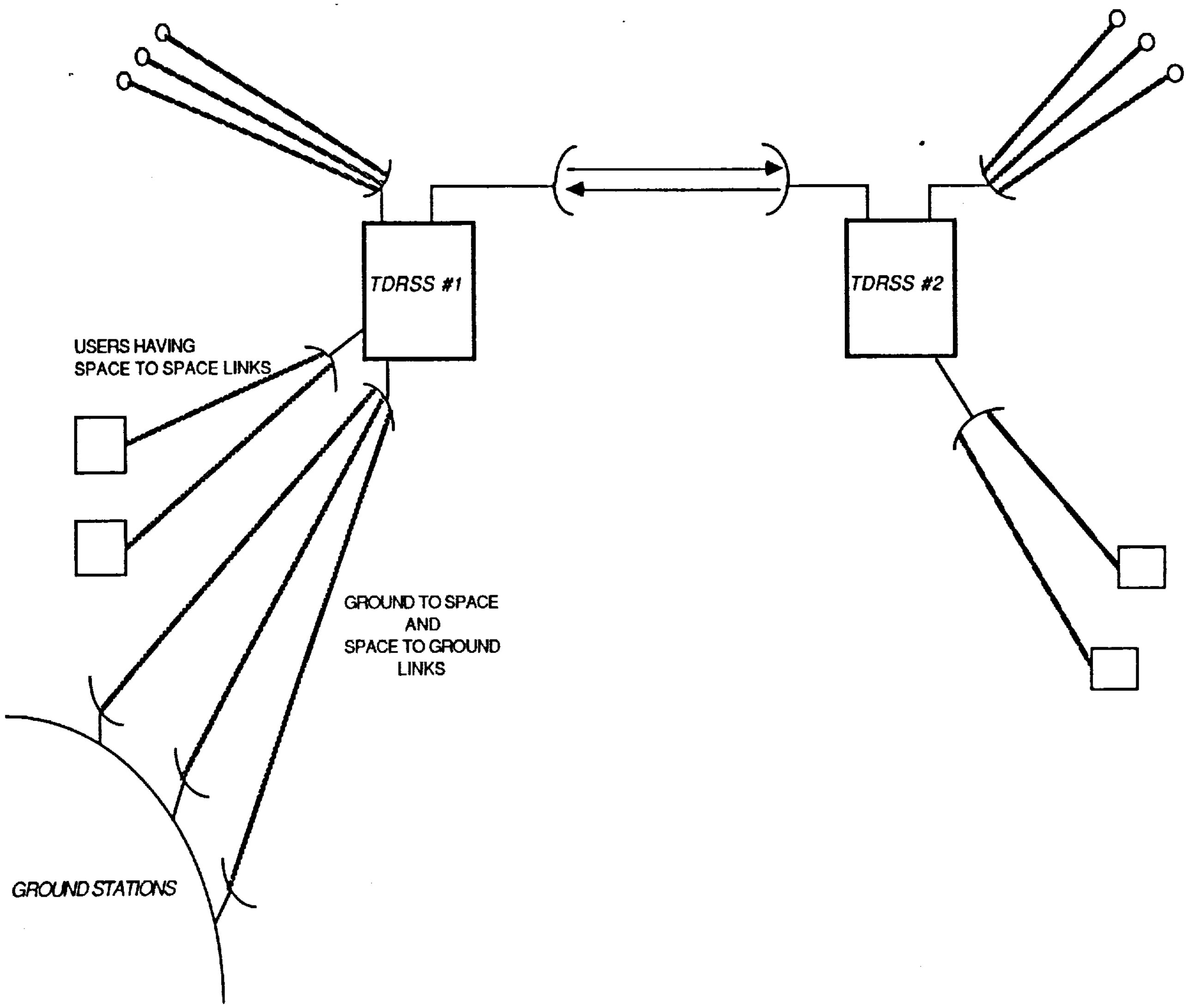

Figure 5.1-1. TDRSS Network

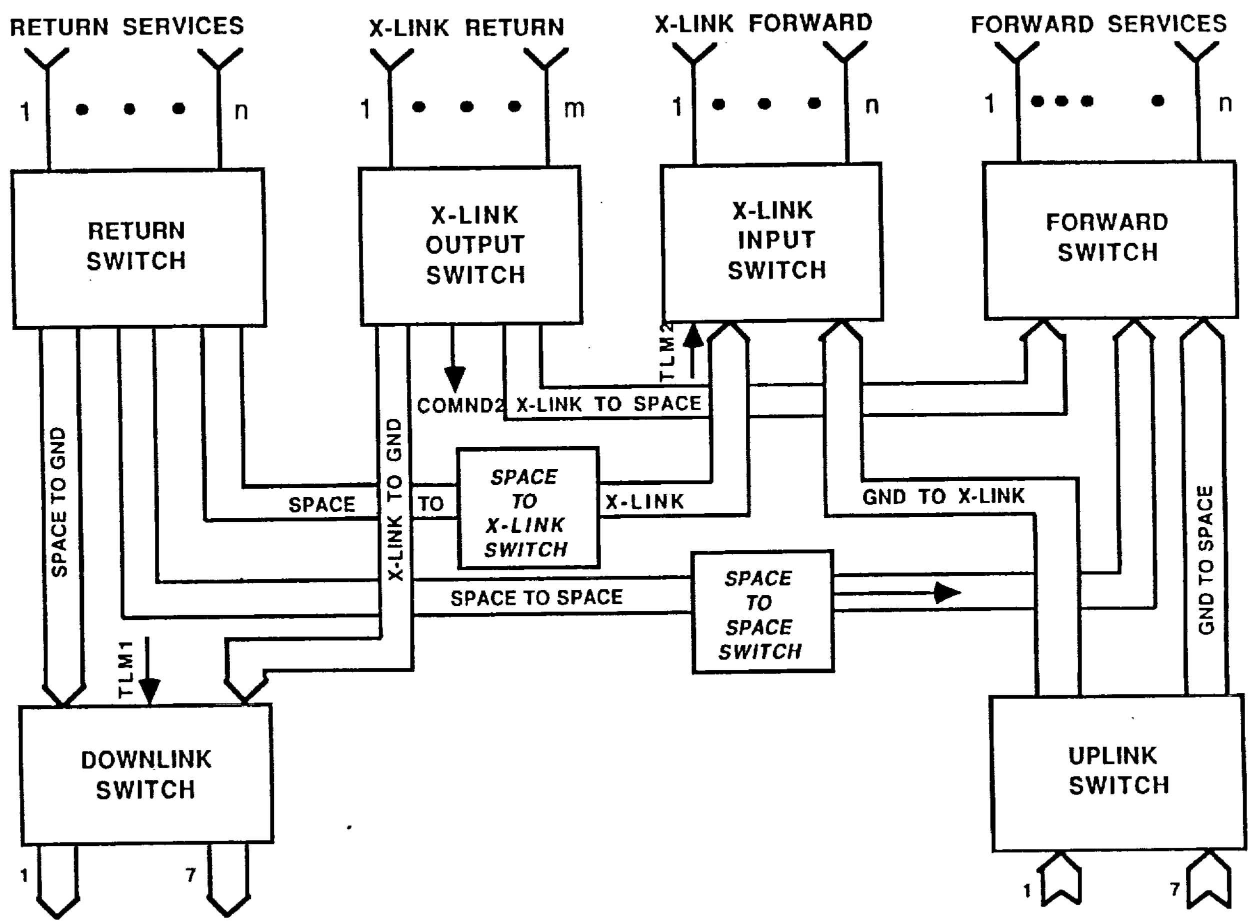

Figure 5.1-2. Functional Partition of the Switch Subsystem

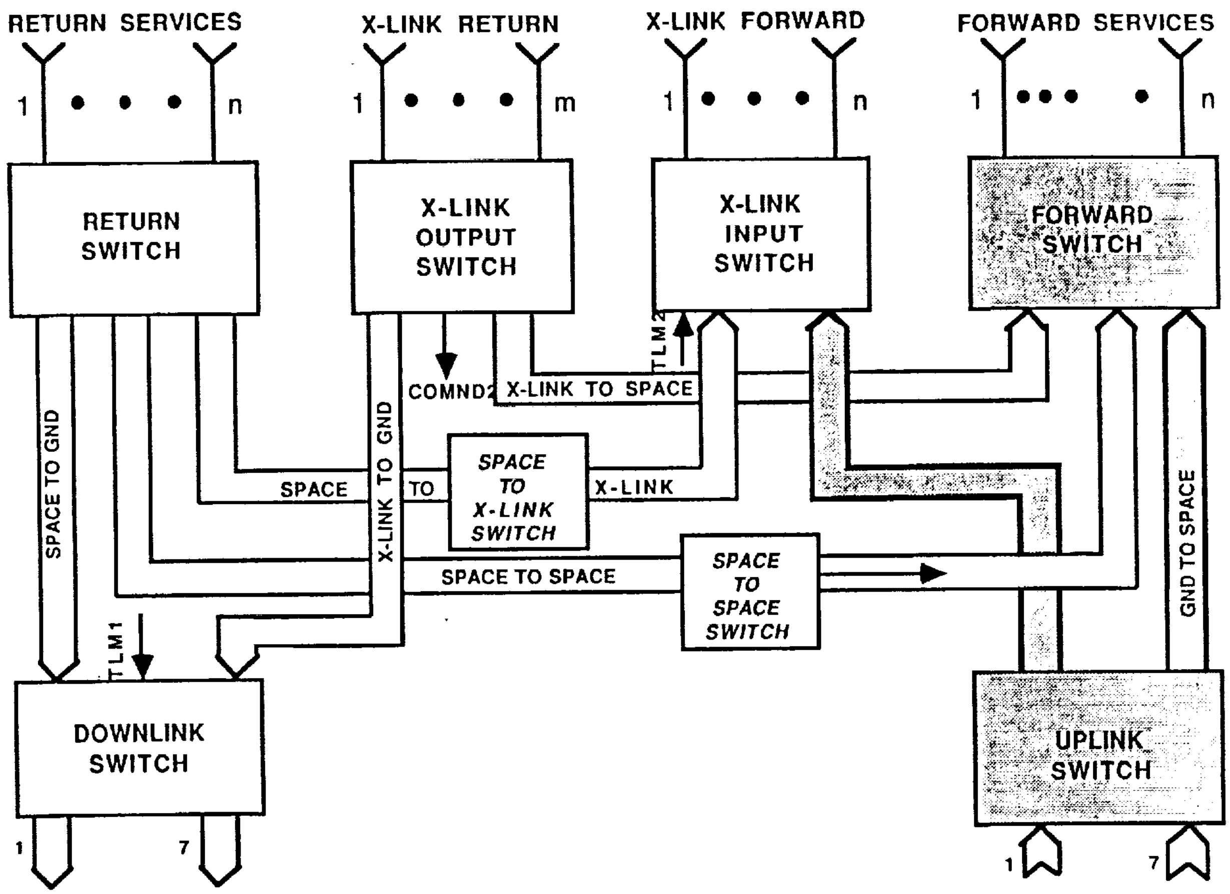

Figure 5.1-3a. Functional Partition of the Switch Subsystem

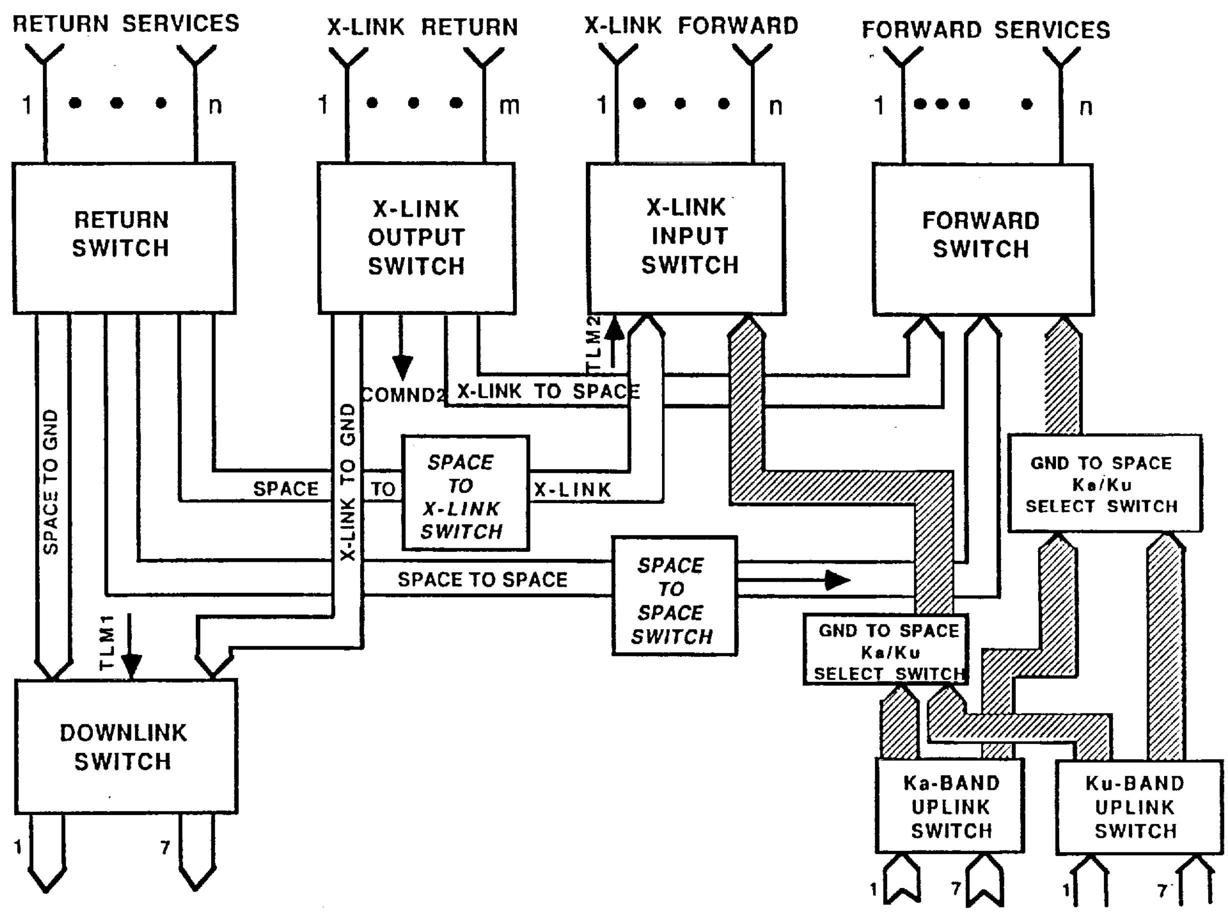

Figure 5.1-3b. Functional Partition of the Switch Subsystem

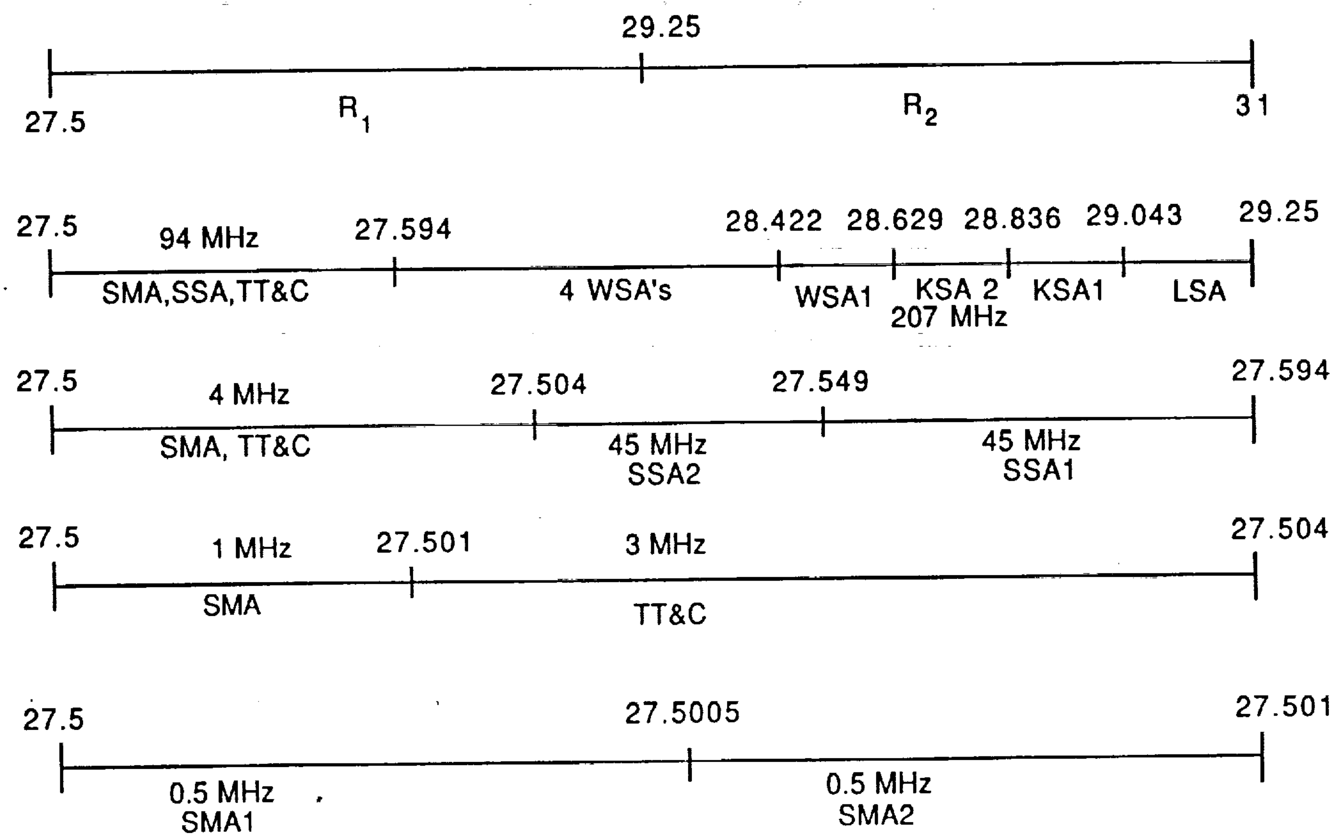

Figure 5.1-4. Frequency Plan, Ka-Band Uplink 1 Baud/4.14 Hz

as assigned by the SOW and as broken down by proposed services. Figure 5.1-4 shows the ground to space band received by the one beam of the antenna. It covers the frequencies from 27.5 to 31.00 GHz. This band is split in two equal portions one from 27.5 to 29.25 GHZ and the other from 29.25 to 31 GHz. The lower subband is R1 and the upper one R2. Each of these subbands contains the same structure of services and the only difference is that band R1 is to be used for the one ATDRS satellite (ATDRS 1), whereas band R2 is received by ATDRS 1 but is directed to be forwarded in its entirety to the other satellite (ATDRS 2) via the crosslink. The splitting of the R1 subband is discussed and then expanded for R2. A simple calculation of the maximum baud rate per the entire bandwidth is obtained by summing the baud rate for each link. This is presented in Table 5.1-1.

Table 5.1-1. Maximum Baud Rate

Service	No. of Services	Max baud Rate	Total baud Rate (Mbaud)
TT&C	2	500K	1.00
SMA	4	10K	0.04
SSA	4	11M	44.00
KSA	4	50M	200.00
WSA	10	50M	500.00
LSA	2	50M	100.00
Total	26		845.04

The equivalent of 1 baud per 4.14 Hz is 845 Mbaud in 3.5 GHz. The purpose of this computation is to show that when breaking the total bandwidth in subbands we have sufficient room to allocate guard bands to help the separation by use of filters. In using contiguous filters the minimum guard band is 10% from the centers of the two filters. Band R1's center is 28.375 and band R2's center is 30.125. The frequency separation between these two centers is 1.75 MHz and 10% of this is 0.175 MHz of which 0.0875 is subtracted from R1 and the same amount from R2. Then the bands are modified to be from 27.5 to 29.1625 GHz for R1 and from 29.3375 to 31 GHz for R2.

The R1 band in Figure 5.1-4 shows there is a low frequency band of 94 MHz containing the services of SMA, SSA, and TT&C. Then from 27.94 to 28.629 GHz there are five WSA services. Next from 28.629 to 28.836 GHz there is KSA2, followed by KSA1 from 28.836 to 29.043 GHz. And finally LSA service from 29.043 to 29.25 GHz.

Figure 5.1-4 contains an expansion of the previous scale for the 94 MHz. Here at the low frequency edge we have allocated 4 MHz (to be discussed later). The two SSA services are shown: SSA2 from 27.504 to 28.549 and SSA1 from 27.549 to 27.594 GHz. Figure 5.1-4 also addresses the 4 MHz, indicating that there are two 50 kHz SMA services located from 27.5 to 27.5005 and from 27.5005 to 27.501 GHz, and one 3 MHz TT&C service from 27.501 to 27.504 GHz.

The separation from one bandwidth to the other is done differently depending on the service bandwidth. The specific separation from R1 and R2 is implemented either by contiguous filters in a diplexer or by means of an isolator and two separate filters (tradeoffs to be done at a later time by filter designers). For the purpose of this discussion a diplexer is assumed. One of the outputs is to be used for the crosslink and then to ATDRS 2 and the other to be used for ATDRS 1.

Figure 5.1-5 is a block diagram illustrating how the signals are separated and shows the equipment needed to perform this separation. The division to bands R1 and R2, which is done by the input multiplexer A, is shown. The signal R1 is downconverted and then split to nine, as shown in Figure 5.1-4. The nine services are LSA, KSA1, KSA2, five WSAs, and the 94 MHz band. This splitting is done in multiplexer B and will be described later. The mixer LO will determine the actual downconverted frequencies. At this time they are not finalized, but for the purpose of describing the principle, they are assumed to be from 8.00 to 9.75 GHz. Since the bandwidth is large, one mixer may not be able to handle it and two or more mixers may be needed, but to illustrate the principle we will continue with the nine bands:

94 MHz BW	from 8.000 GHz	to	8.094 GHz		94 MHz
5 WSAs	from 8.094 GHz	to	9.129 GHz	250 Mbaud	1035 MHz
KSA2	from 9.129 GHz	to	9.336 GHz	50 Mbaud	207 MHz
KSA1	from 9.336 GHz	to	9.543 GHz	50 Mbaud	207 MHz
LSA	from 9.543 GHz	to	9.750 GHz	50 Mbaud	207 MHz

The eight services will be discussed shortly, for now we will continue with the 94 MHz band that contains a 4 MHz band and two services SSA2, SSA1, as shown in Figure 5.1-4. The frequencies are indicated above. To help the filtering process the signals are again downconverted and again the frequency is not finalized but for the sake of illustrating the principle assume the frequency is now at 1.7 GHz. The splitting is done in multiplexer C, which will be explained, and the new frequency bands after the downconversion are:

4 MHz	from 1.700 GHz	to	1.704 GHz		4 MHz
SSA2	from 1.704 GHz	to	1.749 GHz	11 Mbaud	45 MHz
SSA1	from 1.749 GHz	to	1.794 GHz	11 Mbaud	45 MHz

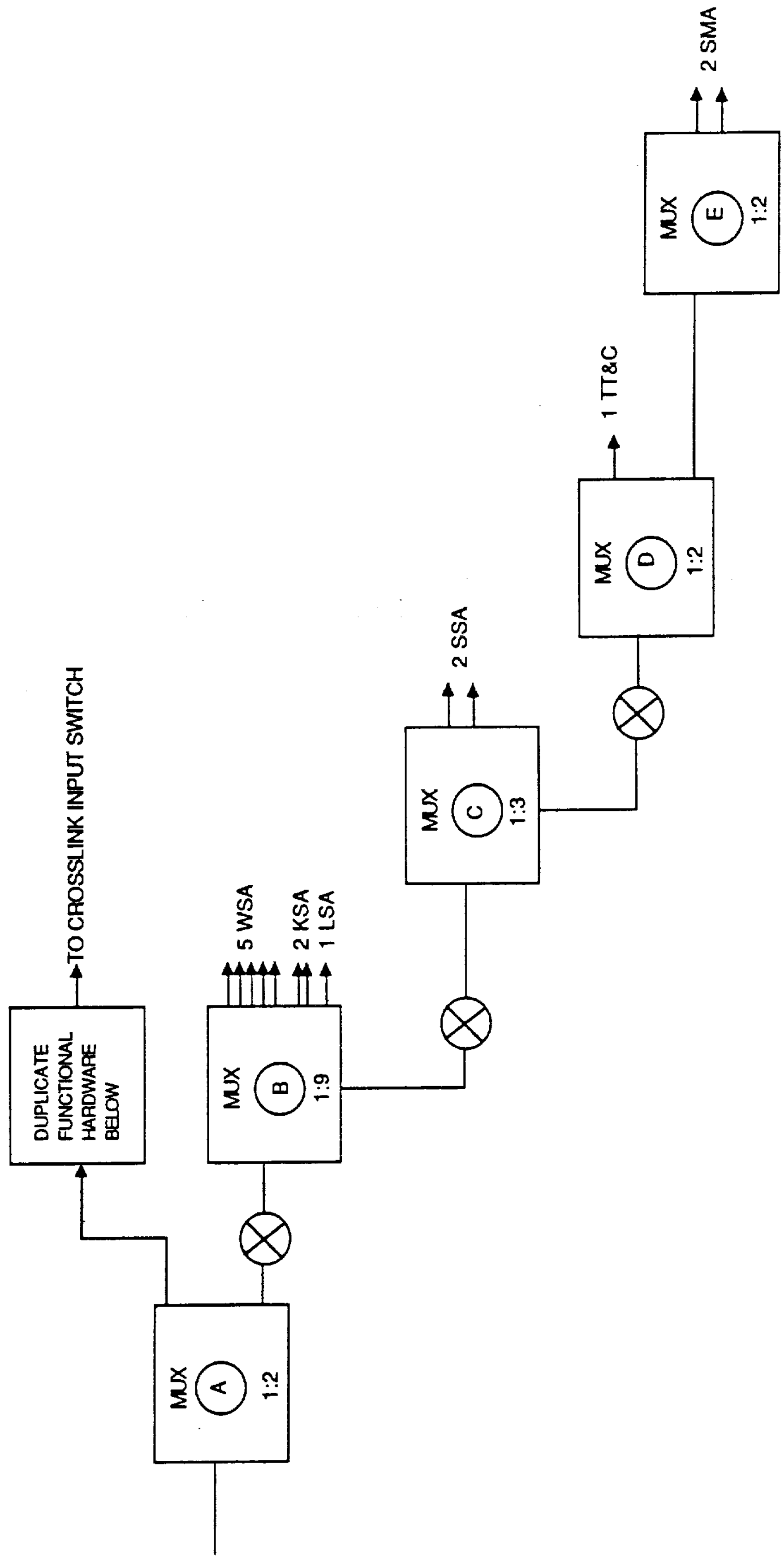

Figure 5.1-5. Forward Services Ground-to-Space Overview

The 4 MHz band also contains SMA1, SMA2, and TT&C. Once more we downconvert to a frequency to be determined later but assumed here as 250 MHz and split to three in multiplexer D then the frequency bands are now:

SMA1	from 250.00 MHz	to	250.50 MHz	10 kbaud	500 kHz
SMA2	from 250.50 MHz	to	251.00 MHz	10 kbaud	500 kHz
TT&C	from 251.00 MHz	to	254.00 MHz	500 kbaud	3000 kHz

The widest band of these three services is demodulated and directed to the command decoder and is used to perform the commands of ATDRS 1. The other output of the hybrid D is once again split in hybrid E and the two SMA services are separated by SAW filters. The separation of all signals has been accomplished and it can be seen how they can be routed for transmission to the users.

Figure 5.1-5 is an overview of the splitting and to be able to follow the signals to the transmitter each portion is presented in a separate figure, basically covering the forward switch. Figure 5.1-6 shows the details of the splitting at multiplexers A and B. At multiplexer B there are nine services. We have discussed the ninth and now we address the eight others, which are five WSAs, KSA2, KSA1, and LSA. (The frequency we suggested was temporarily 8 to 9.75 GHz.) At this time refer to Figure 5.1-7 which shows the continuation of the processing of the channels. Out of the eight outputs five are WSA, 2 KSA and one LSA. There are seven groups like this. Five WSA lines serve as input to a 5 by 5 matrix where any input can be directed to any output. The first output of each of the seven groups serves as input to the WSA 7:1 switch. There are five switches WSA 7:1 producing five outputs. Next in line is the WSA 3:1 switch where three signals can arrive from different places - one from ground, one from the crosslink, and one from space-to-space link. Only one out of the three is selected. There are five such switches. The last one in this chain is a WSA 5:5 switch. There is only one of them and the signals at its output are directed to the WSA transmitters.

Figure 5.1-7 also shows the KSA services in multiplexer B. Immediately after the multiplexer there is a KSA 2:2 switch that allows selection of KSA1 or KSA2 at any of the outputs. Seven groups of these switches exist from the seven ground stations. Next there are two KSA 7:1 switches. Following these there are two KSA 3:1 switches. The three inputs originate from the ground links, from the crosslink, and from space-to-space links. Finally the chain terminates with one KSA 2:2 switch and the output goes to the KSA transmitters.

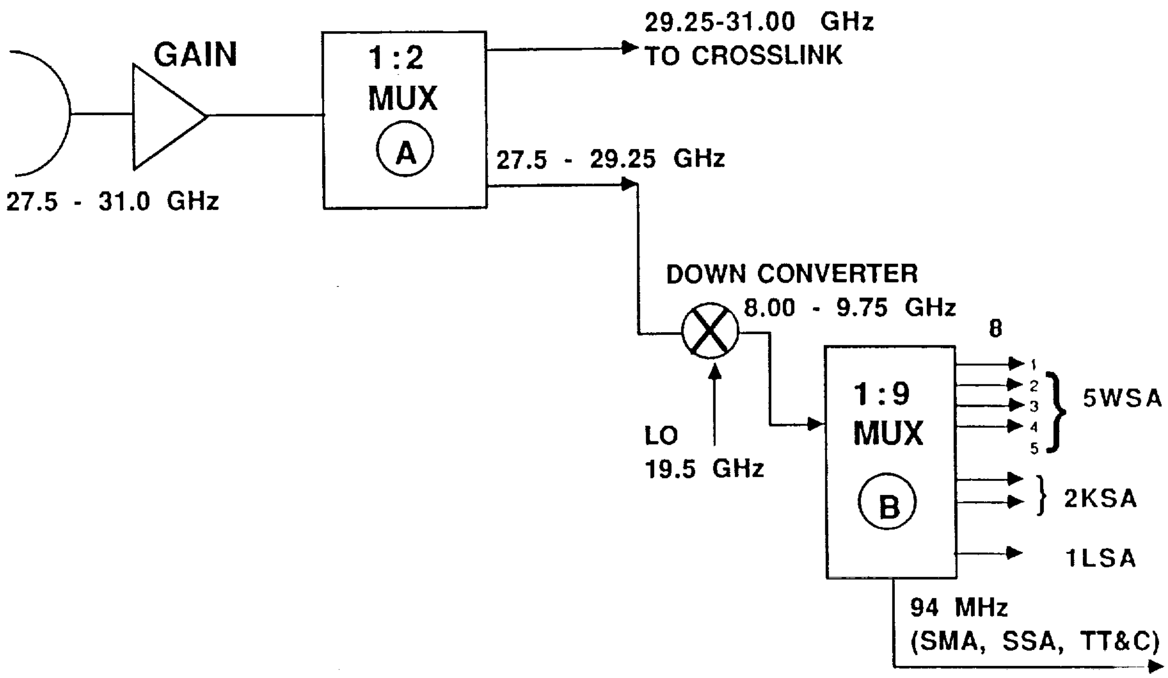

Figure 5.1-6. 26 Forward Services from Ground to TDRSS 1

Returning to the B multiplexer, follow the LSA path. There is one LSA output from the multiplexer, but there are seven of them. One switch, the LSA 7:1, selects one out of the seven. Then the signal is applied to an LSA 2:1 switch - one input from ground and the other from the crosslink. From here the signal is directed to the LSA transmitter. In discussing the switching arrangements, the details of frequency conversion power levels bandwidths, etc. have been ignored.

The block diagram of Figure 5.1-8 shows multiplexer C. The 94 MHz band has been decomposed to one 4 MHz and two SSA services. The frequency was set tentatively to 1.7 GHz. The two SSA signals are applied to a 2:2 switch matrix, and there are seven such matrices. The number 1 output from each of them merge to a switch with seven inputs and one output. There are two 7:1 switches originating at the ground and two others are due to the space-to-space links. The ground and space signals are fed to a 2:1 switch and there are two such units. Another 2:2 switch provides cross-strapping capability, and these two outputs are directed to the antennas.

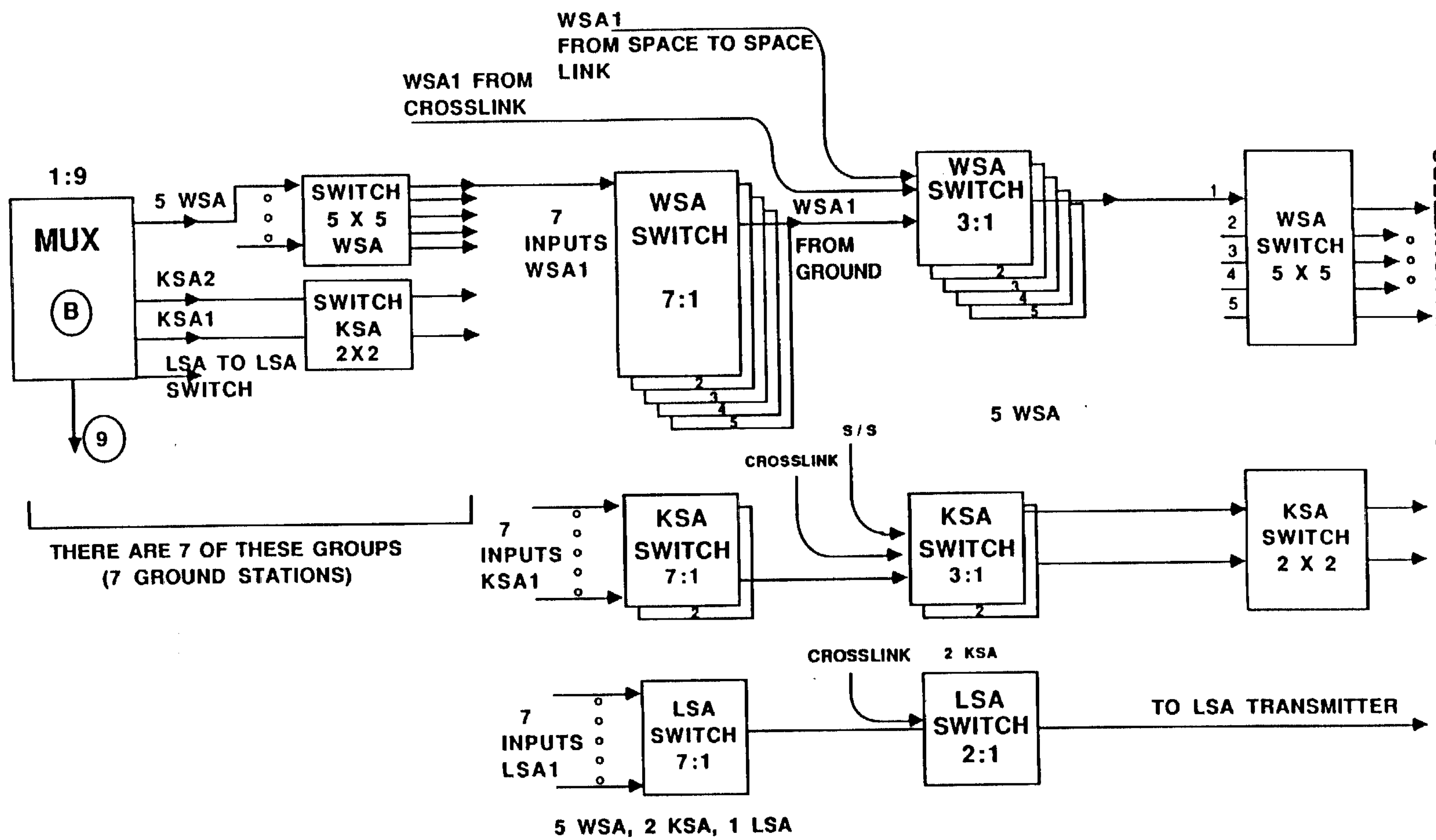

Figure 5.1-7. Expansion from Multiplexer B Forward Services

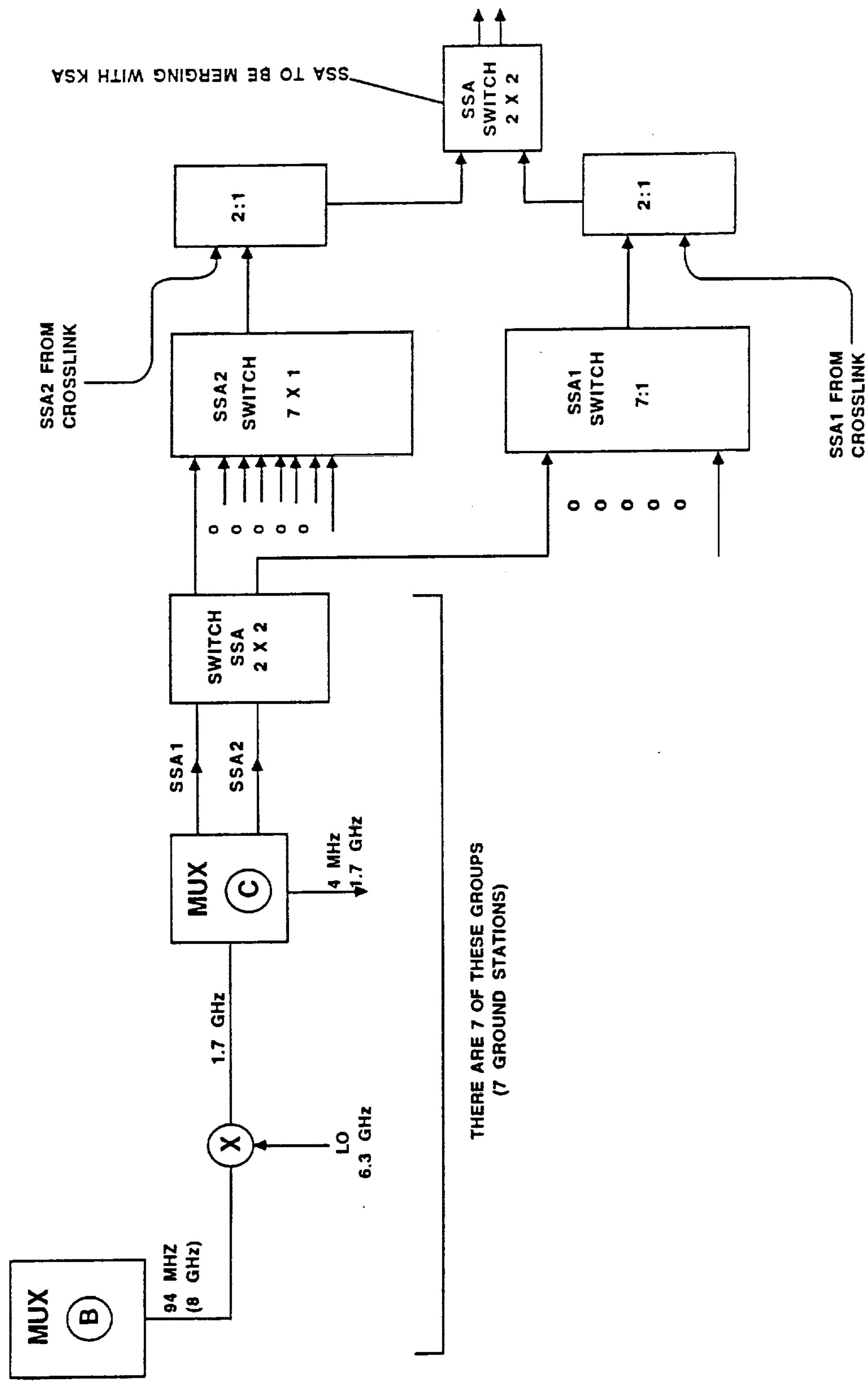

Figure 5.1-8. Expansion from Multiplexer C

The third output of multiplexer C is downconverted to a lower frequency such as 250 MHz as shown in Figure 5.1-9. At this frequency multiplexers are not very practical, thus hybrids are used. Hybrid D produces two outputs, one of which is for the TT&C service and is connected to the command receiver. The other output is split by another hybrid - one leg is a SAW filtered to obtain SMA2, and the second leg is filtered by another SAW filter to obtain SMA1. The two outputs are fed to a two-by-two switch matrix, there are seven such units. The number one output of each of these switches becomes input to a 7:1 switch; there are two of these units. Those services derived from the ground and those from the space-to-space link are brought to a switch of 2:1; there are two of these. Two outputs are applied to 2:2 switch providing cross strapping capability, and the two outputs are directed to the SMA antennas.

Although realization of the components is not part of this discussion, the following is a brief explanation. In the GHz frequencies diplexers or multiplexers are a way to separate different channels. As the frequencies are downconverted diplexers become too big and are replaced by other more suitable components as hybrids and SAW filters.

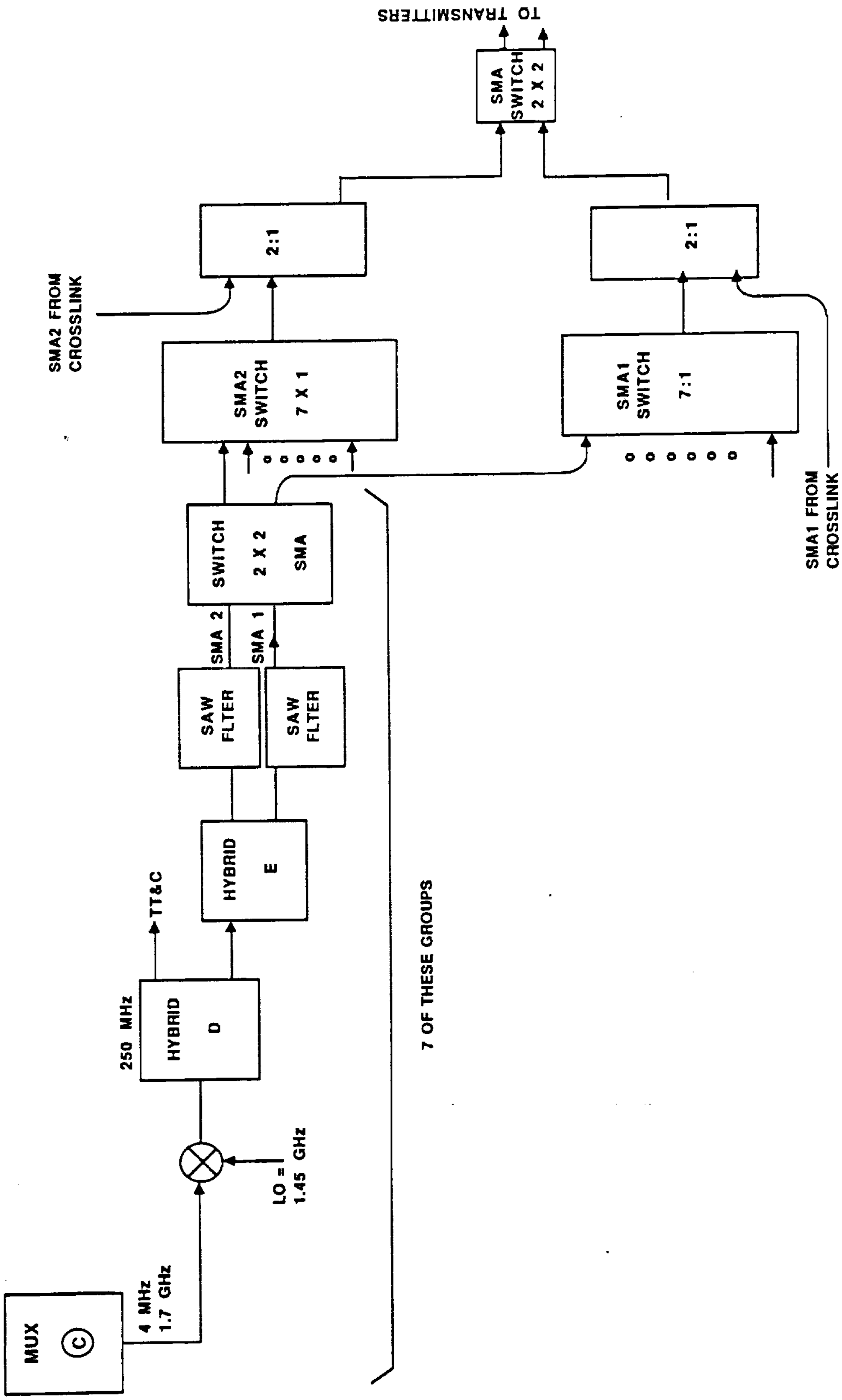

Figure 5.1-9. Expansion from Hybrid D

5.1.2 Return Switch

5.1.2.1 Return Links Frequency Bands Allocation. The return links are all positioned from 17.7 GHz to 21.2 GHz or a bandwidth of 3500 MHz (per SOW). The services to be provided per the SOW (See Table 2, p. 2-14) are 42. These services are split in two - one group is transmitted in one polarization and the other in the other polarization. This is done to be able to position all the services in the available frequency band in a way that they can be separated by filters. In the following discussion we are dealing with 21 services used for one polarization only. Information on these services is presented in Table 5.1-2.

Table 5.1-2. Return Links Frequency Band Allocation for one Polarization

Service	No. of Services	Max. Data Rate Mbaud	Total Mbaud
KSA	2	150	30
SSA	2	6	12
WSA	5	150	750
TLM	1	1.5	1.5
LSA	1	1000	1000
SMA	10	0.1	1
Total	21		2064.5

Since 3500 MHz are available for transmitting 2064.5 Mbaud, 1 baud can have 1.695 Hz. Figure 5.1-10 is a graphical presentation of the various services and the frequency allocations for each of them. This is for one polarization only. The other polarization has identical structure. For a quick reference the services and their allocated frequencies are tabulated here:

Service	Frequency (GHz)
LSA (1)	19.505 to 21.2
WSA (5)	18.23375 to 19.505
KSA (2)	17.72525 to 18.23375
SSA (2)	17.70491 to 17.72525
TT&C (1)	17.702368 to 17.70491
SMA (10)	17.7 to 17.702368

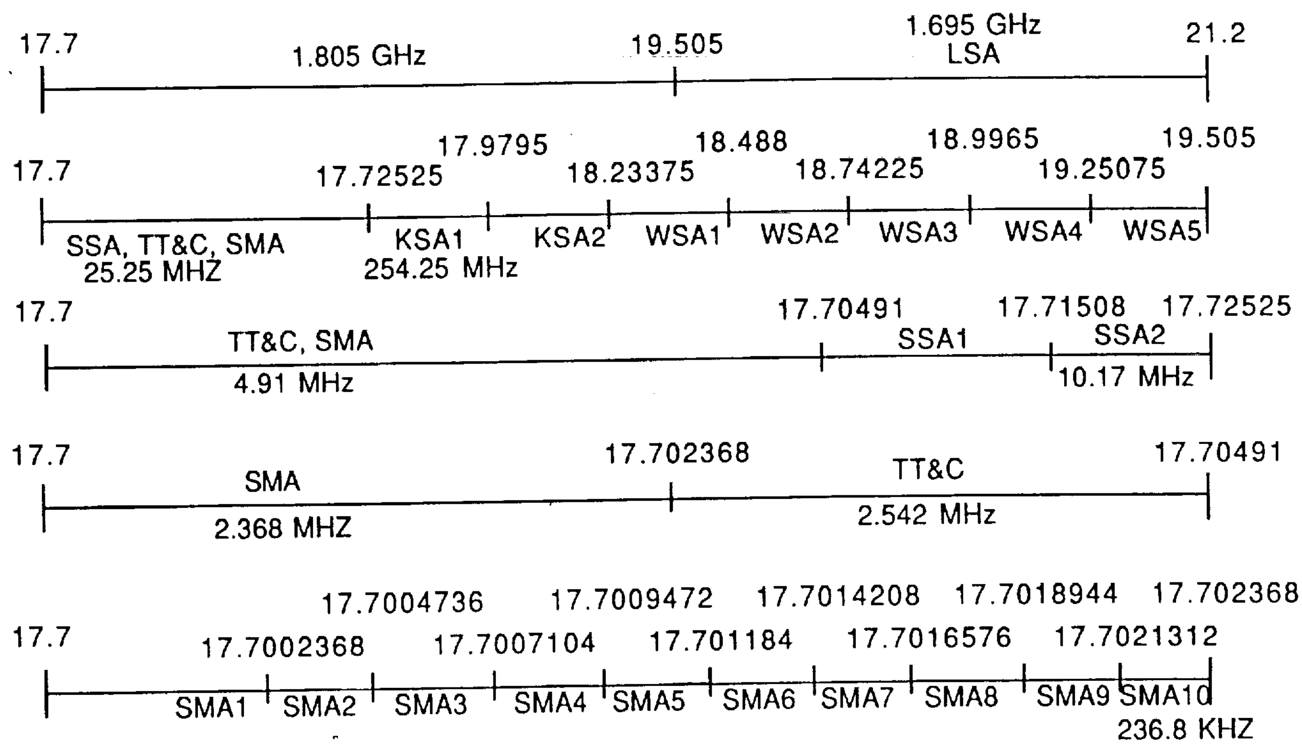

Figure 5.1-10. Frequency Plan, Ka-Band Downlink, 1 Baud/1.695 Hz
Dual Polarization Required

The return services we are about to describe are shown in the darkened areas of the overall block diagram of the switch, Figure 5.1-11a. Shown in Figure 5.1-11b is the inclusion of Ku-band uplinks/downlinks. In this subsection, the discussion is limited to the Ka-band. We are dealing with the received signals originating either from the users or from the crosslink. The destination of these signals are to the ground. From satellite 2, however, the signals arrive from the users and the destination is satellite 1 via the crosslink. The satellites' performance must be constantly kept in mind.

5.1.2.2 **Return/Downlink Description**. The detailed return/downlink switch functional partitioning is presented in Figure 5.1-12. On the left, there are two antennas serving KSA and SSA--one in the eastern and one in the western platforms. Next there are the WSA antennas providing five services, followed by the LSA antenna followed by the SMA antennas providing 10 services. We have included the TT&C which in return really services only telemetry - for ATDRS 1 directed to ground and for ATDRS 2 directed to the crosslink. The figure is very crowded, therefore we have enlarged the drawing of each of the services and described them separately.

Figure 5.1-13 is the enlarged portion of the KSA and SSA service. The incoming frequencies are converted by mixers to a nominal 10 GHz band (tentatively), but in such a way that KSA and SSA will not translate to the same frequencies. Instead they will be adjacent to each other so that they can be handled by the switches. After the mixer there is one switch 1:3 of which one output is directed to ATDRS 1 conducting the signals to ground; the second output is a connection with the Ku-band; and the third output is for operation of ATDRS 2, directing the signals either to crosslink or to space-to-space at point A1. Following the path of ATDRS 1 we have positioned hybrid combiners and splitters capable of providing both KSA and SSA at the same time. Then the signals are directed to a KSA1/SSA1 3:7 switch producing seven outputs destined to the seven ground stations. The A2 output provides connection to the space-to-space switch. KSA2 and SSA2 have exactly the same structure and will not be repeated.

Figure 5.1-14 contains the enlarged portion for the WSA services. Five incoming frequencies are downconverted to some IF of nominal 10 GHz (not finalized at this time). Following the mixer there is a switch 1:3 producing two possible paths: a horizontal to the ground, a second to the Ku-band, and a third for use by ATDRS 2 directing the signals to crosslink or space-to-space operation. Five switches output to one 5:8 switch of which seven outputs are directed to

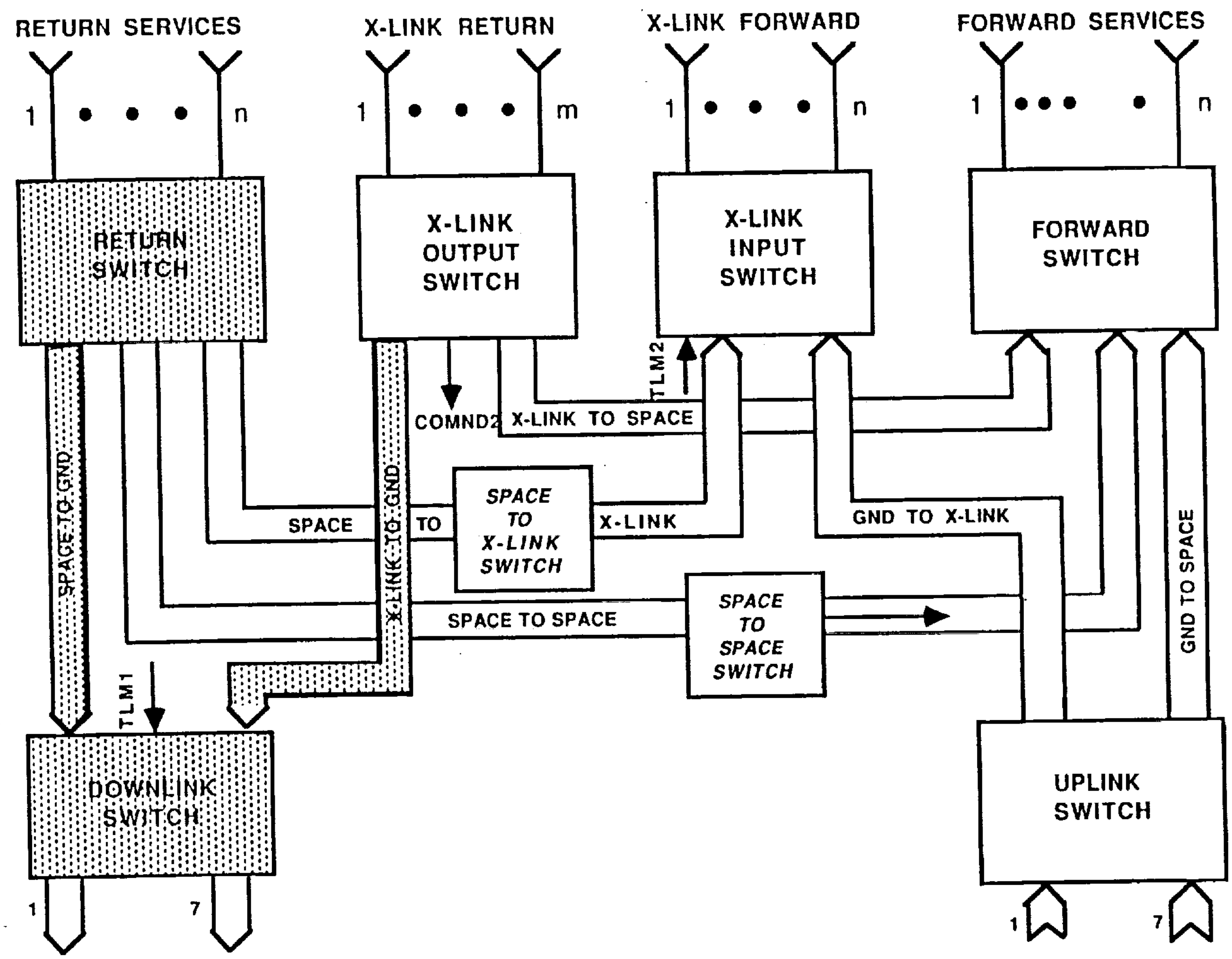

Figure 5.1-11a. Functional Partition of the Switch Subsystem

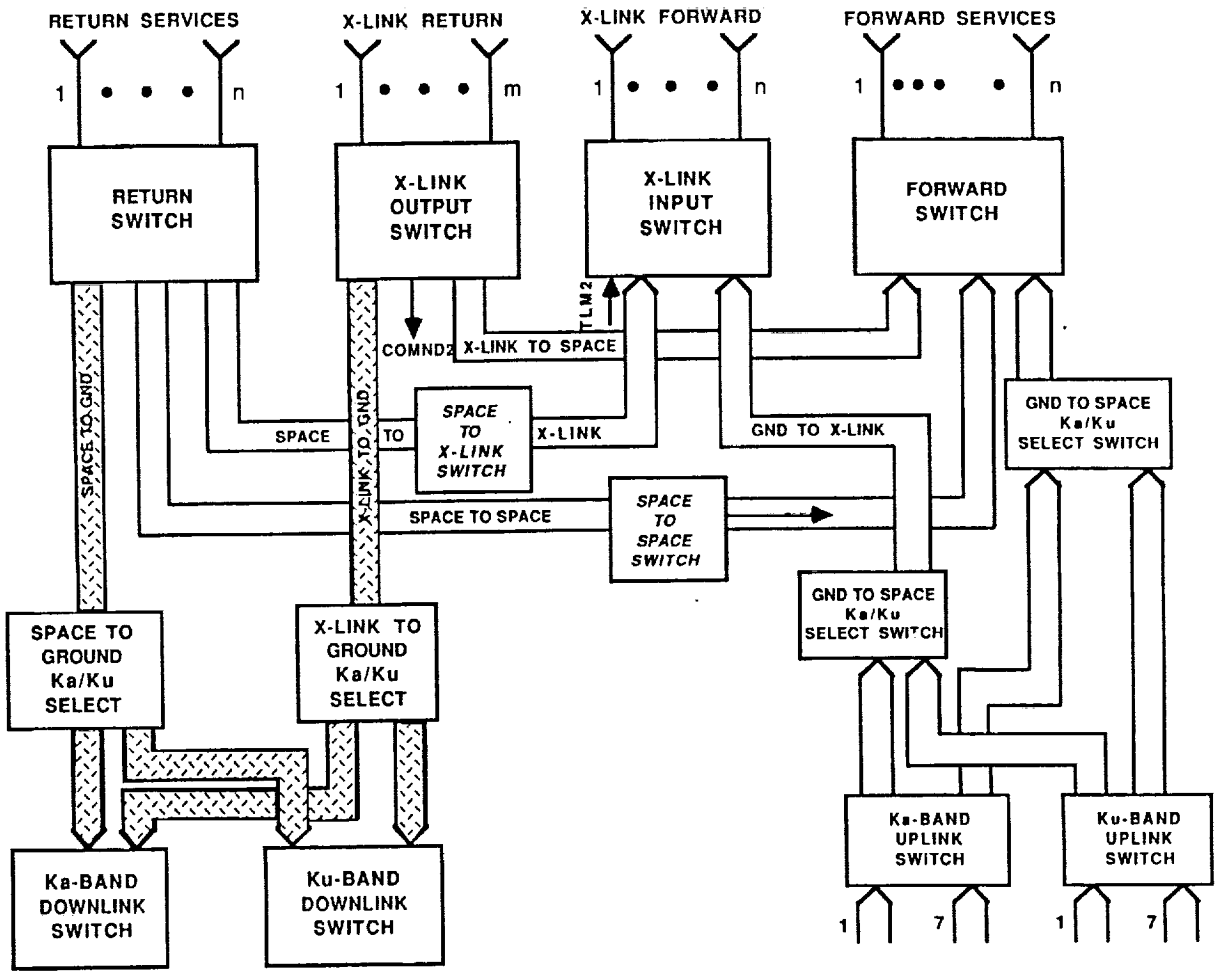

Figure 5.1-11b. Functional Partition of the Switch Subsystem

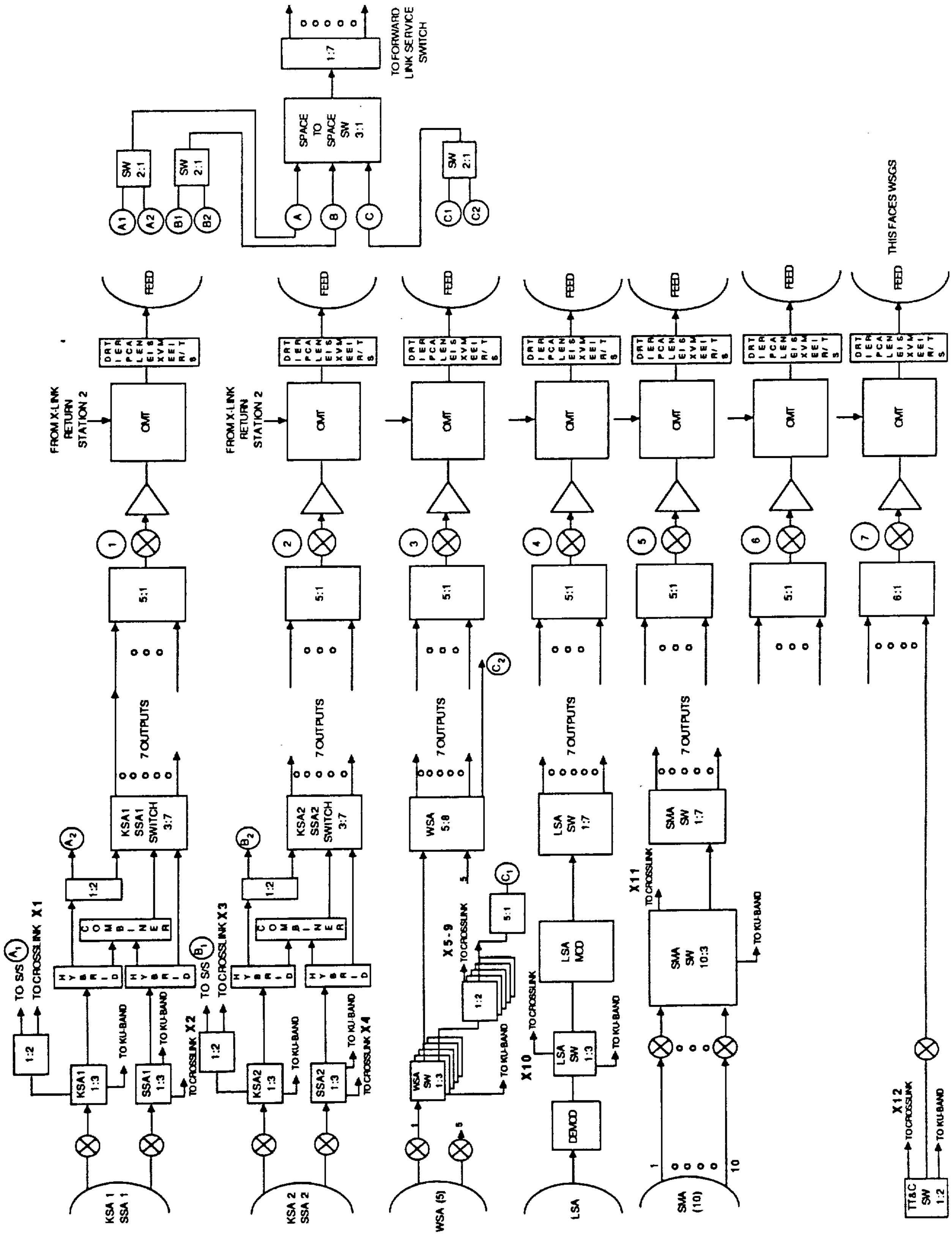

Figure 5.1-12. Ka-Band Return/Downlink Switch Overview

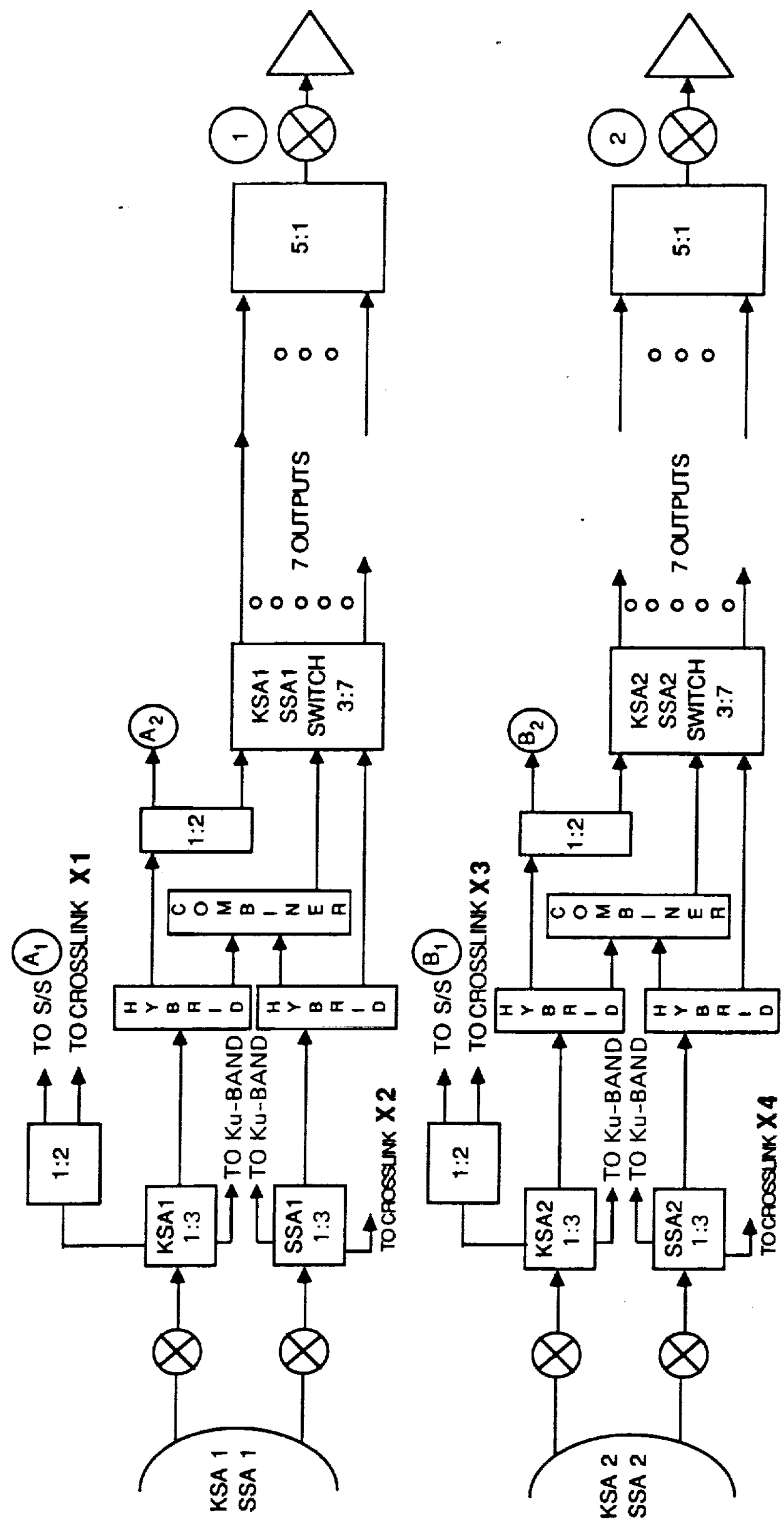

Figure 5.1-13. KSA and SSA Service (Enlarged View)

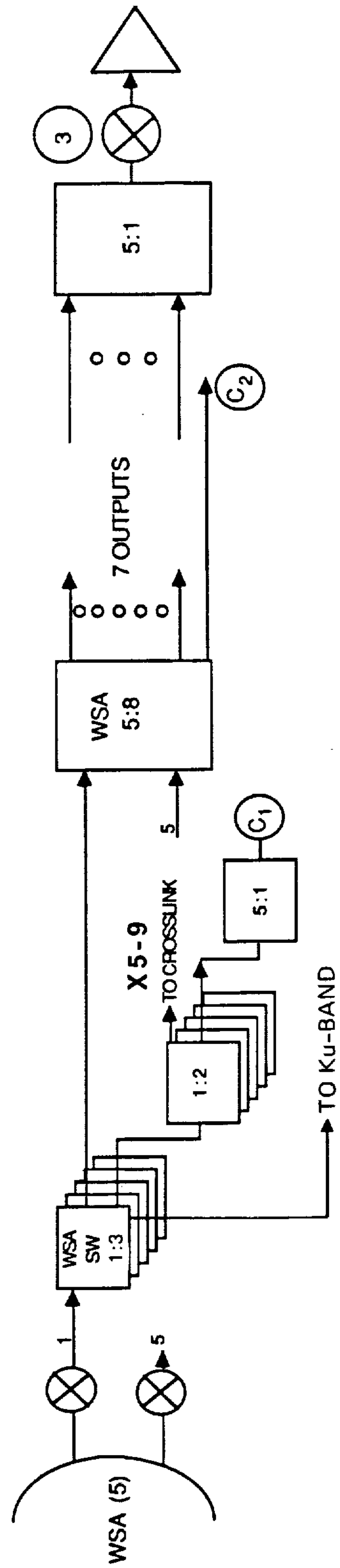

Figure 5.1-14. WSA Services (Enlarged View)

seven antennas, and the eighth is marked C2 intended to direct the signal to the space-to-space switch for ATDRS 1. For ATDRS 2, the input WSA switch 1:3 selects the lower leg to another 1:2 switch. The connection in the top selects the crosslink (five outputs) and the five connections in the bottom merge together in a 5:1 switch with a C1. This continues to the space-to-space switch.

Figure 5.1-15 describes the LSA service. The signal from the antenna is demodulated and the baseband derived. A 1:3 switch splits the signal, directing one signal to the crosslink, the second to Ku-band, and the third after the modulator, to a 1:7 switch. Thus seven outputs are generated.

Figure 5.1-16 is the enlarged diagram describing the SMA services. The antennas receive signals at the same frequency and with the help of the mixers the different services are FDM, placing the 10 channels of information next to each other in the frequency scale. In the combiner all these signals are summed; thus we have one cable with all 10 services. A 1:2 switch selects the signals to send to the crosslink to Ku-band or to the 1:7 switch to be directed to ground.

The TT&C service really provides only telemetry. It is shown in Figure 5.1-17. The signal originates in the command and telemetry portion of the satellite. In ATDRS 1 the TLM signals are modulated and directed to be transmitted to the ground. If, however, TLM is generated in the ATDRS 2, the 1:3 switch directs the signals to the crosslink and to the Ku-band.

At this time we have 5 sources, each one with 7 outputs for a total of 35 connections. At this interface we have provided 7 switching matrices, each having 5 inputs for a total of 35 inputs. The connection between these two groups is shown in the Figure 5.1-18. Seven outputs are created which, after suitable mixing and power amplification, go to the seven beams of the space-to-ground link. All 21 services are applied to an orthomode transducer (OMT) and directed to excite the antennas in one polarization. The other input to the OMT originates from the crosslink and has the same type of signals.

The symbol for power amplifier (usually meaning a single amplifier) is used to drive a separate antenna beam. This may not be the case and it is the topic of other studies.

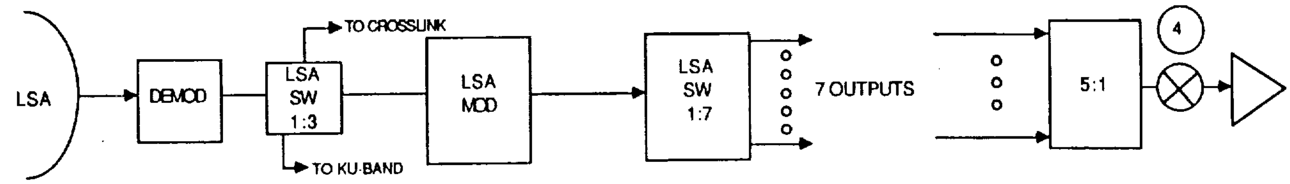

Figure 5.1-15. LSA Service

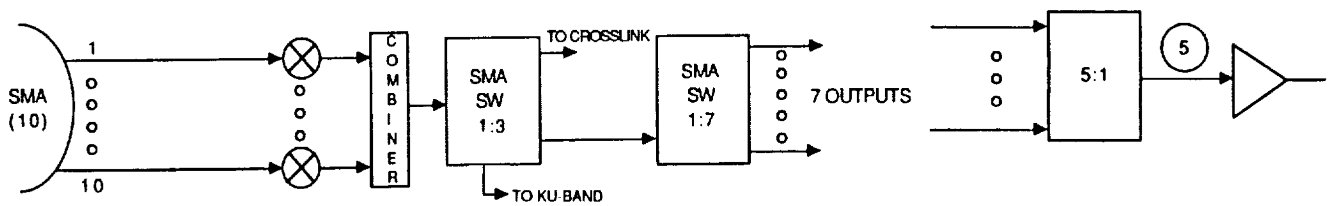

Figure 5.1-16. SMA Services

Figure 5.1-17. TT&C Service

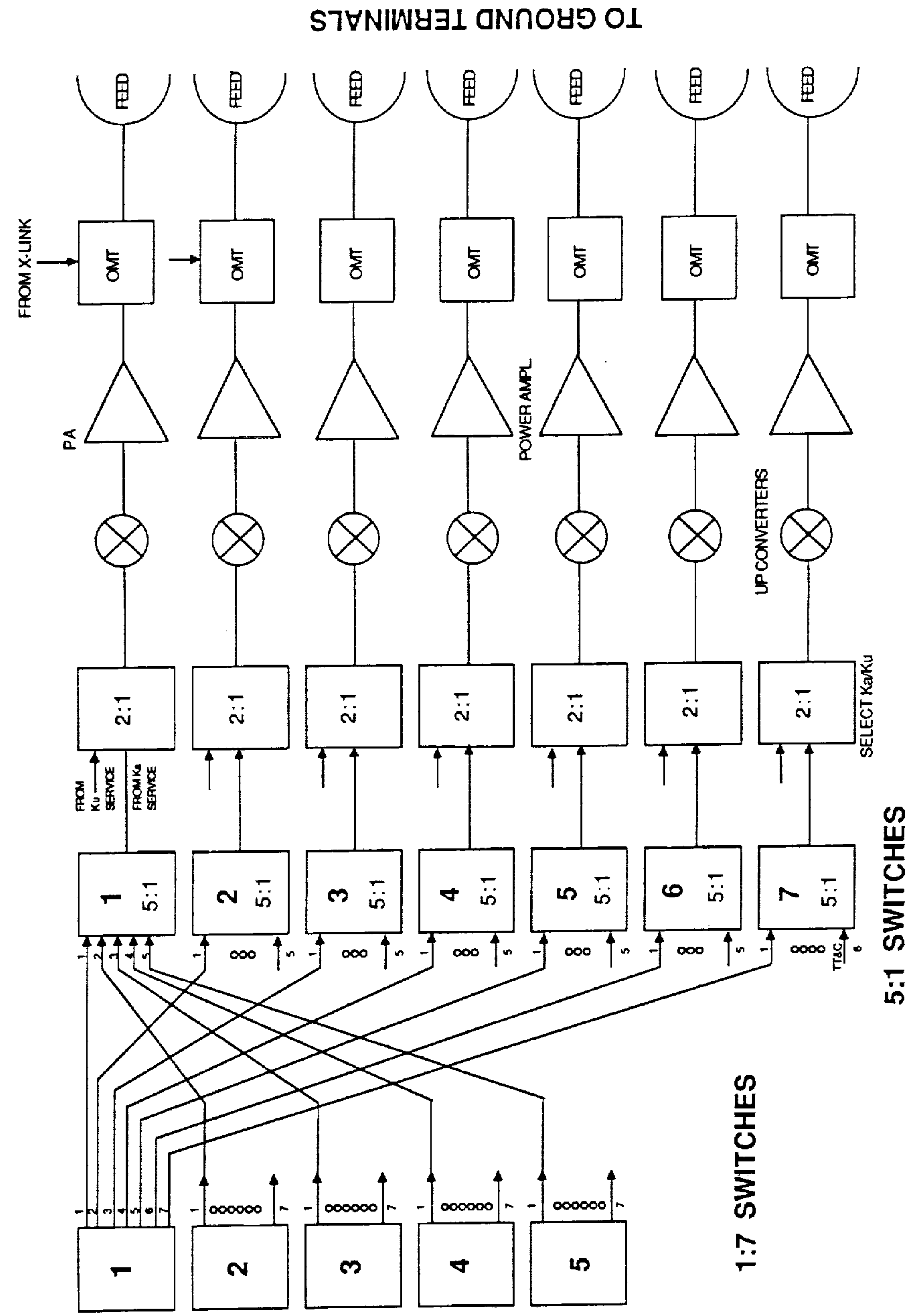

Figure 5.1-18. Downlink Interface and Output Portion

5.1.3 Crosslink Input Switch

The basic function of the crosslink input switch is shown in the shaded area of the functional partition of the switch subassembly (Figure 5.1-19). One group of services originating from the ground is directed to the crosslink - these are forward services. Other service groups coming from users in space are also directed to the crosslink - these are return services.

The 3.5 GHz band is split in half to provide the forward services. One half is used for the forward switch, which is decomposed in detail, and the other goes to the crosslink as indicated. In the latter portion, there are 13 services LSA, 5 WSA, 2 KSA, 2 SSA, 2 SMA and 1 CMD. All these services are first decomposed exactly as in the first portion. For the decomposition of the crosslink switching functions, refer to the baseline block diagram shown in Figure 3 (p. 1-5) of the SOW, which indicates demodulation, baseband multiplexing, and remodulation for transmission on the crosslink. As Figure 5.1-20 shows, each of the signals is first demodulated; thus the baseband of each service is derived. These signals are then multiplexed and positioned in a way to form a very large baseband and then modulates to the frequency of the crosslink (usually 60 GHz). Additional studies will reveal if this is the best method to be used.

The return data links provide 21 services; 1 LSA, 5 WSA, 2 KSA, 2 SSA, 10 SMA, and 1 TLM. These services are received by the satellite, then directed to the crosslink. The signals are first demodulated, then multiplexed, and then modulated.

Forward and return services are applied to a 2:1 switch (operating at 60 GHz) where one only is selected, power amplified, and applied to the antenna.

5.1.4 Crosslink Output Switch

The same signals transmitted on the crosslink by one of the ATDRS satellites are received by the other. The shaded area in Figure 5.1-21 shows the main paths. The forward signals are directed towards the users and the return signals are directed to the downlink.

Figure 5.1-22 shows the crosslink output switch structure. At the antenna input the signals are downconverted to avoid processing at very high frequencies. A switch of 1:2 selects forward or return service. Either way the signals are demodulated, demultiplexed, and remodulated to be positioned in the proper frequency and sent to their destination.

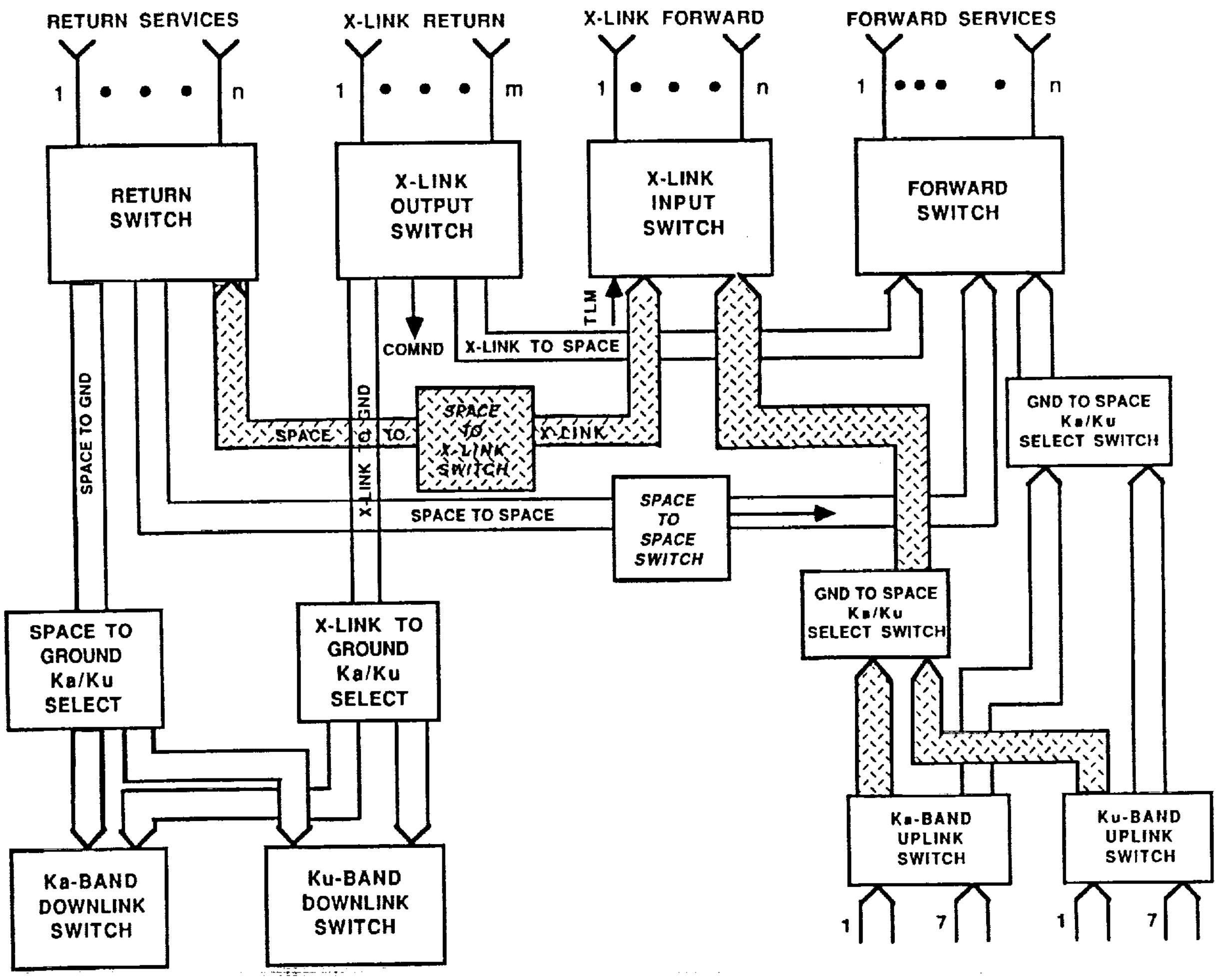

Figure 5.1-19. Functional Partition of the Switch Subsystem

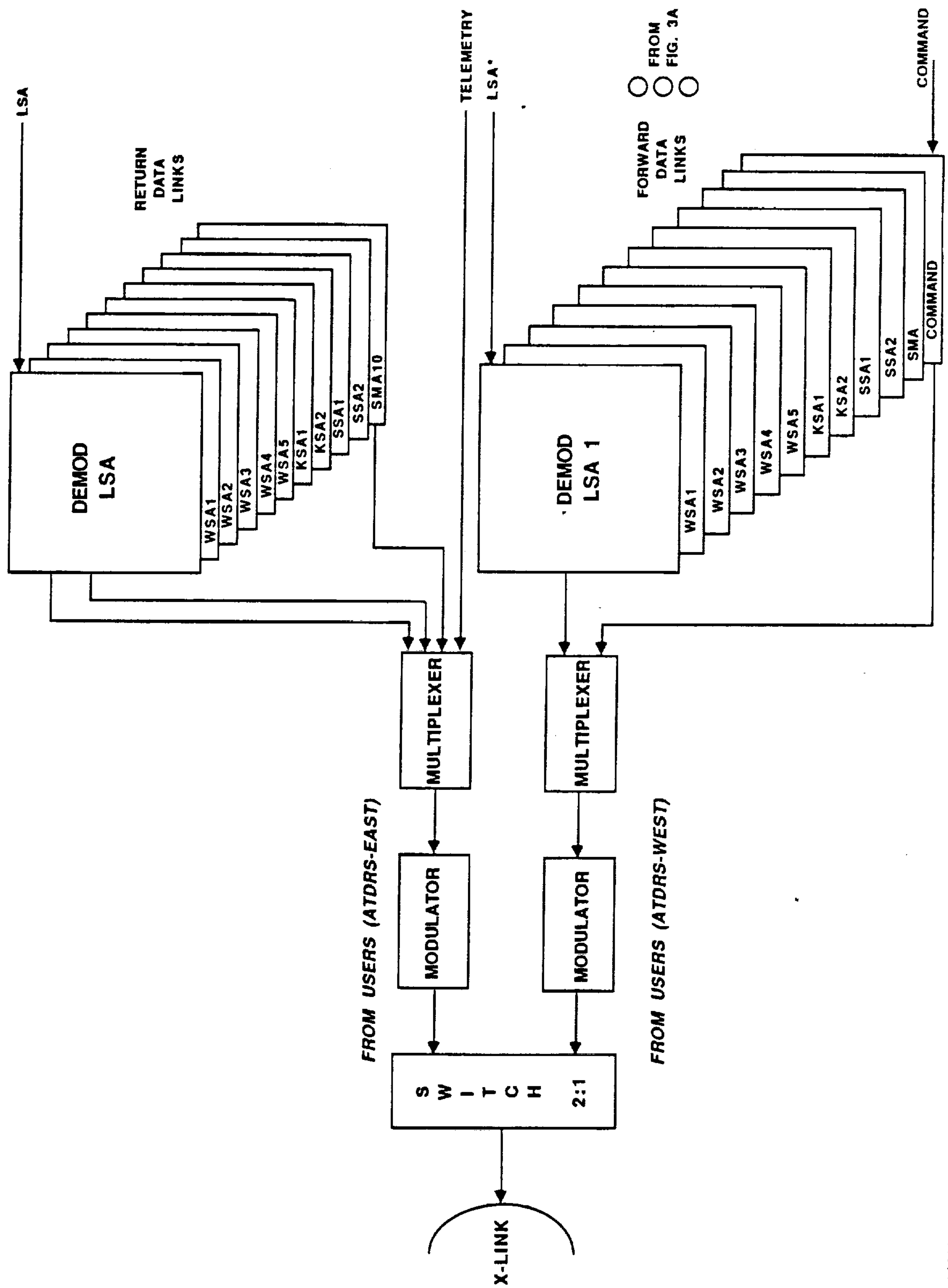

*HARDWARE AS IN UPLINK/FORWARD SWITCH DUPLICATED

Figure 5.1-20. Crosslink Input Switch

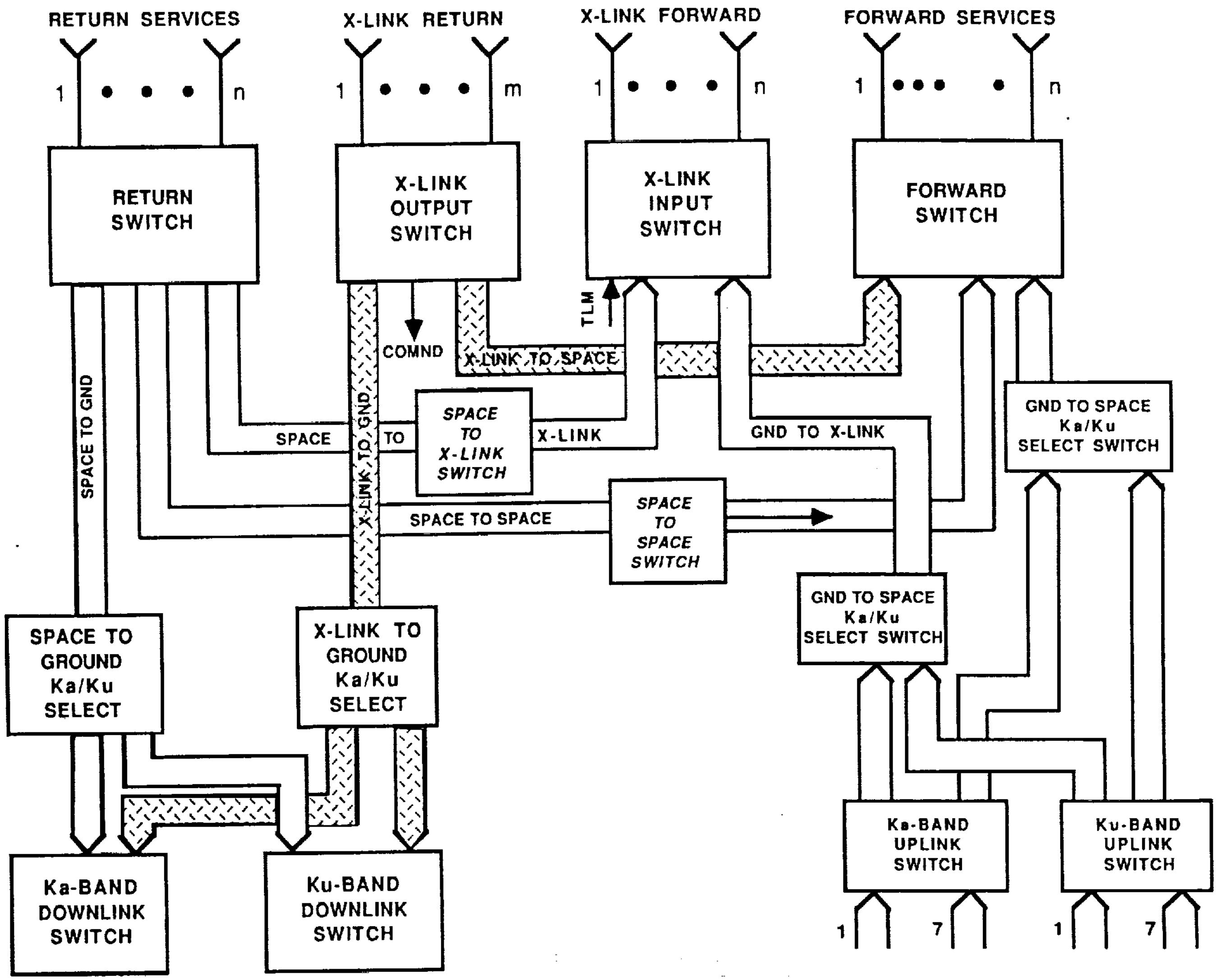

Figure 5.1-21. Functional Partition of the Switch Subsystem

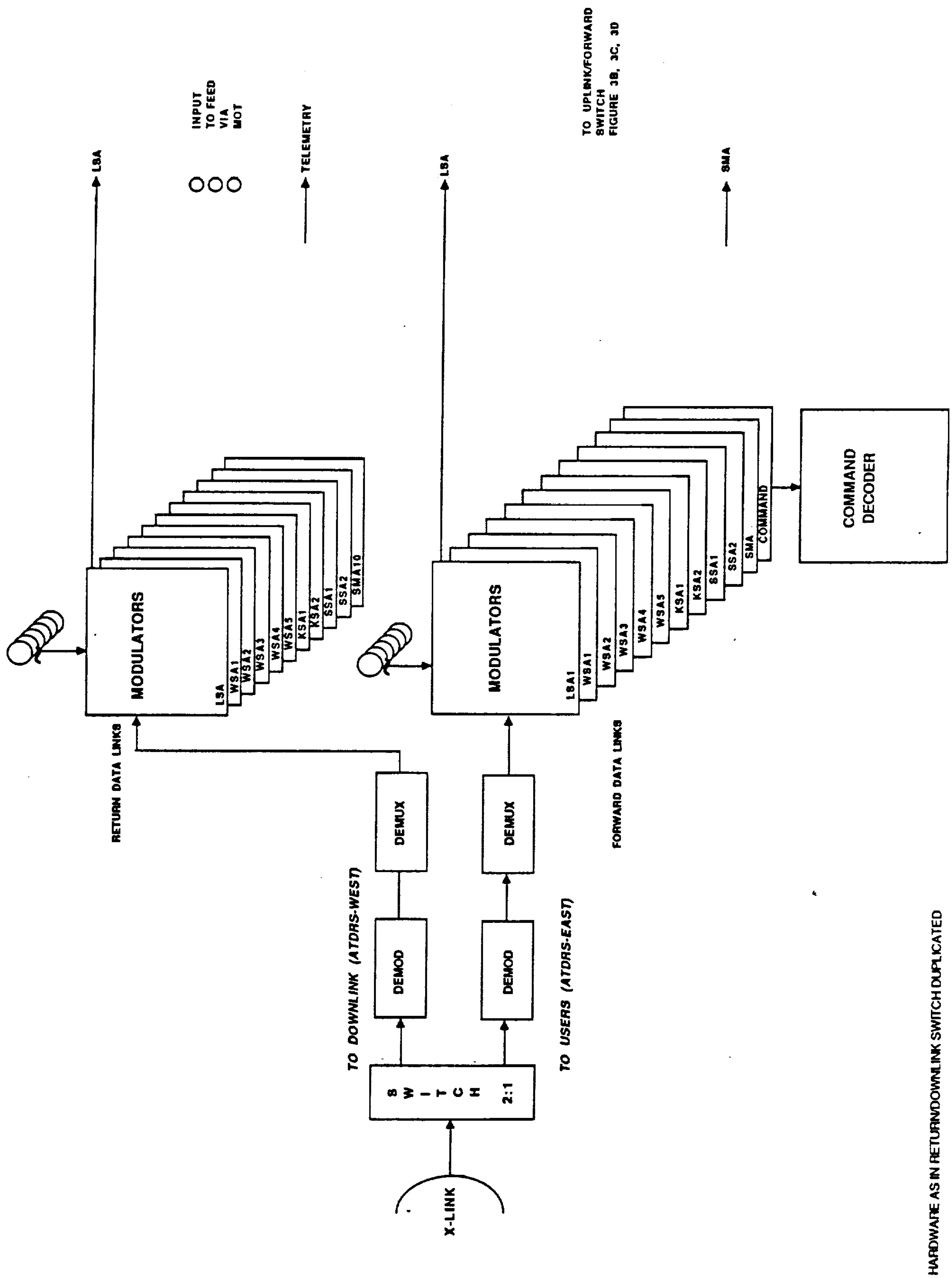

Figure 5.1-22. Crosslink Output Switch

5.2 FUNCTIONAL DECOMPOSITION OF THE Ku-BAND UPLINK/DOWNLINK SWITCHING SYSTEM

Frequency plans, developed in Section 2 for Ku-band uplink/downlink services, are used as a baseline for the functional decomposition of the switching subsystem. The aggregate transmission requirements necessitate the usage of dual antenna polarizations for both uplink and downlink services; the band allocation would be inadequate to provide all the services simultaneously in any given beam coverage area. The functional decomposition of Ku-band uplink/downlink services is described in this subsection.

5.2.1 Ku-Band Uplink Processing System Functional Decomposition

Table 5.2-1 shows the forward links data rate requirements for each of the two polarizations. The Ku-band frequency allocation for the uplink services (as per the SOW) is between the frequencies 14.6 and 14.83 GHz and between 15.15 and 15.35 GHz. This allocation is inadequate for accommodating the aggregate transmission requirements presented in Table 5.2-1. As illustrated by the frequency plan for Ku-band uplink services shown in Figure 5.2-1, this restricts the uplink simultaneous transmission of KSA/LSA/WSA uplink (forward) services to a maximum of five via the Ku-band allocation in any particular beam coverage area.

Table 5.2-1. Forward Links Frequency Band Allocation (for One Polarization)

Service	No. of Services	Max. Data Rate Mbauds	Total Mbauds
TT&C	1	0.5	0.5
SMA	2	0.01	0.02
SSA	2	11	22
KSA	2	50	100
WSA	5	50	250
LSA	1	50	50
Total	13		422.52

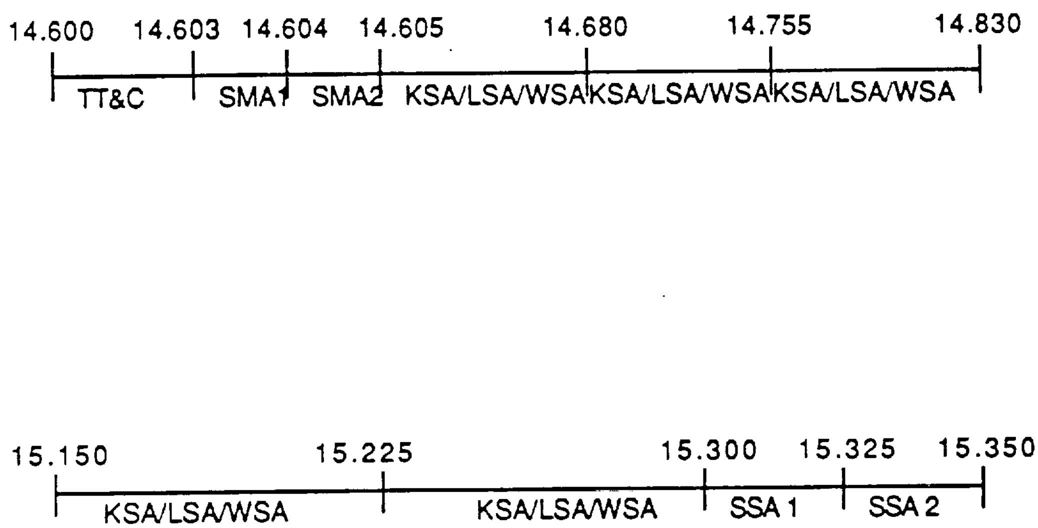

Figure 5.2-1. Frequency Plan, Ku-Band Uplink, Dual-Polarization Required, 1.5 Hz/Baud

A functional decomposition of the Ku-band uplink processing system is illustrated in Figures 5.2-2 through 5.2-7. Each of the seven Ku-band feeds from the seven-beam coverage multiple beam antenna is connected to an OMT, which separates the vertical and horizontal polarizations of the Ku-band signals. The horizontal polarization is nominally assigned for the ATDRS 1 communications. The vertical polarization serves the ATDRS 2 communications via an interface to the intersatellite crosslink communications subsystem. Signals in each of these polarizations pass through a diplexer, which isolates the received signals from the transmitted signals.

The received signals then pass through a low noise amplifier and a downconverter, which nominally downconverts to an IF of about 8 GHz. The input multiplexers separate the individual service channels from one another (note here that several stages of IF conversion and processing may be required for implementing this separation; these stages are summarized in the IF-processing blocks of the diagrams); each of the separated signals then passes through a 2:1 select switch, which selects the Ku- or Ka-band depending on the band of the uplink transmission in a given beam. A 7:1 select switch then selects a beam, determined by the beam of transmission

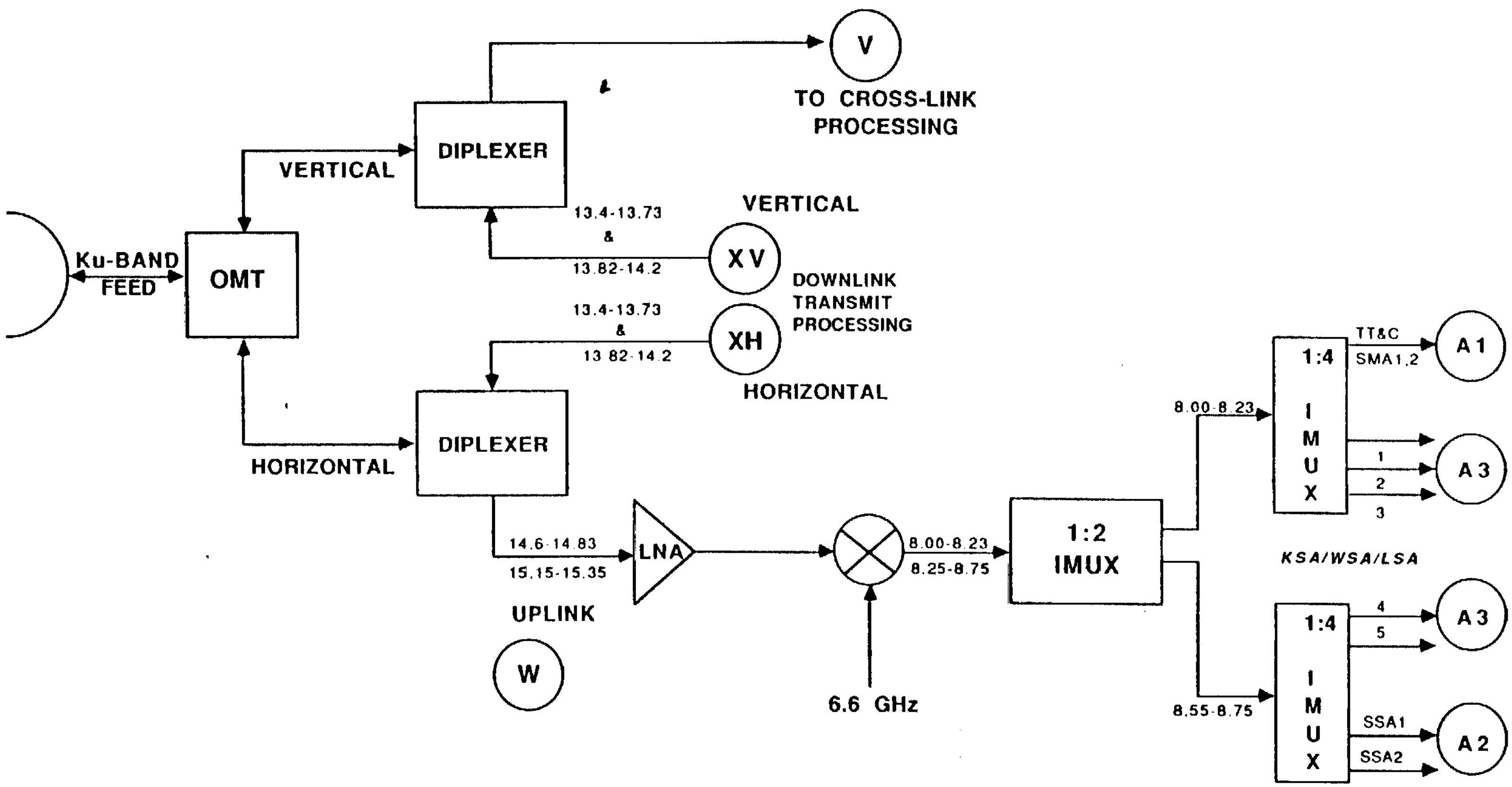

* FUNCTIONAL REPRESENTATION SHOWN HERE IS FOR PROCESSING ONE BEAM COVERAGE; THIS IS TO BE REPLICATED 7 TIMES FOR 7 BEAMS

Figure 5.2-2a. Functional Decomposition of Ku-Band Uplink Processing

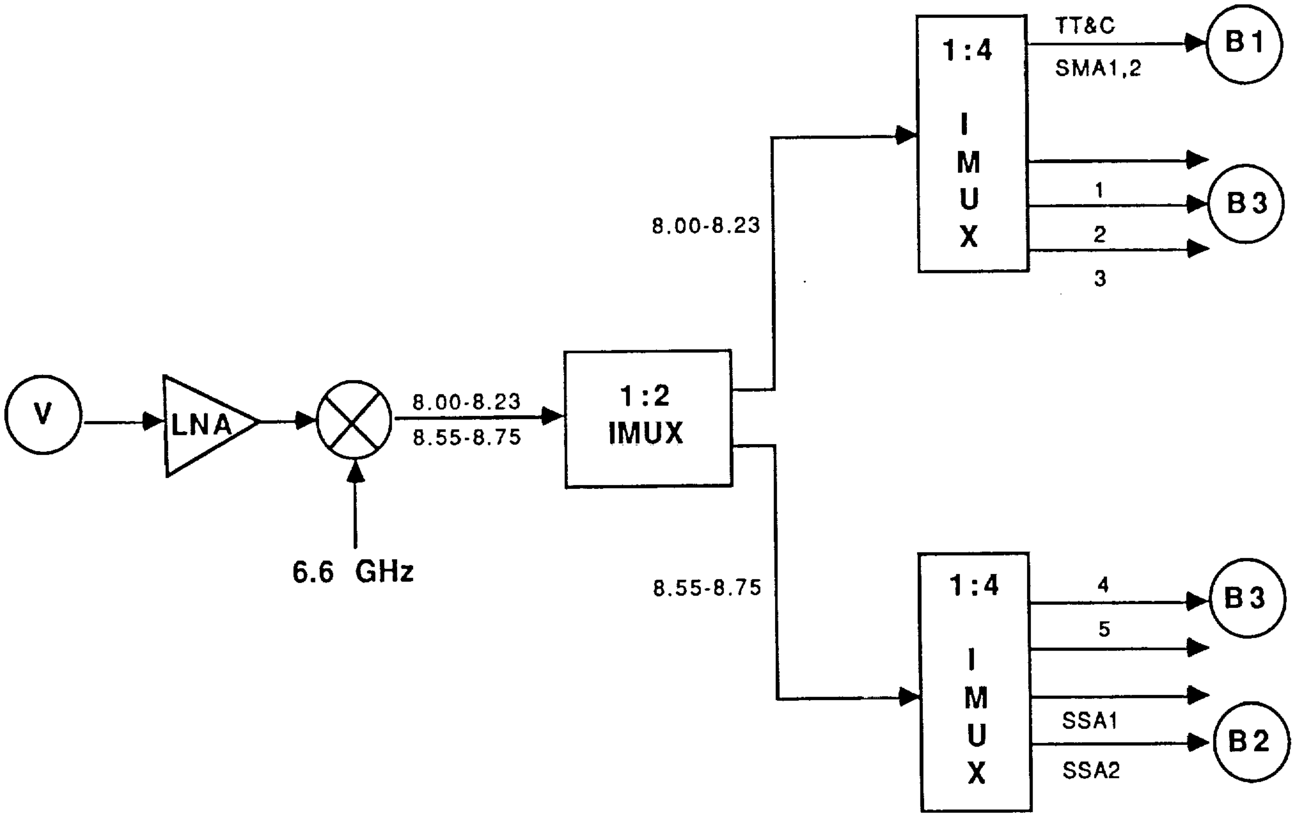

Figure 5.2-2b. Functional Decomposition of Ku-Band Uplink Processing

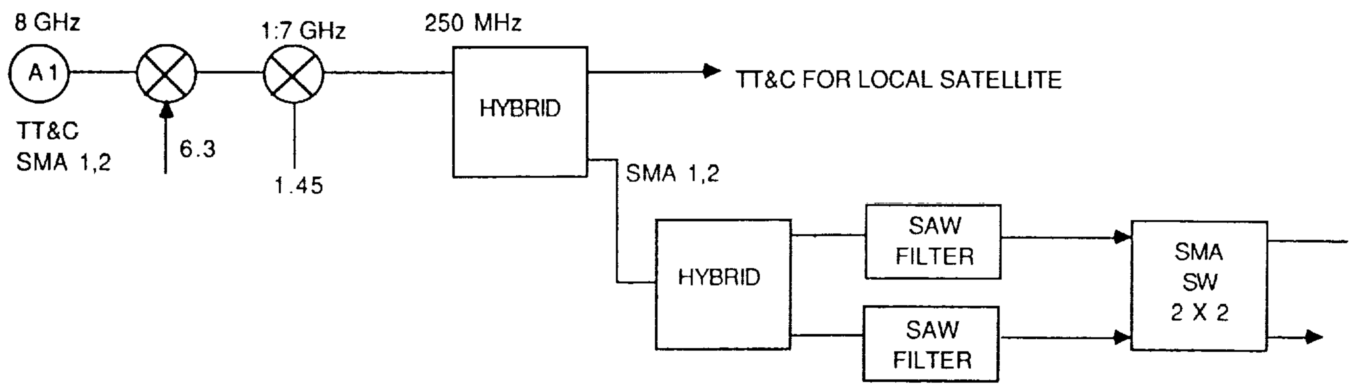

Figure 5.2-3a. Functional Decomposition of Ku-Band Forward Uplink - TT&C and SMA from A1

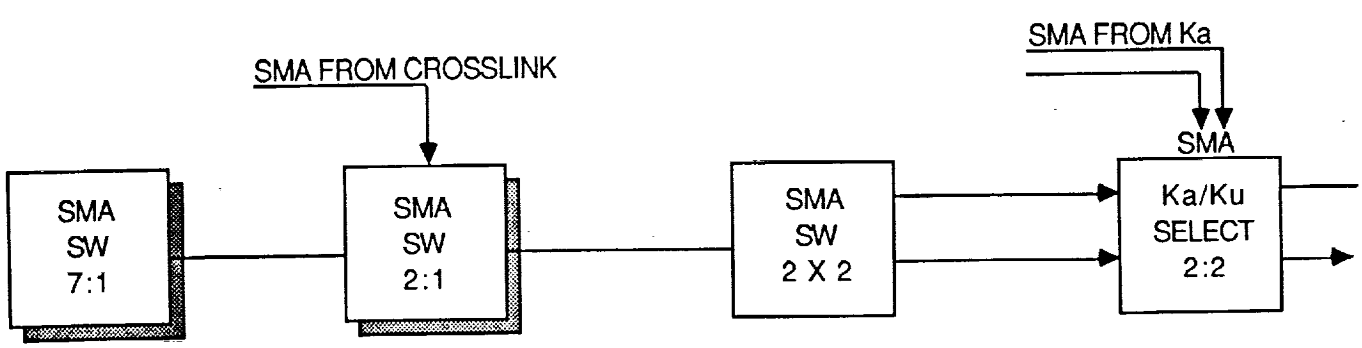

Figure 5.2-3b. Functional Decomposition of Ku-Band Forward Uplink - TT&C and SMA from A1 (Continued)

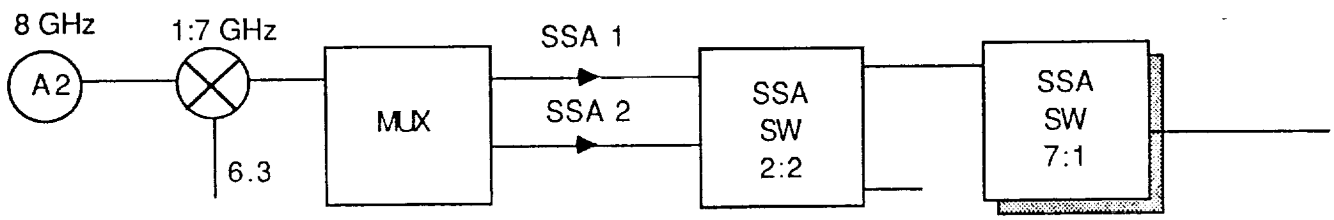

Figure 5.2-4a. Functional Decomposition of Ku-Band Forward Uplink - SSA from A2

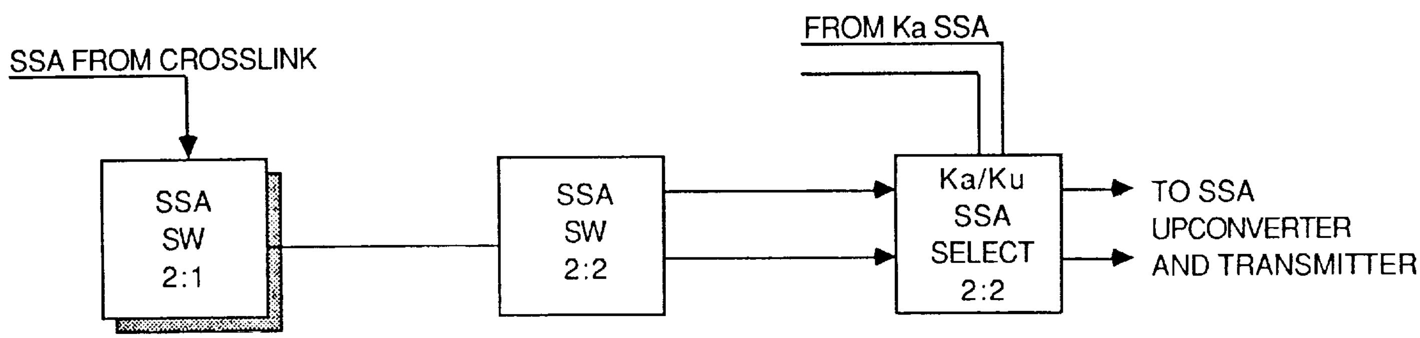

Figure 5.2-4b. Functional Decomposition of Ku-Band Forward Uplink - SSA from A2

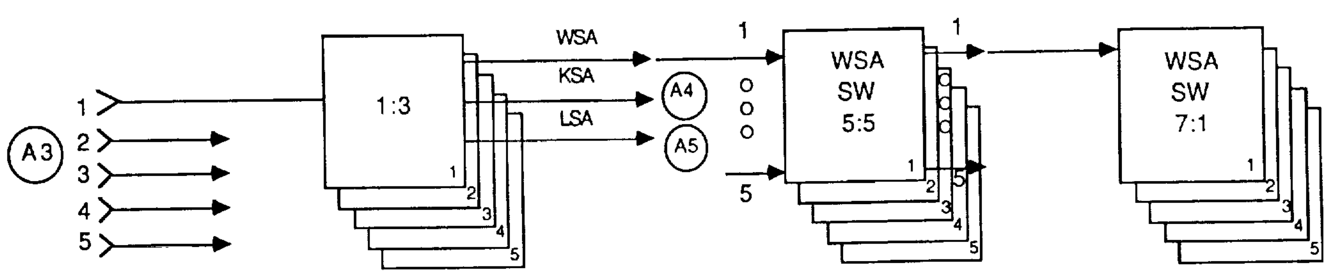

Figure 5.2-4c. Functional Decomposition of Ku-Band Forward Uplink - Continued from A3

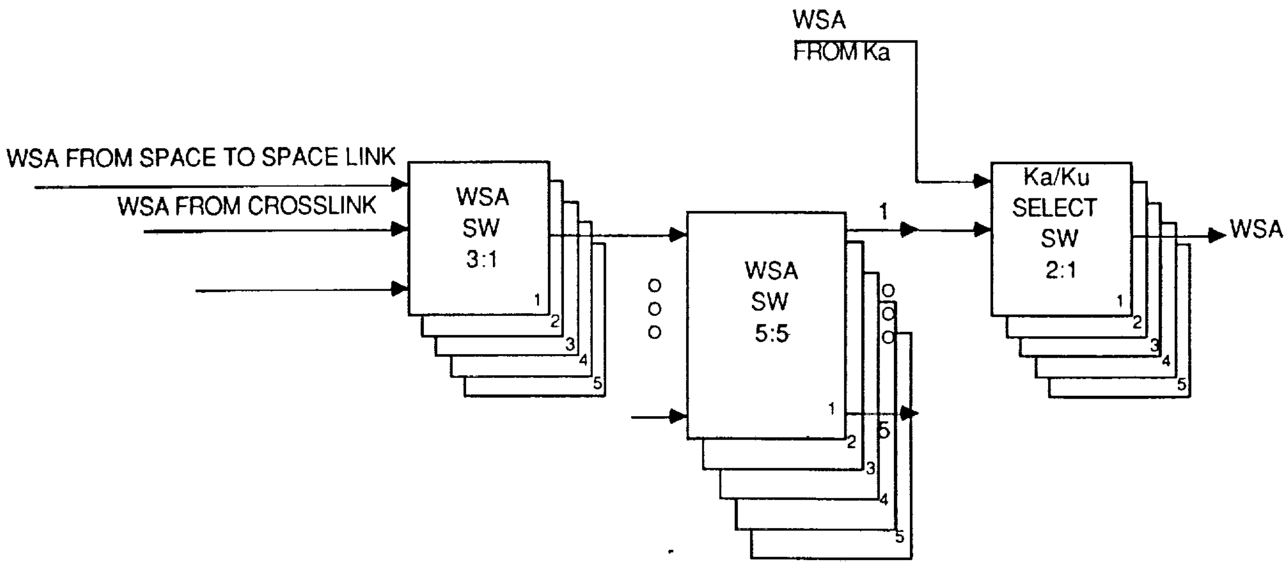

Figure 5.2-4d. Functional Decomposition of Ku-Band Forward Uplink - Continued from A3

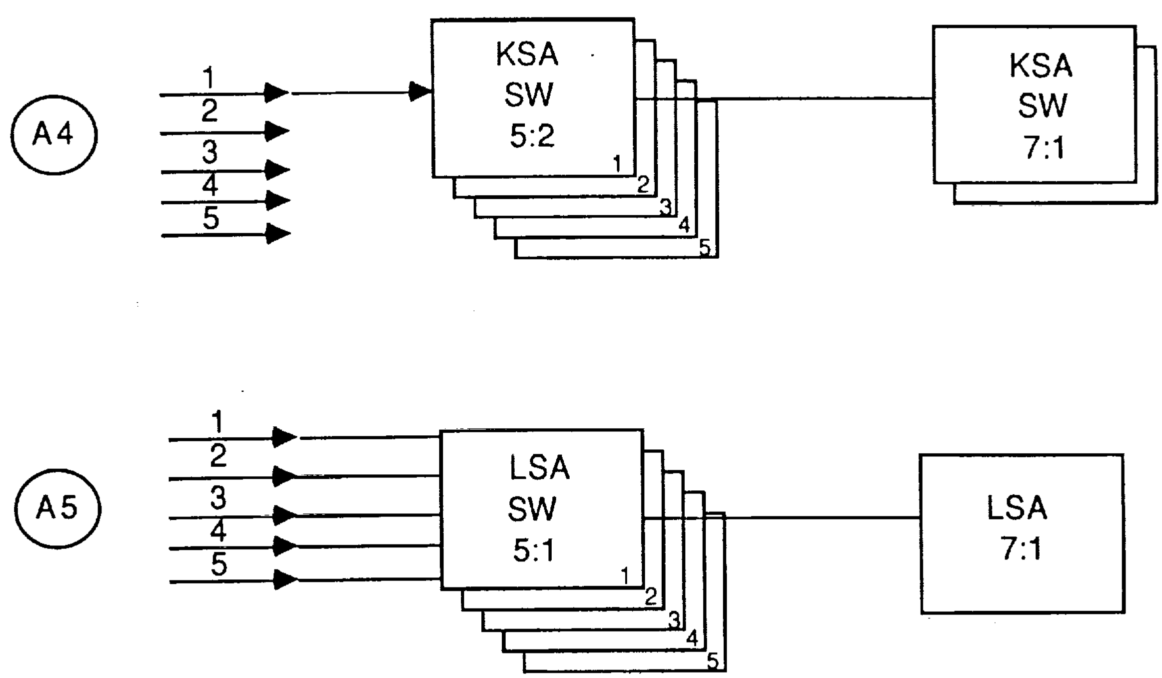

Figure 5.2-5a. Functional Decomposition of Ku-Band Forward Uplink Processing - Starting from A4 and A5

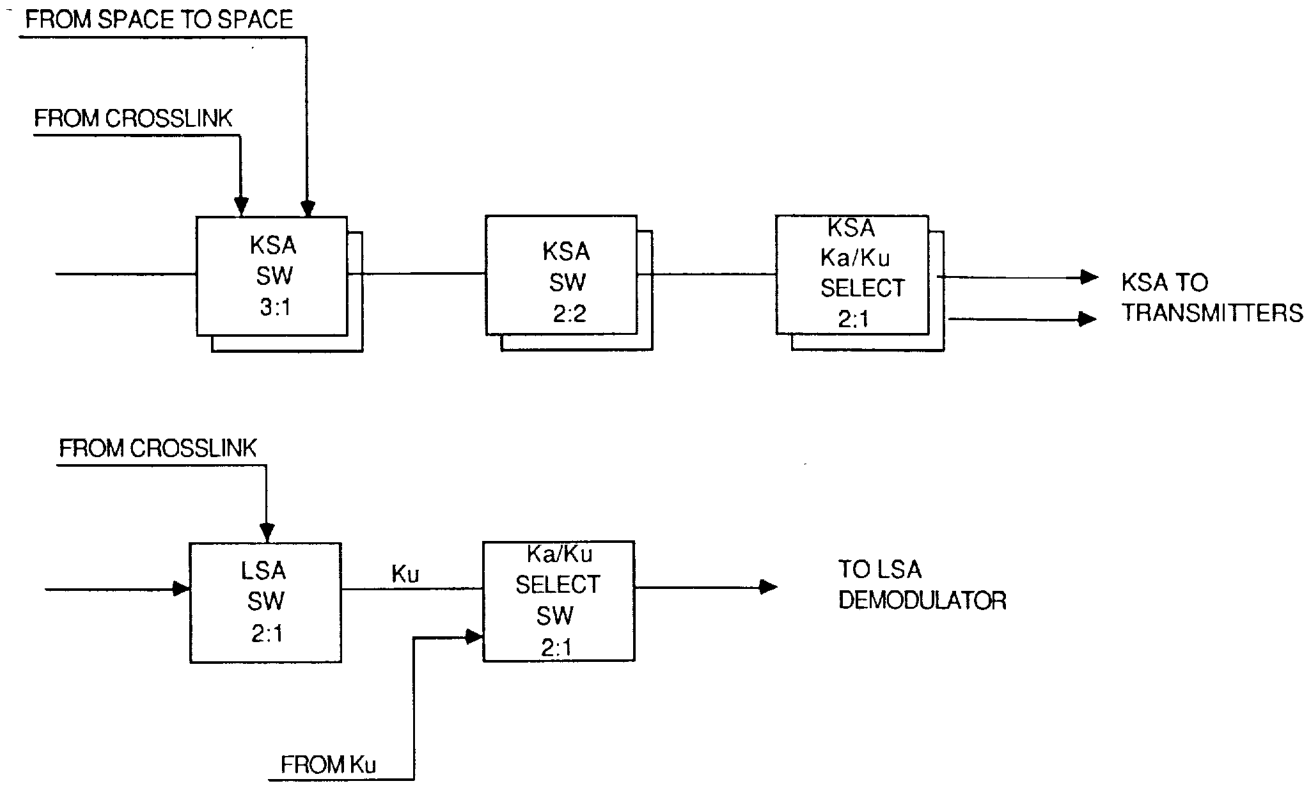

Figure 5.2-5b. Functional Decomposition of Ku-Band Forward Uplink Processing - Starting from A4 and A5 (Continued)

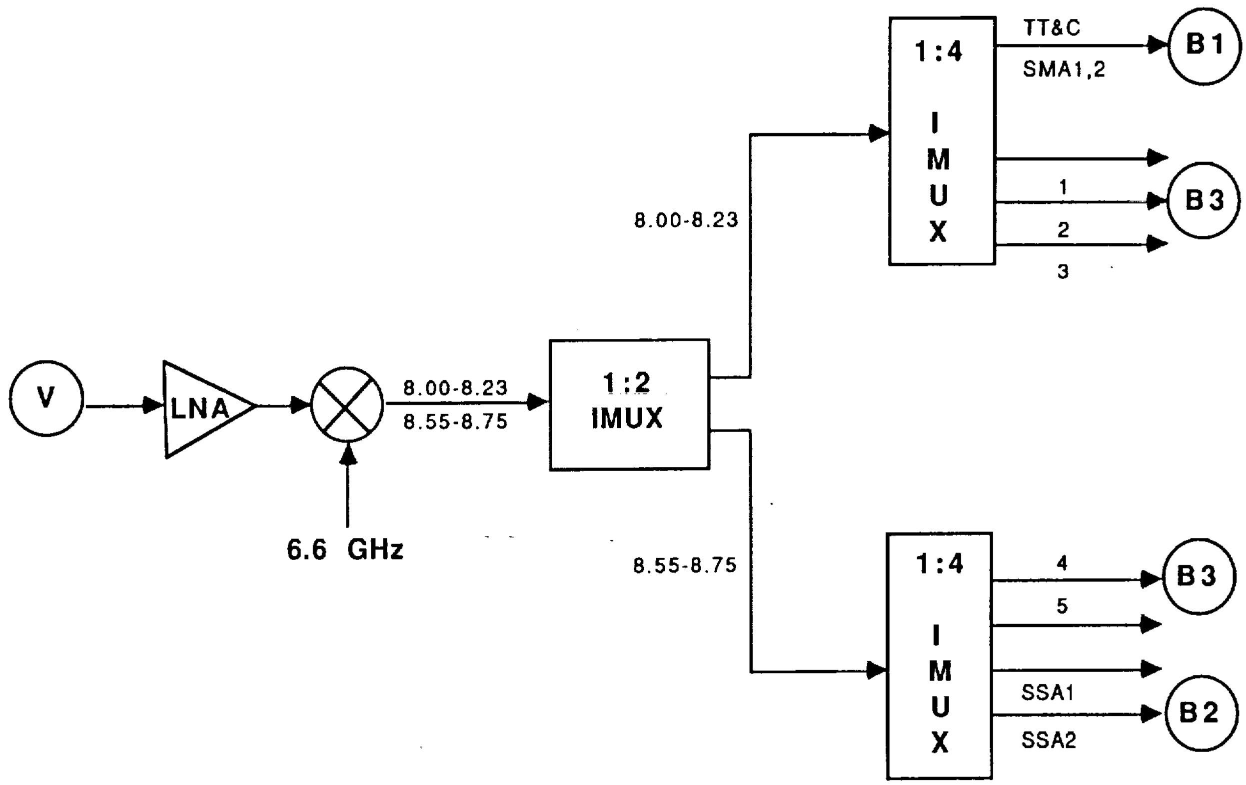

Figure 5.2-6. Functional Decomposition of Ku-Band Forward Uplink from Point V

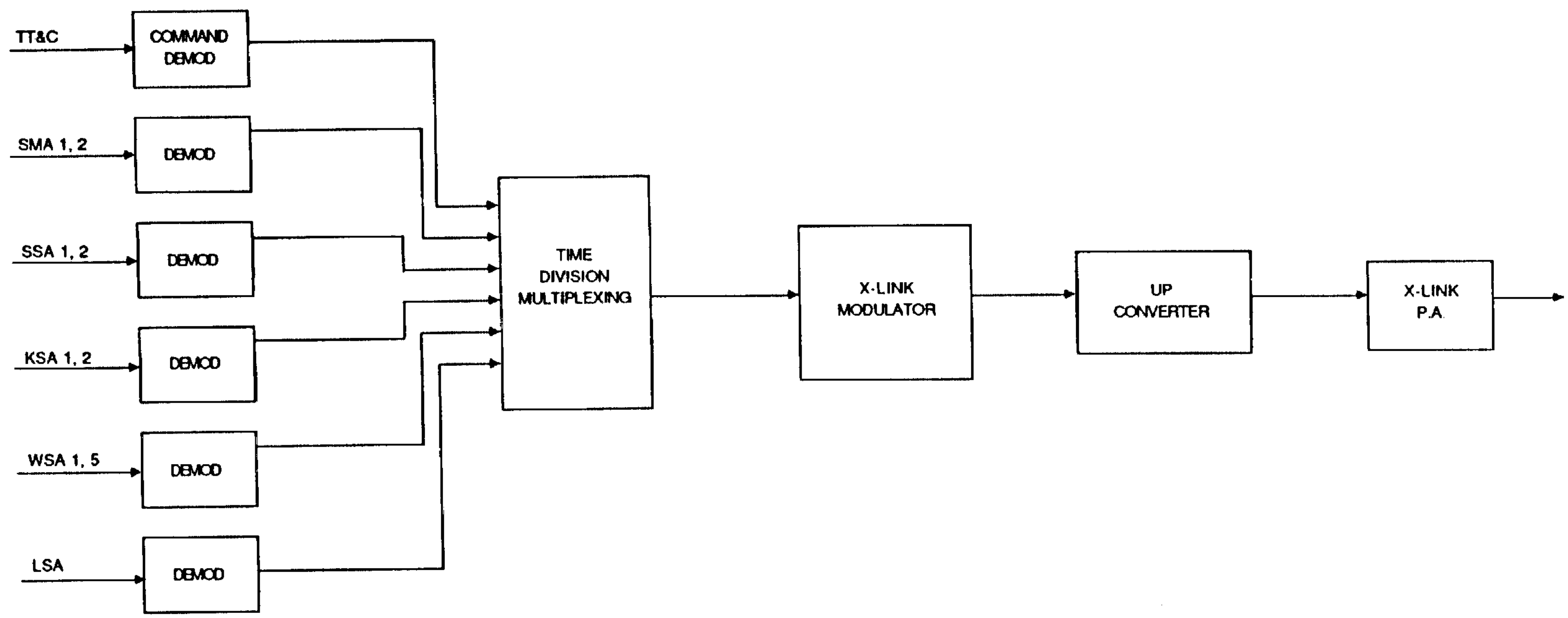

THE DECOMPOSITION OF ALL CROSSLINK SERVICS FROM POINT V IS IDENTICAL TO THE DECOMPOSITION FROM POINT W

Figure 5.2-7. Functional Decomposition of Ku-Band Forward Uplink - from Point V directed to Crosslink

(This philosophy is consistent with the functional decomposition of Ka-band services). Figures 5.2-3 through 5.2-5 show the functional decomposition for ATDRS 1 forward services and Figures 5.2-6 through 5.2-7 illustrate the functional decomposition for ATDRS 2 forward services. As shown in Figures 5.2-4 the channels used for KSA/WSA/LSA forward services must also pass through a 1:3 select switch, which determines the type of these three services; as shown in Figure 5.2-5, the KSA service signals pass through a 7:2 switch to select the appropriate two channels; and the LSA service signals go through a 6:1 switch for selecting the channel of transmission.

This functional decomposition of the Ku-band uplink services demonstrates the additional complexity imposed on the switching and control subsystems by the limited bandwidth and dual-polarization requirements.

5.2.2 Ku-Band Downlink Processing System Functional Decomposition

Table 5.2-2 shows the return link data rate requirements. The Ku-band allocation (as per SOW) for the downlink services is between the frequencies of 13.4-13.73 and 13.82-14.2 GHz. This allocation, even with the use of dual polarization, is not adequate for the aggregate return link services via Ku-band in any particular beam coverage area. A frequency plan, shown in Figure 5.2-8 (described in detail in the July monthly report), is employed. With this plan, when the Ku-band downlink service is required for LSA, all other services in the particular beam coverage area are momentarily suspended for the transmission of LSA return link; also, for each polarization, only three of the KSA/WSA return link communications are accommodated simultaneously for a particular beam coverage area. With the frequency plan shown in Figure 5.2-8 as a baseline, the functional decomposition of the Ku-band downlink services is illustrated in Figures 5.2-9 through 5.2-11. These figures also illustrate the processing required for ATDRS 1 users' return links. As shown in Figure 5.2-11, an RF switch inhibits the transmission of all other services when an LSA transmission is required via Ku-band in any beam coverage area. Also, as shown in Figure 5.2-11, there are a maximum of three out of the five WSA and two KSA return link services for transmission via the Ku-band.

This functional decomposition of the Ku-band downlink services also demonstrates the additional complexity imposed on the switching and control subsystems by the limited bandwidth and dual-polarization requirements.

Table 5.2-2. Return Links Frequency Band Allocation for One Polarization

Service	No. of Services	Max. Data Rate Mbaud	Total Mbaud
KSA	2	150	300
SSA	2	6	12
WSA	5	150	750
TLM	1	1.5	1.5
LSA	1	1000	1000
SMA	10	0.1	1
Total	21		2064.5

5.2.3 Ku-Band Uplink/Downlink Service Impact on Switch Architecture

5.2.3.1 **Introduction**. This paragraph presents some new additions of the switch -- most noticeably, the addition of Ku-band capability for the space-to-ground link (SGL) and the bent pipe version for the crosslink implementation.

5.2.3.2 **Addition of Ku-Band Services**. The addition of Ku-band uplink/downlink services requires the following modifications (see Figures 5.1-3a and 5.1-3b).

Ka/Ku-Band Switches. The Ka SGL and the Ku services are included here. Accordingly Ku switches for receive and transmit and capability for selecting either or both Ka- and Ku-links are included.

5.2.3.3 **Ku-Band Forward Uplink Functional Decomposition**. The satellite is equipped with a Ku-band antenna capable of having seven beams receiving signals from seven ground stations. The services from ground to satellite are the same as in the Ka-band, however, there is only limited band available at Ku-band and the total frequency band is 430 MHz, which is not sufficient to transmit all the information. Frequency reusing--transmitting ground signals using dual polarization--helps somewhat. To be able to use 1.5 Hz per baud as it is usually done at QPSK, two KSA and five WSA services have been assigned three bands. Any of the seven services can use any of the three frequency slots. Since all services cannot be carried at the same time, this self imposed restriction will have a strong impact on the switch.

After downconverting to a nominal 8 GHz the signals are separated by the input multiplexer and three terminals are generated: A1 for TT&C and SMA, A2 for the SSA signals, and A3 for KSA/WSA/LSA signals.

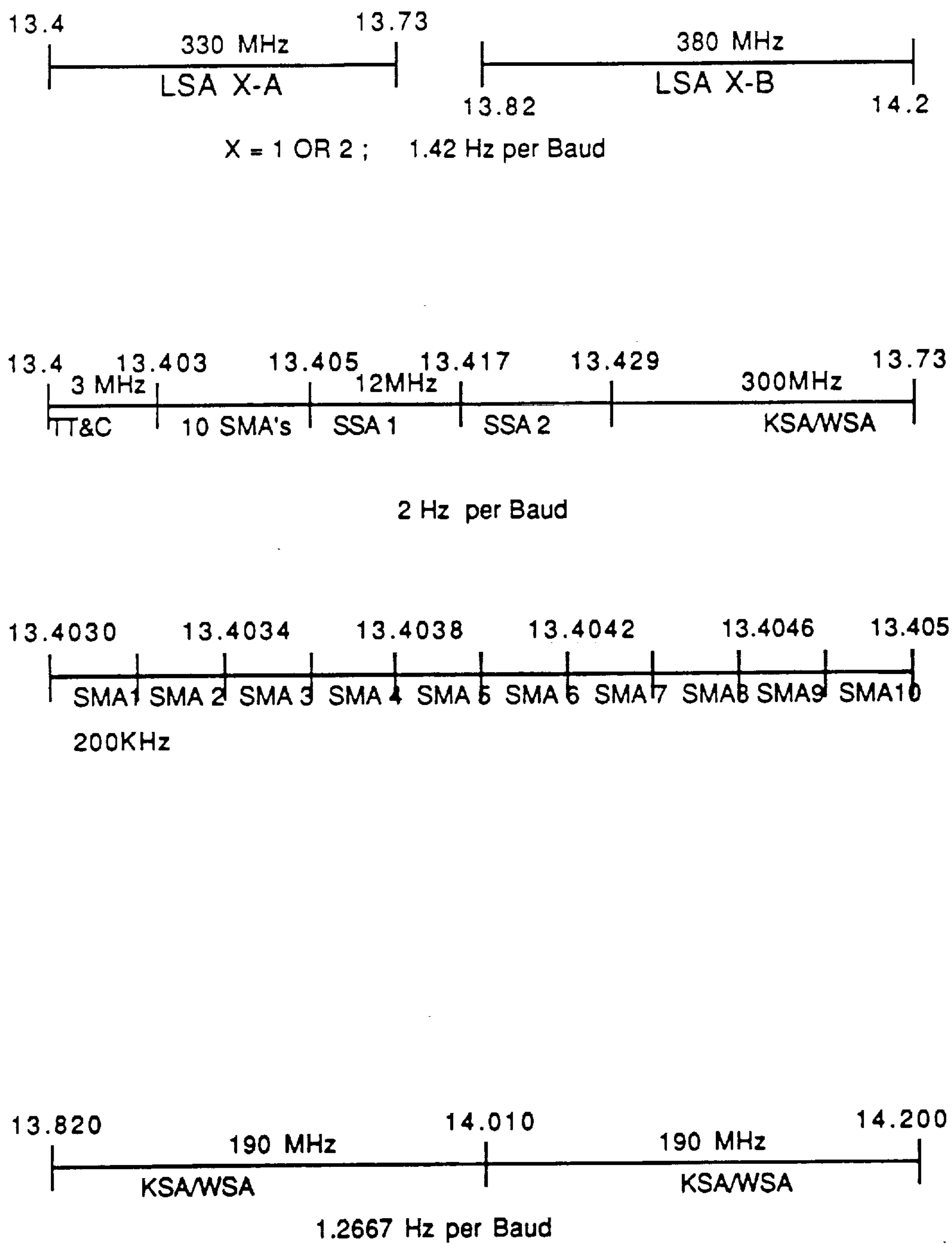

Figure 5.2-8. Frequency Plan, Ku-Band Downlink, Dual Polarization Required

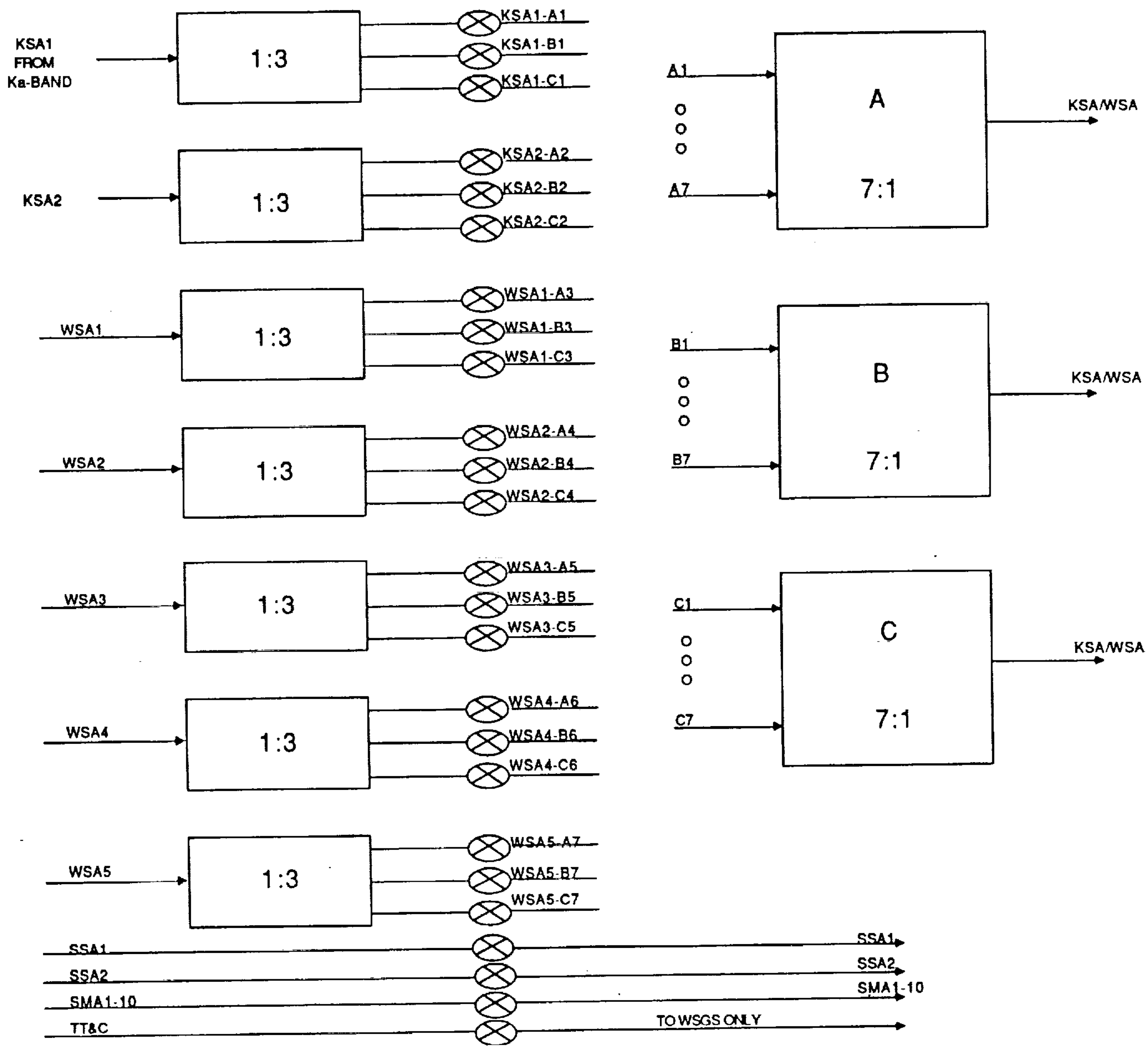

Figure 5.2-9. Ku-Band Return/Downlink Switch Overview (All Services Except LSA)

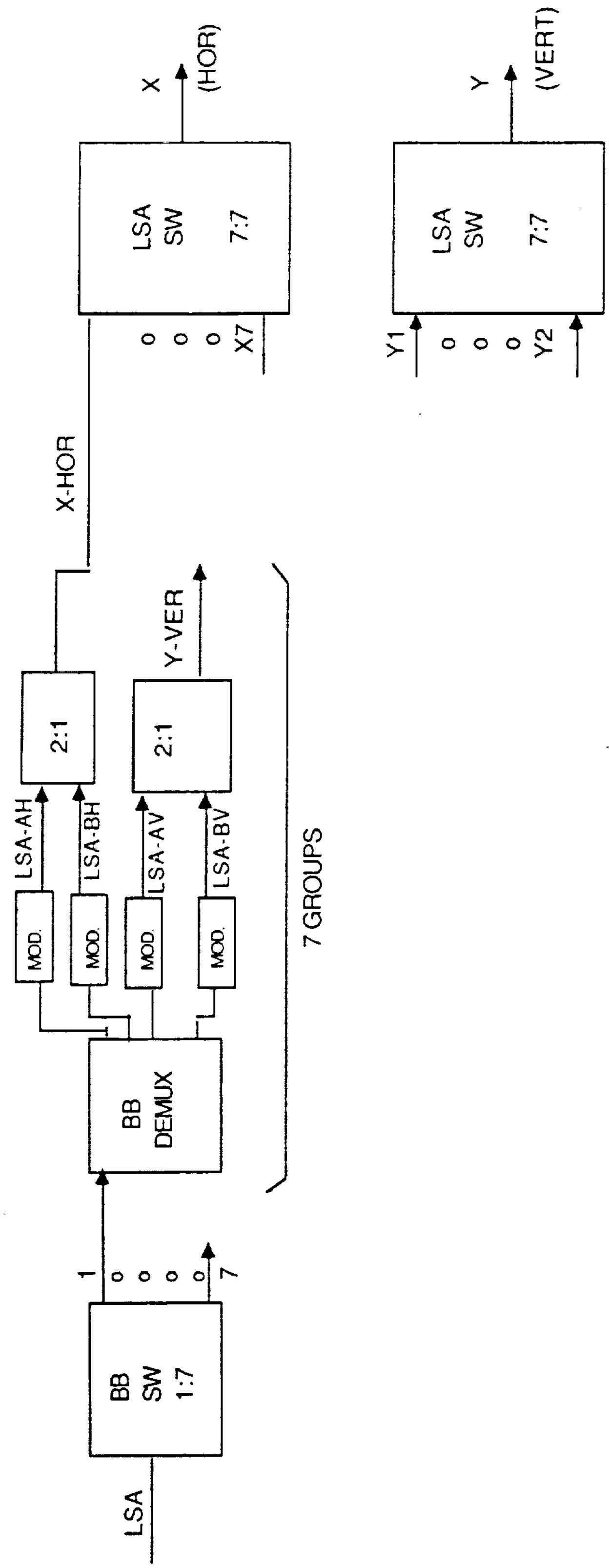

Figure 5.2-10. Ku-Band Return/Downlink Switch-Overview (Continued) (LSA Only)

5.2.3.4 **Ku-Band Return/Downlink** Switch. The frequency allocation for downlink Ku-band includes one band from 13.4 to 13.73 GHz or 330 MHz and a second band from 13.82 to 14.2 GHz or 380 MHz or a total bandwidth of 710 MHz. All of these services used are transmitting 2064.5 bauds. The net result is that if the Ku-band is used, not all services can exist simultaneously. For example, if LSA is to be used, the entire Ku-band will be used and all other services will be inhibited. In addition, the seven KSA and WSA services share three frequency bands and not all of them can exist simultaneously. All these complications impact signal switching.

Figure 5.2-9 shows all services except the LSA. The two KSAs and five WSAs all split in three for possible selection of the three allocated frequency bands. The chart terminates with three combined KSA/WSA outputs, two SSA, one SMA (with all 10 services) and one TT&C (actually TLM) to WSGS only.

Figure 5.2-10 shows the LSA services only. The LSA arriving from the user is demodulated and the baseband signal is split in seven directions going to the seven ground beams. A discussion of one of the seven groups follows. The baseband signal is demultiplexed and four streams of data are separated. They are A (lower frequency band), H-for horizontal transmission, BH, AV, and BV. The data is then modulated to be positioned in the correct frequency slot and grouped horizontally and vertically - thus outputs X1-HOR and Y1-VERT are generated. Next all X signals merge to a 7 X 7 switch and any input can go to any of the seven beams.

The last of the Ku-band return/downlink charts (Figure 5.2-11) deals with the interconnection and the way in which the different inputs are directed to the seven beams of the SGL antenna. This figure shows signals coming from the crosslink. Switches 1:7 split the information from one source to seven possible beams. Switches 6:1 form the beam and select one (or more) to the appropriate beam. Then switch 3:1 performs the select function - if LSA (terminal X from user or XX from crosslink) is active the other signals are inhibited. The signals Y and YY are selected by a 2:1 switch, power amplified, and applied to the OMT in point Z - the vertical polarization. The diplexer for receive transmit separation is also shown.

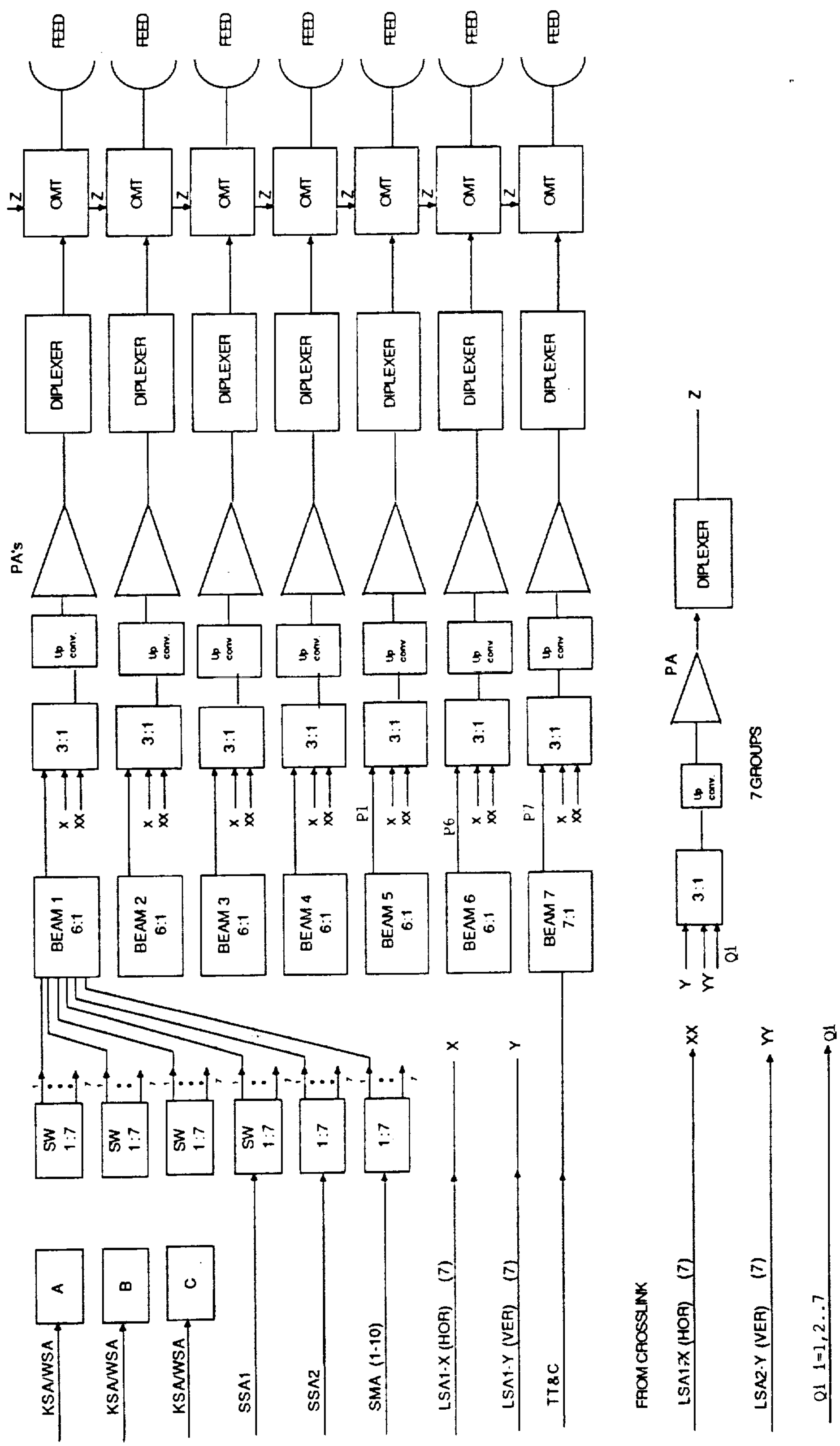

Figure 5.2-11. Ku-Band Return/Downlink Switch - Interconnection

5.3 INTERSATELLITE CROSSLINK INTERMEDIATE FREQUENCY SWITCHING CONCEPT

In this subsection concepts are developed for IF switching of the crosslink communications between the ATDRS 1 and ATDRS 2 for forward and return service processing. This IF switching concept is an alternative to the "demod-remod" approach presented in the baseline.

Figure 5.3-1 shows the crosslink input switch, with the bent-pipe IF switching concept. The 2:1 switch selects one of the two TDRS configurations, i.e., whether the communications payload is on ATDRS 1 or ATDRS 2. The ATDRS 2 receives the various users' return link transmissions, processes them at IF, upconverts, power amplifies, and combines them in a series of output multiplexers for transmission via the crosslink to the ATDRS 1. The ATDRS 1, on the other hand, receives the forward link services (for users of ATDRS 2) from the uplink beams via Ka/Ku bands, downconverts and separates them via a series of input multiplexers and IF stage processors and switching systems; then each of them is separately upconverted, power amplified, and fed to a series of combiners for output multiplexing for transmission over the crosslink.

Figure 5.3-2 shows the crosslink output switch, with the bent-pipe IF switching concept. The 2:1 switch selects one of the two TDRS configurations, i.e., whether the communication payload is on ATDRS 1 or ATDRS 2. The ATDRS 1 receives the various ATDRS 2 users' return link transmissions via the crosslink, downconverts, and separates them at various IF stages by means of input multiplexers and IF processors, selects the appropriate downlink beam and band, upconverts, power amplifies, and combines them in a series of output multiplexers for transmission to the ground stations. The ATDRS 2, on the other hand, receives the forward link services (for users of ATDRS 2) from crosslink, downconverts, and separates them via a series of input multiplexers and IF stage processors; then each of them is separately processed for transmission over the appropriate user's forward link.

5.3.1 Bent-Pipe Crosslink Configurations

Two types of crosslink functional switches are shown: input switch and output switch. The first is for forward services and the second is for return services. In the implementation, however, three types are described, each with its advantages and disadvantages.

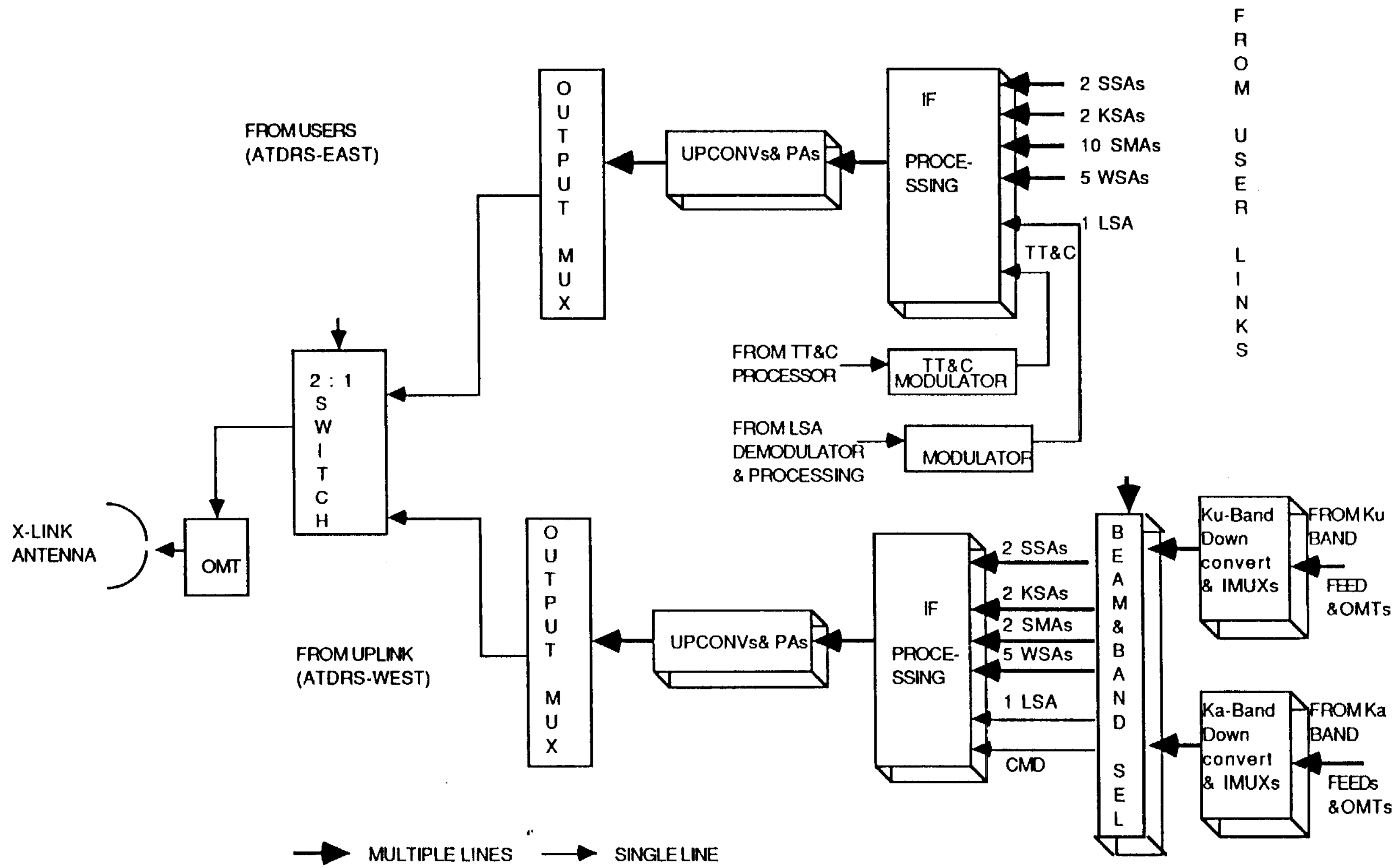

Figure 5.3-1. Crosslink Input Switch IF Switching (Bent-Pipe) Concept

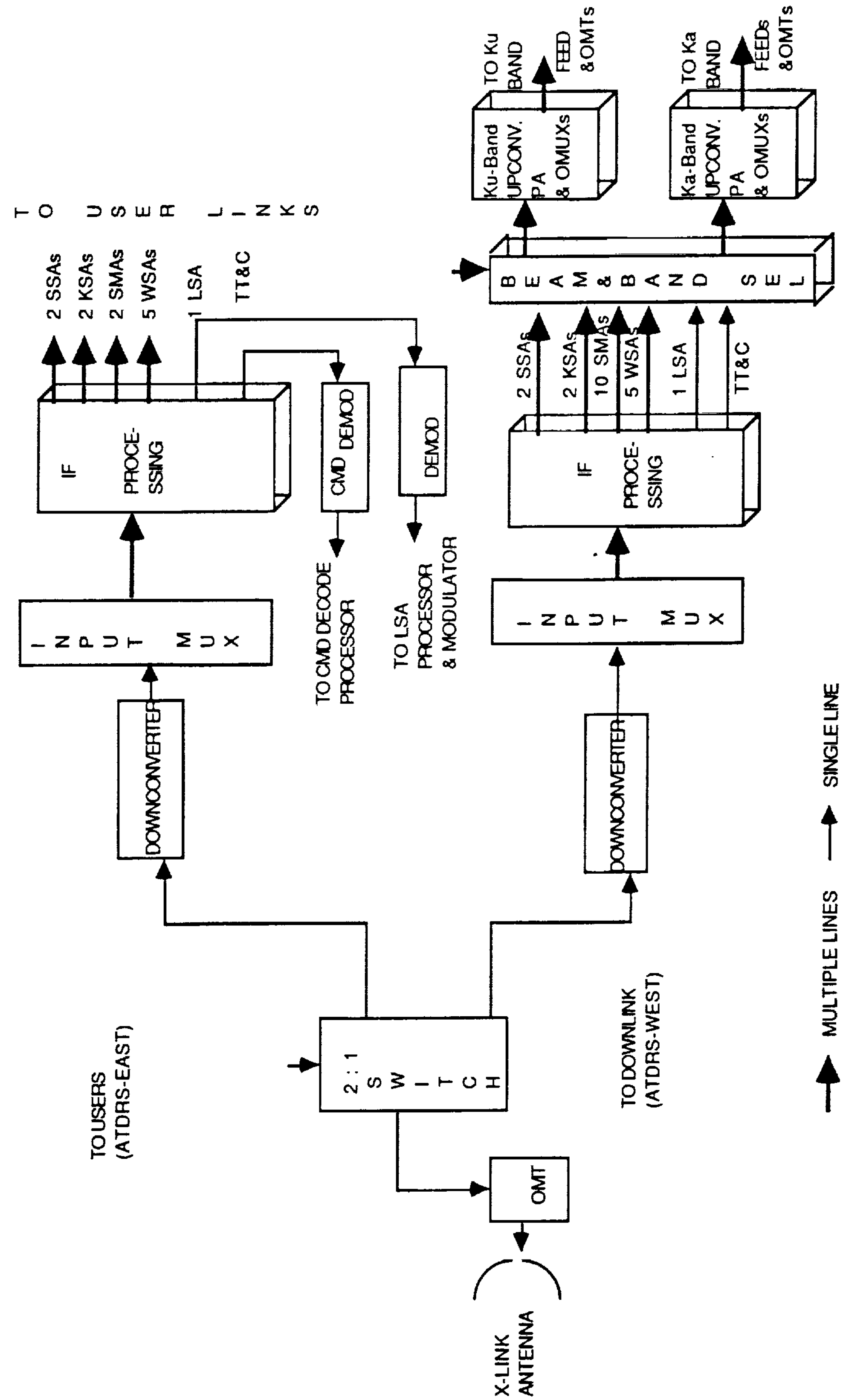

Figure 5.3-2. Crosslink Output Switch IF Switching (Bent-Pipe) Concept

The first implementation is done by the demod/remod method presented previously. The main advantage of this method is the efficient utilization of the frequency band, allowing different levels of modulation and coding to meet the different link requirements. Separate power amplifiers may be used for separate services with low intermodulation products and isolation of the links is possible. However, this method has some disadvantages. Since the data rate is not constant, the demodulators have to handle variable rate, which is difficult and is known to cause degradation in the performance. Research is being done to develop a variable rate demodulator with low degradation in the performance.

A second type of implementation uses the bent-pipe approach and direct frequency translation (see Figure 5.3-3). This method uses inputs from the Ka-band uplink, the Ku-band uplink, and from users (Table 5.3-3). All of the information is upconverted and applied to the power amplifier. The method seems simple enough and on the surface looks attractive. But there are a number of serious disadvantages: the method requires an unusually large bandwidth, it will degrade the signal-to-noise ratio, there will be IM distortion and to avoid or reduce it, the PA has to be grossly oversized. Since the signals in the different services are not equal in amplitude and probably very different, the problem of IM distortion gets further aggravated. This method has possibilities and further investigation is warranted.

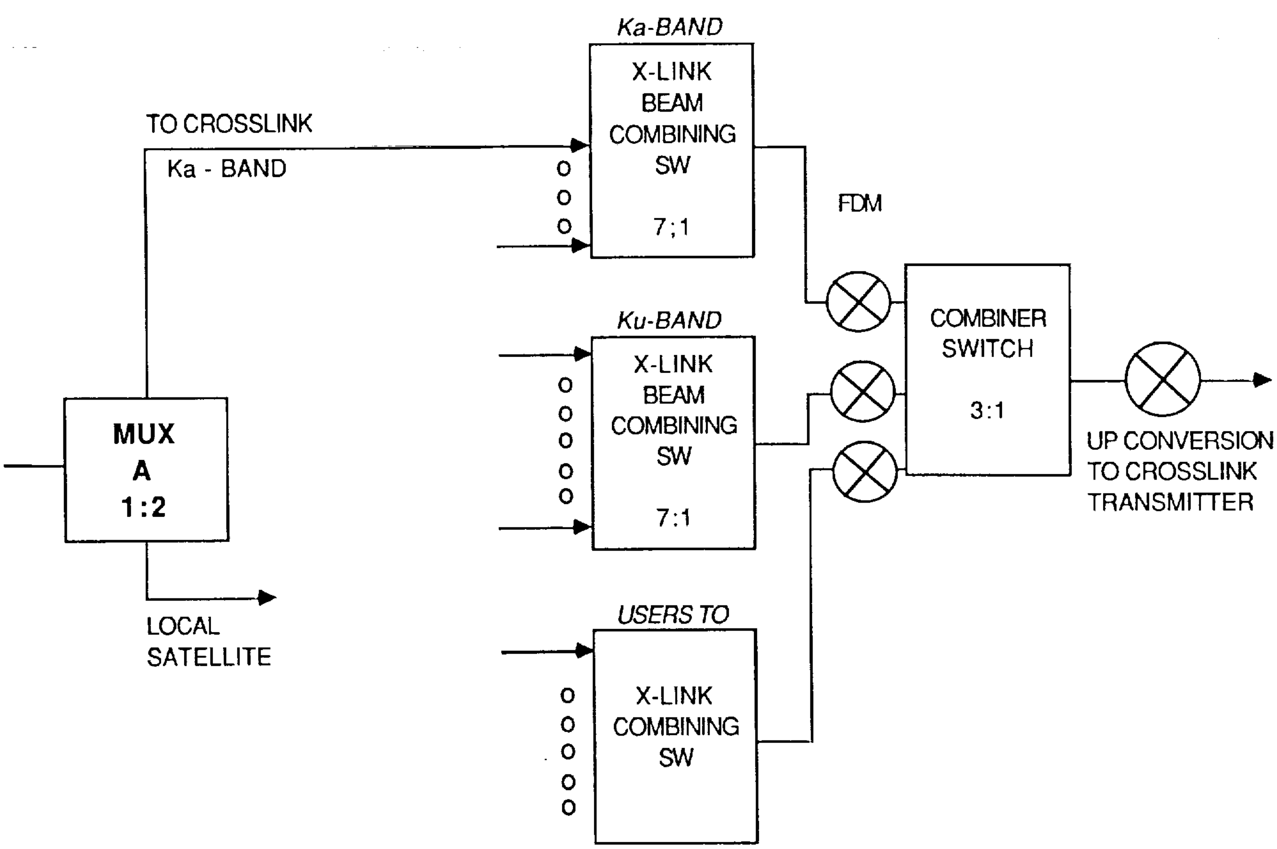

Figure 5.3-3. Bent Pipe by Direct Frequency Translation

Table 5.3-3. Bent-Pipe Concrete Considerations for Bandwidth

- Worst case for crosslink bandwidth is if traffic is coming simultaneously from ground via Ka- and Ku-bands and from users via the space-to-crosslink switch
- Contribution from Ka-band (FORW)
  BW = 1750 MHz 845.04 Mbaud 4.14 Hz/baud
- Contribution from Ku-band (FORW)
  BW = 403 MHz 422.52 Mbaud
  Using 272.52 Mbaud 1.5 Hz/baud
- Contribution from users to crosslink
  BW = 1750 MHz 1032.25 Mbaud 1.7Hz/baud
- Total 3930 MHz 1827.29 Mbaud
- Conclusion BW of 4 GHz is not available

The third method includes decomposition, as shown in Figure 5.3-4, and filtering of each service (Figure 5.3-5). To do this, the signals must be downconverted for filtering. After filtering, the signals will be amplified to a level more or less equal for all the services. Finally all the decomposed IF signals have to be upconverted so that a switch can select any one or any combination of them. The same operation is done for all seven beams of Ka- and Ku-band and for the signals of users. After combining all these signals in FDM, they are all upconverted to 60 GHz and applied to the crosslink transmitter. This method offers advantages: use of variable rate demodulators is eliminated and the losses associated with these demodulators is avoided; noise is contributed only by the active channels; any nonactive channel is switched off, thus the noise contribution is reduced; the amplitudes of the different services are individually controlled and brought to equal it alleviating the IM problem. But there are serious disadvantages also: the bandwidth requirements are still high, in multiple links the degradations are cumulative; this method does not permit optimization of hardware and performance of individual links independently.

In conclusion, the bent-pipe method is a viable alternative and deserves further consideration.

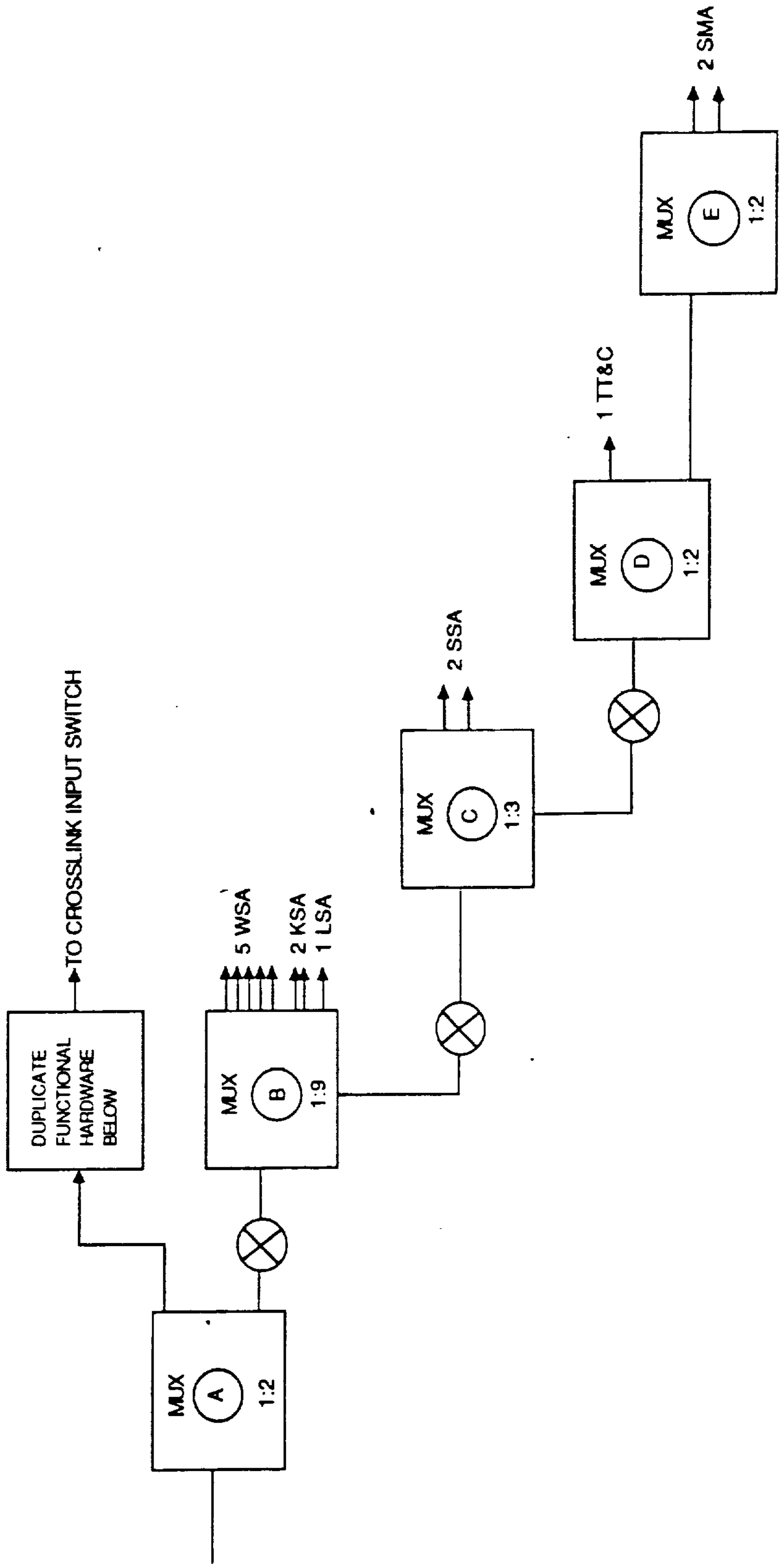

Figure 5.3-4. Forward Services Ground-to-Space Overview

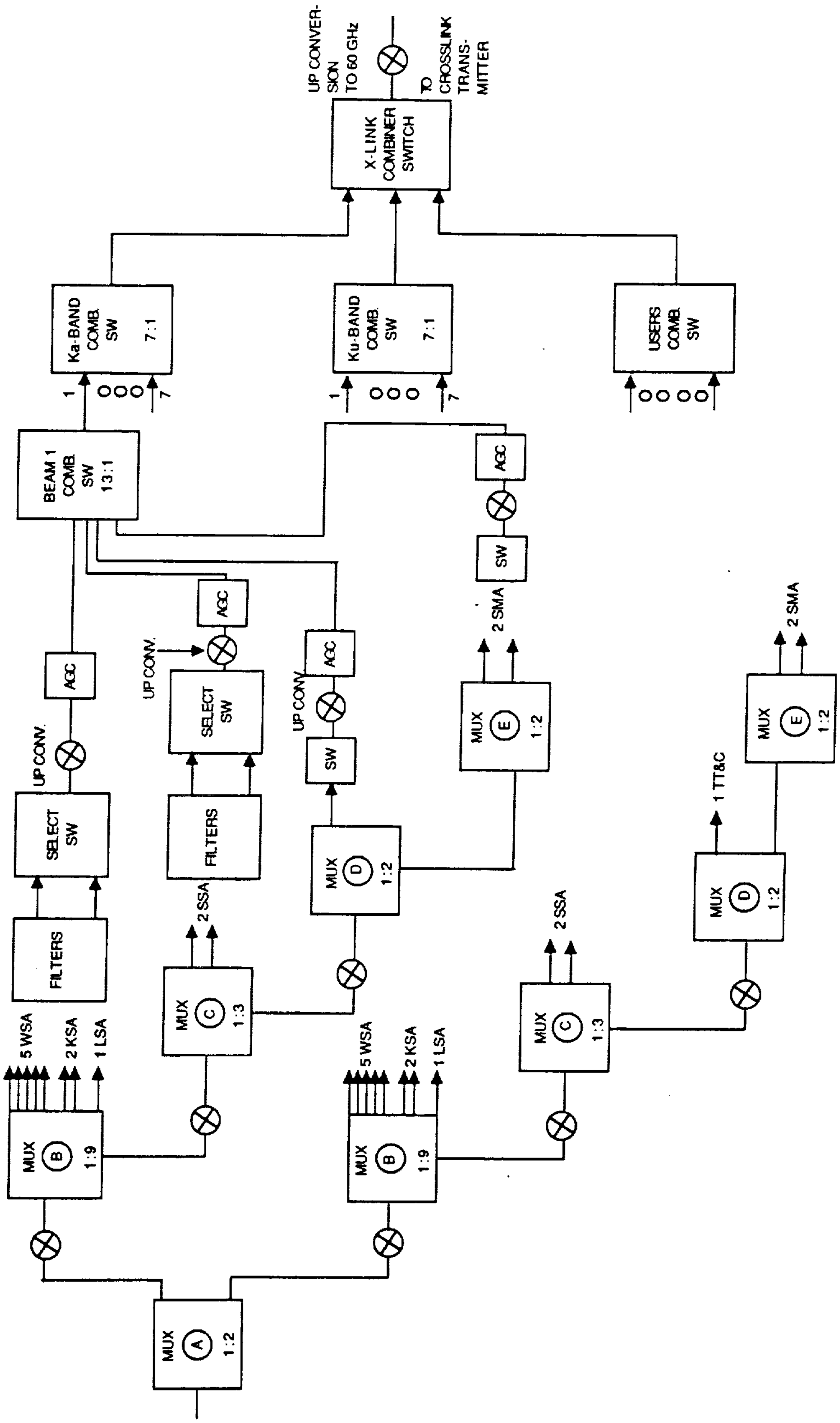

Figure 5.3-5. Crosslink Bent-Pipe Realization

5.4 BASEBAND MULTIPLEXING/DEMULTIPLEXING/SWITCHING ISSUES

In this subsection, the issues related to baseband multiplexing, demultiplexing, and/or switching requirements of the ATDRSS are addressed.

5.4.1 Baseband Switching Requirements of ATDRSS

As previously stated, an option for the ATDRSS crosslink communications is by demodulating, processing, and remodulating onboard the ATDRSS; for transmission over the crosslink for demodulation, processing, and transmission over the appropriate links. As shown in Figures 5.4-1a and in more detail in Figure 5.4-1b, the functional partitioning of the crosslink and space-to-space switching functions require baseband switching, if the above-mentioned onboard processing technique is to be used. Figure 5.4-2 shows the required baseband multiplexing functional blocks and Figure 5.4-3 shows the corresponding baseband demultiplexing functional blocks (hashed) in the crosslink input and output switching blocks respectively.

Baseband switching is also required for LSA forward and return communications. Figure 5.4-4 illustrates the LSA return link, requiring onboard demodulation, baseband switching, and remodulation for transmission over the ATDRSS crosslink or over the appropriate downlink beam.

Figure 5.4-5 portrays a specific case, when the LSA return link communications needs are to be served by downlink Ku-band allocation. Since both bands allocated need to be used in both polarizations for accommodating this service at Ku-band, this in turn requires both baseband switching and demultiplexing for transmission over the appropriate beam, band, and polarization.

5.4.2 Baseband Multiplexing/Demultiplexing Design Considerations

Onboard processing for ATDRSS crosslink communications requires all facets of baseband processing, i.e., baseband switching, multiplexing, demultiplexing and processing. Once the issues concerning this application are understood, the issues related to the baseband processing requirements of other applications such as the LSA communications, depicted in Figures 5.4-4 and 5.4-5 will also be clear. Therefore, the rest of this paragraph will address the issues concerning the onboard processing requirements for ATDRSS crosslink communications.

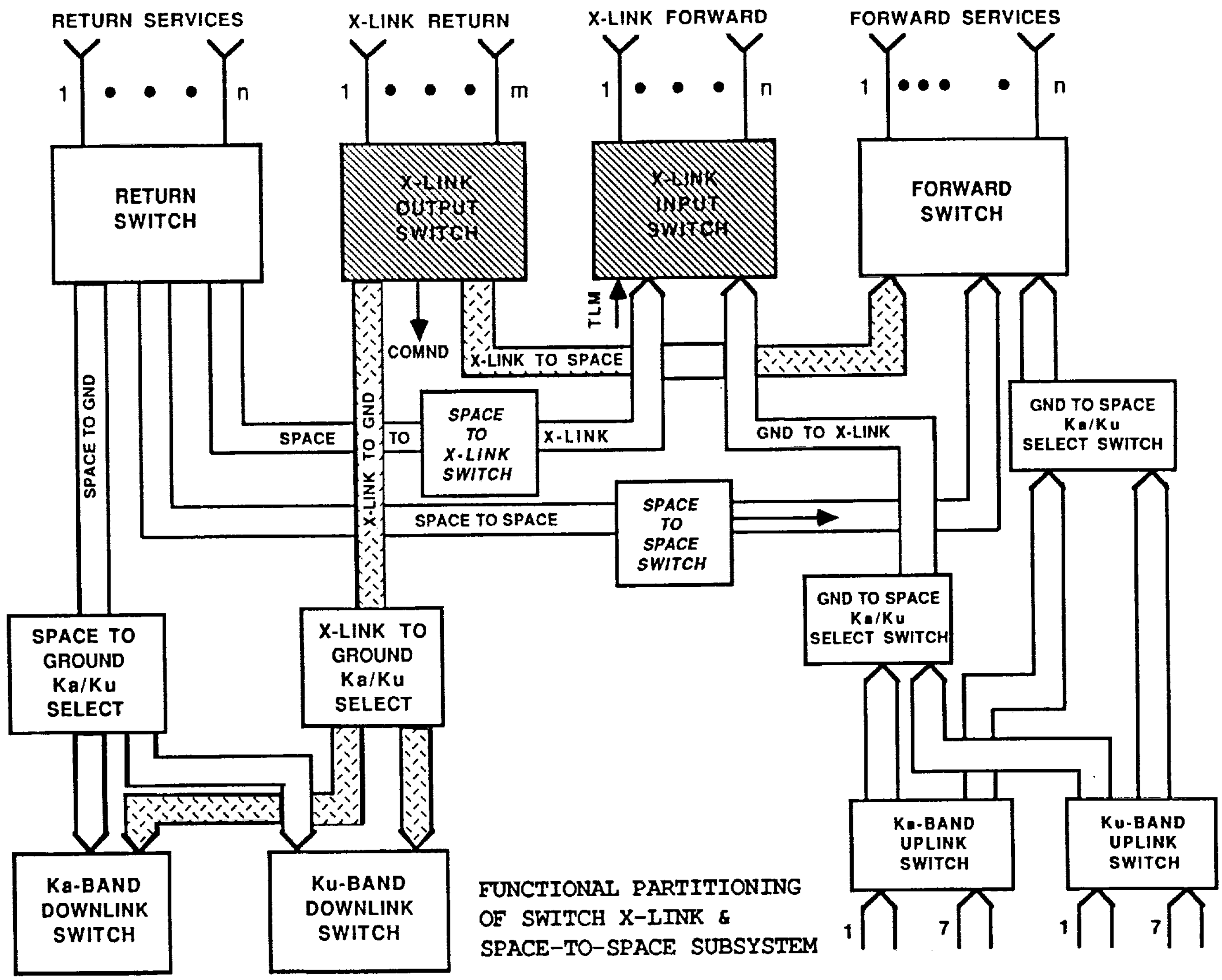

Figure 5.4-1a. Functional Partitioning of Switch X-Link and Space-to-Space Subsystem

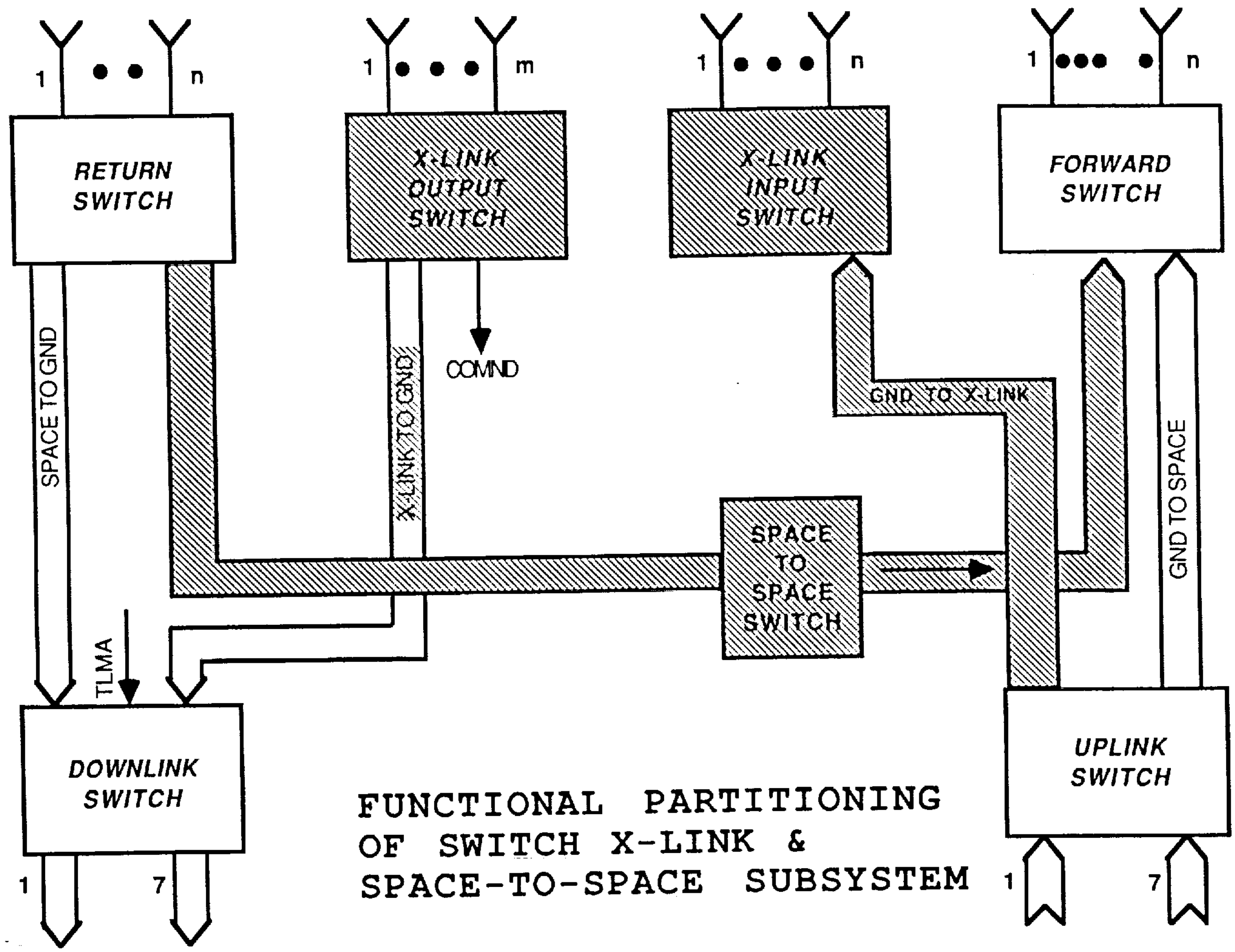

Figure 5.4-1b. Functional Partitioning of Switch X-Link and Space-to-Space Subsystem

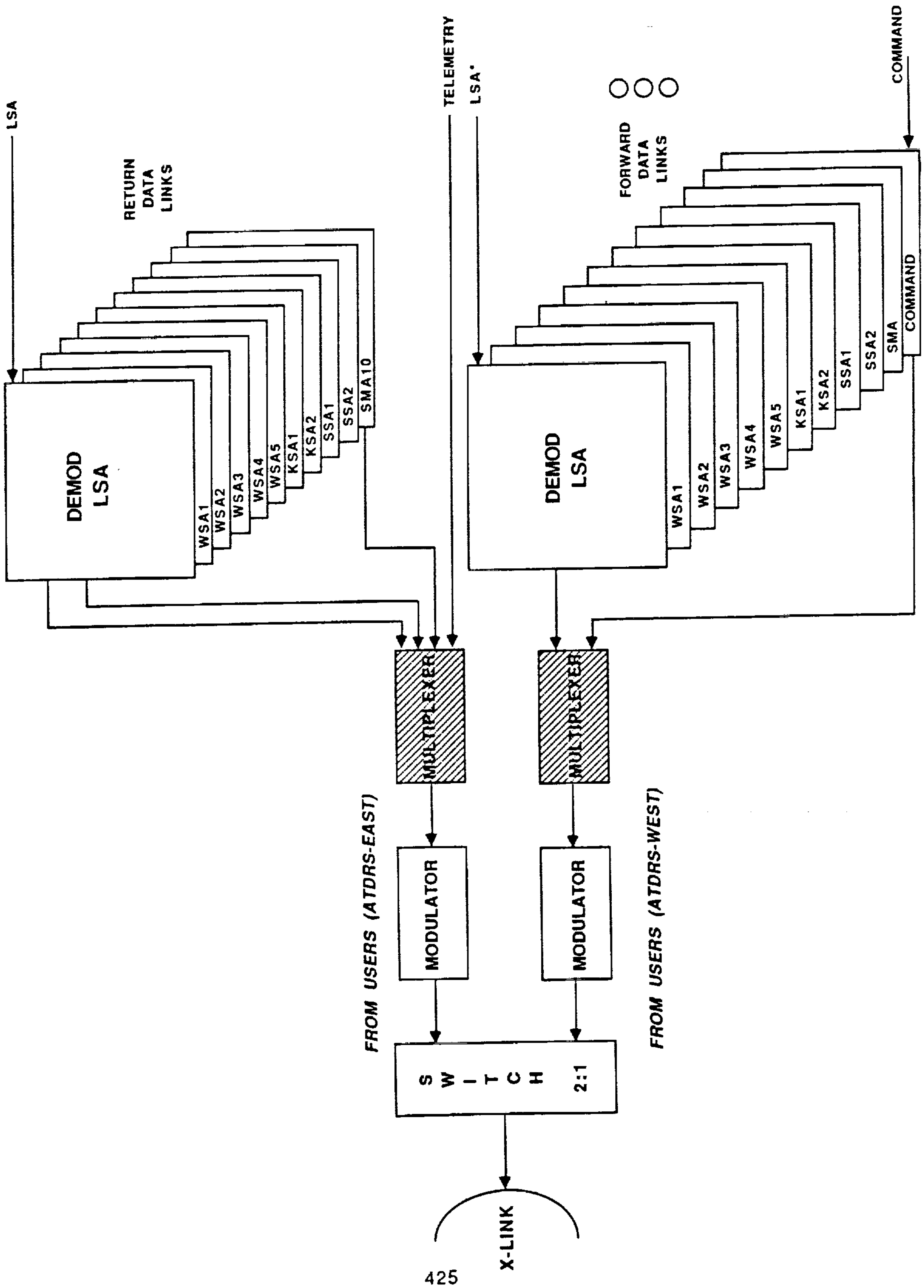

*HARDWARE AS IN UPLINK/FORWARD SWITCH DUPLICATED

Figure 5.4-2. Crosslink Input Switch

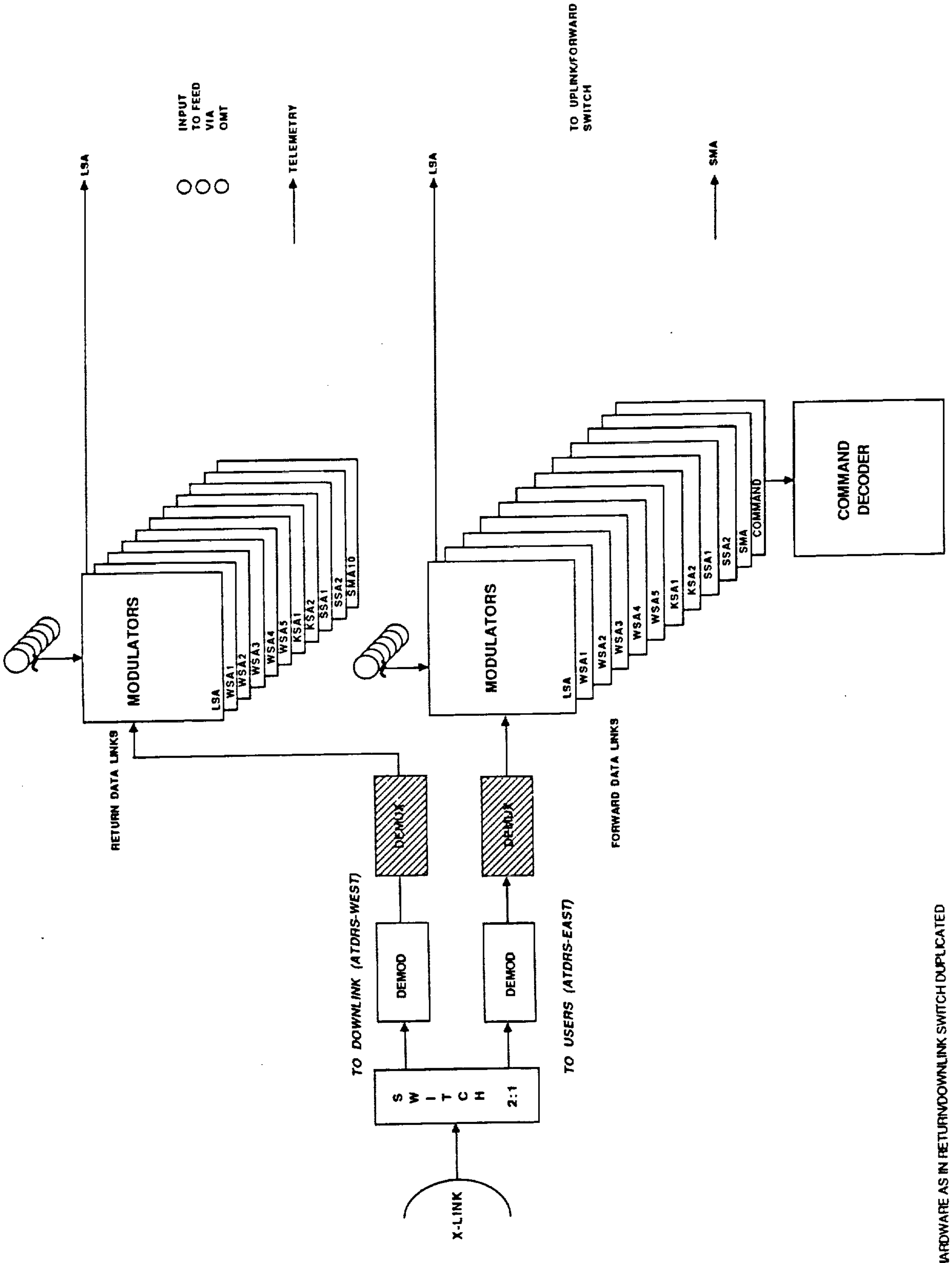

Figure 5.4-3. Crosslink Output Switch

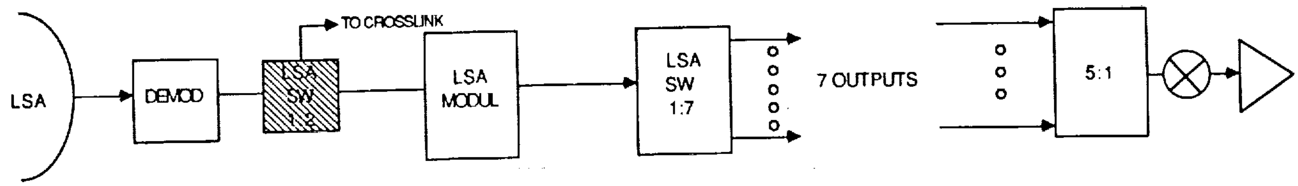

Figure 5.4-4. A Baseband Switching Application

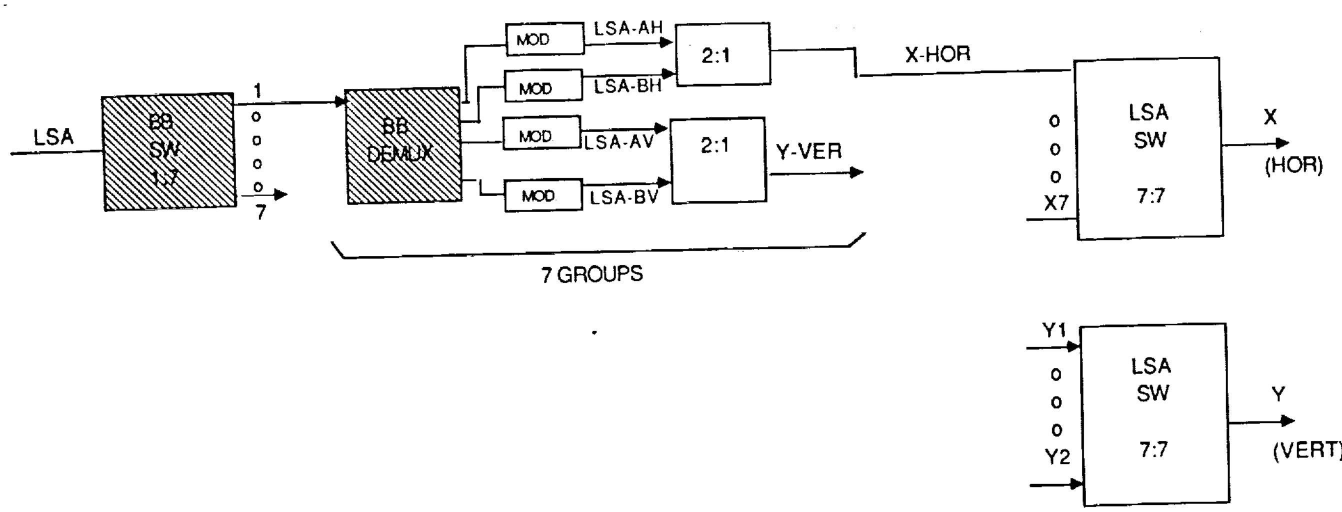

Figure 5.4-5. Ku-Band Return/Downlink Switch Overview (LSA Only)

Baseband multiplexing involves buffering, baseband switching, and time-division-multiplexing (TDM) of various uplinks and user (space-to-space) links appropriately demodulated into the "tributary" bit streams, as depicted in Figure 5.4-6. The TDM frame combiner multiplexes these tributary bit streams into a TDM frame, which in turn may be forward error correction (FEC) encoded and modulated for transmission. The bit streams from each tributary demodulator is typically fed to a "ping-pong" type dual buffer that permits reading of one while the other is being written. These two buffers for each tributary bit stream are read alternately, facilitating the TDM frame formation. The frame synchronization word, which is necessary at the receiving end for proper reception and respective demultiplexing of the tributary streams, is generated for inclusion at the beginning of each frame. In addition, a control word for each block of data is included for usage at the receiver. The corresponding demultiplexing process is depicted in Figure 5.4-7. The input data stream from the FEC decoders feed to the demultiplexer. The sync word correlation precedes the reception of the frame. The control words determine the appropriate switching times of the ping-pong buffers for tributary outputs for further processing and transmission over the appropriate links. The sync word correlation process is illustrated in Figure 5.4-8. In this specific example, a sync word sequence of "01110001001" is selected and correlates with the incoming bit sequence. As depicted in Figure 5.4-8, part a, the autocorrelation process results in a peak amplitude when the sync word is received successfully, which in turn triggers the reception of the remaining frame. In order to minimize the false synchronization, the correlator can be designed to be activated only during the expected "window" of sync word reception.

We begin with the forward link processing requirements, served by the baseband multiplexer (shown in the bottom half of Figure 5.4-2) in the ATDRSS West and by the baseband demultiplexer (shown in bottom half of Figure 5.4-3) in the ATDRSS East. Table 5.4-1 shows the forward link communication requirements for the users of the ATDRSS East (derived from the maximum requirements given in the SOW). It is noted that these requirements are spread over a range of 10 kbaud (for SMA user communications) to 50 Mbaud (KSA/LSA/WSA). Assuming that a quaternary alphabet modulation format is used, this translates to a range of 20 kb/s to 100 Mb/s. Due to such a wide range of requirements, the frame-length would result in a very large number of bits (leading to a bulky hardware configuration). It is therefore convenient to multiplex them in stages (at the ATDRSS West), based on the required communication rates for various services. Figure 5.4-9 shows such an implementation, where the principal frame multiplexer (PFM) multiplexes the high rate user streams (such as the KSA/LSA/WSA), and the super frame multiplexers (SFMs) 1 and 2 multiplex relatively lower rate user streams. SFM 2 multiplexes the low rate SMA streams, and its output is fed to SFM 1, which multiplexes the command, SSA1 and SSA2. The output of SFM 1 is fed to the PFM. The PFM, SFMs 1 and 2 are illustrated in Figures 5.4-10, 5.4-11, and 5.4-12, respectively.

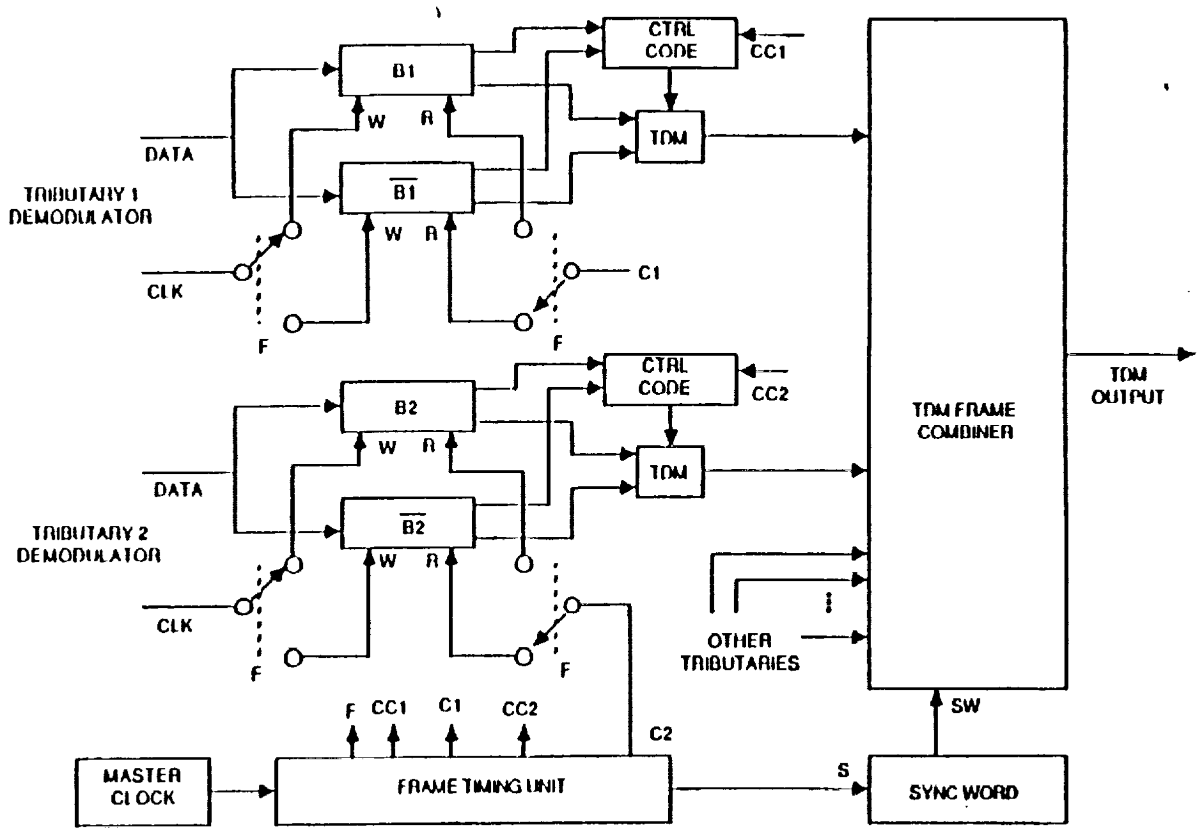

Figure 5.4-6. A Baseband Multiplexer Implementation

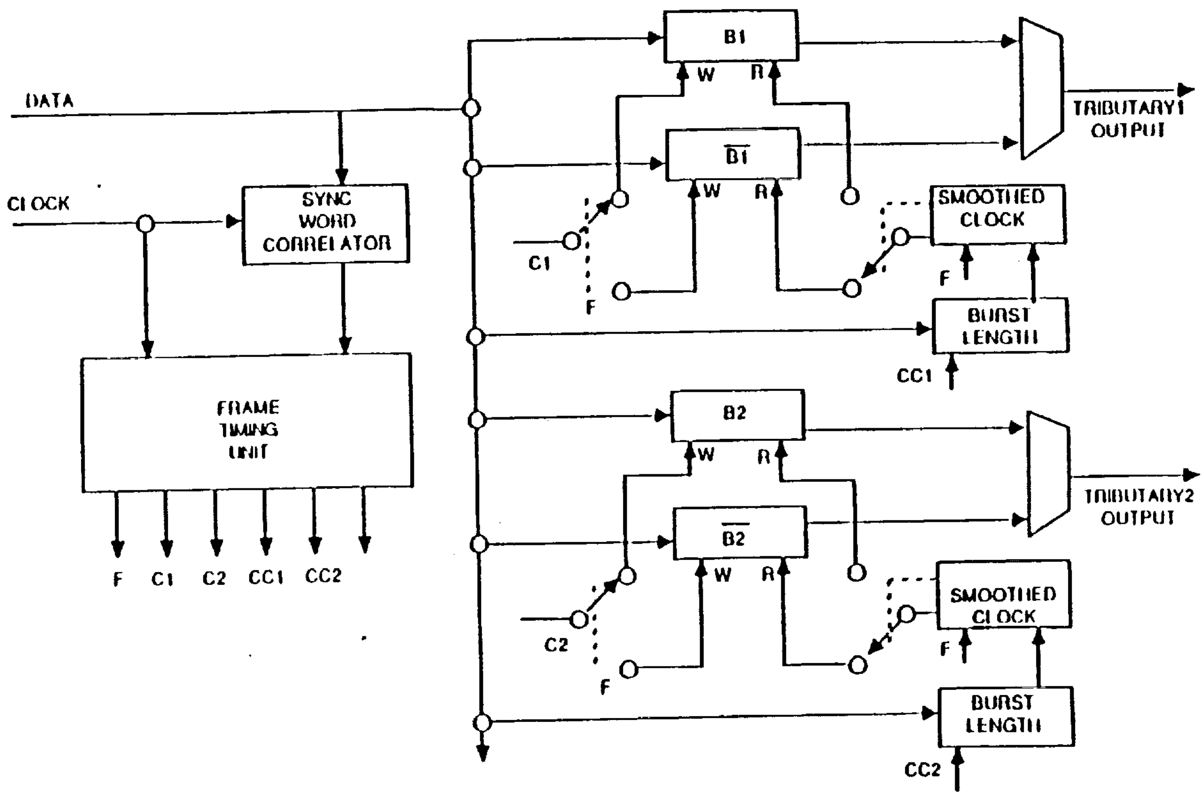

Figure 5.4-7. A Baseband Demultiplexer Implementation

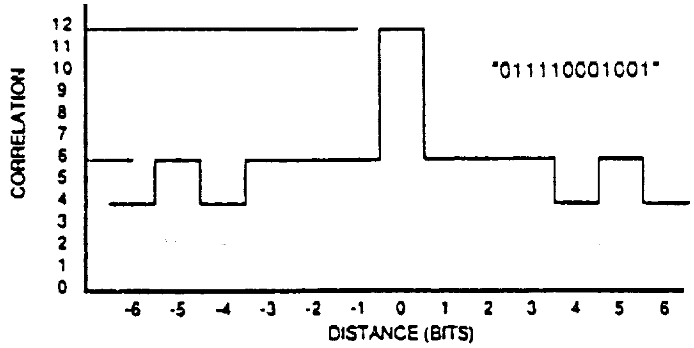

A. AUTOCORRELATION OUTPUT

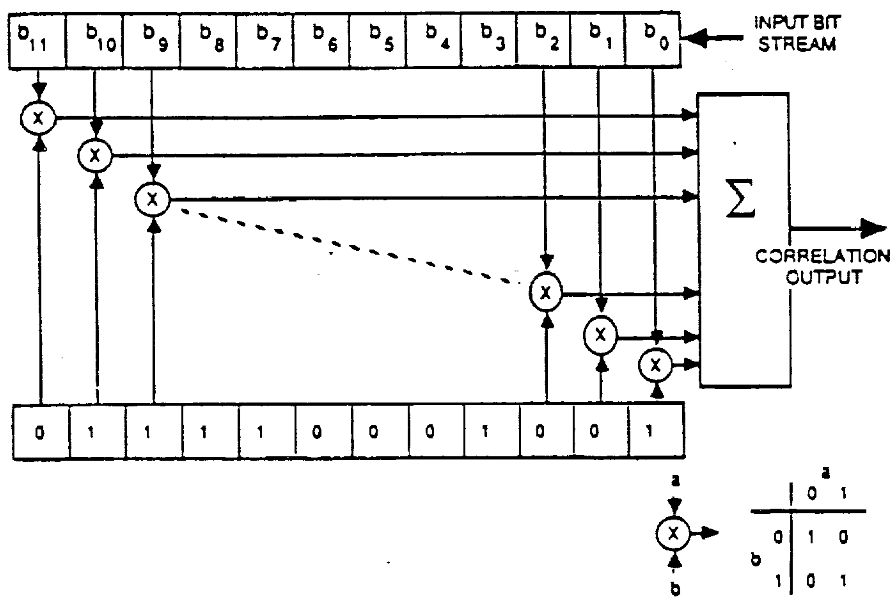

B. TYPICAL SYNCHRONIZATION WORD CORRELATOR

Figure 5.4-8. Sync Word Correlator

Table 5.4-1. Forward Link User Requirements

Service	No. of Services	Max. Data Rate Mbauds	Total Mbauds
TT&C	1	0.5	0.5
SMA	2	0.01	0.02
SSA	2	11	22
KSA	2	50	100
WSA	5	50	250
LSA	1	50	50
Total	13		422.52

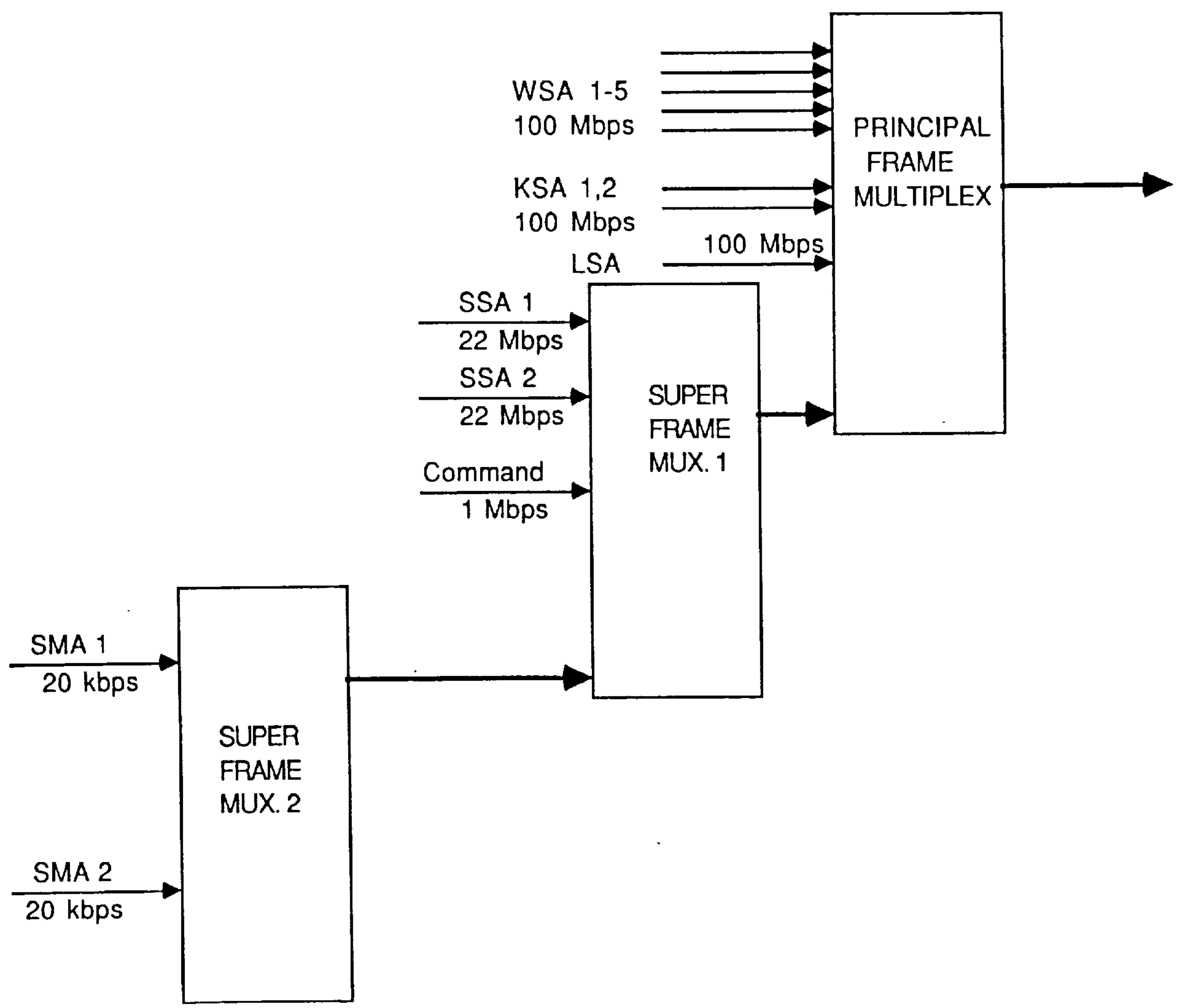

Figure 5.4-9. Forward Multiplexer Implementation

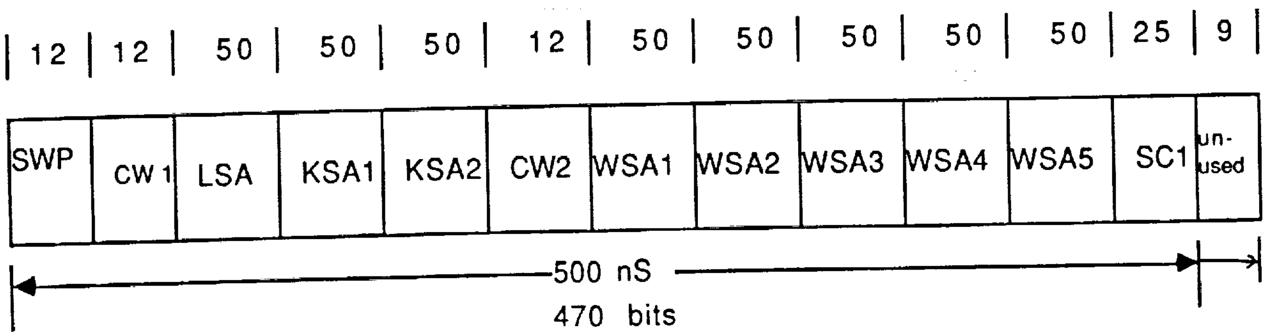

Figure 5.4-10. Principal Multiplex Frame Structure

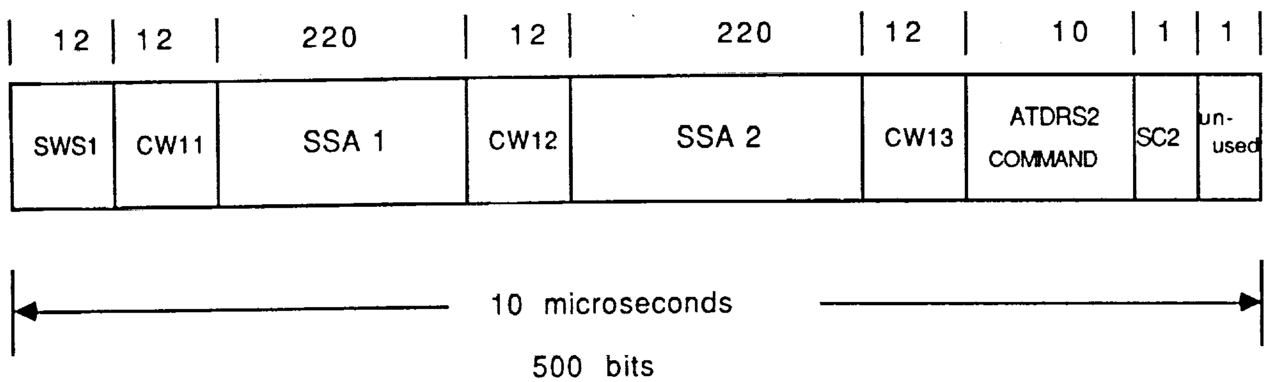

Figure 5.4-11. Structure of Super Frame 1

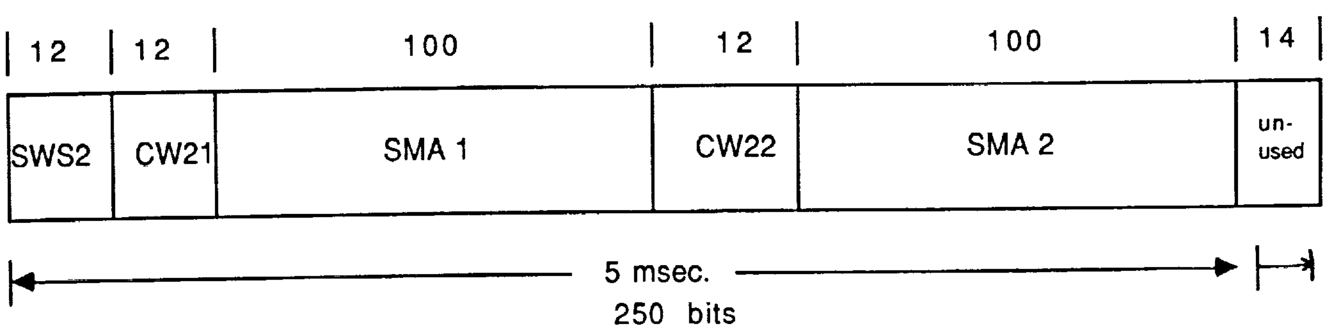

Figure 5.4-12. Structure of Super Frame 2

Table 5.4-2 shows the return link requirements of the users of ATDRSS East. The overall requirements of 2064.5 Mbaud mean that, with a quaternary signaling format, maximum aggregate rates of 4129 Mb/s are to be processed. With an FEC coding of rate of 1/2, this amounts to a coded rate of 8.258 Gb/s. It is unlikely that such high rates will be handled by a single FEC coder/decoder or modulator/demodulator even in the 1993 timeframe. There may be other problems such as the wideband frequency allocation and satisfactory operation of components over the entire band at 60 GHz. Therefore, a separate channel processor has been dedicated for LSA user return communications. This reduces the multiplexer capacity requirements (by 1000 Mbaud) to 1.0645 Gbaud, which may be implementable with 1993 state-of-the-art technologies. We are thus concerned with multiplexing of the remaining return link services.

Figure 5.4-13 shows an implementation of the multiplexer similar to the one shown in Figure 5.4-9 for the forward links. Figures 5.4-14, 5.4-15, and 5.4-16 illustrate the structures of PFM, SFM 1, and SFM 2 respectively for the return link communications.

Table 5.4-2. Return Link User Requirements for One ATDRSS

Service	No. of Services	Max. Data Rate Mbauds	Total Mbauds
KSA	2	150	300
SSA	2	6	12
WSA	5	150	750
TLM	1	1.5	1.5
LSA	1	1000	1000
SMA	10	0.1	1
Total	21		2064.5

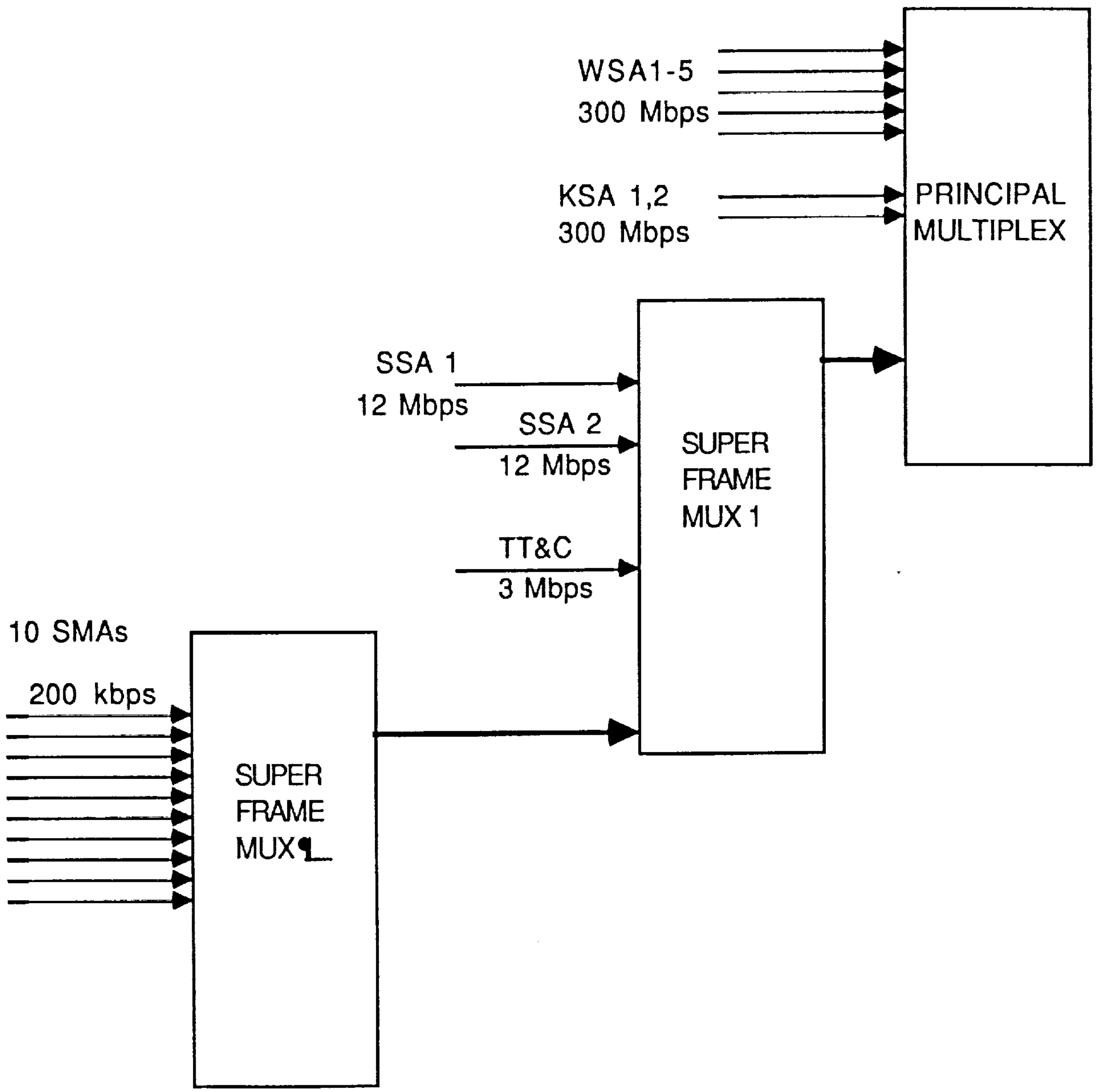

Figure 5.4-13. Return Link Multiplexer Implementation

12	12	50	50	12	50	50	50	50	50	6	8
SWP	CW 1	KSA1	KSA2	CW2	WSA1	WSA2	WSA3	WSA4	WSA5	SC1	un-used

166 nS
400 bits

Figure 5.4-14. Principal Multiplex Frame Structure Return Link Multiplexing

12	12	120	12	120	12	30	27	15
SWS1	CW11	SSA 1	CW12	SSA 2	CW13	ATDRS2 TT&C	SC2	un-used

10 microseconds
360 bits

Figure 5.4-15. Structure of Super Frame 1 Return Link Multiplexing

12	12	50	50	50	50	50	12	50	50	50	50	50	4
SWS2	CW21	SMA1	SMA2	SMA3	SMA4	SMA5	CW22	SMA6	SMA7	SMA8	SMA9	SMA 10	un-used

250 microseconds
540 bits

Figure 5.4-16. Structure of Super Frame 2 Return Link Multiplexing

5.4.3 Implementation Alternatives

The most natural choice for the implementation of the frame multiplexers is to use high-speed random access memories (RAMs). This is not inconceivable because of rapid advances in digital integrated circuit VHSIC implementations. DOD sponsored programs such as DIGIC/MIMIC hopefully permit accelerated results in these areas. An alternative to the implementation with high-speed RAMs would be to use high-speed TDM serial buffers (shift-registers) and high-speed switches. This approach, though viable, is unattractive due to the power and weight requirements imposed by many discrete components. Line delays and noise effects may cripple the operation and redundant switching implementations must be incorporated for reliable operation, which in turn may drive the power and weight requirements still further. The use of the high-speed RAMs with the drivers integrated on board would therefore be the preferred approach.

5.4.4 Technology Considerations

Figure 5.4-17 shows the projected state of the art of the various technology areas. As mentioned in the previous section, the high speed requirements for the baseband multiplexing/demultiplexing and switching functions will limit the technology areas to a few. Gallium Arsenide (GaAs) implementations have the promise for the future in meeting the speed requirements. A possible implementation of the multiplexer function with current state-of-the-art parts is illustrated in Figure 5.4-18. However, the process problems resulting in poor yield must be solved to achieve higher density integrations and avoid the related line delay and noise problems.

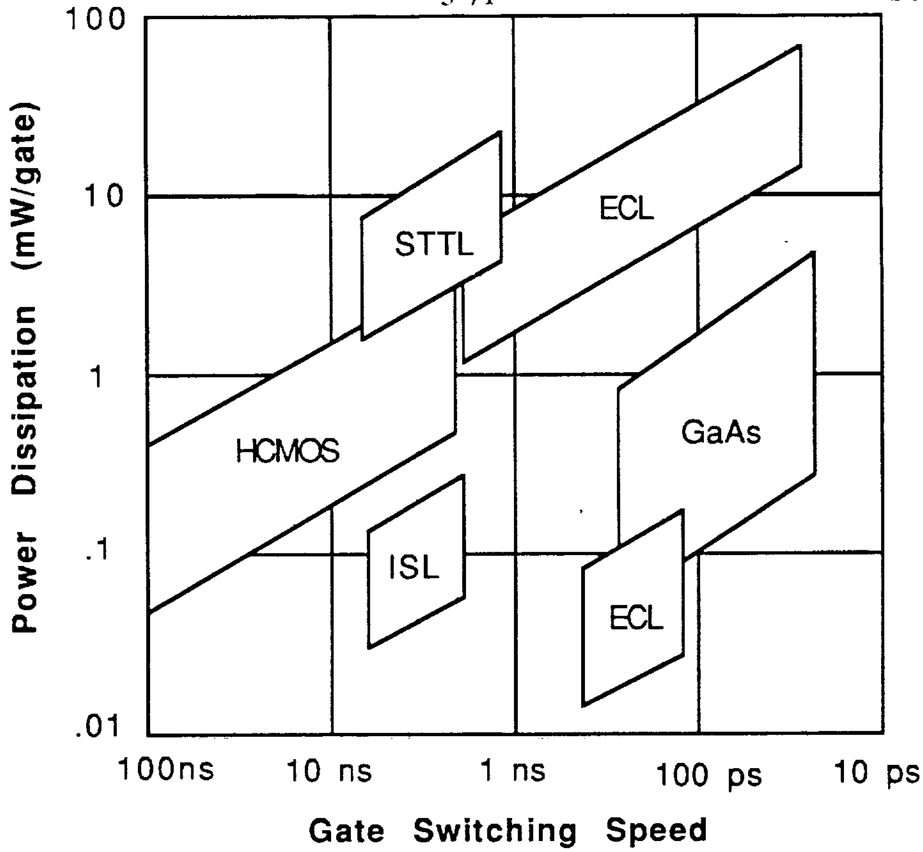

Figure 5.4-17. Comparison of IC Speed and Power

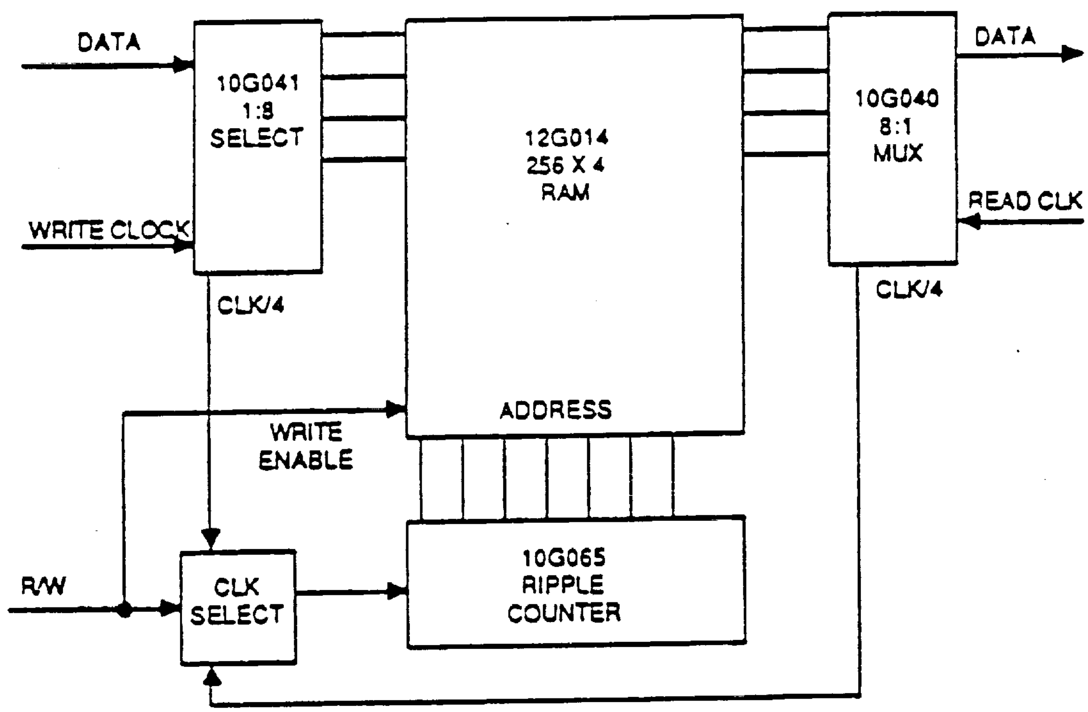

Figure 5.4-18. Buffer Implementation

Emitter-coupled-logic (ECL) bipolar implementations may also satisfy the speed requirements, but the present implementations are power consuming (a 10-fold increase in power requirements compared with GaAs implementations), although it is reported recently that a "geometrical scaling" process may reduce such high power requirements, while permitting higher integrations. Figure 5.4-17 shows this improvement. In this case, hybrid implementations with GaAs drivers and ECL circuits may be feasible in the near future.

Appendix D presents a table of the current state of the art of the cell library and gate array capabilities. Based on this information, it can be stated that by 1993 the state-of-the-art technology will be mature enough to permit implementations meeting the ATDRSS baseband processing requirements.

5.4.5 Size, Weight, and Power

Available technology is a prime driver of the physical attributes, as it not only determines power consumption and size, but also constrains the architecture and algorithms that are practical implementations. In this respect, there has been a recent renaissance in high-speed, low-power technology development. Current technology allows far greater system design flexibility by providing complex integrated circuit solutions with low development risk and high performance.

A prime example of current technology is the 20,000 gate GaAs array offered by Vitesse Semiconductor Corporation. Where previous SSI gate and flip-flop offerings required power on the order of 1 W/package to drive output pins at GHz rates, the new arrays consume 0.33 mW/gate with functions interconnected on the chip. This translates to around 7 W for a 20,000 gate array; in practice, additional power is needed for output drivers, yielding a reasonable power level of around 10 W at this level of complexity. Furthermore, continuing improvements in speed and power consumption may be expected as GaAs technology matures.

The design risk of this technology is greatly reduced by the availability of both standard and custom cells that have been thoroughly tested and optimized to provide building blocks for new designs. High-complexity RAM, Sequencer, ROM, and ALU blocks may be combined with latches and decoders to implement high-complexity designs. This approach takes full advantage of the GaAs gate array by integrating system level functions onto single arrays.

With reference to the return link multiplexer shown in Figure 5.4-13, it is likely that either the principal multiplexer or the super frame multiplexer could be implemented on a single GaAs gate array of 20,000 gate complexity. These chips would be combined with a conventional CMOS-implemented frame multiplexer gate array, yielding a total power of around 20 W for the three packages.

5.5 HARDWARE ASPECTS OF THE SWITCH

5.5.1 Switch Redundancy and Reliability

The information included here is drawn from the experience Ford Aerospace has accumulated from the series of experimental switches it has built, tested, and delivered to NASA Lewis Research Center. The discussion here is limited to the hardware aspects only and covers the redundancy and reliability aspect as well as information of size, weight, and power consumption and presents old and new types of hardware that may be used.

The Ford Aerospace switch matrix uses the coupler crossbar architecture shown in Figure 5.5-1. According to this architecture the inputs are applied to horizontal lines and the outputs are derived from the vertical lines. At the interception of the two lines a crosspoint is generated. A coupler in the horizontal line takes part of the input signal to the switch implemented as a dual-gate two-stage amplifier. If the switch is on the input energy is amplified and applied to a coupler to the vertical line thus providing the desired path for the signal. When the switch is off there is enough isolation so that there is no signal at the output. The small squares at the crosspoints symbolize the existence of couplers and switches and are explicitly shown in Figure 5.5-2.

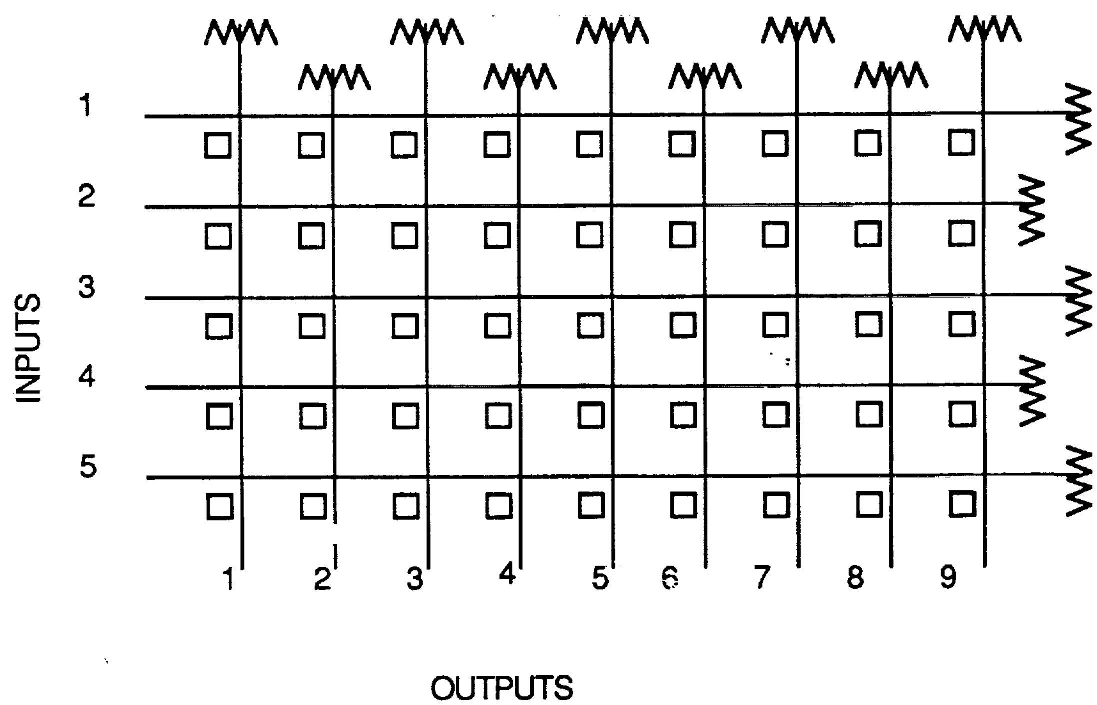

Figure 5.5-1. Ford Aerospace Switch Matrix with Coupler Crossbar Architecture

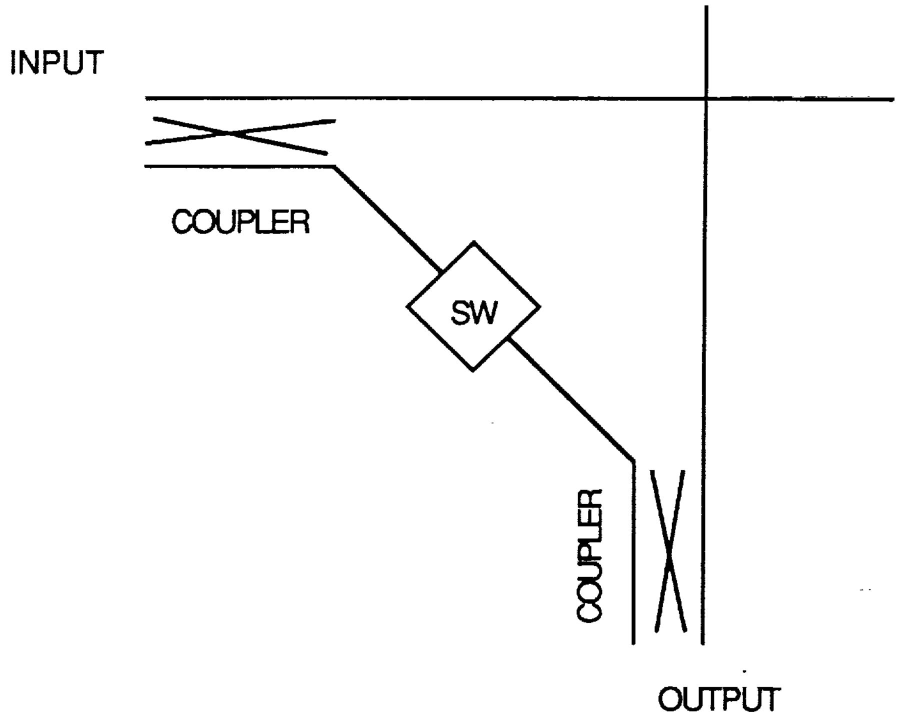

Figure 5.5-2. Couplers and Switches

The transmission lines are usually implemented as microstrip lines and there is an extremely remote possibility for failure. The couplers usually implemented are Lange couplers, being passive devices, they also have a very low probability of failure. The switch, however, uses active devices and therefore is subject to failure depending on the conditions of operation and the device used. Given the finite probability of failure of the switch, the problem is how to implement redundancy to increase the probability of success.

The solution Ford Aerospace presents is simply to add one extra horizontal line and one extra vertical line as shown in Figure 5.5-3. For example, to add redundancy to a 5 by 5 switch matrix, a sixth row and sixth column have been added. In normal operation any of the five inputs can be connected to any of the five outputs. For example, assuming the crosspoint has failed where input number 2 is connected to output number 4, the matrix can be reconfigured to connect input number 2 to output number 6. The sixth output is hard wired to input number 6. Then we connect input 6 to output 4. By going twice through the switch matrix we have established normal operation even when single-point failure has occurred. The reconfigured switch is shown in Figure 5.5-4, and the probability of success is very much increased. In the specific case of the 20 by 20 switch matrix, two more rows and two more columns have been added to increase the probability of success.

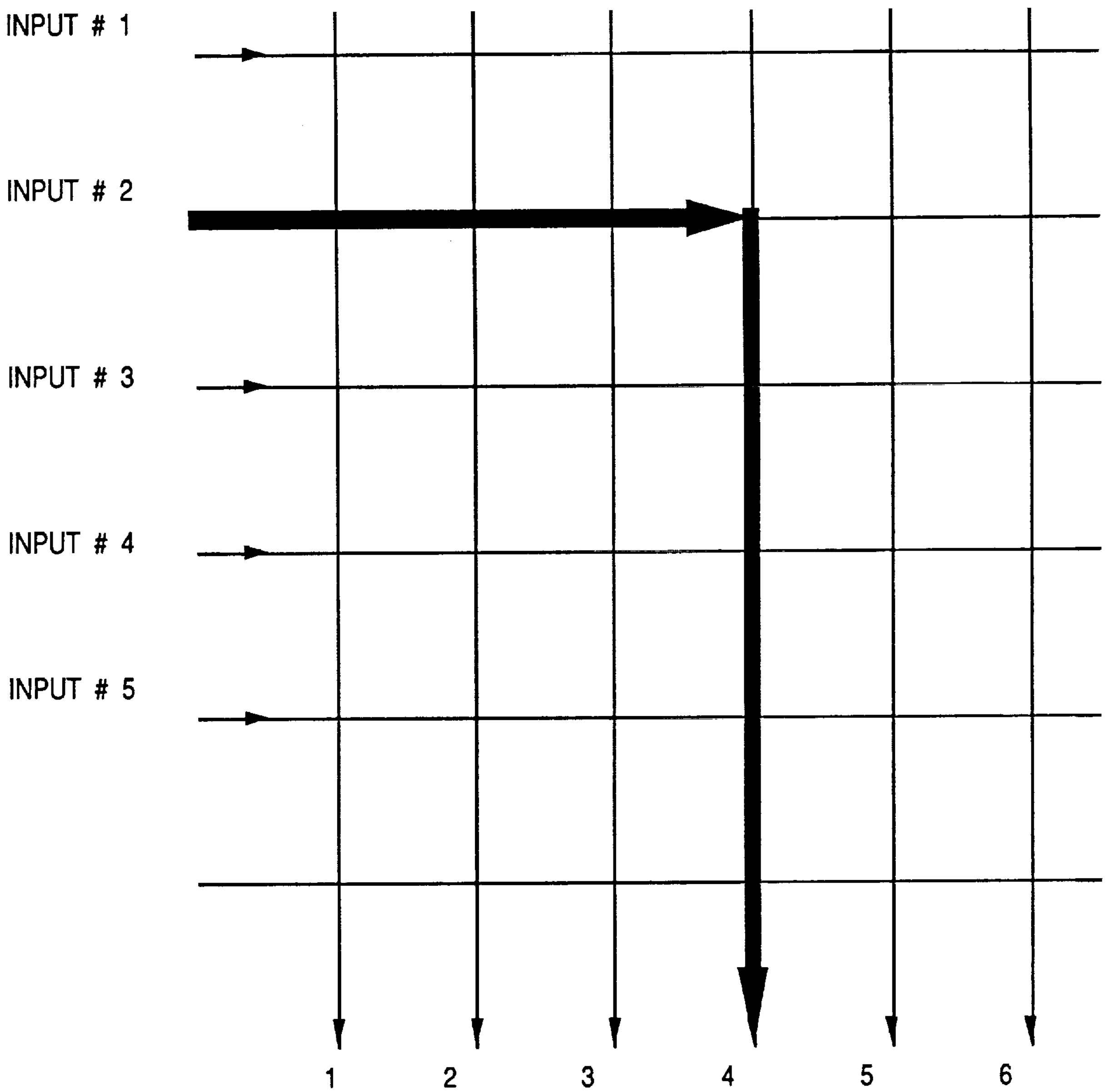

Figure 5.5-3. Switch Configured to Connect Input 2 to Output 4

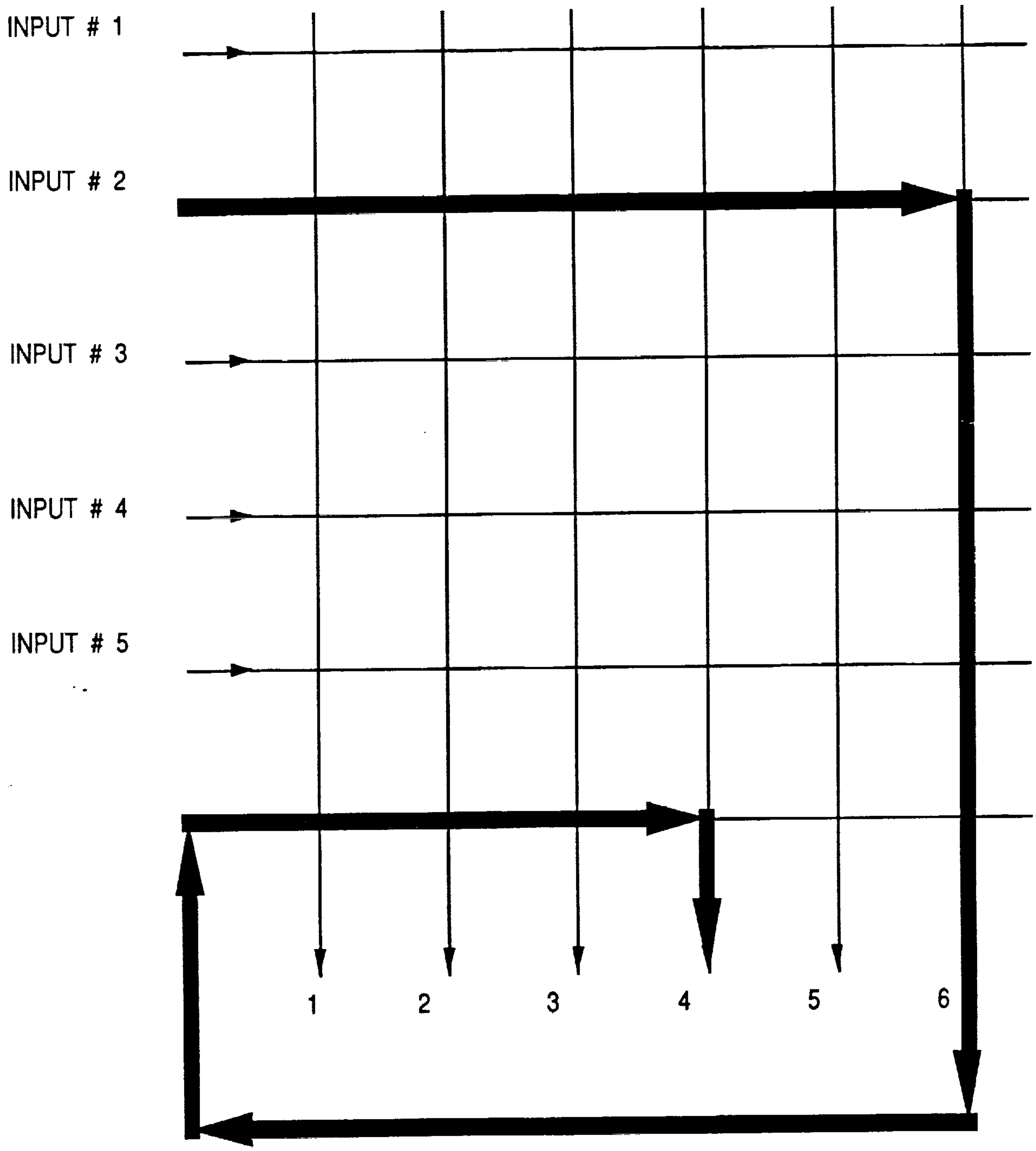

Figure 5.5-4. Reconfigured Switch

In the specific case of the 20 by 20 switch, the probability of failure of a crosspoint was computed for several cases and all for 10 years:

a.	Zero redundancy	0.4466
b.	One extra row and column	0.8069
c.	Two extra rows and columns (baseline)	0.9521
d.	Three extra rows and columns	0.9909

5.5.2 Electrical Performance

Frequency band	3.5 to 6.0 GHz
Ripple	±0.75 dB
Module gain	18 dB
Isolation	64 dB
Switching time	2.5 ns

5.5.3 Power Requirement

The technology used in the 20 by 20 switch matrix was rather old and used the just emerging dual-gate GaAs FET devices. Depending on the numbers of switches in the on position, the power required was changing. Thus a fair quantity can be given for the power required by a single switch. One fully conducting switch required 60 mA from a 5 V supply and 1 mA from a -5 V supply. In the off position of the switch, the power is negligible. With present technology, the on position of the switch requires 4 mA from a +5 V source.

5.5.4 Mechanical Considerations

The full matrix built by Ford Aerospace included the RF portion and a control and distribution unit.

Size:	
RF portion	18-3/4 x 19 x 3-1/4 inches
Control unit	17 x 17 x 3-1/4 inches
Weight:	
RF portion	19335 g (42 lb, 11 oz)
Control unit	4900 g (10 lb, 13 oz)
Interconnect cables	1910 g (4 lb, 3 oz)

With modern technology the reduction in weight is projected to be from 10 to 20 times less.

5.5.5 Projections for the Future

When the available facts are carefully studied the following conclusions may be drawn. Lower power and light weight requirements indicate the need for new components. Some of these components exist. NEC has produced a 2 by 2 switch in one chip. This suggests that a future switch will use some sort of chip as the building block.

Schindler et al [5-1] from Raytheon have reported a DC-20 GHz monolithic switch again indicating the extended capability when MMIC technique is involved.

Hayano et al [5-2] have reported an 8 x 8 switch, again leading to the conclusion that in the future the MMIC components will be the parts to be used.

The use of these or similar components will definitely reduce the size, weight, and power requirement and will make the solutions very attractive; however, none of the components are space approved and a qualification program may be necessary before they are made available for the next generation satellites.

REFERENCES

5-1 M.J. Schindler, M.E. Miller, K.M. Simon. "DC-20 GHz NXM Passive Switches," Raytheon Company Research Division, 131 Spring Street, Lexington, MA 02173 MTT-S Digest, p. 1001, 1988.

5-2 Hayano, Nagashima, Asai, Maeda and Furutsuka. "A GaAs 8x8 Matrix Switch for High-Speed Digital Communications", IEEE GaAs IC Symposium, 1987.

SECTION 6
CONCLUSIONS AND SUGGESTED FUTURE STUDIES

This section draws the conclusions of this study effort and lists suggested further future studies.

6.1 CONCLUSIONS/SUMMARY OF RESULTS

In our study of the MBA/Switch for the SGL uplink and downlink services, several issues related to system engineering, antenna, transmit/receive, and switch systems have been addressed and the results have been provided in the preceding sections. A summary of these results is presented here.

Bandwidth allocation at Ku-band is inadequate to serve the data rate requirements for the forward and return services. These call for the frequency reuse by dual-polarization transmissions. In addition, bandwidth-efficient higher-alphabet signaling schemes need to be considered. It may be necessary to abandon the simple "bent-pipe" IF switching concept and resort to demodulation and remodulation on board each service. This may also affect the link power budgets; this leads to the consideration of power-efficient forward error correction coding techniques.

Rain and depolarization effects at EHF, especially at Ka-band, pose a significant threat to the link availabilities at heavy rain areas such as JSC, KSC, and MSC. The locations of ATDRSS can be optimized to minimize these effects. ZOE is also dependent on the locations of the ATDRSS 1 and 2.

Hardware induced effects such as the nonlinear characteristics of the power amplifiers may necessitate the use of linearizers and limiters. Filter distortion effects, adjacent channel interference, and phase noise effects also degrade the performance and deserve careful consideration.

In addition, the ground stations must be sufficiently separated (at least two beamwidths) to minimize the interbeam interference effects.

It is also important to identify the components that are susceptible to the space radiation effects and shield or redesign them with rad-hard technologies for meeting the requirements of the space environment. In addition, modular design of the component subsystems is desirable for the possible future in-space replacement, servicing, and/or repair.

The MBA requirements can be met by two candidate approaches -- the prime-focus fed torus reflector approach and the shaped dual-offset reflector approach. The phased array approach may not be practical in the desired 1993 technology timeframe due to the slow progress of space-qualified MMICs needed for feasible implementations.

Feed designs, incorporating dual polarizations and multifrequency (14, 20, and 30 GHz) bands are desired. Reflector surface tolerance requirements are tighter for accommodating higher EHF frequency operations. Packaging, stowing, and deployment considerations may require designing and constructing in pieces, and assembling and folding of the torus antenna (for Configuration 2). This may pose other issues such as overall system reliability and gain loss due to possible misalignment of the pieces.

Multiple beam tracking considerations suggest use of flexible feed interconnect schemes such as the coaxial cables; however, coax cables are lossy, especially at EHF. Placement of up- and downconverters at the antenna assembly may raise other issues such as thermal control and radiation protection. Design of tracking mechanisms is simplified if effects of yaw errors can be assumed to be small, leading to a two-degree of freedom implementation. This however, may place the appropriate requirements on the navigation and attitude control system.

Availability of solid-state devices for low noise and power amplifiers may contribute to substantial performance improvement of the transmit/receive systems. In addition, devices such as linearizers and limiters provide additional performance improvements.

To comply with the SGL communications requirements, the switching system architecture must be complex. Redundant switch configurations are desired to improve the system reliability. IF (bent-pipe) switching concept is simple and does not affect the user communications hardware. However, the unavailability of the desired spectrum, especially at Ku-band, may mean that higher alphabet signaling schemes need to be considered. This would, however, affect both the space and ground users' hardware unless on-board demodulation and remodulation with higher alphabet signaling are considered. Major advances in baseband switching hardware technologies are taking place that will make both power and space efficient implementations feasible with 1993 state-of-the-art parts. Space qualification of these parts, however, may be doubtful by the 1993 timeframe; the leading technologies for these applications are, however, gallium arsenide and ECL bipolar semiconductors (gate array) and these technologies are inherently "rad-hard" and space qualification of the baseband switching circuits may not be too difficult.

While advances in all the relevant technology areas are rapidly taking place, it is of particular concern that system level testing be done of implementations with proven technologies.

6.2 PROPOSED FURTHER STUDIES

Further studies of proof concepts in both analog and digital switching hardware are desirable. In the analog switch technology area, the switch topologies must be studied in detail and hardware demonstrations performed. Relevant advanced technologies must be evaluated and the best technologies must be implemented in the proof-of-concept designs.

Digital switch hardware technology is evolving rapidly into a serious contender for the analog switch technology. In this area, there are proof-of-concept studies that are already under way, such as the variable rate modulators/demodulators with programmable modulation formats and data rates. Studies of high-speed FEC coding/decoding schemes are also being implemented. Baseband switching and multiplexing schemes at gigabit data rates deserve proof-of-concept implementation and evaluation studies with various emerging advanced technology such as the power-efficient ECL, GaAs, rad-hard CMOS and other circuit as well as gate-array implementations. Switching topologies and implementations also deserve further studies.

Transmit/receive hardware implementations, using solid-state and integrated devices need to be explored further. A master frequency plan must be developed in a separate study to address all the issues adequately that pertain to the requirements and implementation alternatives of the master frequency generator in its interfaces with other system oscillator requirements. Implementations with MMICs of the transmit/receive equipment deserve further study and proof-of-concept implementations are desirable. In-depth implementation studies of filters and multiplexer/demultiplexer are also to be performed.

In-depth design studies of MBA, including the tradeoffs for various approaches for reflectors (torus, dual reflector, phased arrays, and paraboloids with patch-array feeds), for feed and frequency selective surface designs supporting multiple frequency bands (14, 20, and 30 GHz) and dual polarization with the desired isolations, tracking mechanisms designs and implementations for individual beam coverages, are also desirable.

APPENDIX A
SPACE-TO-GROUND LINK ANALYSES

SGLS Analysis: JSC Ku-Band Downlink

SATELLITE LONGITUDE: 106 deg. West
GROUND STATION : Johnson Space Center
ELEVATION ANGLE : 53.5 degrees

Carrier Frequency: 13.80 GHz

Parameter	Value Units	Remarks
Transmit S/C Power	9.03 dBW	8.00 (W) Backed off Power
Feed Losses	1.00 dB	
Transmit Ant. Gain	48.05 dBi	2.40 (m) Antenna diam. 53.00 (%) Efficiency
EIRP (/Carrier)	56.09 dBW	
Free Space Loss	206.62 dB	37033.70 Range (km)
Rainy sky loss	9.71 dB	For 99.8% Availability
Pointing Loss	0.10 dB	
Polarization Loss	0.10 dB	
Net Path Loss	216.53 dB	
Receive S/C Gain	65.69 dBi	18.29 Meters 60.00 FT. Rcv. Ant. 53 % efficiency
Sys Temp(Rec. Input)	25.33 dB-K	341.00 (K) System Temp
Effective G/T	40.37 dB/K	
Rec'd Carrier Level	-94.75 dBW	
Boltzmann's Constant	-228.60 dBW/Hz-K	
Received C/No	108.52 dB-Hz	
Misc. Hardware Loss	0.00 dB	
ISI Degradation	0.50 dB	
Modem Impl. Loss	2.00 dB	
Symbol Rate	91.76 dB-Hz	1000.00 Mbaud 1.50 BW factor for QPSK
Avail. Eb/No	11.26 dB	
Req'd Eb/No	9.60 dB	1 E-05 Uncoded QPSK BER
Coding Gain	0.00 dB	
MARGIN	**1.66 dB**	
MINIMUM REQUIRED G/T WITH 3 dB MARGIN	41.70 dB/K	

SGL Analysis: Andover Ka-Band Downlink

SATELLITE LONGITUDE: 5.6 deg. West
GROUND STATION : ANDOVER
ELEVATION ANGLE : 9 DEGREES

CARRIER FREQUENCY: 19.45 GHz

Parameter	Value Units	Remarks
Transmit S/C Power	6.02 dBW	4.00 (W) Backed off Power
Feed Losses	1.00 dB	
Transmit Ant. Gain	51.04 dBi	2.40 (m) Antenna diam. 53.00 (%) Efficiency
EIRP (/Carrier)	56.06 dBW	
Free Space Loss	210.36 dB	40437 Range (km)
Rainy sky loss	8.87 dB	For 99.8% Availability
Pointing Loss	0.10 dB	
Polarization Loss	0.10 dB	
Net Path Loss	219.43 dB	
Receive S/C Gain	68.67 dBi	18.29 Meters 60.00 FT. Rcv. Ant. 53 % efficiency
Sys Temp(Rec. Input)	25.33 dB-K	341.00 (K) System Temp
Effective G/T	43.35 dB/K	
Rec'd Carrier Level	-94.70 dBW	
Boltzmann's Constant	-228.60 dBW/Hz-K	
Received C/No	108.57 dB-Hz	
Misc. Hardware Loss	0.00 dB	
ISI Degradation	0.50 dB	
Modem Impl. Loss	2.00 dB	
Symbol Rate	91.76 dB-Hz	1000.00 Mbaud 1.50 BW factor for QPSK
Avail. Eb/No	11.31 dB	
Req'd Eb/No	9.60 dB	1 E-05 Uncoded QPSK BER
Coding Gain	0.00 dB	
MARGIN	**1.71 dB**	

MINIMUM REQUIRED
G/T WITH 3 dB Margin 44.64 dB/K

SGL Analysis: Denver Ka-Band Downlink

SATELLITE LONGITUDE: 32 deg. West
GROUND STATION : DENVER
ELEVATION ANGLE : 9 degrees

Carrier Frequency: 19.45 GHz

Parameter	Value Units	Remarks
Transmit S/C Power	6.02 dBW	4.00 (W) Backed off Power
Feed Losses	1.00 dB	
Transmit Ant. Gain	51.04 dBi	2.40 (m) Antenna diam. 53.00 (%) Efficiency
EIRP (/Carrier)	56.06 dBW	
Free Space Loss	210.36 dB	40437 Range (km)
Rainy sky loss	9.43 dB	For 99.8% Availability
Pointing Loss	0.10 dB	
Polarization Loss	0.10 dB	
Net Path Loss	219.99 dB	
Receive S/C Gain	68.67 dBi	18.29 Meters 60.00 FT. Rcv. Ant. 53 % efficiency
Sys Temp(Rec. Input)	25.33 dB-K	341.00 (K) System Temp
Effective G/T	43.35 dB/K	
Rec'd Carrier Level	-95.26 dBW	
Boltzmann's Constant	-228.60 dBW/Hz-K	
Received C/No	108.01 dB-Hz	
Misc. Hardware Loss	0.00 dB	
ISI Degradation	0.50 dB	
Modem Impl. Loss	2.00 dB	
Symbol Rate	91.76 dB-Hz	1000.00 Mbaud 1.50 BW factor for QPSK
Avail. Eb/No	10.75 dB	
Req'd Eb/No	9.60 dB	1 E-05 Uncoded QPSK BER
Coding Gain	0.00 dB	
MARGIN	**1.15 dB**	
MINIMUM REQUIRED G/T WITH 3 dB Margin	45.20 dB/K	

SGL Analysis: JPL Ka-Band Downlink

SATELLITE LONGITUDE: 53 deg. West
GROUND STATION : JPL
ELEVATION ANGLE : 9 DEGREES

CARRIER FREQUENCY: 19.45 GHz

Parameter	Value Units	Remarks
Transmit S/C Power	6.02 dBW	4.00 (W) Backed off Power
Feed Losses	1.00 dB	
Transmit Ant. Gain	51.04 dBi	2.40 (m) Antenna diam. 53.00 (%) Efficiency
EIRP (/Carrier)	56.06 dBW	
Free Space Loss	210.36 dB	40437 Range (km)
Rainy sky loss	12.97 dB	For 99.8% Availability
Pointing Loss	0.10 dB	
Polarization Loss	0.10 dB	
Net Path Loss	223.53 dB	
Receive S/C Gain	68.67 dBi	18.29 Meters 60.00 FT. Rcv. Ant 53 % efficiency
Sys Temp(Rec. Input)	25.33 dB-K	341.00 (K) System Temp
Effective G/T	43.35 dB/K	
Rec'd Carrier Level	-98.80 dBW	
Boltzmann's Constant	-228.60 dBW/Hz-K	
Received C/No	104.47 dB-Hz	
Misc. Hardware Loss	0.00 dB	
ISI Degradation	0.50 dB	
Modem Impl. Loss	2.00 dB	
Symbol Rate	91.76 dB-Hz	1000.00 Mbaud 1.50 BW factor for QPSK
Avail. Eb/No	7.21 dB	
Req'd Eb/No	9.60 dB	1 E-05 Uncoded QPSK BER
Coding Gain	0.00 dB	
MARGIN	-2.39 dB	
MINIMUM REQUIRED G/T WITH 3 dB Margin	48.74 dB/K	

SGL Analysis: Goddard Ka-Band Downlink

SATELLITE LONGITUDE: 106 deg. West
GROUND STATION : GODDARD
ELEVATION ANGLE : 35.7 deg.

Carrier Frequency: 19.45 GHz

Parameter	Value Units	Remarks
Transmit S/C Power	6.02 dBW	4.00 (W) Backed off Power
Feed Losses	1.00 dB	
Transmit Ant. Gain	51.04 dBi	2.40 (m) Antenna diam. 53.00 (%) Efficiency
EIRP (/Carrier)	56.06 dBW	
Free Space Loss	209.88 dB	38230.04 Range (km)
Rainy sky loss	9.60 dB	For 99.8% Availability
Pointing Loss	0.10 dB	
Polarization Loss	0.10 dB	
Net Path Loss	219.68 dB	
Receive S/C Gain	68.67 dBi	18.29 Meters 60.00 FT. Rcv. Ant. 53 % efficiency
Sys Temp(Rec. Input)	25.33 dB-K	341.00 (K) System Temp
Effective G/T	43.35 dB/K	
Rec'd Carrier Level	-94.95 dBW	
Boltzmann's Constant	-228.60 dBW/Hz-K	
Received C/No	108.33 dB-Hz	
Misc. Hardware Loss	0.00 dB	
ISI Degradation	0.50 dB	
Modem Impl. Loss	2.00 dB	
Symbol Rate	91.76 dB-Hz	1000.00 Mbaud 1.50 BW factor for QPSK
Avail. Eb/No	11.07 dB	
Req'd Eb/No	9.60 dB	1 E-05 Uncoded QPSK BER
Coding Gain	0.00 dB	
MARGIN	**1.47 dB**	
MINIMUM REQUIRED G/T WITH 3dB MARGIN	44.88 dB/K	

SGL Analysis: GSFC Ka-Band Downlink

SATELLITE LONGITUDE: 9 deg. West
GROUND STATION : GODDARD
ELEVATION ANGLE : 8.5 deg.

Carrier Frequency: 19.45 GHz

Parameter	Value Units	Remarks
Transmit S/C Power	6.02 dBW	4.00 (W) Backed off Power
Feed Losses	1.00 dB	
Transmit Ant. Gain	51.04 dBi	2.40 (m) Antenna diam. 53.00 (%) Efficiency
EIRP (/Carrier)	56.06 dBW	
Free Space Loss	210.36 dB	40437 Range (km)
Rainy sky loss	22.02 dB	For 99.8% Availability
Pointing Loss	0.10 dB	
Polarization Loss	0.10 dB	
Net Path Loss	232.58 dB	
Receive S/C Gain	68.67 dBi	18.29 Meters 60.00 FT. Rcv. Ant. 53 % efficiency
Sys Temp(Rec. Input)	25.33 dB-K	341.00 (K) System Temp
Effective G/T	43.35 dB/K	
Rec'd Carrier Level	-107.85 dBW	
Boltzmann's Constant	-228.60 dBW/Hz-K	
Received C/No	95.42 dB-Hz	
Misc. Hardware Loss	0.00 dB	
ISI Degradation	0.50 dB	
Modem Impl. Loss	2.00 dB	
Symbol Rate	91.76 dB-Hz	1000.00 Mbaud 1.50 BW factor for QPSK
Avail. Eb/No	-1.84 dB	
Req'd Eb/No	9.60 dB	1 E-05 Uncoded QPSK BER
Coding Gain	0.00 dB	
MARGIN	**-11.44 dB**	
MINIMUM REQUIRED G/T WITH 3 dB Margin	57.79 dB/K	

SGL Analysis: MFC Ka-Band Downlink

SATELLITE LONGITUDE: 106 deg. West
GROUND STATION : MARSHAL Center
ELEVATION ANGLE : 44.8 degrees

Carrier Frequency: 19.45 GHz

Parameter	Value Units	Remarks
Transmit S/C Power	6.02 dBW	4.00 (W) Backed off Power
Feed Losses	1.00 dB	
Transmit Ant. Gain	51.04 dBi	2.40 (m) Antenna diam. 53.00 (%) Efficiency
EIRP (/Carrier)	56.06 dBW	
Free Space Loss	209.71 dB	37516 Range (km)
Rainy sky loss	15.55 dB	For 99.8% Availability
Pointing Loss	0.10 dB	
Polarization Loss	0.10 dB	
Net Path Loss	225.46 dB	
Receive S/C Gain	68.67 dBi	18.29 Meters 60.00 FT. Rcv. Ant. 53 % efficiency
Sys Temp(Rec. Input)	25.33 dB-K	341.00 (K) System Temp
Effective G/T	43.35 dB/K	
Rec'd Carrier Level	-100.73 dBW	
Boltzmann's Constant	-228.60 dBW/Hz-K	
Received C/No	102.54 dB-Hz	
Misc. Hardware Loss	0.00 dB	
ISI Degradation	0.50 dB	
Modem Impl. Loss	2.00 dB	
Symbol Rate	91.76 dB-Hz	1000.00 Mbaud 1.50 BW factor for QPSK
Avail. Eb/No	5.28 dB	
Req'd Eb/No	9.60 dB	1 E-05 Uncoded QPSK BER
Coding Gain	0.00 dB	
MARGIN	**-4.32 dB**	
MINIMUM REQUIRED G/T WITH 3 dB Margin	50.67 dB/K	

SGL Analysis: MFC Ka-Band Downlink

SATELLITE LONGITUDE: 25.1 deg. West
GROUND STATION : MARSHAL Center
ELEVATION ANGLE : 9 degrees

Carrier Frequency: 19.45 GHz

Parameter	Value Units	Remarks
Transmit S/C Power	6.02 dBW	4.00 (W) Backed off Power
Feed Losses	1.00 dB	
Transmit Ant. Gain	51.04 dBi	2.40 (m) Antenna diam. 53.00 (%) Efficiency
EIRP (/Carrier)	56.06 dBW	
Free Space Loss	210.36 dB	40437 Range (km)
Rainy sky loss	35.45 dB	For 99.8% Availability
Pointing Loss	0.10 dB	
Polarization Loss	0.10 dB	
Net Path Loss	246.01 dB	
Receive S/C Gain	68.67 dBi	18.29 Meters 60.00 FT. Rcv. Ant. 53 % efficiency
Sys Temp(Rec. Input)	25.33 dB-K	341.00 (K) System Temp
Effective G/T	43.35 dB/K	
Rec'd Carrier Level	-121.28 dBW	
Boltzmann's Constant	-228.60 dBW/Hz-K	
Received C/No	81.99 dB-Hz	
Misc. Hardware Loss	0.00 dB	
ISI Degradation	0.50 dB	
Modem Impl. Loss	2.00 dB	
Symbol Rate	91.76 dB-Hz	1000.00 Mbaud 1.50 BW factor for QPSK
Avail. Eb/No	-15.27 dB	
Req'd Eb/No	9.60 dB	1 E-05 Uncoded QPSK BER
Coding Gain	0.00 dB	
MARGIN	**-24.87 dB**	

MINIMUM REQUIRED
G/T WITH 3 dB Margin 71.22 dB/K

SGL Analysis: JSC Ka-Band Downlink

SATELLITE LONGITUDE: 106 deg. West
GROUND STATION : Johnson Space Center
ELEVATION ANGLE : 53.5 degrees

Carrier Frequency: 19.45 GHz

Parameter	Value Units	Remarks
Transmit S/C Power	6.02 dBW	4.00 (W) Backed off Power
Feed Losses	1.00 dB	
Transmit Ant. Gain	51.04 dBi	2.40 (m) Antenna diam. 53.00 (%) Efficiency
EIRP (/Carrier)	56.06 dBW	
Free Space Loss	209.60 dB	37034 Range (km)
Rainy sky loss	16.01 dB	For 99.8% Availability
Pointing Loss	0.10 dB	
Polarization Loss	0.10 dB	
Net Path Loss	225.81 dB	
Receive S/C Gain	68.67 dBi	18.29 Meters 60.00 FT. Rcv. Ant. 53 % efficiency
Sys Temp(Rec. Input)	25.33 dB-K	341.00 (K) System Temp
Effective G/T	43.35 dB/K	
Rec'd Carrier Level	-101.08 dBW	
Boltzmann's Constant	-228.60 dBW/Hz-K	
Received C/No	102.19 dB-Hz	
Misc. Hardware Loss	0.00 dB	
ISI Degradation	0.50 dB	
Modem Impl. Loss	2.00 dB	
Symbol Rate	91.76 dB-Hz	1000.00 Mbaud 1.50 BW factor for QPSK
Avail. Eb/No	4.93 dB	
Req'd Eb/No	9.60 dB	1 E-05 Uncoded QPSK BER
Coding Gain	0.00 dB	
MARGIN	**-4.67 dB**	
MINIMUM REQUIRED G/T WITH 3 dB Margin	51.02 dB/K	

SGL Analysis: JSC Ka-Band Downlink

SATELLITE LONGITUDE: 25 deg. West
GROUND STATION : Johnson Space Center
ELEVATION ANGLE : 9 degrees

Carrier Frequency: 19.45 GHz

Parameter	Value Units	Remarks
Transmit S/C Power	6.02 dBW	4.00 (W) Backed off Power
Feed Losses	1.00 dB	
Transmit Ant. Gain	51.04 dBi	2.40 (m) Antenna diam. 53.00 (%) Efficiency
EIRP (/Carrier)	56.06 dBW	
Free Space Loss	210.36 dB	40437 Range (km)
Rainy sky loss	38.24 dB	For 99.8% Availability
Pointing Loss	0.10 dB	
Polarization Loss	0.10 dB	
Net Path Loss	248.80 dB	
Receive S/C Gain	68.67 dBi	18.29 Meters 60.00 FT. Rcv. Ant. 53 % efficiency
Sys Temp(Rec. Input)	25.33 dB-K	341.00 (K) System Temp
Effective G/T	43.35 dB/K	
Rec'd Carrier Level	-124.07 dBW	
Boltzmann's Constant	-228.60 dBW/Hz-K	
Received C/No	79.20 dB-Hz	
Misc. Hardware Loss	0.00 dB	
ISI Degradation	0.50 dB	
Modem Impl. Loss	2.00 dB	
Symbol Rate	91.76 dB-Hz	1000.00 Mbaud 1.50 BW factor for QPSK
Avail. Eb/No	-18.06 dB	
Req'd Eb/No	9.60 dB	1 E-05 Uncoded QPSK BER
Coding Gain	0.00 dB	
MARGIN	-27.66 dB	

MINIMUM REQUIRED
G/T WITH 3 dB Margin 74.01 dB/K

SGL Analysis: White Sands Ka-Band Downlink

SATELLITE LONGITUDE: 106 deg. West
GROUND STATION : White Sands
ELEVATION ANGLE : 52.3 degrees

Carrier Frequency: 19.45 GHz

Parameter	Value Units	Remarks
Transmit S/C Power	9.03 dBW	8.00 (W) Backed off Power
Feed Losses	1.00 dB	
Transmit Ant. Gain	51.04 dBi	2.40 (m) Antenna diam. 53.00 (%) Efficiency
EIRP (/Carrier)	59.07 dBW	
Free Space Loss	209.61 dB	37067.03 Range (km)
Rainy sky loss	2.27 dB	For 99.8% Availability
Pointing Loss	0.10 dB	
Polarization Loss	0.10 dB	
Net Path Loss	212.08 dB	
Receive S/C Gain	68.67 dBi	18.29 Meters 60.00 FT. Rcv. Ant. 53 % efficiency
Sys Temp(Rec. Input)	25.33 dB-K	341.00 (K) System Temp
Effective G/T	43.35 dB/K	
Rec'd Carrier Level	-84.34 dBW	
Boltzmann's Constant	-228.60 dBW/Hz-K	
Received C/No	118.94 dB-Hz	
Misc. Hardware Loss	0.00 dB	
ISI Degradation	0.50 dB	
Modem Impl. Loss	2.00 dB	
Symbol Rate	94.77 dB-Hz	2000.00 Mbaud 1.50 BW factor for QPSK
Avail. Eb/No	18.66 dB	
Req'd Eb/No	9.60 dB	1 E-05 Uncoded QPSK BER
Coding Gain	0.00 dB	
MARGIN	**9.06 dB**	
MINIMUM REQUIRED G/T WITH 3dB MARGIN	37.28 dB/K	

SGL Analysis: White Sands Ka-Band Downlink

SATELLITE LONGITUDE: 92 deg. West
GROUND STATION : White Sands
ELEVATION ANGLE : 49.2 degrees

Carrier Frequency: 19.45 GHz

Parameter	Value Units	Remarks
Transmit S/C Power	9.03 dBW	8.00 (W) Backed off Power
Feed Losses	1.00 dB	
Transmit Ant. Gain	51.04 dBi	2.40 (m) Antenna diam. 53.00 (%) Efficiency
EIRP (/Carrier)	59.07 dBW	
Free Space Loss	209.64 dB	37190.18 Range (km)
Rainy sky loss	2.48 dB	For 99.8% Availability
Pointing Loss	0.10 dB	
Polarization Loss	0.10 dB	
Net Path Loss	212.32 dB	
Receive S/C Gain	68.67 dBi	18.29 Meters 60.00 FT. Rcv. Ant. 53 % efficiency
Sys Temp(Rec. Input)	25.33 dB-K	341.00 (K) System Temp
Effective G/T	43.35 dB/K	
Rec'd Carrier Level	-84.58 dBW	
Boltzmann's Constant	-228.60 dBW/Hz-K	
Received C/No	118.70 dB-Hz	
Misc. Hardware Loss	0.00 dB	
ISI Degradation	0.50 dB	
Modem Impl. Loss	2.00 dB	
Symbol Rate	94.77 dB-Hz	2000.00 Mbaud 1.50 BW factor for QPSK
Avail. Eb/No	18.43 dB	
Req'd Eb/No	9.60 dB	1 E-05 Uncoded QPSK BER
Coding Gain	0.00 dB	
MARGIN	**8.83 dB**	

MINIMUM REQUIRED
G/T WITH 3dB MARGIN 37.52 dB/K

SGL Analysis: White Sands Ka-Band Downlink

SATELLITE LONGITUDE: 90 deg. West
GROUND STATION : White Sands
ELEVATION ANGLE : 48.3 degrees

Carrier Frequency: 19.45 GHz

Parameter	Value Units	Remarks
Transmit S/C Power	9.03 dBW	8.00 (W) Backed off Power
Feed Losses	1.00 dB	
Transmit Ant. Gain	51.04 dBi	2.40 (m) Antenna diam. 53.00 (%) Efficiency
EIRP (/Carrier)	59.07 dBW	
Free Space Loss	209.65 dB	37256.85 Range (km)
Rainy sky loss	2.47 dB	For 99.8% Availability
Pointing Loss	0.10 dB	
Polarization Loss	0.10 dB	
Net Path Loss	212.32 dB	
Receive S/C Gain	68.67 dBi	18.29 Meters 60.00 FT. Rcv. Ant. 53 % efficiency
Sys Temp(Rec. Input)	25.33 dB-K	341.00 (K) System Temp
Effective G/T	43.35 dB/K	
Rec'd Carrier Level	-84.58 dBW	
Boltzmann's Constant	-228.60 dBW/Hz-K	
Received C/No	118.69 dB-Hz	
Misc. Hardware Loss	0.00 dB	
ISI Degradation	0.50 dB	
Modem Impl. Loss	2.00 dB	
Symbol Rate	94.77 dB-Hz	2000.00 Mbaud 1.50 BW factor for QPSK
Avail. Eb/No	18.42 dB	
Req'd Eb/No	9.60 dB	1E-05 Uncoded QPSK BER
Coding Gain	0.00 dB	
MARGIN	**8.82 dB**	
MINIMUM REQUIRED G/T WITH 3dB MARGIN	37.53 dB/K	

SGL Analysis: White Sands Ka-Band Downlink

SATELLITE	LONGITUDE:	171 deg. West
GROUND	STATION :	White Sands
ELEVATION	ANGLE :	12.8 degrees

Carrier Frequency: 19.45 GHz

Parameter	Value Units	Remarks
Transmit S/C Power	9.03 dBW	8.00 (W) Backed off Power
Feed Losses	1.00 dB	
Transmit Ant. Gain	51.04 dBi	2.40 (m) Antenna diam. 53.00 (%) Efficiency
EIRP (/Carrier)	59.07 dBW	
Free Space Loss	210.29 dB	40097.69 Range (km)
Rainy sky loss	8.26 dB	For 99.8% Availability
Pointing Loss	0.10 dB	
Polarization Loss	0.10 dB	
Net Path Loss	218.75 dB	
Receive S/C Gain	68.67 dBi	18.29 Meters 60.00 FT. Rcv. Ant. 53 % efficiency
Sys Temp(Rec. Input)	25.33 dB-K	341.00 (K) System Temp
Effective G/T	43.35 dB/K	
Rec'd Carrier Level	-91.01 dBW	
Boltzmann's Constant	-228.60 dBW/Hz-K	
Received C/No	112.26 dB-Hz	
Misc. Hardware Loss	0.00 dB	
ISI Degradation	0.50 dB	
Modem Impl. Loss	2.00 dB	
Symbol Rate	94.77 dB-Hz	2000.00 Mbaud 1.50 BW factor for QPSK
Avail. Eb/No	11.99 dB	
Req'd Eb/No	9.60 dB	1 E-05 Uncoded QPSK BER
Coding Gain	0.00 dB	
MARGIN	**2.39 dB**	
MINIMUM REQUIRED G/T WITH 3dB MARGIN	43.96 dB/K	

SGL Analysis: White Sands Ka-Band Downlink

SATELLITE LONGITUDE: 38.2 deg. West
GROUND STATION : White Sands
ELEVATION ANGLE : 10 deg.

Carrier Frequency: 19.45 GHz

Parameter	Value Units	Remarks
Transmit S/C Power	9.03 dBW	8.00 (W) Backed off Power
Feed Losses	1.00 dB	
Transmit Ant. Gain	51.04 dBi	2.40 (m) Antenna diam. 53.00 (%) Efficiency
EIRP (/Carrier)	59.07 dBW	
Free Space Loss	210.33 dB	40279.18 Range (km)
Rainy sky loss	9.82 dB	For 99.8% Availability
Pointing Loss	0.10 dB	
Polarization Loss	0.10 dB	
Net Path Loss	220.35 dB	
Receive S/C Gain	68.67 dBi	18.29 Meters 60.00 FT. Rcv. Ant. 53 % efficiency
Sys Temp(Rec. Input)	25.33 dB-K	341.00 (K) System Temp
Effective G/T	43.35 dB/K	
Rec'd Carrier Level	-92.61 dBW	
Boltzmann's Constant	-228.60 dBW/Hz-K	
Received C/No	110.66 dB-Hz	
Misc. Hardware Loss	0.00 dB	
ISI Degradation	0.50 dB	
Modem Impl. Loss	2.00 dB	
Symbol Rate	94.77 dB-Hz	2000.00 Mbaud 1.50 BW factor for QPSK
Avail. Eb/No	10.39 dB	
Req'd Eb/No	9.60 dB	1E-05 Uncoded QPSK BER
Coding Gain	0.00 dB	
MARGIN	**0.79 dB**	
MINIMUM REQUIRED G/T WITH 3dB MARGIN	45.55 dB/K	

SGL Analysis: White Sands Ka-Band Downlink

SATELLITE LONGITUDE: 37.2 deg. West
GROUND STATION : White Sands
ELEVATION ANGLE : 9 degrees

Carrier Frequency: 19.45 GHz

Parameter	Value Units	Remarks
Transmit S/C Power	9.03 dBW	8.00 (W) Backed off Power
Feed Losses	1.00 dB	
Transmit Ant. Gain	51.04 dBi	2.40 (m) Antenna diam. 53.00 (%) Efficiency
EIRP (/Carrier)	59.07 dBW	
Free Space Loss	210.36 dB	40437 Range (km)
Rainy sky loss	10.62 dB	For 99.8% Availability
Pointing Loss	0.10 dB	
Polarization Loss	0.10 dB	
Net Path Loss	221.18 dB	
Receive S/C Gain	68.67 dBi	18.29 Meters 60.00 FT. Rcv. Ant. 53 % efficiency
Sys Temp(Rec. Input)	25.33 dB-K	341.00 (K) System Temp
Effective G/T	43.35 dB/K	
Rec'd Carrier Level	-93.44 dBW	
Boltzmann's Constant	-228.60 dBW/Hz-K	
Received C/No	109.83 dB-Hz	
Misc. Hardware Loss	0.00 dB	
ISI Degradation	0.50 dB	
Modem Impl. Loss	2.00 dB	
Symbol Rate	94.77 dB-Hz	2000.00 Mbaud 1.50 BW factor for QPSK
Avail. Eb/No	9.56 dB	
Req'd Eb/No	9.60 dB	1 E-05 Uncoded QPSK BER
Coding Gain	0.00 dB	
MARGIN	**-0.04 dB**	

MINIMUM REQUIRED
G/T WITH 3 dB Margin 46.39 dB/K

SGL Analysis: JCS Ku-Band Downlink Case 6

SATELLITE LONGITUDE: 90 deg. West
GROUND STATION : Johnson Space Center
ELEVATION ANGLE : 55.1 deg.

Carrier Frequency: 13.80 GHz

Parameter	Value Units	Remarks
Transmit S/C Power	9.03 dBW	8.00 (W) Backed off Power
Feed Losses	1.00 dB	
Transmit Ant. Gain	48.05 dBi	2.40 (m) Antenna diam. 53.00 (%) Efficiency
EIRP (/Carrier)	56.09 dBW	
Free Space Loss	206.61 dB	36989.25 Range (km)
Rainy sky loss	9.59 dB	For 99.8% Availability
Pointing Loss	0.10 dB	
Polarization Loss	0.10 dB	
Net Path Loss	216.40 dB	
Receive S/C Gain	65.69 dBi	18.29 Meters 60.00 FT. Rcv. Ant. 53 % efficiency
Sys Temp(Rec. Input)	25.33 dB-K	341.00 (K) System Temp
Effective G/T	40.37 dB/K	
Rec'd Carrier Level	-94.62 dBW	
Boltzmann's Constant	-228.60 dBW/Hz-K	
Received C/No	108.65 dB-Hz	
Misc. Hardware Loss	0.00 dB	
ISI Degradation	0.50 dB	
Modem Impl. Loss	2.00 dB	
Symbol Rate	91.76 dB-Hz	1000.00 Mbaud 1.50 BW factor for QPSK
Avail. Eb/No	11.39 dB	
Req'd Eb/No	9.60 dB	1 E-05 Uncoded QPSK BER
Coding Gain	0.00 dB	
MARGIN	**1.79 dB**	
MINIMUM REQUIRED G/T WITH 3 dB MARGIN	41.57 dB/K	

SGL Analysis: JSC Ku-Band Downlink

SATELLITE LONGITUDE: 28 deg. West
GROUND STATION: Johnson Space Center
ELEVATION ANGLE: 11.3 deg.

Carrier Frequency: 13.80 GHz

Parameter	Value Units	Remarks
Transmit S/C Power	9.03 dBW	8.00 (W) Backed off Power
Feed Losses	1.00 dB	
Transmit Ant. Gain	48.05 dBi	2.40 (m) Antenna diam. 53.00 (%) Efficiency
EIRP (/Carrier)	56.09 dBW	
Free Space Loss	207.33 dB	40194.92 Range (km)
Rainy sky loss	19.35 dB	For 99.8% Availability
Pointing Loss	0.10 dB	
Polarization Loss	0.10 dB	
Net Path Loss	226.88 dB	
Receive S/C Gain	65.69 dBi	18.29 Meters 60.00 FT. Rcv. Ant. 53 % efficiency
Sys Temp(Rec. Input)	25.33 dB-K	341.00 (K) System Temp
Effective G/T	40.37 dB/K	
Rec'd Carrier Level	-105.10 dBW	
Boltzmann's Constant	-228.60 dBW/Hz-K	
Received C/No	98.17 dB-Hz	
Misc. Hardware Loss	0.00 dB	
ISI Degradation	0.50 dB	
Modem Impl. Loss	2.00 dB	
Symbol Rate	91.76 dB-Hz	1000.00 Mbaud 1.50 BW factor for QPSK
Avail. Eb/No	0.91 dB	
Req'd Eb/No	9.60 dB	1 E-05 Uncoded QPSK BER
Coding Gain	0.00 dB	
MARGIN	**-8.69 dB**	
MINIMUM REQUIRED G/T WITH 3 dB MARGIN	52.06 dB/K	

SGL Analysis: JSC Ku-Band Downlink

SATELLITE LONGITUDE: 26 deg. West
GROUND STATION : Johnson Space Center
ELEVATION ANGLE : 10 deg.

Carrier Frequency: 13.80 GHz

Parameter	Value Units	Remarks
Transmit S/C Power	9.03 dBW	8.00 (W) Backed off Power
Feed Losses	1.00 dB	
Transmit Ant. Gain	48.05 dBi	2.40 (m) Antenna diam. 53.00 (%) Efficiency
EIRP (/Carrier)	56.09 dBW	
Free Space Loss	207.35 dB	40279.18 Range (km)
Rainy sky loss	20.08 dB	For 99.8% Availability
Pointing Loss	0.10 dB	
Polarization Loss	0.10 dB	
Net Path Loss	227.63 dB	
Receive S/C Gain	65.69 dBi	18.29 Meters 60.00 FT. Rcv. Ant. 5 3 % efficiency
Sys Temp(Rec. Input)	25.33 dB-K	341.00 (K) System Temp
Effective G/T	40.37 dB/K	
Rec'd Carrier Level	-105.85 dBW	
Boltzmann's Constant	-228.60 dBW/Hz-K	
Received C/No	97.42 dB-Hz	
Misc. Hardware Loss	0.00 dB	
ISI Degradation	0.50 dB	
Modem Impl. Loss	2.00 dB	
Symbol Rate	91.76 dB-Hz	1000.00 Mbaud 1.50 BW factor for QPSK
Avail. Eb/No	0.16 dB	
Req'd Eb/No	9.60 dB	1 E-05 Uncoded QPSK BER
Coding Gain	0.00 dB	
MARGIN	**-9.44 dB**	

MINIMUM REQUIRED
G/T WITH 3 dB MARGIN 52.80 dB/K

SGL Analysis: JSC Ku-Band Downlink

SATELLITE LONGITUDE: 25 deg. West
GROUND STATION : Johnson Space Center
ELEVATION ANGLE : 9 degrees

CARRIER FREQUENCY 13.80 GHz

Parameter	Value Units	Remarks
Transmit S/C Power	9.03 dBW	8.00 (W) Backed off Power
Feed Losses	1.00 dB	
Transmit Ant. Gain	48.05 dBi	2.40 (m) Antenna diam. 53.00 (%) Efficiency
EIRP (/Carrier)	56.09 dBW	
Free Space Loss	207.38 dB	40437.00 Range (km)
Rainy sky loss	20.81 dB	For 99.8% Availability
Pointing Loss	0.10 dB	
Polarization Loss	0.10 dB	
Net Path Loss	228.39 dB	
Receive S/C Gain	65.69 dBi	18.29 Meters 60.00 FT. Rcv. Ant. 53 % efficiency
Sys Temp(Rec. Input)	25.33 dB-K	341.00 (K) System Temp
Effective G/T	40.37 dB/K	
Rec'd Carrier Level	-106.61 dBW	
Boltzmann's Constant	-228.60 dBW/Hz-K	
Received C/No	96.66 dB-Hz	
Misc. Hardware Loss	0.00 dB	
ISI Degradation	0.50 dB	
Modem Impl. Loss	2.00 dB	
Symbol Rate	91.76 dB-Hz	1000.00 Mbaud 1.50 BW factor for QPSK
Avail. Eb/No	-0.60 dB	
Req'd Eb/No	9.60 dB	1 E-05 Uncoded QPSK BER
Coding Gain	0.00 dB	
MARGIN	**-10.20 dB**	

MINIMUM REQUIRED
G/T WITH 3 dB Margin 53.57 dB/K

SGL Analysis: White Sands Ku-Band Downlink

SATELLITE LONGITUDE: 171 deg. West
GROUND STATION : White Sands
ELEVATION ANGLE : 12.8 degrees

Carrier Frequency: 13.80 GHz

Parameter	Value Units	Remarks
Transmit S/C Power	9.03 dBW	8.00 (W) Backed off Power
Feed Losses	1.00 dB	
Transmit Ant. Gain	48.05 dBi	2.40 (m) Antenna diam. 53.00 (%) Efficiency
EIRP (/Carrier)	56.09 dBW	
Free Space Loss	207.31 dB	40097.69 Range (km)
Rainy sky loss	4.70 dB	For 99.8% Availability
Pointing Loss	0.10 dB	
Polarization Loss	0.10 dB	
Net Path Loss	212.21 dB	
Receive S/C Gain	65.69 dBi	18.29 Meters 60.00 FT. Rcv. Ant. 53 % efficiency
Sys Temp(Rec. Input)	25.33 dB-K	341.00 (K) System Temp
Effective G/T	40.37 dB/K	
Rec'd Carrier Level	-90.43 dBW	
Boltzmann's Constant	-228.60 dBW/Hz-K	
Received C/No	112.84 dB-Hz	
Misc. Hardware Loss	0.00 dB	
ISI Degradation	0.50 dB	
Modem Impl. Loss	2.00 dB	
Symbol Rate	91.76 dB-Hz	1000.00 Mbaud 1.50 BW factor for QPSK
Avail. Eb/No	15.58 dB	
Req'd Eb/No	9.60 dB	1E-05 Uncoded QPSK BER
Coding Gain	0.00 dB	
MARGIN	**5.98 dB**	

MINIMUM REQUIRED
G/T WITH 3 dB MARGIN 37.39 dB/K

SGL Analysis: White Sands Ku-Band Downlink

SATELLITE LONGITUDE: 106 deg. West
GROUND STATION : White Sands
ELEVATION ANGLE : 52.3 degrees

Carrier Frequency: 13.80 GHz

Parameter	Value Units	Remarks
Transmit S/C Power	9.03 dBW	8.00 (W) Backed off Power
Feed Losses	1.00 dB	
Transmit Ant. Gain	48.05 dBi	2.40 (m) Antenna diam. 53.00 (%) Efficiency
EIRP (/Carrier)	56.09 dBW	
Free Space Loss	206.63 dB	37067.03 Range (km)
Rainy sky loss	1.05 dB	For 99.8% Availability
Pointing Loss	0.10 dB	
Polarization Loss	0.10 dB	
Net Path Loss	207.88 dB	
Receive S/C Gain	65.69 dBi	18.29 Meters 60.00 FT. Rcv. Ant. 5 3 % efficiency
Sys Temp(Rec. Input)	25.33 dB-K	341.00 (K) System Temp
Effective G/T	40.37 dB/K	
Rec'd Carrier Level	-86.10 dBW	
Boltzmann's Constant	-228.60 dBW/Hz-K	
Received C/No	117.17 dB-Hz	
Misc. Hardware Loss	0.00 dB	
ISI Degradation	0.50 dB	
Modem Impl. Loss	2.00 dB	
Symbol Rate	91.76 dB-Hz	1000.00 Mbaud 1.50 BW factor for QPSK
Avail. Eb/No	19.91 dB	
Req'd Eb/No	9.60 dB	1 E-05 Uncoded QPSK BER
Coding Gain	0.00 dB	
MARGIN	**10.31 dB**	

MINIMUM REQUIRED
G/T WITH 3 dB MARGIN 33.05 dB/K

SGL Analysis: Andover Ku-Band Downlink

SATELLITE LONGITUDE: 15 deg. West
GROUND STATION : ANDOVER
ELEVATION ANGLE : 15.3 DEGREES

CARRIER FREQUENCY: 13.80 GHz

Parameter	Value Units	Remarks
Transmit S/C Power	9.03 dBW	8.00 (W) Backed off Power
Feed Losses	1.00 dB	
Transmit Ant. Gain	48.05 dBi	2.40 (m) Antenna diam. 53.00 (%) Efficiency
EIRP (/Carrier)	56.09 dBW	
Free Space Loss	207.27 dB	39936 Range (km)
Rainy sky loss	3.52 dB	For 99.8% Availability
Pointing Loss	0.10 dB	
Polarization Loss	0.10 dB	
Net Path Loss	210.99 dB	
Receive S/C Gain	65.69 dBi	18.29 Meters 60.00 FT. Rcv. Ant. 53 % efficiency
Sys Temp(Rec. Input)	25.33 dB-K	341.00 (K) System Temp
Effective G/T	40.37 dB/K	
Rec'd Carrier Level	-89.22 dBW	
Boltzmann's Constant	-228.60 dBW/Hz-K	
Received C/No	114.06 dB-Hz	
Misc. Hardware Loss	0.00 dB	
ISI Degradation	0.50 dB	
Modem Impl. Loss	2.00 dB	
Symbol Rate	91.76 dB-Hz	1000.00 Mbaud 1.50 BW factor for QPSK
Avail. Eb/No	16.80 dB	
Req'd Eb/No	9.60 dB	1 E-05 Uncoded QPSK BER
Coding Gain	0.00 dB	
MARGIN	**7.20 dB**	

MINIMUM REQUIRED
G/T WITH 3 DB MARGIN 36.17 dB/K

SGL Analysis: Andover Ku-Band Downlink

SATELLITE LONGITUDE: 9 deg. West
GROUND STATION : ANDOVER
ELEVATION ANGLE : 11.2 DEGREES

CARRIER FREQUENCY: 13.80 GHz

Parameter	Value Units	Remarks
Transmit S/C Power	9.03 dBW	8.00 (W) Backed off Power
Feed Losses	1.00 dB	
Transmit Ant. Gain	48.05 dBi	2.40 (m) Antenna diam. 53.00 (%) Efficiency
EIRP (/Carrier)	56.09 dBW	
Free Space Loss	207.33 dB	40201 Range (km)
Rainy sky loss	4.99 dB	For 99.8% Availability
Pointing Loss	0.10 dB	
Polarization Loss	0.10 dB	
Net Path Loss	212.52 dB	
Receive S/C Gain	65.69 dBi	18.29 Meters 60.00 FT. Rcv. Ant. 53 % efficiency
Sys Temp(Rec. Input)	25.33 dB-K	341.00 (K) System Temp
Effective G/T	40.37 dB/K	
Rec'd Carrier Level	-90.74 dBW	
Boltzmann's Constant	-228.60 dBW/Hz-K	
Received C/No	112.53 dB-Hz	
Misc. Hardware Loss	0.00 dB	
ISI Degradation	0.50 dB	
Modem Impl. Loss	2.00 dB	
Symbol Rate	91.76 dB-Hz	1000.00 Mbaud 1.50 BW factor for QPSK
Avail. Eb/No	15.27 dB	
Req'd Eb/No	9.60 dB	1 E-05 Uncoded QPSK BER
Coding Gain	0.00 dB	
MARGIN	**5.67 dB**	

MINIMUM REQUIRED G/T WITH 3 DB MARGIN 37.70 dB/K

SGL Analysis: JPL Ku-Band Downlink

SATELLITE LONGITUDE: 106 deg. West
GROUND STATION : JPL
ELEVATION ANGLE : 48.3 degrees

Carrier Frequency: 13.80 GHz

Parameter	Value Units	Remarks
Transmit S/C Power	9.03 dBW	8.00 (W) Backed off Power
Feed Losses	1.00 dB	
Transmit Ant. Gain	48.05 dBi	2.40 (m) Antenna diam. 53.00 (%) Efficiency
EIRP (/Carrier)	56.09 dBW	
Free Space Loss	206.67 dB	37257 Range (km)
Rainy sky loss	1.97 dB	For 99.8% Availability
Pointing Loss	0.10 dB	
Polarization Loss	0.10 dB	
Net Path Loss	208.84 dB	
Receive S/C Gain	65.69 dBi	18.29 Meters 60.00 FT. Rcv. Ant. 53 % efficiency
Sys Temp(Rec. Input)	25.33 dB-K	341.00 (K) System Temp
Effective G/T	40.37 dB/K	
Rec'd Carrier Level	-87.06 dBW	
Boltzmann's Constant	-228.60 dBW/Hz-K	
Received C/No	116.21 dB-Hz	
Misc. Hardware Loss	0.00 dB	
ISI Degradation	0.50 dB	
Modem Impl. Loss	2.00 dB	
Symbol Rate	91.76 dB-Hz	1000.00 Mbaud 1.50 BW factor for QPSK
Avail. Eb/No	18.95 dB	
Req'd Eb/No	9.60 dB	1 E-05 Uncoded QPSK BER
Coding Gain	0.00 dB	
MARGIN	**9.35 dB**	
MINIMUM REQUIRED G/T WITH 3 dB Margin	34.02 dB/K	

SGL Analysis: Marshall Center Ku-Band Downlink

SATELLITE LONGITUDE: 106 deg. West
GROUND STATION : MARSHALL Center
ELEVATION ANGLE : 44.8 degrees

Carrier Frequency: 13.80 GHz

Parameter	Value Units	Remarks
Transmit S/C Power	9.03 dBW	8.00 (W) Backed off Power
Feed Losses	1.00 dB	
Transmit Ant. Gain	48.05 dBi	2.40 (m) Antenna diam. 53.00 (%) Efficiency
EIRP (/Carrier)	56.09 dBW	
Free Space Loss	206.73 dB	37516.12 Range (km)
Rainy sky loss	9.45 dB	For 99.8% Availability
Pointing Loss	0.10 dB	
Polarization Loss	0.10 dB	
Net Path Loss	216.38 dB	
Receive S/C Gain	65.69 dBi	18.29 Meters 60.00 FT. Rcv. Ant. 53 % efficiency
Sys Temp(Rec. Input)	25.33 dB-K	341.00 (K) System Temp
Effective G/T	40.37 dB/K	
Rec'd Carrier Level	-94.60 dBW	
Boltzmann's Constant	-228.60 dBW/Hz-K	
Received C/No	108.67 dB-Hz	
Misc. Hardware Loss	0.00 dB	
ISI Degradation	0.50 dB	
Modem Impl. Loss	2.00 dB	
Symbol Rate	91.76 dB-Hz	1000.00 Mbaud 1.50 BW factor for QPSK
Avail. Eb/No	11.41 dB	
Req'd Eb/No	9.60 dB	1 E-05 Uncoded QPSK BER
Coding Gain	0.00 dB	
MARGIN	**1.81 dB**	
MINIMUM REQUIRED G/T WITH 3 dB MARGIN	41.56 dB/K	

SGL Analysis: Denver Ku-Band Downlink

SATELLITE LONGITUDE 106 deg. West
GROUND STATION : DENVER
ELEVATION ANGLE : 44.2 degrees

Carrier Frequency: 13.80 GHz

Parameter	Value Units	Remarks
Transmit S/C Power	9.03 dBW	8.00 (W) Backed off Power
Feed Losses	1.00 dB	
Transmit Ant. Gain	48.05 dBi	2.40 (m) Antenna diam. 53.00 (%) Efficiency
EIRP (/Carrier)	56.09 dBW	
Free Space Loss	206.74 dB	37561 Range (km)
Rainy sky loss	1.31 dB	For 99.8% Availability
Pointing Loss	0.10 dB	
Polarization Loss	0.10 dB	
Net Path Loss	208.25 dB	
Receive S/C Gain	65.69 dBi	18.29 Meters 60.00 FT. Rcv. Ant. 53 % efficiency
Sys Temp(Rec. Input)	25.33 dB-K	341.00 (K) System Temp
Effective G/T	40.37 dB/K	
Rec'd Carrier Level	-86.47 dBW	
Boltzmann's Constant	-228.60 dBW/Hz-K	
Received C/No	116.80 dB-Hz	
Misc. Hardware Loss	0.00 dB	
ISI Degradation	0.50 dB	
Modem Impl. Loss	2.00 dB	
Symbol Rate	91.76 dB-Hz	1000.00 Mbaud 1.50 BW factor for QPSK
Avail. Eb/No	19.54 dB	
Req'd Eb/No	9.60 dB	1 E-05 Uncoded QPSK BER
Coding Gain	0.00 dB	
MARGIN	**9.94 dB**	
MINIMUM REQUIRED G/T WITH 3 dB Margin	33.43 dB/K	

SGL Analysis: GSFC Ku-Band Downlink

SATELLITE LONGITUDE: 106 deg. West
GROUND STATION: GODDARD
ELEVATION ANGLE 35.7 deg.

Carrier Frequency: 13.30 GHz

Parameter	Value Units	Remarks
Transmit S/C Power	9.03 dBW	8.00 (W) Backed off Power
Feed Losses	1.00 dB	
Transmit Ant. Gain	48.05 dBi	2.40 (m) Antenna diam. 53.00 (%) Efficiency
EIRP (/Carrier)	56.09 dBW	
Free Space Loss	206.90 dB	38230.04 Range (km)
Rainy sky loss	5.67 dB	For 99.8% Availability
Pointing Loss	0.10 dB	
Polarization Loss	0.10 dB	
Net Path Loss	212.77 dB	
Receive S/C Gain	65.69 dBi	18.29 Meters 60.00 FT. Rcv. Ant. 53 % efficiency
Sys Temp(Rec. Input)	25.33 dB-K	341.00 (K) System Temp
Effective G/T	40.37 dB/K	
Rec'd Carrier Level	-90.99 dBW	
Boltzmann's Constant	-228.60 dBW/Hz-K	
Received C/No	112.29 dB-Hz	
Misc. Hardware Loss	0.00 dB	
ISI Degradation	0.50 dB	
Modem Impl. Loss	2.00 dB	
Symbol Rate	91.76 dB-Hz	1000.00 Mbaud 1.50 BW factor for QPSK
Avail. Eb/No	15.02 dB	
Req'd Eb/No	9.60 dB	1 E-05 Uncoded QPSK BER
Coding Gain	0.00 dB	
MARGIN	**5.42 dB**	

MINIMUM REQUIRED
G/T WITH 3 dB MARGIN 37.94 dB/K

APPENDIX B
THERMAL MANAGEMENT DESIGN PROCEDURES FOR GaAs DIGITAL IC FAMILIES

GBL GigaBit Logic **DESIGNER'S GUIDE**

Thermal Management of PicoLogic™ and NanoRam™ GaAs Digital IC Families

Application Note #3

I. INTRODUCTION

Thermal management of integrated circuits is neccessary in order to ensure long-term device and system reliability and performance. The goals of thermal management are two-fold: to keep individual transistor junction temperatures as low as possible (to maximize device reliability) and to keep device operating temperatures as uniform as possible across the entire system which they comprise (to minimize parametric variations).

Low junction temperatures insure optimum device reliability. MTBFs (Mean Time Between Failures) of greater than 100,000 hours for GaAs ICs can be realized if junction temperatures are maintained at or below 125°C. Junction temperatures lower than this will result in increased reliability while higher temperatures will degrade reliability. This is described by the well known Arrhenius equation and is shown graphically in **Figure 1-a** for an activation energy of 1.4 eV, typical for GaAs ICs. **Figure 1-b** shows FIT (failure unit) rates as a function of temperature. From Figure 1 it is seen that a device operated at 100 °C junction temperature would have an MTBF ten times as great as the 125 °C MTBF. Actual device operating temperatures must be fixed by the system designer after considering such factors as system complexity (i.e., number of devices) and required reliability levels. Reliability of PicoLogic™ ICs is discussed extensively in reference [1].

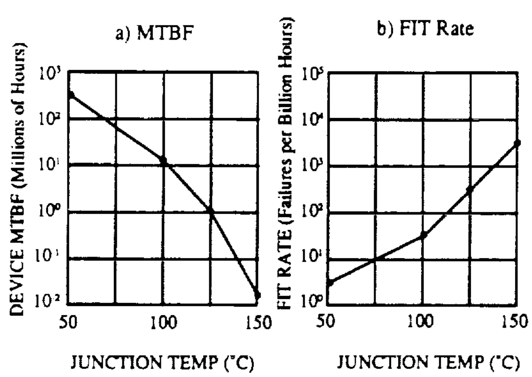

FIGURE 1: Approximate Device MTBF and FIT Rate Junction Temperature for a 1.4 ev Activation Energy

Thermal characteristics of GaAs ICs are similar to those of silicon bipolar ECL ICs. The thermal conductivity of GaAs is low (approximately 1/3 to 1/5 that of silicon, depending on temperature—see **Table 1.**) Board level packing density (and hence power density) will typically be higher for digital GaAs systems to preserve the short propagation delays of the ICs. Despite these minor differences, the thermal management techniques required for GaAs ICs are no different than those required for surface-mount silicon bipolar devices.

This application note provides the information neccessary for the proper thermal management of GigaBit Logic's families of GaAs ICs. **Section II** contains the thermal characteristics of GigaBit Logic devices and packages. **Section III** provides some background on heat transfer, which is needed to describe the thermal path from package to environment. Sample thermal calculations are performed in **Section IV**, based on the data presented in Sections II and III. For those interested in a quick estimate of their thermal management requirements, a simple 4-step method is listed in **Section V**, along with a summary. **Appendix A** provides some technical details on thermal resistance calculations and measurements which may be useful for hybrid thermal design and management and of transient thermal characteristics.

Table 1 lists some material and thermodynamic properties of air and packaging materials which will be used in this report.

TABLE 1: MATERIAL PROPERTIES

Thermodynamics Properties of Air at 100°C

Specific heat (Cp)................ ...	0.941	W/sec g °C
Kinematic viscosity (μ)...........	0.000219	g/sec cm
Thermal conductivity (k)..........	0.000277	W/cm °C
Density (ρ)............................	0.0011	g/cm 3

Thermodynamic Properties of Common Packaging Materials at 100°C

	Thermal Conductivity (W/cm °C)	Coefficient of Thermal Expansion (10⁻⁶/°C)	Specific Heat (W/sec g °C)
Aluminum.............	2.35	25	0.90
Ceramic (alumina)....	0.20	6.5	0.84
Ceramic (beryllia)....	2.20	8.0	1.09
Copper..................	3.90	18.3	0.39
Epoxy (silver filled)..	0.02 to 0.06	40-50	0.24
GaAs.....................	0.35	6.9	0.35
Glass.....................	0.003	12-16	0.80 (est)
Kovar....................	0.20	5.8	0.44
Silicon..................	1.10	2.6	0.70

II. THERMAL RESISTANCES

Junction temperatures of GaAs ICs can be related to device power dissipation by the following approximate relationship:

$$T_j = T_A + 10°C + (\theta_{jc} + \theta_{cA})\,P_D \qquad (1)$$
$$= T_A + 10°C + \theta_{jA} \times P_D$$

where :

T_j = maximum junction temperature (°C)
T_A = maximum ambient temperature (°C)
P_D = maximum device power dissipation (W)
θ_{jc} = ave. die surface to case thermal resistance (°C/W)
θ_{cA} = ave. case to ambient thermal resistance (°C/W)
θ_{jA} = ave. die surface to ambient thermal resistance (°C/W)

Die surface temperature is essentially equivalent to $T_{j(region)}$. The 10°C factor represents the temperature differential between T_j and $T_{j(region)}$, which is typically not a function of overall circuit power dissipation. The surface to case thermal resistance is determined largely by package design whereas the case to ambient thermal resistance is dominated by system-level considerations.

Thermal resistances can be treated as analogous to electrical resistances, with local temperatures and power dissipation as the counterparts to nodal voltages and currents, respectively. This is shown in **Figure 2**. Parallel and series networks of thermal resistances are calculated just as electrical resistive networks would be.

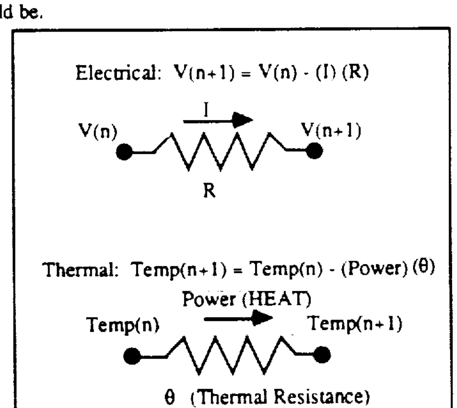

FIGURE 2: Electrical and Thermal Resistances

Package Types and Construction

GigaBit Logic assembles GaAs ICs in four primary package types: 36 and 40 I/O ceramic leadless chip carriers (referred to as L-36 and L-40 in this report), 36 lead glass/metal flatpacks (referred to here as F-36), and 40 lead ceramic "C"-leaded chip carriers (referred to as C-40). Cross-sectional views for these packages are shown in **Figure 3**. Mechanical drawings are shown in **Figure 4**.

The L-36 package is a multi-layer, co-fired, **cavity-up** ceramic package with integral chip capacitors for power supply decoupling and 50 Ω micro-strip transmission lines. The GaAs die is attached to the ceramic chip carrier, which has tungsten-filled thermal vias from the die-attach cavity to the package bottom. Note that these thermal vias (see Figure 4) should be connected to the VSS plane in the printed circuit board. This package is discussed in detail in reference [2]. Although there are actually 40 pads on the bottom of this package, the corner pads are not utilized, and hence it is referred to as a 36 I/O package. The F-36 package is a standard glass sidewall flatpack. To customize the package for gigahertz-rate operation, the GaAs die is mounted on a silicon IC which in turn is mounted in the flatpack. The silicon IC contains decoupling capacitors and 50 coplanar transmission lines [3]. Because of its low thermal resistivity relative to both ceramic and GaAs, the silicon acts as a heat spreader. The flatpack is mountable in either cavity-up or cavity down configurations. The L-40 package is a multi-layer, co-fired **cavity down** ceramic chip carrier which also utilizes the silicon substrate. The C-40 is a leaded version of the L-40 package. Because of their similar thermal characteristics, this application note will not, in general differentiate between the L-40 and C-40 packages. [Note: cavity-up and cavity-down refers to configurations where the die is attached to the package bottom and top surfaces, respectively.]

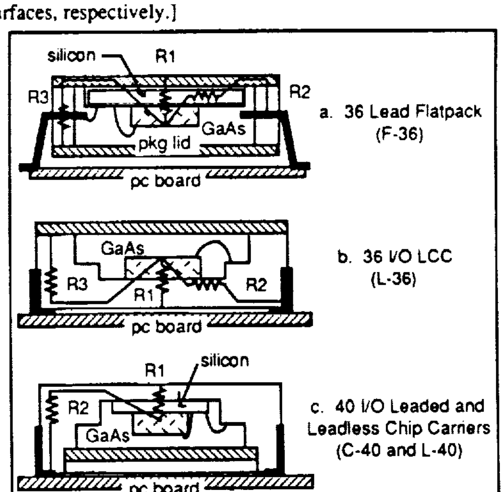

FIGURE 3: Package Cross-Sectional Views with Thermal Resistance Components

Package Thermal Resistance Components

It is useful to decompose the die surface to case thermal

FIGURE 4: PACKAGE AND HEATSINK MECHANICAL DRAWINGS

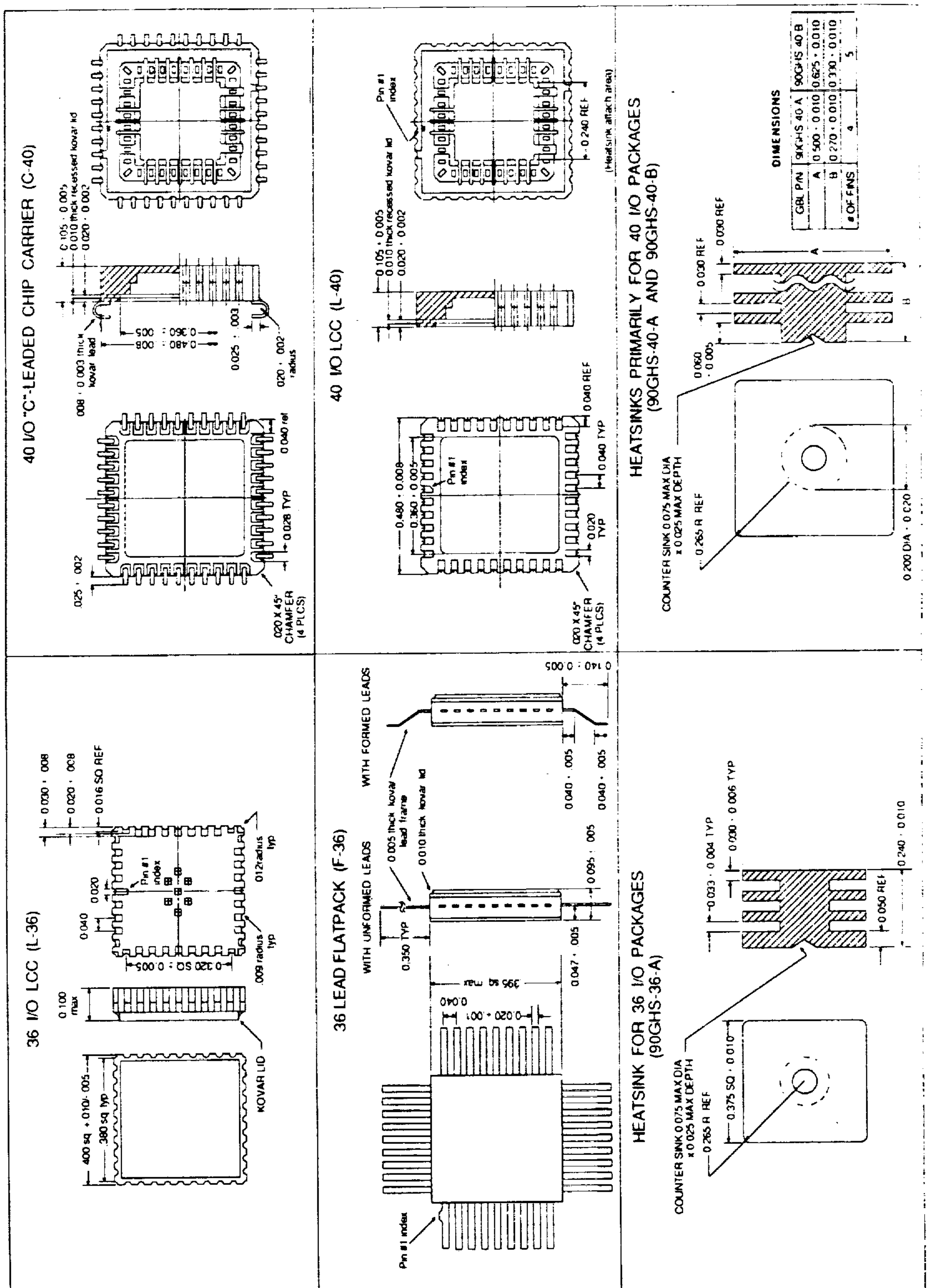

resistance of packaged GaAs devices into 3 components: die surface to package base, die surface to leads, and die surface to lid (referred to here as R1 and R2 and R3, respectively.) This is illustrated in **Figure 3**. Figure 3-a shows the F-36 package mounted in cavity-down configuration. Figure 3-b shows the L-36 package. Because the L-40/C-40 package is inverted, the package "base" is really the top surface, as shown in Figure 3-c. R3 is not shown for this case because the die to package lid thermal resistance path is not significant (the lid is recessed from the pcb surface.) The silicon substrate in the F-36, L-40 and C-40 packages plays a significant role in reducing the R2 thermal resistance. This is discussed, along with other advantages of the silicon substrate in Reference [3]

For the purpose of calculating thermal resistances (and other thermal parameters), PicoLogic™ and NanoRam™ devices can be divided into four groups, based on die size. These are shown in **Table 2**. These device groupings will be referred to throughout this application note.

TABLE 2. DEVICE GROUPS

	GROUP 1	GROUP 2	GROUP 3	GROUP 4
Die Size (mil²)	2000 to 4000	4000 to 6000	6000 to 10000	10000 to 15000
Power Diss.	0.3 to 0.5	0.5 to 1.0	1.0 to 1.8	1.8 to 3.0
Includes	10G000A	10G002	10G022	12G014
	10G001	10G003	10G023	
	10G011B	10G004	10G024	
	10G012B	10G010	10G030	
	10G013	10G021A	10G040A	
	10G060	10G065	10G041A	
	16G010	10G070	10G044	
	16G011	10G181	10G045	
	16G020		10G046	
	16G021		10G061	
			10G100	
			10G101	
			16G040	
			16G044	

The component thermal resistances for the four die size groups and three package types are listed in **Table 3**.

Note that R1 does not vary much between package types. This is because die parameters (size, thickness, material) dominate R1. R2 and R3 depend primarily on package parameters. R2 and R3 are very high for the flatpack because of the thermally insulating package glass sidewalls. **For this reason, it is strongly recommended that the flatpack be mounted cavity-down, i.e., upside down, as shown in Figure 3-a.** Alternatively, the flatpack can be mounted cavity up if the base is in good thermal contact with the pc board. Thermal contact can be guaranteed with solder or thermally conductive epoxy. [CAUTION: the flatpack base is at VSS (nominal -3.4 V) potential while the lid is floating. The lid of the LCC is also at VSS potential. Thus, a conductive heatsink will be electrically "hot" if attached to the flatpack base or LCC lid. Use an anodized aluminum heatsink with electrically non-conductive epoxy to have the heatsink float electrically.]

TABLE 3: PACKAGE THERMAL RESISTANCE COMPONENTS (°C/W)

	GROUP 1	GROUP 2	GROUP 3	GROUP 4
F-36 PACKAGE				
R1	25	13	7	n.a.
R2 [a]	115	110	110	n.a.
R3	220	210	205	n.a.
L-36 PACKAGE				
R1 [b]	29	15	7	6
R2 [a]	58	38	22	20
R3	58	38	24	21
L-40/C-40 PACKAGE				
R1	29	15	7	6
R2 [a,c]	70	46	26	24

NOTES:
a) R2, the surface to leads thermal resistance refers to the parallel sum of all 36 or 40 leads
b) Group 3 devices in the L-36 package do not have the thermal vias.
c) Add about 1.5 to 2.0 °C/W to R2 for the C-40 case.

Case Temperatures

GigaBit Logic GaAs ICs are specified by case temperature. This implies a boundary condition where the device is in contact with an infinite heatsink through the R1 thermal resistance. Thus, for example, if a 0.5 watt Group 1 device in a flatpack has a fixed case temperature of 85°C, then the maximum junction temperature is 85°C + 10°C + 0.5W x 25°C/W = 108°C.

Appendix A discusses the measurements and calculations performed to determine the thermal resistances discussed in this section.

III. HEAT TRANSFER

Heat transfer from die to case, discussed above, is predominantly conductive (and thus is characterized by material thermal conductivities.) Case to ambient thermal resistance is essentially convective (and to a lesser extent, radiative). The convective analog of a thermal conductivity is the heat transfer coefficient, **h** (units are W/cm² °C). Although there are many types of convective cooling of electronic components (i.e., air or liquid, forced or natural, etc.), we will concentrate here on forced air cooling. In general, natural (or "still") air cooling of GaAs ICs is only feasible for devices dissipating less than 1 watt unless special care is taken in designing the sub-assembly or module.

The heat transfer coefficient for forced air convection cooling can be expressed as:

$$h(v) = 0.0011 + 0.036(Cp\ \mu/k)^{.33}\ (v\ L\ p/\mu)^{.8}\ k/L \qquad (2)$$

(assuming turbulent flow) where v is the air velocity in cm/sec, Cp, μ, p, and k are as defined in Table 1, and L is a characteristic dimension of the system [4]. It is reasonable to assign to L the length of the printed circuit board, in cm. **Figure 5** shows the heat transfer coefficient as a function of air velocity for a range of "L" from 5 cm (high curve) to 20 cm (low curve). As a point of reference, 600 to 1000 lfpm air velocities are readily achievable in present-day ECL based systems. State of the art air-cooled systems achieve up to 1800 lfpm.

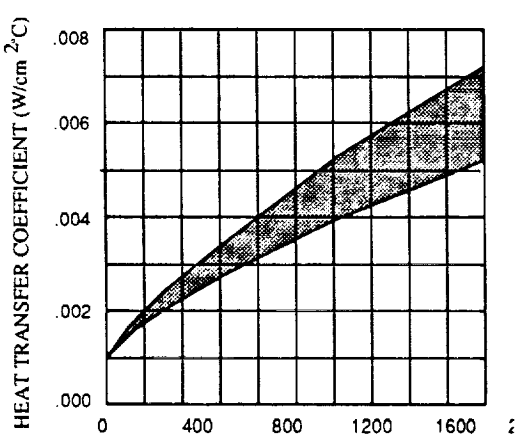

FIGURE 5: Heat Transfer Coefficients vs. Air Velocity

Heatsinks

The thermal resistance to ambient of some object with surface area "A" and heat transfer coefficient "h(v)" is given by:

$$\theta = A/h(v) \qquad (3)$$

The heat transfer coefficient describes both convection from the printed circuit board (through the package leads) and from the device heatsink (through the package body).

Figure 4 shows outlines of three heatsinks designed for use with PicoLogic™ and NanoRam™ packages. The 90GHS-36-A heatsink is intended for use with the 36 I/O packages. The 90GHS-40-A and 90GHS-40-B heatsinks are slightly larger and are intended primarily for use with the 40 I/O packages, although they can be used with the 36 I/O packages (these heatsinks will be referred to as 36A, 40A, and 40B, respectively, throughout this application note.) The effective surface areas of the 36A, 40A and 40B heatsinks are 7 sq cm, 12 sq cm, and 24 sq cm, respectively. Using Figure 5 and equation (3), it is seen that the heatsink to ambient thermal resistances at 600 lfpm are approximately 46, 27, and 13 °C/W, respectively.

Use of a heatsink is strongly recommended for all PicoLogic™ and NanoRam™ ICs, particularly those dissipating more than 1 watt.

The heatsink should be mounted to the package with a thermally conductive, electrically insulating epoxy such as Ablestik 789-4 or 561K, or Thermalloy Thermalbond™. Because heatsinks 40A and 40B are intended primarily for the L-40 and C-40 packages they have a stud to provide clearance for the top surface passive components (terminating resistors and decoupling capacitors) which the package is capable of supporting, as shown in **Figure 6**. The stud does not impact the thermal resistance because it is located directly above the heat-dissipating die. Thermally conductive epoxies such as those listed above will contribute 1 °C/W or less to overall die surface to ambient thermal resistance. Use of thermal grease or heatsink compound instead of conductive epoxy will add 5°C/W or more to overall thermal resistance.

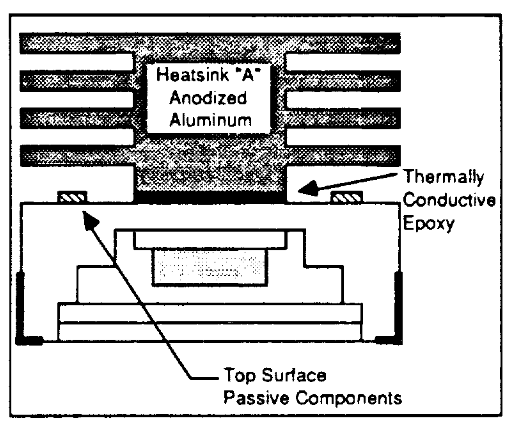

FIGURE 6: 40 I/O LCC with Heatsink

IV. THERMAL MANAGEMENT CALCULATIONS

Most PicoLogic™ and NanoRam™ devices can be maintained at reasonable operating temperatures (i.e., 125°C or lower junction temperatures) with a minimum of effort. The information provided in Sections II and III will allow designers to determine device operating temperatures for the specific system conditions of interest (i.e., device spacing, airflow, board spacing, inlet air temperatures, etc.) **Table 4** shows rule of thumb cooling requirements for the four device groups of Table 2. **Please note that these are only approximations and that actual requirements should be carefully calculated using actual system and device parameters.** Two oz. copper (2.8 mils thick) is recommended for all board power supply planes. This will minimize pc board lateral thermal resistance.

Sample Calculation Parameters

To demonstrate the methodology for more accurately estimating device operating temperatures, a representative sample calculation will be performed. Consider an array of 32 Group 3 devices packaged in 40 I/O LCCs located on .750" centers. Unless otherwise specified, heatsink 90GHS-40-A (of Figure 3) will be assumed. The devices have a nominal power dissipation of 1.0 watt and a maximum power dissipation of 1.4 watts. The maximum ambient temperature is assumed to be 70 °C. The devices are soldered to a multi-layer, single sided (i.e., devices on one side only) printed circuit board with 2 oz. copper planes for each power supply.

TABLE 4: ESTIMATED COOLING REQUIREMENTS FOR PICOLOGIC™ AND NANORAM™ ICs

	W/O HEATSINK	W/ HEATSINK
GROUP 1		
• flatpack	not recommended	still air
• LCC	still air	still air
GROUP 2		
• flatpack	not recommended	200 lfpm
• LCC	400 lfpm	200 lfpm
GROUP 3		
• all pkgs	not recommended	200-600 lfpm
GROUP 4		
• all pkgs	not recommended	600 lfpm or greater

NOTES:
(1) These are only rules of thumb. Actual cooling requirements will be a funct ion of system parameters.
(2) Trade-offs are always possible between heatsink size, device spacing, air velocity, board spacing, etc.

TABLE 5: SAMPLE CALCULATION ASSUMPTIONS

Nominal Device Power Dissipation............	1.0 watts
Maximum Device Power Dissipation...........	1.4 watts
Nominal Operating Junction Temperature......	110 °C
Maximum Operating Junction Temperature....	125 °C
Maximum Ambient Temperature.......	70 °C

System MTBF Calculation

Suppose that it is desired that the sub-system (i.e., the array of 32 devices) has an MTBF of 2 years. It can be shown (though it is not within the scope of this application note) that for a collection of "N" similar components, system MTBF can be estimated by:

$$MTBF_{system} = 0.69 * MTBF_{Component}/N \qquad [4]$$

Thus, for a system MTBF of 2 years we require a device MTBF of approximately 800,000 hours. From Figure 1 it is seen that this requires average maximum junction temperatures of approximately 110 °C.

The thermal management goal for the sample calculation is assumed to be as follows: maximum junction temperatures not to exceed 110 °C under nominal conditions, maximum junction temperatures not to exceed 125 °C under worse case conditions. For this first order calculation we will ignore the board dielectric material and assume that thermal conduction is good between the closely spaced power planes. We will also ignore the temperature and altitude dependence of the parameters of Table 1. The primary assumptions for this sample calculation are summarized in **Table 5**.

If equation [1] is applied to the nominal and worse case conditions, the following conditions result:

Nominal case: $110°C \leq 70°C + 10°C + \theta_{s\text{-}a} \times 1.0$ watts
Worse case: $125°C \leq 70°C + 10°C + \theta_{s\text{-}a} \times 1.4$ watts.
where $\theta_{s\text{-}a}$ is the surface to ambient thermal resistance.

The nominal case requirement is slightly more restrictive than the worse case requirement, calling for a $\theta_{s\text{-}a}$ of 30 °C/W or less.

Calculating Surface to Ambient Thermal Resistance

For Group 3 devices in the L-40 package there are two significant parallel thermal dissipation paths determining $\theta_{s\text{-}a}$: through the package to the pc board and through the package body to the top surface and heatsink—that is, through R2 and R1, respectively. [Note: this will vary from package type to package type.]

Because some of the package pads are connected to short signal traces with relatively small heat dissipating areas, we must derate the die surface to leads thermal resistance. A reasonable estimate would be R2' = 1.5 R2, or R2'=39 °C/W. The surface to ambient thermal resistance is then given by:

$$\theta_{sa} = \frac{1}{\frac{1}{R1 + 1/h(v)\cdot A_{heatsink}} + \frac{1}{R2' + 1/h(v)\cdot A_{board,\ per\ device}}} \quad [5]$$

where h(v) is the heat transfer coefficient as a function of air velocity, $A_{heatsink}$ is the heatsink effective surface area and A_{board} is the pc board effective area per device. Each package has about 6.25 cm^2 of board area (including top and bottom sides, based on our .750" centers assumption) to dissipate heat in addition to the 12 cm^2 of heatsink area. If we assume that the board is 50 square cm in area (i.e., L in equation [2] is 7 cm), and airflow is, for example, 400 lfpm (h=.0027 W/cm^2 °C), then equation [5] reduces to:

$$\theta_{SA} = \frac{1}{\frac{1}{38}\text{ (hs contribution)} + \frac{1}{98}\text{ (pcb contribution)}} \quad [6]$$

$$= 27\ ^\circ C/W$$

It is seen that better than half of the heat generated by the device is dissipated through the heatsink. In the absence of a heatsink, the 12 cm^2 of heat dissipating area in equation [5] would be replaced by 1.5 cm (representing the package top surface area.) The resulting surface to ambient thermal resistance would be 71 °C/W. For a 1 watt device, this represents a 44 °C temperature differential at the device level. **Thus, we see that our system level reliability requirements are met if the heatsink is used, but are significantly missed if a heatsink is not used.** The benefit of using a heatsink is clear.

As a point of reference, a typical 16 pin plastic DIP with an alloy-42 leadframe and an aluminum heat-spreader has a θja of roughly 70 °C/W in forced air. Use of a copper-alloy leadframe and thermally loaded molding compound can lower the thermal resistance to about 25 °C/W [5].

Figure 7 shows the results of the calculation of equation [4] as a function of air velocity for our example for the no heatsink case and for heatsinks 90GHS-40-A and -B. The shaded region represents the conditions required for a surface to ambient thermal resistance of 30 °C/W or less (i.e., for nominal device operating temperatures of 110 °C and maximum device operating temperatures of 125 °C.) It is seen that without a heatsink, no amount of forced air brings thermal resistance low enough to ensure the desired operating temperatures, while for the 40B heatsink, a very nominal amount of air flow (about 100 lfpm) is required. As determined above, about 400 lfpm is required for the 40A heatsink. Of course, these results can vary significantly with different package to package spacings on the printed circuit board.

Table 6 a&b presents the results of the equivalent of equation [5] for most PicoLogic™ device groups, package types and heatsink sizes. Note that Table 6-a assumes a fairly dense board

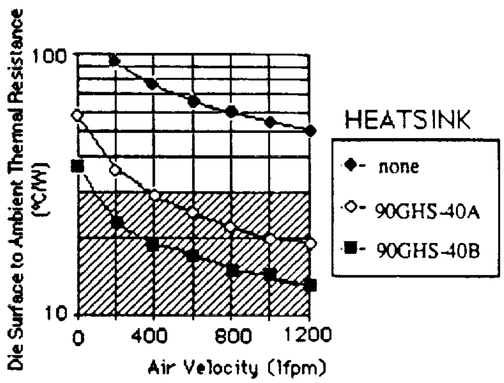

FIGURE 7: Surface to Ambient Thermal Resistance for Group 3 Device in L-40 Package Under Conditions Specified in Text

level density (.750" package centers). Prototyping densities will typically be less, with correspondingly lower thermal resistances due to the increased board area per device. This is shown in Table 6-b, which assumes packages on 1.5" centers. The difference in thermal resistance between the high density and prototype density case ranges from extremely important (for no heatsink and still air) to insignificant (for large heatsinks and high air velocities).

The thermal resistances of Table 6 include first-order temperature dependent effects. These first order effects are most important for the cases with high thermal resistance (clearly, since higher thermal resistances correspond to higher temperatures.) The most important of the first-order temperature dependent effects is that the radiation component of the heat transfer coefficient varies as the fourth power of the case absolute (°K) temperature. To include temperature dependent effects, one must assume a device power dissipation and an ambient temperature. The assumed power dissipation levels are 0.5, 1.0, 1.5 and 2.5 watts, respectively, for Group 1, 2, 3, and 4 devices. The assumed ambient temperature is 55 °C. Wide variations in these values (up

TABLE 7: AMBIENT TEMPERATURE GRADIENT (assumes 0.5 inch board to board spacing)

Air Velocity (lfpm)	ΔT (°C)/W/pkg
200	2.20
400	1.10
600	0.72
800	0.55
1000	0.44
1200	0.40

GBL GigaBit Logic **DESIGNER'S GUIDE**

TABLE 6: PicoLogic™ and NanoRam™ Die Surface to Ambient Thermal Resistances vs. Heatsink Size and Air Velocity

Assumptions:
- 10 cm by 10 cm single sided, multi-layer, 1 oz. copper pcb
- Heatsink eff. surface areas (actual dimensions in Fig. 4) are: 36A: 7 sq. cm. 40A: 12 sq. cm. 40B: 24 sq. cm.
- Flatpack is mounted cavity down (inverted) with base in good thermal contact with pcb.
- Thermal vias are utilized on 36 I/O LCCs
- Nominal power dissipation (W) by device group is given by G1 = 0.5 W G2 = 1.0W G3 = 1.5W G4 = 2.5 W
- Ambient temperature is 55°C

A. HIGH-DENSITY SYSTEM ENVIRONMENTS (packages on 0.75" centers)

	36 LEAD FLATPACK (see Note 2)											
	Device Group 1				Device Group 2				Device Group 3			
HEATSINK...	none	36A	40A	40B	none	36A	40A	40B	none	36A	40A	40B
Air Flow (lfpm)	Rth, s-a (°C/W)				Rth, s-a (°C/W)				Rth, s-a (°C/W)			
0	180	96	74	53	149	81	62	43	130	72	55	38
200	140	67	52	39	125	59	44	30	114	54	39	26
400	123	56	44	34	112	49	36	25	105	45	33	22
600	111	50	40	32	103	43	32	23	98	40	29	19
800	104	46	37	30	97	39	29	21	92	36	26	17
1000	97	43	35	29	91	36	27	20	88	33	24	16
1200	92	41	34	28	87	34	26	19	84	31	22	15

	36 I/O LCC								40 I/O CHIP CARRIER (LEADED OR LEADLESS)					
	Device Group 1				Device Group 2				Device Group 3			Device Group 4		
HEATSINK...	none	36A	40A	40B	none	36A	40A	40B	none	40A	40B	none	40A	40B
Air Flow (lfpm)	Rth, s-a (°C/W)				Rth, s-a (°C/W)				Rth, s-a (°C/W)			Rth, s-a (°C/W)		
0	136	90	77	64	107	74	63	51	100	52	36	80	45	32
200	93	62	54	47	78	52	44	37	81	35	24	69	33	22
400	77	52	46	42	64	43	37	32	70	29	19	62	27	18
600	67	46	42	38	55	37	33	29	63	25	17	57	24	16
800	61	42	39	36	49	34	30	27	57	22	15	53	21	15
1000	56	40	37	34	45	31	28	26	53	21	14	50	20	13
1200	52	38	35	33	42	29	27	24	50	19	13	47	18	13

B. LOW-DENSITY PROTOTYPE/TEST ENVIRONMENTS (packages on 1.50" centers)

	36 LEAD FLATPACK (see Note 2)											
	Device Group 1				Device Group 2				Device Group 3			
HEATSINK...	none	36A	40A	40B	none	36A	40A	40B	none	36A	40A	40B
Air Flow (lfm)	Rth, s-a (°C/W)				Rth, s-a (°C/W)				Rth, s-a (°C/W)			
0	125	77	62	46	112	68	54	38	105	62	49	34
200	106	58	46	35	99	51	39	28	95	48	36	24
400	98	50	40	32	92	44	34	24	89	41	31	21
600	93	46	37	30	87	40	30	22	84	37	27	18
800	88	43	35	28	83	37	28	21	81	34	25	17
1000	85	41	33	28	80	34	26	20	78	31	23	16
1200	82	39	32	27	77	32	25	19	75	29	21	15

	36 I/O LCC								40 I/O CHIP CARRIER (LEADED OR LEADLESS)					
	Device Group 1				Device Group 2				Device Group 3			Device Group 4		
HEATSINK...	none	36A	40A	40B	none	36A	40A	40B	none	40A	40B	none	40A	40B
Air Flow (lfm)	Rth, s-a (°C/W)				Rth, s-a (°C/W)				Rth, s-a (°C/W)			Rth, s-a (°C/W)		
0	60	48	44	39	45	38	34	30	59	37	28	51	33	25
200	45	36	33	30	32	26	24	22	48	27	19	44	25	18
400	40	32	30	28	28	23	21	19	44	23	16	40	22	16
600	37	29	28	26	25	20	19	18	41	20	15	38	19	14
800	35	28	26	25	23	19	18	17	39	19	14	36	18	13
1000	34	27	26	24	22	18	17	16	37	17	13	35	17	12
1200	33	26	25	24	21	17	16	15	36	16	12	33	16	11

NOTES:

(1) Required thermal resistance is given by: $R_{th, s\text{-}a} \leq (T_{j,max} - T_{amb} - 10°C)/(\text{Power dissipation})$

GBL GigaBit Logic **DESIGNER'S GUIDE**

to 50 %) can be tolerated with less than a 10% effect on the thermal resistance value listed in Table 6.

Ambient requirements can have a dramatic impact on air velocity requirements. For example, if the maximum ambient requirement in our example is relaxed by 10°C to 60°C, then the required θ_{sa} becomes 40 °C/W instead of 30 °C/W. The required air velocities for heatsinks 40-A and 40-B become 200 lfpm and still air, respectively, (down from 400 lfpm and 100 lfpm).

Inlet Temperatures vs. Ambient Temperatures

Ambient temperature is defined as the air temperature in the immediate vicinity of the device. In applications where the board-level power density is high, the effect of nearby devices raising the ambient temperature above inlet temperature must be considered. In the example above, the 50 sq cm board contains 32 devices, for a total power dissipation of 32 watts. The rise in air temperature across the board can be expressed as:

$$\Delta T\ (^{\circ}C) = 1.76 * P_{board}/CFM \qquad [6]$$

where CFM is the air volumetric flow rate in cubic feet per minute [6]. Table 7 shows the temperature rise per package per watt of power dissipation as determined by equation [4] for 0.5 inch board-to-board spacing. For example, if the 32 devices on the example board are arranged 4 wide by 8 deep (deep referring to the direction of air flow), then the air in the vicinity of the last device will be 8 x 1.1 = 9 °C warmer than at the first device, assuming 400 lfpm air velocity. Thus, to insure ambients of 70 °C, the inlet temperature would have to be 61 °C or less. [Note: this ignores any temperature rise from system inlet to the beginning of the pcb of interest. In many applications this factor can represent a significant adder, up to 15 °C or more.]

Maximum ambient temperature is esstentially equivalent to system outlet temperature.

V. SUMMARY

This application note has provided the information required for proper thermal management of the PicoLogic™ and NanoRam GaAs digital IC families. The thermal characteristics of all GigaBit devices and packages have been presented, along with some background on heat transfer. A detailed sample calculation was performed to demonstrate a thermal management methodology. This methodology along with the general results shown in Table 6 can be used to estimate cooling requirements for any PicoLogic or NanoRam device as shown below:

1. Determine the desired maximum operating junction temperature and the maximum ambient (i.e., outlet) temperature.
2. Determine the device group of interest from Table 2, the package type, and the maximum power dissipation from the device data sheet.
3. Determine $\theta_{s\text{-}a,\,required}$ from the following equation:
   $\theta_{s\text{-}a,\,required} \leq (Tj{,}max - Tamb - 10\ ^{\circ}C)/P_{diss}$
4. Determine an acceptable heatsink/air velocity combination from Table 6 which satisfies
   $\theta_{s\text{-}a,\,required}$.

Some of the important points to remember about the thermal management of PicoLogic™ and NanoRam™ digital ICs are:

- Most PicoLogic™ and NanoRam™ devices will require a heatsink and forced air in high-density systems environ-ments. In general, a small heatsink and 600 lfpm of air will be sufficient. In low density prototyping environments, a heatsink alone may be adequate.
- When using a heatsink with the flatpack package, always mount the package upside down. This is the most efficient means of removing heat from this package.
- Understand the tradeoffs between board-level density, heatsink size, air velocity, and temperature requirements. There are many ways to achieve thermal management needs.

APPENDIX A: THERMAL RESISTANCE MEASURLMENTS AND CALCULATIONS

This appendix will provide some backround material describing how the thermal resistances of Section II were derived. This information will be helpful to hybrid designers or those performing custom assembly of PicoLogic™ and NanoRam™ ICs. The transient thermal behavior of GaAs ICs will also be discussed, which has important implications for testing and characterization.

Thermal Resistance Measurements

There are a number of techniques for measuring thermal resistance from junction (or die surface) to a specified reference point (case, heatsink, ambient, etc.) A number of these techniques are discussed in MIL-STD-883C, METHOD 1012.1—THERMAL CHARACTERISTICS. The die surface temperature discussed in this application note is essentially equivalent to $T_{j(Repos)}$ in the MIL-STD. Typically, the reference point temperature is measured by direct means with a thermocouple. The die surface temperature can be measured directly (with liquid crystal indicators or IR microradiametry) or indirectly by measuring some temperature sensitive parameter (TSP) on the integrated circuit.

Most of the thermal resistance measurements reported in this application note were made by using the forward biased I-V characteristic of an isolated diode on the surface of the GaAs IC as the TSP. The diode is calibrated over temperature in an oven to determine the forward-bias voltage drop required to maintain a constant 250 µA current. This calibration provides the TSP temperature coefficient, $\Delta V_f/\Delta T$ (mv/°C). This coefficient will be referred to as C_{TSP}.

To measure, say, the surface to ambient thermal resistance for a particular device under test (DUT), the ambient temperature V_f @250 µA is measured with no power applied. A known amount of power, P, is applied to the DUT. After allowing several minutes for the DUT to thermally stabilize, the new V_f required to maintain the 250 µA is measured. The surface to ambient thermal resistance of the DUT is then given by:

$$\theta sa = [V_{f,init} - V_{f,final}]/[(C_{TSP})(P)] \qquad (A\text{-}1)$$

Thermal Resistance Calculations

The thermal resistance through a path of cross-sectional area A and thickness t, as shown in **Figure A-1** is given by:

$$\theta = t/(K\,A) \qquad (A\text{-}2)$$

where K is the material thermal conductivity (see Table 1).

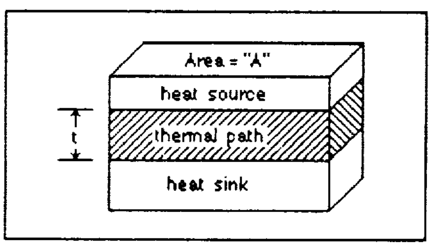

FIGURE A-1: Thermal Resistance Path

However, when the cross-sectional area of the heat source is less than that of the thermal conductor on which is it sits (as is the case for an IC mounted on a package or hybrid substrate), then thermal spreading takes place. This is shown in **Figure A-2**. For most cases it is adequate to assume a spreading angle of 45°. The cross-sectional area to use in equation [A-2] is then the average of the heat source cross-sectional area and the projected cross-sectional area of the thermal spreading path on the heat sink.

As mentioned in Section II, thermal resistance networks can be treated as electrical resistance networks. Thus, the large number of tools available for analyzing electrical networks can be utilized for thermal analysis of complex structures. For example,

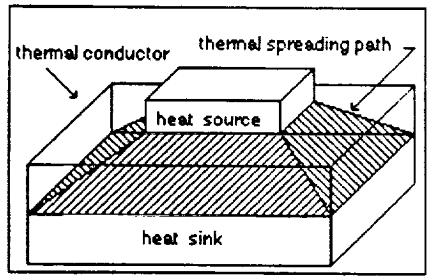

FIGURE A-2: Thermal Spreading

a resistive network like that shown in **Figure A-3** can by studied by an electrical analysis program such as SPICE. The value of the individual resistors is determined by the thermal conductivity of the material and by the "grid size" of the network. If the heat source is modeled by a current source whose value in amperes is equal to the power dissipated in watts, then the nodal voltages at a given point will correspond to the temperature differential from heat source to that point. More than one current source can be used to model either power distribution across an IC surface or muti-chip hybrids. Any number of material layers can be modeled. Programs such as SPICE can analyze networks with hundreds or thousands of nodes and resistors.

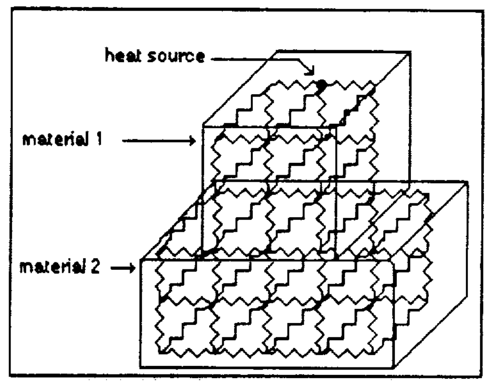

FIGURE A-3: Network for Thermal Analysis

Transient Behavior

When power is applied to an IC, it does not instantaneously realize its equilibrium temperature. This is because the heat is initially absorbed by the thermal capacities of the materials in the thermal path. The thermal capacity of a material is given by the product of its specific heat (see Table 1) and its mass. Thermal capacitances and resistances can be analyzed as if they were electrical capacitances and resistances. Thus, an equivalent circuit to analyze the transient thermal behavior of a packaged IC is shown in **Figure A-4**.

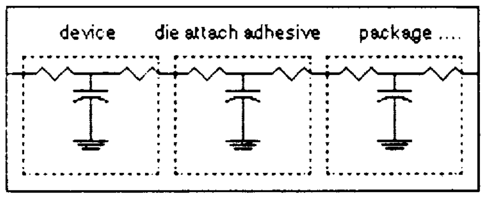

FIGURE A-4: Equivalent Circuit for Transient Analysis

With a model such as that in Figure A-4, the device transient or "turn-on" thermal behavior can be studied. Figure A-5 shows the turn-on thermal behavior of a 1.5 watt Group 3 device in 40 I/O LCC withot and without heatsink. It is seen that up to about 1 second, there is no difference in junction temperature between the heatsink and no heatsink case. However, the junction temperaure of the device without heatsink rises rapidly after about 1 second and stabilizes after about 2 minutes. The device with a heatsink takes longer to stabilize (about 10 minutes) due to the large thermal capacity of the heatsink.

This transient thermal behavior (not significantly different from that of silicon ICs) is important to keep in mind when testing, characterizing, and "cold-starting" PicoLogic™ and NanoRam™ ICs. For example, during a short test, case temperature or heatsink temperature may not be a good indicator of junction temperature.

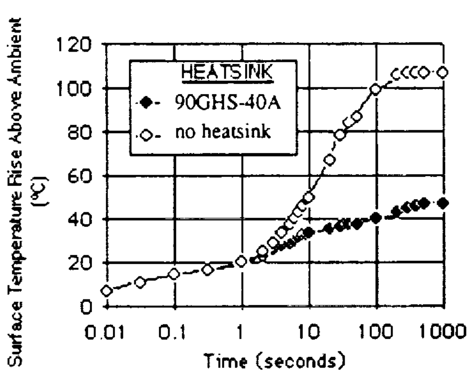

FIGURE A-5: Transient Turn-On Response of a 1.5 Watt Group 3 Device in 40 I/O LCC with and without Heatsink

REFERENCES

1. Reliability and Quality Assurance Handbook, GigaBit Logic, Inc.

2. Advanced Packaging for Ultra-Fast GaAs Devices, S. Cherensky, **WESCON-85 Technical Program**, November, 1985.

3. Packages for Ultra-High Speed GaAs ICs, Tushar Gheewala, **IEEE GaAs IC Symposium Proceedings**, November, 1985.

4. **Essentials of Engineering Fluid Mechanics**, Third Edition, Ruben M. Olson.,(New York: Harper and Row, 1973), Chapter 16.

5. Thermal Management in Semiconductor Device Packaging, M. Mahalingam, **Proceedings of the IEEE**, Vol. 73, No. 9, September, 1985.

6. Forced Air Cooling in High-Density Systems, G. Taylor, Reprinted in **Microelectronics Interconnection and Packaging**, J. Lyman, Ed., (New York: McGraw Hill, 1980), p. 237.

APPENDIX C
EXAMPLE OF CONTIGUOUS MULTIPLEXER REALIZABILITY

EXAMPLE OF CONTIGUOUS MULTIPLEXER REALIZABILITY

The rule for realization of contiguous filters is that the guard band between the two filters must be at least 10% of the distance between the center frequency of the two adjacent bands. We will illustrate this by an example.

In our report # 4 we discussed the Ka-Band uplink and indicated we have the frequency band from 27.5 GHz to 31 GHz and further we suggested to split it in two: the one band from 27.5 to 29.25 GHz and the other from 29.25 to 31 GHz. The center frequency of the lower band is 28.375 and the center frequency of the upper band is 30.125 GHz. The distance (in frequency) between the two bands is 1.75 GHz. Now we have to create a guard bad between the two channels of at least 10 % or 0.175 GHz. One half of this value is taken away from the lower band thus its frequency is from 27.5 to 29.1625 and one half is removed from the upper band resulting in the band from 29.3375 to 31 GHz. with this minimum guard band the diplexer is realizable. In real life a slight increase of the guard band is to be expected.

MULTIPLEXER REALIZATION

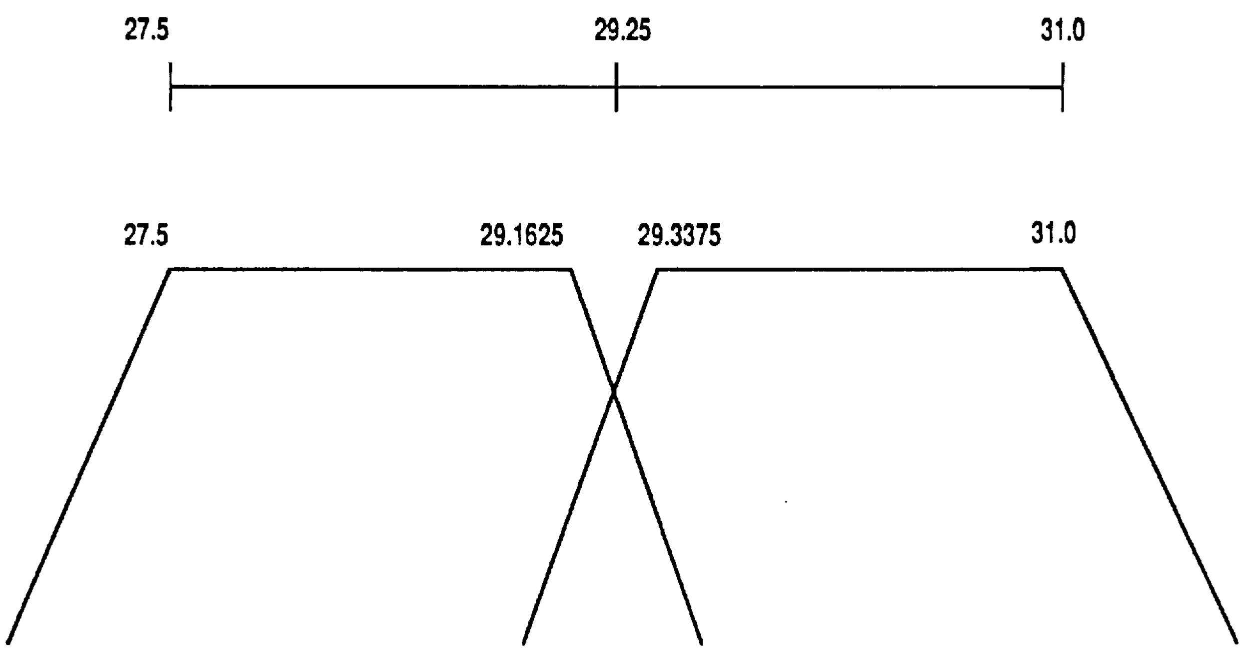

APPENDIX D
GATE ARRAY AND CELL LIBRARIES

Gate Array and Cell Library Vendor Profiles

Company	Products	Customer interface					CAD system access					Nonrecurring expense ($K)		Turnaround (weeks)		Minimum production contract
		Functional	Generic	Converted	Netlist	Layout	CAD system hardware	On-site	Remote	Off-site	Work-stations, simulators, and layout supported	GA	SC	GA	SC	
VLSI Technology	CMOS gate arrays and cell libraries			•	•	•	Apollo Elxsi HP MicroVAX Sun VAX	•	•	•	HP Daisy Mentor FutureNet	16-150	n s	3	5-6	Contact sales
VTC	CMOS and bipolar gate arrays and cell libraries			•	•		Apollo IBM PC	•	•	•	Mentor Daisy	25	50	6	12	None
WaferScale Integration	CMOS cell library	•	•	•	•		VAX	•	•	•	Daisy Intergraph	–	60		16	Contact sales
Xerox Microelectronics Center	CMOS and ECL gate arrays, CMOS and ECL cell libraries	•	•				VAX 11/78x or 8600 (some software) Xerox 6085 workstations	•	•		Xerox 6085	20-35	40-55	4-10	6-12	None
Xilinx	CMOS gate arrays		•	•	n a	n a	IBM PC Apollo Sun Daisy	n a	n a	n a	Daisy Mentor IDEA Valid PC	–	n a	–	n s	None
Zymos	CMOS cell libraries		•	•	•		IBM PC Prime	•	•	•	Case	n a	Contact sales	n a	Varies	Contact sales

Directory of Gate Arrays

[illegible]	Technology Line width	Program-mable Layers	Typical performance			Complexity		Interface levels[4]			Temp. ranges[5]			Second sources
			MHz[1]	mW[2]	ns[3]	Gates	I/Os	C	T	ECL	C	I	M	
Actel Corp.	Act1 (2) Si-gate CMOS 2 µm	M1 6 µm M2 7 µm	70	n/s	2.7	1200-2000	57-69	•	•		•			None
Advanced Micro Devices	Am3500 Bipolar OI (ECL) 1.5 µm	M1 6 µm M2 9 µm	650	1-4	0.4-0.6	4988	134			10K, 100K	•			None
	Am3525 Bipolar OI (ECL) 1.5 µm	M1 6 µm M2 9 µm	650	1–4	0.4–0.6	3718 + 1152 bits RAM	135			10K, 100K	•			None
	Am3550 (5) Bipolar OI (TTL, STTL, ECL) 1.5µm	M1 6 µm M2 9 µm	560	2	0.4	1568–5228	48–124		•	10KH, 100K	•			None
	Am3530 Bipolar OI (TTL, STTL, ECL) 1.5 µm	M1 6 µm M2 9 µm	560	2	0.4	410	20		•	10KH, 100K	•			None

1. Flip-flop toggle rate 2. Gate power at frequency. 3. 2-in NAND delay, FO = 2, 1 mm wire 4. C = CMOS, T = TTL 5. C = commercial, I = industrial, M = military.

Directory of Gate Arrays (continued)

Company	Product Technology Line width	Programmable Layers	Typical Parameters MHz[1]	mW[2]	ns[3]	Components Gates	I/Os	Interface levels[4] C	T	ECL	Temp. ranges[5] C	I	M	Second Sources
Applied Micro Circuits	Q5000 (5) Bipolar OI (TTL, STTL, ECL) 2 µm	M1 5.6 µm M2 8.0 µm M3 (only on Q5000T)	800	0.9	0.35	1300–5000	76–160		•	10K, 100K	•	•	•	Sig-netics - Philips
	Q14000 (4) Si-gate CMOS and bipolar OI (TTL, ECL) 1.5 µm	M1 4.5 µm M2 4.5 µm M3 6 µm	240	0.02	0.67	2100–14,000	80–226	•	•	10K, 100K	•	•	•	S-MOS
	Q20000 (3) Bipolar trench isolation 1 µm	M1 4 µm M2 5 µm M3 7 µm	1.5 GHz	0.5	0.09	2000-16,000	244		•	•	•	•	•	Plessey
AT&T Micro-electronics	ALA-200 Bipolar JI (IIV) 1.5 µm	M1 5 µm M2 10 µm	4.5 GHz	n/a	n/a	111-222 active 501-998 passive	36-48		•	•	•	•	•	None
	ALA-300 Bipolar JI (90V) 8 µm	M1 10 µm M2 10 µm	250	n/a	n/a	29-116 active 111-444 passive	30-32		•	•	•	•	•	None
	ALA-400 Bipolar JI (30 V) 4 µm	M1 8 µm M2 8 µm	250	n/a	n/a	122-208 active 417-670 passive	38-42	•	•	•	•	•	•	None
	DBIC gate array (TTL, ECL)	M1 5 µm M2 5 µm	600	1.25	0.2	2000-6000	72-120			10K				n/s
Barvon BiCMOS Technology	BC9000 (1) BiCMOS (bipolar and Si-gate CMOS) 2 µm	M1 M2	100	n/s	1.5	2000 gates 18 analog 900 passive	68 total	•	•		•	•	•	None
California Micro Devices	C3000 (4) Si-gate CMOS 3.5 µm	P1 7 µm M1 7 µm	15	0.44	2.1	500–2000	40–80	•	•		•	•	•	None
	C2000 (8) Si-gate CMOS 2 µm	M1 4.5 µm M2 5.5 µm	30	0.8	1.2	1500–10,000	72–250	•	•		•	•	•	None
Cherry Semi-conductor	1200, 1300, 1400 Bipolar JI (I^2L) 4 µm	M1 16 µm	3	0.7	50	192–288 gates 50–106 active	24–28 2–6 analog	•	•	•	•	•		Exar
	Genesis (4) Bipolar JI (I^2L) 4 µm	M1 16 µm	3	0.4	50	64–256 gates 143–69 active 345–200 passive	10—18 16–22 analog	•	•		•	•	•	Exar
Commodore Semi-conductor	4100 Series Si-gate CMOS 2 µm	M1 5 µm M2 7 µm	80	1	1.2	500–6000	40–152	•	•		•			None
Control Data	VLSI-6200 Si-gate CMOS 2 µm	M1 5.5 µm M2 7 µm	40	0.24	0.85	8500	154	•	•		•	•	•	National, VTC
	VLSI-6100 Si-gate CMOS 1.25 µm	M1 3.5 µm M2 4.5 µm	40	0.2	0.8	8500	154	•	•		•	•	•	National, VTC
	VLSI-7000 Si-gate CMOS 1.25 µm	M1 2.5 µm M2 2.5 µm	75	0.2	0.5	20,000	238	•	•		•	•	•	Honey-well Digital Products
Custom Arrays	MM 20 V bipolar (9) Bipolar JI 6 µm	M1	n/s	n/s	n/s	45–280 active 100–1150 passive	14–46		•	•	•	•	•	Ferranti Inter-design
	MV 40 V bipolar (5) Bipolar JI 6 µm	M1	n/s	n/s	n/s	68–340 active 360–1400 passive	20-44		•	•	•	•	•	Ferranti Inter-design

1. Flip-flop toggle rate 2. Gate power at frequency 3. 2-in NAND delay, FO = 2, 1 mm wire 4. C = CMOS, T = TTL 5. C = commercial, I = industrial, M = military

Directory of Gate Arrays (continued)

Company	Product Technology Line width	Program-mable Layers	Typical Parameters MHz[1]	mW[2]	ns[3]	Components Gates	I/Os	Interface levels[4] C	T	ECL	Temp. ranges[5] C	I	M	Second Sources
Custom Silicon	SLA-8000 (10) Si-gate CMOS 1.2 μm	M1 3.5 μm M2 5 μm	120	1.45	.52	5000-130,000	86-308	•	•		•	•	•	Seiko
	HCA 62A00 (8) Si-gate CMOS 2 μm	M1 5.25 μm M2 6 μm	50	1	1.5	648-8568	44–168	•	•		•	•	•	Motorola, NCR
	MH–15 Volt (8) Si-gate CMOS 4 μm	M1 8 μm	40	n/s	Depends on voltage	70-1600 gates 8-84 active	18-84	•	•		•	•	•	Plessey
	SLA–1.5 Volt (6) Si-gate CMOS 2 μm	M1 M2	10 @ 3 V 1 @ 1.5 V	2.2	8.5 @ 1.5 V	1632–8000	78–178	•	•		•	•	•	Seiko
	HDC 100 (10) Si-gate CMOS 1 μm	M1 3.6 μm M2 4 μm M3 4 μm	175	1	0.45	5670-104,832	99-512	•	•		•			Motorola
	MM–15 Volt (9) Bipolar JI 5 μm	M1 18 μm	350[6]	n/s	n/s	41-276 active 50-369 passive	14-46 analog I/O	•	•	all	•	•	•	Plessey
	MV-40 Volt (5) Bipolar JI 5 μm	M1	n/s	n/s	n/s	58-203 active 216-924 passive	16-36 analog I/O	•	•	all	•	•	•	Plessey
Data Linear	DL104–650 analog arrays (5) Bipolar DI 5 μm	M1 15 μm	0.5–1 GHz[6]	n/s	2	56–347 active 28–173 passive	14–34 analog	•	•	10K, 100K	•	•	•	None
	SP1104 Bipolar DI 4 μm	M1 7 μm M2 15 μm	npn, 1 GHz; pnp, 0.6 GHz	20 V; 35 V	n/s	444 active NiCr 800 KΩ Pinch 1.2 MΩ 14 MOS caps 6 zeners	24	•	•		•	•	•	None
	SP1204 Bipolar DI with JFETS 4 μm	M1 7 μm M2 15 μm	npn, 1 GHz, pnp, 0.6 GHz	20 V 35 V	n/s	440 active 16 JFETS 2 zeners pinch 400 KΩ NiCr 800 kΩ or SiCr 6 MΩ	40	•	•	•	•	•	•	None
Design Devices	CMOS gate arrays Si-gate CMOS 2 μm	M1 6 μm M2 9 μm	50	1.05	1.75	300–13,500	44–200	•	•		•	•	•	None
	Si-gate CMOS 1.5 μm	M1 5.6 μm M2 6 μm	150	0.14	0.7	5300-129,000	70-370	•	•		•	•		None
Electronic Technology	A5S (13) Bipolar OI (TTL) 5 μm	M1 10 μm	1	4	n/s	37–298 active	14–40	•	•		•	•	•	Exar
	D2D, D3D, D5S (6) Si-gate CMOS	M1 M2	65	0.56	0.9/1.4	600–5000	44–124	•	•		•	•	•	Motorola, NCR, Gould
	Bipolar linear (15) Bipolar JI 7 μm	n/s	n/s	n/s	n/s	n/s	14–40		n/s		•	•	•	Exar
Exar	Flexar Bipolar (analog) 3 μm	M1 M2	1 GHz[6]	n/s	n/s	800	48	•	•	•	•	•	•	Rohm
Ford Micro-electronics	Gate array (1) GaAs E/D MESFET (proprietary Ford logic) 1.5 μm	M1 5 μm M2 4 μm	1 GHz	0.6	170 ps	3000	68			100K	•			n/s

1. Flip-flop toggle rate 2. Gate power at frequency 3. 2-in NAND delay, FO = 2, 1 mm wire 4. C = CMOS, T = TTL 5. C = commercial, I = industrial, M = military 6. f_T

Company	Product Technology Line width	Programmable Layers	Typical Parameters MHz[1]	mW[2]	ns[3]	Components Gates	I/Os	Interface levels[4] C	T	ECL	Temp. ranges[5] C	I	M	Second Sources
Fujitsu Microelectronics	ET-H ECL (1) Bipolar ECL 0 5 μm	M1 4.5 μm M2 4.5 μm M3 4.5 μm	1000	1.62	.100	9856	200			10K. 100K	•			None
	ET ECL (5) Bipolar OI (ECL) 1 μm	M1 · 5 μm M2 5 μm	800	1.83	0.22	1056–6160	64–136		•	10K. 100K	•			None
	ETM ECL (2) Bipolar OI (ECL) 1 μm	M1 .5 μm M2 5 μm	800	1.83	0.25	2640–3960 4.6–9.2K RAM	136		•	10K, 100K	•			None
	BC-H (1) BiCMOS 1 μm	M1 4 μm M2 4 μm M3 4 μm	250	4.5	.57	11968	200		•	•	•			None
	BiCMOS (4) Si-gate CMOS and bipolar JI 1 5 μm	M1 6 μm M2 6 μm	180	4.5	0.65	645–3240	52–112		•		•	•		None
	HB-LSTTL (2) Bipolar JI (STTL) 2 μm	M1 6 μm M2 9 μm	70	0.8	2.4	528–1080	60–88		•		•	•		None
	H-LSTTL (5) Bipolar JI (STTL) 2 μm	M1 6 μm M2 9 μm	150	0.8	1.25	360–3162	40–112		•		•	•	•	Texas Instruments
	AV CMOS (5) Si-gate CMOS 1.8 μm	M1 6 μm M2 9 μm	85	2.2	1.4	2600–8000	106–160	•	•		•	•	•	None
	AVB CMOS (6) Si-gate CMOS 1.8 μm	M1 6 μm M2 8 μm	85	2.2	1.4	350–2000	42–92	•	•		•	•	•	None
	AVM CMOS (3) Si-gate CMOS 1.8 μm	M1 6 μm M2 8 μm	85	2.2	1.4	1500–4000 2K RAM	114–127	•	•		•	•	•	None
	UH CMOS (1) Si-gate CMOS 1.5 μm	M1 4.5 μm M2 6 μm M3 9 μm	105	2.1	1.0	20,000	220	•	•		•	•		None
	UHB CMOS (11) Si-gate CMOS 1.5 μm	M1 4.5 μm M2 6 μm M3 9 μm	115	2.3	0.9	330–12,000	60–220	•	•		•	•		None
	UM CMOS (2) Si-gate CMOS 1.5 μm	M1 4.5 μm M2 6 μm M3 9 μm	105	2.1	1.0	10,000– 15,000 6–12K RAM	219	•	•		•	•		None
	AU CMOS (5) Si-gate CMOS 1.2 μm	M1 3.5 μm M2 5 μm M3 7 μm	120	2.4	0.7	30,000– 100,000	200–350	•	•		•	•		None
	AVL CMOS (6) Si-gate CMOS 2.3 μm	M1 6 μm M2 8 μm	10	n/s	10.8	350–2000	42–92	•			•	•		None
Gain Electronics	GFL2000, GFL4000, GFL7000 (3) GaAs E/D MESFET (GFL patent pending) 1 μm	M1 M2	1000	1.2	247	2000–7000	80–176		•	10K	•			n/s
GE Microelectronics Center	GEGATEAGC-40000 TAGC40000 CMOS and megarad version "T" (CMOS/SOS rad-hard process also available) 1.25 μm	M1 3 μm M2 4 μm	40	0.5	0.7	1700–13,500	60–172	•	•				•	None
Genesis Microchip	SCX6B (9) Si-gate CMOS 1.5 μm	M1 M2	100	n/s	0.6	400–15,000	28–200	•	•		•	•	•	National

1 Flip-flop toggle rate. 2 Gate power at frequency. 3 2-in NAND delay, FO = 2, 1 mm wire. 4 C = CMOS, T = TTL. 5 C = commercial, I = industrial, M = military

Directory of Gate Arrays (continued)

Company	Product Technology Line width	Programmable Layers	Typical Parameters MHz[1]	mW[2]	ns[3]	Components Gates	I/Os	Interface levels[4] C	T	ECL	Temp. ranges[5] C	I	M	Second Sources
Gennum	LA250 (3) Bipolar JI (analog) 8 µm	M1 8 µm	20	n a	20	96–207 active 38–132 passive	24–40	•	•	•	•	•	•	Polycore
	LA200 (3) Bipolar JI (analog) 8 µm	M1 8 µm	20	n a	20	37–122 active 26–58 passive	14–24	•	•	•	•	•	•	Polycore
	GA900 Bipolar (analog) 4 µm	M1 4 µm	200	n a	2	140-280 active 110 passive	28-48	•	•	•	•	•	•	None
GE Solid State	PA60 000 (2) Si-gate SOS 4 µm	M1 10 µm	10	0 15	2	650–1200	78–106	•			•	•	•	None
	PA40.000 (6) Si-gate CMOS 3 µm	M1 10 µm	10	0 2	2 5	250–1200	76–106	•	•		•	•	•	None
	PA50.000 (6) Si-gate CMOS 3 µm	M1 10 µm M2 13 µm	15	0 3	2 5	680–6000	74–180	•	•		•	•	•	LSI Logic
	CGA10 (6) Si-gate CMOS 2 µm	M1 5 8 µm M2 7 5 µm	50	20	1 1	960-8000	56-140	•	•		•	•	•	VLSI Technology
	CGA200 (13) Si-gate CMOS 1 5 µm	M1 4 8 µm M2 6 2 µm	250	1.5	0 8	960-54,000	48-348	•	•		•	•	•	VLSI Technology
Gould Semiconductor	B (7) Si-gate CMOS 2 µm	M1 5 µm M2 7 µm	50	2	1 3	1000–10 000	68-208	•	•		•	•		Contact company
	Si-gate CMOS 1 25 µm	M1 M3	100	n s	0.6	2000-14,000	52–152	•	•		•	•		Contact company
Holt Integrated Circuits	HI 5100 (1) Si-gate CMOS 3 µm	M1 8 µm	20	0 2	6	73 gates 254 active 255 passive	12 40 analog	•	•		•	•	•	None
	HI 5300 Si-gate CMOS 3 µm	M1 8 µm	20	0 2	6	178 gates op amps comparators current source, 86 passive 1 bipolar transmitter	64	•	•		•	•	•	None
Honeywell Solid State Electronics Division	HCT5000 Si-gate CMOS 1 2 µm	M1 M2	40	0 24	0 3	5000	96	•	•		•	•	•	None
	HCT15000 Si-gate CMOS 1 2 µm	M1 M2	40	0 24	0 3	15,000	144	•	•		•	•	•	None
	HC20000 Si-gate CMOS 1 2 µm	M1 M2	50	0 30	0 3	20 000	238	•	•		•	•	•	None
	HC40000 Si-gate CMOS 1.2 µm	M1 M2	50	0 30	0 3	40 000	300	•	•		•	•	•	None
	HCS15000 Si-gate CMOS 1 2 µm	M1 M2	25	0 30	0 4	12 000	144	•	•				•	None
	HM3500 Bipolar OI 2 5 µm	M1 M2	500	2 0	0 3	3500	120		•	•	•	•	•	None
	HVM10000 Bipolar OI 1.2 µm	M1 M2	300	0 4	0 2	10,000	256		•	•	•	•	•	None
	HE12000 Bipolar OI 1 2 µm	M1 M2	600	0	0 1	12,000	256		•	•	•			None

1 Flip-flop toggle rate 2 Gate power at frequency 3 2-in NAND delay FO 2, 1 mm wire 4 C CMOS. T TTL 5 C commercial. I industrial, M military

Company	Product Technology Line width	Programmable Layers	Typical Parameters MHz[1]	mW[2]	ns[3]	Components Gates	I/Os	Interface levels[4] C	T	ECL	Temp. ranges[5] C	I	M	Second Sources
Hughes Aircraft	U series (11) Si-gate CMOS 2 µm	M1 5 µm M2 7 µm	200	1.2	1.2	1000–41,000	40–248	•	•		•	•	•	None
	HL5000 (8) Si-gate CMOS 3 µm	M1 M2	n/s	0.02/MHz	2.4	504–6000	52–180	•	•		•	•	•	LSI Logic
	HL7000 (8) Si-gate CMOS 2 µm	M1 M2	n/s	0.02/MHz	1.4	880–10,013	68–232	•	•		•	•	•	LSI Logic
	HL9000 (8) Si-gate CMOS 1.5 µm	M1 M2	n/s	0.02/MHz	1.0	880–10,013	68–232	•	•		•	•	•	LSI Logic
	HL10,000 (4) Si-gate CMOS 1.5 µm	M1 M2	n/s	0.01/MHz	0.7	50,000–129,000	120–256	•	•		•	•	•	LSI Logic
ICI Array Technology	DHS (10), HCD (3) Si-gate CMOS 1.5, 2, and 3 µm	P1 M1 1.5, 2, 3 µm	40	0.07	2	150–2650	38–86	•	•		•			None
Integrated Circuit Systems	VGT10 Si-gate CMOS 2 µm	M1 6µm M2 6µm	70	0.2	1.0	800–10,000	40–140	•	•		•	•	•	VLSI Technology
	VGT100 Si-gate CMOS 1.5 µm	M1 6µm M2 6µm	85	0.13	0.7	3700–66,000	84–384	•	•		•	•	•	VLSI Technology
	SCX Si-gate CMOS 2 µm	M1 6µm M2 6µm	66	0.2	1.0	600–8,700	40–155	•	•		•	•	•	National Semiconuctor
Integrated Logic Systems	CA15 (6) Si-gate CMOS 1.5 µm	M1 7 µm M2 7 µm	150	1	0.7	1960-41,568	48–194	•	•		•	•	•	None
	15GH (5) Si-gate CMOS 1.5 µm	M1 6 µm M2 6 µm	150	1	0.7	30,400–100,512	146–260	•	•		•	•	•	None
International MicroCircuits	G4000 (8) Me-gate CMOS 8 µm	M1	2.0	0.015	70	75–600	23–53	•	•		•	•	•	S-MOS Systems
	G70000 Si-gate CMOS 3.5 µm	P1 M1	42	0.42	3.3	135–2535	28–88	•	•		•	•	•	S-MOS Systems
	IMI6000 (7) Si-gate CMOS 2 µm	P1 M1 M2	60	0.6	1.4	820–6204	60–158	•	•		•	•	•	S-MOS Systems
	IMI7000 Si-gate CMOS 1.5 µm	P1 M1 M2	100	n/s	0.75	1632-8000	70-170	•	•		•	•	•	S-MOS Systems
International Micro-Electronic Products	Si-gate CMOS (5) 1.2 µm	M1 4 µm M2 4.5 µm	40	1.4	1	800–15,000	40–110	•	•		•	•		National Semiconductor, VLSI Technology
LSI Logic	LCA100K (3) Si-gate CMOS 0.7 µm	M1 M2 M3	n/s	0.01/MHz	0.46	50,000–100,000	316-418	•	•		•	•	•	Contact company

1 Flip-flop toggle rate. 2 Gate power at frequency. 3 2-in NAND delay, FO = 2, 1 mm wire. 4 C = CMOS, T = TTL. 5 C = commercial, I = industrial, M = military

Directory of Gate Arrays (continued)

Company	Product Technology Line width	Program-mable Layers	Typical Parameters MHz[1]	mW[2]	ns[3]	Components Gates	I/Os	Interface levels[4] C	T	ECL	Temp. ranges[5] C	I	M	Second Sources
LSI Logic	LMA9000 (10) Si-gate CMOS 1.5 µm	M1 M2	n.s	0.012 MHz	0.57	700-15,000	41-174	•	•		•	•	•	Contact company
	LCA10000 (6) Si-gate CMOS 1.5 µm	M1 M2 M3	n.s	0.012 MHz	0.57	10,000 50,000	76-256	•	•		•	•	•	Contact company
	LSA1500 (4) Si-gate CMOS 1.5 µm	M1 M2	n.s	0.012 MHz	0.57	22,000 38,000 18K 32K RAM	234	•	•		•	•	•	Contact company
	LL9000 (8) Si-gate CMOS 1.5 µm	M1 M2	n.s	0.018 MHz	1.0	880-10,013	68-232	•	•		•	•	•	Contact company
	LL7000 (8) Si-gate CMOS 2 µm	M1 M2	n.s	0.018 MHz	1.4	880-10,013	68-232	•	•		•	•	•	Contact company
	LSA2000 (11) Si-gate CMOS 2 µm	M1 M2	n.s	0.018 MHz	1.4	4000-6900 2K-9K RAM	190	•	•		•	•	•	Contact company
	LDD10000 (6) Si-gate BiCMOS 1.5 µm	M1 M2	n.s	0.012 MHz	0.57	8000-43,500 CMOS 375-1330 biCMOS	144-256	•	•		•	•	•	Contact company
Marconi Electronic Devices	MA2000A (5) Si-gate CMOS 3 µm	M1 8 µm M2 8 µm	60	0.18	1.6	1120-6864	48-128	•	•		•	•	•	None
	MA9000 (3) Si-gate CMOS-SOS 2.5 µm	M1 8 µm M2 8 µm	60	0.1	1.2	748-4048	48-106	•	•		•	•	•	None
	MA8304 (1) Si-gate CMOS 3 µm	P1 6 µm M1 6.5 µm	35	0.11	3	392	26	•	•		•	•	•	United Microelectronics
	MA4000 (4) Si-gate CMOS 2 µm	M1 6 µm M2 6 µm	100	0.2	0.9	3904 10,044	96-160	•	•		•	•	•	None
Matra Design Semiconductor	MA (4) Si-gate CMOS 2.5 µm	P1 6.5 µm M1 10 µm	25	0.018 MHz	2	228-1139	32-62	•	•		•	•	•	None
	MB (9) Si-gate CMOS 2 µm	P1 4 µm M1 6 µm M2 9 µm	45	0.015 MHz	1	810-7500	73-191	•	•		•	•	•	Plessey
MCE Semiconductor	MCE Uniray Bipolar JI (analog) 5 µm	M1 11 µm	50	20	15	38-220 71-592 active	n.s	•	•	•	•	•	•	Ferranti Interdesign
	MCE MGC (7) Me-gate CMOS 5 µm	M1 10 µm	5	2	16	75-984	22-68	•	•		•	•	•	Master Logic
Micro Linear	FB900 (6) Bipolar JI (analog) 5 µm	M1 20 µm	30	n.s	10	50-205 active 120-607 passive	18-28	•	•	10K	•	•	•	Cherry Exar Ferranti Interdesign MCE
	FB300 (5) Bipolar JI (analog digital) 4 µm	M1 16 µm M2 22 µm	100	n.a	4	120 gates 252-319 active 741-907 passive	22 digital 24-44 analog	•	•	10K	•	•	•	None
	FB3600 (3) Bipolar JI (analog digital)	M1 14 µm M2 22 µm	100	n.a	4	256-720 active 678-1816 passive	24-44 digital or analog	•	•	10K	•	•	•	None
	FB3400 (2) Bipolar JI (analog)	M1 20 µm M2 22 µm	30	n.a	10	200-540 active 508-1362 passive	28-44 analog or digital	•	•	10K	•	•	•	None

[illegible]

Company	Product Technology Line width	Programmable layers	Typical parameters MHz[1]	mW[2]	ns[3]	Components Gates	I/Os	Interface levels[4] C	T	ECL	Temp. ranges[5] C	I	M	Second sources
Micro LSI	μGA Si-Gate CMOS 3 μm	P1 5 μm M1 7 μm	90	3.5	1.1	200–3500	120	•	•		•	•		None
	ULSI 20 Si-gate CMOS 2 μm	M1 6 μm M2 8 μm	90	3.5	1.1	200	26 10% analog	•	•			•		None
Mietec	MTC CMOS Si-gate CMOS 2.4 μm	P1 4.8 μm P2 4.8 μm M1 5.6 μm M2 4.2 μm	60	0.2	2.0	n.s	n.s	•	•		•	•	•	Inter-metall (Frei-bourg)
	MTC biMOS Bipolar JI + CMOS 3 μm	P1 7 μm M1 8 μm M2 9 μm	40	0.2	4.5	n.s	n.s	•	•		•	•	•	None
Mitsubishi Electronics America	M6001x (9) Si-gate CMOS 2 μm	M1 4 μm M2 7.5 μm	100	0.015	1.4	500–8100	54–190	•	•		•	•		None
	M6002x (6) Si-gate CMOS 1.3 μm	M1 4 μm M2 6 μm	175	0.01	0.9	200–2400	22–72	•	•		•	•		None
	M6003x (6) Si-gate CMOS 1.3 μm	M1 4 μm M2 6 μm	175	0.01	0.9	3200–20,000	88–256	•	•		•	•		None
	M6004x (2) Si-gate CMOS 1.3 μm	M1 4 μm M2 6 μm	175	0.01	0.9	4100-6300	182-222 (for high I.O pin count)	•	•		•	•		None
Motorola	MCA I ECL (2) Bipolar OI (ECL) 3 μm	M1 8 μm M2 16 μm	250	3.3	0.8	625–1192	46–60			10K, 10KH	•			None
	MCA II ECL (3) Bipolar OI (ECL) 2 μm	M1 6 μm M2 10 μm (M3 fixed)	770	3.2	0.25	902–2760 1K RAM	54–120			10K, 10KH, 100K	•			None
	MCA I ALS (2) Bipolar OI (STTL) 3 μm	M1 8 μm M2 16 μm	80	1.0	1.4	533–1280	57–75		•		•			None
	MCA II ALS (2) Bipolar OI (STTL) 2 μm	M1 6 μm M2 10 μm (M3 fixed)	150	1.2	0.7	1800–2860 16 · 8 RAM	120		•		•			None
	HCA 62A00 (8) Si-gate CMOS 2 μm	M1 5.4 μm M2 6 μm	85	1.0	1.5	648–8568	44–168	•	•		•	•	•	NCR
	MCA III ECL (2) Bipolar OI (ECL) 1.5 μm	M1 4 μm M2 6 μm (M3 fixed)	1000	1.0-3.0, pro-gram-mable	0.1	1500–10,332	108–256			10K, 10KH, 100K	•			None
	BiMOS (3) Si-gate CMOS and bipolar OI (STTL) 1.5 μm	M1 4 μm M2 5 μm	150	0.022 MHz	0.6	704–6144	44–228	•	•	10K, 10KH, 100K	•			None
	HDC series (5) Si-gate CMOS 1 μm	M1 3.6 μm M2 4 μm M3 4 μm	150	0.006 MHz	0.4	8208-104,832	100-267	•	•		•	•	•	None
National Semiconductor	SCX 6200 (2) Si-gate CMOS 2 μm	M1 4.75 μm M2 6.25 μm	100	2.75	0.9	600–8736	49-155	•	•		•	•	•	IMP
	10K VHSIC Si-gate CMOS 1.25 μm	M1 3 μm M2 4 μm	200	0.12	0.4	10,000	152	•	•				•	Westinghouse
	SCX6Bxx (1) Si-gate CMOS 1.5 μm	M1 3.5 μm M2 4.75 μm	150	3	0.65	400-15,000	28-200	•	•		•	•	•	None
	FGE (5) Bipolar OI (ECL) 1.5 μm	M1 5 μm M2 9 μm M3 13 μm	1000	4.5	0.23	100-6300	21-220		•	10K, 100K	•	•	•	Honeywell
	FGA (3) Bipolar OI (ECL) 1.5 μm	M1 5 μm M2 5 μm M3 9 μm	1800	3.7	0.12	1300-15,000	72-300		•	•	•	•	•	None

1 Flip-flop toggle rate 2 Gate power at frequency 3 2-in NAND delay, FO 2, 1 mm wire 4 C CMOS, T TTL 5 C commercial, I industrial, M military

Directory of Gate Arrays (continued)

Company	Product Technology Line width	Programmable layers	Typical parameters MHz[1]	mW[2]	ns[3]	Components Gates	I/Os	Interface levels[4] C	T	ECL	Temp. ranges[5] C	I	M	Second sources
NCM	3000 (3) Me-gate CMOS 7 μm	M1 12.5 μm	5	n/s	18	235–500	38–48	•	•		•	•	•	None
	7300, 7500 Si-gate CMOS 3, 5 μm	P1 10 μm M1 10 μm	18, 12	n/s	5, 8	780 gates 8 active	62	•	•		•	•	•	None
	5000 Bipolar JI 5 μm	M1 12.5 μm	40	n/s	3	78–132 active 227–296 passive	18–24		•	•	•	•	•	Exar, Ferranti Inter- design
NCR Micro-Electronics	62A00 (8) Si-gate CMOS 2 μm	M1 M2	85	1.6	1.5	600–8500	44–168	•	•		•	•	•	Motorola
NEC Electronics	CMOS-5 5A (13) Si-gate CMOS 1.2 μm	M1 3.6 μm M2 4.6 μm M3 7.2 μm	250	3.0	0.52	2000– 45,000	88–334	•	•		•	•		None
	CMOS-4 4A 4R (16) Si-gate CMOS 1.5 μm	M1 5.4 μm M2 7 μm	140	2.1	0.9	320–19,551	54–266	•	•		•	•		None
	CMOS-4L (6) Si-gate CMOS 1.5 μm	M1 5.4 μm M2 7 μm	25	0.08	7	860-5600	62-138	•			•			None
	BiCMOS-5 (5) Si-gate CMOS 1.3 μm Bipolar 1.2 μm	M1 M2	300	5.4	0.45	5000– 20,000	148-280	•	•	10KH, 100K	•	•		None
	BiCMOS-4 4A (6) Si-gate CMOS 1.5 μm Bipolar 2 μm	M1 5.4 μm M2 7 μm	200	3.6	0.67	600–10,000	64–228	•	•		•	•		None
	ECL-4A (5) Bipolar (ECL) 1.2 μm	M1 M2 M3 (power)	1200	4.85	0.15	2400-35,000	108-236		•	10KH, 100K	•			None
	ECL-4 (2) Bipolar (ECL) 1.2 μm	M1 M2 M3 (power)	1700	6.75	0.14	600-4400	56–108			10KH, 100K	•			None
	ECL-3A 3B (5) Bipolar (ECL) 1.4 μm	M1 M2 M3 (power)	450	4.35	0.5	2400-9600	120-172		•	10KH, 100K	•			None
	ECL-3 (3) Bipolar (ECL) 3 μm	M1 8 μm M2 M3 (power)	300	1.1	0.7	1200-3000	48-180			10K	•			None
	ECL-2 (3) Bipolar (ECL) 3 μm	M1 8 μm M2 M3 (power)	450-750	4.5	0.05	300-2000	28-108			100K	•			None
Oki Semi-conductor	MSM7H000 CMOS 2 μm drawn	M1 8 μm M2 11 μm	40	6	1.8	301-10,008	32-188 4-18 mA 48 mA max	•	•		•	•		None
	MSM7nV000 CMOS 1.5 μm drawn	M1 5 μm M2 7.5 μm	50	5	1	700-10,008	74-188 4-8 mA 24 mA max	•	•		•	•		None
	MSM10V000 CMOS 1.5 μm drawn	M1 5 μm M2 7.5 μm	65	4.5	0.8	5500-100,500	74-188 4-12 mA 24 mA max	•	•		•	•		None
	MSM7U000 CMOS 1.2 μm drawn	M1 4.5 μm M2 6 μm	80	4	0.5	1632-30,384 cells (6 transistors)	60-252 + 8 power 4-12 mA 24 mA max	•	•		•	•		None
Panasonic	MN 51000 (8) Si-gate CMOS 2.5 μm	M1 3.6 μm M2 5 μm	120	0.025	1.9	312–4000	46–164	•	•		•	•		None
	MN 52000 (5) Si-gate CMOS 2 μm	M1 2.7 μm M2 3.8 μm	160	0.02	1.4	2014– 10,000	94–234	•	•		•	•		None
	MN 53000 (13) Si-gate CMOS 1.5 μm	M1 2.4 μm M2 2.8 μm	200	0.015	1	315–20,064	42-256	•	•		•	•		None

1 Flip-flop toggle rate 2 Gate power at frequency 3 2-in NAND delay, FO = 2, 1 mm wire 4 C = CMOS, T = TTL 5 C = commercial, I = industrial, M = military.

Company	Product Technology Line width	Program-mable layers	Typical parameters			Components		Interface levels[4]			Temp. ranges[5]			Second sources
			MHz[1]	mW[2]	ns[3]	Gates	I/Os	C	T	ECL	C	I	M	
Plessey Semi-conductor	CLA 5000 (8) Si-gate CMOS 2 μm	M1 6 μm M2 6 μm	100	0.35	1.2	640–10,044	44–176	•	•		•	•	•	Matra-Harris
	ELA60000 (4) Bipolar (ECL) 1.5 μm	M1 5 μm M2 5 μm M3 7 μm (power only)	2000	7	0.3	600–4500	48–120	•	•	10K, 100K	•	•	•	None
	MVX (5) Bipolar JI (analog) 10 μm	M1 18 μm	n/s	n/s	n/s	62–213 active	20–44	•	•	•	•	•	•	Custom Arrays
	MFX (5) Bipolar JI 4 μm	M1 18 μm	n/s	n/s	n/s	100–170 gates 160–650 active	16–48	•	•	•	•	•	•	None
	MMX (9) Bipolar JI 10 μm	M1 18 μm	n/s	n/s	n/s	36–434 active	14–48	•	•	•	•	•	•	Custom Arrays
	ULA Digilin G (7) Bipolar CDI 4 μm	M1 8 μm	0.66	0.002	230	30–578 gates 124–436 active	10–36	•	•		•	•	•	None
	ULA Digilin P Bipolar CDI (10) 3 μm	M1 8 μm	4.8	0.001	40	128–1152 gates 444–1088 active	16–44	•	•		•	•	•	None
	ULA R (28) Bipolar CDI 2.5 μm	M1 8 μm	65	350	2.2	130–2000	20–72	•	•		•	•	•	None
	ULA DS (30) Bipolar CDI 1.5 μm	M1 6 μm	250	0.33	1.0	630–10,000	32–138	•	•		•	•	•	None
	MLX (2) Me-gate CMOS 7 μm	n/s	n/s	n/s	n/s	64 gates 312–842 active	30–42	•	•		•	•	•	None
	MC (7) Me-gate CMOS 6 μm	M1 10 μm	18	0.125	15	140–800	29–58	•	•		•	•	•	MCE, Master Logic, Hytek
	MH (8) Si-gate CMOS 4 μm	M1 8 μm	40	0.1	n/s	70–1600	18–84	•	•		•	•	•	None
Polycore Electronics	Maxi chip (8) Bipolar JI (analog) 5 μm	M1 15 μm	n/s	n/s	n/s	17–165 active 24–280 passive	10–40		•	all	•			Gennum
Raytheon Semi-conductor	CGA 300 Bipolar JI (STTL) 5 μm	M1 15 μm M2 15 μm	25	5	6	300	48		•		•	•	•	None
	CGA 800-2500 Bipolar JI (ISL) 3 μm	M1 10 μm M2 15 μm	100	0.4	2.2	800–2400	48–84		•		•	•	•	None
	CGA 3,500, 5,000 Bipolar OI (ISL) 2 μm	M1 6 μm M2 9 μm	150	0.16	1.2	3500, 5000	120, 150		•		•	•	•	None
	CGA70E18 Bipolar (ECL) 2 μm	M1 4 μm M2 4 μm	1000	300	0.3	12,800	176	•	•	10KH, 100K	•	•	•	None
	RL 7000 series Si-gate CMOS 2 μm	M1 7 μm M2 9 μm	40	0.72	1.4	880–10,013	68–232	•	•		•	•	•	LSI Logic
	CGA40E12 Bipolar (ECL) 2 μm	M1 4 μm M2 4 μm	1000	300	.3	7752	120		•	10KH, 000053	•	•	•	None
	CGA1ME12 Bipolar (ECL) 2 μm	M1 4 μm M2 4 μm	1000	300	.3	4584 1280 bits of RAM	120		•	10KH, 100K	•	•	•	None
	RL1050–H1200 NCMOS 1.25 μm	M1 4 μm M2 6 μm	250	8 mW/ MHz/ gate	0.95	5670–20, 440–160	90	•	•		•	•	•	None
Siliconix	ISO5 (9) Si-gate CMOS 4.8 μm	M1 10 μm	10	0.09	2.8	180–2400	30–90	•	•		•	•	•	Universal

1 Flip-flop toggle rate 2 Gate power at frequency 3 2-in NAND delay, FO = 2, 1 mm wire 4 C = CMOS, T = TTL 5 C = commercial, I = industrial, M = military

Directory of Gate Arrays (continued)

Company	Product Technology Line width	Program-mable Layers	Typical Parameters MHz[1]	mW[2]	ns[3]	Components Gates	I/Os	Interface levels[4] C	T	ECL	Temp. ranges[5] C	I	M	Second Sources
Silicon Systems	SSI 6600 (6) Si-gate CMOS and bipolar JI (CML) 3 μm	P1 6 μm M1 8 μm	25	n/s	5	0–545 179–294 active 224–712 passive	28–62 analog	•	•		•	•	•	None
	BK MSA6900 Bipolar JI (STTL) 3 μm	M1 8.8 μm M2 12 μm	>100	n/s	1.5	n/s	n/s	•	•	•	•	•	•	None
	MSA6700 (4) Si-gate CMOS 3.8 μm	P1 M1	20	0.01/MHz	5	80–600 gates 190–601 active 600–1200 passive	32–52 8–12 analog	•	•		•	•		None
	SSI 6900 (4) Bipolar JI (STTL, ECL, CML) 2.5 μm	M1 8 μm M2 14 μm	100	n/s	n/s	20–80 gates 144–168 active 24–56 passive	16–32 8 analog	•	•	•	•	•		Ferranti Inter-design
Silicon West	SWI 1000 (4) Si-gate CMOS 2 μm	M1 M2	100	0.6	1.2	360–10,000	40–161	•	•		•	•		None
S-MOS Systems	SLA 6000 (10) Si-gate CMOS 2 μm	M1 7 μm M2 9.8 μm	70	0.8	1.7	513–6206	60–154	•	•		•			IMI
	SLA 7000 (5) Si-gate CMOS 1.5 μm	M1 5.2 μm M2 7.4 μm	100	1.2	0.9	2232–16,250	90–188	•	•		•			IMI
	SLA 8000 (6) Si-gate CMOS 1.2 μm	M1 3.5 μm M2 5 μm	120	1.45	0.7	5904–38,550	82–218	•	•		•			None
Tektronix	QuickChip 4 Bipolar JI (ECL CML) 4 μm	M1 7 μm M2 7 μm	500	1	0.4	300	n/s			all	•	•		None
Texas Instruments	TGC100 series Si-gate CMOS 1 μm	M1 4.8 μm M2 5.4 μm	150	0.018/MHz	0.5	3200–18620	84–216	•	•		•	•	•	None
TLSI	TA CMOS (6) Si-gate CMOS 5 μm	M1 10 μm	10	n/s	6	300–1260	37–75	•	•		•	•	•	
	TA CMOSII (5) Si-gate CMOS 3 μm	M1 7 μm	36	n/s	3	540–2500	37–81	•	•		•	•	•	Gould
	TA CMOSIID (4) Si-gate CMOS 3 μm	M1 7 μm M2 8 μm	40	n/s	2.5	1000–4012	61–117	•	•		•	•	•	Gould
Toshiba America	TC110G Si-gate CMOS 1.5 μm	M1 5.6 μm M2 6 μm	150	0.14	0.6	3498–129,000	68–368	•	•		•	•		LSI Logic
	TC120G Si-gate CMOS 1 μm	M1 5.6 μm M2 6 μm	200	Contact company	0.4	37,932–129,042	19–368	•	•			n/s		None
TriQuint Semi-conductor	TQ3000 GaAs E/D MESFET 1 μm	M1 2 μm M2 3 μm	1000	2.5	0.18	2000–4200	84	•	•	all	•	•	•	None
Unicorn Micro-electronics	UM1200 (4) Si-gate CMOS 3 μm	M1 P1	20	0.4	3.0	200–910 gates 36–68 passive	28–58	•	•		•	•		United Micro-elec-tronics
	UM1300 (4) Si-gate CMOS 2 μm	P1 M1 M2	30	0.9	2	1320–3060 gates 58–102 passive	54–92	•	•		•	•		United Micro-elec-tronics
United Technologies Micro-electronics Center	UTB (5) Si-gate CMOS 3 μm	M1 7.5 μm M2 7.5 μm	115	2.25	2.2	1000–7600	40–144	•	•				•	None
	UTD (4) Si-gate CMOS 1.5 μm	M1 6 μm M2 6 μm	250	7.5	0.63	3400–11,000	116–212	•	•				•	None

1 Flip-flop toggle rate 2 Gate power at frequency 3 2-in NAND delay, FO = 2, 1 mm wire 4 C = CMOS, T = TTL 5 C = commercial, I = industrial, M = military

Company	Product Technology Line width	Program-mable Layers	Typical Parameters MHz[1]	mW[2]	ns[3]	Components Gates	I/Os	Interface levels[4] C	T	ECL	Temp. ranges[5] C	I	M	Second Sources
Vitesse Semi-conductor	VSC4500 (1) GaAs E/D-MESFET (DCFL) 1.2 μm	M1 4 μm M2 8 μm	600 single-ended, 850 differential	6.2	0.240	4000	120		•	10K, 100K	•	•	•	None
	VSC1500 (1) Mixed D-and E/D-MESFET (DCFL; source-coupled FET logic) 1.2 μm	M1 4 μm M2 8 μm	2000	DCFL 0.42, SCFL 0.23[6]	DCFL 0.545, SCFL 0.235[6]	1500	35			10K, 100K	•	•	•	None
VLSI Technology	VGT200 (13) Si-gate CMOS 1.5 μm	M1 4 μm M2 5.6 μm	250	15	0.560	960–54,000	48–348	•	•		•	•	•	Philips, GE
	VGT-100 (13) Si-gate CMOS 1.5 μm	M1 4 μm M2 5.6 μm	175	3.5	0.8	1600–66,500	56–348	•	•		•	•	•	GE
	VGT10 (6) Si-gate CMOS 2 μm	M1 6 μm M2 6 μm	120	2.4	1.2	1600–10,648	56–140	•	•		•	•	•	GE
VTC	VJ800 (4) Bipolar JI 3 μm	M1 8 μm M2 12 μm	50	2.25	2	50 28–40	28–68 active		•	10K, CML	•	•	•	None
	Si-gate CMOS 1 μm	M1 4 μm M2 6 μm	200	n/s	0.7	6000	n/s	•	•		•	•	•	Motorola
	VG6000 Si-gate CMOS 1.6 μm	M1 M2	200	n/s	1	6000	172	•	•		•	•	•	National
	VJ900 (3) Bipolar OI 2 μm	M1 8 μm M2 12 μm	250	2.25	0.42	30–572	16–68		•	10K	•	•	•	None
Xerox Micro-electronics Center	SCX 6200 (2) Si-gate CMOS 2 μm	M1 4.75 μm M2 6.25 μm	>100	2.75	0.9	600–8736	49-155	•	•		•	•	•	IMP
	10K VHSIC Si-gate CMOS 1.25 μm	M1 3 μm M2 4 μm	200	0.12	0.4	10,000	152	•	•				•	Westing-house
	SCX6Bxx (1) Si-gate CMOS 1.5 μm	M1 3.5 μm M2 4.75 μm	>150	3	0.65	400-15,000	28-200	•	•		•	•	•	None
	FGE (5) Bipolar OI (ECL) 1.5 μm	M1 5 μm M2 9 μm M3 13 μm	1000	4.5	0.23	100-6300	21-220		•	10K, 100K	•	•	•	Honeywell
	FGA (3) Bipolar OI (ECL) 1.5 μm	M1 5 μm M2 5 μm M3 9 μm	1800	3.7	0.12	1300-15,000	72-300		•	•	•	•	•	None
Xilinx	XC2000/XC3000 (7) Si-gate CMOS 1.2 μm	n/a	70	1.0	2	1200-9000	58-144	•	•		•	•	•	AMD

1 Flip-flop toggle rate 2 Gate power at frequency 3 2-in NAND delay, FO 2, 1 mm wire 4 C CMOS, T TTL 5 C commercial, I industrial, M military 6 For a 2-in NOR gate

Directory of Cell Libraries

Company	Product Technology Line width	Wiring layers	Typical parameters MHz[1]	mW[2]	ns[3]	Cells Simple	Complex	Interface levels[4] C	T	ECL	Temp. ranges[5] C	I	M	Second sources
ABB HAFO	MEG 6 Me-gate CMOS 5 μm	M1 10 μm	10	0.5	10	55 gates 10 MSI 15 analog 20 I/O	RAM, ROM, PLA	•	•		•	•	•	GE
	SOS3 Si-gate SOS 4 μm	P1 8 μm M1 8 μm	35	0.1	2.5	55 gates 10 MSI 10 I/O	RAM, ROM, PLA	•	•		•	•	•	GE

1 Flip-flop toggle rate 2 Gate power at frequency 3 2-in NAND delay, FO 2, 1-mm wire 4 C CMOS, T TTL 5 C commercial, I industrial, M military

APPENDIX E
MULTIPLE BEAM ANTENNA EXTENDED ANALYSES

APPENDIX E
MULTIPLE BEAM ANTENNA EXTENDED ANALYSES

E.1 INTRODUCTION

Extended analysis on two of the configurations, the torus reflector and the single parabolic reflector, was performed to provide an in-depth comparison of the proposed MBAs. The initial analysis of the torus was done with simplifying assumptions, and for only two feed sizes. This analysis has been extended to cover a range of feed sizes from 1 to 3 inches at both 14 and 29 GHz, using a corrugated horn feed to produce better sidelobes in all planes. This would allow closer spacing of adjacent beams without degrading isolation.

Another effort was undertaken to explore an alternate technique for overcoming the effects of defocussing when scanning off the focal point for a simple parabolic reflector. This approach was suggested by results from another project in which an array of small feeds was used to shape an off-axis beam using such a reflector.

The results of these two efforts are documented in the following sections.

E.2 TORUS ANTENNA CALCULATIONS

The original torus design reported earlier was for a unit capable of scanning ±7.5° in azimuth, somewhat more than required for Configuration 2 (±6.4°), but represents coverage for all stations with elevation angles above 30°. Corresponding size reductions are possible for designs with less scanning capability as follows:

Maximum scan in azimuth (degrees)	0	±3	±6.4	±7.5
Torus width required (in.)	96	128	164	176

Thus while the problem of deploying a 176 inch reflector from a launch vehicle that will accommodate only a 143 inch structure without folding is apparent*, the real requirements need to be verified, and then the possibility of modifying the design to meet these restrictions needs to be examined. Perhaps a shorter focal length could be accepted, with a slightly lower gain at the edges of scan; or the possibility of two separate reflectors could be considered, particularly for Configuration 2 where the need for intermediate stations between scan extremes has not been established.

*Minomo and Yasaka of NTT Electrical Communications Labs, Yokosuka, Japan, have studied the problem of deploying a large (3.5 M) circular reflector by folding in 3 sections from a structural viewpoint, although no electrical data appears to be available.

In order to examine the effect of varying feed sizes for the torus antenna over the frequency extremes of Ku- and Ka-bands, and to explore the sidelobe structure for a more symmetric feed type, patterns were calculated for a 96 x 170-inch torus, with a 144-inch focal length and 300-inch radius (as utilized previously), at both 14 and 29 GHz, with a corrugated horn feed. This feed equalizes E- and H-plane patterns and generally results in lower sidelobes. Feed aperture sizes from 1 to 3 inches in diameter were used (except at 14 GHz, where the 1 inch size was beyond cutoff). Calculations were made both for the on-axis beam and for one scanned 7.5° off axis in the plane of the torus long dimension (so-called "horizontal", or azimuth plane), for vertical linear polarization. Results are shown in Figures E-1 through E-4. Only the horizontal cut ($\phi = 90°$) was calculated for the scan beam because of difficulty locating the exact feed position to pass through the beam peak in the vertical plane. A summary of the gain and beamwidth characteristics calculated is given in Table E-1.

Another important parameter of interest in frequency-reuse communication systems is the isolation between beams. The calculated patterns of Figures E-1 through E-4 may be used to determine both the isolation between adjacent beams achievable when feed horns producing these beams are actually touching each other (minimum separation), as well as the separation required to achieve a desired isolation value (such as 27 dB, as required for the INTELSAT V system). These values are listed in Table E-2. For example, at 14 GHz with a 2-inch feed horn, the minimum separation

Table E-1. Calculated Gain and Beamwidth of Torus Antenna

Horn Size, In	Zero Scan Gain, dBi	Scan Loss dB*	Beamwidth @ Zero Scan	Beamwidth @ 7.5 Scan
TORUS @ 14 GHz				
3.0	51.24	-.21	.50°	.51°
2.5	51.53	-.34	.45°	.47°
2.0	51.24	-.48	.40°	.44°
1.5	50.19	-.60	.38°	.41°
TORUS @ 29 GHz				
3.0	51.83	.02	.49	.49
2.5	53.84	.02	.39	.39
2.0	55.65	-.04	.30	.31
1.5	56.58	-.09	.26	.29
1.0	56.01	-.09	.25	.28

*Estimated, since calculated scan pattern did not pass through beam peak.

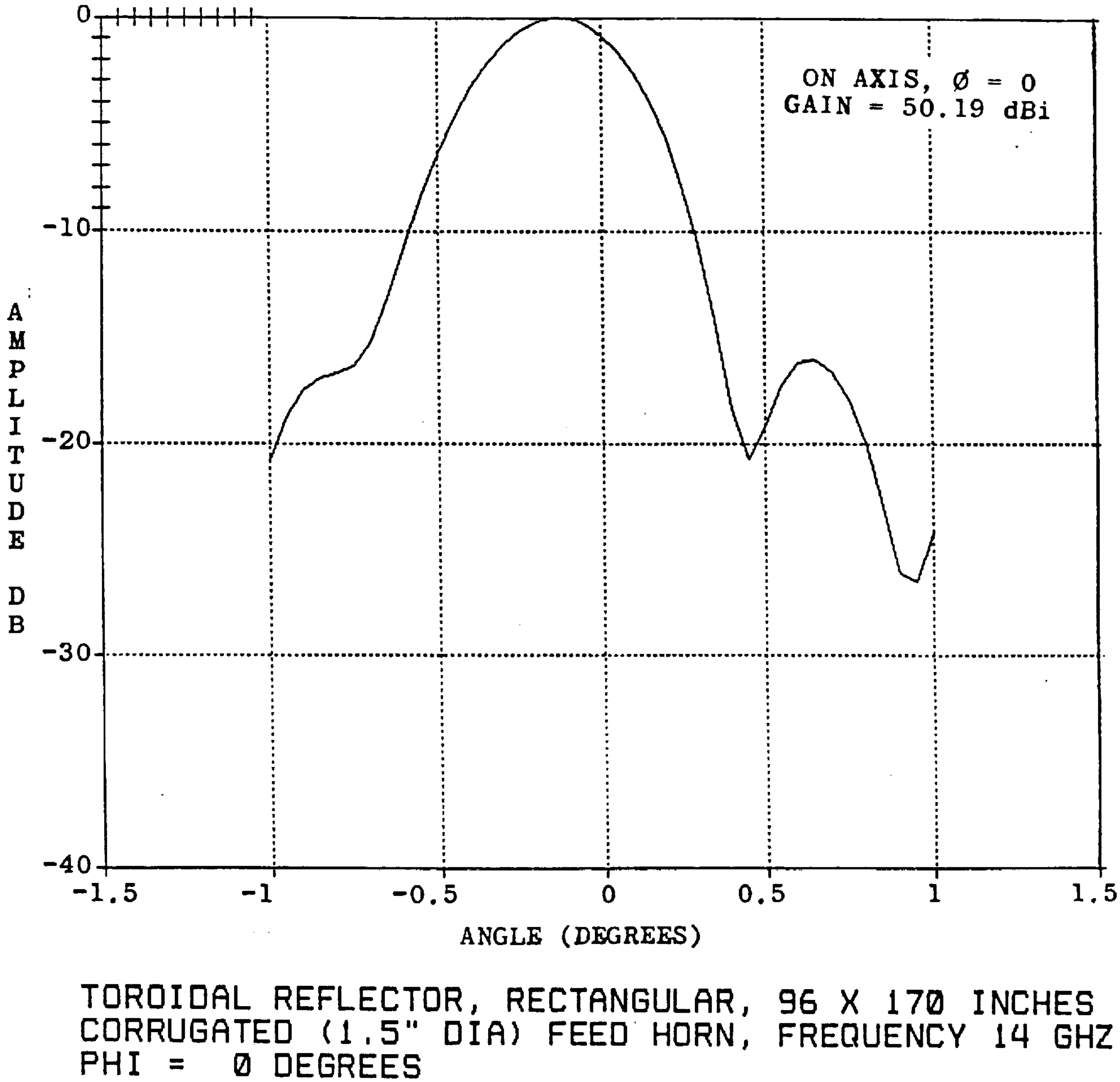

Figure E-1. Toroidal Reflector Patterns at Zero Scan, 14 GHz

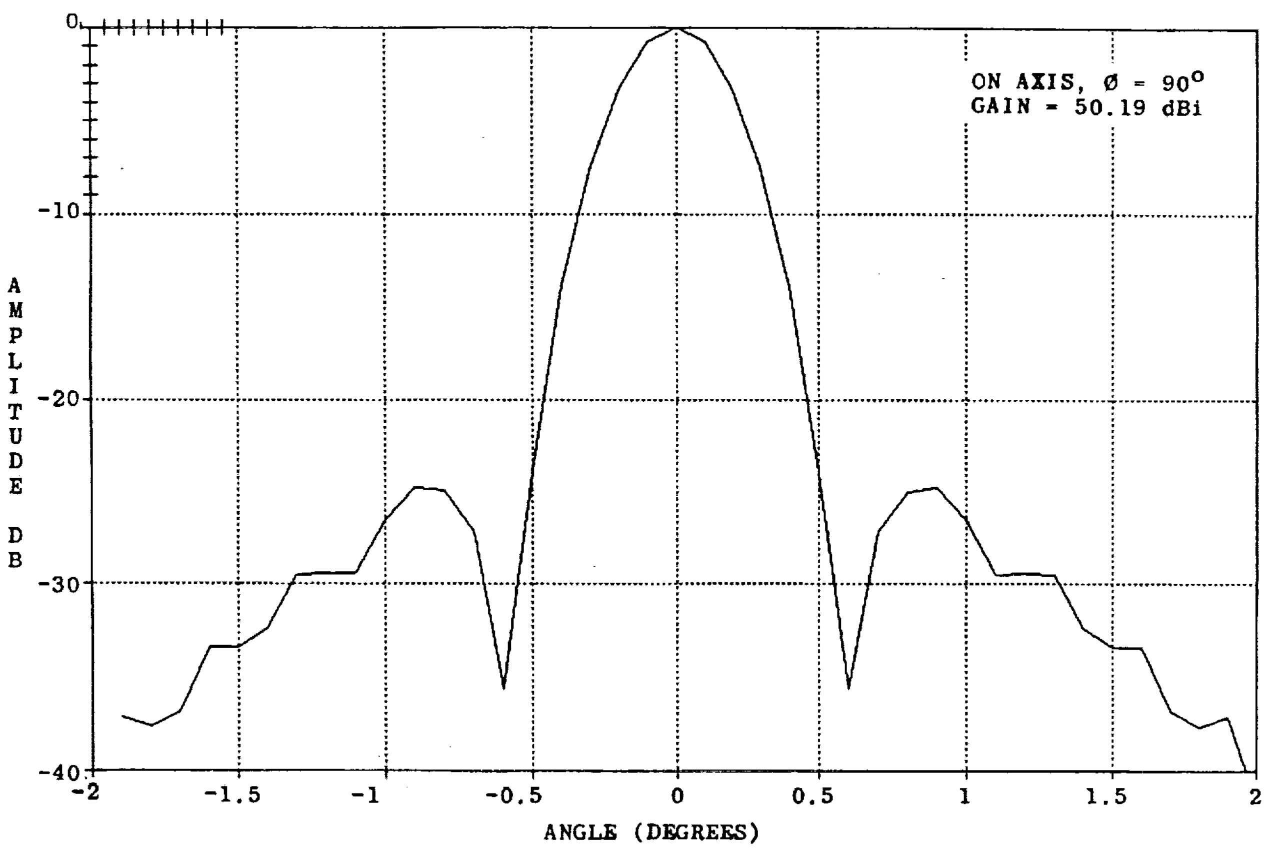

TOROIDAL REFLECTOR, RECTANGULAR, 96 X 170 INCHES
CORRUGATED (1.5" DIA) FEED HORN, FREQUENCY 14 GHZ
PHI = 90 DEGREES

Figure E-1. Toroidal Reflector Patterns at Zero Scan, 14 GHz (Continued)

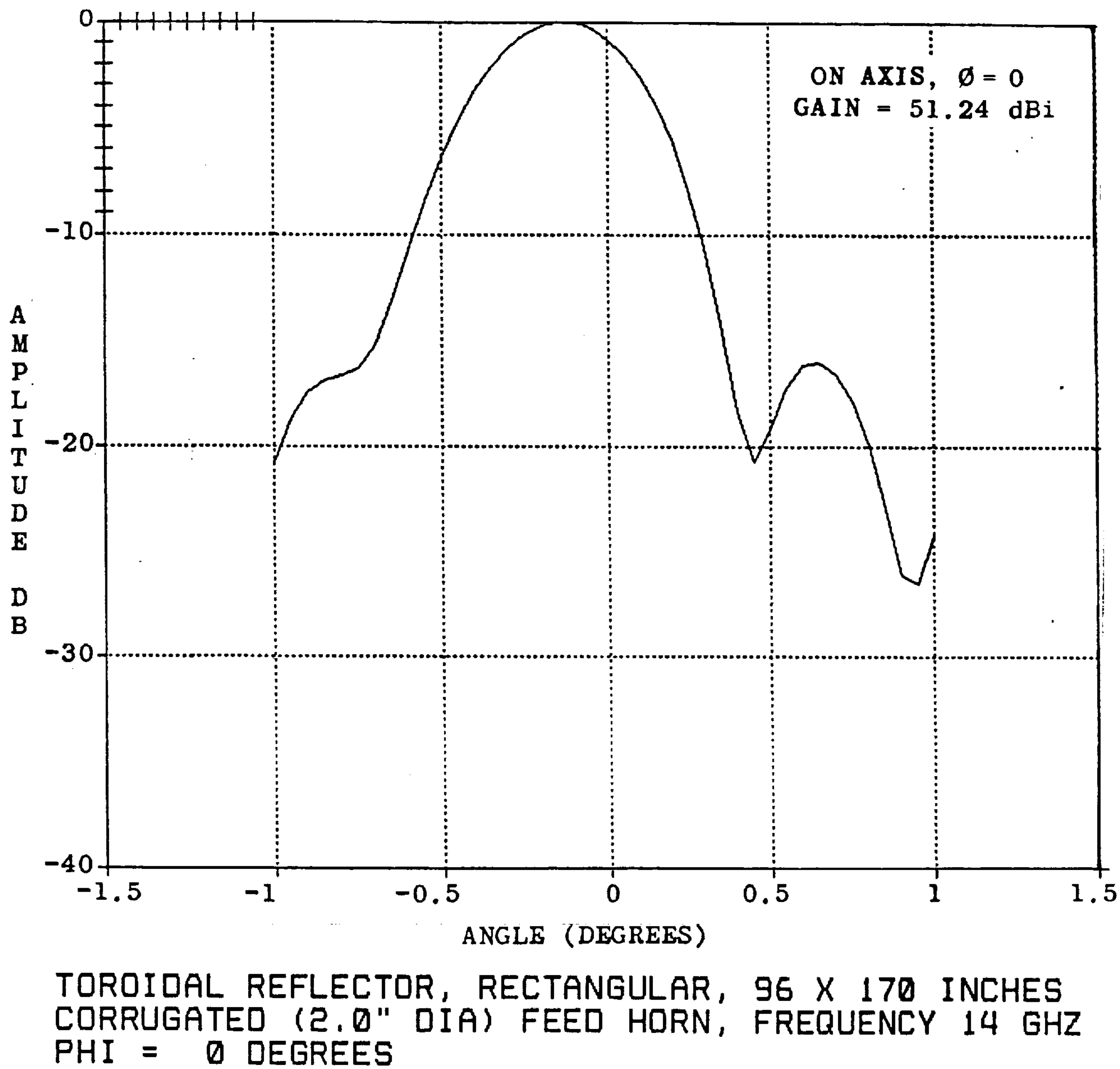

Figure E-1. Toroidal Reflector Patterns at Zero Scan, 14 GHz (Continued)

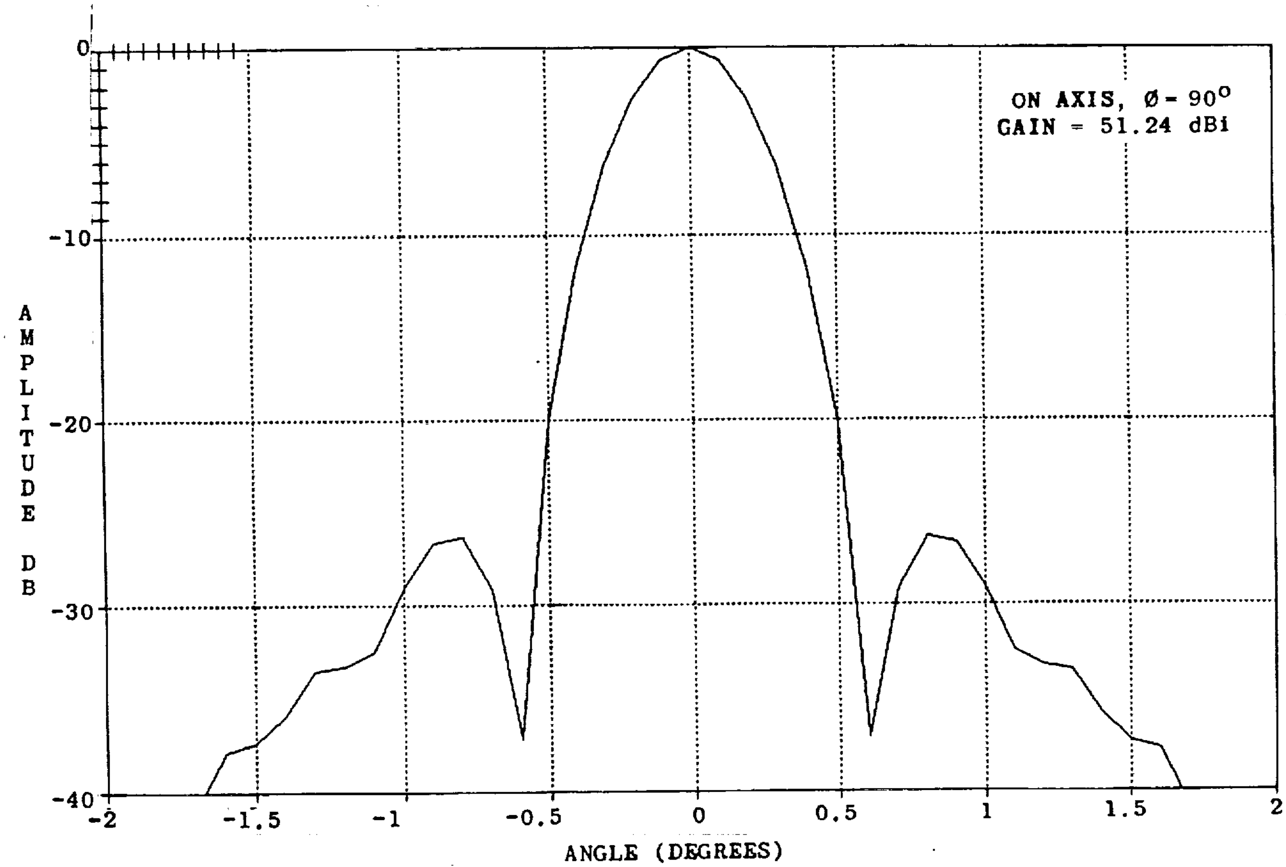

TOROIDAL REFLECTOR, RECTANGULAR, 96 X 170 INCHES
CORRUGATED (2" DIA) FEED HORN, FREQUENCY 14 GHZ
PHI = 90 DEGREES

Figure E-1. Toroidal Reflector Patterns at Zero Scan, 14 GHz (Continued)

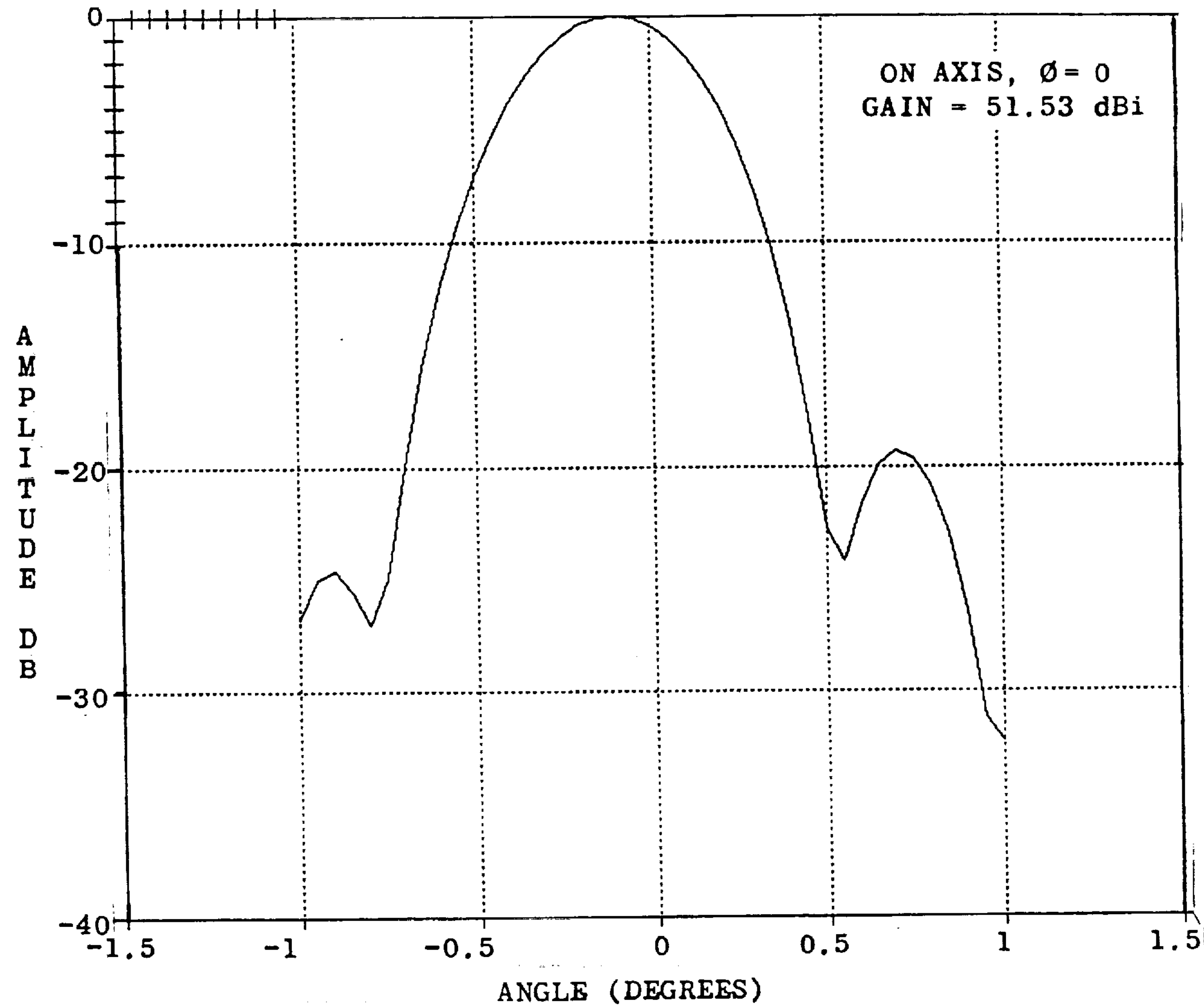

TOROIDAL REFLECTOR, RECTANGULAR, 96 X 170 INCHES
CORRUGATED (2.5" DIA) FEED HORN, FREQUENCY 14 GHZ
PHI = 0 DEGREES

Figure E-1. Toroidal Reflector Patterns at Zero Scan, 14 GHz (Continued)

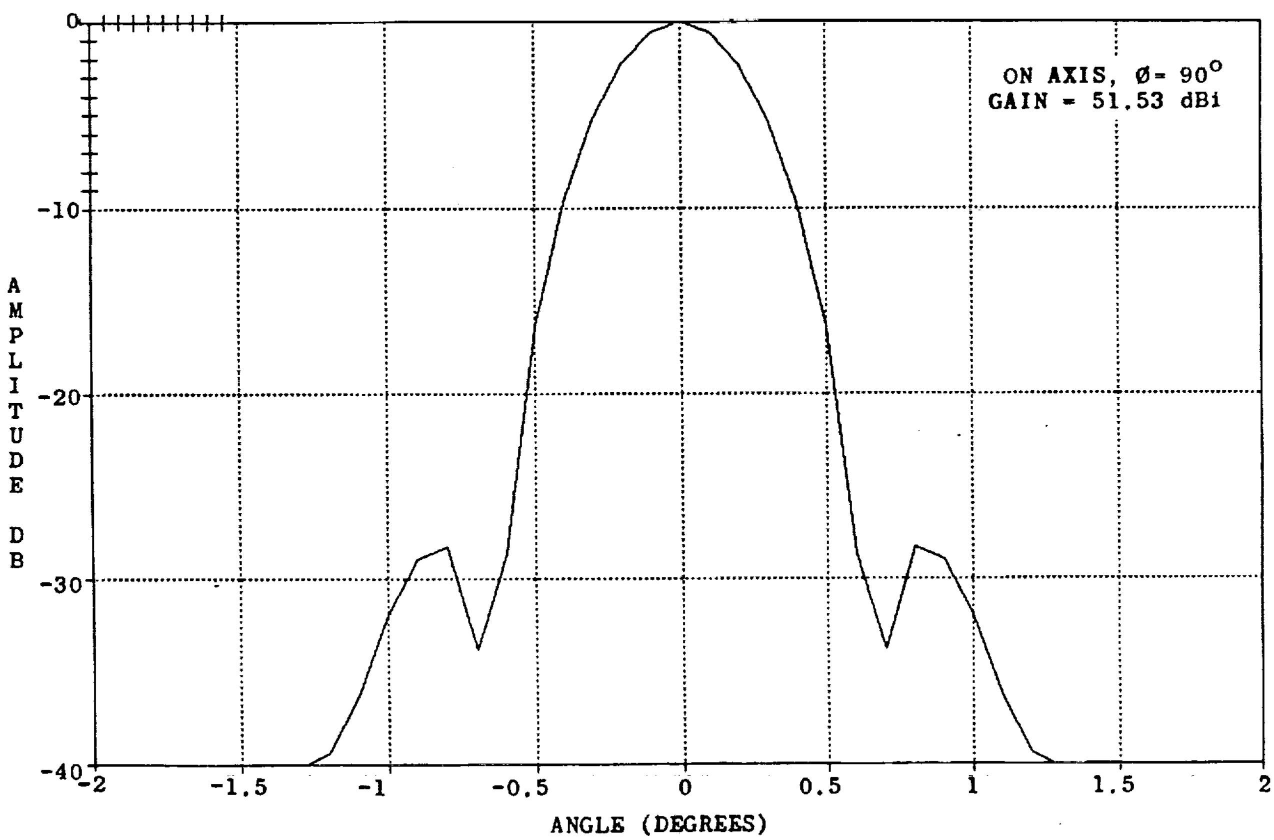

TOROIDAL REFLECTOR, RECTANGULAR, 96 X 170 INCHES
CORRUGATED (2.5" DIA) FEED HORN, FREQUENCY 14 GHZ
PHI = 90 DEGREES

Figure E-1. Toroidal Reflector Patterns at Zero Scan, 14 GHz (Continued)

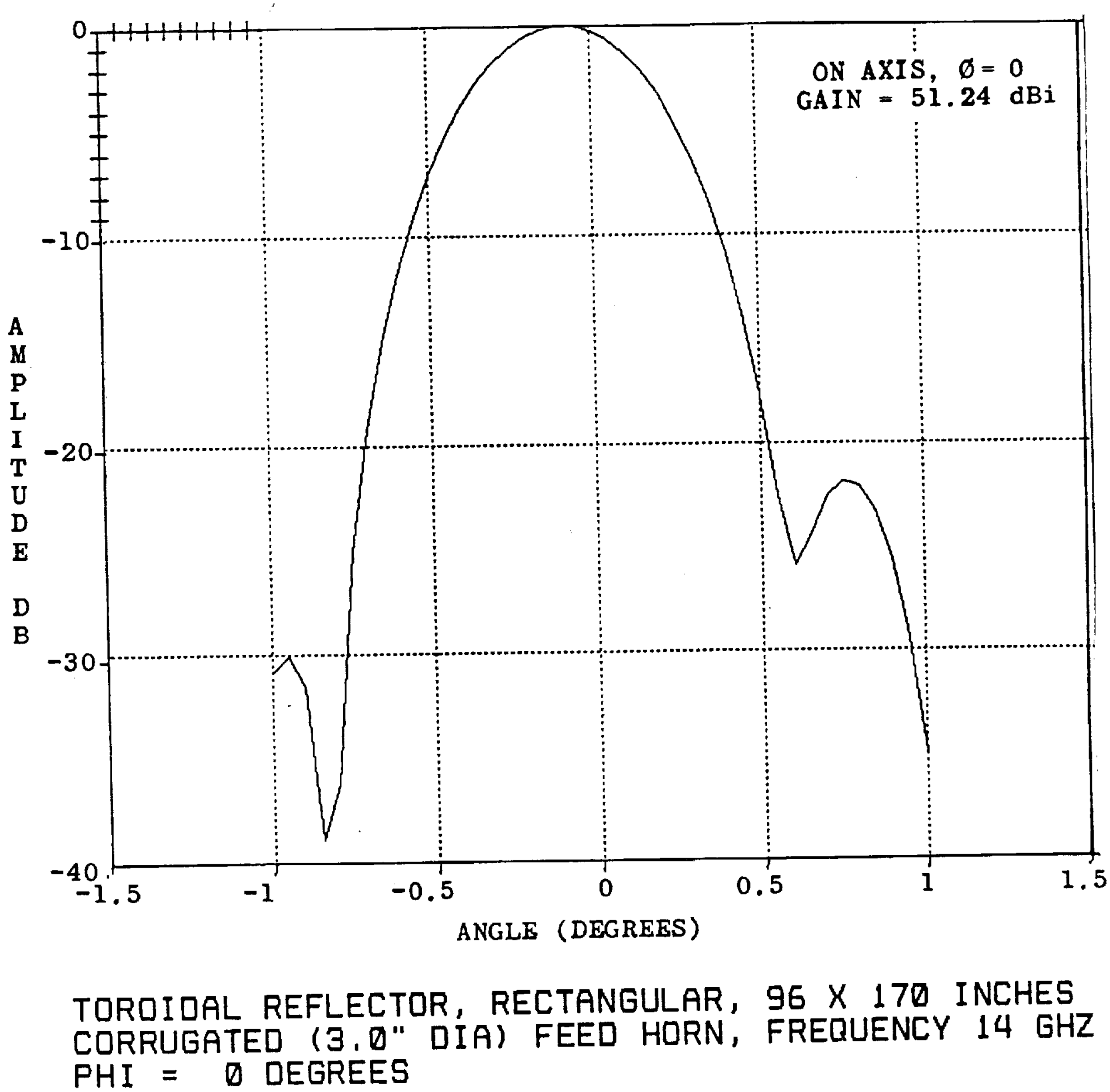

Figure E-1. Toroidal Reflector Patterns at Zero Scan, 14 GHz (Continued)

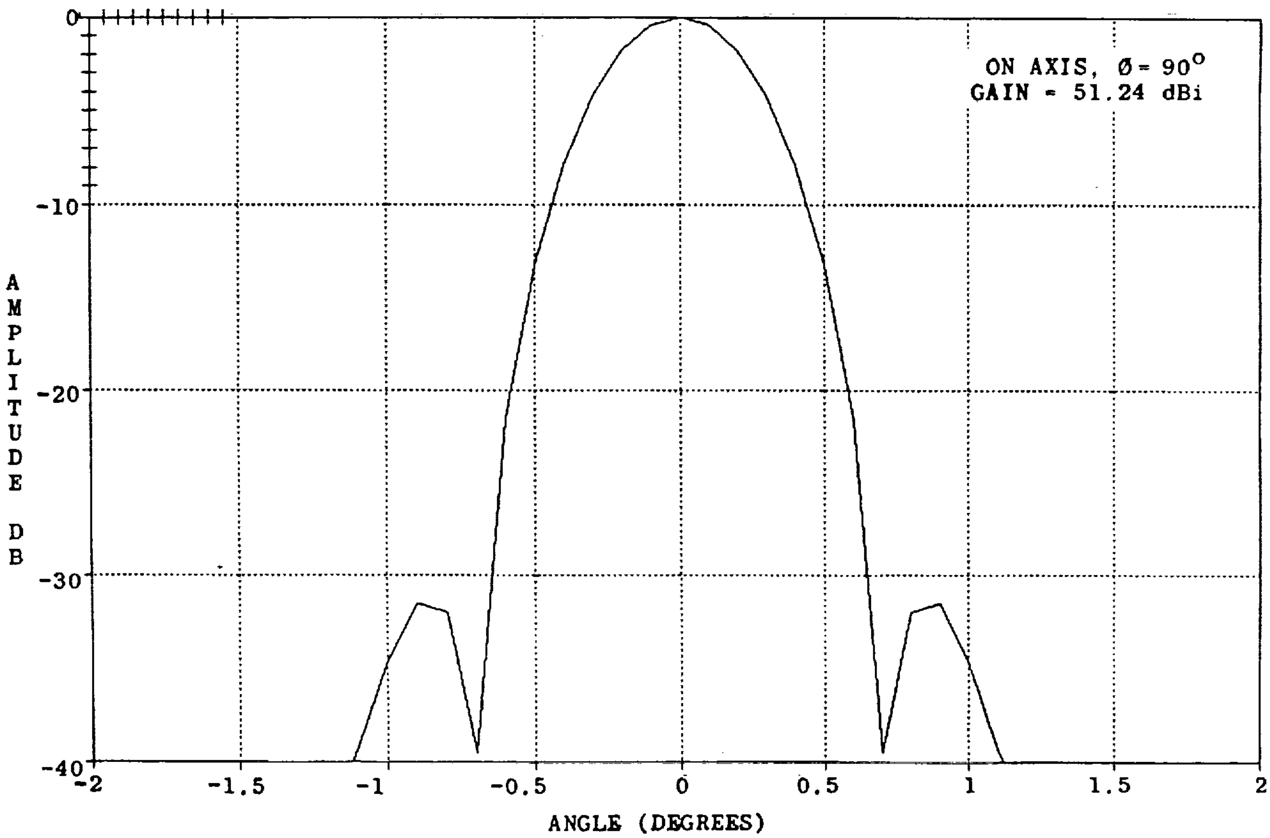

TOROIDAL REFLECTOR, RECTANGULAR, 96 X 170 INCHES
CORRUGATED (3" DIA) FEED HORN, FREQUENCY 14 GHZ
PHI = 90 DEGREES

Figure E-1. Toroidal Reflector Patterns at Zero Scan, 14 GHz (Continued)

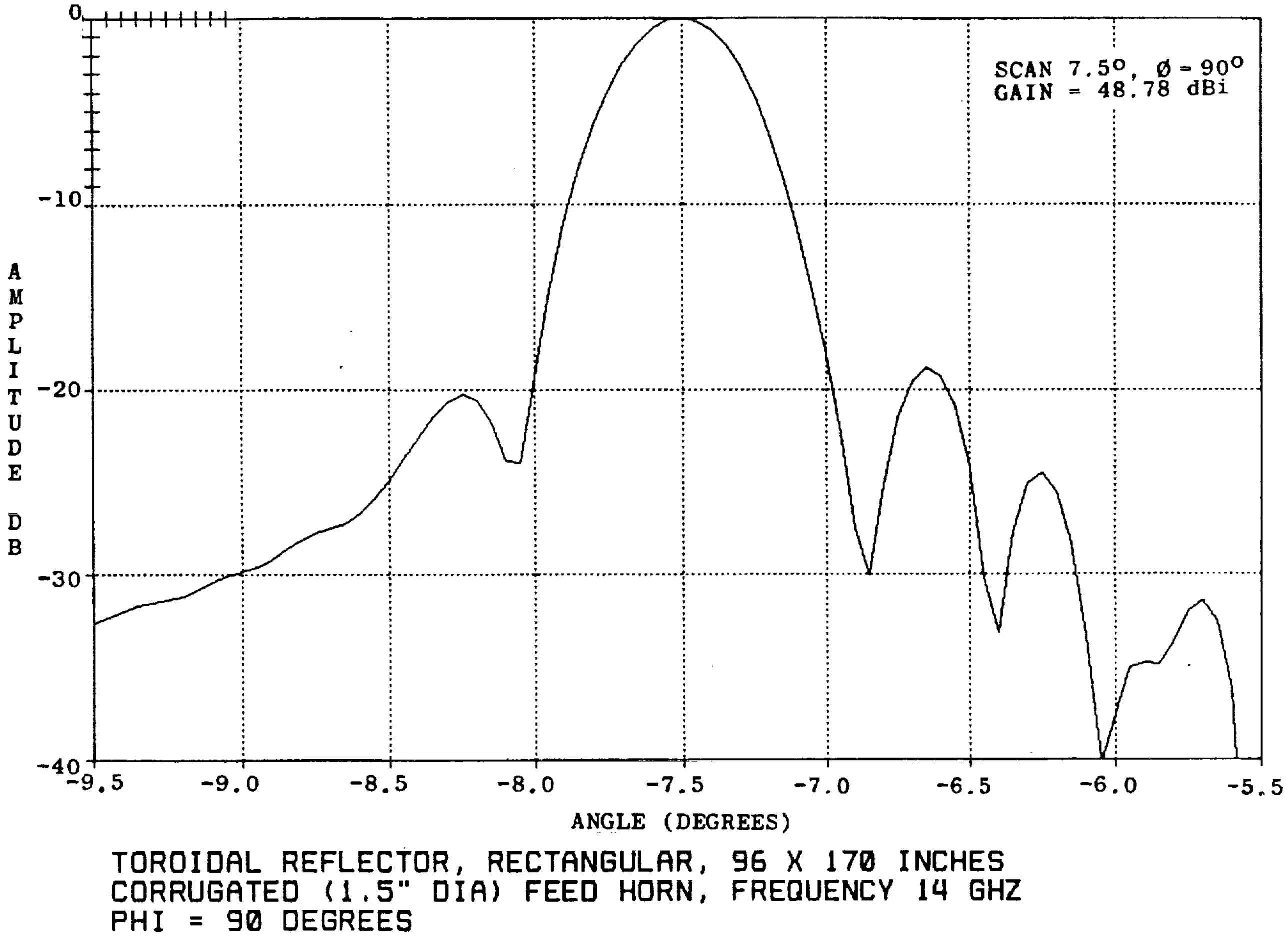

Figure E-2. Toroidal Reflector Patterns at 7.5° Scan, 14 GHz

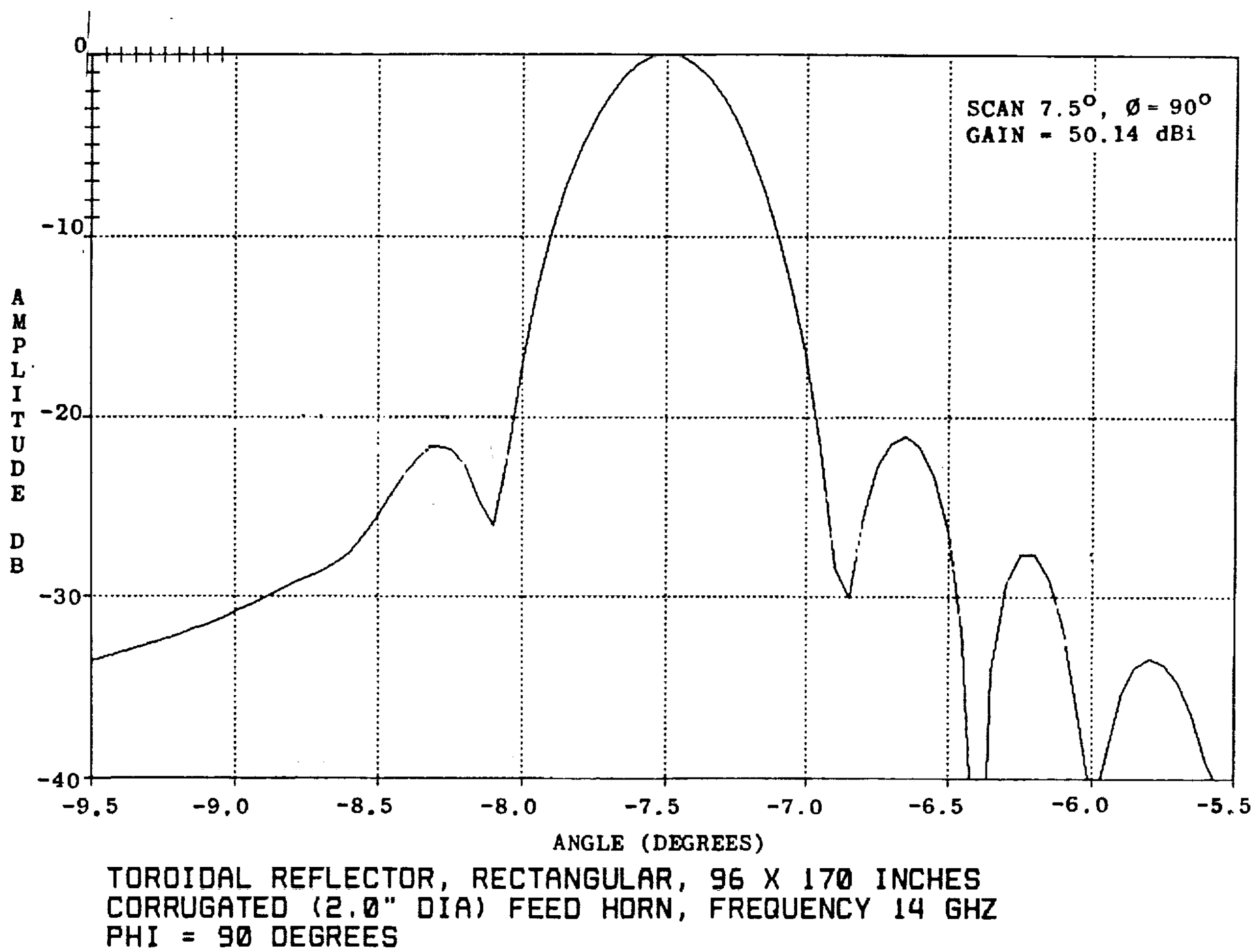

Figure E-2. Toroidal Reflector Patterns at 7.5° Scan, 14 GHz (Continued)

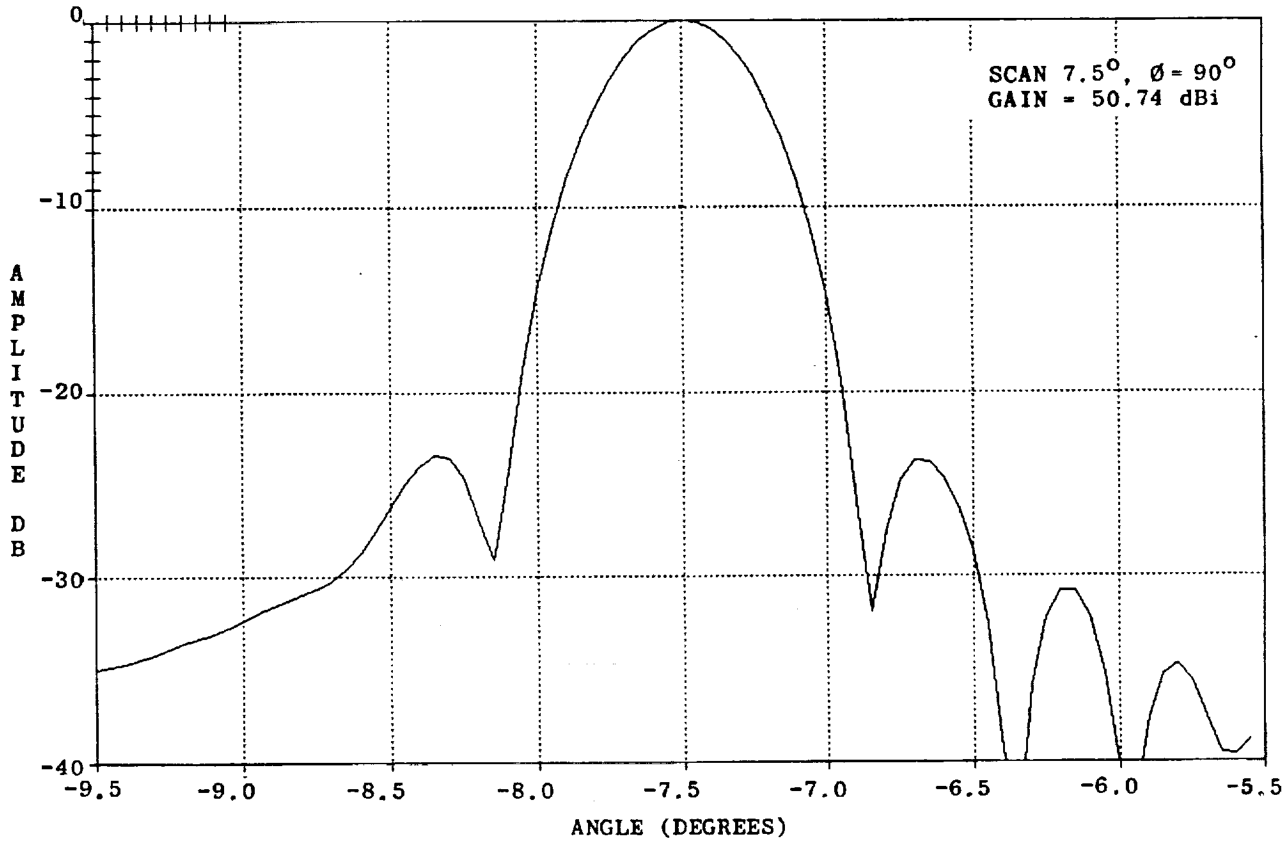

TOROIDAL REFLECTOR, RECTANGULAR, 96 X 170 INCHES
CORRUGATED (2.5" DIA) FEED HORN, FREQUENCY 14 GHZ
PHI = 90 DEGREES

Figure E-2. Toroidal Reflector Patterns at 7.5° Scan, 14 GHz (Continued)

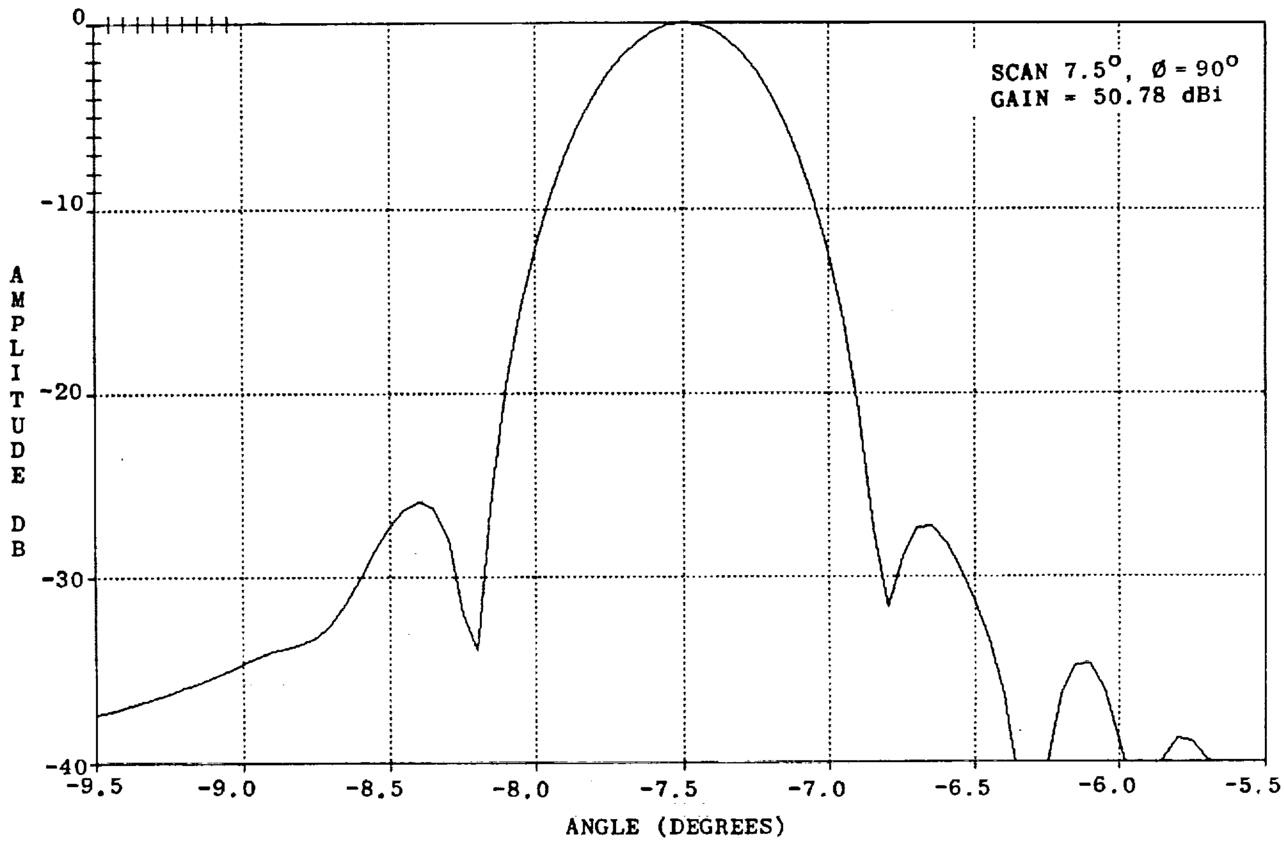

TOROIDAL REFLECTOR, RECTANGULAR, 96 X 170 INCHES
CORRUGATED (3.0" DIA) FEED HORN, FREQUENCY 14 GHZ
PHI = 90 DEGREES

Figure E-2. Toroidal Reflector Patterns at 7.5° Scan, 14 GHz (Continued)

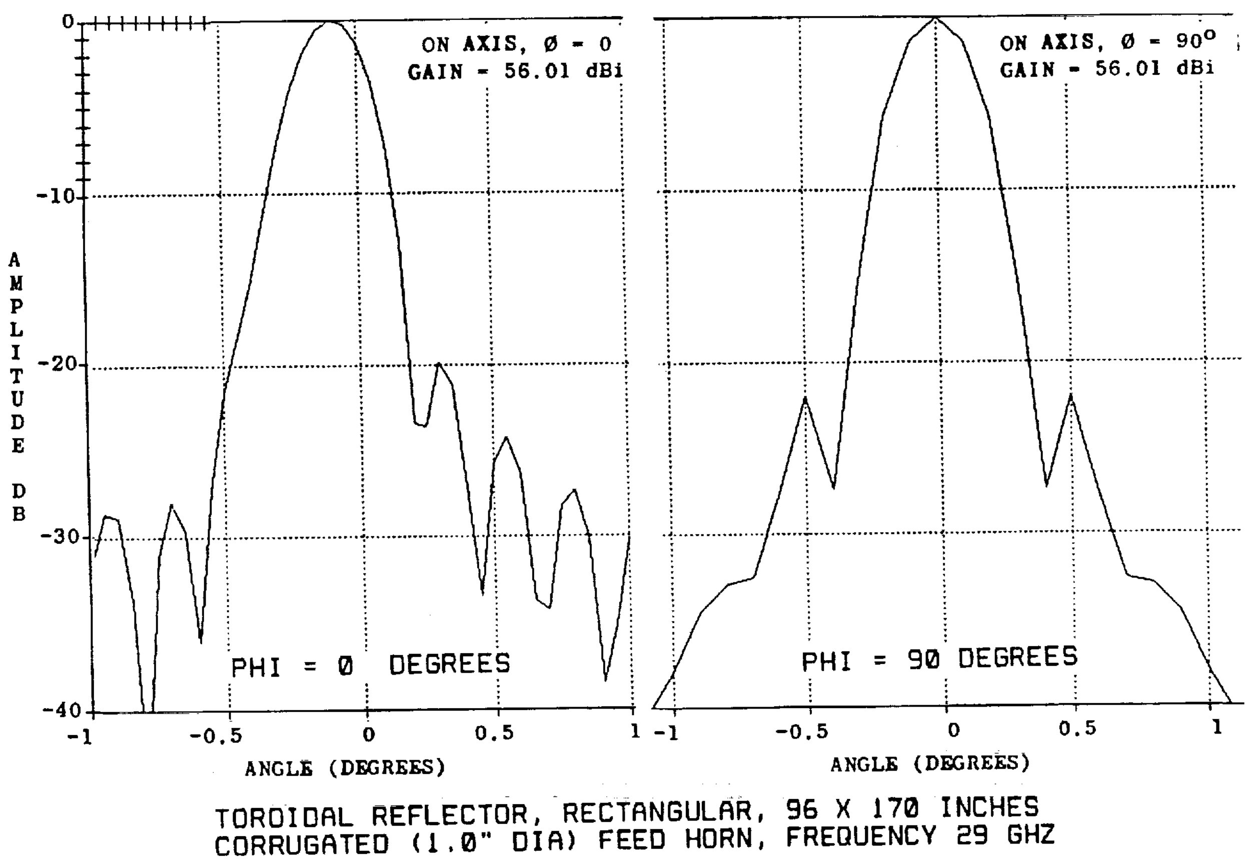

Figure E-3. Toroidal Reflector Patterns at Zero Scan, 29 GHz

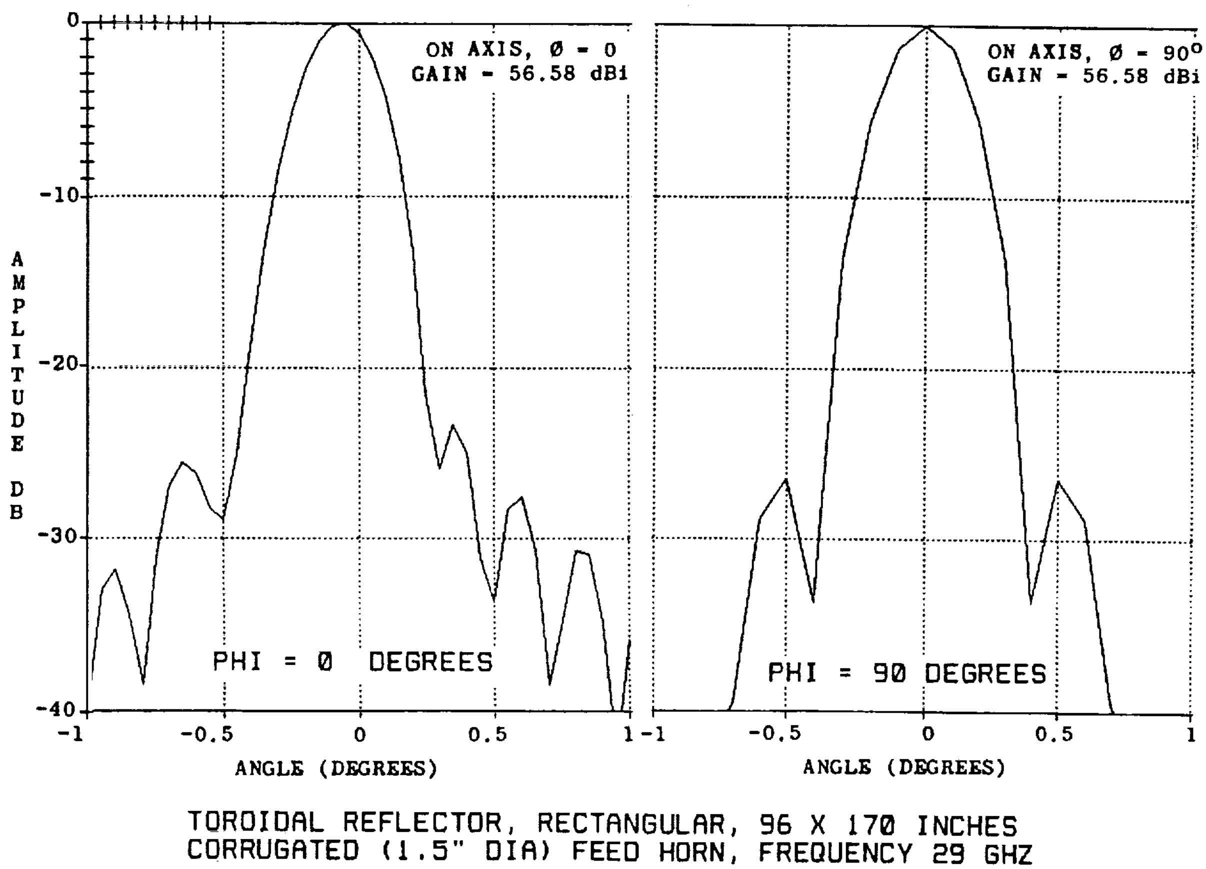

Figure E-3. Toroidal Reflector Patterns at Zero Scan, 29 GHz (Continued)

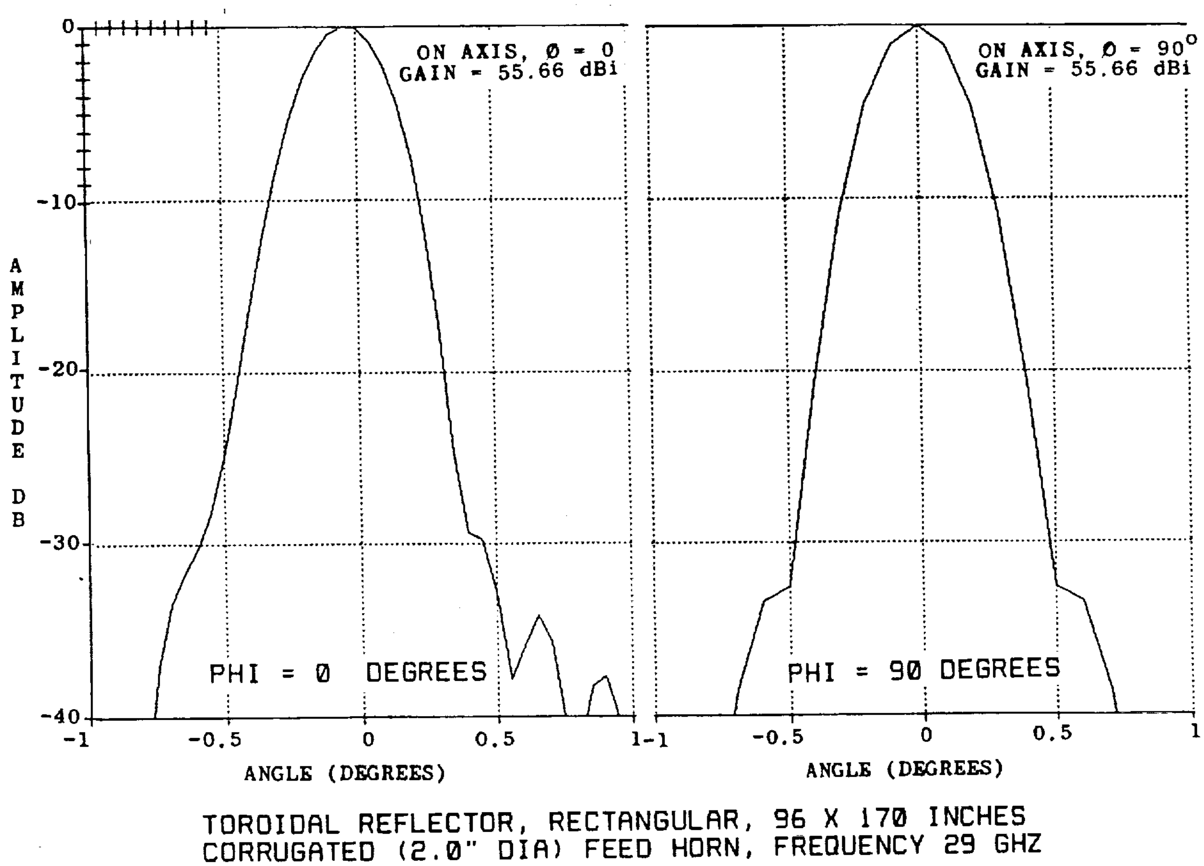

Figure E-3. Toroidal Reflector Patterns at Zero Scan, 29 GHz (Continued)

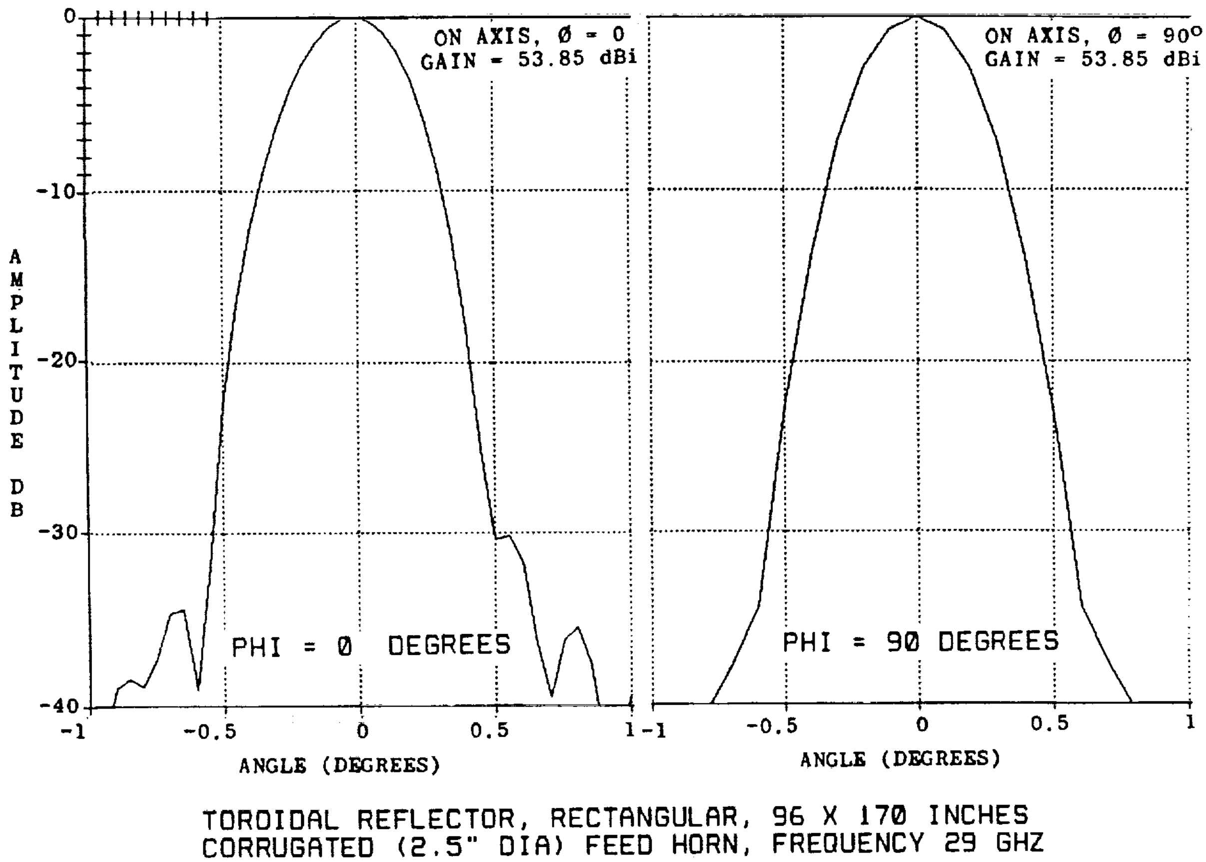

Figure E-3. Toroidal Reflector Patterns at Zero Scan, 29 GHz (Continued)

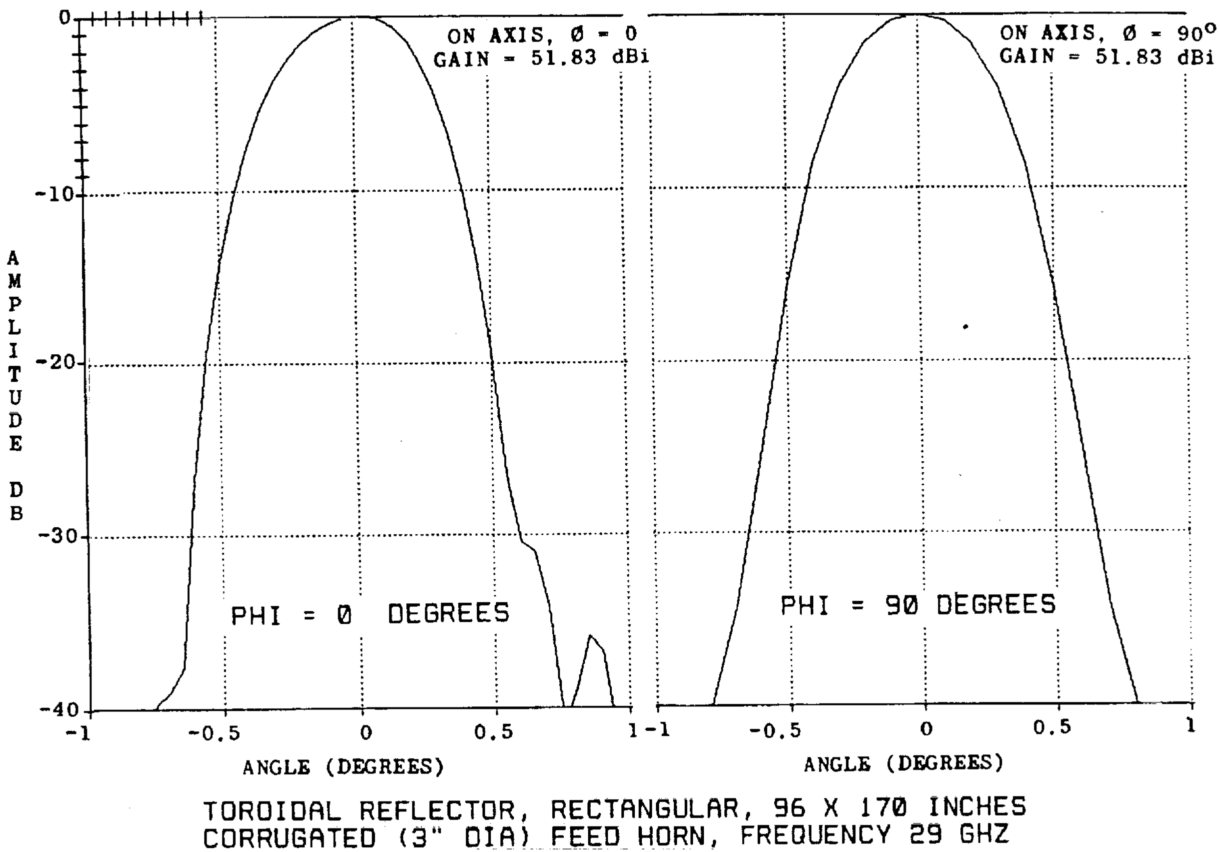

Figure E-3. Toroidal Reflector Patterns at Zero Scan, 29 GHz (Continued)

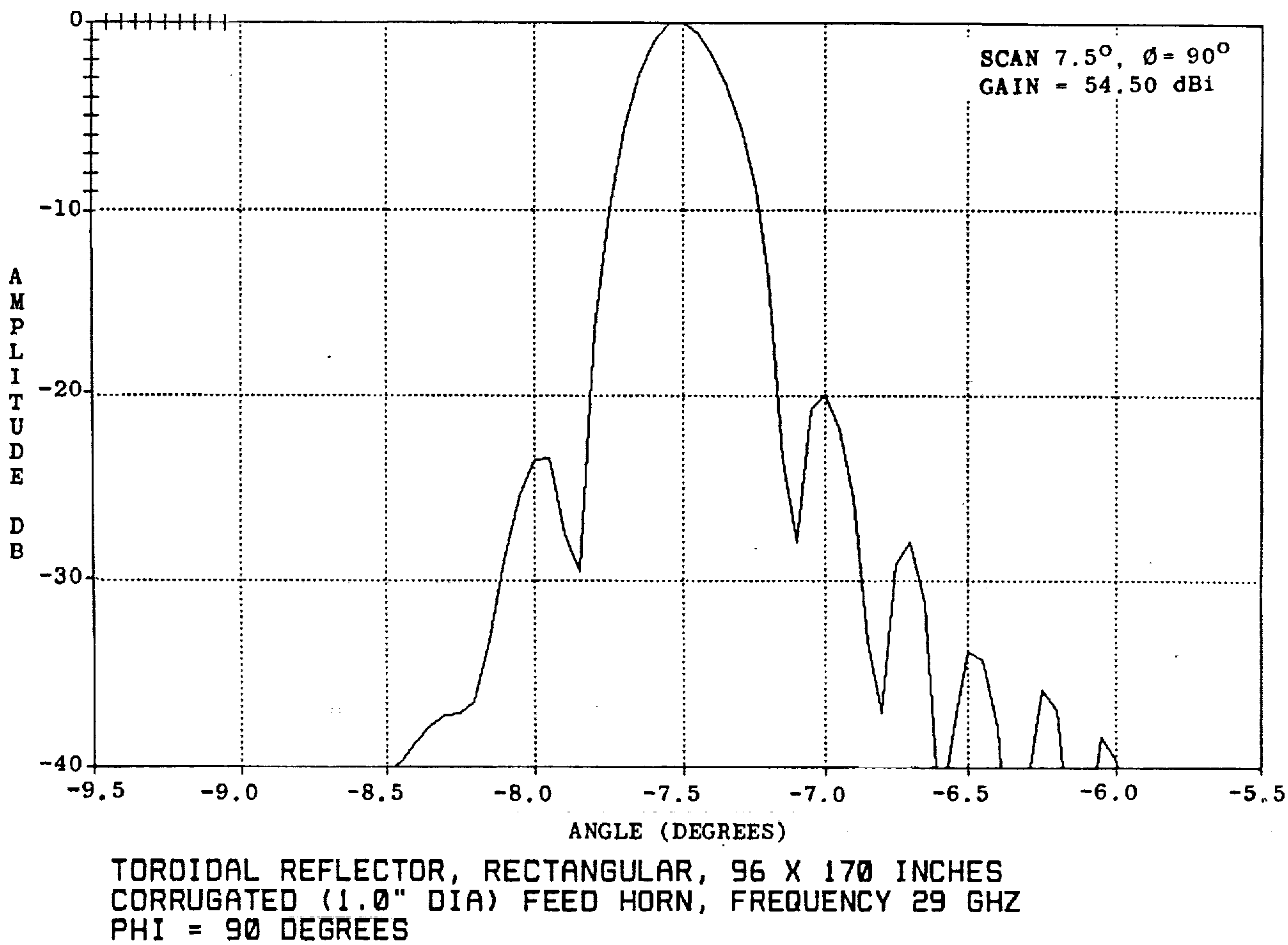

Figure E-4. Toroidal Reflector Patterns at 7.5° Scan, 29 GHz

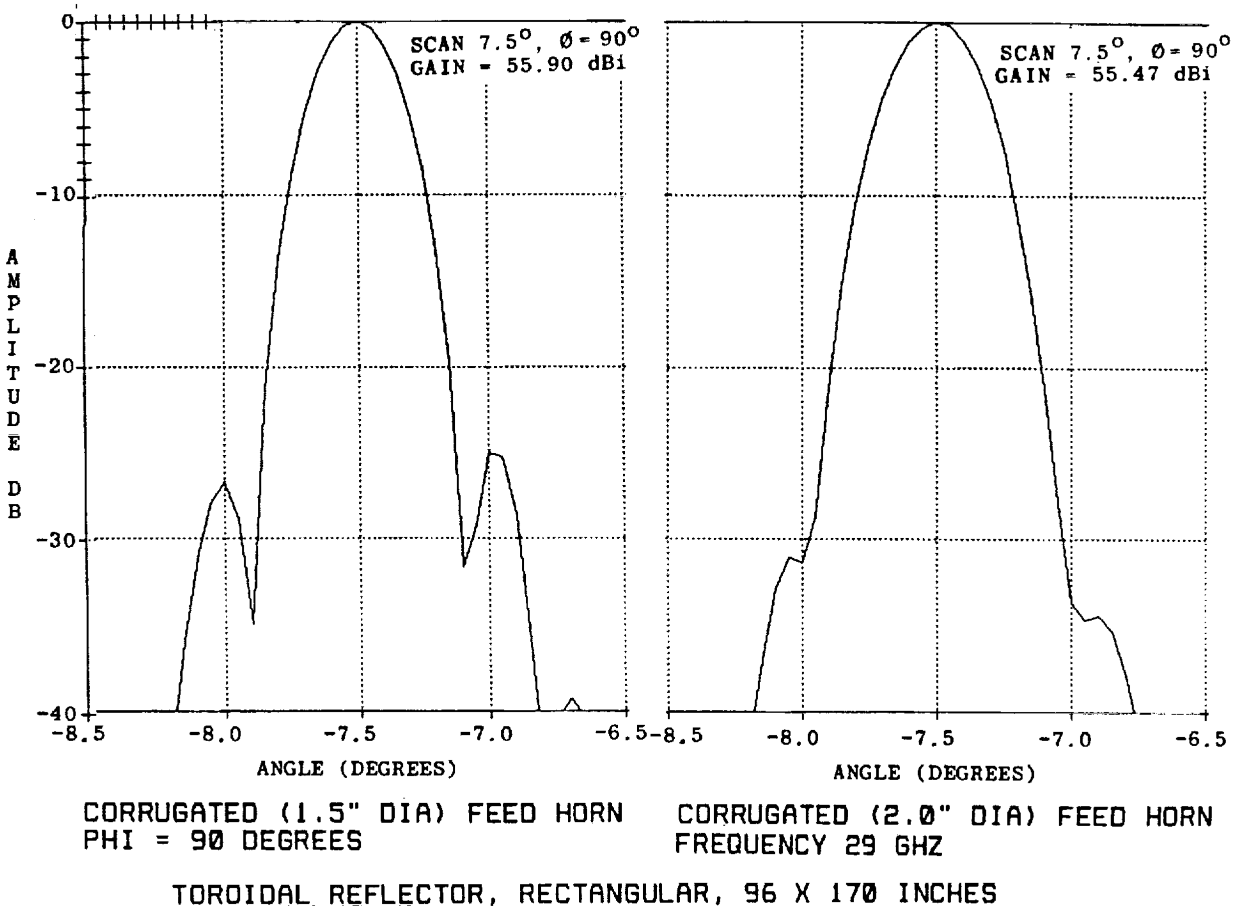

Figure E-4. Toroidal Reflector Patterns at 7.5° Scan, 29 GHz (Continued)

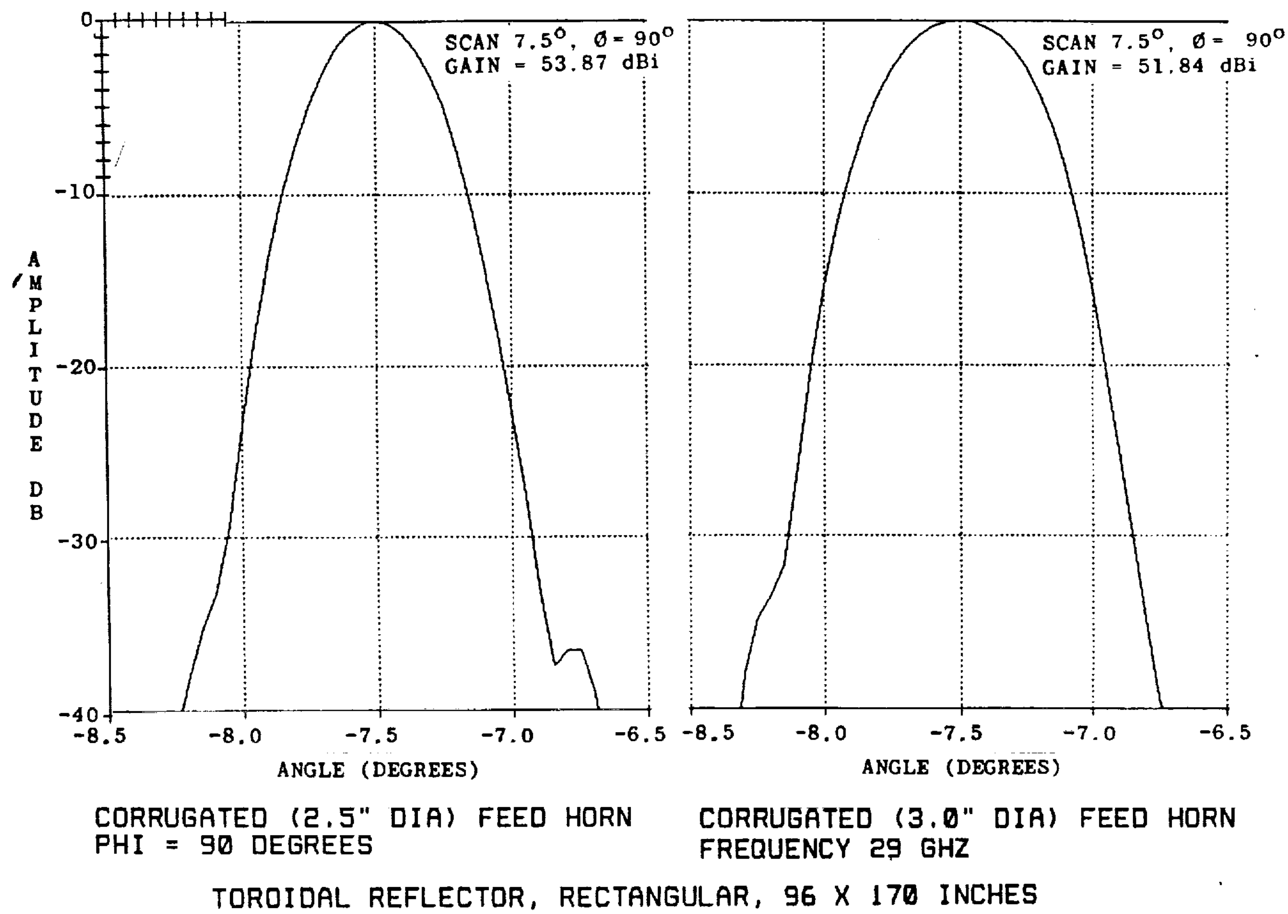

Figure E-4. Toroidal Reflector Patterns at 7.5° Scan, 29 GHz (Continued)

Table E-2. Beam Spacing and Isolation for 170" Torus

Horn Size, In.		Beam Spacing Scan @ Zero	Beam Spacing Scan @ 7.5°	Isolation, dB Scan @ Zero	Isolation, dB Scan @ 7.5°	Beam Spacing for 27 dB Isolation Scan @ Zero	Beam Spacing for 27 dB Isolation Scan @ 7.5°
@ 14 GHz							
1.	3.0	1.32°	1.32°	>27.0	25.0	1.32°	1.35°
2.	2.5	1.13°	1.13°	26.0	20.0	1.19°	1.4°
3.	2.0	0.94°	0.94°	20.2	18.0	1.25°	1.6°
4.	1.5	0.75°	0.75°	21.0	15.5	1.5°	1.7°
@ 29 GHz							
1.	3.0	1.32°	1.32°	>27.0	>27.0	1.2°	1.32°
2.	2.5	1.13°	1.13°	>27.0	>27.0	1.13°	1.13°
3.	2.0	0.94°	0.94°	>27.0	>27.0	0.94°	0.94°
4.	1.5	0.75°	0.75°	26.0	27.0	0.78°	0.75°
5.	1.0	0.56°	0.56°	19.0	17.0	0.81°	1.0°

between beams for two adjacent feed horns is 0.94°, for which the isolation is only 20.2 dB. In order to achieve 27 dB isolation, the beams must be separated by 1.25°, at zero scan. This separation must be increased to 1.6° for a scan beam 7.5 ° off axis. Also, there appears to be an optimum horn size for minimum spacing to achieve the desired isolation. These optima appear to be as follows, together with the associated beam separations:

Table E-3. Optimum Horn Sizes for 27 dB Isolation (Torus Reflector)

Frequency GHz	Zero Scan Horn Size (inch)	Zero Scan Beam Separation (degree)	7.5° Scan Horn Size (inch)	7.5° Scan Beam Separation (degree)
14	2.5	1.19	3.0	1.35
29	1.5	0.78	1.5	0.75

It appears that these horn sizes also result in maximum gain, as listed in Table E-1, which may be more than a coincidence.

E.3 PARABOLIC REFLECTOR WITH ARRAY FEED

A conventional focussed reflector antenna system shows considerable degradation in patterns and gain for beams off the focal axis, because of optical aberrations. Hung and Mittra [E-1] have analyzed one means for alleviating this scan loss by using an array feed, and adjusting the phase and amplitude of the individual elements to achieve a conjugate match to the focal field variations. Figure E-5 shows a plot of their calculated focal field distribution for a beam scanned 48 beamwidths off axis, with an array of 27 small (0.6-wavelength) feed elements superimposed. Using this array, their calculated scan loss at 48 beamwidths scan was only 6 dB. This is an improvement of 7 dB relative to the gain achievable at the same scan with a single feed, as seen from a reproduction of their calculated scan patterns in Figure E-6.

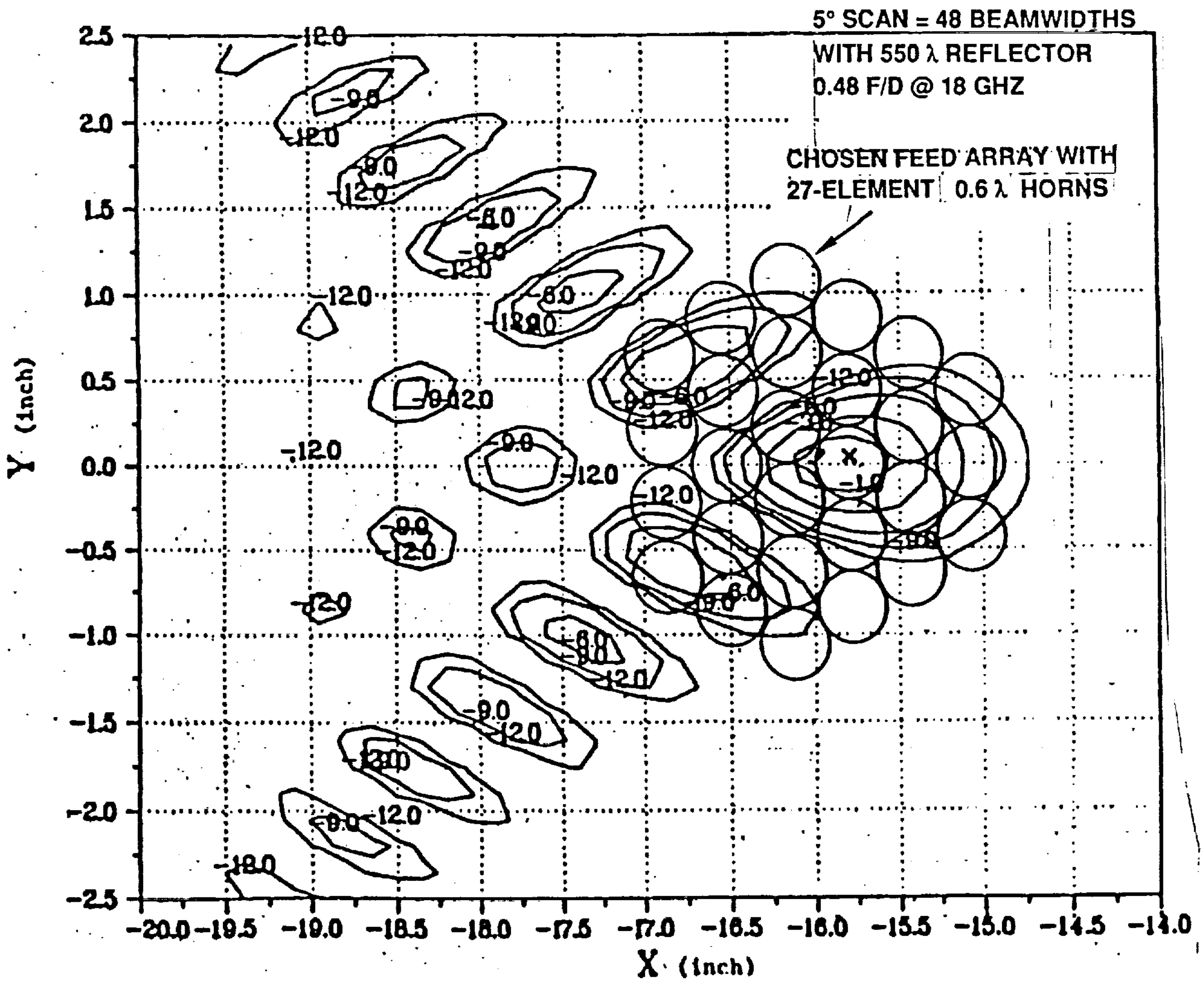

Figure E-5. Calculated Focal Plane Distribution - Hung and Mittra 1983

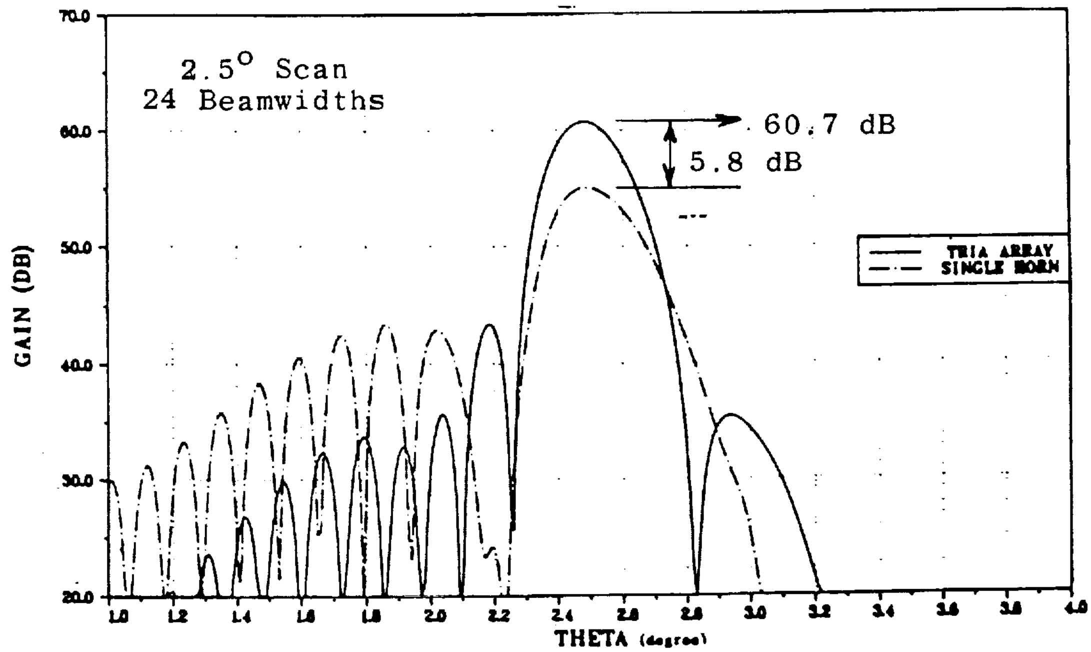

IDEAL (MAX.) GAIN = 64.85 dB

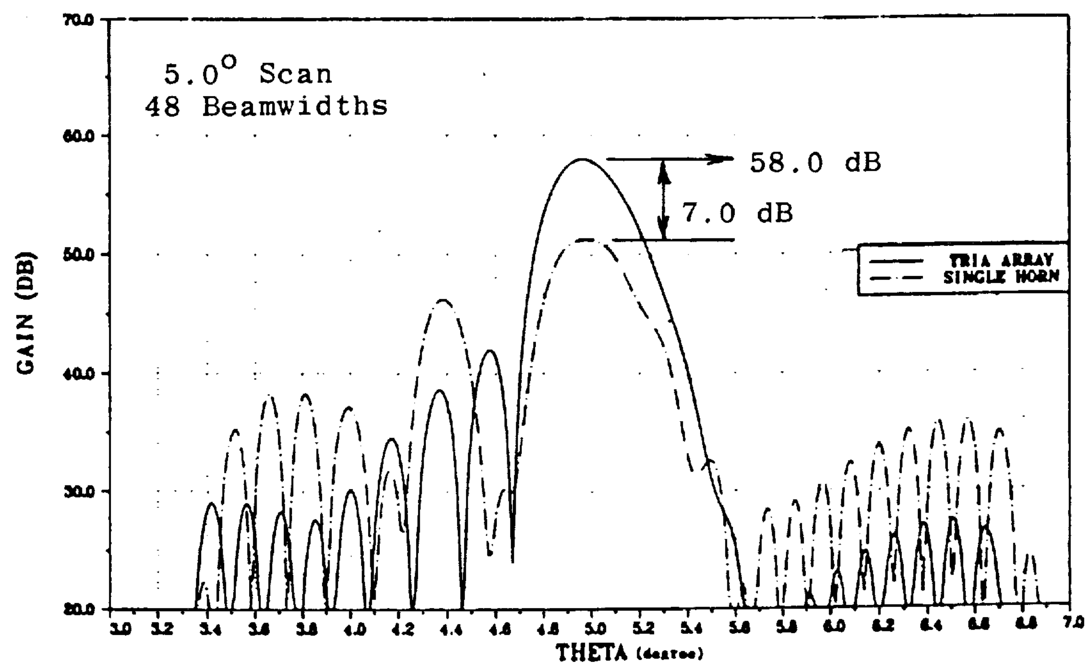

Figure E-6. Hunt and Mittra's Calculated Scan Patterns for 27-Element Feed Array

In applying this technique to our MBA application, we decided to analyze first the case of a 19-element feed array (one central element surrounded by two contiguous rings), for an offset-fed 96-inch diameter parabolic reflector with f/D = 1.0, at an operating frequency of 29 GHz. In order to reduce computational time, performance estimates were first generated for only a single row of five elements (representing extreme positions within the full array), positioned to produce a beam scanned 8.5° off axis, corresponding to edge-of-the-earth coverage from synchronous orbit, a worst case. Using 0.75-inch diameter circular feed horns, a total 19-element array gain of 51.3 dBi was predicted, some 6 dB below the ideal maximum on-axis gain of 57.4 dB for this size reflector. This case represents a scan of about 29 beamwidths, so the results are not as good as could be expected from the above reference. Consequently, it was decided to consider a case with a larger f/D = 2.0, which shows less aberration for a given scan. The geometry selected is shown in Figure E-7. We felt that the larger focal length could be accommodated by deploying the reflector from an extended support structure off one side of the spacecraft, with the feed array mounted directly on the spacecraft. Since the antenna must handle three separate bands (14, 19, and 29 GHz), the optimum configuration seems to be the one shown, using an FSS to separate one of the bands (the upper, 29 GHz) from the other two, so that an optimum feed array may be selected for each.

For this dual arrangement, optimum feed horn sizes were selected for the band extremes using the method outlined above, evaluating the performance with five feed horns along one axis in the direction of scan. These results seemed to indicate that near maximum gain at 8.6° scan could be achieved at 29 GHz with 0.5 in^2 feed horns, and at 14 GHz with 0.75 in^2 horns. These horn sizes were selected for a complete evaluation of the 19-element array at 14, 19, and 29 GHz. The feed arrays were located in a plane centered at the focal point (for zero scan) and tilted up 21.2° towards the center of the reflector (as shown on Figure E-7). For maximum 8.6° scan, the feed array was moved 30.32 inches in a direction perpendicular to the plane of Figure E-7, or P(x,y,z) = (0,30.32,192). The 0.5 inch array was also evaluated at 14 GHz. Calculated patterns are shown in Figures E-8 through E-11, and a summary of the array gains is given in Table E-4.

A number of patterns were also calculated for single feed horns (the center ones in each array), for comparative purposes; these are shown in Figures E-12 through E-14.

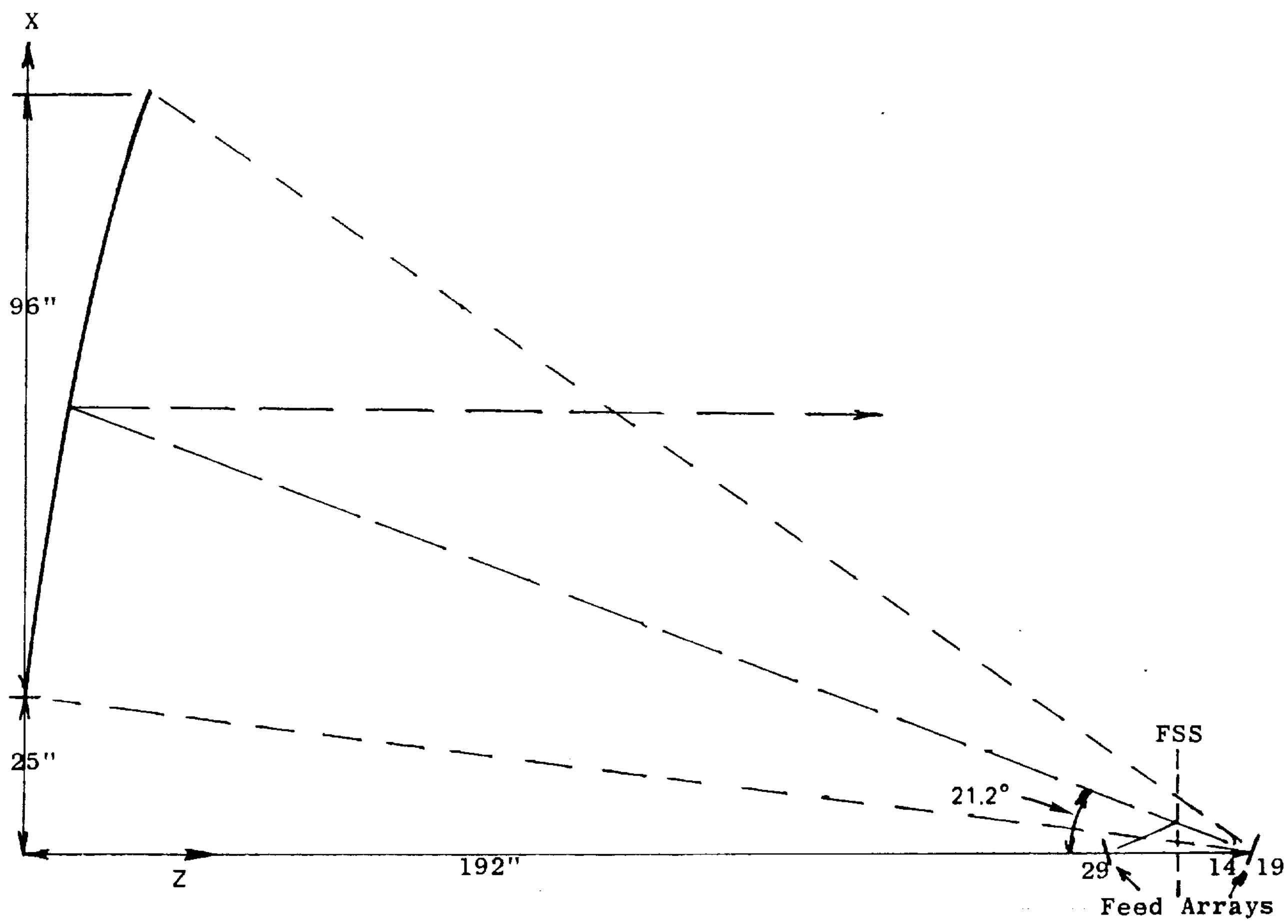

Figure E-7. Selected Antenna Geometry

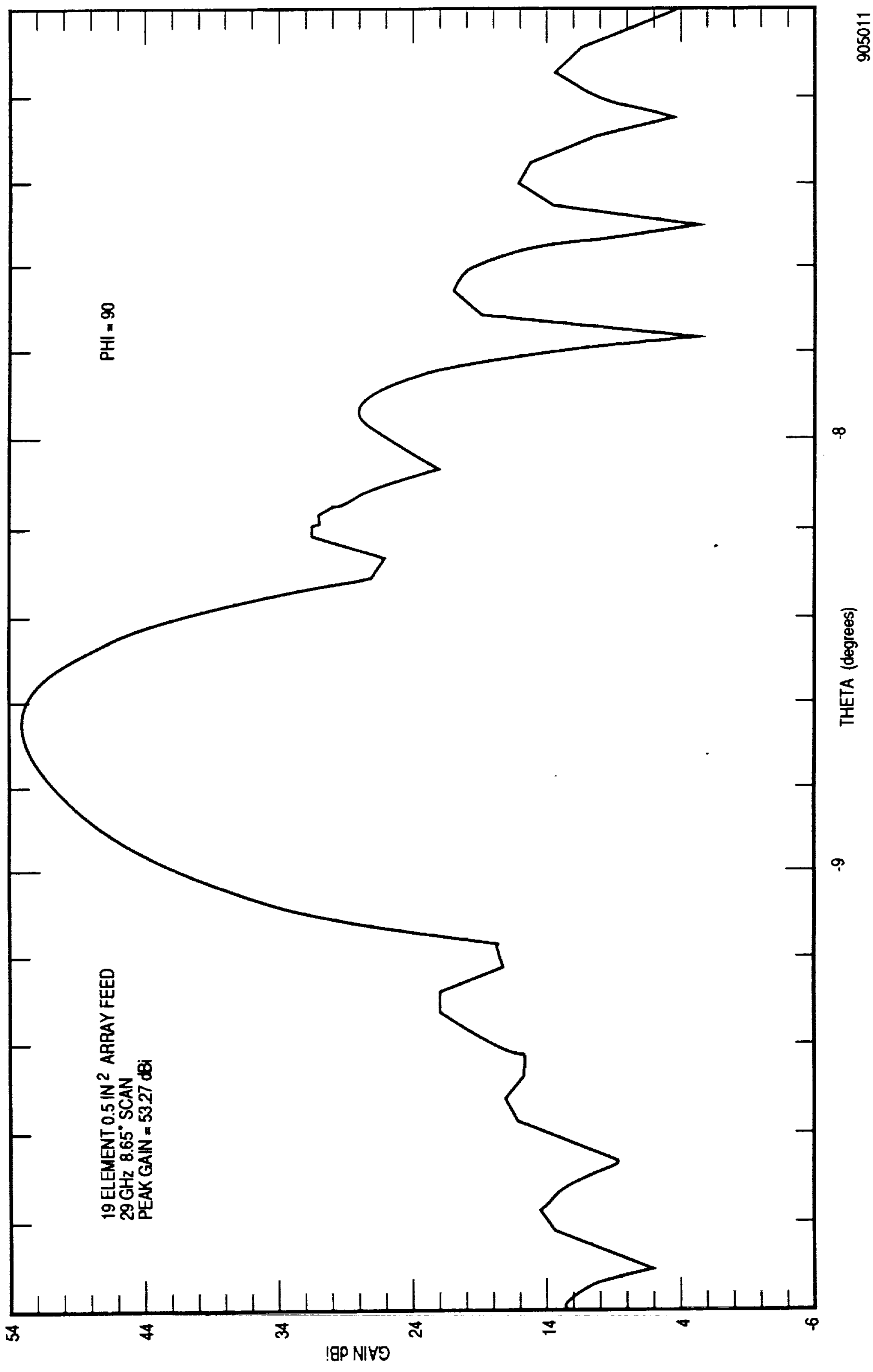

Figure E-8. Calculated Scan Pattern at 29 GHz

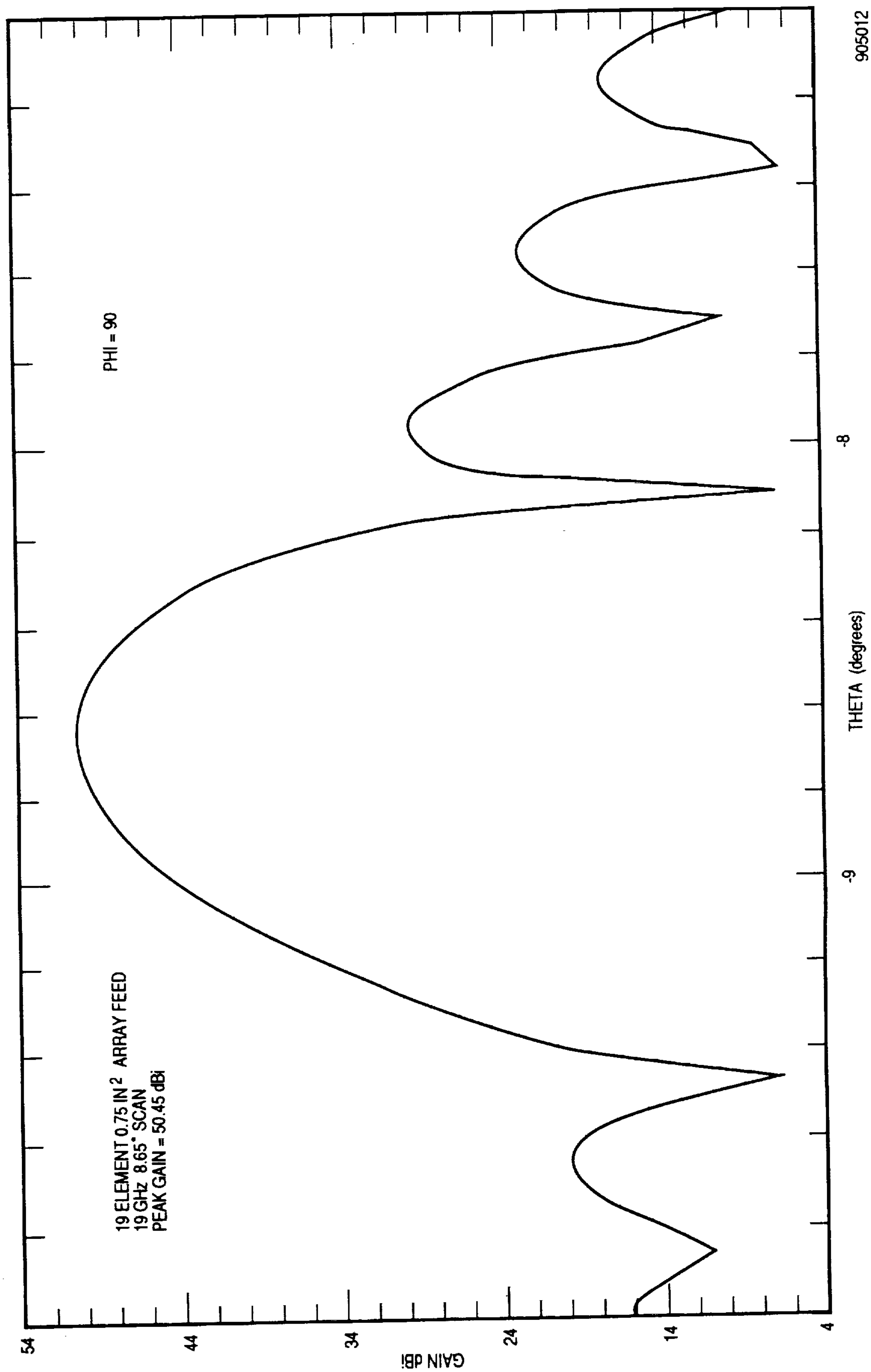

Figure E-9. Calculated Scan Pattern at 19 GHz

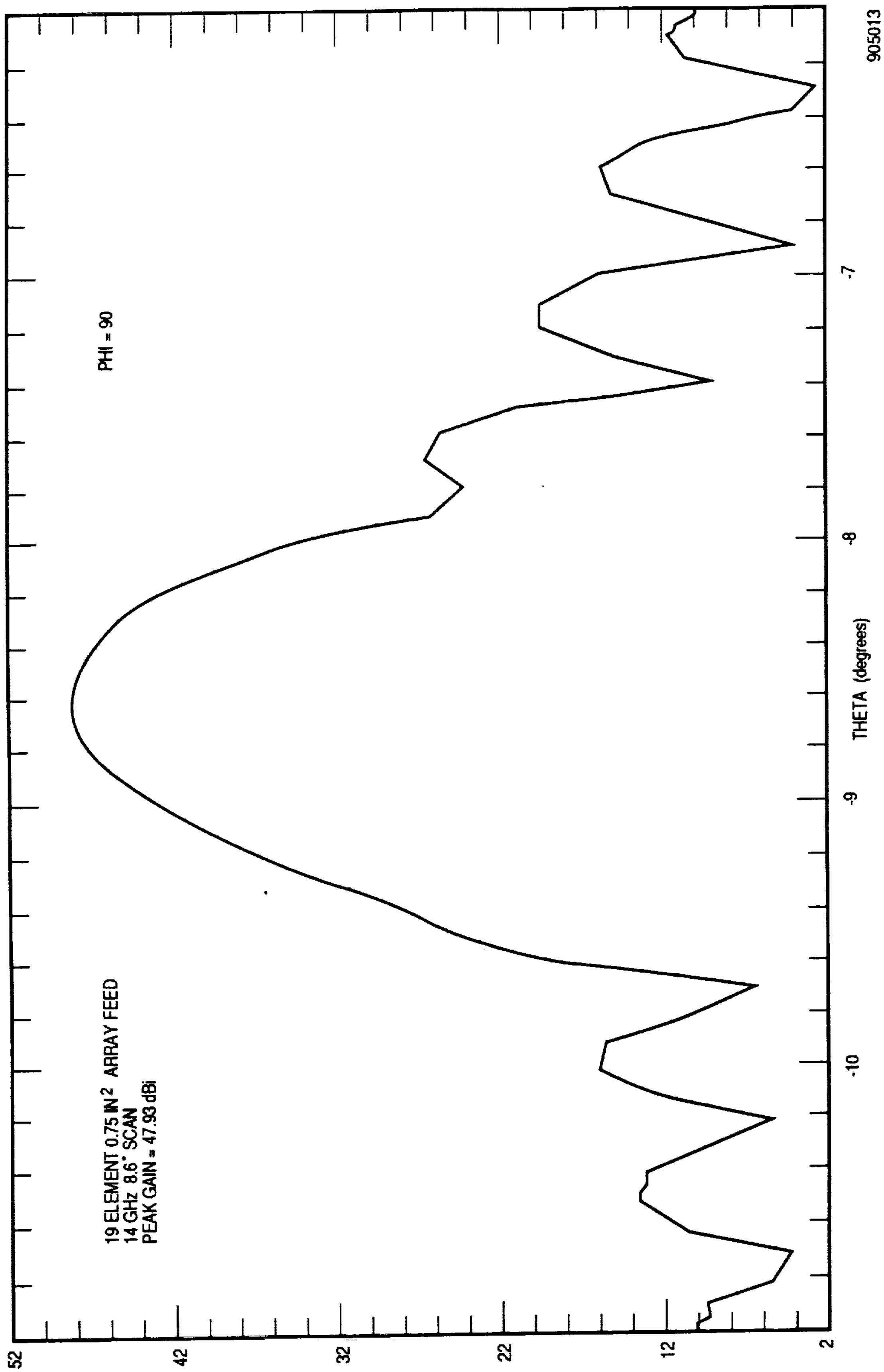

Figure E-10. Calculated Scan Pattern at 14 GHz, 0.75inch Elements

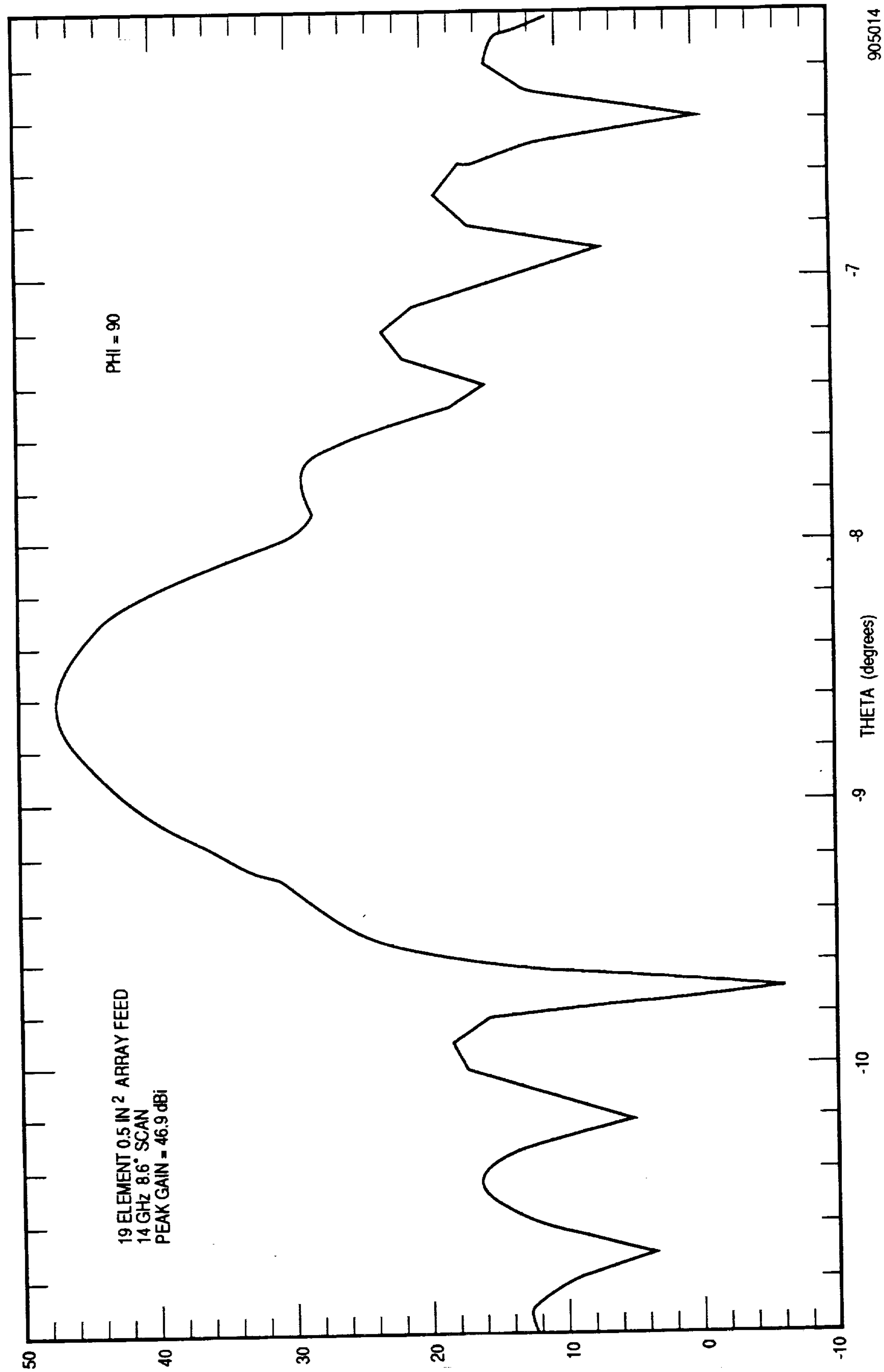

Figure E-11. Calculated Scan Pattern at 14 GHz, 0.5 inch Elements

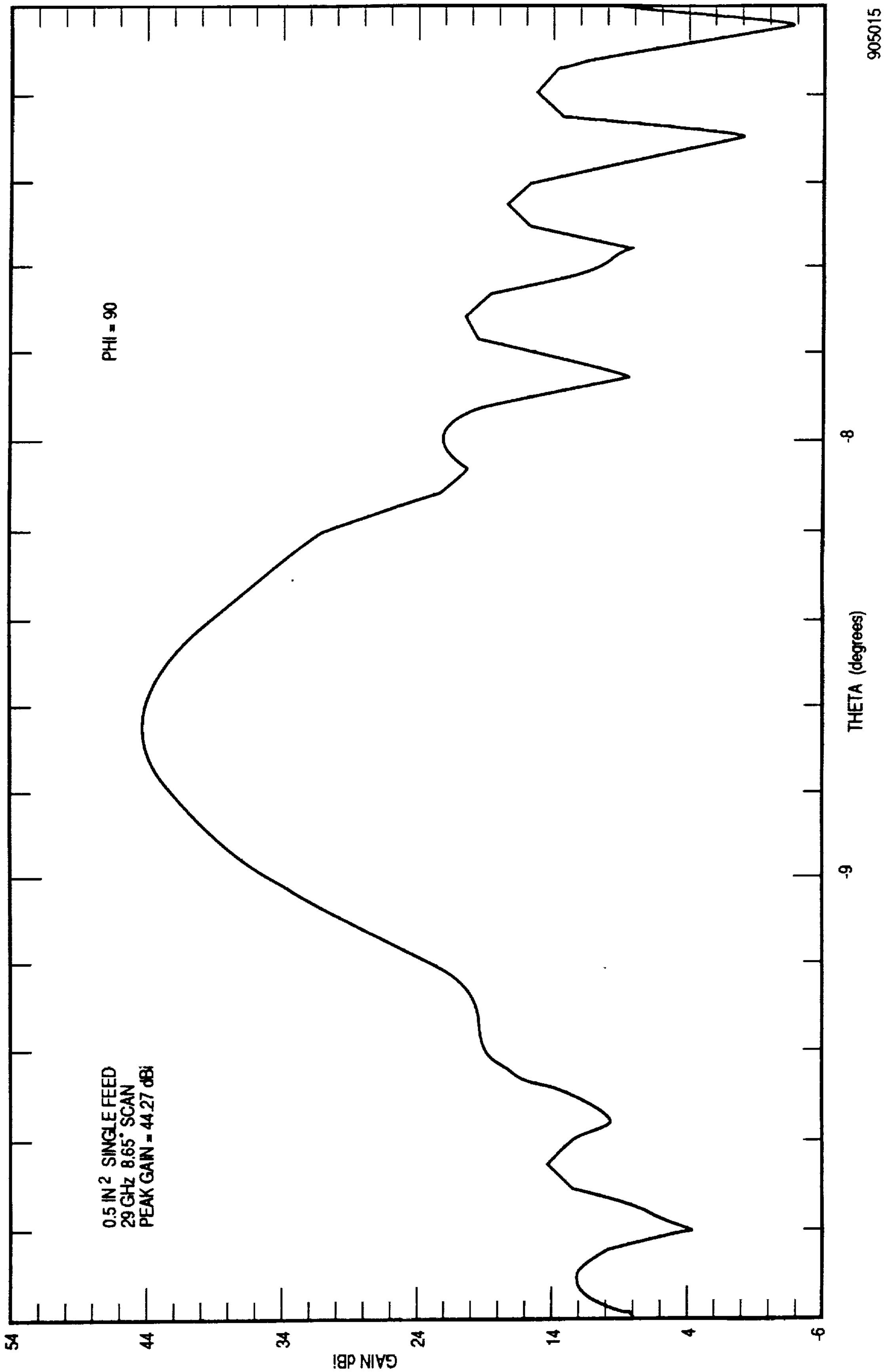

Figure E-12. Calculated Singlet Scan Pattern at 29 GHz

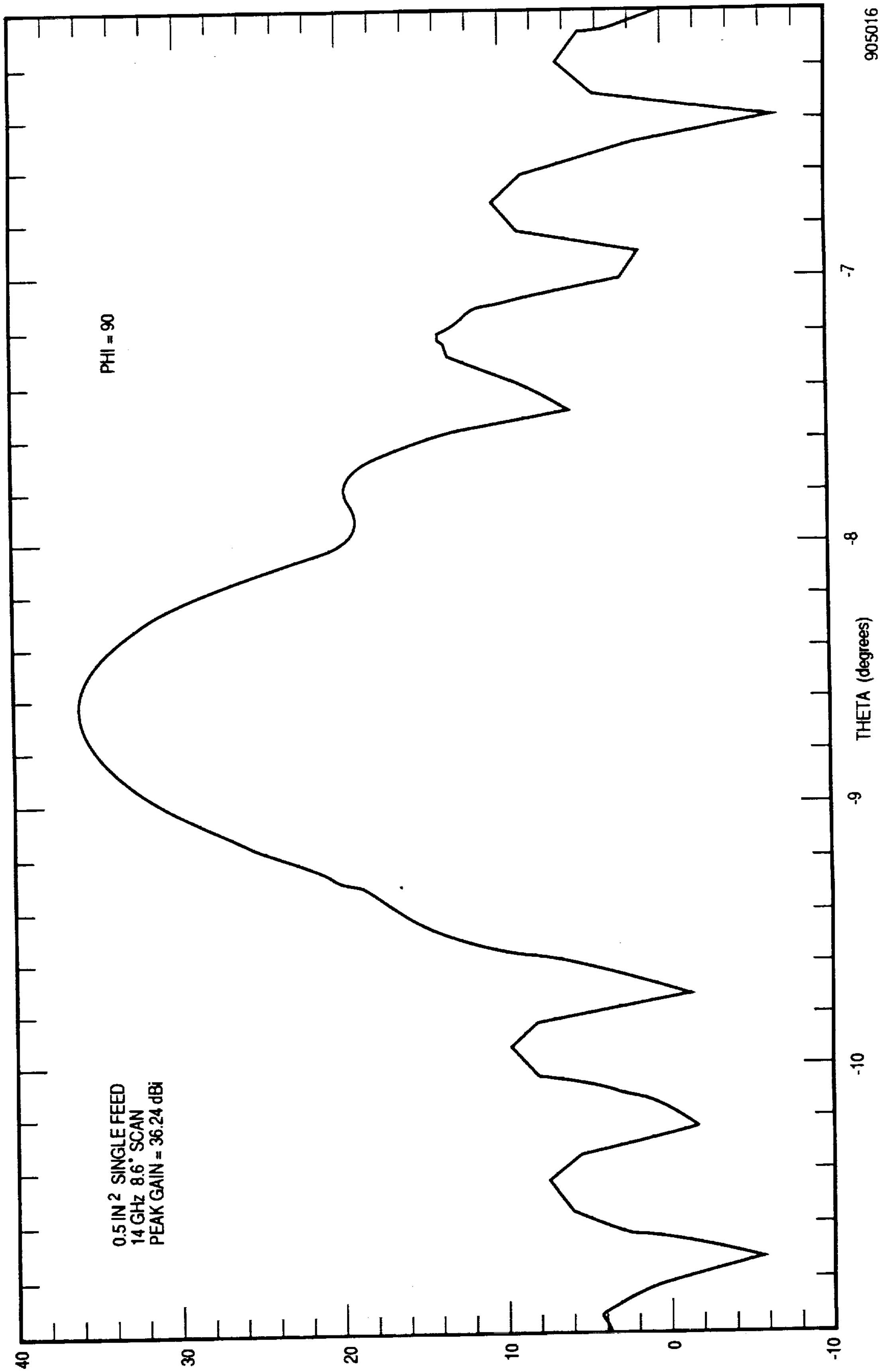

Figure E-13. Calculated Singlet Scan Pattern at 14 GHz

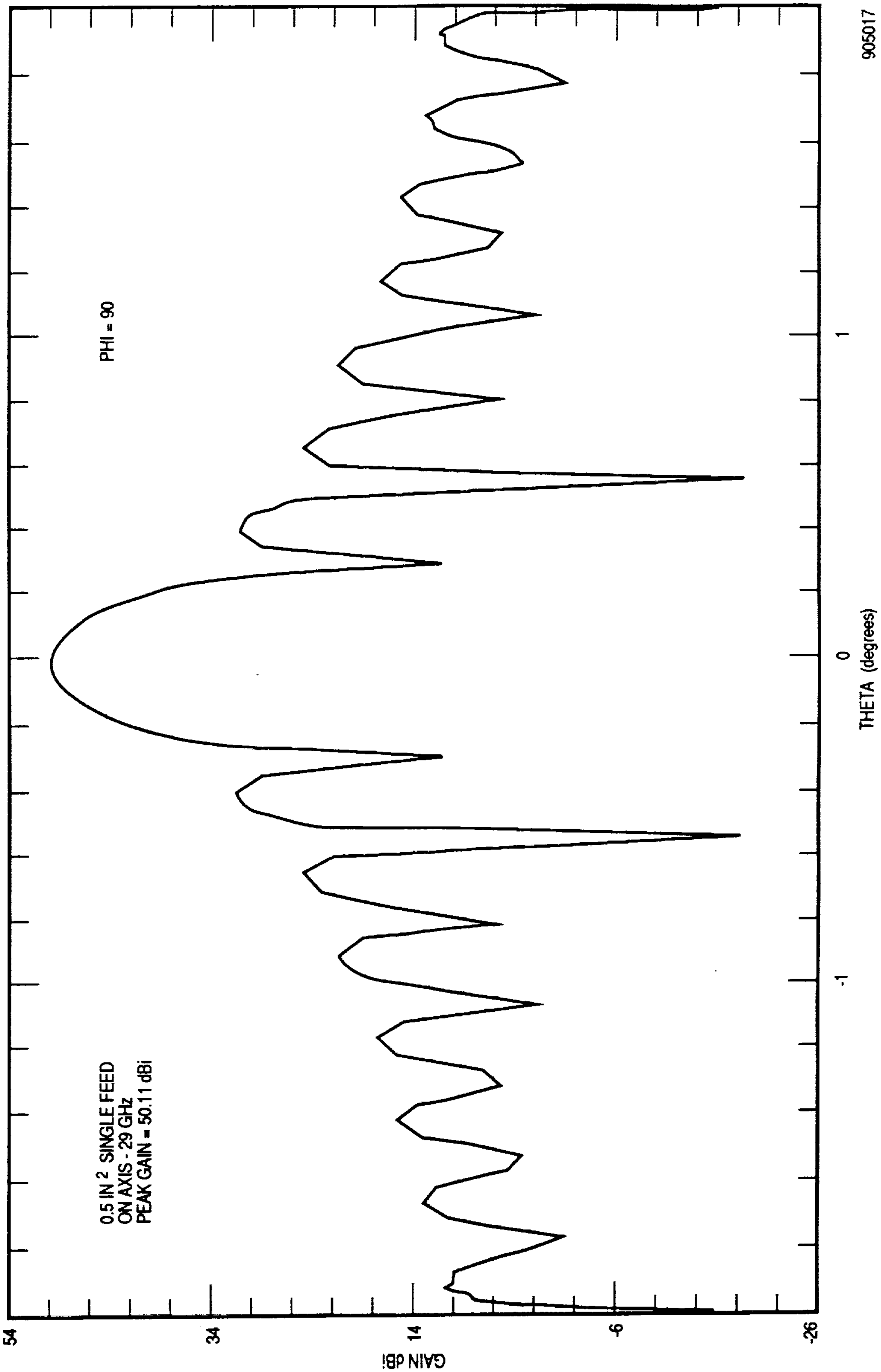

Figure E-14. Calculated On-Axis Singlet Pattern at 29 GHz

An indication of the effectiveness of the 19-element array, and of the extent of the focal field distribution, may be obtained by examining the relative excitations of individual elements in the feed array. These are shown in Figures E-15 through E-18 for the four cases studied in detail; they show the actual gain of the center horn in each case, and the excitations of the surrounding horns relative to this value. It is apparent, for instance, that 0.5 inch horns are too small at 14 GHz, since excitations of some of the edge elements of the array are only 2 dB below the center horns, so that significant amounts of energy must be lost outside the given array.

The scan losses listed in Table E-4 naturally apply to the 19-element feed array using the horn sizes indicated, and for a scan angle of 8.6°. Undoubtedly somewhat lower losses could be obtained through further optimization of horn sizes, and by using a larger feed array (more than 19 elements). However, a larger array would require a more complex feed network, which would be larger, heavier and more lossy. Furthermore, the scan loss would be proportionately lower for less scan. An estimate of this reduction is listed in Table E-5, based on extrapolating other data from Reference E-1. These values also do not include effects of feed network losses, which may be considerable, depending upon the type of controls required (fixed or variable). Such losses may indicate that an even smaller array would be desirable, with a simpler feed network. However, losses of a fixed waveguide network for the 19-element case should not exceed 1 dB, so that this technique may constitute a desirable candidate for the multibeam downlink antenna desired.

Table E-4. Comparative Results of Array Gain Calculations

Freq. (GHz)	Feed Size (in)	Scan Angle	Array Gain (dBi)	Max Aperture Gain (dBi)	Array Loss From Ideal (dBi)	Apparent Aperture Efficiency (%)	Center Horn Gain (dBi)	Array Gain (dB)
29	0.5	8.65°	53.27	57.4	-4.13	38.6	44.27	9.0
19	0.75	8.65°	50.45	53.74	-3.27	47.1	43.32	10.4
14	0.75	8.6°	47.93	51.07	-3.14	48.5	39.5	8.43
14	0.5	8.6°	46.90	51.07	-4.17	38.3	36.24	10.66
29	0.5	0	---	57.4	---	---	50.11	---

Table E-5. Estimated Scan Loss of Array - Fed Reflector Versus Scan Angle - (Values in dB Below Max. Aperture Gain)

Freq. (GHz)	Scan Angle:	0°	3°	6°	8.6°
14		0.4	0.5	2.4	3.15
19		0.4	0.5	2.5	3.27
29		0.5	0.6	3.1	4.1

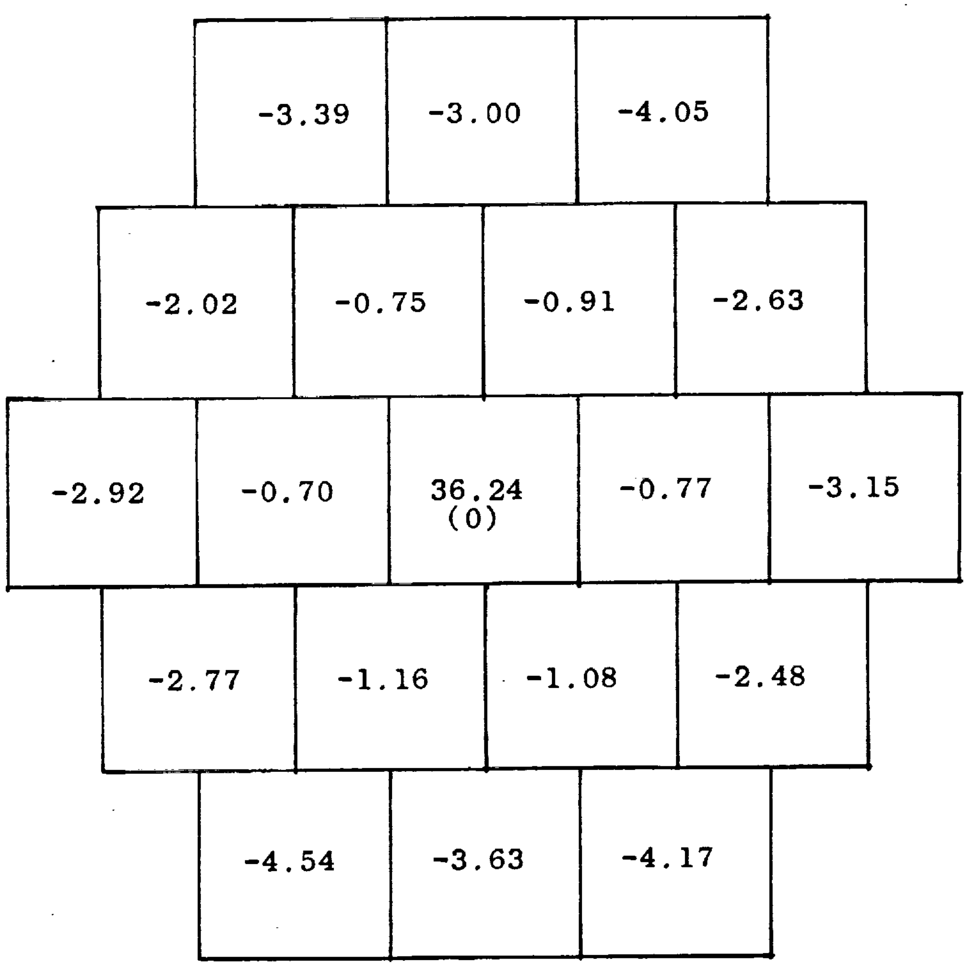

Figure E-15. Element Excitations at 14 GHz, 0.5 inch Feeds

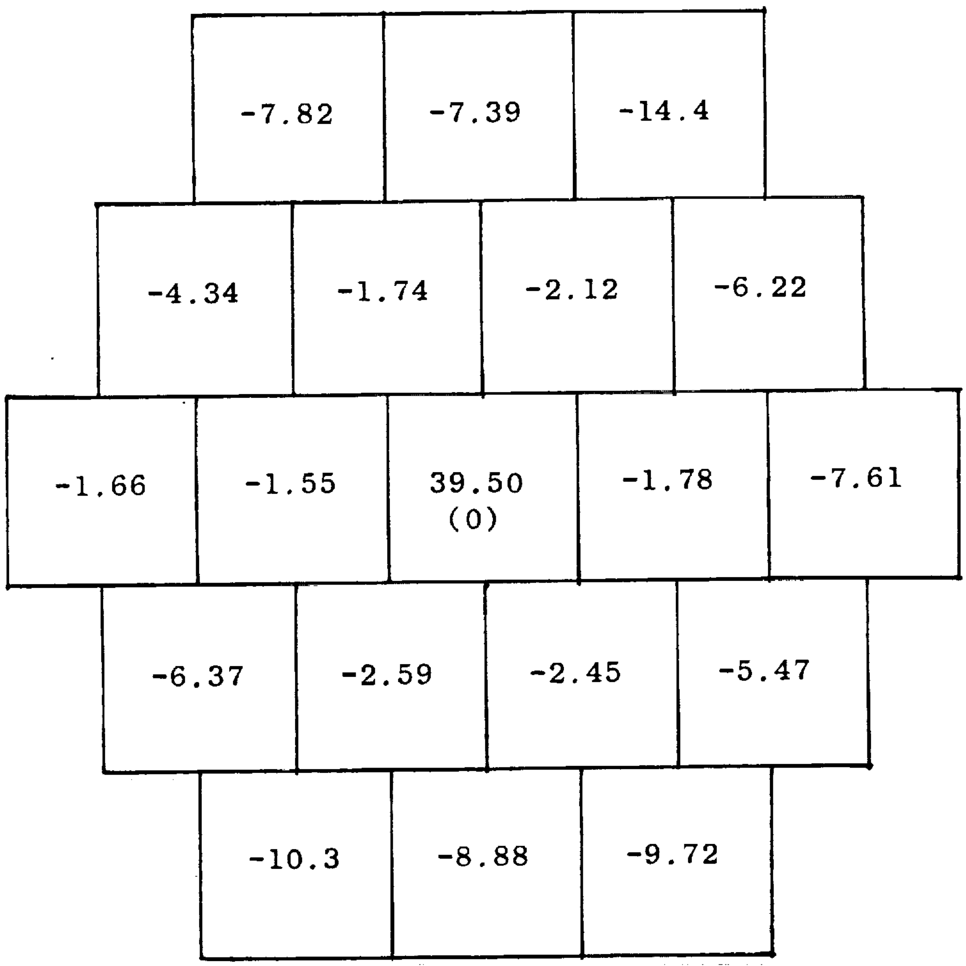

Figure E-16. Element Excitations at 14 GHz, 0.75 inch Feeds

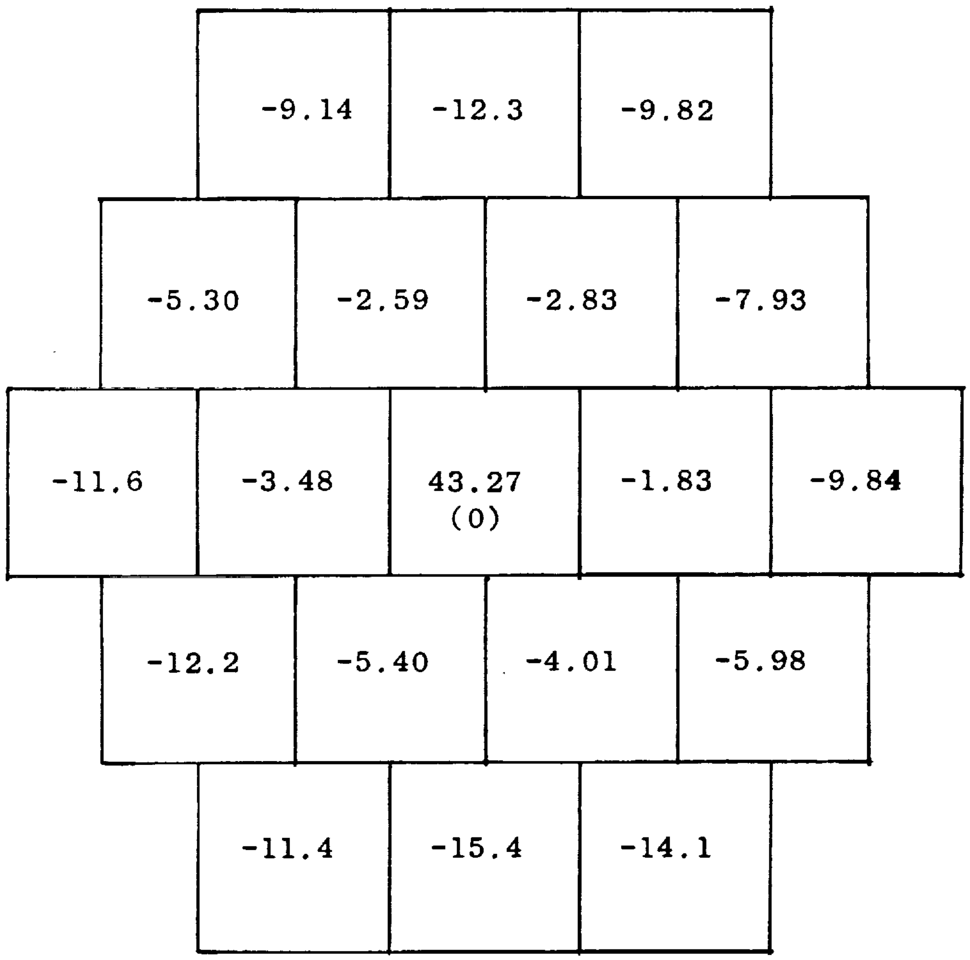

Figure E-17. Element Excitations at 19 GHz, 0.75 inch Feeds

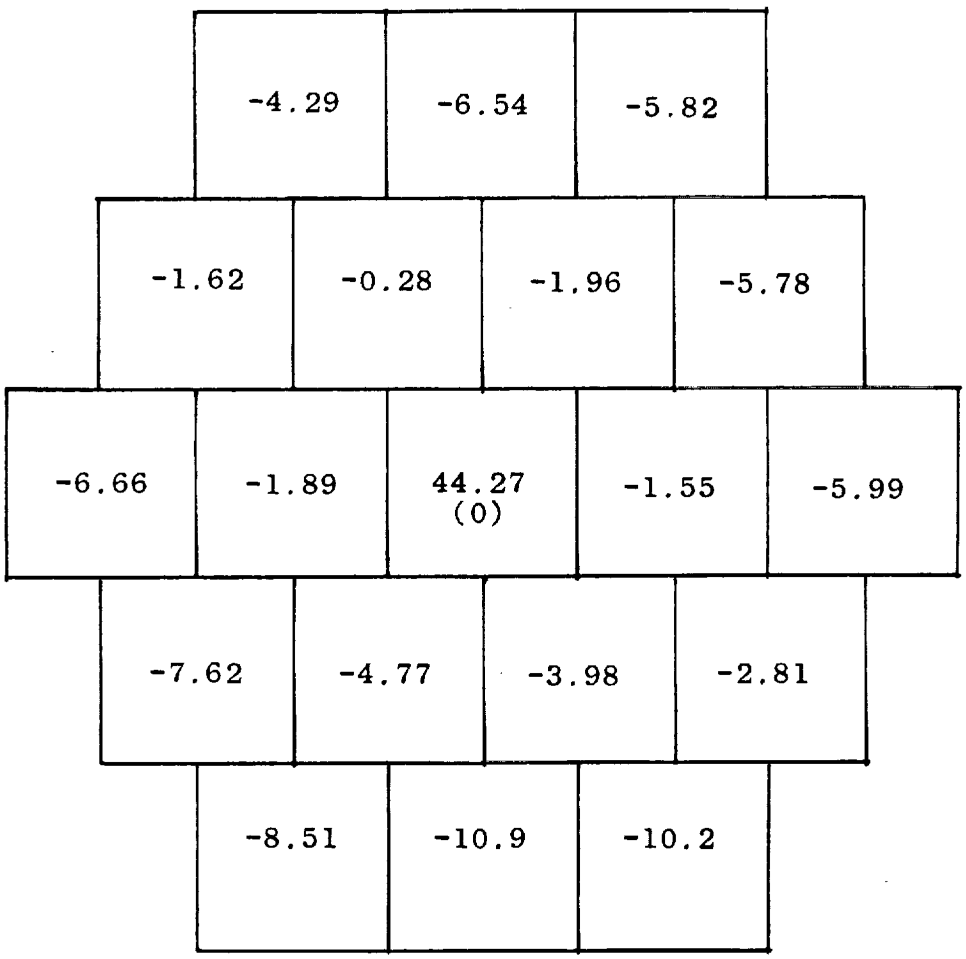

Figure E-18. Element Excitations at 29 GHz, 0.5 inch Feeds

REFERENCES

E-1. C. C. Hung and R. Mittra. "Secondary Pattern and Focal Region Distribution of Reflector Antennas Under Wide Angle Scanning," IEEE Trans. A&P, Sept 1983.

APPENDIX F
Ka/Ku-BAND TRAFFIC TRADES

APPENDIX F
Ka/Ku-BAND TRAFFIC TRADES

In our previous studies, the bandwidth allocations either at Ku-band or at Ka-band were exclusively utilized to serve the entire forward and return service SGL communications needs. While this allowed the initial feasibility study, and resulted in the worst case sizing of the required hardware, it is quite important to study the efficient use of both bands for serving the entire SGL communications needs, based upon the following observations:

- The allocation of bandwidth at Ku-band is insufficient for forward/return link communications requirements even with the use of dual polarizations and frequency reuse, whereas relatively larger bandwidth allocations are made at Ka-band. In addition, Ku-band allocation is in two separate bands for each direction of SGL communications (i.e., two bands for uplink and two bands for downlink) as contrasted with a contiguous Ka-band allocation for each direction of communications.
- Ka-band transmissions undergo more severe degradations (both co-polarization and cross-polarization degradations) due to rain when compared with Ku-band transmissions, especially at the ground stations experiencing heavy rains, such as JSFC, KSFC, and MSFC.
- For a given size of the ATDRSS/SGL Multiple Beam Antenna, the beamwidths at Ku-band are considerably larger than those at Ka-band, thereby requiring much larger ground station separations in order to meet the same interbeam interference specification and allow frequency reuse. With a 2.4 meter antenna, for example, the beamwidths at 30 GHz, 20 GHz, and 15 GHz are respectively 0.30°, 0.45°, and 0.60°. If the adjacent beams are to be located beyond the first sidelobe, the minimum station separation is approximately 2.3 times the corresponding beamwidth at each frequency band. Thus, a minimum station separation at 15 GHz of approximately 1.4° is required as contrasted with a 0.7° separation at 30 GHz.
- Efficient use of bandwidth allocations at each band will perhaps result in less complicated ATDRSS/SGL (especially the switching) hardware.

From the observations listed above, it is desirable to use Ka-band and Ku-band allocations in such a way that the ground stations experiencing worst rainfall use Ku-band, while others use Ka-band for SGL forward/return communications needs. However, some ground stations such as JSFC, MSFC, and KSFC, which experience severe rain attenuations, are within the 2.3 beamwidths (1.4° @ 15 GHz) of each other at Ku-band, even from an ATDRSS located right over the CONUS (e.g., 90° W).

One alternative, then, is to use Ku-band for communications needs of some of these stations (e.g., JSFC and KSFC), and use Ka-band for the other potentially interfering beam covering another ground station (e.g., MSFC). This simplifies a cost-effective ground station design to either Ka-band or Ku-band capability depending on the location where it is used. This alternative, however, does not compensate for the degradation due to rain attenuation encountered at the Ka-band ground terminals.

Another alternative is to provide both Ku-band and Ka-band communications capabilities at each ground station, and use Ka-band at each ground station and switch to Ku-band only when severe rain attenuation is encountered. In addition, if two ground stations are within 2.3 beamwidths (1° @ 20 GHz) of each other, then the station experiencing relatively severe rain attenuation at any given time will have to use Ku-band, while the other station uses Ka-band. Additionally, this approach permits the mobile ground station to enter any fixed beam coverage area, and the mobile coverage beam uses the band not used for the fixed beam services. This approach is implementable; however, both the ground terminal and ATDRSS hardware are more complex than the previous approach and the associated cost factor may be significant.

Another alternative is to use one (e.g., horizontal) polarization of Ka-band and Ku-band capabilities for one ground terminal communications needs and use the other (vertical) polarization for another ground station in an interfering beam. This approach also permits the mobile ground station to enter any fixed beam coverage area, and the mobile coverage beam reuses the bands with polarizations not used for the fixed beam services. Rain attenuation and depolarization effects at Ka-band, however, are still problem areas with this alternative. The approach, then, is to identify the essential and nonessential forward and return services, and route the essential services over the Ku-band and the nonessential services over the Ka-band during the rainy situations.

It is important to recall here that, wherever Ku-band is exclusively used for communications, the insufficient bandwidth allocation in two separate bands limits the simultaneous communications capabilities. In such a case, it is important to carefully address the forward/return link communications needs of each of the ground terminals in order to assess the adequacy of the bandwidth for communications needs in the beam coverage area of that terminal, thereby permitting optimal design choices.

APPENDIX G
USER GROUND TERMINAL CONSIDERATIONS

APPENDIX G
USER GROUND TERMINAL CONSIDERATIONS

For the purpose of the MBA/Switch Study, it is specified that five fixed CONUS ground stations and a mobile CONUS ground station are to be considered. The locations of these ground stations, however, are not specified. Their impact on the performance of ATDRSS system is addressed here.

First, it is to be noted that the rain attenuation and cross-polarization degradation effects at Ka-band are significantly more pronounced at Ka-band (in the order of 20 to 30 dB) than at Ku-band (less than 10 dB). It is therefore important to identify all the ground terminal locations that are subject to heavy rainfall. Figure G-1 shows the various regions, categorized according to the expected annual rainfall figures. It may be desirable for the locations in the heavy rainfall regions to use Ku-band rather than Ka-band for all the forward/return communications requirements.

The bandwidth allocation at Ku-band, on the other hand, is inadequate for serving all the forward/return link communications needs simultaneously for any beam coverage area. In addition, for a given SGL downlink Multiple Beam Antenna (main) reflector size, the beamwidths at Ku-band are relatively larger than those at Ka-band, and the station separation requirements at Ku-band are consequently larger. (A more detailed discussion of this issue is presented in Appendix F.

Figure G-2 shows the ground station separation requirements for frequency reuse with multiple isolation beams, each covering a potential ground user site, and for various satellite locations. The dotted circles correspond to the station separation requirements at Ku-band and the solid circle lines specify the separation requirements at Ka-band.

It is therefore important to select the locations of the ground stations, based on separation requirements at the lowest frequency band of operation (i.e., at Ku-band or at Ka-band) and, if possible, in the regions experiencing low rainfall rates. This, in turn, may require construction, operation, and maintenance of remote ground stations at some distance from actual location of the users. For instance, Johnson Space Center (JSC) and Marshall Space Center (MSFC) are far enough apart from each other so that the station separation requirements at Ka-band are met (refer to Figure G-2); however, both these locations experience heavy rains. Therefore, it is better if they both could use Ku-band for forward/return link communications. On the other hand, they do not meet the station separation requirements at Ku-band. In addition, JSC and White Sands Ground Terminal (WSGT) also do not meet the separation requirements at Ku-band. One solution

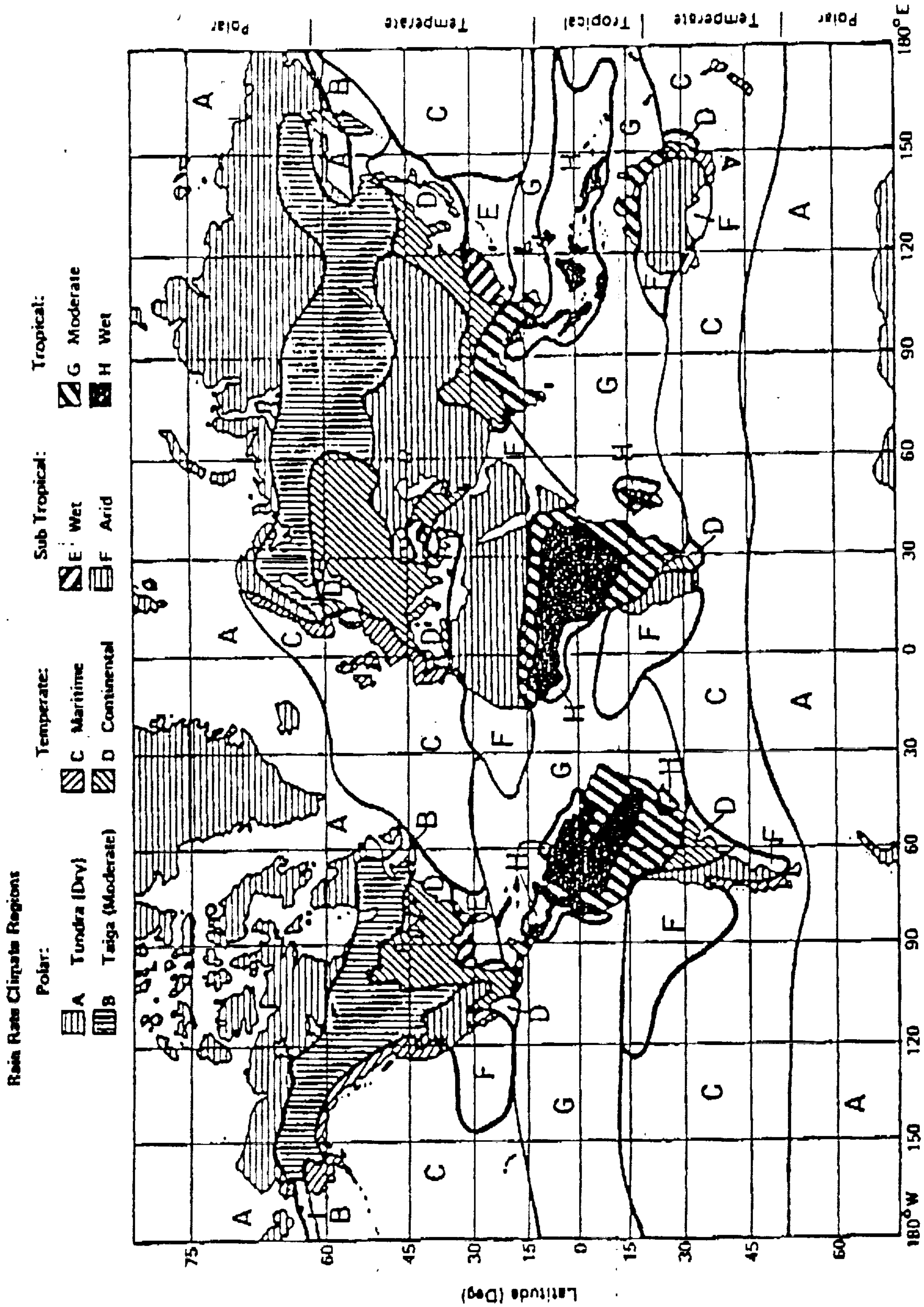

Figure G-1. Rain Rate Climate Regions

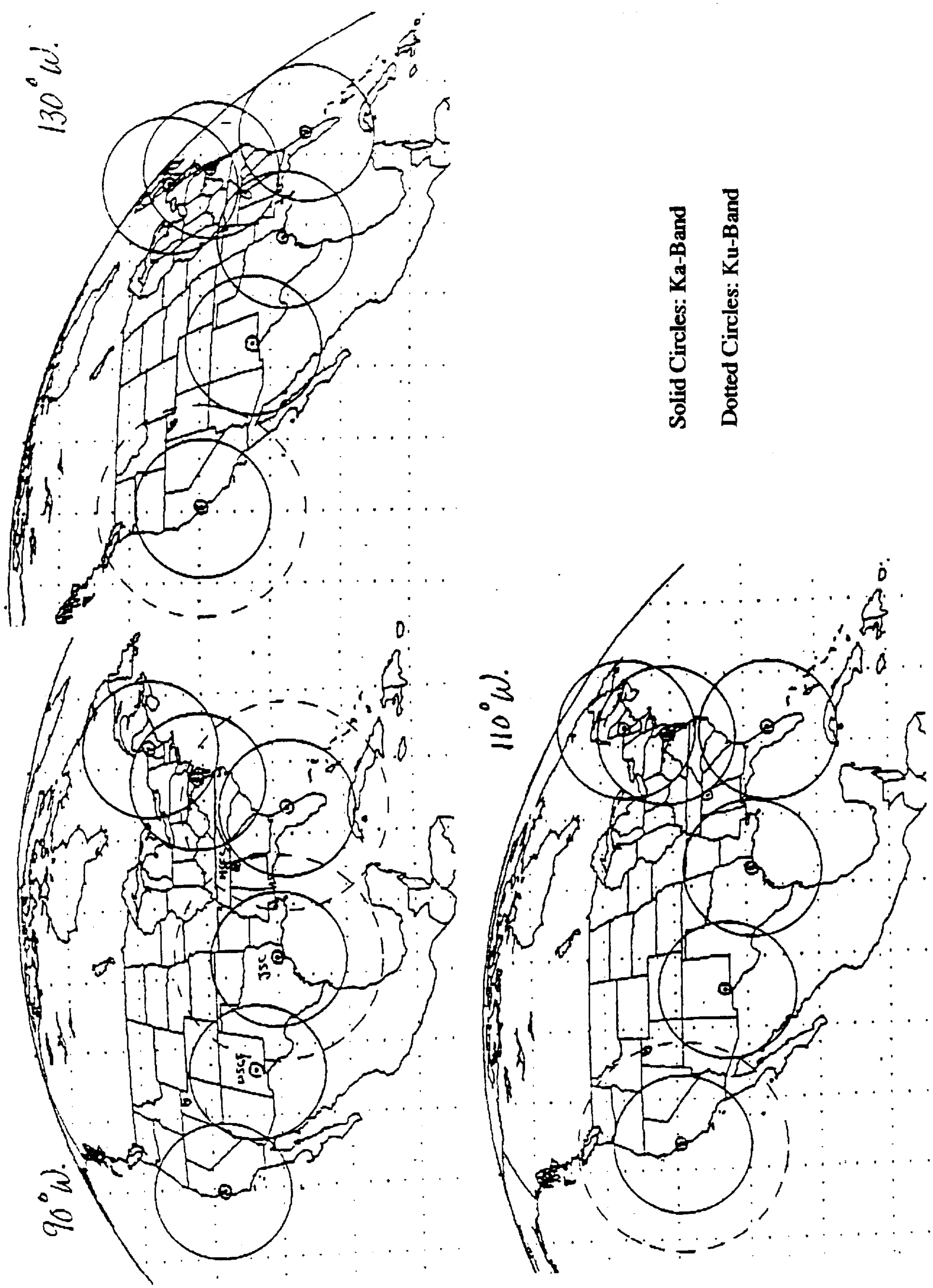

Figure G-2. Ground Station Separation Requirements for this problem is to allocate Ku-band for JSC and allocate Ka-band for WSGT and MSFC. This concept meets the station separation requirements at each band of utilization. Since WSGT experiences low rain rates, there is no concern in utilizing Ka-band for WSGT beam. However, MSFC experiences heavy rains. If MSFC has the communications requirements, needing a separate beam (and frequency reuse), then it would be necessary to place the ground terminal site (remotely) in a nearby area that experiences relatively low rainfall, and deploy ground-based wirelines for communications between the actual user site at MSFC and the remote ground terminal in the nearby low rain region. Of course, this concept poses the associated cost considerations and other related issues, and therefore deserves further studies and planning prior to the system design decisions.

In conclusion, it can be stated that the station separation and rain attenuation requirements at Ka-band and Ku-band, as well as the cost and system performance considerations, require that the individual ground user's forward/return link ATDRSS communications requirements be assessed prior to the determination of the ground terminal locations and the system planning.

APPENDIX H
REDUCING THE COMPLEXITY OF THE SWITCH

APPENDIX H
REDUCING THE COMPLEXITY OF THE SWITCH

The sections describing the architecture of the switch lead to the conclusion that the MBA switch is extremely complicated; unless simplified it will be very difficult or impossible to accomplish. On the other hand, every step taken was done to comply with requirements. The requirements must be simplified to accomplish the solution. We are hoping that in some cases our suggestions will be acceptable and will reduce the complexity without compromising the requirement; in other cases a change in requirements will sacrifice the operation and, therefore, will not be acceptable. The purpose of these discussions is to find a way to simplify the solution without sacrificing the operation.

The requirements of the SOW call for 26 incoming and 42 outgoing services. A switch matrix with 26 inputs and 42 outputs permits every input service to be directed to every output service. A switch like this will have 26 times 42 crossing points or 1092 switching elements. This device can serve the forward direction only, since our microwave switch is a unilateral device and for the return services we need another switch of the same size for a total of 2184 switching elements. These numbers are astronomical and the configuration still does not comply with the requirements. Because there are seven beams in the space-to-ground link, the forward and return services are complicated. Figure 3 of the SOW shows that we have done nothing yet for the space-to-space switch, or for the Ka-band, and everything has to be repeated to include the operation on the Ku-band. This is obviously not a viable solution.

It appears that a square or rectangular switching system, while connecting every possible input to every possible output, is not the best configuration and we decided to look for possible partitioning of the switch in many but smaller groups that are more manageable. This provides a simpler and more elegant configuration.

Since some of the units must split or combine the various signals, it seems necessary to replace a group of switches with combiners. For example, Figure 5.1-8 contains switches 7:1. This switch, if replaced by a 7:1 combiner with passive devices, will be simplified and the size and weight of the equipment will be reduced. The same figure shows the existence of seven 2:2 switches in the input and one in the output. The purpose of these switches is to provide cross connection. However, if the seven switches in the input are completely eliminated we still have the cross-connection capability provided by the output 2:2 switch and have reduced the amount of hardware. If this method is applied to all out switch diagrams we are positive there will be a substantial simplification.

Another possible way to simplify the switch is to establish a more realistic requirement for the connectivity needs. At present every possible signal can be directed to every possible destination at any possible frequency. This may be unnecessary. The SOW indicates that the TNGT ground station is capable of handling higher data rate (4 Gbauds) while the RGT station can handle half of the data rate (2 Gbauds). In this context, it seems that one station can be equipped with more equipment than the other. It may be that some of the ground stations may be designated to operate at Ka-band only, others at Ku-band only, and still others with both capabilities. If this is an acceptable solution the switching equipment can be greatly simplified. A typical example is when an LSA service has to be directed to ground via Ku-band. The complexity of squeezing a very large baud rate per link to a relatively small frequency band causes problems to the switch and contributes to its complexity. We know that one beam should be directed to a mobile station. It is quite possible that the mobile station cannot be equipped with all the frequency bands and in that case the switch as well as other equipment in the satellite can be simplified

When all simplifications have been done that can be without reducing the capabilities, another simplification is possible by using advanced components. MMICs are much smaller, much lighter, and consume less power. Switches are an ideal area for standardization. One design - for instance one chip containing an 8 by 8 switch - can be used for all the applications. There will be a minimum of development and the results will be most satisfactory.

APPENDIX I
GLOSSARY

APPENDIX I
GLOSSARY

Term	Meaning
ABCR	As-Built Configuration Report
A/C	Air Conditioning
ACE	Ancillary Aerospace Equipment
ACN	Ascension Island, STDN Station
ACS	Attitude Control System
ACU	Availability Control Unit
ADC	Actual Direct Cost
ADE	Autotrack Detector Equipment
ADP	Acceptance Data Package
ADPE	Automatic Data Processing Equipment
ADR	Aerospace Data Rate
ADS	Aerospace Data System
ADSS	Aerospace Data System Standard
AFC	Automatic Frequency Control
AFD	Aft Flight Deck
AFETR	Air Force Eastern Test Range
AFETRM	Air Force Eastern Test Range Manual
AFSCF	Air Force Satellite Control Facility
AFSC/SD	Air Force System Command/Space Division
AGC	Automatic Gain Control
AGE	Aerospace Ground Equipment
AGO	Santiago, Chile, STDN Station
AI	Action Item
AIP	Autotrack Interface Processor (computer)
AL	Acronym List
ALC	Automatic Level Control
ALU	Automatic Logic Unit
AM	Amplitude Modulation
AM	Antenna Module
AM/AM	AM to AM Conversion
AM/PM	AM to PM Conversion
ANK	Alphanumeric Keyboard
ANT	Antenna
AOS	Acquisition of Signal
APE	Analog Processing Electronics
APM	Assistant Project Manager
A/R	Axial Ratio
ARIA	Advanced Range Instrument Aircraft
ASC	American Standard Code
ASCII	American Standard Code for Information Interchange
ASE	Airborn Support Equipment
ASSY	Assembly
A&T	Assembly & Test (spacecraft)
ATDRSS	Advanced TDRSS
ATSP	ATDRSS Study Project
ATP	Acceptance Test Procedures
AVE	Aerospace Vehicle Equipment
AW	Advanced WESTAR
AWGN	Additive White Gaussian Noise
AZ	Azimuth

Term	Meaning
BAC	Boeing Aircraft Corporation
BARF	Boeing Aircraft Research Facility
BB	Baseband
B/B	Brass Board
BCD	Binary Coded Decimal
BCL	Basis Control Logic
BCWP	Budgeted Cost of Work Performed
BCWS	Budgeted Cost of Work Scheduled
Bd	Baud
BDA	Bermuda, STDN Station
BEC	Bit Error Comparator
BEP	Budgeted Expenditure Plan
BERTS	Bit Error Rate Test Set
BITE	Built-in Test Equipment
BOD	Beneficial Occupancy Date
BOE	Basis of Estimate
BOI	Break of Inspection
BOL	Beginning of Life
BPF	Bandpass Filter
BPOCC	Backup Payload Operations Control Center
BPSK	Biphase Shift Keying
BRT	Bilateration Ranging Transponder (S-band)
BRTS	Bilateration Ranging Transponder System
BSR	Bit Slip Rate
BTE	Bench Test Equipment
BU	Backup
BW	Bandwidth
C	Celsius, Centigrade
CA	Contract Amendment
CAD	Computer Aided Design
CAD	Coherent Amplitude Detector
CADM	Configuration Data Management
CAIN	Caution, Alarm, Information (message) Notification
CAL	Calibration
C-Band	3.9 to 6.2 GHz
CDR	Critical Design Review
CDRL	Contractor Data Requirements List
CMO	Configuration Management Office
CMOS	Complementary Metal Oxide Semiconductor
CMS	Command Management System
C/N	Carrier to Noise Ratio
C/No	Carrier Power to Noise Spectral Density Ratio (dB/Hz)
COMSEC	Communication Security
COTR	Contracting Officers' Technical Representatives
CP	Computer Program
CP	Circular Polarization
CPC	Contamination Protective Cover
CPE	Control Processor Unit
CR	Card Reader
CR	Change Request
CSCSC	Cost Schedule Control System Criteria

Term	Meaning
CST	Comprehensive System Test
C&T	Communications and Tracking
CTFS	Common Time and Frequency Standard
CTS	Control Test Set
CTU	Command and Telemetry Unit
CTV	Compatibility Test Van
CW	Continuous Wave
CA	Data Acknowledge
DB	Data Base
dB	Decibel
DBE	Data Bus Equipment
dBM	Decibel Relative to One Milliwatt
DBRB	Data Base Review Board
dBW	Decibel Relative to One Watt
DC	Direct Current
D/C, DC	Down Converter
DCAS	Defense Contract Administration Services
DCE	Data Control Equipment
DCE	Drive Command Electronics
DDPS	Digital Data Processing System
DEC	Digital Equipment Corporation
DATA	Data Evaluation Laboratory
DG	Data Group or Display Generator
DG1	Data Group 1
DG2	Data Group 2
DI	Discrete Interface
DID	Data Item Description
DIU	Digital Interface Unit
DMA	Direct Memory Access
DMIU	Dual Image Interface Unit
DOD	Department of Defense
DOMSAT	Domestic Satellite
DOY	Day of Year
DP	Data Poll
DP	Data Processor
DPM	Data Processing Management
DPR	Design Problem Report
DPSK	Delta Phase Shift Keyed
DR	Data Rate
DR	Data Reply (data bus)
DR	Discrepancy Report
DRL	Data Requirements List
DRM	Design Reference Mission (IUS)
DSI	DECOM Systems, Inc.
DSN	Deep Space Network
DSRC	Data System Requirements Committee
DTE	Data Terminal Equipment (NASCOM)
DTM	Dual Thruster Module
DV	Data Valid
DVM	Design Verification Model
DVRB	Design Verification Review Board

Term	Meaning
E	Electric Field Strength
Eb/No	Bit Energy-to-Noise Spectral Density Ratio (dB-Hz)
ECC	Error Correction Calculation
ECC	Emitter Coupled Logic
ECD	Engineering Change Directive
ECP	Engineering Change Proposal
ECR	Engineering Change Request
ECRB	Engineering Change Review Board
EEC	Extendable Engine Cone (IUS)
EED	Electro-Explosive Device
EGSE	Electronic Group Support Equipment
EIA	Electrical (Electronic) Industry Association
EIRP	Effective Isotropic Radiated Power (dBW)
EL	Elevation
ELS	Eastern Launch Site
EMS	Electromagnetic Compatibility
EMI	Electromagnetic Interference
EO	Engineering Order
EOL	End of Life
EPROM	Erasable Programmable Read Only Memory
EQUIP	Equipment
ERVS	Emergency Routine Verification SHO
ESA	Earth Sensor Assembly
ESP	Error Signal Processor (autotrack)
ESPE	Emergency Support Period Extension
ESSE	Emergency Support Schedule Changes
ESTL	Electronic System Test Laboratory (JSC)
ET	External Tank
ETC	Engineering Training Center STDN Station, Greenbelt, Maryland, USA
ETO	Emergency Time Out
ETR	Eastern Test Range
EXCON	Executive Control (software component)
°F	Degrees Fahrenheit
F	Transmit Carrier Frequency (Hz)
FAA	Federal Aviation Administration
FAB	Fabrication
FAC	Ford Aerospace Corporation
f_b	Bias Frequency
f_d	Doppler Frequency
F/G	Focal Length-to-Diameter Ratio (antenna)
FDA	Final Design Audit
FDA	Frequency Distribution Amplifier
FDM	Frequency Division Multiplexing
FDR	Final Design Review
FDS	Flight Dynamics System
FEC	Forward Error Correction
FET	Field Effect Transistor
FH	Frequency Hop
FM	Frequency Modulation
f_o	Nominal Center Frequency

Term	Meaning
FOSA	Flight Operations Support Annex
FOV	Field of View (degrees)
FPP	Floating Point Processor
FPS	Feet per Second
FR	User S/C Return Center Frequency
FR	Failure Report
FRB	Failure Review Board
FRR	Flight Readiness Review
FSS	Fixed Service Structure
FST	Functional System Test
FST	Fail Safe Timer
FT	Failover Table
FU	Failed Unit
FWD	Forward
G	Gain (dB)
GaAs	Gallium Arsenide
GCA	GCE Control and Access
GCE	Ground Communications Equipment
GCS	Ground Communications Subsystem
GCU	General Communications Unit
GDA	Gimbal Drive Assembly
GDE	Gimbal Drive Electronics
GDS	Goldstone, CA, USA, STDN Station
GET	Ground Elapsed Time
GFE	Government Furnished Equipment
GHz	Gigahertz (1000 MHz)
GIE	Gyro Interface Electronics
GMI	Goddard Management Instruction
GMIL	Spaceflight Tracking and Data Network Station (KSC)
GMT	Greenwich Mean Time
GOE	Ground Operational Equipment
GOWG	Ground Operations Working Group
GPTE	General Purpose Test Equipment
GRA	Gyro Reference Assembly
GSE	Ground Support Equipment
GSFC	Goddard Space Flight Center
GSTDN	Ground/Space Tracking Data Network
GTF	Ground Terminal Forward
GTOS	Ground Terminal Operations and Support Component
H	Orbital Altitude (used for LEO)
HEMT	High Electron Mobility Transistor
HPA	High Power Amplifier
HRD	High Rate Demodulator
HSI	H/W-S/W Integration
HST	Hardware Status Table
Hz	Hertz (Cycles per Second)
I	In-Phase Channel (QPSK)
IC	Integrated Circuit
ICD	Interface Control Document

Term	Meaning
ICG	Interface Control Group
ICP	Interface Control Plan
ICR	Interface Change Request
ICWG	Interface Control Working Group
ID	Identification
ID	Interface Documentation
ID	Identifier
IDF	Internal Data Format (document)
IF	Intermediate Frequency (also a name of a class of TDRSS service)
I/F	Interface
IFJ	In-flight Jumper
IFL	Interfacility Link
IFV	Interface Verification
IGS	Internal Ground Segment
IGWA	Intergroup Work Authorization
IIRv	Improved Interrange Vector
IMD	Intermodulation Distortion
IMP	Intermodulation Products
IMU	Inertial Measurement Unit
I/O	Input/Output
IOU	Input Output Unit
IPM	Interprocessor Multiplexer (computer)
IRAC	Interdepartmental Radio Advisory Committee
IRIG	Interrange Instrumentation Group
IRN	Interface Revision Notice
ISL	Intersatellite Link
IST	Integrated System Test
I&T	Integration and Test
ITU	International Telecommunications Union
IUI	IFFI, UNIVAC Interface
IVCS	Intrasite Voice Communications Subsystem
J	Joule (unit of energy)
JPL	Jet Propulsion Laboratory
JSC	Johnson Space Center (Texas)
k	Boltzmann's Constant, -228.6 dBW/Hz-K
K	Constraint Length of Convolutional Code
K	Degrees Kelvin
K-band	10.9 to 36 GHz
KBPS	Kilobits per second (also Kbps, kb/s, Kb/sec)
KDD	KSA Despreader Demodulator (for KSAR DG1)
kHz	Kilohertz (also KHz, KHZ)
km	Kilometer (also Km)
KSA	K-band Single Access
KSAF	KSA Forward
KSAR	KSA Return
KSC	Kennedy Space Center (Florida)
KSH	K Shuttle

Term	Meaning
L/C	Launch Complex
LCC	Launch Control Center
LEO	Low Earth Orbit
LDT	Local Data Terminal
LO	Local Oscillator
LOLFE	Loss of Link Forward Equipment
LOS	Loss of Signal
LOS	Line of Sight
LPC	Logical Processing Capabilities
LPS	Launch Processing System
LRD	Low Rate Demodulator
LRR	Launch Readiness Review
LRT	Link Readiness Test
LSA	Laser Single Access
LSB	Least Significant Bit
LSD	Least Significant Digit
LSI	Large Scale Integration
LSSP	Launch Site Support Plan
L/V	Launch Vehicle
MA	Multiple Access
MACP	Multiple Access Command and Pilot (e.g., combiner)
MA-CSE	MA Calibrator Signal Equipment
MAD	Madrid, Spain, STDN Station
MAF	Multiple Access Forward
MAG	Multiple Access Ground
MAGE	Multiple Access Ground Equipment
MAR	Multiple Access Receiver
MARFE	Multiple Access RF Equipment
MASP	Multiple Access Signal Processor
MBA	Multiple Beam Antenna
MBS	Megabits per Second
MCC	Message Class Code
MCC	Mission Control Center
MCG	Manual Command Generator
MCI	Memory-to-Computer Interface
Mc/s	Megachips per Second (also Mc/sec)
MDAC	McDonnell Douglas Aeronautics Company
MDM	Multiplexer/Demultiplexer
MECO	Main Engine Cutoff
MFG	Master Frequency Generator
MFR	Multifunction Receiver (part of GSTDN)
MGSE	Mechanical Ground Support Equipment
MHz	Megahertz (10^6 Hz)
MIC	Microwave Integrated Circuit
MILA	Merritt Island, Florida, STDN Station
MIPS	Million Instructions per Second
MIU	MAGE Interface Unit
MLA	Microwave Link Analyzer
MLP	Mobile Launcher Platform
MMA	Martin-Marietta Aerospace
MMI	Man/Machine Interface

Term	Meaning
MMIC	Monolithic Microwave Integrated Circuit
MMSE	Multiuse Mission Support Equipment
MMT	Multimode Transponder
MOS	Metal Oxide Semiconductor
MPA	Maneuver Planning Algorithm
MPL	Master Program Library
MRB	Material Review Board
MRBS	Medium Rate Bit Synchronizer
MRD	Medium Rate Demodulator
MS	Millisecond
MSA	Microwave System Analyzer
MSB	Most Significant Bit
MSFC	Marshall Space Flight Center (Alabama)
MSG	Message Stream Generator
MSM	Mission Simulation Model
MSOCC	Multisatellite Operations Control Center
MSU	Main Storage Unit
MTA	Measurement Tolerance Allowed
MTAS	Microwave Transistor Amplifiers
MTBF	Mean Time Between Failures
N/A	Not Applicable; Not Available
NASA	National Aeronautics and Space Administration
NASCOM	NASA Communication Network
NBS	National Bureau of Standards
NCC	Network Control Center (at GSFC)
NCE	Network Communications Engineer
ND	Network Director
NDTP	Network Development Test Plan
NEC	Nippon Electric Corporation
NEI	Nonexplosive Initiator
NF	Noise Figure
NGE	Noise Generator Equipment
NGT	NASA Ground Terminal (at WSGT)
NIMS	NASA Interface Monitoring System
NIU	NASCOM Interface Unit
NMI	NASA Management Instruction
NNTT	NASA Network Test Team
NOCC	Network Operations Control Center
NOD	Network Operations Division
NOSP	Network Operations Support Plan
NOSS	Network Operations Support Specialist
NPR	Nonprocessor Request
NRT	Network Readiness Test
NRZ	Nonreturn to Zero
L,M,S	Nonreturn to Zero Level, Mark, Space
NSCI	NASA System Control Interfaces
NSE	Network System Engineer
NSM	Network Support Manager
NSP	Network Support Plan
NSTI	NASA Simulation Traffic Interface
NTTF	Network Test and Training Facility, GFSC

Term	Meaning
NUTI	NASA User Traffic Interface
NVR	Nonvolatile Residue
OBC	Onboard Computer
OGF	Orbit Determination Facility
ODM	Operational Data Message
OFT	Orbital Flight Test (Shuttle)
OI	Operational Instrumentation
OIWG	Operations Interface Working Group
O&M	Operations and Maintenance
OMT	Orthomode Transducer
OPF	Orbiter Processing Facility
OPI	Orbiter Payload Interface
OPID	Operations Procedure Interface Document
OPM	Operations Procedure Message
OPS	Operations
OR	Operations Requirements (Document)
ORB	Orbiter
ORB SIM	Orbiter Simulator
ORD	Orbital Requirements Document
ORR	Orroral Valley, Australia, STDN Station
O/S	Operating System
OSCF	Operations Support Computing Facility (at GSFC)
OSF	Office of Space Flight
OSHA	Occupational Safety and Health Act
OSID	Operational System Interface Document
OSTDS	Office of Space Tracking Data System
OTDA	Office of Tracking and Data Acquisition
PA	Power Amplifier
Pacq	Probability of Correct Acquisition
PAG	Portable Address Generator
PAM	Pulse Amplitude Modulation
PAOTS	Power and Ordnance Test Set
PARAMP	Parametric Amplifier
PB	Parallel Binary
PCI	Periodic Convolutional Interleaving
PCIS	Product Configuration Information System
PCM	Pulse Code Modulation
PCMMU	Pulse Code Modulation Master Unit
PCR	Payload Changeout Room (at Launch Complex 39)
PCU	Power Control Unit
PDA	Pin Diode Attenuator
PDA	Preliminary Design Audit
PDF	Project Data Format
PDI	Project Data Interleaver (on Orbiter)
PDM	Propellant Distribution Module
PDM	Pulse Duration Modulation
PDP	Parallel Data Processor
PDR	Preliminary Design Review
PDVF	Payload Design Verification Facility
PERT	Project Evaluation Review Technique (schedule network)

Term	Meaning
PET	Performance Evaluation Test
PET	Phase Elapsed Time
PGHM	Payload Ground Handling Mechanism
PI	Payload Interrogator (Orbiter)
PIP	Payload Interrogator Plan
PIRN	Preliminary Interface Revision Notice
PLL	Phase Locked Loop
PLS	Primary Landing Site
PM	Phase Modulation
PM	Preventive Maintenance
PMA	Property Movement Authorization
PMCD	Part Material Control Document
PMP	Parts, Materials and Processes
PMR	Performance Measurement Report
PMS	Performance Measurement System
PMT	Phase Modulated Transmitter
PN	Pseudo-Random Noise
PN	Pseudo-Random Number
PNP	Preliminary Network Plan
PO	Parallel Output
POCC	Project Operations Control Center (at GSFC)
POWG	Program Operations Working Group
PPLU	Pressurant and Propellant Loading Unit
PPR	Pre-Paramp Redundancy (switch on TDRS)
PPSS	Pressurant and Propellant Service System
PROG	Program
PRD	Program Requirements Document
PROM	Programmable Read Only Memory
PRN	Pseudo-Random Noise
PR&R	Project Review and Reporting
PRT	Project Readiness Test
PSD	Power Spectral Density
PSE	Power Switching Electronics
PSK	Phase Shift Keyed
PSP	Payload Signal Processor
PSP	Program Support Plan
PSS	Portable Simulation System (simulate user of NCC)
PTCR	Pad Terminal Connection Room
PTM	Propellant-Pressurant Tank Module
PWR	Power
QDSB	Quadrature Double Sideband
QPSK	Quadriphase Shift Key
QU	Quarterly
QUI	Quito, Ecuador, STDN Station
R	Range
R.	Range Rate
R..	Range Acceleration
R...	Rate of Change of Range Acceleration
RAAN	Right Ascension Ascending Node
RAM	Random Access Memory

Term	Meaning
RAVE	Ranging Aerospace Vehicle Equipment
RC	Receive Component
RCP	Right Hand Circular Polarization
RCS	Reaction Control System
RCTU	Remote Command and Telemetry Unit
RCU	RMDU Control Unit
RD	Receive Data
RDR	Return Data Relay
RDRM	Return Data Relay Measurement
RF	Radio Frequency
RFI	Radio Frequency Interference
RFP	Request for Proposal
RFPU	RF Processor Unit
RFSOC	RF Spacecraft Operations Center
R-GOE	Ranging Ground Operational Equipment
RGT	Regional Ground Terminal
RHC	Right-Hand Circular
RM	Rate Multiplier
R/M	Reliability/Maintainability
RMA	Reliability/Maintainability & Availability
RMDU	Remote Multiplexer/Demultiplexer Unit
RMS	Root Mean Square
RNIU	Reverse NASCOM Interface Unit (test set)
ROM	Rough Order of Magnitude
ROM	Read Only Memory
ROS	Rosman, North Carolina, USA, STDN Station
R&RR	Range and Range Rate
RSS	Rotating Service Structure
RSSC	Routine Support Schedule Changes
RT	Receive Timing
RTN	Return
RTS	Remote Tracking Station (AFSCF)
RV	Routine Verification
RVCF	Vehicle Checkout Facility
RVE	Routine Verification Equipment
RVS	Routine Verification SHO
RWA	Reaction Wheel Assembly
RX	Receiver
RZ	Return to Zero
SA	Single Access
SAA	Single Access Antenna
S&A	Safe and Arm
SAI	Standard Analog Interface
SAC	Single Access Compartment
SADA	Solar Array Drive Assembly
SAEF-2	Spacecraft Assembly and Encapsulation Facility 2
SAMSO	Space and Missile Systems Organization
SAT	Service Acceptance Test
SAWG	Spacecraft Anatomy Working Group
S-band	1550 to 5200 MHz
SBS	S-band Switch

Term	Meaning
SC	Segment Control (computer)
S/C	Spacecraft
SCC	Segment Control Computer
SCC	Spacecraft Control Center
SCCC	System Control and Computing Component
SCDC	Sampled Channel Doppler Corrector
SCDRL	Subcontract Data Requirements List
SCE	Spacecraft Command Encoder
SCF	Satellite Control Facility
SCN	Specification Change Notice
SCPB	Sample Change Pulse Blanker
SCU	Service Control Unit
SCU	Signal Conditioning Unit
SD	Serial Decimal
SDE	SADA Drive Electronics
SDI	Standard Discrete Interface
SDPF	Sensor Data Processing Facility
SDR	System Design Review
SDS	System Demonstration Scenario
SD&TE	SCC, DBE and TOCC Equipment
SDU	Signal Distribution Unit
SE	Simulation Equipment
SE	Support Equipment
SEC	Spacecraft Equipment Converter
SER	Symbol Error Rate
SGL	Space Ground Link
SGLS	Space Ground Link Subsystem (AFSCF)
SHO	Service Schedule Orders
SIC	Service Identification Code
SID	System Interface Document (within space segment)
SIITP	System Implementation, Integration and Test Plan
SIM	Simulation
SIM/CAL	Simulation Calibration Component
SIMS	Simulation SHO
SIM/VER	Self-Check Function of Simulation and Verification
SINC	Spacecraft Integration Contractor (BAC)
SIR	Supplier Information Report
SIRD	System Instrumentation Requirements Document
SIT	Select In Test
SIU	Signal Interface Unit
SIU	Storage Interface Unit
SLR	Status Level Report (Equipment Status Report)
SLS	Status Level Status
SLS	Secondary Landing Site
SMA	S-band Multiple Access
SM GPC	System Management/General Purpose Computer
SMM	Solar Maximum Mission
SMU	System Maintenance Unit
S/N	Signal-to-Noise Ratio
S:(N+1)	Signal-to-Noise Plus Interference Ratio
SNR	Signal-to-Noise Ratio
SOC	Simulations Operations Center, GSFC

Term	Meaning
SOI	Synchronous Orbit Injection
SPEC	Specification
SPI	Supervised Parallel Input
SPIDPO	Shuttle Payload Integration Development Project Office
SPIF	Shuttle Payload Interface Facility
SPO	Supervised Parallel Output
SPR	Software Problem Report
SPS	Symbols per Second
SQPN	Staggered Quadriphase Pseudo-Random Noise
SQPSK	Staggered Quadriphase Phase-Shift Keyed
SRAD	System Requirements Allocation Document
SRE	STDN Ranging Equipment
SRM	Solid Rocket Motor
SRO	System Review Office
SRT	Station Readiness Test
S/S	Space Segment
SSA	S-band Single Access
SSAF	SSA Forward
SSAR	SSA Return
SSH	SSA Shuttle
SSIT	Software System Integration and Test
SSMCC	Space Shuttle Mission Control Center
SSO	Space Shuttle Orbiter
SSP	Software Standards and Procedures
SSTDMA	Spacecraft Switched TDMA (AW payload)
SSTDRSS	Shared Service TDRSS
SSV	Space Shuttle Vehicle
STAR	Shuttle Turnaround Analysis Report
STC	Satellite Test Center of AFSCF
STC	System Test Controller
STDN	Spaceflight Tracking and Data Network
STDS	Space Tracking and Data Systems
STGT	Second TDRSS Ground Terminal
STR	Software Task Requirements
STS	Shuttle Tracking Services
STS	Space Transportation System (Space Shuttle)
STU	System Transition Unit
STV	Structural Test Vehicle
SUPIDEN	Support Identification Code
S/W	Software
T	Noise Temperature (in °K)
TA	Time Acquire
TACQ	Time to Acquire (seconds)
TBD	To be Determined
TBR	To be Resolved (or Revised)
TBS	To be Supplied
TC	Transmit Component
T&C	Telemetry and Command
TCM	Technical Coordination Meeting
TCXO	Temperature-Compensated Crystal Oscillator
T&DA	Tracking and Data Acquisition

Term	Meaning
TDA	Tunnel Diode Amplifier
TDAS	Tracking and Data Acquisition System
TDM	Time Division Multiplexing
TDMA	Time Division Multiple Access
TDN	Test Distortion Network (Harris)
TDR	Test Discrepancy Report
TDR	Time Domain Reflectometer
TDR	Tracking and Data Relay
TDRE	Tracking Delay Relay Experiment
TDRS	Tracking Data Relay Satellite
TDRSS	Tracking Data Relay Satellite System
TDY	Teledyne
TELOPS	Telemetry On-Line Processing System
TEM	Test Evaluation Matrix
TLC	Test Loop Component
TLM	Telemetry
TLP	Transmission Level Point
TNGT	ATDRSS Network Ground Control
TO	TDRS Operations (software component)
TO	Time Zero
TOCC	TDRSS Operations Control Center
TOD	Time of Day
TPD	TRW Project Drawing
TPF	Telemetry Processing Facility (at GSFC)
TPID	Telecommunications Performance and Interface Document
TPM	Technical Parameter Monitor (computer program)
TPSR	Team Program Status Review
TR	Trouble Report
TRB	Test Review Board
TRVM	Test Requirement Verification Matrix
TRW	Thompson, Ramo, and Wooldridge
TS	System Noise Temperature
TS	TDRS Support Component (software)
TSDM	Tracking Service Data Message
TSGLT	ATDRSS SGL Terminal
TSS	Test Support System
TSWG	Test Scenario Working Group
TT	Terminal Timing
TT&C	Telemetry, Tracking and Command
TTG	Test Traffic Generator (simulator)
TTGE	Test Traffic Generator Equipment
TT&S	Traffic Tracking & Simulation
TTY	Teletype
TWG	Test Working Group
TWTA	Traveling Wave Tube Amplifier
TX	Transmitter
UASC	User Assignment Switch Control
UBC	Ultra High Bit Rate Converter
UBS	Universal Breadboard Simulator (Harris)
UCI	Unsupervised Command Interface, Unsupervised Control Interface
UDI	Unsupervised Data Interface

Term	Meaning
UDF	Unit Development Folder (software)
UDS	Universal Documentation System
UHRBS	Ultra High Rate Bit Synchronizer
UHRD	Ultra High Rate Demodulator
ULA	Fairbanks, Alaska, USA, STDN Station
UPN	Universal PN
UPS	Uninterruptible Power Supply (facility power)
UQPSK	Unbalanced Quadriphase Shift Key
US	User Service
USB	Unified S-band
USC	User Spacecraft
USCS	User Spacecraft Simulator
USCSC	User Spacecraft Simulator Component
USNO	U.S. Naval Observatory, Washington, D.C.
USR	Upper Saddle River
USRT	Universal Station Readiness Test
USS	User Service Support (software)
USSE	User Spacecraft Simulator Equipment
UTC	Universal Time Coordinated
UTDF	Universal Tracking Data Format
UTF	Universal Tracking Format
UTLFE	User Traffic Forward Equipment
UTFL	User Traffic Forward Link
UTLRE	User Traffic Link Return Equipment
UVSC	User Verification and Simulation Component
VAB	Vehicle Assembly Building
VAR	Variance Analysis Report
VCM	Volatile Condensible Materials
VCO	Voltage Controlled Oscillator
VCXO	Voltage Controlled Crystal Oscillator
VDE	Valve Drive Electronics
VDS	Video Distribution Switch
VER	Verification
VGHM	Vertical Ground Handling Mechanism
VHF	Very High Frequency
VITS	Vertical Internal Test Signals
VPE	Vertical Processing Facility
VSWR	Voltage Standing Wave Ratio
VT	Video Terminal
WARC	World Administrative Radio Conference
WBD	Wideband Data
WBDI	Wideband Data Interface
WBDI	Wideband Data Interleaver
WBS	Work Breakdown Structure
WD	Wideband Discrimination (Shuttle service)
WESTAR	Western Union Communications Satellite
WS	White Sands
WSA	60 GHz Single Access
WSGS	White Sands Ground Station
WSGT	White Sands Ground Terminal

Term	Meaning
WSNGT	White Sands NASA Ground Terminal
WSTF	White Sands Test Facility
WTR	Western Test Range
WU	Western Union
WU	Western Union Space Communications, Inc.
WUDF	Western Union Director of Facilities
WUSCI	Western Union Spacecom, Inc.
WUTCO	Western Union Telegraph Company
X	Spacecraft Roll Axis (direction of flight for on-orbit TDRS)
XLR	Translator
Y	Spacecraft Pitch Axis (points south for on-orbit TDRS)
Z	Spacecraft Yaw Axis (points to earth for on-orbit TDRS)
Z	Zulu Time (same as GMT)
ZOE	Zone of Exclusion